Origin and evolution of mafic volcanics of Sumatra (Indonesia): their mantle sources, and the roles of subducted oceanic sediments and crustal contamination.

by

Massimo Gasparon

Dottore in Scienze Geologiche
University of Firenze

Submitted in fulfilment of the requirements
for the degree of
Doctor of Philosophy (Geology)
University of Tasmania

October, 1993

STATEMENT

This thesis contains the result of research done in the Geology Department, University of Tasmania, between 1989 and 1993. This thesis contains no material which has been accepted or submitted for the award of any other higher degree or graduate diploma in any tertiary institution, and to the best of the author's knowledge and belief, the thesis contains no material previously published or written by another person, except where due reference is made in the text of the thesis.

Massimo Gasparon
University of Tasmania
October 1993

CONTENTS

LIST OF TABLES

LIST OF FIGURES

Acknowledgments

Many people from several corners of the world have helped me in different ways to complete this thesis.

- My supervisor, Dr Rick Varne, invited me to Tasmania while I was still an undergraduate student in Firenze, provided continuous and enthusiastic support and supervision, arranged substantial financial support during my last year in Hobart, and, most of all, gave me a chance to broaden my scientific and personal experience.

- Professors Piero Manetti (Department of Geology - University of Firenze) and Angelo Peccerillo (Department of Geology - University of Messina) helped me at various stages before and during my stay in Hobart, and Prof Manetti also provided some financial support. Drs Sandro Conticelli and Lorella Francalanci were invaluable in keeping me in touch with everyone and everything in Firenze.

- Field work in Indonesia was made possible through the help of the Indonesian Embassy in Roma, the Indonesian Institute of Science (LIPI), and the Geological Research and Development Centre (GRDC) in Bandung. Dr Rab Sukamto, Director of GRDC, sponsored the field work in Sumatra, provided logistic support and gave me free access to the GRDC facilities. Mr Kardana Hardjadinata and Sigit Maryanto were a great help in the field in Sumatra, and Mr Turisman drove us safely on a 6000 km journey from Bandung to Medan. Special thanks to all the locals who helped me to get where I wanted to by whatever means, and who made my stay in Sumatra extremely enjoyable and profitable.

- Professor Hans Friedrichsen invited me to the Department of Geochemistry of the Free University of Berlin, and gave me free access to the laboratory facilities, and together with Drs Konrad Hammerschmidt, David Hilton, Stephan Teufel, and Ms Monika Feth and Carla Weniger helped me at various times during my stay in Berlin and provided an excellent working environment. I am particularly grateful to Dr David Hilton, who shared with me the thrill and pleasure of field work in Sumatra and quite a few beers and discussions in various parts of the world, and who arranged my visit to Berlin and gave permission to use some of his unpublished He isotope data in this thesis, and to Dr Stephan Teufel, who taught me how to pull apart (and then put back together) a Finnigan MAT 261 mass spectrometer, and all I know about mass spectrometry.

- Dr Vadim (Dima) Kamenetsky initiated me to the wonders of mineral chemistry and to the hidden beauty of olivine crystals, and gave me an enormous help with the separation and analysis of mineral grains, and with the melt inclusion experiments. Most of all, I thank Dima and his family for their genuine friendship and enthusiasm.

- Dr Tony Crawford made some very useful comments to some of the chapters of this thesis and was a constant source of encouragement.

- Drs John Foden and Simon Turner, and many others at the Department of Geology of the University of Adelaide, helped with some of the Sr and Nd isotope analyses and with the setting of a Sr-Nd separation laboratory in Hobart.

- Mr Phil Robinson and Aung Pwa helped with the XRF analyses and the Sr and Nd isotope separation. Mr Aung Pwa was great in preparing all those samples for Sr and Nd isotope analysis.

- Mr Wislaw Jablonski kept the Cameca SX 50 electron microprobe "hot 'n running" at top levels.

- Mr Simon Stephens and the lapidary staff are thanked for countless thin sections. Mr Peter Cornish and the secretaries, Ms Jeanette Hankin and Julie Beattie, helped in various situations.

- My fellow postgraduate students and many post-doctoral fellows created a good and friendly working environment, and shared with me many discussions, beers, and late-night home delivered pizzas. I particularly wish to acknowledge all the students who shared the room with me at the University during these years - Ingvar Sigurdsson (my long-time flat-mate), Ruth Lanyon, Greg Yaxley, Fernando Della Pasqua, Alicia Verbeeten, Geoff Nichols, Mike Seitz, and many others, including Drs Russell Sweeney, Steve Eggins, Leonid Danyushevsky, Bob Musgrave, and Udi Hartono, Sampan Singarajwarapan, Anthea Hill, Kim Hein, Marcel Kampermann, Andrew McNeill, Paul Kitto, Russell Fulton, Mark Doyle, Alex Andronikov, Ai Yang.

- Thanks to all the friends in Hobart and Firenze (they know who they are - no need to list their names here), including people mentioned above, and especially all the friends who wrote me so many letters and e-mails, and who came all the way from Firenze (or Melbourne) to visit me.

- Special thanks to Teodor and Ariella Flonta, who "adopted" me in their family and provided me a job which helped me substantially to survive above the poverty line, and students and staff at the Department of Italian of the University of Tasmania.

- I wish to thank Louise for making me feel at home in Hobart, for her patience during the last stages of this thesis, for her help with English ("a clumsy adaptation of a barbarian language to a civilised alphabet", as I defined it), and finally, for coming home to Firenze with me.

Finally, I dedicate this thesis to my parents and my sister, who always supported and encouraged me.

Abstract

The Quaternary volcanoes along the Sunda arc of Indonesia are a well known example of subduction-related volcanism. Relatively primitive rocks in the arc are rare, so that in the last two decades much attention has been dedicated to the study of the isotopic systematics of the mafic volcanics. These suggest that sediments - or fluids derived from the sediments - subducted along the Sunda Trench have some effect on the chemistry of the arc volcanics only in some sectors of the arc, whereas the isotopic signature of other sectors mainly reflects the composition of their mantle source. However, very little is known about the composition of the mantle beneath the arc, and good quality, representative analyses of oceanic sediments from the northeastern Indian Ocean are scarce. Moreover, the importance of crustal contamination has not been sufficiently tested, at least partly due to the lack of exposure of arc basement in the best studied areas.

Good-quality, modern analyses of volcanic rocks from the Sunda arc mainly come from the relatively easily-accessible areas, but little is known about the least accessible volcanoes in the largest island in the arc, Sumatra, despite the fact that the occurrence of both granitic rocks and very primitive basalts was reported some 70 years ago.

In the first part of this thesis, after a brief review of the studies on the volcanism in the Sunda-Banda arc, an attempt is made to define the chemical and isotopic composition of "typical" oceanic sediments, and continental crust, for use in the modelling of contamination processes along the Sunda Trench.

"Basement" granitoids and arc-related granitoids from several localities in Sumatra were investigated and described, and compared with the better known granitoids of peninsular southeast Asia.

Two groups of granitoids have been identified. Arc-related granitoids, generally older than the Quaternary arc volcanics, are found along the arc, follow the calcalkaline trend of arc rocks, and have Sr, Nd, and Pb isotope systematics similar to those of Indian Ocean basalts (including basalts from south Sumatra). East of the Semangko fault, granitoids and pyroclastic rocks are mainly of "S-type", and have considerably high initial $^{87}Sr/^{86}Sr$ values, similar to those found in the Central Granitoid Province of Southeast Asia. Therefore, the Semangko fault and the Quaternary arc may represent an important tectonic boundary, defining the southeastern margin of the

SIBUMASU terrane. No systematic variations in geochemical and isotopic composition from north to south Sumatra have been observed in the two groups of granitoids. This suggests that there are no major variations in the isotopic composition of the source of arc volcanism and of the continental crust from north to south Sumatra.

Oceanic basalts from the Northeastern Indian Ocean were studied to test the possibility of the existence, beneath the Sunda arc, of mantle sources with OIB composition and "enriched" (EM, HIMU) isotopic signatures.

Basalts with an isotopically "enriched" component are described for the first time in three new locations in the Northeastern Indian Ocean: the Cocos Plateau, the Investigator Ridge, and site DSDP 22 211. Only the occurrence of this type of basalts along the Investigator Ridge is consistent with a "fixed hot spot" model of evolution of the Northeastern Indian Ocean. Pre-"Gondwana rifting" basalts in the Argo Abyssal Plain seem to have isotope systematics similar to Atlantic and Pacific MORB.

For the sediments, the large (but qualitatively poor) existing database was integrated with new data to provide a more precise picture of variations of chemical and isotopic composition of the sedimentary cover in time and distance from and along the arc.

The variability in major and trace element composition observed in oceanic sediments can be modelled as the result of variable degrees of dilution of a detrital component by organogenic calcite and silica. Pb isotopes can distinguish between pre- and post-Miocene sediments, and the Sr, Nd, and Pb isotope systematics in old sediments are consistent with their derivation from volcanogenic material with isotope systematics similar to those of Indian Ocean basalts, and material from pre-Mesozoic continental crust similar to that found in Sumatra. On the other hand, post-Miocene sediments seem to be enriched in a U-rich component.

Using the new data, the distribution of volcanism along Sumatra and the west Sunda arc and the effects of crustal and sediment contamination are briefly reviewed and discussed.

These data suggest that neither contamination of the mantle source by bulk sediment nor bulk assimilation of crustal material by an uprising melt can satisfactorily account for the Sr, Nd, and Pb isotope systematics observed in most arc rocks in the west

Sunda arc.

Fluids released from the subducted sediments do not seem to be able to reproduce the range and spatial distribution of $^{87}Sr/^{86}Sr$ - $^{143}Nd/^{144}Nd$ values in the west Sunda volcanic rocks. Pb isotopic values and their variations along the arc also suggest that subducted sediments did not have important effects on the Pb systematics of the west Sunda volcanic rocks.

On the contrary, assimilation of partial melts of crustal material by uprising magmas can account for the Sr, Nd, and Pb isotope systematics in the Sumatran and Jawanese arc rocks, and is consistent with the spatial distribution of Sr, Nd, and Pb isotope values observed from north Sumatra to Lombok. This model requires that Indian Ocean OIB-like mantle, as well as MORB mantle, be present in the mantle wedge, and also requires the existence of pre-Mesozoic continental crust in Sumatra and west Jawa, but its absence in the Bali sector from east Jawa to Lombok.

Relatively low $^{3}He/^{4}He$, and high B/Be and $\partial^{18}O$ values, usually interpreted as evidence for metasomatism of the mantle wedge by slab-derived material, are rare in the west Sunda volcanics, and are best explained by processes occurring at shallow levels (degassing of the magma, percolation of meteoric fluids, assimilation of crustal material), in the magma chamber or at near-surface levels. $^{230}Th/^{232}Th$ values in Holocene rocks are indicative of an OIB source, and there is no evidence for ^{230}Th - ^{238}U disequilibrium and metasomatism of the mantle source by slab-derived fluids.

In the second part of this thesis, all three localities in Sumatra where olivine-phyric basalts had been previously reported (Sukadana, Bukit Telor, and Bukit Mapas) have been studied, together with other alleged occurrences of olivine-phyric basalts elsewhere in Indonesia. Whole rock major, trace and Sr, Nd and Pb isotope analyses, together with detailed mineralogical studies, were carried out to determine the composition of the source and the evolution of these isotopically and compositionally rather unusual (in an arc environment) rocks, and their similarity to OIB and MORB basalts from the Indian Ocean and Australia is evaluated

The basaltic andesites of Bukit Mapas are olivine-phyric, but closely resemble the other Sumatran arc volcanics in their mineral and whole-rock composition, and Sr, Nd, and Pb isotope systematics. These rocks are characterised by the coexistence of Al-spinel and Cr-spinel inclusions in olivine phenocrysts, probably as the result of mixing at relatively shallow depth between a "normal" basaltic melt and a high-Al

melt derived from the melting of crustal material.

Two types of olivine-bearing basalts (Sukadana basalts) were identified in south Sumatra. The high-Ti basalts have $TiO_2 > 2.3\%$, are slightly alkaline, and have HFSE, and MREE and HREE concentrations similar to those of OIB, but are relatively depleted in LILE and LREE. Isotopically they resemble basalts from the Ninetyeast Ridge and some Indian Ocean MORB, and there is no evidence for their derivation from isotopically strongly enriched hot spot magmas. Despite their proximity to the arc, there is no evidence for metasomatism of their source by subducted sediments, and the depletion in LREE and LILE suggests that their source might have suffered a previous episode of depletion: maybe the extraction of arc melts, as suggested by the fact that these rocks are spatially and temporally associated with arc rocks, and that arc-related granitoids in Sumatra derived from an isotopically similar source.

Low-Ti basalts have $TiO_2 < 1.6\%$, are tholeiitic, and have variable major and trace element composition, with the most "depleted" samples showing trace element composition similar to E-MORB, but with negative HFSE peaks and depleted HREE. The low-Ti basalts may derive from a source similar to that of the high-Ti basalts through a combination of two processes: higher degrees of partial melting, responsible for the lower content in incompatible elements, and crustal contamination, which accounts for the Sr, Nd, and Pb isotopic variations, and for the correlation between isotope ratios and LILE/HFSE values. The composition of some spinel inclusions in the low-Ti basalts suggests that relatively large degrees of crustal contamination may produce melts which may have major and trace elements and Sr, Nd, and Pb isotopic ratios very similar to those of arc basalts.

Basalts from Bukit Telor in central Sumatra are rich in mantle xenoliths (lherzolite) and resemble the high-Ti basalts of Sukadana, but are overall more primitive and more alkaline, and probably represent the composition of the unmetasomatised mantle wedge at some distance from the volcanic arc. Isotopically, they resemble basalts of the Ninetyeast Ridge and of some Indian Ocean MORB.

In general, the basalts from Sukadana and Bukit Telor have trace element and isotopic characteristics similar to those of tholeiitic to mildly alkaline basalts from Kerguelen, the Ninetyeast Ridge, and from the eastern Australian volcanic province. Similar magmatism may also occur within the southeast part of the Eurasian plate (Karimunjawa Islands, and Quaternary volcanics in central and western Kalimantan).

CHAPTER 1

Sunda-Banda arc volcanism: how to solve one equation with many variables

1.1 General introduction

The Quaternary volcanoes along the Sunda arc of Indonesia are a well-known example of subduction-related volcanism. Much of the interest in subduction-related volcanic rocks arises because their composition is unlike that of the volcanism of the ocean basins and continents, yet also seems to be related to their tectonic setting. Indeed, one of the factors that was most influential in the early acceptance of the "new global tectonics" was the demonstration of the "K-h" relationship. However, it has proved difficult to identify the sources of arc volcanism, or even to achieve agreement on an explanation for the "K-h" relationship, and the tectonic processes of orogenic zones would certainly be much better understood if the compositions of arc magmas could be used to identify the composition, origin, and conditions of melting of their source materials. Indeed, the importance attached to the solution of this problem goes beyond its tectonic implications. Subduction zones are the major site of crustal recycling on the Earth, and it is the recycling of crustal material into the mantle that might be one of the key processes in the continuing chemical differentiation of the planet. A knowledge of the flux of material into the deep mantle is therefore essential to the study of global chemical geodynamics, and this requires a knowledge of the amount of the subducted material which is fixed within the subduction zone by subduction-related magmatism.

Relatively primitive subduction-related magmas that might be melts of material beneath the volcanic arc, unmodified by post-melting processes, are rare, so that much attention has been dedicated in the last two decades to the study of the isotopic systematics of the mafic volcanics as a means of identifying their source materials. These suggest that sediments - or fluids derived from the sediments - subducted along the Sunda Trench might have an effect on the composition of the Sunda-Banda arc volcanics. However, the isotopic signature of mafic volcanics in some sectors of the arc resembles that of basalts from Indian Ocean volcanoes, and is seemingly little-affected by recently-subducted continent-derived sedimentary material. Yet very little is known about the composition of the mantle beneath the Sunda arc, and good-quality, representative analyses of oceanic sediments from the Northeastern Indian Ocean are scarce, so that the compositions of two of the most likely source

components are difficult to constrain. Moreover, the importance of crustal contamination has not been sufficiently tested in the Sunda-Banda arc at least partly due to the lack of exposure of arc basement in the best-studied areas, and little is known about the igneous rocks of the largest island in the arc, Sumatra, despite the presence of relatively old granitic basement rocks and primitive basalts.

This thesis has two main aims.

First, it attempts to identify the mantle sources which may be present in the mantle wedge of the Sunda arc, particularly in south Sumatra and in the west Sunda arc. Basalts of the Northeastern Indian Ocean and the South China Sea are characterised by a distinctive isotopic signature, and by inference this isotopic signature is present in their mantle sources. The Sunda arc is therefore unlike most volcanic arcs of the world in that involvement of this mantle in the arc volcanism should be betrayed by the appearance of these distinctive isotopic characteristics.

Second, this thesis is a study of the influence of the crustal component in the arc magmatism, and an attempt to distinguish the results of crustal contamination of arc magmas from those of sediment contamination of the mantle source. Again, the Sunda arc is an ideal location for the study of crustal contamination of arc magmas, because it offers a chance to compare volcanics from an arc sector with thick and old continental crust (Sumatra) with volcanics in other sectors of the arc with transitional crust, and relatively young and thin oceanic crust (Bali, Lombok).

If a study is to be made of crust-magma and sediment-mantle interactions in the Sunda arc, it is first necessary to investigate the composition of the different endmembers. This thesis evaluates the composition of the continental crust of Sumatra; it explores the compositions of olivine basalts which occur within and behind the Sunda-Banda arc in several localities in Indonesia, and uses them to consider the composition of the mantle wedge beneath Sumatra and west Jawa; and it assesses the composition of the lithosphere of the Northeastern Indian Ocean, including the sediments, as a guide to the composition of the crustal material being subducted beneath the arc.

In addition, it is necessary to detect and explain temporal and spatial variations in the composition of the endmembers. This is particularly important, because even if we cannot clearly understand the mechanisms of the contamination/metasomatism processes, we might be able to correlate the temporal and spatial compositional

variations in the arc volcanics with temporal and spatial variations in the composition of the endmembers.

While it is difficult to predict the behaviour of many important trace elements during contamination/metasomatism processes, it is generally believed that isotopic ratios of elements such as Sr, Nd, and Pb are unlikely to be changed by the processes. In other words, the Sr, Rb, REE, and Th-U-Pb concentrations in a mixture are dependent on the concentrations of these elements in the endmembers, on the relative proportions of the endmembers, and on the mixing process, whereas the isotopic composition of the mixture is only dependent on the isotopic composition of the endmembers and the relative proportions of the endmembers, when the effects of radioactive decay are taken into account. For these reasons, many of the arguments discussed in this thesis are based on evidence from isotopic data.

1.2 A review of Sunda-Banda arc volcanism

The first detailed and comprehensive synthesis of the geology of Indonesia was published by van Bemmelen (1949), and a IAVCEI catalogue of the active volcanoes followed in 1951, compiled by Neumann van Padang (later revised and updated by Kusumadinata 1979). However, the first of these two fundamental publications, extremely rich in information and bibliographic material, mainly describes the geology (i.e. stratigraphy and paleontology) and, as far as the volcanoes are concerned, the morphology and type of activity of the volcanic structures, and the second includes only a few petrological and geochemical descriptions of the volcanic rocks. Other early works include a summary and review of the Sumatran volcanism by Westerveld (1952), and a discussion of the relationship between tectonic setting and magmatic activity by Rittman (1953), which anticipated aspects of the "K-h" relationship formulated by Dickinson & Hatherton (1967).

The work of van Bemmelen (1949) is essentially based on pre-plate tectonics ideas, and for a plate-tectonic synthesis of the geodynamic evolution of the Sunda-Banda arc we have to wait until the late seventies, when Warren Hamilton integrated the previous knowledge of the geology of Indonesia with a wealth of modern geophysical and geological data and observations, and interpreted them within the paradigm of modern plate tectonics, producing a detailed geo-tectonic map of the Indonesian region and a work (Hamilton 1979) that has been, and still is, a fundamental reference for any study of the Indonesian volcanism.

However, the Banda arc and the eastern portion of the Sunda arc had already attracted the attention of Hamilton and other workers[1], and the tectonic complexity of this subduction zone was also the subject of a number of articles, many of which were presented during a thematic international meeting in 1979 in Bandung[2], and this area has continued to be of interest[3].

A much smaller number of articles discuss the tectonic evolution of the western part of the Sunda arc (including Jawa and Sumatra), and deal mainly with the activity of the Semangko fault in Sumatra, the formation and evolution of the Sumatran fore-arc, and the position of Sumatra relative to other terranes in Southeast Asia (see Chapter 2 and Chapter 5 for a brief discussion and references).

Studies of the petrology and the volcanic activity of the Indonesian arc have also concentrated on the volcanoes of the eastern Sunda and Banda arcs (see Figure 1.1 for the location of the volcanic centres mentioned in this chapter. A more detailed location map of the Sumatran volcanoes is reported in Appendix C), Jawa, and on two major problems, namely the K_2O variations across the arc and the petrology of the high-K volcanoes.

Early studies of Sunda-Banda arc petrology and geochemistry were devoted to the testing of the positive correlation, observed and studied in some volcanic arcs, including the Sunda-Banda arc, by several authors (e.g.Rittman 1953; Kuno 1959; Sugimura 1960; Dickinson & Hatherton 1967; Hatherton & Dickinson 1969; Ninkovich & Hays 1972; Nielson & Stoiber 1973), between the K_2O content in an arc rock (for a given SiO_2 content) and the corresponding depth of the Benioff zone.

1 e.g. Vening Meinesz 1954; Raitt 1967; Hatherton & Dickinson 1969; Fitch 1970; Fitch & Molnar 1970; Hamilton 1970; Katili 1971; Audley-Charles et al. 1972; Fitch 1972; Hamilton 1972; Ben Avraham & Emery 1973; Hamilton 1973; Hutchison 1973; Katili 1973; Tjia et al. 1974; Molnar & Tapponnier 1975; Barber & Audley-Charles 1976; Carey 1976; Carter et al 1976; Hamilton 1976; Crostella 1977; Curray et al. 1977; Hamilton 1977; Holcombe 1977a, b; Purdy et al. 1977; Cardwell & Isacks 1978; Hamilton 1978; Silver & Moore 1978; Audley-Charles et al. 1979; Green et al. 1979; Jacobson et al. 1979; Norvick 1979; von der Borch 1979

2 e.g. Bowin et al. 1980; Cardwell et al. 1980; Kierckhefer et al. 1980; McCaffrey et al. 1980; Moore et al. 1980; Abbott & Chamalaun 1981; Audley-Charles 1981; Barber 1981; Berry & Grady 1981; Burollet & Salle 1981; Cardwell & Isacks 1981; Haile 1981; Hamilton 1981; Johnston 1981; McCaffrey 1981; McCaffrey et al. 1981; Nishimura et al. 1981; Untung & Barlow 1981

3 e.g. Alzwar et al. 1981; McCaffrey 1982; Moore & Silver 1982; Pigram & Panggabean 1983; Silver et al. 1983; McCaffrey & Nabelek 1984a,b; McCaffrey et al. 1985; Silver et al. 1985; Charlton 1986; Lee & McCabe 1986; Nishimura & Suparka 1986; Reed et al. 1986; Karig et al. 1987; McBride & Karig 1987; van Gool et al. 1987; Eva et al. 1988; Hamilton 1988; Masson 1988; McCaffrey 1988; Charlton 1991

Figure 1.1 Sketch map of the Sunda-Banda arc (excluding Sumatra), showing the location of active volcanic centres (according to Neumann van Padang 1951), and other volcanoes discussed in this thesis. Symbols are: filled circle - volcanoes with magma or phreatic eruptions; open circles - volcanoes in fumarolic stage, no eruptions known; crosses - solfatara or fumarole fields; Mu - Muriah; RB - Ringgit Beser; W - Watukubu; M - Mandiri.

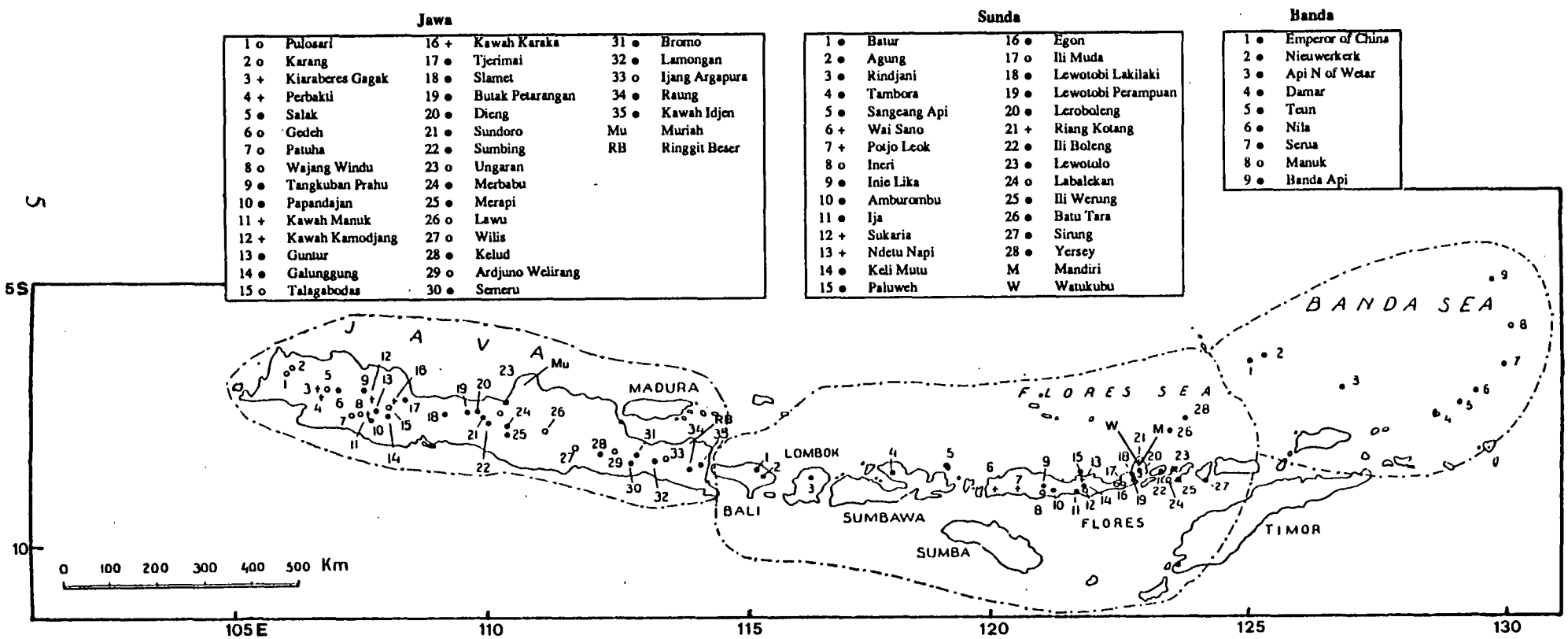

The discovery of this correlation, for which there is still no generally-accepted explanation, was particularly important to adherents of the "new global tectonics" which incorporated the controversial new concept of subduction, because it offered independent evidence that the process existed.

Using rocks with composition ranging from arc tholeiitic to calcalkaline to high-K alkaline from Jawa and Bali, Whitford & Nicholls (1976) showed that for some volcanoes a very good correlation exists between the depth of the Benioff zone and K55 (a parameter defined by K_2O wt % content 55 wt %. SiO_2), especially for the rocks with relatively low $^{87}Sr/^{86}Sr$ values (Whitford 1975), and concluded that such a correlation is consistent with the derivation of the magma, modified by the addition of material from the subducted oceanic crust, from the mantle wedge above the subduction zone. Whitford & Nicholls (1976) also identified two different volcanic series in the high-K volcano Muriah in West Jawa, one of which is totally independent of the observed K_2O/depth relationship. Because of its "unusual" composition, Muriah has been the most studied volcano in the Sunda arc, and the genesis and evolution of the alkaline K and high-K lavas of the Muriah volcano have been the subject of a number of works (e.g. Iddings & Morley 1915; Ferrara et al. 1981; Calanchi et al. 1983; Nicholls & Whitford 1983; Edwards et al. 1991)

Using data from Neumann van Padang (1951), Hadikusumo (1961), and Whitford (1975), Hutchison (1975, 1976) independently reached similar conclusions, and, following the approach of Palacios & Oyarzun (1975), showed that Sr and Rb contents, like K_2O, increase with the depth of the Benioff zone.

Based on these studies, Nicholls & Whitford (1976) discussed the origin and evolution of the andesites in Jawa and Bali, and concluded that these cannot directly derive from primary magmas produced by melting of peridotitic mantle or eclogite in subducted mafic crust, but must have had a complex history of crystal fractionation of olivine from a primary olivine-tholeiite to produce the observed basalts, followed by low-pressure (less than 10 kbar), fractionation of olivine, ortho- and clinopyroxene, amphibole, plagioclase and titanomagnetite, to produce the more evolved andesitic and dacitic volcanics.

However, these early conclusions were based on a quantitatively and qualitatively small database (old wet-chemistry analyses were processed together with modern data obtained by XRF), and probably many of the rocks discussed had been sampled and analysed mainly because they were unusual, so that the data bank was not

suitable to explain general processes.

Like arc volcanics worldwide, very few Sunda-Banda basalts and andesites can be considered to be melts of their source materials which have been little-modified by later events, but seem generally to be the result of the superimposition of several magmatic processes, and even complex models of magmatic differentiation may be over-simplifications. The use of Sr, Nd, and Pb isotopes allowed an examination from another perspective of the genesis of arc andesites, and most studies on the Sunda-Banda volcanics since the late seventies have used isotopic, major element and trace element evidence to discuss:

1) the possible role of contamination, from the crust and from fluids/material derived from the subducted slab, of the mantle source in the production of the observed geochemical and isotopic characteristics. Does the slab melt and do the products of this melting then mix with the mantle? Or, is it simply a source of water or fluid that lowers the temperature of melting of a mantle that has already acquired the geochemical characteristics of the arc rocks?

2) the derivation, starting from the most primitive samples available, of primary liquid compositions and, from these, primary mantle compositions.

Magaritz et al. (1977) showed that Banda arc andesites have high $^{87}Sr/^{86}Sr$ values and that these correlate with high $\partial^{18}O$ values. Taking into account the existence of the so-called "ambonites", which with their cordierite, their very high $^{87}Sr/^{86}Sr$ values, and their heavy oxygen, seem likely to have formed by melting of pelitic material, and Hamilton's belief that the Banda arc is built on oceanic crust, Magaritz et al. (1977) suggested that the andesites might have been produced by mixing between mantle-derived and sialic (continentally-derived sediments or continental crust) components. According to Jezek & Hutchison (1978) two distinct volcanic groups (Nila-Teun-Damar, and Banda-Manuk-Serua) can be recognised in the Banda arc, and the cordierite-bearing dacites in Ambon have a crustal origin, whereas the young tholeiites in Ambon and Banda are related to a shallow subduction zone dipping southwards from Seram.

Earlier, Whitford (1975) had pointed out the range in Sr isotope ratios in the Sunda arc and the complex relationship between major and trace elements and Sr isotopic ratios, and observed that geochemically similar volcanic rocks from the same volcano might have different Sr isotope systematics. Whitford (1975) also observed a

decrease in $^{87}Sr/^{86}Sr$ values along the arc from west Jawa to Bali and an increase with increasing depth to the Benioff zone, and suggested different mechanisms of enrichment in ^{87}Sr for the different magmatic associations: interaction between oceanic crust and sea-water, and disequilibrium melting in the slab/mantle for the tholeiitic and low-^{87}Sr calcalkaline rocks, a further sialic contamination for the high-^{87}Sr calcalkaline volcanics, and a mantle origin for the high-K alkaline volcanics.

Magaritz et al. (1978) further discussed the problems identified by Magaritz et al. (1977), and concluded that a process whereby sediments of continental origin partially melted in the subduction zone and mixed with the overlying mantle material might best explain the Sr and O isotope systematics in the Banda arc.

In the Sunda arc, Whitford et al. (1977) showed that Sr isotopic ratios in the eastern Sunda arc are higher than in the western Sunda arc, and explained the observed isotopic systematics with the subduction and involvement in the magma genesis of either sediments or continental crust, but also suggested, as an alternative but unlikely explanation, that the magmatic source might be heterogeneous and highly enriched in ^{87}Sr. In fact, Whitford et al. (1978) showed that some centres in Lombok and Sumbawa do not follow the K_2O/depth trend observed for some volcanoes in Jawa and Bali, that Sr isotopic ratio variations are not simply a function of the K_2O content in the rock, and that overall there seems to be no correlation between major and trace element abundances, depth to the Benioff zone, and $^{87}Sr/^{86}Sr$ values. Whitford et al. (1978) also observed that mafic and ultramafic xenoliths found in some volcanics have higher $^{87}Sr/^{86}Sr$ than most volcanics in Lombok and Sumbawa.

Whitford et al. (1979) summarised these early studies and concluded that the rocks in Jawa and Bali are not the result of partial melting of the crustal component of the subducted lithosphere and that few of them represent primary mantle-derived melts, but that most were affected by variable degrees of crystal fractionation. They suggested that the parent magmas formed from a geochemically zoned mantle by progressively lower degrees of partial melting with increasing depths, and that the zoning of the mantle was the result of the addition of a small fraction of melt deriving from the crustal component of the subducted lithosphere; however, it was recognised that the models for this contamination are "ad hoc" and not entirely satisfactory. Using evidence from REE distributions, Nicholls et al. (1980), further discussed the conclusions reached by Nicholls & Whitford (1976) and then-current ideas on slab/mantle interactions, and pointed out that simple variations in the conditions of magma genesis cannot explain the observed change in LREE patterns in volcanics for

increasing depth of the Benioff zone, and that the variation in incompatible elements in the magma sources is likely to be somehow related to the dehydration and partial melting of the subducted oceanic crust.

These conclusions were further discussed in Whitford & Jezek (1979) and Morris & Hart (1980), and in more detail in Hutchison (1981), Nishimura et al. (1981), Whitford et al. (1981), and Whitford & Jezek (1982). Considering also Nd and Pb isotope data, it was suggested (Whitford & Jezek 1979; Morris & Hart 1980; Whitford et al. 1981; Whitford & Jezek 1982) that terrigenous sediments from the Precambrian shields of India and Australia are most likely responsible for the isotopic signature observed in the volcanics of the Sunda arc, and especially in some calcalkaline lavas from Jawa, also enriched in K. Contamination by a continental crust with the same age and composition would produce the same effects, but the available geological and geophysical data seemed to suggest that such crust does not exist beneath Jawa (van Bemmelen 1949; ben Avraham & Emery 1973; Hutchison 1973; Katili 1975; Curray et al. 1977), although it is now generally believed, based on the isotopic and geophysical data, that there is a transition from continental to oceanic basement going eastward from West Jawa to Bali. On the other hand, Sr and Nd isotopes in the Banda arc suggest mixing with upper continental crust and not subducted sediments.

Nishimura et al. (1981) studied the distribution of earthquakes along the Sunda-Banda arc, and pointed out that a major tectonic, geochemical, and isotopic discontinuity between Sumbawa and Flores separates eastern Indonesia from western Indonesia.

Using a different approach, other workers carried out a detailed study of the geochemical and isotopic composition of one or a few volcanic centres from a small area, and tried to extend their conclusions to other centres.

Foden & Varne (1981a), and Foden (1983) identified two groups of rocks in the Rinjani volcano in Lombok, and showed that crystal fractionation of the observed phenocryst phases can explain the variation from ankaramites to high-Al basalts and from andesites to dacites. Also, they discussed the physical conditions required for the crystallisation of the andesites from the high-Al basalts, and concluded that the source of the entire suite of rocks observed is in the mantle wedge above the subduction zone.

Foden & Varne (1980, 1981b; see also Foden 1986) and Varne & Foden (1986) also described the compositionally extremely wide range of volcanics in Lombok and Sumbawa, and pointed out that these do not show any K/depth correlation. In this sector of the arc the depth of the Benioff zone beneath volcanoes that produced different magmatic associations is not significantly different, and therefore the observed compositional array cannot be the result of pressure-dependent phase relationships, either in the slab or in the mantle, nor of variations in the thickness of mantle traversed by the magmas to get to the surface; instead, the geochemical and isotopic variations reflect the heterogeneity of the mantle-source.

However, it might be that the unusual distribution of the volcanism in Sumbawa reflects the existence of a large-scale cross-arc transcurrent fracture that extends from Sumbawa to Flores as a result of the different tectonic evolution of the Banda arc with respect to the eastern Sunda arc (see also Audley-Charles 1975; Alzwar et al. 1981; Nishimura et al. 1981). Silver et al. (1983) also stressed the importance of the spatial association between cross-arc faults and active volcanoes in the east Sunda arc, and observed that "the gross trend of the arc from Jawa to Alor is a gentle convex southward arc, but this arc is interrupted at eastern Sumbawa and western Flores. Here the volcanic edifice is gently convex northward." (page 7445). Silver et al. (1983) recognised the existence of the Pantar fracture zone but, discussing the existence of the Sumba fracture zone, pointed out that "Cardwell & Isacks (1978) found no indication of a break in the seismic zone across this offset [the Sumba fracture zone] and available seismic reflection profiles have not documented its existence in the upper plate." (page 7431). Silver et al. (1983), however, ignored the studies of Nishimura et al. (1981) and Alzwar et al. (1981).

Varne (1985) described the threefold increase in K, Rb, Sr, Ba, La, and Nb contents, going from Bali to Flores, and its correlation with increasing Sr and decreasing Nd isotopic ratios, and proposed two separate sources for the arc volcanics: 1) a high $^{143}Nd/^{144}Nd$, and low $^{87}Sr/^{86}Sr$ and K (and related elements) source (suboceanic mantle), most evident in the Bali-Lombok sector, and 2) a low $^{143}Nd/^{144}Nd$, and high K and $^{87}Sr/^{86}Sr$, showing some similarities with K-rich ultramafics in northwest Australia (but different in the Ti-group elements), and considered to derive from an ancient K-rich subcontinental mantle involved in the collision zone. Varne & Foden (1986), also using Pb, O, and Be isotope data, for the first time examined in detail the effects of a postulated contamination by altered oceanic crust and Indian Ocean sediments, and suggested that the compositional variations observed in the Sunda arc may be the result of large-scale tectonic mixing of suboceanic (the same

source as that of the Indian Ocean basalts) and subcontinental OIB-like mantles around the collision zone, and that there is strong evidence for the involvement of recently subducted upper crustal material in the Banda arc but not in the Sunda arc.

Wheller et al. (1987) considerably expanded the existing database of chemical analyses, and divided the Sunda-Banda arc (excluding Sumatra) into four sectors, with boundaries that correspond to important changes in regional tectonic setting and geological history: west Jawa, Bali and Flores, where the volcanics become progressively more K-rich in each sector going eastward, and the Banda sector, where they have generally lower K contents which decrease going northeastward. According to Wheller et al. (1987), the rocks in each sector show different correlation trends between Sr isotopes and geochemical composition, and such trends are believed to be the result of at least three geochemically and isotopically distinct components in the source regions of the volcanic rocks of the arc: 1) a dominant low-K and low-$^{87}Sr/^{86}Sr$ source, believed to be peridotitic suboceanic mantle, common to all the sectors; 2) a high-K, low-$^{87}Sr/^{86}Sr$ source, most evident in the Bali sector, and believed to be closely associated with the DUPAL mantle anomaly and not the result of the incorporation into the mantle of recently subducted continent-derived sialic material (this conclusion was also based on U-Th isotopic data; see also Williams et al. 1983); 3) a low-K, high-$^{87}Sr/^{86}Sr$, probably crustal material (most likely continental crust, and not recently subducted sediments), most evident in the Banda sector, but also detectable in West Jawa, where continental crust underneath the arc is likely to exist, and in the Flores sectors, which is close to the arc-continent collision zone. Wheller et al. (1987)'s zonation of the arc did not take into account the K-rich volcanics of Ringgit Beser in the centre of their Bali sector.

Stolz et al. (1990) further discussed the problem of the sources of the volcanic rocks in the Flores-Lembata sector, and reached the following conclusions: 1) the low-K tholeiites were formed by relatively large degrees of partial melting of depleted MORB mantle (source 1 of Wheller et al. 1987), modified by subduction-related fluids (seawater); 2) the K-rich rocks (Stolz et al. 1988) were derived from an OIB source, possibly modified by a subduction-related melt component; 3) the trace-element and isotopic geochemistry of the medium- to high-K calcalkaline volcanics may reflect derivation from a complex mixture of OIB-source, MORB-source, and melt/fluids derived from subducted oceanic sediments; 4) the low-Ti content in the rocks believed to have an OIB source is the result of the involvement of a residual Ti-rich accessory phase (rutile? ilmenite? perovskite?).

Varekamp et al. (1989) also recognised the existence of the arc sectors described by Wheller et al. (1987), and concluded that the volcanoes in the eastern Sunda arc (Sirung, Lewotolo, Boleng and Batu Tara) have geochemical characteristics transitional between the rocks of the western Banda arc and the Bali-Lombok sector, as a result of the increasing contribution of subducted crustal/sedimentary material going eastward, and decreasing contribution of the same material for increasing depth of the Benioff zone, where an enriched, K-rich mantle is the dominant source. Varekamp et al. (submitted for publication) further studied the problem of the sources of the high-K volcanics in the eastern Sunda arc, and suggested that sediment subduction occurs predominantly where the subducting slab is affected by major tectonic disruptions, through which the mantle fluids can migrate to the mantle wedge; in fact, both Batu Tara and Muriah are situated along major cross-arc fractures in the Sunda arc (respectively the Pantar fracture and a cross-arc lineament which has been interpreted as the trace of a Cretaceous subduction zone - see e.g. Katili 1975, and Untung & Sato 1978).

In the Banda arc van Bergen et al. (1989) identified some systematic spatial variations along and across the arc, with progressively increasing K and other incompatible elements contents towards the arc-continent collision area near Timor for the volcanoes situated above a depth of 100-150 km to the Benioff zone, and, in the westernmost Adonara-Pantar sector, a further increase in the content of the same elements for increasing depths of the Benioff zone. However, because of the lack of correlation between isotopic systematics and geochemistry, they suggested that the volcanism in the collision zone near Timor is affected not only by the continental sediment/crust subduction, but also by the tectonic framework.

Only a few volcanic centres in the western Sunda arc have been studied in detail.

Wheller & Varne (1986) described the volcanic activity of Batur volcano in Bali, the compositional changes in the geochemistry accompanying the formation of the caldera, and the processes of differentiation in a magma chamber, but not the origin and the source of the magmas. However, they pointed out that O and Sr isotope systematics bear no evidence for the assimilation of crustal country rock. ^{238}U decay series systematics of basalts and dacites from Batur were also studied in detail (Rubin et al. 1989 - see also Chapter 5 for a brief summary of the studies about U and Th radionuclides systematics in the Sunda arc).

With the exception of Muriah, only two volcanoes have been studied in some detail in Jawa, and both are situated in the West Jawa sector as defined by Wheller et al. (1987).

Vukadinovic & Nicholls (1989) discussed the trace element, and Zr/Nb and $^{87}Sr/^{86}Sr$ values in the volcanic rocks of Slamet volcano in central Jawa, and identified two types of magmas, generated by different degrees of melting of a mantle wedge which, before the metasomatism by the underlying lithosphere, was chemically similar to "transitional-MORB" source mantle. The metasomatising agent, identified using immobile/mobile element ratios, REE abundances and Sr isotope ratios, was believed to derive from the subducted slab (basalts and sediments), and several models of interaction between the mantle wedge and this metasomatising agent were tested. Vukadinovic & Nicholls (1989) concluded that 1) bulk mixing of oceanic basalts and sediments with the mantle wedge does not satisfactorily explain the observed characteristics of the arc rocks; 2) to match the composition of the arc volcanics, the mixing between melts derived from the subducted slab and the mantle wedge would require the precipitation of a Ti-bearing phase (rutile?); 3) aqueous slab-derived fluids rich in incompatible and mobile elements are the most likely metasomatising agent; however, these cannot explain the HREE contents observed in the arc volcanics, and the calculations are based on a number of assumptions made about the concentrations of the mobile elements before the metasomatising event; 4) crustal assimilation can account for the observed range in $^{87}Sr/^{86}Sr$ values, but the estimate of the effects of crustal contamination is strongly dependent on the assumptions made about the metasomatising agent. Vukadinovic et al. (1988) reached similar conclusions for other centres in West Jawa (Dieng, Sundoro, Sumbing).

The Galunggung volcano in West Jawa in 1982-83 erupted volcanic rocks with compositions ranging from typical calcalkaline arc dacites and andesites to high-Mg, primitive basalts. The origin and evolution of the products of this unusually long eruption (approximately nine months) were studied by Gerbe et al. (1992) and Harmon & Gerbe (1992). The basalts are among the most primitive found in West Jawa, with 10 to 12 % MgO, 180 to 200 ppm Ni and 550 to 700 ppm Cr, and Fo values up to 90, and the more evolved volcanics were shown to be the result of crystal fractionation from these basalts, with the formation of gabbroic cumulates (plagioclase + olivine + clinopyroxene ± titanomagnetite ± amphibole), possibly with some mixing among the magmas with different degrees of evolution (and between these and the cumulates). This is also suggested by the constant O, Th, Sr, Nd, and Pb isotopic values in basalts, andesites, and dacites; only some of the andesites might

have been slightly contaminated (as suggested by the slightly higher O and Sr isotopic values) by meteoric water, but there is no evidence for the introduction of ^{18}O-rich material from the crust. The basalts, which might represent a primary mantle melt, all have the typical characteristics of calcalkaline arc rocks, but also unusual isotope systematics, with O isotope values typical of MORB, and high Sr and low Nd isotopic ratios. The higher ^{87}Sr and lower ^{143}Nd contents (relative to Pacific MORB) for constant $\partial^{18}O$ values were interpreted as the result of contamination of the mantle wedge by minor amounts of subducted sediments (or fluid/melt derivates).

During the last few years other isotope systematics provided different ways of looking at the problem of the identification of metasomatising agents and processes. Among these, only the $^3He/^4He$ values measured in volcanic gases and hot springs, and in olivine and pyroxene phenocrysts in volcanic rocks have been extensively used in the Indonesia region. In particular, He isotopes measured in phenocrysts (olivine and clinopyroxene are the most suitable common mineral in volcanic rocks because, due to their crystalline structure, they retain He more efficiently than other minerals) are believed to reflect the He isotopic composition of the magma at the moment of the crystallisation, provided this has not been modified by non-magmatic (e.g. mixing) processes. The analytical techniques, and the significance and range of He isotope ratios have been described in a number of articles (see the articles cited in the next paragraph and the references therein), and will not be further discussed here.

Poreda & Craig (1989) first observed that all the volcanoes in the Banda (Serua, Teun, Damar) and eastern Sunda (Sirung, Lewotolo) arc analysed for He isotopes have extremely low (Banda arc) and very low (eastern Sunda arc) R/RA values (R/RA is the ratio between the measured $^3He/^4He$ value in the sample and the atmospheric $^3He/^4He$ value), lower than any other values measured in circum-Pacific volcanic arcs, and suggested that most of the He is derived from subducting continental crust associated with a Precambrian craton; nevertheless, they also observed that He in the other circum-Pacific arcs is almost entirely derived from a dominant Pacific MORB component in the mantle wedge, and that values different from typical MORB values (R/RA = 8 ± 1) can be found in hotspots (e.g. R/RA 11-30 in Hawaii, Iceland, Samoa, and R/RA 5-8 in Jan Mayen, Açores, Gough).

Hilton & Craig (1989), and Hilton et al. (1992) studied in detail the $^3He/^4He$ distribution in the Sunda and Banda arc, and in the transition from the Sunda to the Banda arc, and reached the following conclusions: 1) a sharp but complex transition in He isotope values exists from the Banda arc (extremely low R/RA) to the Sunda

arc (relatively high R/RA); this He isotope transition corresponds with a transition in other geochemical parameters, and is interpreted to be due to the involvement of crustal material in the Sunda/Banda arc; 2) the main source of He in the crustal component is not terrigenous sedimentary material from Australia, but, more likely, the degassing of the Australian continental crust (see Chapter 5); 3) the amount of the radiogenic crustal He component decreases with the distance from the arc-continent collision zone and with increasing depth to the Benioff zone; 4) He isotopes are decoupled from Sr isotopes and other geochemical characteristics along the Banda arc; 5) R/RA values in the west Sunda arc are considerably higher than in the Banda arc and in the east Sunda arc, and range from 5.7 up to 8.8 in Bali.

Poorter et al. (1989a,b; 1991) also studied the chemical and isotopic composition (He, C, S, H, and O isotopes) of volcanic gases, hot springs, and fumaroles in the volcanoes of the east Sunda and Banda arc. These authors concluded that all the studied isotopic systematics are consistent with the involvement of a continental component in the genesis of the arc magmatism, but they did not clearly specify the nature of this component (i.e. crust or sediments), although they seemed to favour a sedimentary origin (in conflict with the interpretation of Hilton et al. 1992).

New unpublished data on the He isotopic composition of the active volcanoes in Sumatra and the west Sunda arc will be briefly referred to in Chapter 5.

The potential use of ^{10}Be as a tracer of recently subducted sedimentary material in the source of the Indonesian arc magmas was discussed by Tera et al. (1986), who found low ^{10}Be concentrations in the Sunda arc volcanics, and concluded that either there is no (in detectable amounts) sedimentary material in the Sunda volcanic rocks, or that the young sediments (rich in ^{10}Be) are not subducted, or that the subduction is slow enough for ^{10}Be to decay to undetectable levels before the slab/mantle interaction. The lack of ^{10}Be in the Sunda volcanics is strong evidence against the involvement of recently subducted young sedimentary material.

Morris et al. (1990) showed that the study of B/Be coupled with Be isotope systematics in four volcanic arc (Aleutians, Central America, Andes, Bismarck) suggests that the subducted component is homogeneous. This is contrary to expectations, as the $^{10}Be/Be$ value in a sedimentary column is a function of age (and stratigraphic level). Homogenisation could be consistent with one of the following possibilities: 1) in all the arcs the metasomatising fluids derive from the same stratigraphic level; 2) the sedimentary column is homogenised during the subduction;

3) the process of formation and migration of fluids is an effective agent for the homogenisation of the sedimentary column. Also, Morris et al. (1990) noted that subducted B is not stored in the sub-arc mantle, and concluded that there must be a process through which the B added to the mantle is quickly brought back to the surface.

Edwards et al. (1993) applied the B/Be and Be isotope systematics to the Sunda arc, and found that while alkaline volcanics (Muriah, Ringgit Beser) have B/Be values similar to OIB and MORB (3 to 5), consistent with a derivation from a mantle which has not been affected by recent subduction, calcalkaline lavas from Guntur and Seram in Jawa, and several volcanoes in eastern Flores, have high B/Be values, interpreted as the result of a strong interaction of the mantle wedge with a "subduction zone component" (sediment + altered oceanic basalt). These results will be discussed in more detail in Chapter 5.

Following this review, it is concluded that any study of Sunda-Banda arc magmatism should take into account the following conclusions:

1) The Sunda-Banda arc is not a single tectonic unit: the composition of the mantle wedge and any magmatic/metasomatising processes that might affect the mantle source(s) of the magmatism may differ from one sector to the other, and from one volcanic centre to the other.

2) With very few possible exceptions, the volcanic rocks in the Sunda-Banda arc do not represent primary magma compositions, and any attempted recalculation of notional primary magma compositions is strongly dependent on the assumptions made about a) the composition of the mantle; b) the type and extent of magmatic processes (e.g. amount and composition of the crystals fractionated, degree of partial melting, variations of physical parameters during the magmatic processes); c) the type and extent of lithospheric contamination (crust/sediments).

3) It is generally believed that the source (or at least one of the sources) of the Sunda-Banda arc magmatism (and of arc volcanics in general) is similar to a MORB (or to a source depleted after the generation of MORB melts) source, before the addition of material/fluids from the subducted slab. Given this assumption, it becomes absolutely necessary to add an "enriched" (compared with MORB) component to explain the geochemical and isotopic characteristics of the arc magmatism. However, there is no direct evidence to believe that the source of the arc rocks is uniquely a MORB-like

source.

Maury et al. (1992) described the first studied occurrence of mantle xenoliths immediately below an active arc (Luzon arc, Philippines), and showed that the trace element patterns in these harzburgitic xenoliths (originated within the mantle wedge at a depth of about 30 km) reflect metasomatism by a hydrous fluid (not a melt) of a mantle originally more depleted than the source of MORBs. They therefore explained the observed HFSE depletion in arc volcanics as the combination of two factors, namely the original depletion in HFSE in the mantle before the metasomatism, and the inability of the metasomatising hydrous fluids to transport these elements to the surface. Nevertheless, they pointed out that these xenoliths do not represent the actual source of the arc rocks, but both the mantle from which the xenoliths derived and the source of the arc volcanics were affected by the same metasomatising process. Furthermore, the conclusions reached for the Philippines may not be applicable to other arcs.

From the isotopic point of view, it is now widely accepted that the Indian Ocean MORB have a distinct isotopic composition compared with Atlantic and Pacific MORB, and this must be taken into account in the models involving isotopic calculations. Again, we do not know whether the (allegedly) MORB source underneath the Indonesian arc has Atlantic/Pacific-type or Indian-type isotopic systematics.

As an alternative (or complementary) to a MORB source, an OIB source (or some OIB sources) is potentially able to explain the LILE and LREE enrichment, and the "enriched" isotopic systematics of the arc rocks, and has been proposed by various workers for the Sunda (e.g. Stolz et al. 1990, and references therein) and other arcs (e.g. Morris & Hart 1983; Reagan & Gill 1989). However, the derivation of the arc rocks from an OIB source requires the crystallisation of phases able to fractionate the HFSE, and the behaviour of the HFSE and the stability fields of the HFSE-bearing phases in the arc environment are poorly known and extremely controversial (e.g. Pearce & Norry 1979; Green 1981; Arculus & Powell 1986; Tatsumi et al. 1986; Ryerson & Watson 1987; Hofmann 1988; Salters & Shimizu 1988; Jochum et al. 1989; Foley & Wheller 1990; Hoffman 1990; Kelemen et al. 1990; McCulloch & Gamble 1991).

4) The nature and origin of the metasomatising agent(s), if any, are even more obscure than the composition of the source mantle.

In general, and with a few notable exceptions (ben Othman et al. 1989; Dia et al. 1992; Plank & Ludden 1992; Plank & Langmuir 1993) the geochemical and isotopic composition of the sedimentary material in the Northeastern Indian Ocean is not known, and the models of sediment contamination are generally based on average compositions or on sediments sampled in sedimentary basins that are not "feeders" to the Sunda arc. The geochemical and isotopic characterisation of the sediment-derived metasomatising fluid is even more difficult (e.g. Lin 1992, and references therein), and although now most authors agree that the metasomatising agent is a sediment-derived "fluid", the bulk addition of sediments is still regarded as a possible process in some arcs (e.g. McDermott et al. 1993; Plank & Langmuir 1993).

5) Geophysical and geological evidence show that at least Sumatra and West Jawa are built on continental crust, and small fragments of continental crust can, in principle, exist underneath some segments of the eastern Sunda arc (e.g. Hamilton 1979; Varne 1985). However, the geochemical and isotopic composition of the continental crust in Sumatra and Jawa was not known before this study, and models of crustal contamination had to rely on estimated average composition of crustal materials deduced from other areas.

CHAPTER 2

Sumatran granitoids and their relationship to Southeast Asian terranes

2.1 Introduction

Three subparallel, N-S trending granitoid provinces occur in SE Asia: the Eastern Granitoid Province of peninsular Malaysia; the Central Granitoid Province, extending from northwestern Thailand to the western part of peninsular Malaysia and to the "Tin Islands" (Indonesia); and the Western Granitoid Province, in western Thailand and Burma. Each of these granitoid provinces is restricted to one of the Southeast Asian terranes defined using Gondwanan Palaeozoic stratigraphic relations and faunal distributions. Very little is known about possible continuations of these terranes in Sumatra, and the aim of this chapter is to identify the geochemical and isotopic composition of the Sumatran continental lithosphere, and to detect any temporal and spatial compositional variations of the Sumatran lithosphere which may help in identifying a possible crustal input in the arc volcanics.

In general, where granitoids are composed partly or wholly of crustal melts, then the granitoid compositions will reflect the compositions of their crustal source rocks. If these crustal melts are derived from deep in the continental lithosphere, then lateral discontinuities in granitoid compositions such as those observed in peninsular Malaysia might correspond with changes in composition in the deep crust. The term "granite basement terrane" has been applied to regions defined by granitoid compositional boundaries (Chappell et al. 1988).

Following the "granite basement terrane" concept, granites of any age that are derived by melting of the same crustal source rocks are likely to share similar isotopic and geochemical characteristics. Although repeated melting of the same source materials will lead to changes in the geochemical characteristics of the melts, the changes are likely to be fairly systematic, and amenable to modelling using a batch melting approach. Similarly, changes in source isotopic ratios such as $^{87}Sr/^{86}Sr$ values will occur with passing time, but again, such changes are likely to be predictable.

The "granite basement terrane" concept also implies that even if deep-seated crustal discontinuities are concealed by younger cover, as they might be in Sumatra, the

granitoids could still betray the characteristics of the buried basement, and its regional affinities.

In this chapter geological, petrological, geochemical and isotopic data for some Sumatran granitoids are discussed, and the Sumatran granitoids are compared with the granitoid belts of Southeast Asia. It will be demonstrated that some may have shared similar source rocks, and may therefore define "granite basement terranes". Possible locations for the boundaries of the Southeast Asian "granite basement terranes", corresponding with existing tectonic features, will be defined, and their regional significance will be discussed.

The geochemical and isotopic composition of the two different types of granitoids found in Sumatra, and their age and spatial distribution, will be used to model the effects of crustal contamination of melts formed in the Sumatran mantle wedge (Chapter 5), and to constrain the isotopic composition of the Sumatran mantle wedge (Chapter 6).

2.2 Granitoid provinces and terranes of Southeast Asia

Partly due to the tin mineralisation associated with them, the granitic bodies of Thailand, Malaysia and Bangka Island (Indonesia) have been the subject of a number of geological studies during the last twenty years (e.g. Mitchell 1977; Beckinsale et al. 1979; Hutchison 1883; Cobbing et al. 1986), and although the geotectonic evolution of mainland Southeast Asia has yet to be completely understood, it seems clear that granitoids with different ages and tectonic settings are present.

The granitoid bodies of peninsular Malaysia have been subdivided (Hutchison 1978; Hutchison & Taylor 1978; Hutchison 1983; Cobbing et al. 1986) into three subparallel, N-S trending granitoid provinces (Figure 2.1). These belts have been defined mainly on the basis of tectonic and structural characteristics, and good quality chemical analyses and absolute age determinations are scarce. As can be seen from the data summarised by Hutchison (1983), and Cobbing et al. (1986), there is a range in major and trace element compositions in each province, but each province shows distinctive isotopic and geochemical characteristics, summarised in Table 2.1.

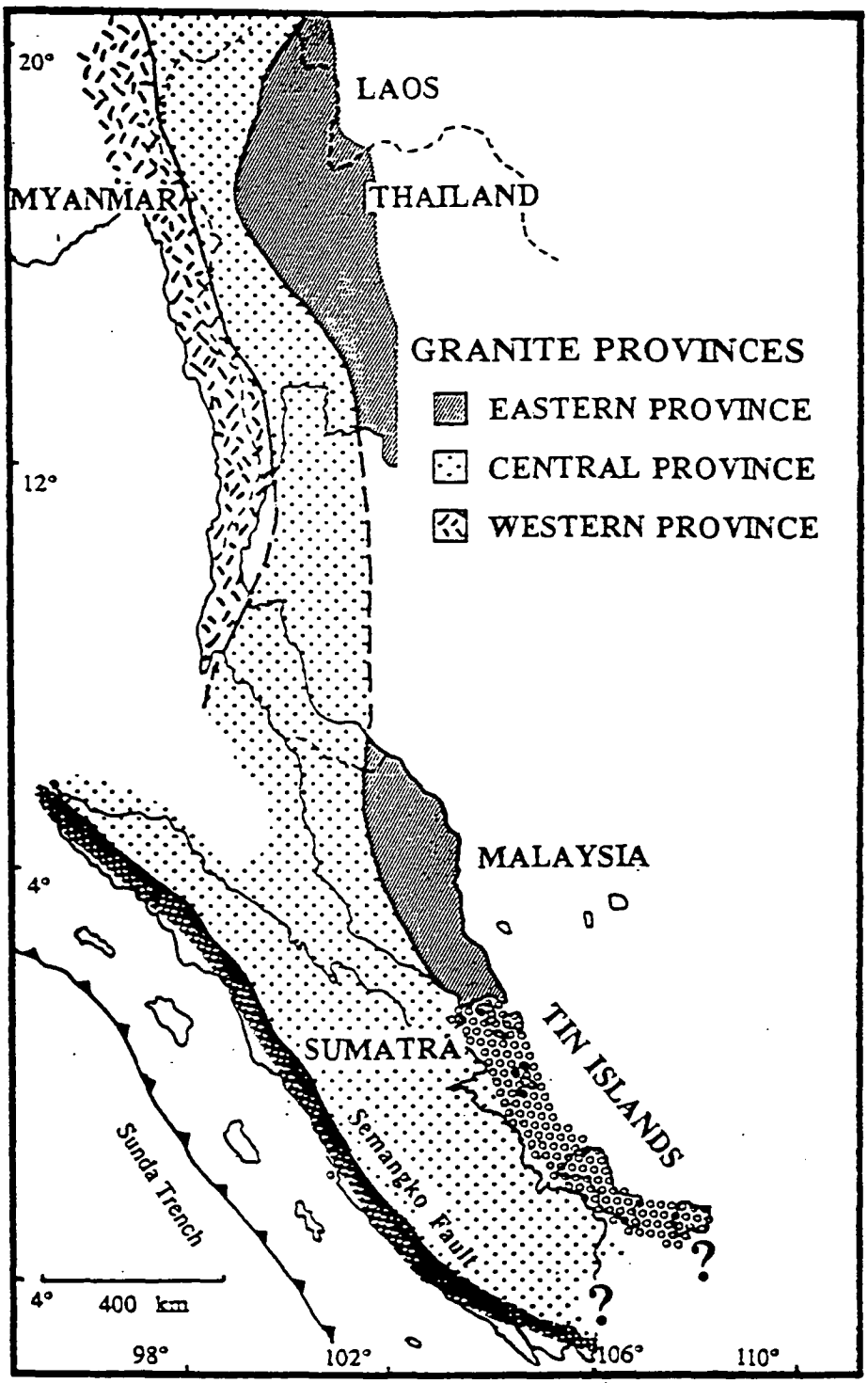

Figure 2.1. General tectonic sketch map of Sumatra and Southeast Asia, showing the different granitoid provinces (simplified and modified after Cobbing et al. 1986). The Central Province has been extended into Sumatra as a result of this study. The heavy shaded area marks the southwestern boundary of the SIBUMASU* terrane in Sumatra. The boundary (small circles in the map) between the Central and Eastern Provinces appears to be gradational and to run through the "Tin Islands". In west Sumatra, the margin of the SIBUMASU terrane coincides with the Semangko Fault and the Quaternary arc. In south Sumatra it is not yet clear whether the SIBUMASU terrane continues into west Jawa or the Sunda Strait marks its southern margin.

* SIBUMASU (= SIam-BUrma-MAlaysia-SUmatra) terrane of Metcalfe (1984)

Area	Granitoid Type	Age (Ma)	Initial 87Sr/86Sr
Southeast Asia Granitoid Provinces			
Western Province	S + I	82 - 98 (Upper Cretaceous)	0.714 - 0.740
Central Province	S	200 - 230 (Upper Triassic)	0.711 - 0.719
Eastern Province	I	200 - 280; 70 - 80 (Permian/Triassic; Upper Cretaceous)	0.708 - 0.712
Sumatran Granitoids EAST of the Semangko fault			
Tin Islands	S	200 - 230 (Upper Triassic)	0.715
Bukit Batu	S	Jurassic ?	0.715
Jambi basement	S?	max. 247 - 298 (Permian/Triassic)	?
Hatapang	S	80 (Upper Cretaceous)	0.715
Sijunjung	S	247 (Lower Triassic)	?
Sibolga	S?	257 (Upper Permian)	?
Toba tuffs and associated volcanics	Andesites, dacites, rhyolitic tuffs	Pliocene/Quaternary	0.710 - 0.714
Arc Granitoids - WEST OF, OR ALONG, the Semangko fault (including localities from references quoted in the text, and new data from this work.)			
Arc granitoids	I	Jurassic/Cretaceous to Tertiary; mainly Upper Cretaceous to Middle Miocene	0.704 - 0.706
Fragmental deposits and associated volcanics			
Maninjau	Andesites, dacites, rhyolitic tuffs	Pliocene/Quaternary	0.705 - 0.707
Ranau	Andesites, dacites, rhyolitic tuffs	Pliocene/Quaternary	0.705 - 0.707
Lampung	Andesites, dacites, rhyolitic tuffs	Pliocene/Quaternary	0.705

Table 2.1 Main features of the three granitoid provinces of Southeast Asia (after Cobbing et al. 1986; Metcalfe, pers. comm.) and Sumatra. Data from this study and references quoted in the text.

The Eastern Granitoid Province of peninsular Malaysia is made essentially of I-type, Permian to Upper Cretaceous granites with initial $^{87}Sr/^{86}Sr$ values ranging from 0.708 to 0.712. The Central Province extends from northwestern Thailand, to the western part of peninsular Malaysia, and is made of S-type, syn- to post-collisional, Upper Triassic granitoids, with initial $^{87}Sr/^{86}Sr$ values (0.711 - 0.719) slightly higher than those of the Eastern Province. This granitoid belt is considered to be the result of collision in Upper Triassic times between eastern Malaysia and a composite terrane that includes the Shan States, northwestern Thailand, peninsular Burma and Thailand, western Malaysia and eastern Sumatra (e.g. Burrett 1974; Mitchell 1977; Metcalfe 1988). Page et al. (1979) also showed that north Sumatra, at least, has the same Carboniferous to Triassic stratigraphy as the Central Province. Finally, the Western Granitoid Province, in western Thailand and Burma, is characterised by having both S- and I-type Upper Cretaceous granitoids with extremely high initial $^{87}Sr/^{86}Sr$ values (0.714 - 0.740).

Each of these provinces corresponds spatially with Southeast Asian terranes defined by Paleozoic faunal distributions (e.g. Asnachinda 1978; Bunopas 1981; Gatinsky et al. 1984; Metcalfe 1984; Burrett & Stait 1985). These Palaeozoic terranes, termed the West Burma (= Western Granitoid Province), Shan Thai (or SIBUMASU)* (= Central Granitoid Province), and Indochina (= Eastern Granitoid Province) Terranes, were accreted to the SE Asian margin in pre-Tertiary times, and possibly were rifted off the Gondwanan supercontinent (for a review of the evolution of the peri-Gondwanan Asian terranes, see e.g. Audley-Charles 1988, Metcalfe 1988, Sengor et al. 1988, and Hutchison 1989).

2.3 Sumatra and its relationship to the terranes of Southeast Asia

The occurrence in Sumatra of granites and other intrusive bodies, of crystalline schists believed to be part of a pre-Mesozoic basement, and of sedimentary units as old as Carboniferous, are the basis for considering Sumatra to be mainly composed of relatively old continental crust (van Bemmelen 1949; Hamilton 1979). Part of the Sumatran crust therefore predates the opening of the Indian Ocean, and is thus Gondwanan in its affinities.

The tectonic evolution of Sumatra within the Southeast Asia region is still a matter of debate (see Chapter 5), and it is not yet clear whether Sumatra has always been

* SIBUMASU (= SIam-BUrma-MAlaysia-SUmatra) terrane of Metcalfe (1984)

tectonically part of the Sundaland, or has become part of it only in relatively recent times (after the Late Triassic).

If Sumatra has been joined to peninsular Malaysia and Thailand at least since the late Carboniferous/Permian, we might expect the Sumatran lithosphere to be tectonically and compositionally similar to peninsular Malaysia and the granitoid belts observed in the Malaysian peninsula to continue into Sumatra. Alternatively, and more important for this study, the composition and the age of the crust in Sumatra may change from north to south - what is now a single island may be the result of the fusion of originally different terranes, possibly at different times. In this case we might expect to see differences in the composition of the Sumatran plutonic bodies.

Little is known about the extension of the Southeast Asian terrane boundaries into Sumatra, and the differing extrapolations are based on very limited, and often contradictory, geotectonic and paleontological evidence (e.g. van Bemmelen 1949; Hamilton 1979; Hutchison 1983; Metcalfe 1984; Burrett & Stait 1985; Wikarno et al. 1988; Hamilton 1989). It is commonly accepted that a southern continuation of the boundary between the Eastern and the Central Province might be found in Sumatra, but Wikarno et al. (1988) believes that the boundary corresponds to the "Tin Islands", implying that all eastern Sumatra belongs to the SIBUMASU block, whereas other workers (e.g. Hamilton 1989) suggest that the boundary could swing SW and divide Sumatra transversely into two different terranes.

2.4 Previous studies of the plutonic rocks of Sumatra

A large number of plutonic bodies, many associated with important Sn-W-Sb primary and alluvial mineralisation, exist in Sumatra (see Figure 2.2 for the location of the granitoids listed in this section). Among the best known are the granites of the so-called "Tin Islands" (Belitung, Bangka, Singkep and the Riau Archipelago), which account for a large proportion of the world's tin production.

Although these granites are believed to be part of the Central Granitoid Province, some important differences exist between the granites of the "Tin Islands" and the other granites of the Central Province. I-type granites, similar to those found in the Eastern Province in Malaysia, are common in the "Tin Islands", and all the plutonic bodies seem to have much the same age as the rocks they intrude. In contrast, the granitoids of the Central Province in Malaysia and Thailand are essentially of highly

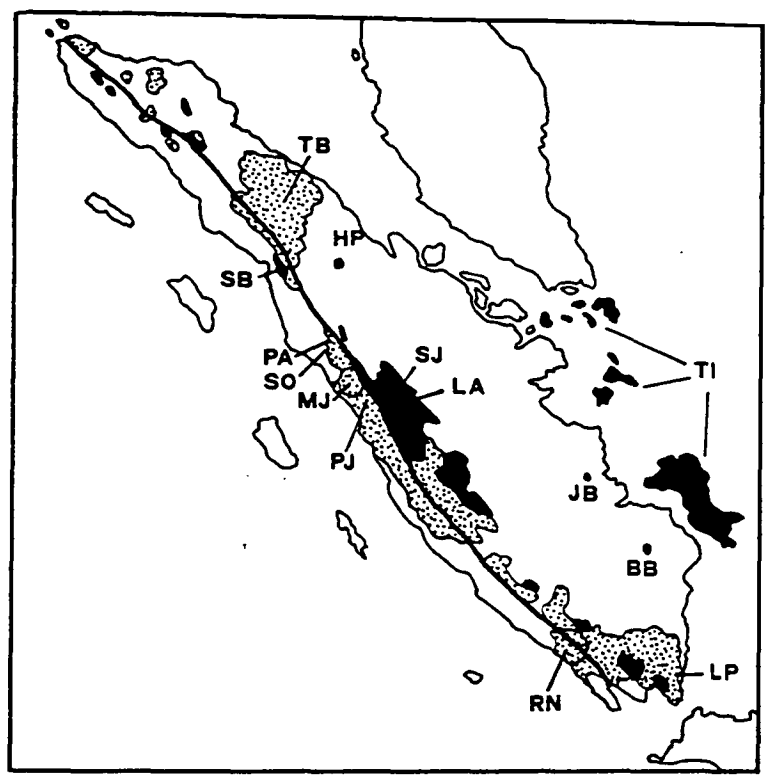

Figure 2.2. Location of the Sumatran granitoids mentioned in the text. Abbreviations are: TI=Tin Islands; LP=Lampung; RN=Ranau; BB=Bukit Batu; JB=Jambi (basement); LA=Lassi; SJ=Sijunjung; PJ=Padangpanjang; MJ=Maninjau; So=Sontang; Pa=Panti; SB=Sibolga; HP=Hatapang; TB=Toba. Also shown are the major outcrops of granitoids (black areas) and Quaternary arc rocks (dotted areas).

evolved S-type, and about 150 Ma younger than their envelope (Cobbing et al. 1986).

Relatively little is known about the plutonic bodies in mainland Sumatra. According to the information reported in Katili (1973) and in the geological maps (see also Hehuwat 1976), several granitoids ranging in age from Permian to Neogene outcrop along the volcanic arc from north to south Sumatra, but only a few of them have been studied in any detail.

Katili (1973) reported some K/Ar and Rb/Sr ages for several igneous rocks in mainland Sumatra and the Sunda Shelf, and pointed out the existence of Middle Tertiary (Panti granodiorite, 42.7 Ma, and Sontang granodiorite, 47.7 Ma) and, further west, Upper Cretaceous (Sontang granite, 89 Ma) plutons on the west coast of central Sumatra (Hutanopan area), and a Lower Cretaceous granite in central Sumatra (Lassi granite in the Padang area, 112 Ma). At least some of these ages have been shown to be too old by Sato (1991). Katili (1973) also noticed that "the Upper Cretaceous granites occur apparently more to the east side than the Middle Tertiary granites". Rb/Sr ages for the granites in south Sumatra (Lampung Province) range from 84 to 88.7 Ma (Katili, 1973), i.e. slightly older than their stratigraphic age according to the geological map (Amin et al. 1988), and samples of granitic rocks and graphitic schists cored from the basement in the Jambi area gave K/Ar and Rb/Sr ages ranging from 298 ± 39 Ma to 247 ± 10 Ma (Katili 1973).

K/Ar and Rb/Sr dating of the Hatapang granite, SE of Lake Toba (Clarke & Beddoe-Stephens, 1987) gave a concordant age of 80 ± 1 Ma, and an initial $^{87}Sr/^{86}Sr$ value of 0.7151 similar to the value of 0.7152 reported for the granites in Belitung, Bangka, and the Tujuh Islands by Priem et al. (1975). Clarke & Beddoe-Stephens (1987) based their suggestion that this granite may belong to the Western Province on its age, which is considerably younger than the age of the granites of the Central Province, and on the occurrence of W mineralisation, which is more common in granites of the Western Province. However, the major and trace element data show that the granite is of S-type, like most granites in the Central Province, and its initial $^{87}Sr/^{86}Sr$ value is low for Western Province granites, which are characterised by having extremely high initial $^{87}Sr/^{86}Sr$ values (0.714 to 0.740, according to Putthapiban & Gray 1983) compared with the Eastern and Central Province (0.708 to 0.719; Hutchison 1977. For a review of initial $^{87}Sr/^{86}Sr$ values see also Hutchison 1989).

For the Padang area in central Sumatra, Sato (1991) reported three K/Ar ages of 64 ± 3 Ma, 56 ± 3 Ma and 247 ± 12 Ma for three different granites (respectively Padangpanjang, Lassi and Sijunjung), and concluded that the two younger plutons belong to the same magmatic episode but differ, both in age and in composition, from the Hatapang granite. Similar K/Ar Paleocene ages (Suensilpong et al. 1983) have been reported for some granites of Phuket, in the Western Province. The older Sijunjung pluton, together with the Sibolga granite for which a Rb/Sr age of 257 ± 24 Ma has been reported by Katili (1973), is tentatively correlated by Sato (1991) with the Permian-Triassic granitoids of the Eastern Province (Malay peninsula), but,

as with the correlation of the two Paleocene and the Hatapang granites with the granites of respectively Phuket and the Western Province, this is only based on the age of the pluton, and not on its geochemistry.

Finally, a number of minor stocks and small batholiths of granitic to dioritic composition have been described in north Sumatra (Page et al. 1979; Rock et al. 1982). Some of these gave lower to middle Miocene K/Ar ages and initial $^{87}Sr/^{86}Sr$ values in the range 0.7042 - 0.7046 (Bennett et al. 1981a, b). These plutons have no equivalents elsewhere in Southeast Asia, and as it will be argued, their generation is believed to be closely related to the subduction of Indian Ocean lithosphere.

2.5 Previous studies of the fragmental deposits of Sumatra

Compared with the other islands of the Indonesian arc, Sumatra is rich in young fragmental felsic volcanic rocks associated with major caldera-forming events, and commonly believed to have involved the melting of upper crustal material (e.g. Hamilton 1979).

Four major Pliocene to Quaternary pyroclastic deposits are known in Sumatra: the Toba tuffs in north Sumatra, the Padang tuffs in central Sumatra, and the Ranau and Lampung tuffs in south Sumatra (Figure 2.2). Three of these deposits are associated with large eruptions that formed the calderas now occupied by three of the major lakes of Sumatra (Lake Toba, Maninjau and Ranau). The location of the site of the fourth eruption, of the Lampung tuffs in south Sumatra, may be in the Sunda Strait (Nishimura et al. 1986). The Toba tuffs have been studied in some detail, but the other major recent pyroclastic deposits have received scant (Maninjau caldera and tuffs in the Padang area - Leo et al. 1980) or no attention (Lake Ranau tuffs and the Lampung Formation in South Sumatra).

Whitford (1975) first suggested, on the basis of a single $^{87}Sr/^{86}Sr$ value of 0.71392, that the Toba tuffs have a crustal origin. Most of the studies on the Toba caldera have dealt with the chronology and stratigraphy of the different ignimbrites (e.g. Ninkovich et al. 1978a, b; Knight et al. 1986; Chesner et al. 1991; Chesner & Rose 1991), and relatively little is known about the geochemical and Pb/Sr/Nd isotopic composition of the Toba tuffs, but Whitford's interpretation is generally accepted.

K/Ar whole-rock age determinations for the andesitic centres and tuffs surrounding the Maninjau caldera range from 0.83 ± 0.42 Ma for the older, pre-caldera andesites, to 0.28 ± 0.12 Ma for the youngest rhyolitic ash-flows (Leo et al. 1980). For the same samples, $^{87}Sr/^{86}Sr$ values are in the range 0.7056 - 0.7066. These values are considerably higher than those of most andesitic centres elsewhere in the Sunda arc and in Sumatra (Whitford 1975), and it is suggested that they reflect the extensive involvement of sialic crustal material. Nevertheless, it should be noted that these $^{87}Sr/^{86}Sr$ values are considerably lower than those reported for the Toba tuffs.

Very little is known about the Ranau and Lampung tuffs. Westerveld (1952) briefly discussed some major element analyses of tuffs from several localities (including the Ranau and Lampung tuffs) in his review of Sumatran volcanism, and pointed out similarities between the Sumatran Pliocene and Quaternary tuffs and the Taupo ignimbrites in New Zealand.

For the Lampung tuffs, Nishimura (1980) and Nishimura et al. (1984, 1986) obtained a fission track age of 0.09 ± 0.01 Ma, and an older age (1 ± 0.2 Ma) for an ignimbrite sampled close to Kotaagung at the southern end of the Semangko fault. Based on major and trace element evidence, they concluded that these ignimbrites are similar in composition (but not in age, nor in isotopic composition, as the new data show) to the tuffs in the Lake Toba area and in central and West Jawa, and considered them as the result of the remelting of the lower crust.

2.6 Analytical results

New analytical data for some Sumatran plutonic and volcanic rocks associated with pyroclastic deposits are presented here, and compared with published data.

The analytical techniques are decribed in Appendix A, and the major and trace element, and isotopic compositions are listed in Table 2.2. A brief petrographic description of the samples is given in Appendix B. The lithology and geology of the granitoids and fragmental volcanic formations have been described in the explanatory notes of the 1:250,000 geologic maps (and in the references quoted therein, and elsewhere in this text; see Appendix B for the location of the samples).

Fragmental deposits

Sample	75212	75220	75221	75222	75223	75224	75225	75226	75218	75219	75230
SiO2	75.37	67.90	71.72	70.80	72.04	73.87	71.20	74.73	79.75	57.09	69.11
TiO2	0.13	0.21	0.17	0.17	0.17	0.17	0.21	0.16	1.00	1.05	0.30
Al2O3	13.19	16.28	13.49	14.12	14.00	14.19	13.73	14.24	12.42	18.11	15.92
Fe2O3	1.33	1.95	0.82	1.18	1.14	1.00	1.03	0.72	0.75	8.62	2.45
MnO	0.03	0.10	0.01	0.12	0.12	0.05	0.02	0.04	0.01	0.07	0.09
MgO	0.02	0.38	0.21	0.26	0.15	0.11	0.26	0.09	0.40	2.69	0.55
CaO	0.82	1.45	1.50	1.03	1.02	1.07	1.46	1.06	0.01	0.58	2.06
Na2O	4.05	2.33	3.05	3.23	4.27	5.02	3.56	4.99	0.01	0.98	3.53
K2O	3.93	3.13	4.01	4.06	3.64	3.24	3.59	3.25	4.11	3.63	2.49
P2O5	0.00	0.05	0.02	0.05	0.03	0.07	0.02	0.06	0.02	0.14	0.05
LOI	0.85	6.33	5.39	4.79	2.93	1.15	4.64	0.87	2.18	7.29	3.04
Total	99.72	100.11	100.39	99.81	99.51	99.94	99.72	100.21	99.76	100.25	99.59
Rb	135	127	213	148	99	93	244	95			194
Ba	477	542	870	596	620	648	868	639	266	713	497
Sr	83	244	302	165	162	169	278	165			182
Pb	16		9	15	15	16	11	15	6		
Cs	3.25			4.08							
Zr	126	203	154	160	159	162	159	159			143
Hf	3.04		2.75	3.73							
Nb	9	13	12	12	12	12	12	12			5
Ta	1.08		0.9	0.96							
Y	17	26	42	24	23	31	39	25			14
Th	17.5		10.86	11.75	13	13	11	13	18		
U	4		3	5	5	3	4	3	4		
La	26.7		46	27.1	30				27		
Ce	43.7		93.6	55.6	57				48		
Nd	15.6		41.6	22.7	25				17		
Sm	2.85		8.32	4.36							
Eu	0.52		1.49	0.88							
Tb	0.45		1.18	0.63							
Ho	0.63		1.47	0.87							
Yb	1.9		4.38	2.49							
Lu	0.27		0.63	0.37							
Cr	3	1	2	2	1	1	3	1	1	39	1
Ni	2	1	1	1	1	2	1	1	2	19	3
V	6	4	21	4	2	3	18	2	7	190	30
Sc	2	3	4	2	2	2	4	2	2	23	7

All Fe is reported as Fe_2O_3 wt %.

Table 2.2 Major and trace element analyses, and isotopic data for fragmental and intrusive volcanic rocks in Sumatra. All elements analysed by XRF except Cs, Hf, Ta, and Th (only where the REE are reported). REEs by INAA, except where only La, Ce, and Nd are reported (XRF). The initial $^{87}Sr/^{86}Sr$ values have been recalculated from the measured Rb/Sr and $^{87}Sr/^{86}Sr$ values, and the age has been estimated from the stratigraphic age reported in the geological maps. The error reported here is an estimate of the maximum variation due to the age uncertainty. For these recalculations, samples 75221 and 75222 have been considered to be Quaternary, as field evidence suggests that they belong to the Lampung Formation and not to the Tarahan Formation as reported in the geological map. A recalculation of their initial $^{87}Sr/^{86}Sr$ values based on the age of the Tarahan Formation would produce improbably low initial $^{87}Sr/^{86}Sr$ values ($<< 0.704$).

Measured Pb and Nd isotopic ratios have not been recalculated. Measured Nd isotopic ratios should not differ significantly from initial ratios, due to the relatively young age and high Nd/Sm of all the samples. On the other hand, initial Pb isotope values might be significantly different from the measured values, especially in the older samples (> 40-50 Ma) with high U/Pb and Th/Pb and low Pb concentrations. Note also that the differences between the two samples from Bukit Batu can be explained by assuming that with time the observed differences in their Th, U and Pb contents caused the differences in their measured Pb isotope ratios, starting from similar initial Pb isotopic ratios.

Further information about the samples, including their location, stratigraphic position, age and petrographic information, if available, is provided in Appendices B and C.

Fragmental deposits

Sample	75231	75241	75242	75246	75290	75291	75292	75293	75306	75307	75308
SiO2	72.36	62.26	64.29	67.92	69.98	57.90	61.77	53.59	69.99	71.02	71.51
TiO2	0.20	0.86	0.18	0.47	0.11	1.00	0.80	0.98	0.19	0.19	0.13
Al2O3	13.56	18.11	12.09	16.10	11.87	17.38	17.31	19.91	15.46	14.48	12.64
Fe2O3	1.81	4.86	1.29	3.79	0.85	7.82	5.70	7.77	2.13	1.35	1.53
MnO	0.08	0.04	0.06	0.02	0.05	0.13	0.09	0.13	0.07	0.05	0.07
MgO	0.41	0.72	0.29	0.18	0.09	2.82	1.42	2.66	0.39	0.31	0.18
CaO	1.89	3.20	1.68	0.32	0.85	6.78	4.26	5.61	1.53	1.73	1.14
Na2O	3.88	1.73	3.13	4.53	2.35	3.22	4.18	2.82	3.18	3.19	2.62
K2O	3.32	0.33	2.88	4.78	4.57	1.67	1.94	1.04	4.09	4.62	4.75
P2O5	0.07	0.18	0.00	0.01	0.02	0.19	0.33	0.18	0.03	0.01	0.00
LOI	2.75	8.04	13.94	1.42	9.83	0.52	1.66	4.86	3.08	2.91	5.30
Total	100.33	100.33	99.83	99.54	100.57	99.43	99.46	99.55	100.14	99.86	99.87
Rb	142	9		107	189	64	67	27	217	215	
Ba	432	208	448	693	586	339	522	733	457	612	306
Sr	153	288		274	96	352	321	315	111	128	
Pb	13		17			10	13				
Cs	6.9										
Zr	113	147		376	76	189	265	229	150	144	
Hf	2.95										
Nb	6	6		15	8	4	7	6	18	15	
Ta	1.46										
Y	13	42		39	16	32	52	49	36	29	
Th	18.53		18			7	9				
U	4		4								
La	19.6					21	55				
Ce	38.9					43	56				
Nd	15.8					23	72				
Sm	2.39										
Eu	0.42										
Tb	0.47										
Ho	0.66										
Yb	1.73										
Lu	0.22										
Cr	3	5	2	1	1	15	2	5	5	4	3
Ni	3	12	1	2	1	13	5	11	4	1	2
V	17	156	13	14	2	224	42	110	18	9	10
Sc	4	23	4	7	3	27	16	23	5	4	3

Intrusives

Sample	75415	75412	75413	75414	75247	75248	75249	75250	75251	76100	76101
SiO2	75.47	71.17	63.50	68.85	67.54	58.37	77.23	65.38	57.06	57.75	61.05
TiO2	0.04	0.23	0.58	0.31	0.70	0.82	0.10	0.05	0.87	0.59	0.51
Al2O3	13.61	14.90	17.02	16.30	14.42	14.22	12.93	19.67	16.55	16.04	17.32
Fe2O3	0.52	1.93	4.13	2.23	5.83	7.03	0.52	0.98	5.72	10.87	5.42
MnO	0.01	0.05	0.08	0.04	0.04	0.27	0.02	0.02	0.17	0.52	0.18
MgO	0.03	0.57	1.33	0.88	0.48	3.05	0.18	0.26	2.56	0.35	0.55
CaO	0.82	2.38	3.07	3.49	2.89	12.04	0.33	4.89	11.30	3.15	2.19
Na2O	4.49	4.20	4.52	4.32	4.12	3.45	4.53	5.61	3.83	4.06	3.64
K2O	3.53	3.18	4.12	2.18	2.24	0.33	3.97	2.16	0.84	5.05	7.38
P2O5	0.02	0.08	0.21	0.15	0.26	0.27	0.08	0.04	0.24	0.06	0.12
LOI	1.43	0.78	1.21	0.83	1.25	0.27	0.57	0.52	0.35	0.41	1.23
Total	99.97	99.47	99.77	99.58	99.77	100.12	100.46	99.58	99.49	98.85	99.58
Rb	237	77	68	51	100	5	80	52	16	113	181
Ba	12	535	937	448	344	173	878	633	216	45	43
Sr	14	464	490	826	286	421	116	445	454	32	70
Pb	46		16		8	7	13	10		27	36
Cs	5.1		1.3			0.27		0.36	0.47		
Zr	119	89	333	99	169	130	68	60	178	1535	956
Hf	5.82		7.05			3.32		1.9	4.32		
Nb	37	13	15	7	5	7	11	3	8	35	41
Ta	8.99		1.02			0.79		1.01	0.8		
Y	7	15	22	8	43	30	12	12	32	23	31
Th	34.9		5.91		5	5.44	12	4	6.96	184	151
U	25		2		3	4	3	2		11	8
La	3.23		35.4			19		11.6	21.7	718	865
Ce	7.18		74			40.9		23	47.3	1104	1240
Nd	4.05		30.6			21.5		11.2	25.6	375	393
Sm	1.07		5.66			4.82		2.29	5.09		
Eu	0.19		1.05			1.48		0.75	1.49		
Tb	0.22		0.58			0.74		0.38	0.77		
Ho	0.36		0.79			0.96		0.5	1.12		
Yb	1.35		1.86			2.51		1.29	3.06		
Lu	0.24		0.24			0.37		0.19	0.48		
Cr	3	3	10	11	4	56	1	4	46	1	1
Ni	1	2	12	6	3	25	1	3	20	4	1
V	4	25	53	45	25	150	4	19	139	1	1
Sc	3	4	9	7	20	19	2	8	20	18	19

Intrusives

Sample	75286	75287	75289	75309	75411	75409	75410	75403	75402	75398	75391
SiO2	71.14	70.66	49.36	59.10	67.98	67.80	76.81	65.38	75.63	51.07	67.56
TiO2	0.24	0.28	1.15	0.66	0.42	0.42	0.11	0.48	0.06	0.83	0.28
Al2O3	15.16	15.52	15.61	17.06	15.73	15.40	12.27	16.09	13.61	18.05	15.59
Fe2O3	1.71	1.76	8.77	6.65	2.84	2.86	0.98	3.65	0.51	9.10	2.91
MnO	0.03	0.03	0.13	0.14	0.08	0.09	0.02	0.06	0.01	0.20	0.07
MgO	0.61	0.68	7.91	2.94	0.85	0.82	0.36	2.09	0.04	5.39	1.23
CaO	2.22	3.13	8.59	6.29	2.21	2.28	0.24	4.13	1.04	4.52	5.10
Na2O	4.30	4.61	3.27	2.51	4.16	4.16	2.69	4.45	4.81	5.76	4.17
K2O	3.13	1.79	1.24	2.33	4.88	4.63	5.46	2.35	2.10	0.52	1.87
P2O5	0.11	0.08	0.30	0.17	0.19	0.14	0.03	0.18	0.05	0.15	0.09
LOI	0.87	0.99	3.20	1.84	0.44	0.91	0.90	0.64	1.58	3.84	0.58
Total	99.52	99.53	99.53	99.69	99.78	99.51	99.87	99.50	99.44	99.43	99.45
Rb	48	26	28	81	131	143	169	55	53	19	34
Ba	603	304	302	592	784	665	440	366	10	636	397
Sr	447	641	514	285	315	296	146	727	41	719	402
Pb			5				23				
Cs											
Zr	105	99	116	142	170	192	62	113	58	58	74
Hf											
Nb	2	2	8	8	11	11	7	7	9	1	3
Ta											
Y	6	6	21	29	20	21	14	12	3	23	11
Th			4				14				
U			2				4				
La			17								
Ce			41								
Nd			20								
Sm											
Eu											
Tb											
Ho											
Yb											
Lu											
Cr	5	6	349	5	4	1	4	45	1	46	7
Ni	3	3	129	6	4	4	2	37	1	26	4
V	31	38	225	135	34	35	15	76	6	261	56
Sc	4	4	33	22	5	6	3	10	1	25	10

Sample name	75212	75221	75222	75231	75415	75413	75248	75250
87Sr/86Sr	0.70453	0.70494	0.70495	0.70652		0.70477	0.70560	0.70537
Estimated age (Ma)	1±1	1±1	1±1	1±1		60±20	20±4	15±3
Estimated initial 87Sr/86Sr	0.70446±7	0.70491±3	0.70491±3	0.70648±4		0.70443±11	0.70559±0	0.70530±2
143Nd/144Nd	0.512804	0.512691	0.512690	0.512575	0.5127	0.512746	0.512768	0.512732
208Pb/204Pb	38.757	38.770	38.805	39.204	38.545	38.421	38.801	38.913
207Pb/204Pb	15.623	15.630	15.636	15.701	15.614	15.580	15.622	15.650
206Pb/204Pb	18.596	18.598	18.605	18.817	19.108	18.417	18.688	18.681

Sample name	75251	76100	76101	75286	75289	75410	75403	75391
87Sr/86Sr	0.70555	0.74036	0.73287	0.70406	0.70473	0.71026	0.70418	0.70466
Estimated age (Ma)	15±3	170±35	170±35	25±25	1±1	135±20	97.7±0.7	14.3±0.5
Estimated initial 87Sr/86Sr	0.70555±1	0.71564±510	0.71477±375	0.70395±11	0.70473±0	0.70383±100	0.70388±0	0.70461±0
143Nd/144Nd	0.512726	0.51221	0.512219	0.512931	0.512751	0.512481	0.512849	0.512860
208Pb/204Pb	38.803	44.815	42.427	38.071	38.482	39.114	38.175	38.282
207Pb/204Pb	15.617	15.812	15.788	15.520	15.577	15.695	15.539	15.563
206Pb/204Pb	18.673	19.765	19.289	18.193	18.447	19.047	18.286	18.292

2.7 Granitoids and fragmental deposits of the volcanic arc and west of the Semangko fault

The compositions of most igneous rocks from centres in the volcanic arc and west of the Semangko fault, as well as the previously analysed pyroclastites (Westerveld 1952), fall within the calcalkaline differentiation trend (Debon & Le Fort 1988), with a complete overlap between intrusive and generally more differentiated pyroclastic rocks (Figures 2.3 and 2.4).

Most rocks have a composition intermediate between peraluminous (S-type) and metaluminous (I-type). The scatter in the "alumina index" (Figure 2.4) partly reflects some slight alteration, particularly of some of the fragmental rocks. The set of samples includes highly differentiated granites, pumices and fragmental deposits, and clasts sampled within pyroclastic units, with andesitic compositions indistinguishable from the Quaternary andesitic lavas.

In general, despite their compositional and textural variability:

1) all the samples follow a typical calcalkaline differentiation trend, which overlaps the one observed for the basalt-andesite-dacite series of the Quaternary volcanic arc;
2) compared with the three granitoid provinces of Southeast Asia, they have considerably lower Rb/Sr values, usually « 1, and generally lower Pb (5 to 17 ppm) and U (2 to 5 ppm) contents;
3) the Na_2O/K_2O values are always ≥ 1, except in the samples where this ratio has been slightly modified by alteration (fragmental deposits and samples with very high L.O.I. values, i.e. 75219, 75220, 75221, 75222, and 75290, and slightly altered granitoids, i.e. 75409 and 75411);
4) on a Nb+Y/Rb diagram (Figure 2.5), useful in the discrimination of granitic rocks from various tectonic settings (Pearce et al. 1984), all the samples fall within the field of volcanic arc intrusives;
5) no systematic variations in major and trace element composition have been observed with age and location;
6) all the samples have a remarkably constant isotopic composition, despite their differences in age and the very large area of provenance. Their Sr and Nd isotopic composition is similar to that of the arc volcanics, with the initial $^{87}Sr/^{86}Sr$ values of fragmental volcanics tending to be slightly more radiogenic than those of the plutonic rocks (Figure 2.6).

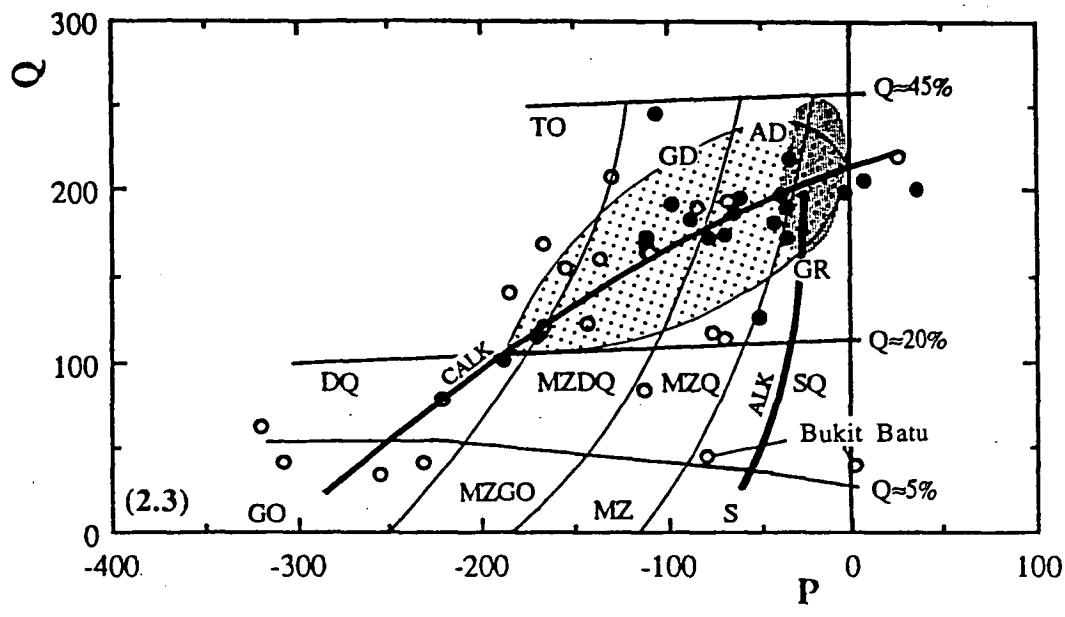

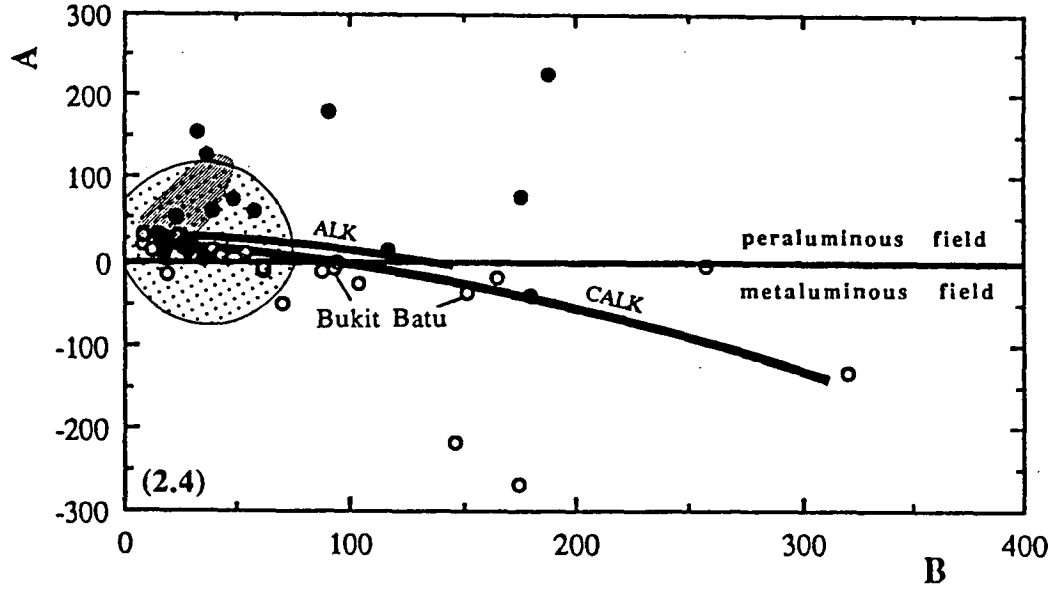

Figures 2.3 and 2.4. Debon-Le Fort (1983, 1988) classification diagrams (Q-P and A-B) for the Sumatran granitoids and fragmental rocks. Data from this study, and from references quoted in the text. A=Al-(K+Na+2Ca); B=Fe+Mg+Ti; P=K-(Na+Ca); Q=Si/3-(K+Na+2Ca/3). Open and closed circles are respectively intrusives and fragmental deposits. Lines labelled CALK and ALK are respectively typical calcalkaline and alkaline trends. Note that among the granitoids of this study, only those from Bukit Batu follow an alkaline trend. Light dotted area is the field of Sumatran granitoids and fragmental deposits from earlier works. Shaded area is the field of most granites from the Central Province, Hatapang, Sijunjung, and the "Tin Islands". In Figure 2.3: TO=tonalite; GD=granodiorite; AD=adamellite; GR=granite; DQ=quartz diorite; MZDQ=quartz monzodiorite; MZQ=quartz monzonite; SQ=quartz syenite; GO=gabbro; MZGO=monzogabbro; MZ=monzonite; S=syenite. Lines labelled Q=5%, Q=20%, and Q=45% are empirical estimates of quartz/(quartz+feldspars+muscovite) values, in volume pecentages.

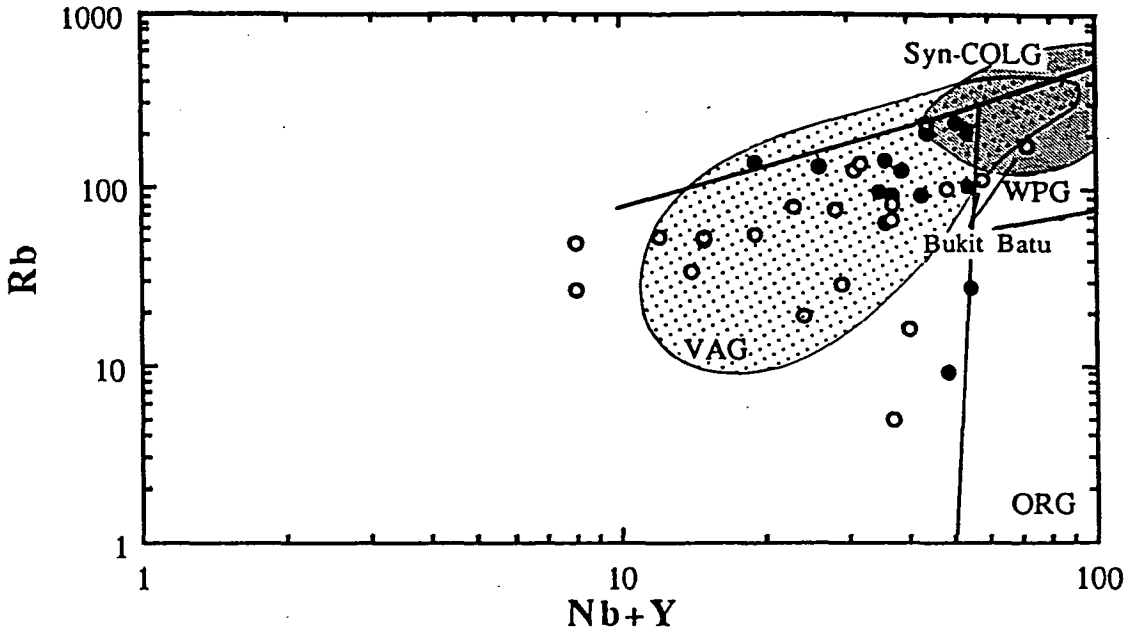

Figure 2.5. Nb+Y vs. Rb classification diagram (Pearce et al. 1984) for the Sumatran granitoids and fragmental rocks. Data from this study, and from references quoted in the text. Symbols as in Figure 2.3 and 2.4. Shaded and dotted areas are respectively the fields of granitoids of the Central and Eastern Province. VAG=volcanic arc granites; ORG=ocean ridge granites; Syn-COLG=syn-collisional granites; WPG=within plate granites.

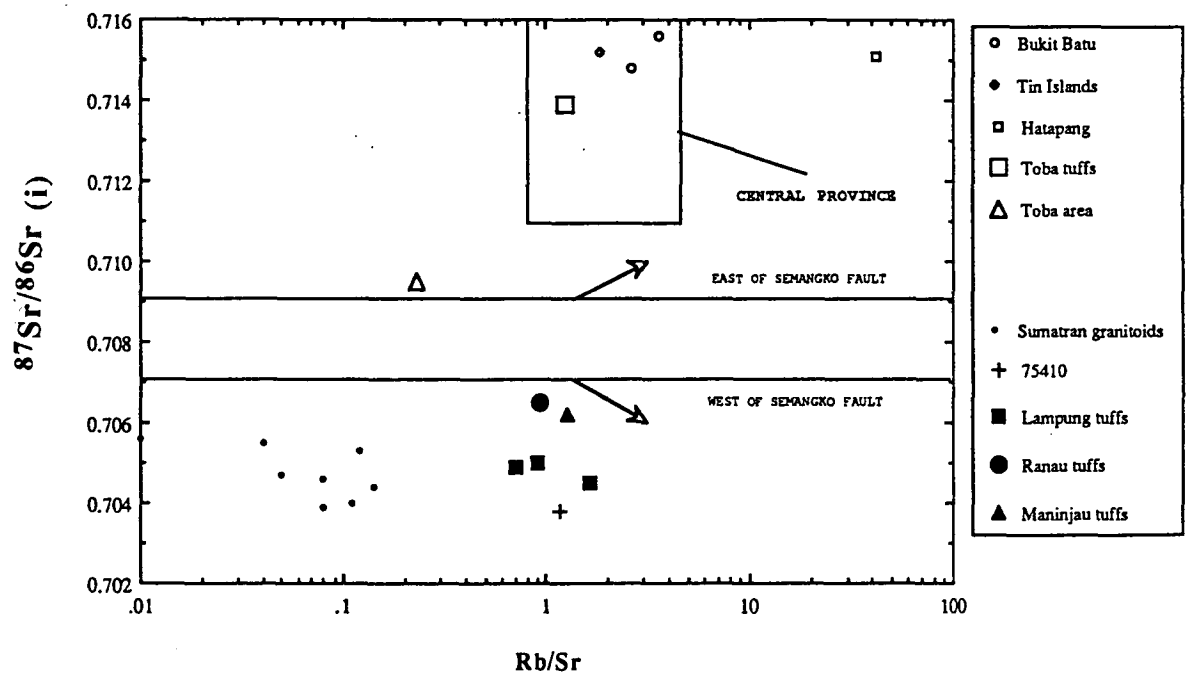

Figure 2.6. $^{87}Sr/^{86}Sr$ - Rb/Sr diagram for the Sumatran granitoids and fragmental rocks. Data from this study, and from references quoted in the text. Note the gap in $^{87}Sr/^{86}Sr$ values from 0.707 to 0.709 that clearly separates the plutons and pyroclastic deposits east of the Semangko fault from those along the volcanic arc, and the considerably high $^{87}Sr/^{86}Sr$ values of andesitic-dacitic volcanoes in the Toba area, compared with values in the range 0.704 to 0.706 for most andesitic volcanoes in the Sumatran arc (see Appendix C).

Initial $^{87}Sr/^{86}Sr$ values range from 0.7039 to 0.7056 for the granitoids and from 0.7045 to 0.7065 for the fragmental deposits of Lake Maninjau, Lake Ranau and the Lampung Formation. These values are substantially lower than the lowest values observed in the granitoid provinces of Southeast Asia. Nd and Pb isotopes also show remarkably constant compositions. The only exceptions are two granitoids. Sample 75415, a granodiorite in south Sumatra, has an unusually high $^{206}Pb/^{204}Pb$ isotopic value, although its Nd isotopic ratio is similar to the other granitoids. This sample also has unusually high Pb, Th and U contents (46, 34.9 and 25 ppm respectively), which are not likely to be of primary magmatic origin, so that the measured Pb ratios might well have grown in to their present-day values following Pb-Th-U-bearing hydrothermal mineralisation. Another sample from the same pluton (75413) has an isotopic composition more typical of the other granitoids. Sample 75410, a granite in north Sumatra, is unusual in having $^{87}Sr/^{86}Sr$ values similar to the other granitoids, but remarkably lower Nd and higher Pb isotope ratios, and relatively low Na_2O/K_2O (about 0.5) and high Rb/Sr (>1) values.

The age of most plutons is only approximately known, and therefore the initial isotopic ratios cannot be calculated very accurately (see note in Table 2.2). Nevertheless, even taking into account the large uncertainties, the conclusions outlined in the following discussion remain valid.

2.8 Bukit Batu and Lake Toba

Bukit Batu (Rock Hill) is one of two small outcrops (less than 10 square km each) of granite, situated in the east Sumatran flood plain close to the town of Tulung Selapan in the West Sumatra Province, about 220 km NE of the volcanic arc, and less than 100 km SW of Bangka Island (in the "Tin Islands").

The granitoids of Bukit Batu have a geochemical and isotopic composition very unlike granitoids of the arc. Although their SiO_2 contents are unusually low for S-type granites, they do not follow the calcalkaline differentiation trend of the other granitoids (Figure 2.3), they have very high K_2O contents, low (« 1) Na_2O/K_2O values, high (» 2) Rb/Sr values, and very high Pb-Th-U and REE contents. These geochemical characteristics reflect high concentrations of Pb-Th-U-Zr and LREE-bearing accessory phases in the rocks. Their low Ba and high Nb and Zr values are also unusual, and unlike any other plutons in Southeast Asia. On a Nb+Y/Rb

diagram (Figure 2.5), they fall in the field of within-plate granites, typical of granitoids of the Central Province (Cobbing et al. 1986).

Calculated initial $^{87}Sr/^{86}Sr$ values are high (0.715), $^{143}Nd/^{144}Nd$ values are low, and Pb isotopic ratios high, compared with those of the granitoids along the volcanic arc and west of the Semangko fault, and the calculated initial $^{87}Sr/^{86}Sr$ values are well within the range of granitoids of the Central Province (Figure 2.6).

Despite the differences in measured Pb isotope ratios, a calculation (based on the age of the rocks and their U-Pb-Th content) of their initial $^{208}Pb/^{204}Pb$ and $^{206}Pb/^{204}Pb$ gives concordant values, respectively 39.4 ± 0.2 and 18.3 ± 0.1. This simplistic approach and the evidence in the field (the two samples were collected about 10 cm from each other) suggest that the differences in Pb isotopic ratios between the two samples are due only to the different contents of Th-U bearing phases, and not to original isotopic heterogeneities. Jones et al. (1977) reported similar values for two samples of galena from Belitung (average of the two analyses: $^{208}Pb/^{204}Pb$ = 18.553 ± 0.056; $^{207}Pb/^{204}Pb$ = 15.713 ± 0.002; $^{206}Pb/^{204}Pb$ = 38.913 ± 0.035).

The samples of tuffs collected in the Lake Toba area (75306, 75307, and 75308) are compositionally similar to the tuff for which Whitford (1975) reported an initial $^{87}Sr/^{86}Sr$ value of 0.71392, and have low Na_2O/K_2O and high Rb/Sr and Nb values, typical of the S-type granites of the Central Province, and, like the granites of the Central Province, they plot close to the syn-collisional/within plate/volcanic arc granites triple point in a Nb+Y/Rb diagram (Figure 2.5). The only sample of granodiorite from the Lake Toba area (75309) has a more I-type affinity, having a Na_2O/K_2O value close to 1, and low Rb, Nb and Rb/Sr values.

2.9 Discussion

Despite differences in age (ranging from 247 Ma of the Sijunjung pluton to the Quaternary Toba tuffs), chemical composition (for example, the variable Rb/Sr and Na_2O/K_2O values), and type of mineralisation (Sn-W in Hatapang, Sn in the Tin Islands, and no significant mineralisation in Bukit Batu, Sijunjung and the Toba area), the remarkably constant initial $^{87}Sr/^{86}Sr$ values of the granitoids east of the Semangko fault suggest derivation from a common source. The very different ages of the plutons and silicic fragmental deposits do not imply the existence of different terranes, but may simply be the result of the extraction of melts from the same source

at different times. The consistency of the available data suggests that marked geochemical and isotopic fractionation did not occur.

A range of initial $^{87}Sr/^{86}Sr$ values might imply either 1) derivation from originally different sources, or 2) derivation from a common source that had suffered several episodes of marked Rb/Sr fractionation over a long period, perhaps as a result of melting; as a consequence, the different Rb/Sr values in the residual source might have evolved to different $^{87}Sr/^{86}Sr$ values. The uniformly high initial $^{87}Sr/^{86}Sr$ values are unlikely to be coincidental, and are better explained by the derivation of the rocks from a common source whose Rb/Sr has not been significantly modified.

The Toba tuffs are (Whitford 1975) isotopically (and possibly compositionally) similar to the granitoids exposed in east Sumatra suggesting that little or no juvenile material participated in the formation of the Toba tuffs, and that these are mainly the result of melting of the crust. On the other hand, the Quaternary volcanoes in the Lake Toba area, to the north of it, and the Toba granodiorite, all located east of the Semangko fault and some far from it, show a rather variable isotopic composition, with values ranging from close to those found in the arc andesites elsewhere in Sumatra, to rather more radiogenic, suggestive of varying amounts of interaction between the same juvenile material that forms the arc andesites and the east Sumatran upper continental crust.

At the other end of the spectrum, all the granitoids and tuffs sampled in localities situated on the volcanic arc along and within the Semangko fault zone or to its west have major and trace element chemical compositions typical of volcanic arcs built on continental crust. Their isotopic composition differs remarkably from the three granitoid provinces of Southeast Asia, and from the Sumatran granitoids and tuffs from east of the Semangko fault: despite the large area from which samples were taken, the relatively large number of samples and the differences in ages, the plutons show a rather narrow isotopic and compositional range (apart from the variations due to different degrees of fractionation), and their initial $^{87}Sr/^{86}Sr$ values, which vary from 0.704 to 0.706, are consistently low and similar to those of the arc andesites (Figure 2.7). Also, their isotopic systematics are unusual (Figures 2.7, 2.8, 2.9), with values intermediate between the Quaternary andesites and the OIB basalts in south and central Sumatra (see Chapter 6).

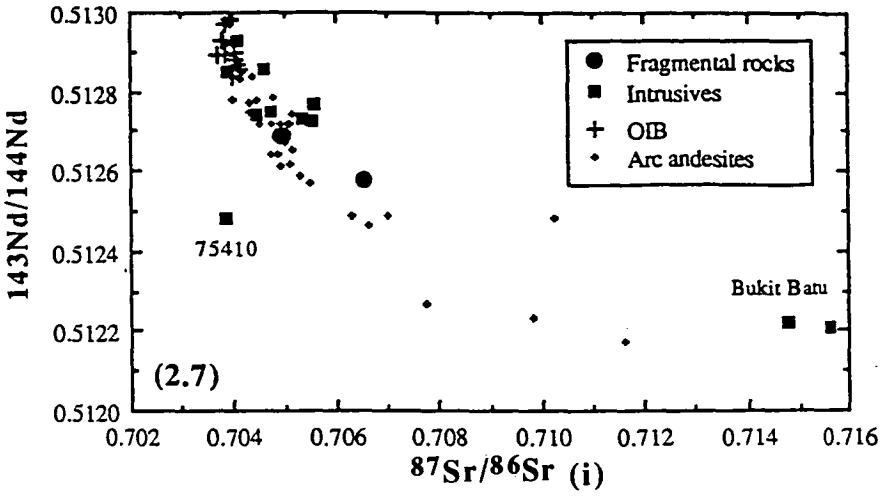

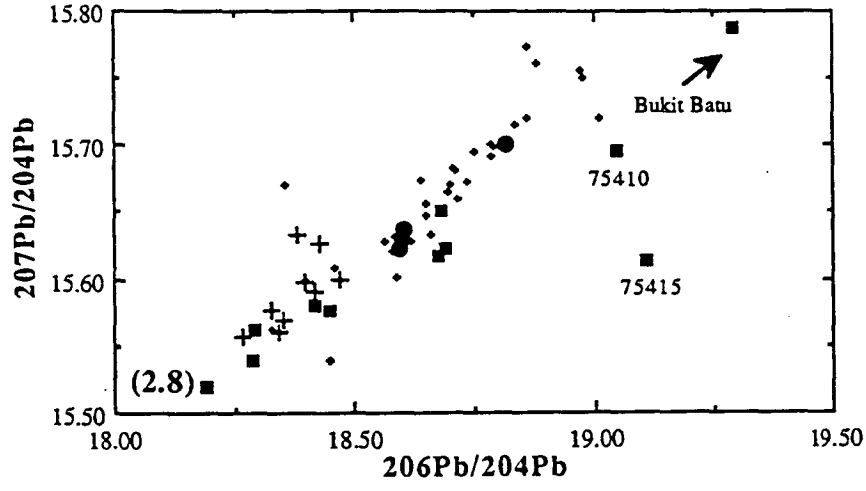

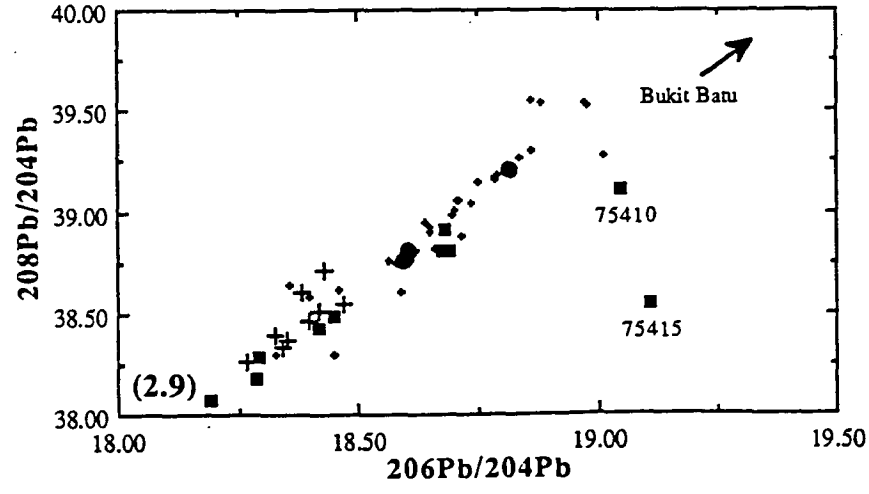

Figures 2.7, 2.8, 2.9. Sr, Nd and Pb isotope ratios diagrams for the Sumatran granitoids and fragmental rocks, OIB, and arc andesites. The only Sumatran arc andesites and dacites with $^{87}Sr/^{86}Sr$ higher than 0.706 are from the lake Toba area ($^{87}Sr/^{86}Sr$ = 0.707 to 0.712) and other centres situated east of the Semangko fault (Pulau Weh; $^{87}Sr/^{86}Sr$ = 0.707 to 0.708), and from centres associated with large pyroclastic deposits in the Maninjau area ($^{87}Sr/^{86}Sr$ = 0.705 to 0.707). These also have the lowest $^{143}Nd/^{144}Nd$ and highest $^{208}Pb/^{204}Pb$, $^{207}Pb/^{204}Pb$, and $^{206}Pb/^{204}Pb$ values.

This seems clear evidence that the compositional characteristics of the sources of the granitoid and related rocks change abruptly across the Semangko fault zone. If granitoids reflect the nature of their lower crustal sources, then the Semangko fault zone represents a marked change in the composition of the basement, because east of the fault zone the granitoids have much higher $^{87}Sr/^{86}Sr$ values.

Pyroclastic rocks associated with the two calderas of Lake Maninjau and Lake Ranau show slightly more radiogenic isotopic values, but still considerably lower than those of the east Sumatran granitoids and in the Toba area - despite their very similar major and trace element composition. The Quaternary arc andesites also tend to have slightly more radiogenic isotopic ratios in the vicinity of these calderas.

The Semangko fault zone is the most marked of a regional system of dextral wrench-faults which is developing as a result of the oblique convergence between the Southeast Asian and Indian Ocean plate boundaries. The volcanoes of the Sumatran volcanic arc follow the Semangko fault zone, and it is generally thought that the fault has developed in the Sumatran crust where it is more plastic, due to the magmatism. However, the simplest interpretation of the new data is that the Semangko fault zone follows the southwestern boundary of the SIBUMASU terrane in Sumatra, and is actually located along a profound compositional discontinuity in the Sumatran lithosphere, possibly at the original Southeast Asian continental boundary that was formed following the rifting of this part of Gondwanaland.

The Quaternary volcanic arc also follows the terrane boundary. None of the analysed samples of granites outcropping within the volcanic arc or west of it bears the crustal signature typical of east Sumatra, nor of any of the Southeast Asian Granitoid Provinces, and the granitoids, fragmental deposits and Quaternary arc andesites seem to be isotopically very closely correlated. The only known exception to the observed distribution is sample 75410, and possibly the Sn- and W-bearing (Aspden et al. 1982) Sibolga granite, situated west of the Semangko fault and for which a Rb/Sr age of 257 ± 24 Ma (older than any of the other granites found west of the Semangko fault, and within the age range of the Central Province) has been reported by Katili (1973).

It has been pointed out (see e. g. the summary of the tectonic evolution of north Sumatra in Wajzer et al. 1991) that part of Sumatra west of the Semangko fault is composed of a number of continental microplates ("Woyla Group"), each "with distinctive stratigraphic sequences and structural, metamorphic and magmatic

histories" (Wajzer et al. 1991), and the complex nature of the ophiolite belt running parallel to the Semangko fault was also pointed out by Sengupta et al. (1990), who recognised lithologies typical of seamounts among the material forming the ophiolites.

Sample 75410 is the oldest among the granitoids sampled west of the Semangko fault, and therefore it is not surprising that its isotopic composition differs from the isotopically homogeneous post-Lower Cretaceous, arc-related granitoids; the same is probably true for the Sibolga granite, although no isotopic data are available to test this conclusion.

Despite the compositional heterogeneity of the terranes forming the western part of Sumatra, the source of the granitoids seems to have been isotopically homogeneous since the Lower Cretaceous, and only the pre-Lower Cretaceous plutons may carry the original isotopic characteristics of their microplate. Because the microplates bear different compositional signatures, we should expect to see an array of isotopic compositions in the granitoids and arc andesites, if these were derived from the melting of these microplates which now are part of the upper crust, or if there had been strong interaction of microplate-derived material with material from a juvenile, deeper source, but the lack of a strong microplate-derived crustal signature in the granites and in most of the arc andesites suggests little (but significant) interaction between the juvenile material and the upper crust.

On the other hand, the similarity in isotopic composition between the granitoids along and west of the Semangko fault and the OIB from south (Sukadana basalts, isotopically similar to some Indian Ocean volcanics - see Chapter 6) and central (Bukit Telor basalts) Sumatra (Figures 2.7, 2.8, 2.9) suggests involvement in the granitoid sources of material derived from the same mantle that produced the OIB. The oldest Sukadana-like isotopic values occur in Lower Cretaceous granitoids, showing that mantle signatures similar to those of Indian Ocean basalts have existed beneath Sumatra over a very large area, and with a remarkably constant isotopic composition in time. The petrogenetic implications of this apparent relationship between OIB and western Sumatran granitoids are explored in Chapter 6.

In the southernmost part of the island, the Semangko fault zone splays into the zone of extension marked by the Sunda Strait, and the width of the Quaternary volcanic arc is considerably greater. Here, the distinction between eastern and western Sumatran granitoids is also less clear. The Lampung and Tarahan Formation, and the granites

of the Seputih batholith, east of the Semangko fault, are isotopically similar to the arc volcanics. This could imply that SIBUMASU-type basement typical of east Sumatra may not be present, and that the Sunda Strait marks an approximate southern limit to the SIBUMASU terrane.

2.10 Conclusions

Two different types of granitoids and fragmental deposits have been recognised in Sumatra.

West of the Semangko fault and along the Quaternary volcanic arc as far south as the Sunda Strait, the granitoids and fragmental deposits define a differentiation trend typical of calcalkaline associations in continental arcs. They are younger than the granitoids of eastern Sumatra, and have considerably lower initial $^{87}Sr/^{86}Sr$ values, Pb isotopic values similar to the OIB basalts in south and central Sumatra, and Sr and Nd isotopes intermediate between the Quaternary arc andesites and the OIB basalt source. A complex array of continental and oceanic microplates may form part of the lithosphere of western Sumatra, but most of the granitoids resemble the products of the young arc volcanism and only the older granitoids display isotopic and geochemical signatures that might betray involvement of microplate-derived material.

The granitoids in east Sumatra, east of the Semangko fault zone, including those of the "Tin Islands", Bukit Batu close to Palembang, the Hatapang pluton and granodiorites and fragmental volcanics of the Lake Toba area, and possibly Sijunjung pluton south of Lake Toba, all share high $^{87}Sr/^{86}Sr$ values and other isotopic and compositional similarities, and seem to be related to the Central Granitoid Province S-type granitoids of the Malay peninsula, suggesting that they are derived from the same granite basement terrane. This granite basement terrane roughly corresponds with the SIBUMASU tectonic terrane and may therefore form its deep basement. This interpretation does not preclude the possibility that there is more than one terrane in eastern Sumatra, nor that any such terranes were assembled at different times, but the granitoid data and the granite basement terrane concept offer no support for this interpretation. Neither do the available data exclude the possibility that a single Gondwanan basement block was pulled apart, and the fragments later accreted at various times to form eastern Sumatra. However, the simplest interpretation of the data is that the entire eastern (east of the volcanic arc) part of Sumatra, with the exception of the "Jambi Nappe", apparently derived from peninsular east Malaysia

(van Bemmelen 1949), belongs to a single granite basement terrane which corresponds with the SIBUMASU tectonic terrane.

The lack of systematic compositional and isotopic variations in arc-related granitoids and arc volcanics from north to south Sumatra also suggests that no major tectonic boundaries exist across Sumatra. Furthermore, the similarity between the Sr, Nd, and Pb isotopic composition in the arc-related granitoids, the OIB basalts of south Sumatra, and, as will be shown in Chapter 6, some of the volcanics in the eastern portion of the Sunda arc, suggests that the same mantle wedge component can be identified from north Sumatra to the east Sunda arc.

Granitoids that are geochemically and isotopically similar to those of the Western Province are not yet known in Sumatra, and granitoids similar to those of the Eastern Province are rare, implying that the boundary between the Central and the Eastern Granitoid Provinces runs through the "Tin Islands", and that the boundary between the Central and the Western Granitoid Provinces does not occur within Sumatra. The Semangko fault zone and the Sunda Strait mark the southwestern and southern limits of this granite basement terrane, suggesting that the Semangko fault zone formed and developed along the southwestern boundary of the granite basement terrane, which corresponds with the southwestern boundary of the SIBUMASU terrane.

Based on the data discussed in this chapter, the likely composition of the Sumatran SIBUMASU crust will be estimated in Chapter 5, and the effects of contamination by crustal material on the Sr, Nd, and Pb isotopic composition of melts generated in the Sumatran mantle wedge will be illustrated.

CHAPTER 3

Distribution of OIB and basalts with an "enriched mantle" component in the Northeastern Indian Ocean

3.1 Introduction

3.1.1 Aims of the chapter

The aim of this chapter is to investigate the composition of fresh and altered basalts in the Northeastern Indian Ocean, and to provide an estimate of the geochemical and isotopic composition of the mantle source of basalts in the Northeastern Indian Ocean in the proximity of the Sunda arc. This chapter is also an attempt to answer two questions. First, can the study of the disrtibution of OIB in the Indian Ocean provide any evidence for the existence of an isotopically "enriched" (i.e. with an EM or a HIMU component) mantle component in the source of the arc volcanics in the Sunda arc? Second, is the isotopic signature of the depleted MORB component of the mantle source of the arc volcanics in the Sunda arc likely to be similar to that of Indian Ocean MORB?

Since the early cruises of the HMAS "Diamantina" in the middle sixties, much geophysical and geological data have been obtained on the Northeastern Indian Ocean. The results of the studies made on samples of volcanic rocks collected mainly during the DSDP and ODP cruises, and syntheses of the geological and tectonic history of the NE Indian Ocean have been published in a number of articles and regional reports (Initial Reports of the Deep Sea Drilling Project vol. 22 and 27, 1974; Curray et al. 1982; Schlich 1982; Kolla & Kidd 1982; Initial Reports of the Ocean Drilling Program vol. 118 to 123, 1991-92; Scientific Results of the Ocean Drilling Program vol. 118 to 123, 1991-92). The new major and trace element data presented here for the DSDP samples reinforce the conclusions reached by others, and will therefore be discussed only briefly here. However, the data from the Cocos Plateau and the Investigator Ridge, and the new isotopic data, provide new information on previously unknown areas.

3.1.2 Petrological background

OIB in the Indian Ocean are characterised by distinctive isotopic signatures, which, as other OIBs, can be described as the result of mixing between four hypothetical mantle components, defined by Zindler & Hart (1986) and Hart & Zindler (1989) as DMM (Depleted MORB Mantle, with relatively high $^{143}Nd/^{144}Nd$ values, and low $^{87}Sr/^{86}Sr$ and $^{206}Pb/^{204}Pb$ values), HIMU (High U/Pb (= μ) mantle, with low $^{87}Sr/^{86}Sr$ and intermediate $^{143}Nd/^{144}Nd$, but very high $^{206}Pb/^{204}Pb$ values) and two "enriched" mantle components, EM1 and EM2 (Enriched Mantle I, with intermediate $^{87}Sr/^{86}Sr$ values and low $^{143}Nd/^{144}Nd$ values, and Enriched Mantle II, with very high $^{87}Sr/^{86}Sr$ values and intermediate $^{143}Nd/^{144}Nd$ values). Falloon et al. (submitted for publication) recognised a HIMU-EM1 array in the volcanics of Christmas Island, and Weis et al. (1993) suggested that the source of the Kerguelen volcanics (the Kerguelen Plume) may be a mixture of EM1 and EM2. Although a DUPAL (after Dupré & Allègre 1983) mantle source was initially defined as a source with $^{87}Sr/^{86}Sr > 0.705$ and $\Delta 8/4 > 60$ (see Hart 1984), the term DUPAL is now applied to "OIB [situated] beween the equator and 50°S, isotopically characterised by high proportions of the EM1, EM2, and HIMU mantle components " (Hart et al. 1992, page 520), and many authors recognised a DUPAL component in the source of some Indian Ocean basalts (see the next paragraphs).

Varne & Foden (1986), and Stolz et al. (1990) suggested that OIB mantle is present, together with MORB or depleted MORB mantle, in the mantle wedge of the Sunda arc, and other workers evaluated the possibility that an OIB component in the mantle source of arc volcanics may exist in other arcs (e.g. Morris & Hart 1983; Reagan & Gill 1989).

Data from active ridges (Le Roex et al. 1983; Le Roex 1985; Le Roex et al. 1989; Hamelin & Allègre 1985; Hamelin et al. 1985-86; Michard et al. 1986; Price et al. 1986; Dosso et al. 1988; Mahoney et al. 1992) clearly show that Indian Ocean MORB are isotopically characterised by having higher $^{87}Sr/^{86}Sr$, $^{208}Pb/^{206}Pb$ and $^{207}Pb/^{206}Pb$ ratios than those of Atlantic and Pacific MORB (e.g. Dupré & Allègre 1983; Hamelin et al. 1985-86; Ito et al. 1987).

These differences in isotopic compositions are believed (e.g. Storey et al. 1989; Gautier et al. 1990) to be the result of the contamination of the Indian Ocean asthenosphere by an isotopically enriched mantle plume. During the last decade, much attention has been given to the study of the isotopic composition of oceanic

ridges and plateaux, in an attempt to understand the geochemical and isotopic origin and evolution of this anomaly, and to reconstruct the tectonic evolution of the Indian Ocean.

It is generally believed that the Kerguelen mantle plume has been continuously active during the last 120 Ma (Storey et al. 1989; Weis et al. 1989; Weis et al. 1991; Storey et al. 1992; Müller et al. 1993), and there is a general consensus that a record of more or less strong interaction of the Kerguelen plume (and possibly other similar plumes) with "normal" Indian Ocean asthenosphere, and possibly lithosphere, is preserved by the Kerguelen-Heard Island Plateau (Davies et al. 1989; Storey et al. 1988, 1989; Gautier et al. 1990; Salters et al. 1992; Storey et al. 1992), the Ninetyeast Ridge (Frey et al. 1991; Saunders et al. 1991; Weis & Frey 1991; Weis et al. 1991), and some areas in northeast India (Rajmahal Traps - Sarkar et al. 1980; Paul & Potts 1981; Mahoney et al. 1983; Baksi et al. 1987; Middlemost et al. 1988), Antarctica (Prince Charles Mountains lamprophyres - Sheraton 1983), and Australia (Bunbury basalts and Naturaliste Plateau - Burgess 1978; Coleman et al. 1982).

Yet, the origin of the isotopic signature of the plume, its geographic extent and its depth within the mantle are still matters of debate. Recently, for example, Curray & Munasinghe (1991) proposed that the Rajmahal Traps in India, the 85° E Ridge and the Afanasy Nikitin Seamount are not related to the Kerguelen plume, but instead follow the trace of a different plume, the Crozet hotspot. Müller et al. (1993) also suggested that the 85° E Ridge may have been formed by a distinct hotspot, and that the Kerguelen hotspot was located south of the Rajmahal Traps between 130 and 84 Ma.

At the eastern boundary of the Indian - Australian plate, it is not clear whether the isotopic signature of the East Australian Basalts (e.g. Ewart et al. 1988; Johnson 1989) is the result of mantle-crust interactions, or it represents the trace of at least five N-S trending hotspot traces. In the northern hemisphere, Flower et al. (1992) and Tu et al. (1992) recognised a DUPAL component in Pb isotopic ratios in the South China Basin and in the Hainan basalts.

Today, a great deal of isotopic data exists for volcanic rocks from the Indian Ocean plateaux and from active and inactive ridges, but, with the exception of Christmas Island, virtually no isotopic and very scarce good quality trace element data are available for areas distant from the main tectonic features and close to the Sunda arc. Therefore, the possibility that mantle with an isotopically "enriched" (EM, HIMU)

component is present in the proximity of the Sunda arc, evaluated by Varne & Foden (1986) and Stolz et al. (1990) (see Chapter 1) has yet to be tested.

3.2 Geography and geomorphology of the Northeastern Indian Ocean: definition of the area of study

The Northeastern Indian Ocean is physically defined by several topographic sea-floor characteristics (Figure 3.1). Its northern boundary is the Indonesian archipelago itself. The Sunda Trench runs parallel to the Andaman and Nicobar Islands, and then to Sumatra, Jawa, Bali, Lombok, Sumbawa and Sumba, ending just east of Sumba.

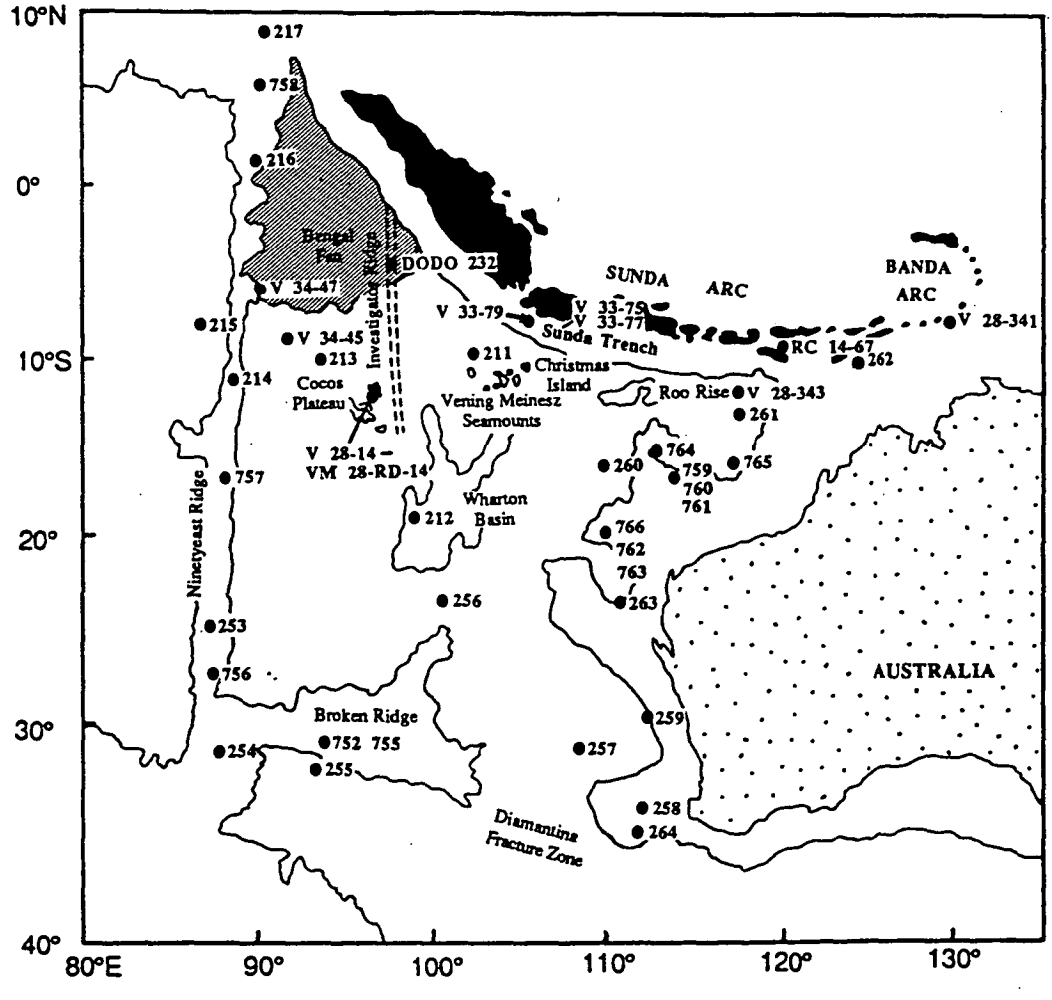

Figure 3.1. Sketch map of the Northeastern portion of the Indian Ocean, with approximate locations of the DSDP, ODP, and dredge haul sites discussed in this thesis. The contour line marks the margins of only the most prominent topographic features and approximates the 4000 m depth contour (depth of the sea floor buried under the Bengal Fan sediments where these are present, and actual depth of the sea floor elsewhere). The lightly ruled area represents the portion of the Bengal Fan where sediments are more than 2000 m thick.

Its depth averages 6000-6500 m, ranging from a maximum of 7130 m off central Jawa, to 5000-6000 m off southern-central Sumatra, to 2500-5000 m off the Andaman and Nicobar Islands, where the trench is partially filled by sediments of the Ganges - Brahmaputra fluvial system. Its distance from the coast varies from about 100 km (off Sumba) to about 200 km (off Bali and central Jawa) with an average of about 150 km.

The Timor Trough, which runs northeast from Timor towards the Kai Trench (off the Kai archipelago), is the topographic continuation of the Sunda Trench, but is separated from it by a shallow saddle south of Sawu and Roti islands. The depth of the Timor Trough varies from a maximum of about 3300 m, off the northernmost tip of Timor, to less than 1000 m off the northern part of the Tanimbar archipelago, with an average of 2000 to 2500 m; its distance from both the archipelago and the Australian continent ranges from a few tens to more than 100 km, with an average of about 50 km.

The Bali Trough runs parallel to the Sunda Trench from western Jawa to Sumba; its depth varies from 3000-3500 m off Jawa to 4000-4500 m off Bali, Lombok and Sumbawa, where it is separated from the Sunda Trench by a shallow (600 to 2000 m) submarine chain (Roo Rise). The Bali Trough is abruptly interrupted by the Sumba island, but topographically continues E of it, running parallel and very close to the arc (10 to 30 km) from Flores to the Banda islands. Due to the complexity of the topography, this trough can be considered as a single unit only as a first approximation, however. A feature similar to the Bali Trough, although much shallower (1500 to 200 m) and more discontinuous, runs parallel to the western coast of Sumatra, separated from the Sunda Trench by a well developed fore-arc, in places exposed subaerially as the Mentawai Archipelago, that can be viewed as a continuation of the submarine chain that separates the Bali Trough from the Sunda Trench.

The Australian continental margin marks the eastern boundary of the Northeastern Indian Ocean. The sector of the arc from Sumba eastward actually lies on the "contact" between the Australian and the Banda plates, with virtually no intervening oceanic crust.

Finally, two submarine mountain chains, the Broken Plateau and the Ninetyeast Ridge, form the southern and the western boundary of the Northeastern Indian Ocean.

The Broken Plateau runs from approximately 31° S 88° W (where it merges with the Ninetyeast Ridge) to 32° S 101° W, and its elevation above the surrounding sea floor ranges from 2500 to less than 500 m. A large gap (Diamantina Fracture zone) exists between the eastern termination of the Broken Ridge and the Naturaliste Plateau, off western Australia.

The Ninetyeast Ridge is one of the most prominent structures of the Indian Ocean. It runs continuously from approximately 31°S 88°W to 9°N 90°W (where it is very close to the northernmost end of the Sunda Trench) with a depth ranging from 3000 m to less than 500 m, with an average of 2000-2500 m. The northern parts of the Sunda Trench and Ninetyeast Ridge are buried under the Ganges-Brahmaputra delta sediments.

Description and discussion of the geophysical and petrographic characteristics of the Ninetyeast Ridge and of the Broken Plateau are outside the scope of this thesis (for summaries, see e.g. Veevers 1977; Luyendyk 1977; Frey et al. 1977; Schlich 1982, and, more recently, ODP Scientific Results, vol. 118 to 123, 1991-1992).

Several seamounts rise from the seafloor, the Wharton Basin, in the area between 10°S to 15°S and 95°W to 110°W, but only in two cases (Cocos and Christmas islands) do they reach the surface. Apart from these and the plateaux situated off the Australian coast (Exmouth, Wallaby and Naturaliste Plateaux), several other minor characteristics make the topography of the Wharton Basin fairly rugged, but normally the depth of the basin ranges from more than 6000 m - the deepest part of the Indian Ocean apart from the Sunda Trench - to 5000-5500 m at the base of the plateaux (for a summary of the characteristics and significance of the different structures see e.g. Schlich 1982, Udintsev 1975, and Masson et al. 1990).

In this thesis, the term "Northeastern Indian Ocean" refers to the area as defined herein.

3.3 Basalts in the Northeastern Indian Ocean: a review

Subbarao et al. (1979) summarised several important conclusions on the results of the studies made on the samples collected during the DSDP legs 22 and 27.

Firstly, with only a very small number of $^{87}Sr/^{86}Sr$ isotope data available, and well before the DUPAL anomaly was recognised, it was clear that the tholeiitic basalts of the Mid-Indian Ocean Ridge (MIOR) are relatively enriched in LILE, LREE, and $^{87}Sr/^{86}Sr$ compared with Atlantic and Pacific MORB, and have more variable geochemical and isotopic composition. The isotopic heterogeneity was later shown to be (Batiza 1984; Holness & Richter 1989) a function of the spreading rate of the ridge: it seems that fast-spreading ridges may efficiently homogenise the small scale heterogeneities in the mantle, whereas in the slow-spreading ridges - like those of the Indian Ocean - original mantle heterogeneities may persist in the oceanic basalts.

Secondly, the peculiarly alkaline composition of the basalts and andesites of the Ninetyeast Ridge, characterised by high TiO_2, K_2O, LILE and $^{87}Sr/^{86}Sr$ values, was pointed out (see also Kempe 1975), and it was proposed that 1) the Ninetyeast Ridge, Broken Ridge, Naturaliste Plateau, Kerguelen Plateau, and St Paul - Amsterdam islands were originally joined together, forming a single ridge system produced from two fixed hot spots, and 2) the same type of mantle was the source for the Cocos Islands and Christmas Island, and of the sill and basement in site 211.

The mantle sources of the basalts in the Indian Ocean were thus divided into two groups, alkali-poor, from spreading ridges, and alkali-rich, including quartz tholeiites from aseismic ridges, and alkali-olivine basalts from oceanic islands, with seamounts and "abyssal hills" having variable compositions. Among the analysed sites, eight out of twenty were considered related to hotspot activity, and three to mixed hotspot and spreading activity. In several cases (sites 211, 253, and 261 - see the site description in Appendix D, and also Kempe 1975) - inconsistencies between geochemistry and tectonic models were observed.

Summary descriptions of the DSDP and ODP sites, and dredge hauls located within the margins of the Northeastern Indian Ocean are reported in Appendix E, and include a brief petrographic description of the samples analysed for this study.

3.4 Definition of the database

New analyses of basalts from the Northeastern Indian Ocean are presented in Table 3.1 and Appendix D. Many of the samples, or splits from the same cores and units, have already been analysed for major and some trace elements by Engel et al. (1965), Hekinian (1974), Robinson & Whitford (1974), Frey et al. (1977), and their

Sample	DSDP 22 211 12-1:23-25	DSDP 22 211 12-1:125-127	DSDP 22 211 12-2:16-18	DSDP 22 211 12-2:112-115	DSDP 22 211 15-3:57-59	DSDP 22 211 15-4:70-73	DSDP 22 211 15-4:73-75	DSDP 22 211 15-4:94-96
SiO2	45.54	44.87	44.76	44.78	42.21	45.31	45.16	40.79
TiO2	2.19	2.28	2.27	2.35	2.68	2.37	2.44	2.54
Al2O3	15.21	14.87	14.96	15.06	17.48	16.42	16.23	16.93
Fe2O3	10.82	10.70	10.59	10.64	9.56	9.05	8.87	9.49
MnO	0.16	0.15	0.14	0.20	0.11	0.14	0.12	0.08
MgO	10.13	9.28	8.80	7.07	4.52	6.43	5.58	3.06
CaO	6.57	5.87	5.82	8.47	8.79	7.53	8.18	9.24
Na2O	2.97	3.84	4.08	2.93	3.28	3.10	3.16	2.70
K2O	1.54	1.79	1.90	2.38	1.89	2.94	3.09	2.71
P2O5	0.67	0.65	0.62	0.64	0.78	0.70	0.71	0.76
L.O.I.	4.27	5.83	5.94	5.25	8.78	6.31	6.36	11.75
Total	100.07	100.13	99.88	99.77	100.08	100.30	99.90	100.05
Mg#	64.97	63.21	62.21	56.82	48.36	58.46	55.48	38.97
Rb	36	39	39	52	40	52	56	42
Ba	468	578	611	565	312	448	480	444
Sr	455	513	523	502	400	416	422	412
Pb	3	2.52	2	4	3	4	3	3
Cs								
Zr	182	190	198	196	343	289	292	304
Hf								
Nb	54	54	57	57	72	63	60	64
Ta								
Y	24	25	24	24	35	31	29	32
Th	5	6	5	4	5	5	6	6
La	**47.5**					**32.8**		
Ce	**74**					**82**		
Nd	**28**					**37**		
Sm	**6.12**					**6.76**		
Eu	**1.95**					**2.19**		
Tb	**1.0**					**1.0**		
Ho	**1.1**					**0.85**		
Yb	**2.6**					**2.8**		
Lu	**0.29**					**0.37**		
Cr	314	303	292	230	93	98	88	102
Ni	163	137	136	131	85	117	117	94
V	183	176	176	181	160	160	161	208
Sc	13	17	15	19	21	18	18	19
Co	**30**					**21**		

Measured isotope ratios

87Sr/86Sr	0.70567
143Nd/144Nd	0.512693
208Pb/204Pb	38.710
207Pb/204Pb	15.578
206Pb/204Pb	18.445

Table 3.1. Chemical analyses of samples of volcanic rocks from the Northeastern Indian Ocean from this study. Data in **bold** (Co, REE for all the DSDP samples) are from Frey et al. (1977). Some glassy samples reported in Appendix D were not analysed for major and trace elements. Mg# is calculated assuming $Fe_2O_3/FeO = 0.10$.

"Vening Meinesz" is an average of 3 analyses (only major elements available) of altered volcanic rocks dredged from Vening Meinesz seamounts (data from Williams 1992).

Table 3.1 cont.

Sample	DSDP 22 212 39-3:145-147	DSDP 22 213 18-2:50-53	DSDP 22 213 18-2:115-117	DSDP 27 260 18-2:140-142	DSDP 27 260 20-1:16-18	DSDP 27 261 33cc 6-8	DSDP 27 261 34-1:75-77
SiO2	46.70	46.48	48.19	48.28	49.43	48.46	50.06
TiO2	0.62	1.12	1.00	2.14	1.86	1.35	1.35
Al2O3	17.58	19.26	17.84	17.46	15.06	14.52	14.98
Fe2O3	8.54	11.78	10.35	10.57	12.28	11.74	10.00
MnO	0.15	0.20	0.16	0.31	0.28	0.21	0.21
MgO	7.02	2.06	5.24	6.59	6.94	6.85	8.11
CaO	6.49	10.11	12.04	6.90	7.72	10.76	10.90
Na2O	1.46	2.78	2.64	4.06	3.45	2.45	2.61
K2O	3.98	2.29	0.43	0.40	0.19	0.81	0.54
P2O5	0.10	0.12	0.07	0.21	0.20	0.12	0.10
L.O.I.	7.16	3.91	1.92	2.85	2.38	2.75	1.15
Total	99.80	100.11	99.88	99.77	99.79	100.02	100.01
Mg#	61.95	25.73	50.07	55.25	52.82	53.61	61.63
Rb	32	16	7	3	1	23	10
Ba	128	71	21	95	71	17	17
Sr	100	158	123	132	114	87	88
Pb	1	1	2	1	1	1	1
Cs							
Zr	29	72	61	131	114	73	75
Hf							
Nb	2	2	2	6	6	1	2
Ta							
Y	18	25	25	36	41	35	39
Th	1	2		2		1	1
La	2.3		2.2	7.7	6.0		2.34
Ce	6.0		7.6	20.0	17.0		11.0
Nd	3.6		6.2	13.0	9.7		7.1
Sm	1.29		2.18	4.03	3.75		3.11
Eu	0.52		0.85	1.32	1.21		1.03
Tb	0.38		0.64				0.73
Ho	0.55		0.86	1.3	1.7		1.5
Yb	1.75		2.55	3.7	4.1		3.4
Lu	0.27		0.41	0.68	0.65		0.62
Cr	949	311	366	163	128	208	208
Ni	164	83	80	217	46	67	74
V	240	311	264	553	464	356	381
Sc	54	57	43	92	67	54	59
Co	33		33	110	36		50
Measured isotope ratios							
87Sr/86Sr			0.70321				
143Nd/144Nd			0.512994				
208Pb/204Pb							
207Pb/204Pb							
206Pb/204Pb							

Table 3.1 cont.

Sample	DSDP 27 261 34-2:100-102	DSDP 27 261 35-2:83-86	DSDP 27 261 35-2:120-123	DSDP 27 261 35-3:124-126	DSDP 27 261 35-4:102-105	DSDP 27 261 39-1:11-13	DSDP 27 261 39-1:44-48	DODO 232E
SiO2	49.73	48.85	46.29	45.96	44.36	49.54	48.58	49.29
TiO2	1.37	1.35	3.21	3.14	3.15	1.39	1.43	1.82
Al2O3	14.24	14.90	14.89	13.97	13.71	14.74	14.24	15.94
Fe2O3	11.73	11.56	12.61	13.51	16.12	9.87	12.25	9.40
MnO	0.26	0.20	0.46	0.26	0.15	0.19	0.25	0.13
MgO	7.09	7.09	5.74	7.19	6.02	7.21	6.66	5.43
CaO	12.10	10.92	5.25	7.14	5.68	11.16	10.51	10.39
Na2O	2.22	2.33	2.82	2.98	3.06	2.63	2.45	3.30
K2O	0.04	0.52	1.80	0.60	1.21	0.40	0.69	1.08
P2O5	0.10	0.09	0.39	0.29	0.27	0.12	0.12	0.44
L.O.I.	1.20	2.27	6.55	5.01	5.67	2.15	2.93	2.76
Total	100.08	100.08	100.01	100.05	99.40	99.40	100.11	99.98
Mg#	54.49	54.85	47.41	51.32	42.52	59.13	51.85	53.36
Rb	1	10	14	5	23	6	16	19
Ba	15	18	44	47	86	12	19	177
Sr	89	91	99	100	104	86	83	302
Pb	1	1	3	3	1	3	1	2
Cs								
Zr	73	73	199	194	188	73	76	171
Hf								
Nb	2		8	8	7	1	1	19
Ta								
Y	35	35	67	65	63	35	35	41
Th	1	1		1	1	1	1	3
La						2.45		
Ce						9.0		
Nd						7.8		
Sm						3.16		
Eu						1.17		
Tb						0.79		
Ho						1.5		
Yb						3.9		
Lu						0.60		
Cr	213	227	50	33	38	190	191	65
Ni	66	56	57	46	42	76	55	31
V	381	383	529	521	553	379	381	275
Sc	57	56	69	57	63	54	57	42
Co			13			41		

Measured isotope ratios

87Sr/86Sr	0.70409
143Nd/144Nd	0.513078
208Pb/204Pb	37.438
207Pb/204Pb	15.509
206Pb/204Pb	18.145

Table 3.1 cont.

Sample	DODO 232G fresh	DODO 232G altered	DODO 232J	DODO 232K	DODO 232N	V 28 14A	V 28 14B	VM 28 RD 14-1
SiO2	49.44	48.70	49.01	49.42	49.05	39.45	39.65	45.84
TiO2	1.49	1.47	1.77	1.86	1.75	2.70	2.91	2.87
Al2O3	18.29	18.09	15.47	16.15	15.36	13.16	13.04	14.03
Fe2O3	9.15	10.17	9.51	9.55	9.18	8.49	12.51	14.03
MnO	0.11	0.15	0.11	0.13	0.12	0.16	0.14	0.35
MgO	4.06	3.68	5.70	5.10	5.84	2.06	2.85	2.38
CaO	11.08	10.16	10.25	10.13	10.27	15.64	11.08	7.56
Na2O	3.08	3.27	3.15	3.26	3.14	3.49	3.12	4.27
K2O	0.94	1.18	1.04	0.98	0.93	1.85	2.14	2.33
P2O5	0.33	0.26	0.44	0.44	0.38	2.39	5.70	2.52
L.O.I.	2.24	2.54	3.35	3.08	3.47	10.15	6.48	3.58
Total	100.21	99.67	99.80	100.10	99.49	99.54	99.62	99.76
Mg#	46.78	41.75	54.28	51.40	55.75	32.46	31.09	25.15
Rb	16	20	24	19	19	33	44	56
Ba	133	150	170	161	164	910	816	1944
Sr	305	313	294	312	291	729	809	813
Pb	1	1	1	2	1	3	4	3
Cs					1.62	2.01		1.93
Zr	133	130	164	174	164	245	223	260
Hf					4.05	5.96		5.66
Nb	16	13	18	19	18	69	67	73
Ta					1.35	4.28		4.15
Y	31	29	37	41	35	57	101	56
Th	2	3	2	1	3	6	5	5
La					17.9	63.4		60.9
Ce					35.0	130.0		125.0
Nd					20.2	66.5		65.6
Sm					4.73	14.10		13.60
Eu					1.56	6.64		6.33
Tb					0.84	1.56		1.49
Ho					1.08	1.40		1.34
Yb					2.77	3.06		2.98
Lu					0.42	0.50		0.42
Cr	75	69	63	69	65	5	7	6
Ni	38	43	46	47	52	32	39	40
V	247	220	269	261	272	123	117	146
Sc	46	43	42	48	42	27	26	26
Co								
Measured isotope ratios								
87Sr/86Sr					0.70398	0.70415		
143Nd/144Nd					0.512848	0.512847		
208Pb/204Pb					38.499	39.513		
207Pb/204Pb					15.561	15.633		
206Pb/204Pb					18.269	19.376		

Table 3.1 cont.

Sample	VM 28 RD 14-2	VM 28 RD 14-3	VM 28 RD 14-4 "fresh"	VM 28 RD 14-4 altered	Vening Meinesz
SiO2	44.41	43.23	38.39	39.44	47.66
TiO2	2.87	2.95	2.79	2.87	3.06
Al2O3	14.12	14.80	12.88	12.99	16.63
Fe2O3	11.41	12.07	11.50	12.63	11.12
MnO	0.15	0.16	0.21	0.32	0.15
MgO	2.82	3.23	2.55	2.92	4.64
CaO	9.92	8.51	12.83	10.87	7.29
Na2O	3.90	3.37	3.33	3.19	3.46
K2O	2.07	1.76	2.08	1.87	1.89
P2O5	1.80	2.84	6.88	5.40	0.59
L.O.I.	6.17	7.49	6.56	7.12	3.80
Total	99.64	100.41	100.00	99.62	100.29
Mg#	32.86	34.64	30.52	31.41	45.2
Rb	67	38	41	47	
Ba	955	723	754	681	
Sr	741	760	817	727	
Pb	5	2	2	10	
Cs					
Zr	257	261	220	242	
Hf					
Nb	72	74	64	69	
Ta					
Y	48	49	100	95	
Th	5	4	5	4	
La					
Ce					
Nd					
Sm					
Eu					
Tb					
Ho					
Yb					
Lu					
Cr	4	8	6	9	
Ni	13	38	79	145	
V	116	109	111	119	
Sc	28	29	29	28	
Co					

results agree reasonably well with the new analyses, apart from the elements most sensitive to alteration and within the large analytical inter-laboratory uncertainty (analyses performed in different laboratories, using different standards and analytical techniques). Where more than one analysis is available (at least for some elements) for the same core section, the data set which seemed more reliable and complete was included in the database. In a few cases, partial information coming from different sources for a particular sample was merged into one single analysis in order to use that particular sample in diagrams and calculations. All the samples but those from site DSDP 22 213 and V28 14 are relatively fresh in thin section, compared with most oceanic basalts, and there is a number of reasons to believe that their composition - including their isotopic composition - was not strongly modified by alteration. More details on the effects of alteration are given in the following discussion.

REE and trace element patterns of samples from the different sites are shown in Figures 3.2 to 3.4, and will be discussed in the next section.

The discussion of the distribution of OIB and basalts with an "enriched mantle" component in the Northeastern Indian Ocean is based on data from the Northeastern Indian Ocean (as defined in paragraph 3.2) and its margins, and also on data from the Indian Ocean ridges and oceanic islands. All the analyses published in the references cited have been taken into account in the discussion. The main literature sources for the database of basalts of the Northeastern Indian Ocean and Ninetyeast Ridge are: Engel et al. (1965); Hekinian (1968); Vinogradov et al. (1969); Initial Reports of the Deep Sea Drilling Project vol. 22, 26, and 27 (1974), and references therein; Frey & Dickey (1977); Frey et al. (1977); Heezen et al. (1977); Subbarao et al. (1977); Thompson et al. (1978); Viswanatha Reddy et al. (1978); Subbarao et al. (1979); Initial Reports of the Ocean Drilling Program vol. 118-123, (1991-92); Scientific Results of the Ocean Drilling Program vol. 118-123, (1991-92).

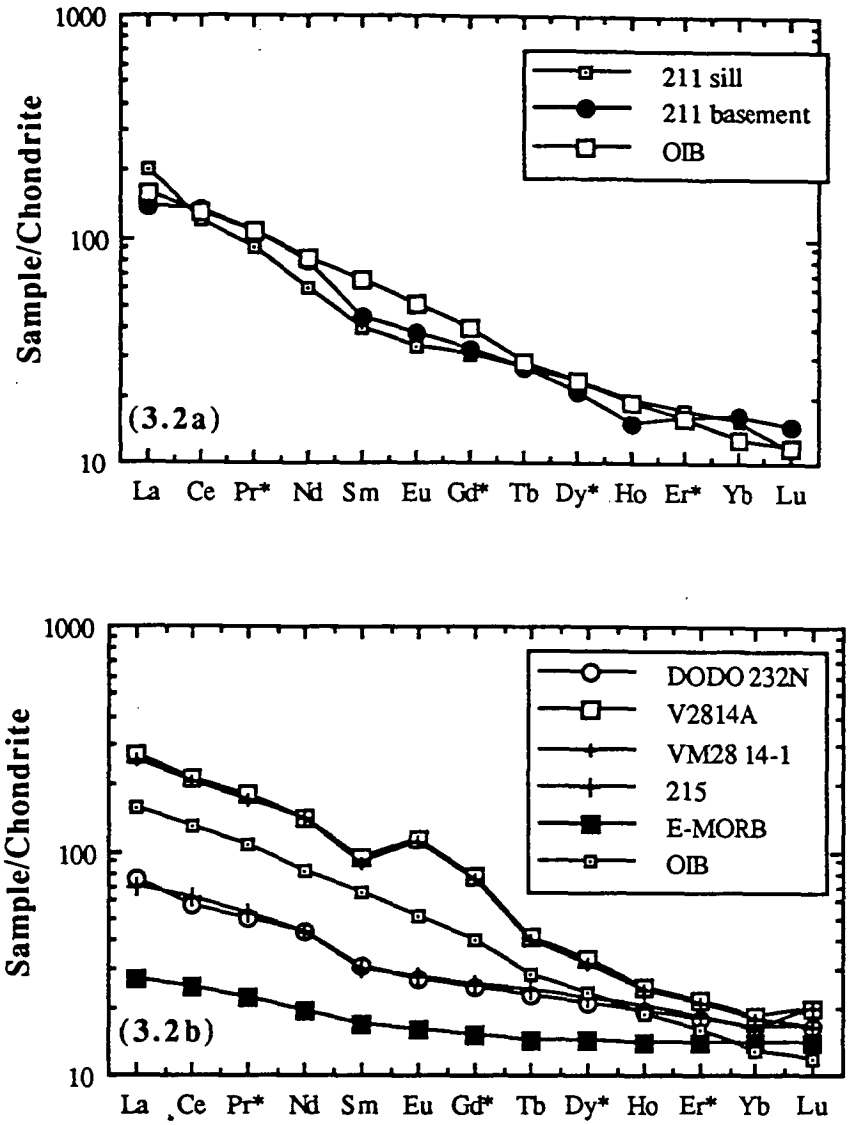

Figures 3.2a-g. Chondrite-normalised REE patterns for the different sites and basaltic units in the Northeastern Indian Ocean. Chondrite, MORB, and OIB REE values are from Sun & McDonough (1989). Elements labelled "*" are, apart from a few exceptions, interpolated from the other measured REEs. In Figure 3.2b note the positive Eu anomaly of the Vema (V28 14A and VM 28 14-1) samples (the high Gd* values are an artefact of the recalculation), and the similarity between DODO 232N and site DSDP 215. The kink in the REE pattern between Sm and Nd, more evident in the diagram in the DODO 232N and DSDP 215 samples, has also been observed in site 211 and in the other rocks belonging to Group III (see text), including the Upper and Lower and Middle Volcanic Series in Christmas Island, and also in Kerguelen and East Australia. Note that the DODO 232N - DSDP 215 - DSDP 256 show a very slight HREE depletion (typical of OIB), and their HREE patterns are subparallel to MORB. In contrast, samples from the Vema dredge are more strongly HREE-depleted. In Figure 3.2c note the similarity between DODO 232N and DSDP 256 En (= enriched, while Dep = depleted, according to the distinction by Subbarao et al. 1979). The scatter in LREE is probably due to alteration. In this smaller-scale plot, a kink between Ce and La, probably due to alteration, can be observed in the REE pattern of DODO 232N.

Within the analytical error of REE analyses performed more than 10 years ago, REE patterns of sites DSDP 257, 259, and 213 are virtually identical to N-MORB, whereas site DSDP 212 shows a slight depletion (and probably some enrichment in LREE because of alteration) (Figures 3.2d-e). The large variations and the unusual REE pattern of the two samples from site DSDP 260 (Figure 3.2f) are also an artefact of low-precision analyses. In Figure 3.2g the thick line represents ODP sites 765 and 766 unit 4 and 5, and the thick dotted line is the average of units A and C in site DSDP 261. Data from this study and references quoted in text.

Figure 3.2 cont.

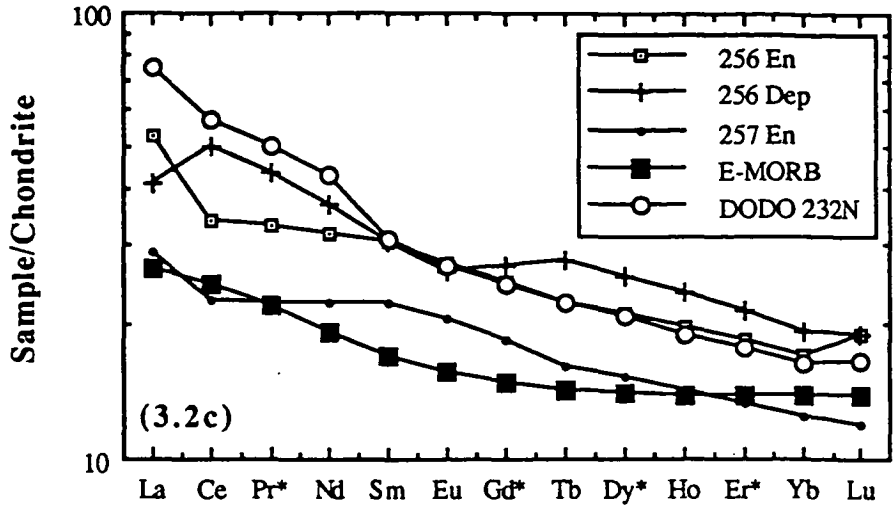

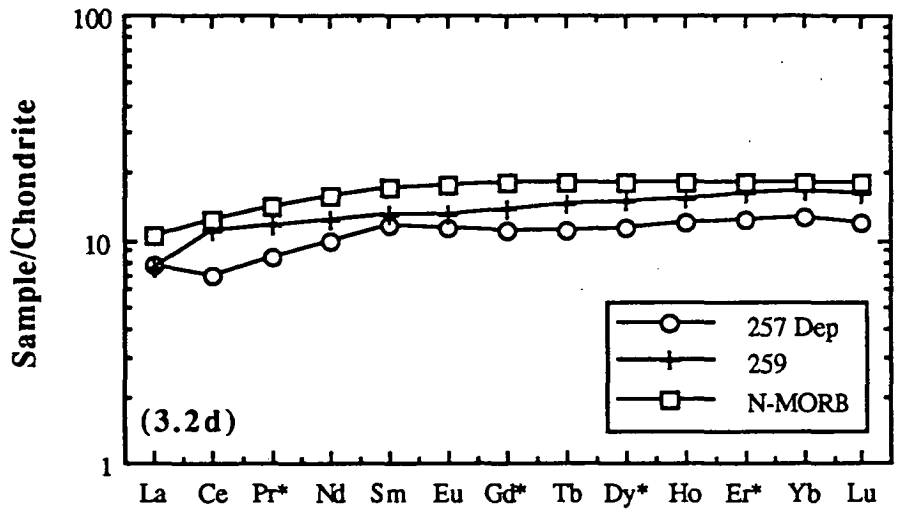

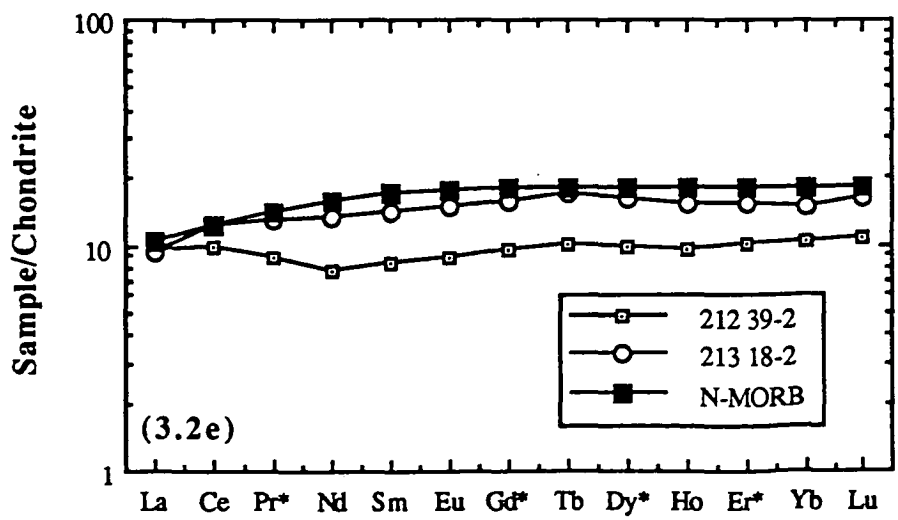

Figure 3.2 cont.

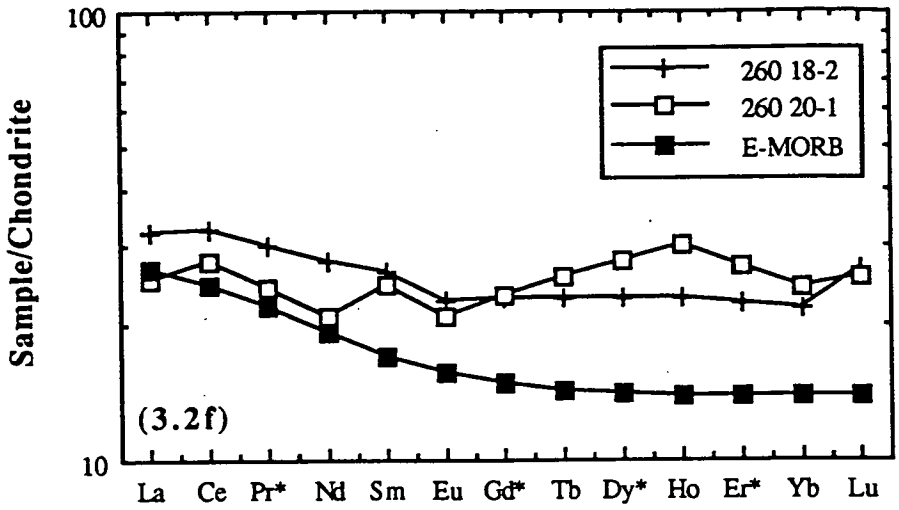

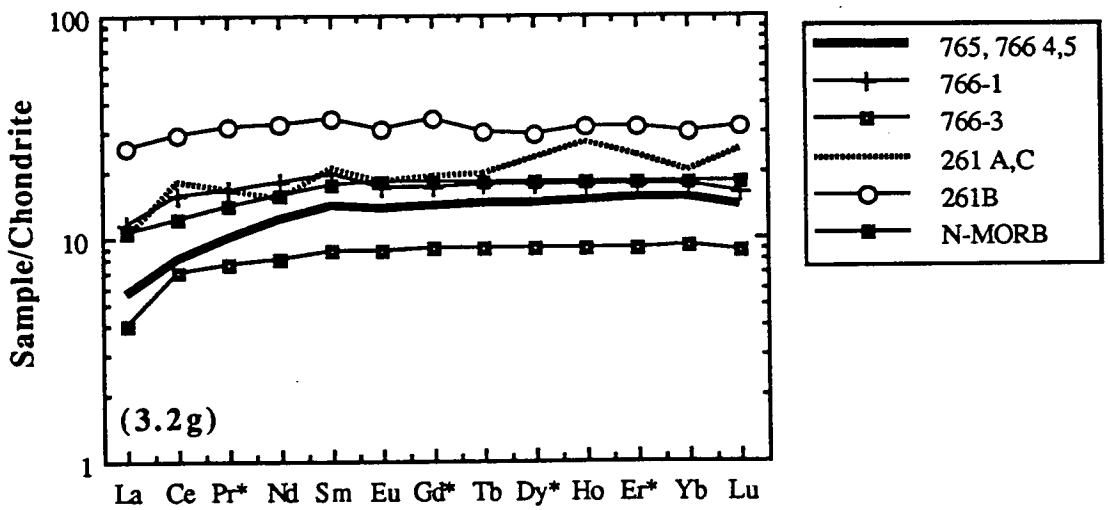

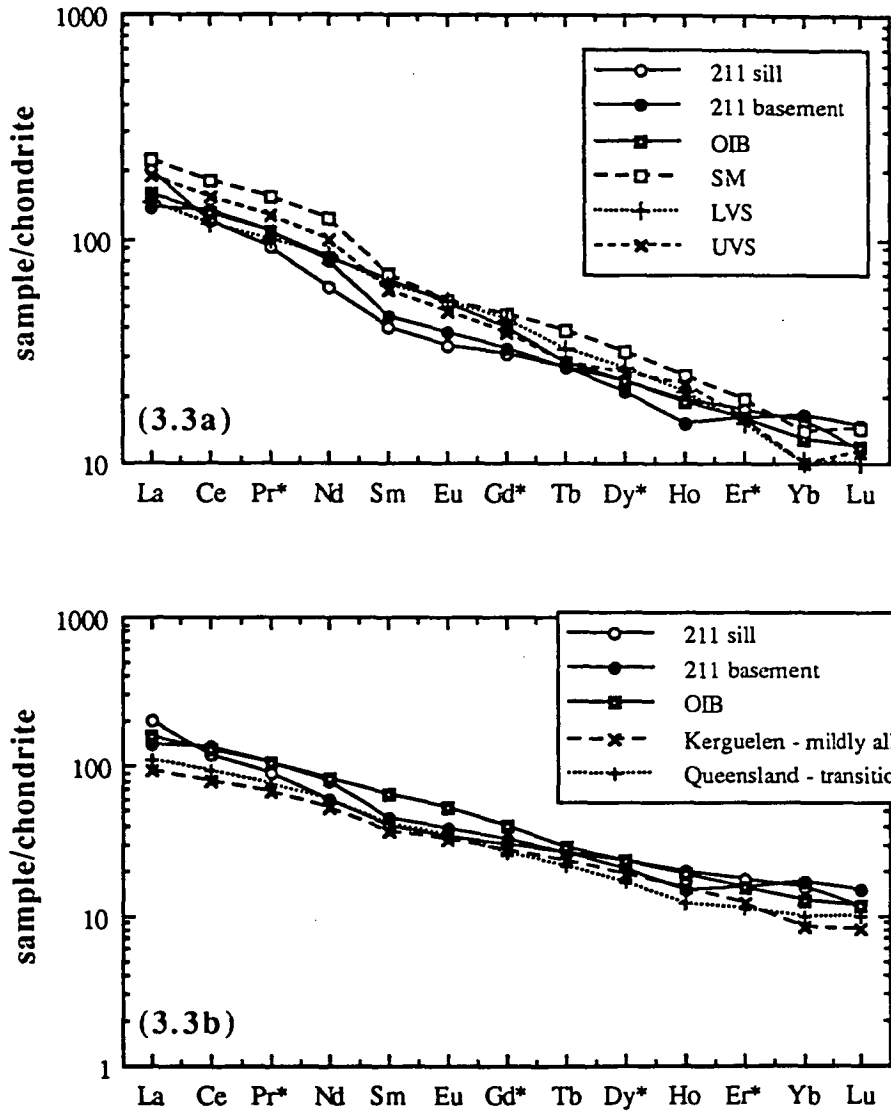

Figures 3.3a-d. REEs and trace element patterns of DSDP 211 sill and basement. Chondrite (for REEs) and primitive mantle (for trace elements) normalising values from Sun & McDonough (1989). Elements labelled "*" are interpolated from the other measured REEs. Pb and Th are not plotted because low concentrations and a large analytical error would produce artificial Pb and Th anomalies. East Australia, Kerguelen, and Christmas Island (and the Vening Meinesz seamount) data are respectively from Ewart et al. (1988), Gautier et al. (1990), and Falloon et al. (submitted for publication) - and references therein. LVS - Christmas Island Lower and Middle Volcanic Series; UVS - Christmas Island Upper Volcanic Series; SM - Vening Meinesz seamount.

Note the high Rb and K in 211 basement compared with the sill, probably due to alteration, and the negative Sr anomaly in both sill and basement. The basalts at site 211 have similar trace elements and REE contents like those of compositionally similar rocks from Kerguelen (mildly alkaline basalts), East Australia (Queensland transitional basalts), and Christmas Island (Lower and Middle Volcanic Series).

Figure 3.3 cont.

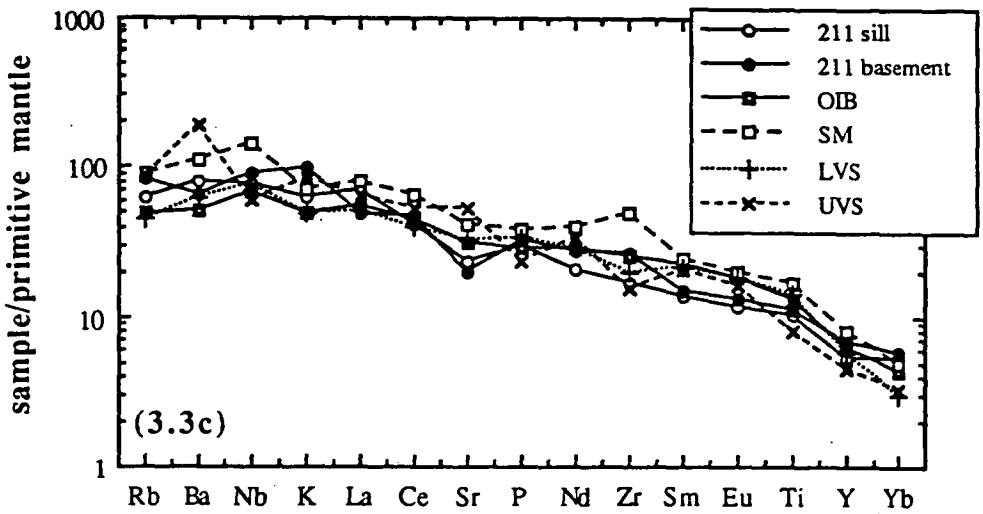

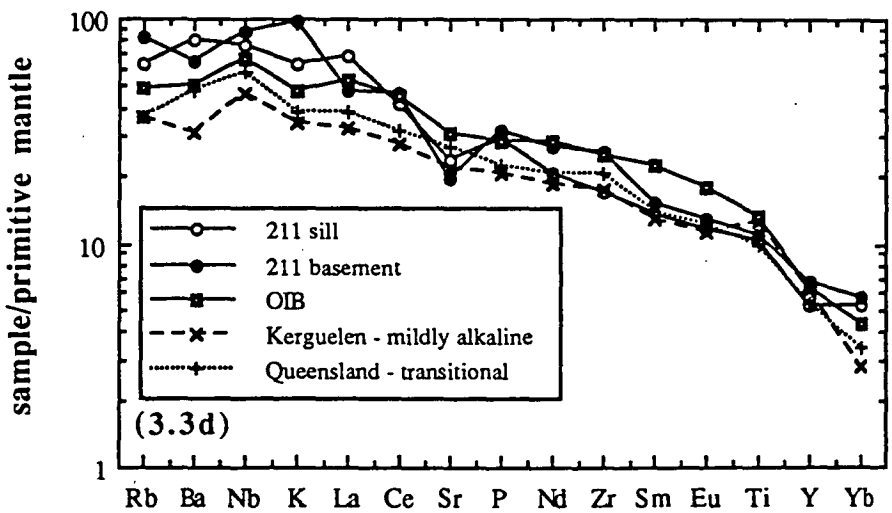

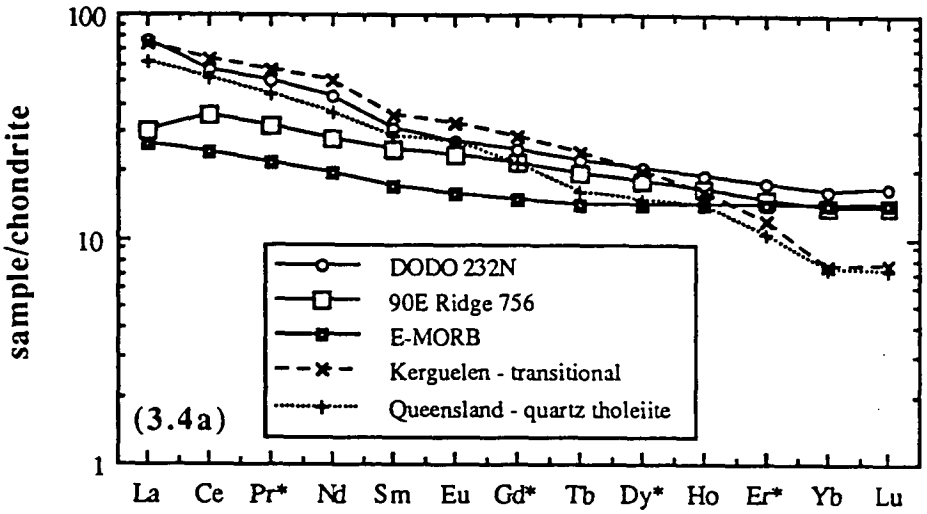

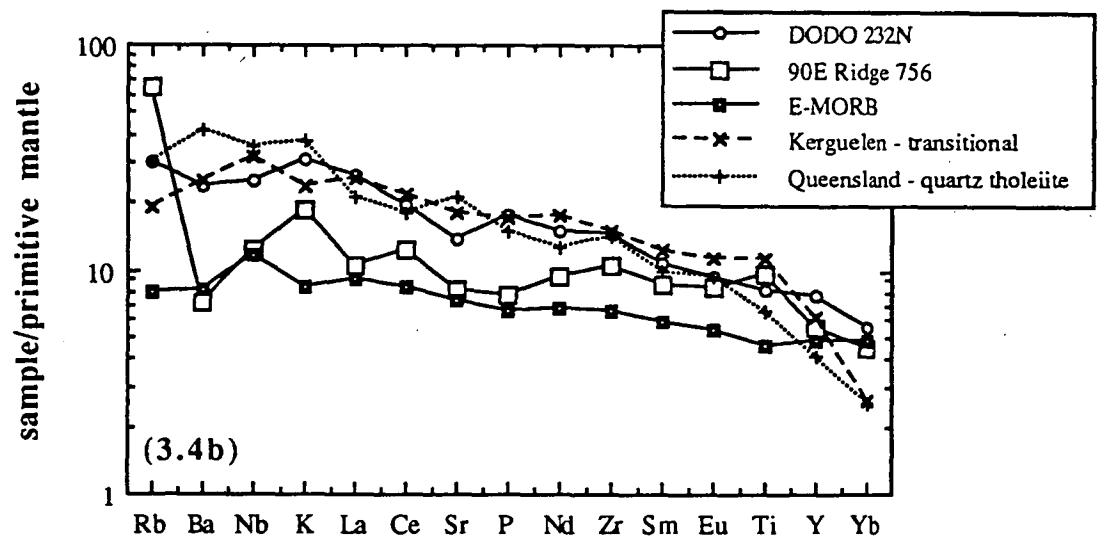

Figures 3.4a-b. REEs and trace element patterns of DODO 232 basalts. Chondrite (for REEs) and primitive mantle (for trace elements) normalising values from Sun & McDonough (1989). Elements labelled "*" are interpolated from the other measured REEs. Pb and Th are not plotted because low concentrations and a large analytical error would produce artificial Pb and Th anomalies. East Australia, Kerguelen, and Ninetyeast Ridge (ODP site 756) data are respectively from Ewart et al. (1988), Gautier et al. (1990), and Frey et al. (1991), Falloon et al. (submitted for publication) - and references therein.

The DODO 232 samples have LREE and MREE values similar to transitional and quartz-tholeiitic basalts from Kerguelen and East Australia, but do not show the HREE depletion typical of OIB volcanism. In fact, their REE pattern is similar, apart from the LREE enrichment due to alteration, to the REEs distribution in some lavas from the Ninetyeast Ridge (site 756). However, the trace element distribution in site 756 is similar to E-MORB (apart from the anomalous K and Br enrichment due to alteration), whereas the DODO 232 rocks are considerably more enriched.

3.5 Discussion

3.5.1 Effects of alteration

Most oceanic basalts are more or less strongly altered as a consequence of low-temperature interaction with seawater, and precipitation of secondary minerals (calcite, clays, zeolites and Fe/Mn-rich oxides) in veins and vesicles. Stronger degrees of alteration lead to replacement of crystals and glass by secondary phases such as calcite, smectites, and chlorites. Alteration usually affects the surface of the rock and, to a lesser extent, the interior, and the degree of alteration is dependent on a number of factors such as the time of exposure of the rock to seawater, and the grain size, porosity and permeability of the rock, and the composition of the overlying sediments and circulating fluids.

In general, it has been observed that oceanic basalts are subject to alteration for a long period of time after their emplacement: for example, Hart and Staudigel (1986) showed that fluids precipitating calcite and celadonites may interact with the basalt for tens of millions of years after its emplacement.

As a result, the scatter observed in the major and trace element composition within a unit and among different units and sites is probably a function not only of original differences in the source of the rock, but also of magmatic and post-magmatic (i.e. phenocryst redistribution during and after eruption) processes, and of variable degrees and types of alteration.

In general, those elements that because of their higher solubility in fluids are mobile during magmatic processes (LILE, LREE) are also enriched in alteration materials. Among the major elements, Ca (unless significant amounts of calcite, which is Ca, P, and Y-HREE-rich, are precipitated in veins and cavities) and Na are usually depleted and K and Al enriched. Fe^{3+}/Fe^{2+} values are also modified as a result of the increased volatile content, and the high volatile content also has a dilution effect on other major elements.

Ti is the only major element that is not modified by low-temperature alteration and at the same time is a good indicator of genetic differences in oceanic basalts and, at least for relatively magnesian basalts, is not strongly affected by crystal fractionation. It must be pointed out that Ti and the other HFSE can be strongly modified by high-temperature alteration; however, this type of alteration is easily recognisable and

quantitatively rare (only a few examples are reported in the literature from the Northeastern Indian Ocean, and these have not been taken into account in the following discussion).

An example of the effects of alteration is given in Figures 3.5 and 3.6. Basalts from sites DODO and DSDP 22 215 are relatively fresh and show no variations in CaO and K_2O, and their CaO, K_2O, and TiO_2 values probably represent the true magmatic values.

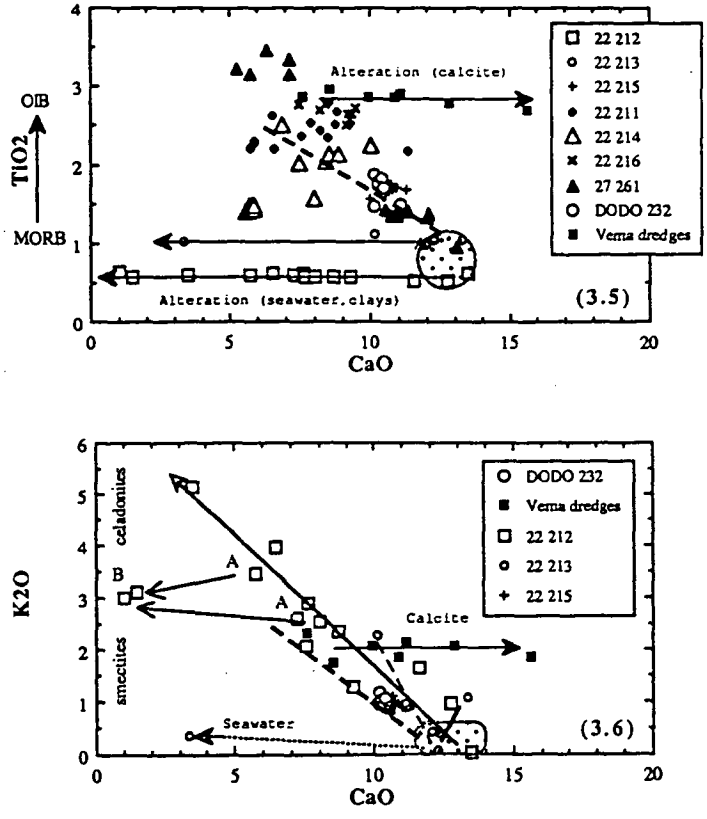

Figures 3.5 and 3.6. Whole-rock CaO-TiO_2 and CaO-K_2O diagrams showing the different effects of low-temperature alteration on basalts from some sites of the Northeastern Indian Ocean. Data from this study and references quoted in the text. Sites DSDP 214 and 216 are from the central part of the Ninetyeast Ridge, and site DSDP 215 is from the western flank of the Ninetyeast Ridge. Notice the similar chemical composition of the basalts from the DODO dredge and DSDP site 215. Points enclosed in the dotted areas are fresh glasses from DSDP sites 212 and 213. Note that TiO_2 is not affected by any type of low-temperature alteration (large CaO and K_2O variations for constant TiO_2). Within-site TiO_2 variations have a magmatic origin, whereas TiO_2 differences among sites reflect different source compositions, from TiO_2-poor (MORB) to TiO_2-rich (OIB). Thick broken line is the approximate locus of relatively unaltered basalts ranging in composition from MORB to OIB (best fitting of the CaO, K_2O, and TiO_2 values reported in Table 3.2 for the three groups).

In Figure 3.6 A and B are respectively pillow basalts cores and rims. Alteration produces CaO and K_2O trends towards the fields of smectites (low CaO and relatively low - ≤ 4% - K_2O) and celadonites (low CaO and relatively high K_2O), except for the Vema dredge rocks, where the increase in CaO with alteration is the result of organogenic calcite-apatite accumulation. Different types and degrees of alteration can also be seen in samples from the same site (dotted line - seawater alteration; broken line - smectite alteration; thick line - minor calcite/smectite alteration).

Fresh glasses from sites DSDP 22 212 and 22 213 have high CaO and very low K_2O, but the altered samples from the same sites have progressively lower CaO and higher K_2O (seawater alteration and precipitation of smectites) or simply lower CaO (seawater alteration without precipitation of secondary clays), while TiO_2 is unmodified. Accumulation of calcite and apatite in veins and cavities shifted CaO towards higher contents in the Vema dredged basalts, again leaving K_2O and TiO_2 unmodified.

Irrespective of the type and extent of alteration, TiO_2 contents can still discriminate the different types of basalts - from the low-Ti N-MORB of sites DSDP 22 212 and 22 213, to the more enriched basalts in sites DSDP 27 261, 22 215, DODO, to the OIBs in the Ninetyeast Ridge, Cocos Plateau (Vema dredges), the alkaline sill in site DSDP 22 211, and the enriched basalts in site DSDP 27 261 (unit B).

Of particular interest for its implications on the isotope systematics is the behaviour of Rb-Sr, Sm-Nd, and Pb-Th-U during alteration. Recycled old sediments and altered oceanic crust are believed to be responsible for the large scale isotopic heterogeneities in the mantle (for a review see e.g. Albarede & Michard 1989; Hart & Staudigel 1989; White 1989; and references therein), and although a discussion of the origin and significance of the different isotopic anomalies (HIMU, EM1, EM2) found in the oceanic basalts is outside the scope of this thesis, a discussion of the possible effects of alteration is relevant to the evaluation of the new isotopic data presented in the next paragraph.

Verma (1992) studied in detail the effects of low-temperature hydrothermal alteration on basalts, and showed that crystalline and glassy samples behave in different ways during alteration. Verma's results are in general agreement with previous studies of the effects of alteration on oceanic basalts (see references in Verma 1992; Albarede & Michard 1989, Hart & Staudigel 1989 and references therein), and can be summarised as follows:

1) all the REE (not only the LREE) are altered in both crystalline and glassy rocks. Crystalline altered basalts have higher REE abundances and are relatively enriched in LREE, whereas glassy rocks are generally slightly depleted in LREE and MREE compared with the fresh glass. As a result, La/Yb values increase during alteration in crystalline basalts, but decrease during palagonitisation. Despite the LREE/HREE and the absolute REE variations, Sm/Nd values in both crystalline and glassy basalts do not change significantly because of alteration.

Sm/Nd values and Nd isotopes in altered oceanic crust should therefore not differ from those of the unaltered material. A slight but systematic decrease in $^{143}Nd/^{144}Nd$ was observed in the palagonitised basalts, but this effect will not be taken into account both because the variation is very small (within the analytical error), because basaltic glass is only a fraction of the oceanic crust, and because the decrease may reflect actual variations in unaltered glasses. In general, no differences are observed in Nd isotopes in samples analysed before and after leaching, and it is assumed that the measured $^{143}Nd/^{144}Nd$ values have not been affected by alteration.

Negative Ce anomalies in altered basalts are inherited from both seawater (negative Ce anomalies but very low REE concentrations) and carbonaceous sediments (e.g. calcite veins - negative Ce anomalies inherited from sediments and relatively higher Ce concentrations). The negative Eu anomaly in seawater does not produce any significant changes in the Eu abundances in the altered basalts.

2) K and Rb increase in both crystalline and glassy altered basalts, but Cs and Sr show differing behaviours. Sr shows a slight increase in crystalline rocks but a decrease in glasses, whereas Cs shows the opposite behaviour. The absolute and relative abundances of these elements are highly variable and span a large range; in particular, Sr concentrations will be also dependent on the direct intake of Sr from seawater and on the amount of secondary calcite deposited in veins and vesicles.

Increase in $^{87}Sr/^{86}Sr$ values as a result of alteration is a well documented but complex process. In general, alteration as the result of interaction with Sr-rich material in isotopic equilibrium with seawater (pelagic oozes, seawater, secondary minerals formed by basalt/seawater interaction) will produce high $^{87}Sr/^{86}Sr$ values but presumably not higher than those of seawater (approximately 0.709-0.710), and no age corrections will be necessary because of the high Sr/Rb values. Obviously, the effects of alteration will be stronger in low-Rb and low-Sr basalts (i.e. enrichment stronger in N-MORB than in OIB).

In summary, measured $^{87}Sr/^{86}Sr$ values are dependent on secondary alteration, and because of the high solubility of both Sr and Rb, even the $^{87}Sr/^{86}Sr$ values measured on accurately leached samples should be treated with caution.

3) Pb, Th, and U also have a complex geochemical behaviour, and because of their low concentrations only relatively few good-quality data are available in the literature. In general, their concentrations all increase during alteration, but the U/Pb and Th/Pb

will also increase, thus producing higher $^{206}Pb/^{204}Pb$, $^{207}Pb/^{204}Pb$, and $^{208}Pb/^{204}Pb$ values (see also Hart & Staudigel 1989).

3.5.2 Basalts in the Northeastern Indian Ocean: N-MORB, E-MORB, and OIB?

Despite the variable degree and type of alteration, the original geochemical characteristics of the oceanic basalts in the different sites can still be recognised using the relatively "immobile" elements.

TiO2, Zr, and Nb contents, and Ti/Zr and Zr/Nb values are very different in N-MORB, E-MORB and OIB, and the oceanic basalts samples within the Northeastern Indian Ocean have been subdivided into three groups according to these values and ratios (Table 3.2, and Figures 3.7 and 3.8). Only samples with MgO (normalised H_2O-free) content higher than 5 % were considered, so as to minimise the effect of HFSE fractionation in evolved rocks (mainly because of titanomagnetite crystallisation), and all the analyses for which neither Zr nor Nb were reported were also discarded.

Despite its location outside the Northeastern Indian Ocean, site DSDP 215 has been included in the database because of its close similarity with the DODO dredge. After this selection, a total of one hundred and twenty-one analyses (including averages of a number of analyses) were left in the database, but most trace elements are only available for a small fraction of these samples.

Within Group I (sixty-nine analyses, most of them from sites DSDP 261 and ODP 765) fall most samples from sites cored in abyssal plains (DSDP 212, 213, 257, 259, 260, 261, and ODP 765 and 766) with the exception of Unit B in site 261, and several samples from site 257. It seems that all the samples of basaltic basement located at a reasonable distance from ridges, seamounts, and other topographic or geophysical structures fall within Group I. All the basalts are believed to be relatively old (i.e. approximately of the same age as the basement).

Unlike Group I, Group II (forty-six analyses) is geochemically not very well defined, and the average composition reported in Table 3.2 does not adequately represent the large variations within samples of the same site and among sites observed in this group. Apart from some analyses of basalts from site 213, 259 and 260 (note that most analyses from these sites, including the most accurate, fall within Group I), the

	Group I	std	Group II	std	Group III	std
SiO2	49.95	1.13	49.53	1.83	45.07	0.32
TiO2	1.37	0.27	1.56	0.67	2.32	0.09
Al2O3	14.76	1.23	15.55	1.28	15.46	0.68
FeO*	11.12	1.15	9.40	2.83	10.11	0.90
MnO	0.21	0.05	0.21	0.07	0.15	0.03
MgO	6.97	1.03	7.12	1.19	7.88	1.78
CaO	11.48	1.30	10.48	2.39	7.07	1.15
Na2O	2.28	0.30	2.69	0.50	3.35	0.49
K2O	0.62	0.67	0.49	0.43	2.27	0.64
P2O5	0.11	0.02	0.20	0.12	0.67	0.04
L.O.I.	2.09	2.84	3.00	1.33	5.66	0.79
Total	100.95		100.22		100.01	
Rb	12	11	18	15	46	9
Ba	17	23	163	193	525	68
Sr	91	30	211	158	472	47
Pb	1	1	2	1	3	1
Zr	73	20	143	31	225	51
Hf	1.90	0.50	4.38	0.46		
Nb	2	1	12	6	58	4
Y	32	7	43	9	26	3
Th	1	0	2	1	5	1
U	0.10		0.48	0.21		
La	2.2	1.0	7.9	5.5	40.2	10.4
Ce	7.8	3.1	19.1	12.8	78.0	5.7
Nd	6.1	2.4	12.5	5.5	32.5	6.4
Sm	2.10	0.65	3.49	1.35	6.44	0.45
Eu	0.79	0.20	1.18	0.44	2.07	0.17
Tb	0.53	0.18	0.73	0.29	1.00	0.00
Ho	0.95	0.34	1.28	0.34	0.98	0.18
Yb	2.66	0.82	2.84	0.90	2.70	0.14
Lu	0.43	0.14	0.45	0.17	0.33	0.06
Cr	263	181	195	106	221	103
Ni	84	28	97	39	134	17
V	342	83	346	104	173	10
Sc	52	6	49	19	17	2
Co	36	9	50	22	26	6
V/Ti	0.044	0.010	0.037	0.013	0.012	0.001
Ti/Zr	113	16	74	20	68	12
Sc/Y	1.950	0.718	1.178	0.414	0.640	0.088

Table 3.2. Average composition of basalts in the Northeastern Indian Ocean. See text for explanations. Standard deviation not reported for U of Group I (only 1 analysis). The reported element ratios are averages of ratios. Data from this study and references quoted in text. Samples have been subdivided into three groups with Ti, Zr, and Nb contents and Ti/Zr and Zr/Nb values similar to N-MORB (Group I), E-MORB (Group II), and OIB (Group III). Basalts of Group I have (values in ppm, Ti normalised L.O.I.-free) Ti = 8354±1657; Zr = 73±20; Nb = 2±1; Ti/Zr = 113±16; Zr/Nb = 42±12. Group II: Ti = 9712±4278; Zr = 143±31; Nb = 12±6; Ti/Zr = 74±20; Zr/Nb = 17±7. Group III: Ti = 14725±659; Zr = 225±51; Nb = 58±4; Ti/Zr = 68±12; Zr/Nb = 4±1.

rocks in this group come from inactive ridges (DODO - Investigator Ridge; DSDP 215 - western flank of the Ninetyeast Ridge; DSDP 256 - related to the Broken Ridge), and volcanic sills emplaced after the formation of the basement (unit B of site 261).

The basement and dolerite sill of site 211 have very enriched LILE and HFSE and are the only rocks in Group III (six analyses). However, the rocks from the Vema dredge (Cocos Plateau, samples V28-14 A-B, and VM28 RD 14 1-4), which were not considered in the calculations because of their low MgO content, are extremely enriched in HFSE and have low Ti/Zr (average 76) and very low Zr/Nb, V/Ti, and Sc/Y (respectively 3.5, 0.006, and 0.5, excluding two excessively high Y values), are relatively depleted in HREE, and should also be classified in Group III.

Rocks dredged from the Vening Meinesz Seamounts south of Jawa have been described by Williams (1992) and Falloon et al. (submitted for publication). The dredged basalts reported by Falloon et al. (submitted for publication) are altered but have typical OIB REE pattern (but with higher REE values probably as a result of alteration), similar to the sill of site 211 and the three volcanic series of Christmas Island (Figure 3.3a), and show the characteristic Sm and Eu depletion already observed in site 211, Cocos Island, and Christmas Island. Other trace elements (Figure 3.3c) are generally more enriched than in site 211 but follow the same pattern, except for Ba (very high values, up to >> 700 ppm, similar to the Upper Volcanic Series of Christmas Island). Although Zr and Nb are also considerably enriched, incompatible trace element data (e.g. Ti/Zr, Zr/Nb, La/Sm) are also typical of OIB and similar to the Vema dredges and site 211. Other rocks dredged from the Vening Meinesz Seamounts (Williams 1992) also have major element composition (Table 3.1) similar to the DSDP 211 basement and dolerite and the Vema dredges.

Hart (1984; 1988; 1989) and Falloon et al. (submitted for publication) studied the volcanic rocks of Christmas Island, the only island with volcanic sequences in the Northeastern Indian Ocean, and recognised three different volcanic series. The Lower (approximately 40 Ma) and Middle (approximately 34 Ma) Volcanic Series are made of typical OIB alkaline basalts (and minor trachytes) resembling alkaline volcanic rocks from Heard and Kerguelen Islands, but, according to Falloon et al. (submitted for publication), with lower $^{87}Sr/^{86}Sr$ and Pb isotope values, and higher $^{143}Nd/^{144}Nd$.

The Upper Volcanic Series is considerably younger (3 to 5 Ma), relatively potassic and strongly ne-normative, extremely enriched in Ba (> 1200 ppm) and with lower HFSE and higher LILE compared with the older series. Some rocks have high Mg#, MgO and Ni, contain spinel-lherzolite xenoliths, and are believed to be primary melts. Sr and Nd isotope ratios are similar to the alkaline basalts in Kerguelen, but Pb isotopic ratios, and especially $^{206}Pb/^{204}Pb$, are considerably lower.

It is important to note that all the samples from seamounts in the northern part of the Northeastern Indian Ocean, and the sill and basement at site 211, show an OIB affinity and isotope systematics different from typical Indian MORB, and with a clear "enriched mantle" (EM, HIMU) component (Figures 3.2a-b, 3.3, and 3.8, 3.9, 3.10, and 3.11).

From Table 3.2 and Figure 3.7 it is clear that the basalts of Group I resemble N-MORB, although Rb, K, Th, Pb, and Ba (and U and Cs) contents are enriched, probably as a result of alteration. In contrast, the average LREE do not seem to have been strongly modified by alteration. Despite the relatively large standard deviations, the average composition of this group is very well defined. Incompatible element ratios - Ti/Zr, V/Ti, and Sc/Y, as studied by Woodhead et al. (1993) - also fall within typical N-MORB values (the average Sc/Y is slightly higher, but still similar to N-MORB within the standard deviation).

In contrast, basalts of Group II have very variable composition, and form a very heterogeneous group. Compared with E-MORB, they are generally enriched in all the incompatible elements, and relatively enriched in LILE, although the enrichment is less obvious than in Group I because of the relatively higher (compared to N-MORB) trace element content in the fresh basalts. As in Group I, the LREE do not seem to have been strongly affected by alteration. The K depletion and Zr enrichment are probably not a primary characteristic of the group, but an artificial effect introduced by averaging compositionally diverse samples.

In summary, although these Group II samples are generally similar to an "enriched", altered E-MORB, mostly with compositions intermediate between E-MORB and OIB, the average composition in Table 2 does not adequately represent the diversity within the group. The extreme geochemical and isotopic variability among (and often within) sites is a characteristic of compositionally similar basalts from the Ninetyeast Ridge.

The effects of alteration are even less evident in the basalts of Group III, both because the fresh basalts are relatively more enriched in LILE than the other groups, and because they are less altered. Their average chemical composition is similar to OIB and, as has already been pointed out, OIB with similar isotopic composition can be found in several other localities in the southern hemisphere (Indian Ocean, Kerguelen, East Australia).

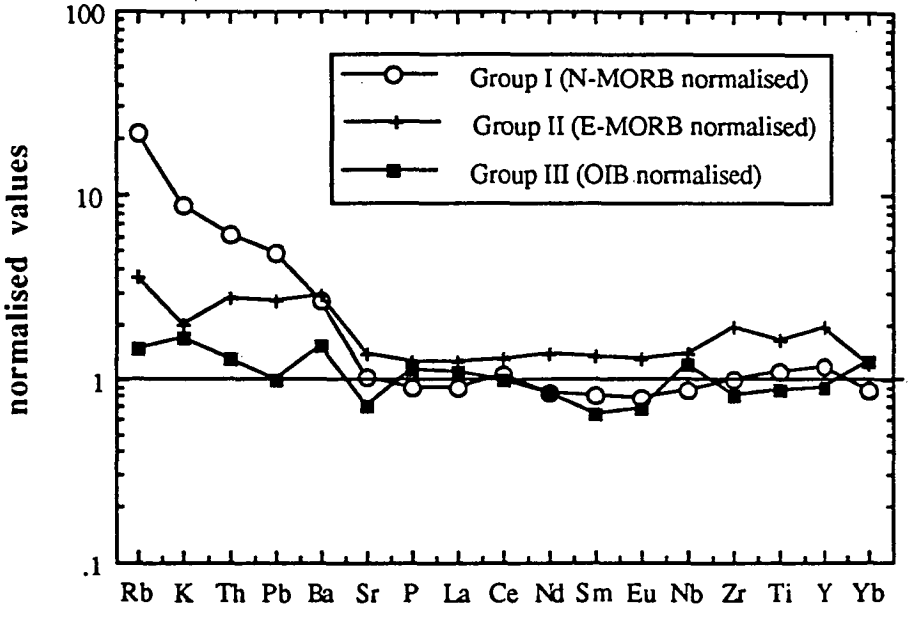

Figure 3.7. Average composition of Group I, II, and III basalts (from Table 3.1) normalised to N-MORB (Group I), E-MORB (Group II), and OIB (GROUP III). Normalising values from Sun & McDonough (1989). Elements are listed according to McCulloch & Gamble (1991) from "slab-derived" (more volatile and subject to increase by alteration), and enriched in most arc-lavas, to more immobile, that reflect the original composition of the source. The order is slightly modified to include P, La, and Eu in the plot, and the elements from Rb to Sr are listed for decreasing values of Group I. Notice the strong enrichment in elements from Rb to Ba in the basalts of Group I relative to Group II and II, and the relatively flat pattern from Sr to Yb for all the groups. However, in Group I and III the ratio Group I : N-MORB and Group III : OIB for the more immobile elements (Sr to Yb) is very close to 1, indicating that the source of Group I and III is geochemically very similar to - respectively - an N-MORB and an OIB source. On the contrary, the "immobile" trace element content of Group II is systematically higher than in E-MORB but parallel to it, suggesting that the source of this group is similar to an "enriched" E-MORB. However, it should not be forgotten that Group II is extremely heterogeneous and cannot simply be defined as a single group, and this is also suggested by the irregular K and HFSE elements distribution.

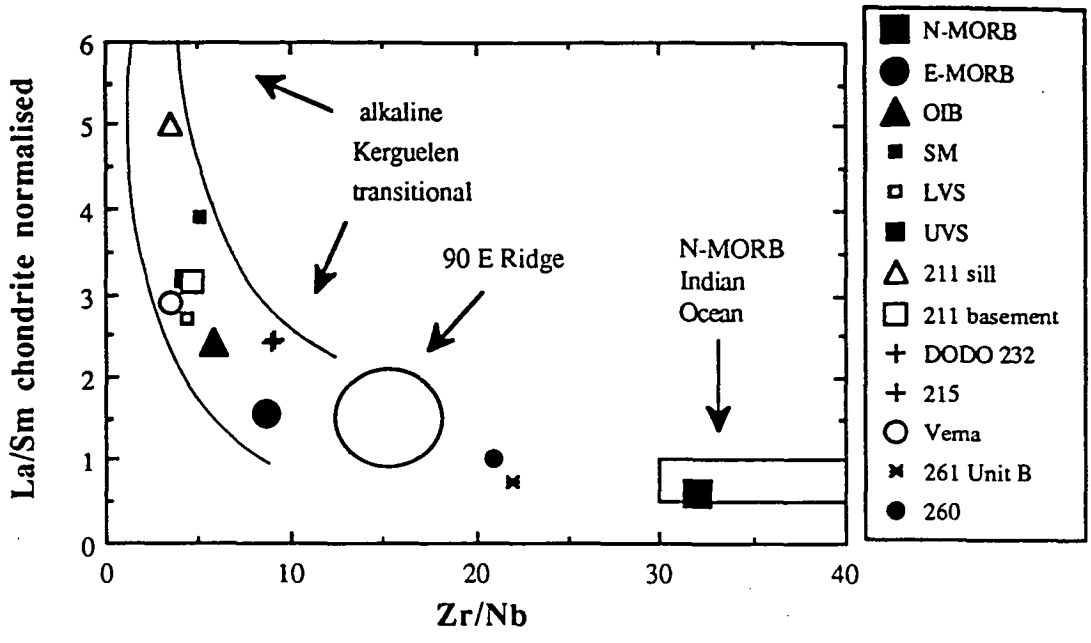

Figure 3.8. Chondrite-normalised La/Sm vs Zr/Nb. Data for Kerguelen, Ninetyeast Ridge, N-MORB Indian Ocean and Christmas Island are from references quoted in text. LVS - Christmas Island Lower and Middle Volcanic Series; UVS - Christmas Island Upper Volcanic Series; SM - Vening Meinesz seamount. The N-MORB Indian Ocean field includes sites 212, 213, 257, 259, 261 unit A and C, 765, 766. No Nb nor Ta data are available for site 256 (approximate normalised La/Sm 1.5). Notice the progressive enrichment (low Zr/Nb and high La/Sm) from N-MORB to 261 unit B (with La/Sm <1), to site 260, intermediate between N-MORB and E-MORB (other samples from this site plot within the N-MORB field), to DODO 232 and site 215 (the two sites plot at the same point) intermediate between E-MORB and OIB and similar to Kerguelen transitional basalts, to the more enriched rocks from Christmas Island, the Vema dredge (samples V28 14A and VM28 RD 14-1) and site 211, which are more "enriched" than OIB and plot in the field of mildly alkaline basalts of Kerguelen. Notice also that the basalts from the Ninetyeast Ridge are depleted compared with DODO 232N and 215, and plot just outside the field of the most depleted Kerguelen tholeiites.

3.5.3 New geochemistry and isotope data

The basaltic sill from site 22 211 has a trace element content typical of OIB (Figures 3.2a, and 3.3), and a typical DUPAL isotopic signature (Figures 3.9 to 3.11), similar to those samples from Kerguelen with similar geochemistry. This is not the result of the interaction with the surrounding sediments, because only the chilled margins of the sill show evidence of reaction with them, and the composition of the sediments is such that even a very strong interaction with them could not produce the observed isotopic ratios (see Chapter 4).

The underlying basement has a $^{87}Sr/^{86}Sr$ value of 0.7040 (measured for the altered amphibole-bearing basalt of the basement and reported in Subbarao et al. 1979, and corresponding to an approximate initial ratio of 0.7037), and, like the sill, seems to have an OIB signature (e.g. Zr/Nb = 4.5-5, Ti/Zr = 45-50; see also Figure 3.2a). Furthermore, titanaugite, abundant in the sill, has been observed at least in one of the flows (core 15-4, 73-75 cm) that form the basement, and very high TiO_2 content (up to 5%) in fresh glass was estimated (using EDS on the microprobe) in core 15-2, 38-40 cm. As was observed by Subbarao et al. (1979), in this site there is no consistency between geological setting and chemical composition, as the site is located in the middle of a topographic low (water depth >5500 m), and far away from seamounts enough to be unlikely part of a flow originated from these, and despite its location displays typical OIB characteristics.

The DODO 232 samples were dredged from the flank of a large structure situated on the western flank of the Investigator Ridge, which marks the location of a dextral transform fault, parallel to but less prominent than the Ninetyeast Ridge. Compared with those of site DSDP 22 211 these basalts are considerably less enriched, and show a trace element pattern intermediate between OIB and E-MORB (Figures 3.2b-c, and 3.4), slightly enriched, compared with Indian MORB, Pb isotopic values (Figures 3.9 to 3.11), but lower $^{87}Sr/^{86}Sr$ and higher $^{143}Nd/^{144}Nd$ isotopic ratios. These rocks closely resemble basalts from the Ninetyeast Ridge, and especially those from site DSDP 22 215, cored just west of the Ninetyeast Ridge, and with a Sr isotopic ratio of approximately 0.7043 (initial ratio estimated from data reported by Subbarao 1979), and therefore slightly higher than in the DODO 232 sample.

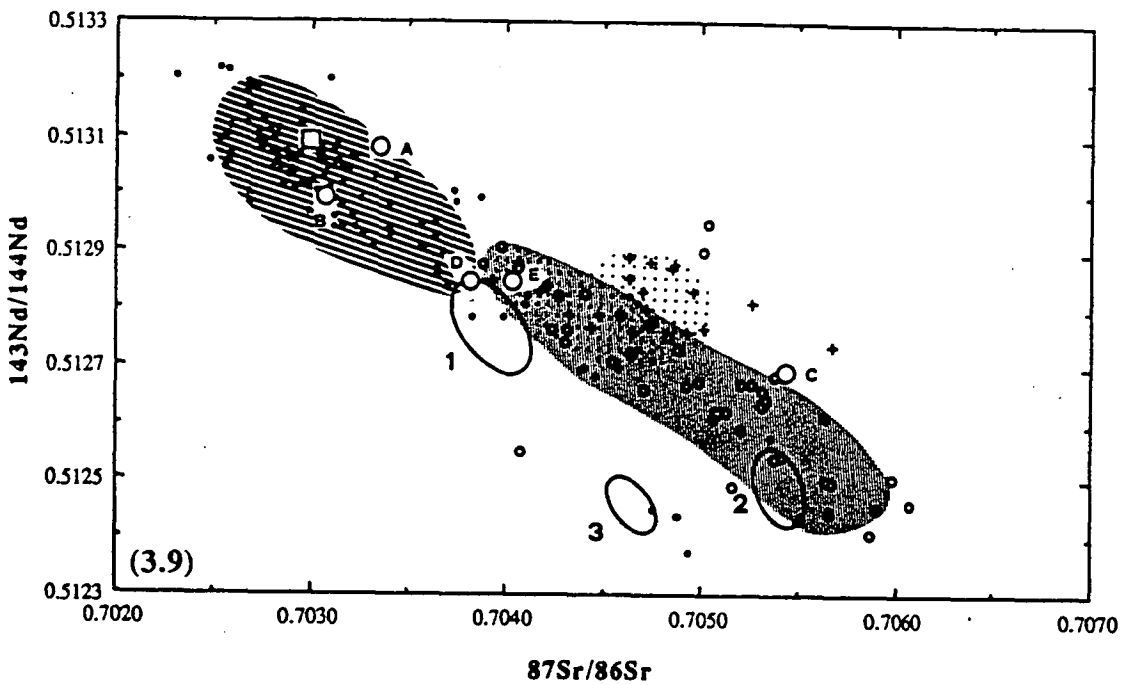

Figures 3.9, 3.10, and 3.11. Fields of Sr, Nd, and Pb isotope for basalts from the Indian Ocean (mainly from SEIR and SWIR - dots), Kerguelen (small circles), and Ninetyeast Ridge (crosses). 1, 2, and 3 are fields of Christmas Island (respectively: Lower and Middle Volcanic Series, Upper Volcanic Series, and Vening Meinesz seamounts). Diagonal heavily ruled, vertical lightly ruled, and stippled areas are the fields of, respectively, "typical" basalts from SEIR and SWIR, Kerguelen, and the Ninetyeast Ridge.

The new data are shown by the large circles (A - site 261; B - site 213; C - sill at site 211; D - DODO 232; E - Vema dredge). Large square in Figure 9 is the average of the analyses at site 765.

Other estimated initial $^{87}Sr/^{86}Sr$ values (omitted from the diagram due to lack of Nd isotope data) for the sites discussed here are: site 215 - 0.7043; basement of site 211 - 0.7037; site 260 - 0.7041; site 261 Unit B - 0.7033; site 766 - 0.7030-0.7033 (data for Sr isotope values, Rb and Sr concentrations, and estimated ages of the sites from Subbarao et al. 1979; Royer et al. 1991; Ishiwatari 1992; Ludden 1992; Ludden & Dionne 1992; Sager et al. 1992; this study).

Initial $^{87}Sr/^{86}Sr$ have been calculated based on the stratigraphic (radiometric, when available) age of the samples and on the Rb/Sr values of the samples (when available) or on the average Rb/Sr for a specific site. As has been pointed out elsewhere, the stratigraphic age deduced for the DODO and Vema dredges is probably a maximum age, and therefore the correction made is a maximum correction. However, the Rb/Sr values for these samples are fairly low, so that even if the age correction applied here has been excessive, the correct initial $^{87}Sr/^{86}Sr$ value would be similar to the value used here. For site 213 the recalculation is based on an approximate age and subject to large errors, due to the low Rb concentrations - lower concentrations are affected by larger errors. For Unit A at site 261 a Rb content of 5 ppm was assumed for the recalculation of the initial $^{87}Sr/^{86}Sr$ value, which is probably lower than the true Rb content (the isotope and major and trace element analyses of site 261 section 34-2:100-102 are from different fragments, and the section shows different degrees of alteration on a millimetric scale). Therefore the "true" initial $^{87}Sr/^{86}Sr$ value for site 261 is likely to be close to that of site 213, or lower, similar to the values reported for site 765.

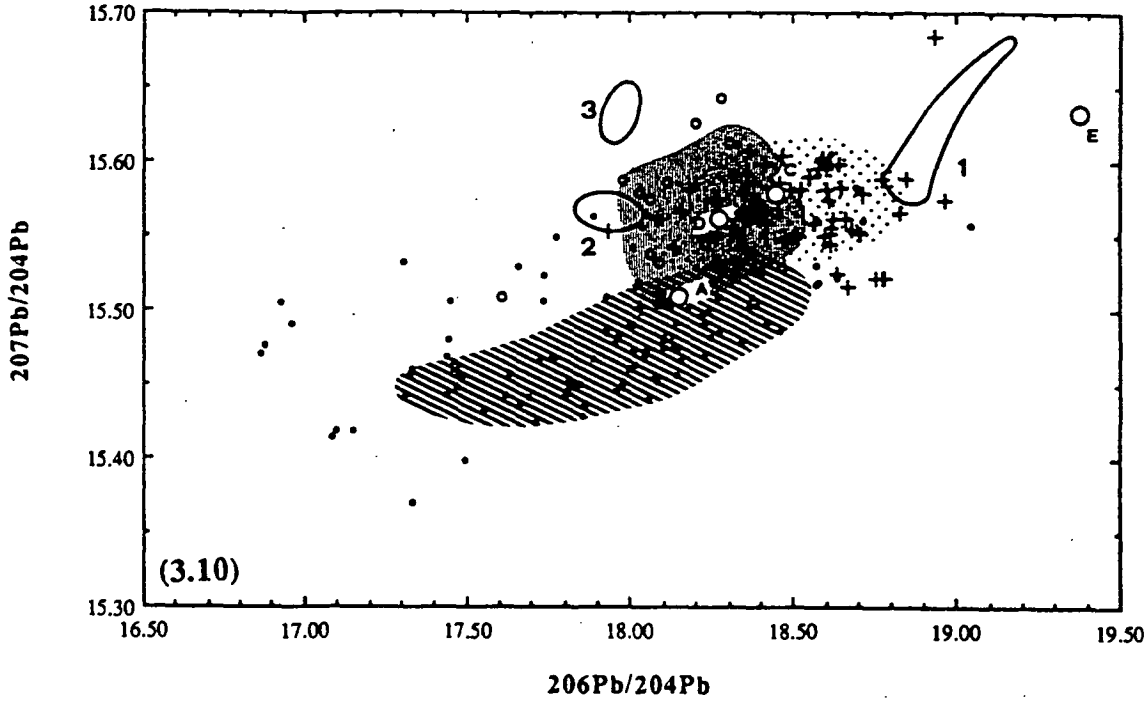
15.70
15.60
15.50
15.40
15.30
207Pb/204Pb
16.50
17.00
17.50
18.00
18.50
19.00
19.50
206Pb/204Pb
(3.10)
1
2
3
A
C
D
E

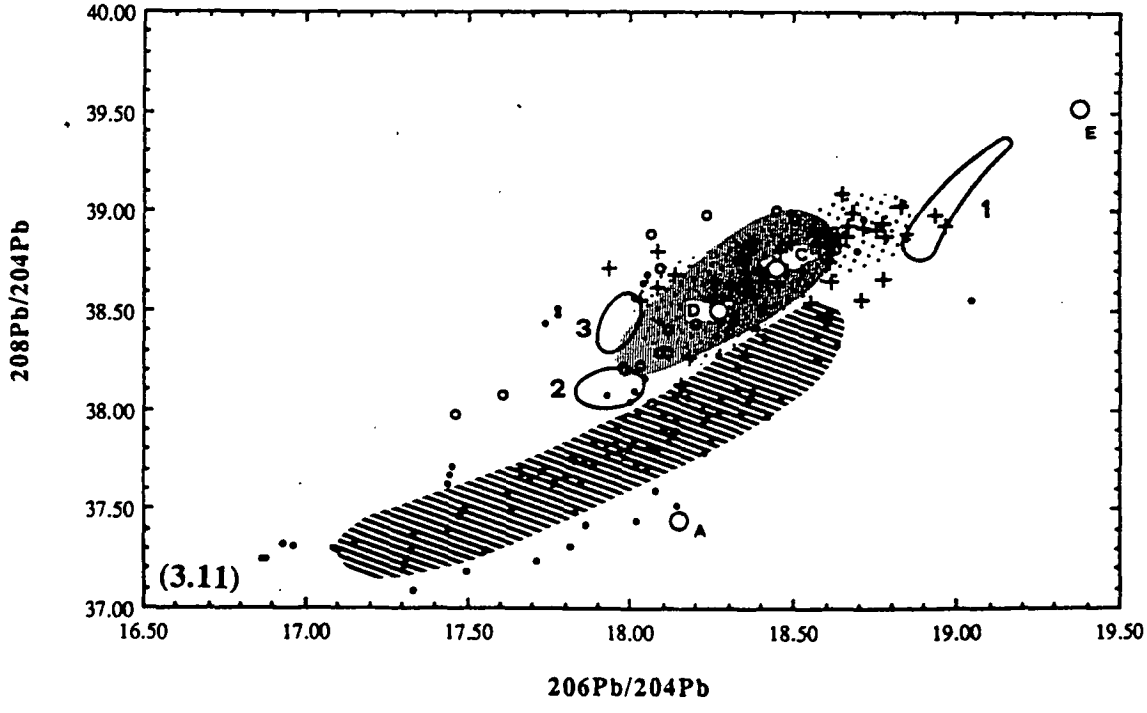
40.00
39.50
39.00
38.50
38.00
37.50
37.00
208Pb/204Pb
16.50
17.00
17.50
18.00
18.50
19.00
19.50
206Pb/204Pb
(3.11)
1
2
3
A
C
D
E

The Sr and Nd, and typically high $^{208}Pb/^{204}Pb$ and $^{207}Pb/^{204}Pb$ values are similar to tholeiitic Kerguelen volcanics and plot within the field of basalts from the Ninetyeast Ridge, and can be interpreted as the result of a smaller degree of interaction of a Kerguelen-type plume with Indian Ocean asthenospheric mantle. No significant differences in major element composition were observed between the new analyses presented here and those reported by Engel et al. (1965).

Compared with the basalts of site DSDP 22 215, the DODO 232 basalts have systematically slightly lower contents of MgO, Cr, Ni, Ba and Sr - which is consistent with shallow-level fractionation of small amounts (up to 2 -3 %) of olivine and plagioclase (and possibly minor amounts of clinopyroxene) from DSDP 22 215 type rocks. Alternatively, the differences between the two sets of samples may simply be due to slightly different contents of phenocrysts. Apart from these minor differences, basalts of sites DSDP 22 215 and DODO 232 appear to be identical, and therefore originated from the same source. On the other hand, site DSDP 256 has REE patterns similar to DODO and DSDP 215 (Figure 3.2c) but, like most sites cored in the Broken Ridge, is relatively enriched in FeO and depleted in K_2O.

The DODO 232 dredge site is geographically very close but chemically very different from the rocks of DSDP site 22 213 that show an N-MORB composition (Figure 3.2e), apart from the enrichment in LILE due to a slight alteration. Basalts from site 22 213 - consistently with their chemical composition - seem to have a typical Indian Ocean MORB isotopic signature, with higher $^{143}Nd/^{144}Nd$ and lower $^{87}Sr/^{86}Sr$ values (Figure 3.9; the measured $^{87}Sr/^{86}Sr$ value has probably been slightly increased by alteration). The differences in geochemical and isotopic composition are not surprising, as the two sites are located in very different tectonic environments (transform ridge in DODO 232, pillow lavas that form the oceanic floor in one of the deepest areas in the Northeastern Indian Ocean, the Wharton Basin, in site DSDP 22 213).

Chemically and isotopically similar to samples from site DSDP 22 213 is unit A - another sill intruded between the basement basalt and the overlying sediments - of site 27 261 (Figures 3.2g and 3.9) cored in the northeastern part of the Argo Abyssal Plain. The age of the sill is not precisely known, but sediments overlying the sill and the basaltic basement in this area of the Indian Ocean are as old as Upper Berriasian (139 Ma - ODP Initial Reports 123 765, 1989), and an age of 159 Ma - considerably older than the overlying sediments, was discussed and proposed by Sager et al.

(1992) and therefore the volcanic basement in this area is the oldest known in the Northeastern Indian Ocean.

The gap between the age of the oldest sediments and the age of the basement, also observed in nearby site 765, was explained as a result of the combination of low Jurassic sedimentation rates, sedimentation below the CCD (at least in site 765), and, possibly, minor errors in the geophysical parameters used in the model. Hart & Staudigel (1986) obtained a Rb/Sr age of 121.4 Ma for secondary celadonite and smectite veins in the underlying basalts of unit B, and suggested that these veins might have formed just after (and as a consequence of) the emplacement of the sill.

Interestingly, the same veins did not yield U enough for dating, that suggests that at the time of formation of unit A the site was too far from the ridge to suffer the enrichment in U (and depletion in Pb) typical of hydrothermally-altered ocean ridge basalts. This is true for samples DODO 232N and DSDP 22 211 as well, because they were emplaced in areas far from the ridge. For a sample from unit B, Frey et al. (1977) reported a $^{87}Sr/^{86}Sr$ value of 0.7039 (corresponding to an approximate initial ratio of 0.70330), similar to that measured in unit A. In the vicinity of site 261, $^{87}Sr/^{86}Sr$ values range from 0.7027 to 0.7033 (sites 765 and 766 - Ishiwatari 1992; Ludden & Dionne 1992), whereas site 260 seems to have a higher value (approximately 0.70412 - initial ratio estimated from the values reported in Subbarao 1979).

Site 261 also shows a rather peculiar Pb isotopic signature (Figures 3.10 and 3.11), with measured $^{208}Pb/^{204}Pb$ values considerably lower than most Indian Ocean basalts and similar to Atlantic and Pacific MORB. It seems that even when an approximate estimated correction for a maximum age of 160 Ma is considered the sample maintains an unenriched Pb isotope signature.

This value has important implications for the geotectonic reconstruction of the Northeastern Indian Ocean, because it may imply that the process responsible for the high Pb isotopic values observed in the Indian Ocean started to be active about 121-139 Ma ago, i.e. after the formation of a small portion of the Northeastern Indian Ocean - the Argo Abyssal Plain, where sites 261 and 765 are situated - but before the separation of India from Antarctica-Australia (based on the age of the Rajmahal Traps and the Prince Charles Mountains lamprophyres).

However, precise Pb, Th, U data and isotopic values are required to constrain this hypothesis. Ludden & Dionne (1992) also reported some Pb isotope data for nearby site 765, and concluded that site 765 has the same Pb (and Sr, Nd) isotopic signature as modern Mid Indian Ocean Ridges, with the implication that Indian Ocean mantle with high Pb isotopic values already existed at least 160 Ma ago and before the break-up of Gondwana. However, the Pb data reported by Ludden & Dionne (1992) are very inconsistent (i.e. inconsistent ^{206}Pb - ^{207}Pb - ^{208}Pb variations) and the Pb isotopic values range from Atlantic-Pacific MORB to more enriched values similar to those observed in some Kerguelen basalts. The origin of such large variations was not explained by Ludden & Dionne (1992), and their data will not be considered in the following discussion. Possible explanations include sample contamination, and whole-rock/glass fractionation of U, Th, and Pb which after 160 Ma led to significantly different Pb isotope ratios.

The samples dredged from the Cocos Islands (V28 RD 14-1/2/3/4 and V 28 14 A/B) are extremely altered. However, no other rocks have been described from the pedestal on which the young Cocos reef is built, so the analytical data are of interest. They appear to be undersaturated and strongly fractionated rocks, with high L.O.I. and organogenic P_2O_5 contents.

Although the geochemical composition of these samples has been modified by alteration, they still show typical OIB - but very enriched - REE patterns (Figure 3.2b), with depleted HREE, and incompatible element ratios (e.g. Zr/Nb = 3.5, Ti/Zr = 71), and Nd and Sr isotopic values indistinguishable from those of the DODO 232 basalts (Figure 3.9). The positive Eu anomaly and the high Sr contents are clearly due to plagioclase accumulation.

The absence of correlation between Sr and P_2O_5 suggests that apatite is enriched in REEs (good positive correlation P_2O_5 - Y) but not in Sr, and therefore only a very small portion of the excess Sr (approximately 10 % compared with typical OIB), taking into account the excess Sr due to plagioclase accumulation, might be secondary. This could explain the lack of ^{87}Sr enrichment that we would expect in such a strongly altered rock. On the other hand, the high Ba and Rb values could be due to the abundant clayey secondary material, also usually enriched in Pb, Th and U, and maybe responsible to some extent for the enriched Pb isotopic ratios (Figures 3.10 and 3.11). Plagioclase in these rocks is mainly andesine (optical microscope and EDS microprobe determination) and therefore is not likely to strongly fractionate Rb and Ba.

These rocks have Ba/Nb and Ba/La values similar to those of the relatively fresh and primitive basalts of the Upper Volcanic Series in Christmas Island, which are rich in Ba. If the Ba enrichment and the relatively high Pb isotopic ratios were a primary characteristic of these rocks, then they would resemble the Upper Volcanic Series of Christmas Island in their Ba/Nb and Ba/La values, but the Lower Volcanic Series in their Sr, Nd, and Pb isotopic values.

However, as has been shown before, Ba is extremely mobile during alteration processes, and it is extremely likely that some Ba, K, Rb, U and Th have been added to these samples. Assuming that the HFSE content and Sr and Nd isotopic values have not been modified by alteration nor by crystal fractionation, these rocks seem to have HFSE ratios and Sr and Nd isotope values similar to those observed in rocks with a HIMU component, and this HIMU component would also account for their high Pb isotopic ratios. If approximately 15-20% of their Ba, K, Rb, and Th has been added during alteration, then also their LILE/LILE values would resemble HIMU values.

In summary, these evolved and altered rocks have HFSE values typical of OIB, but with Sr and Nd isotopic ratios similar to tholeiitic or transitional rocks in many other sites in the Indian Ocean (DODO 232, Kerguelen tholeiitic, Ninetyeast Ridge), and to the Lower Volcanic Series of Christmas Island. If the measured Pb isotopic ratios have not been strongly modified by alteration, then they also resemble those of the Lower Volcanic Series of Christmas Island, and suggest that a HIMU component is present in the source of these rocks.

3.5.4 Isotopic composition of MORB in the Argo Abyssal Plain

After a long dispute over the discrepancy between the age of the oldest known sedimentary rocks at sites DSDP 261 and ODP 765, and the estimated age of the basement based on magnetic anomalies, Ludden (1992) and Sager et al. (1992) concluded that seafloor spreading in the Argo Abyssal Plain began just before 163 Ma. The Argo spreading centre then propagated northwards and was subducted under the Jawa Trench. During the Lower Cretaceous, approximately at 132 Ma, spreading began between Australia and India.

The Argo Abyssal Plain is therefore older than the rest of the Northeastern Indian Ocean, and was formed in a different geo-tectonic environment. All the available data

- including the new data reported here - seem to show that all the MORB that formed during and after the rifting between Australia and India have an isotopic composition characterised by relatively high Pb isotopic ratios than those of Atlantic and Pacific MORB. Was the mantle source of Indian MORB enriched in ^{206}Pb, ^{207}Pb, and ^{208}Pb before the 132 Ma rifting?

The only samples of oceanic crust considerably older than 132 Ma are the basement at site 765, and Unit A and C at site 261. Reported initial $^{87}Sr/^{86}Sr$ values for site 765 range from 0.7027 to 0.7030 (Ishiwatari 1992; Ludden & Dionne 1992). The new analysis of site 261 Unit A gave a higher initial $^{87}Sr/^{86}Sr$ value of approximately 0.7033 but, as was pointed out, the relatively high value could be due to alteration, and the true value may be closer to 0.7030. In contrast, the sites younger than 132 Ma, and not related to ridges or seamounts (i.e. the basement at site 211, 213, and 260, Unit B at site 261, and site 766) have $^{87}Sr/^{86}Sr$ values in the range 0.7030 to 0.7041.

$^{143}Nd/^{144}Nd$ values for the older samples are in the range 0.51308 - 0.51309, and are also considerably higher than the value of 0.51300 for site 213, and the lower values for MORB and OIB from the Ninetyeast Ridge, Kerguelen Plateau, and Indian Ocean Seamounts (Christmas Island, Vening Meinesz seamounts, Cocos Island).

In summary, the basalts older than 132 Ma have systematically lower $^{87}Sr/^{86}Sr$ and higher $^{143}Nd/^{144}Nd$ values than those of basalts younger than 132 Ma; and also plot within the field where Atlantic and Indian MORB overlap, and actually at the least "enriched" end of the Indian Ocean MORB field.

Excluding the Pb isotope data published by Ludden & Dionne (1992) for the reasons explained in paragraph 3.5.3 (however, the whole-rock Pb isotope analyses reported by Ludden & Dionne 1992 for site 765 are similar to those presented here), the only Pb isotope value for rocks older than 132 Ma is the new analysis of site 261 Unit A, for which values were obtained for $^{206}Pb/^{204}Pb$ and $^{207}Pb/^{204}Pb$ which lie within the fields of Indian and Atlantic-Pacific MORB, but for which the $^{208}Pb/^{204}Pb$ value is definitely lower than Indian MORB and more typical of Atlantic-Pacific MORB.

Although these new Pb data are likely to need a correction for age and - possibly - minor alteration, the Sr, Nd, and Pb isotopic data seem to suggest that Northeastern Indian Ocean basalts older than 132 Ma are similar to Atlantic-Pacific MORB, in contrast with the conclusions by Ludden & Dionne (1992). Accordingly, the

appearance of the isotopic signature characteristic of Indian Ocean MORB is probably related to the major tectonic disturbance that caused the rifting between Australia and India, and its presence beneath the Argo Abyssal Plain after 132 Ma is only supported by the slightly higher $^{87}Sr/^{86}Sr$ values measured at sites 261 Unit B and 766. However, neither basalts with an isotopically enriched component (EM, HIMU), nor OIB have been found in this portion of the Northeastern Indian Ocean.

3.5.5 The trail of the Kerguelen mantle plume

It is generally accepted (but see Müller et al. 1993) that the trace of the Kerguelen mantle plume can be followed from Kerguelen to the Ninetyeast Ridge and the Rajmahal Traps going north, and to the Bunbury basalts, Prince Charles Mountains lamprophyres, and probably the Naturaliste Plateau and the other plateaux off the coast of Western Australia (probably the remnants of a pre-Gondwanan rift basaltic plateau; see e.g. Storey et al. 1992), going south.

The geochemical and isotopic characteristics of the volcanics attributed to the plume are interpreted to be a result of different degrees of mixing between a "normal" mantle source, isotopically and geochemically similar to the source of MORB, and the isotopically "enriched" (relatively high Sr and Pb, and low Nd isotopic ratios) alkaline material from the plume: the strongly alkaline rocks are isotopically more "enriched", and indicate a larger amount of plume component.

Continental lithosphere was probably involved at least in the marginal basalts (Rajmahal Traps, Bunbury basalts and Australian seamounts, Antarctica) and is still disputed in Kerguelen (e.g. Storey et al. 1992), but not in the intra-oceanic areas, which formed when the Gondwanan rift was already well developed.

This model is conceptually very simple, and is based on the assumption that one single isotopically-"enriched" fixed hotspot, the Kerguelen mantle plume, active since at least 132 Ma, contaminated the mantle source of the Indian Ocean MORB, which was previously isotopically similar to the source of Atlantic MORB. According to this model, only the rocks that are now situated directly on the trail of the Kerguelen plume should have a significant plume component, and were formed at the moment of the passage over the plume of the plate on which they are located. Therefore, the existence of rocks with isotope characteristics different from typical Indian Ocean MORB is spatially and temporally constrained.

To date, none of the existing geodynamic models of evolution of the Northeastern Indian Ocean includes the localities of DSDP 22 211, DODO 232, the Cocos and Christmas Islands, and the Vening Meinesz seamounts in the trail of the Kerguelen plume or other similar plumes. The possibility that these localities owe their "anomalous" (relative to Indian Ocean MORB) isotopic signature to interaction with continental crust or subducted sediments can be ruled out, as there is no evidence for the presence of an overlying continental or somehow isotopically "enriched" crust, nor for the existence of active or fossil subduction zones in the vicinity of these sites.

The new data seem to show that basalts with an isotopically "enriched" (EM, HIMU) component are not confined to the trail of the Kerguelen plume or other recognised mantle plumes, and may indeed be more widespread throughout the Northeastern Indian Ocean than was suspected.

The Investigator Ridge is a structure similar to the Ninetyeast Ridge, but is topographically less prominent and partially buried under sediments from the Ganges-Brahmaputra system. Yet, its continuation into North Sumatra is a major tectonic and geochemical boundary (see Chapter 6). If the only available data (DODO 232) can be taken as representative of the whole ridge, then the Investigator Ridge is a "duplicate" of the Ninetyeast Ridge, parallel to it and probably with the same origin.

Other sub-parallel hotspot trails have been described in the Indian Ocean (Crozet-85°E Ridge, Réunion, Marion, and Laccadive-Maldive Ridge; see e.g. Duncan 1981; Duncan & Hargraves 1990; Curray & Munasinghe 1991; Duncan 1991), and the new data presented here suggest that the Investigator Ridge may be the trail of another previously unrecognised hotspot.

On the other hand, the Cocos Plateau, despite being located very close to the Investigator Ridge, has a strong geochemical and isotopic affinity with the Lower and Middle Volcanic Series of Christmas Island, the Vening Meinesz seamounts, some volcanoes in the Sunda arc, and the sill at site 211, and, together with the Roo Rise, forms an almost east-west trending arch which has no equivalents in the Indian Ocean. The seamounts off the coast of central Jawa are situated over a bulge that formed, according to Hamilton (1979), as a result of the downward bending and fracturing of the Indian Ocean crust approaching the trench.

Normal tensional faults have been observed in the subducting oceanic crust as it bends downward into the subduction zone (Masson et al. 1990), but the distribution

of these seamounts is too irregular and cannot be explained by such a simple mechanism (see also Falloon et al. submitted for publication). More likely, these seamounts formed in a regional field of tensional stress in an area "characterised by an extremely high level of intraplate deformations" (Cloetingh et al. 1992), but it is not clear whether the enriched mantle which originated these seamounts is always present at some depth and only comes up in a particular tectonic situation, or the seamounts are a trail of a yet-to-be-found mantle hotspot transverse to all the other hotspot trails in the Indian Ocean, or possibly one (or more) 'blobs' drifting northeast from the Kerguelen hotspot.

There are two consequences of the fixed hotspot model. Firstly, the age of volcanism along the ridges is consistent with the movement of the plates; that is, the age of volcanism must increase regularly with distance from the hotspot. This appears to be true for the Ninetyeast Ridge (age of volcanism increasing northward; but see Müller et al. 1993) and the other hotspot trails in the Indian Ocean, and may also be true for the Investigator Ridge, although no age determinations are available for this ridge, but is probably not true for the seamounts (from the Cocos Plateau to the Roo Rise), and is definitely not consistent with the three episodes of volcanism on Christmas Island. Secondly, if the enriched mantle always remained in a fixed position, the mantle now beneath the Ninetyeast and Investigator Ridges and the Sunda arc is probably "normal" Indian Ocean mantle.

However, it is possible that material from the Kerguelen plume (or other similar plumes) was trapped beneath the Sunda arc either because the plume might have been located underneath the Sunda arc before 100 Ma (see discussion in Müller et al. 1993), or because asthenospheric material "detached" from the Kerguelen plume might have flowed northeasterly under the Indian Ocean, and might have been trapped under the Sunda arc before subduction began.

Although little is known about the location of the Sunda arc and the Kerguelen hotspot before subduction began in the Sunda arc, the seamounts in the central part of the Northeastern Indian Ocean (including Christmas Island) and the sill at site 211 define a NE-SW trend, and show that mantle with an isotopically enriched endmember (HIMU in the Lower and Middle Volcanic Series of Christmas Island and in the Cocos Plateau, EM1 in the Upper Volcanic Series of Christmas Island and at least one of the Vening Meinesz seamounts, and EM2 at site 211) was present at some stage in the Northeastern Indian Ocean, thus suggesting that mantle material from the Kerguelen hotspot might indeed have drifted northeastwards.

In summary, the distribution in time and space of magmatism along the seamounts in the central part of the Northeastern Indian Ocean and, as will be shown in Chapter 6, in south Sumatra, is not consistent with a single fixed hotspot model and with simple models of mixing between mantle sources with different isotopic signatures ("normal" Indian Ocean mantle, EM1, EM2, HIMU), as proposed for Christmas Island (Falloon et al. submitted for publication), neither the observed variations in Sr, Nd, and Pb isotopes appear to be the result of simple radioactive decay, as argued by Class et al. (1993) for the Ninetyeast Ridge. At this stage, because of the very small amount of samples studied and the poor understanding of the geodynamic evolution of this part of the Indian Ocean, it is not clear whether the isotopically "enriched" OIB volcanism in this area is the result of secondary "blobs" of mantle drifting from the Kerguelen hotspot (and possibly from other hotspots) or the manifestation of a vertically (at least) zoned mantle.

In any case, the volcanism of these seamounts, and especially the young volcanics of the Upper Volcanic Series in Christmas Island and the Quaternary Sukadana basalts in south Sumatra (Chapter 6) are a clear manifestation of the existence of mantle capable of generating isotopically "enriched" OIB in the vicinity and beneath the Sunda arc in recent times. The spatial extension of this mantle beneath the Sunda arc will be further discussed in Chapters 5 and 6.

3.6 Conclusions

1) Basalts with a large range of chemical compositions are found in the Northeastern Indian Ocean. In general, their Rb, K, Th, Pb, and Ba (and presumably Cs and U), contents have been increased to varying extents by alteration, and the effects of alteration are more evident in the rocks which were originally more depleted in LILE. In general, the LREE seem to be relatively unmodified by alteration. Unlike the other major elements, Ti appears to be unaffected by low-temperature hydrothermal alteration, and due to its distinctive content in the different types of basalts, is, together with the other HFSE, a good indicator of the original geochemistry of the rock. Using HFSE contents and ratios, three groups of basalts can be identified in the Northeastern Indian Ocean. Each group appears to be systematically associated with a particular tectonic environment.

2) Basalts of Group I are found in the basement of the tectonically inactive, deep areas of the Northeastern Indian Ocean, away from ridges, plateaux and seamounts,

and seem to be the most common. Although minor variations can be observed from site to site, this group is compositionally very homogeneous, and resembles a typical, low-temperature hydrothermally altered N-MORB, with considerably enriched (compared with the original low values) LILE because of alteration, but unmodified - compared to N-MORB - Sr, P, REE (including LREE), and HFSE. Isotopically, these basalts are similar to typical N-MORB erupted from Mid Indian Ocean Ridges. However, the basalts cored in the Argo Abyssal Plain are considerably older than the estimated age of the Gondwana rifting, and apparently do not show the distinct Pb isotopic signature which characterises MORB of the Indian Ocean.

3) In contrast with Group I, Group II is extremely heterogeneous, and the basalts of this group range in composition from strongly enriched E-MORB to types transitional between E-MORB and OIB. The effects of alteration are less evident, seemingly due to the originally higher LILE content. Most samples of this group are from inactive ridges or sills emplaced in the older basement. Compared with the basalts of the Ninetyeast Ridge, these basalts are geochemically more enriched and resemble tholeiitic and transitional basalts from Kerguelen and East Australia, but do not show the HREE depletion typical of OIB. Isotopically, these rocks are indistinguishable from transitional and tholeiitic basalts found in Kerguelen, East Australia, south Sumatra (Chapter 6), and the Ninetyeast Ridge, and are consistent with a stronger (compared to Group I) interaction between normal Indian Ocean mantle and an isotopically enriched (EM, HIMU) mantle plume.

4) All the seamounts for which data are available, including the Cocos Islands, Christmas Island, the Vening Meinesz seamounts, and the dolerite sill and basement found at site 211, show HFSE contents typical of OIB, and similar to those of transitional and mildly alkaline rocks from Kerguelen, East Australia, and south Sumatra. Unlike their rather homogeneous geochemical compositions, their Sr, Nd, and Pb isotope systematics are very variable in time (in Christmas Island) and space. The observed range is, in principle, consistent with a four mantle components model ("normal" Indian Ocean mantle, EM1, EM2, and HIMU).

5) At present, the very small amount of data and the poor understanding of the geodynamic evolution of the Northeastern Indian Ocean do not allow us to map the extent of the mantle plume (or plumes) responsible for the isotopic anomalies in this area. While the Investigator Ridge (and possibly the 85°E Ridge), near-parallel and similar to the Ninetyeast Ridge, might be consistent with a "fixed hotspots" (one

hotspot is required for each ridge) model, the seamounts off the coast of the Sunda arc require a different explanation.

It is not clear whether the isotopically "enriched" endmembers are always present at some depth in the area and only generate melts in particular geotectonic situations, or whether the observed volcanism is the manifestation of drifting "blobs" of "enriched" mantle. However, the available data indicate that a mantle capable of generating OIB with a more or less strong EM and HIMU signature must have existed in the area at least from approximately 70 Ma ago (age of the sill at site 211) to 5 Ma ago (age of the Upper Volcanic Series on Christmas Island). Chapter 6 will evaluate the evidence that similar mantle currently forms part of the mantle wedge beneath the Sunda arc, at least in south Sumatra.

CHAPTER 4

Geochemical and isotopic composition of sediments in the Northeastern Indian Ocean

4.1 Introduction

The subduction of oceanic sediments, except where the sediments are accreted in the fore-arc, and their recycling into the mantle are implicit in the plate tectonic model of genesis and evolution of volcanic arcs.

In general, most oceanic sediments are enriched, compared to what is believed to be the "normal" composition of the mantle source of the arc rocks, in those elements that also have high concentrations in arc rocks. Also, most sediments have Sr, Nd, and Pb isotope systematics different from those of typical depleted and MORB mantle (e.g. Hart & Zindler 1989), and many arc rocks in many localities plot along mixing curves that go from a low $^{87}Sr/^{86}Sr$, $^{208}Pb/^{204}Pb$, $^{207}Pb/^{204}Pb$, $^{206}Pb/^{204}Pb$, and high $^{143}Nd/^{144}Nd$ mantle source to high $^{87}Sr/^{86}Sr$, $^{208}Pb/^{204}Pb$, $^{207}Pb/^{204}Pb$, $^{206}Pb/^{204}Pb$, and low $^{143}Nd/^{144}Nd$ sediments, altered oceanic crust, or not well defined "subduction-related fluids".

However, as was outlined in Chapter 1, the evidence for the involvement of subducted material is, in general, indirect and model dependent. In other words, because of the large variations in the geochemical and isotopic composition of sediments, it is always possible to select the "right" sediment and mix it with the "right" mantle to obtain the required composition.

Two prerequisites are essential if sediments are to be used in modelling the sources of arc magmatism. Firstly, the composition of the sedimentary cover must be known, and it is then necessary to characterise the composition of "typical" sediments, taking into account their volume, age, and provenance. Secondly, we need to know the composition of the material contaminating the source of the arc rocks.

During subduction, sediments suffer complex metamorphic and dehydration processes which strongly modify their original chemical composition and texture. The extent of element mobility is strongly dependent on the grain size and mineralogical composition of the sediments. In general, by knowing the composition

of the starting material (i.e. the "typical" sediment cored from the sea-floor), making a number of assumptions about several interdependent parameters (like pressure and temperature gradients in the subducting slab, porosity and permeability of the sedimentary column, element mobility), and using direct evidence (that is, comparing the sea-floor sediment with old subducted material occasionally brought back to the surface, or with xenoliths believed to derive from subducted sediments), we could estimate the compositions for the sediment-derived contaminating material, but these estimates are extremely model-dependent (e.g. Lin 1992, and references therein).

The Sr, Nd, and Pb isotopic signature of arc volcanics is often used as strong and conclusive evidence for sediment (or sediment-derived fluid) contamination, and, as isotopic compositions are likely to be less sensitive to change by processes occurring during the subduction, it can be assumed that the Sr, Nd, and Pb isotope ratios measured on cored samples of sediments are maintained unchanged in the subducted material, provided - as is likely in most cases - that the timing of recycling is short enough not to produce isotope variations following parent-daughter element fractionation during subduction.

This chapter is an attempt to define realistic geochemical and isotopic compositions of oceanic sediments which might be involved in the magmatism in the Sunda arc, and is based on new analyses and on the existing database of geochemical and isotopic analyses of sediments in the Northeastern Indian Ocean, and not on selected and arguably unrepresentative analyses of sediments from distant areas. In particular, the discussion will focus on the Sr, Nd, and Pb isotopic variations as a function of the composition and age of the sediments.

In the next chapter the spatial and temporal variations in Sr, Nd, and Pb isotopes in sediments of the Northeastern Indian Ocean will be compared with the spatial isotopic variations observed in the Quaternary volcanics of the west Sunda arc.

4.2 Previous studies

Using a statistical approach and major and trace element data from five sites in the eastern portion of the Eastern Indian Ocean, Cook (1974) showed that two groups of sediments, namely "clays" and "calcareous oozes", can be easily distinguished, and that elements and oxides can be subdivided into groups which correspond with different mineral phases. Also, it was pointed out that the trace element contents of

both groups are generally lower than those of pelagic sediments in other oceans.

Importantly, Cook (1974) noticed that the dilution effect of $CaCO_3$ is by far the most important factor in a multi-variable statistical analysis, and that the two groups are similar to each other when considered on a carbonate- and water-free basis. In other words, Cook (1974) showed that carbonates are compositionally equivalent to clays diluted by mainly $CaCO_3$.

Plank & Ludden (1992) analysed in detail the major and trace element composition of sediments cored at ODP site 765 in the Argo Abyssal Plain, and reached virtually the same conclusions, that the geochemical variability observed in the sediments is a consequence of the different degrees of dilution of a relatively homogeneous detrital component - similar to Average Post-Archaean Australian Shale (PAAS) - by biogenic silica and $CaCO_3$. The similarity between the sediments in this particular site and PAAS is not surprising, as the site is located very close to the Australian continental shelf where post-Archaean shales outcrop, and no other major landmasses are present in its proximity, and therefore the sediments in the Argo Abyssal Plain are likely to be predominantly PAAS turbidites and aeolian deposits (see e.g. Windom 1975) diluted by biogenic marine material.

Only recently have sediments from the Northeastern Indian Ocean been analysed for isotopes. Ben Othman et al. (1989), McLennan et al. (1990), and Dia et al. (1992) reported analyses of Sr, Nd, and Pb isotopes from surface and subsurface sediments from several localities in the Northeastern Indian Ocean, including some turbidites and fore-arc sediments. The depth in the sedimentary column, age, composition, and distance of the analysed sediment from the trench are important for the understanding of the provenance of the sediment and also have important implications for the sediment-recycling models in arc volcanism: they will be discussed in detail later in this chapter.

4.3 New analytical data

Samples from several DSDP and ODP cores have been analysed for major and trace elements and Sr, Nd, and Pb isotopes, and the results are reported in Table 4.1. Also, together with other samples from the same piston-cores, some of the samples analysed by Ben Othman et al. (1989) have been re-analysed, as no major element compositional data were published in that article. A brief description of the lithology

is given in Appendix D, and the stratigraphy of the DSDP and ODP cores has been summarised in Appendix E.

Sample	DSDP 22 211 13-1:10-12	DSDP 22 213 1-3:30-32	DSDP 22 213 1-4:67-69	DSDP 22 213 7-2:88-90	DSDP 22 213 7-5:71-73	DSDP 22 213 10-2:60-62
Lithology	Nanno Ooze	Diatom Ooze	Diatom Ooze	Diatom Ooze	Diatom Ooze	Clay
Age	Upper Cretaceous	Quaternary	Quaternary	Upper Miocene	Upper Miocene	Middle Miocene
SiO2	51.40	57.80	61.75	56.10	54.17	48.68
TiO2	1.34	0.52	0.36	0.53	0.55	0.45
Al2O3	14.92	13.18	9.97	15.64	15.79	14.81
Fe2O3	9.05	5.33	4.11	5.81	5.96	6.04
MnO	0.32	0.94	0.29	0.17	0.46	1.69
MgO	3.47	2.02	1.73	2.04	2.29	3.30
CaO	3.23	0.72	0.59	0.73	0.75	1.18
Na2O	1.70	4.94	5.35	4.30	4.92	4.38
K2O	3.74	1.69	1.23	2.03	1.60	1.45
P2O5	0.16	0.16	0.10	0.21	0.25	0.59
L.O.I.	10.10	12.90	14.58	11.84	13.19	17.11
Total	99.43	100.20	100.06	99.40	99.93	99.68
Rb	122	51	43	80	64	53
Ba	279	654	1453	398	230	326
Sr	126	110	101	87	90	129
Pb	18	26	19	30	30	42
Cs	3.52	3.96	2.81	6.49	4.41	5.83
Zr	344	98	80	119	112	133
Hf	8.10	2.98	1.98	3.50	3.00	4.73
Nb	41	7	6	9	8	8
Ta	2.62	0.65	0.40	1.54	1.03	0.50
Y	47	27	18	46	48	116
Th	14.50	10.30	7.32	13.80	12.60	15.50
U						
La	47.3	25.4	15.6	37.7	36.4	68.6
Ce	124.0	74.8	50.9	81.1	80.7	149.0
Nd	51.9	34.4	18.0	44.6	48.5	95.5
Sm	10.6	6.7	4.4	9.8	10.3	22.7
Eu	2.36	1.49	1.31	2.42	2.36	5.39
Gd						
Tb	1.44	0.74	0.75	1.30	1.33	3.11
Dy						
Ho	1.60	1.05	0.89	1.76	1.85	4.47
Er						
Yb	4.24	2.74	2.00	4.41	5.03	11.70
Lu	0.63	0.35	0.29	0.69	0.73	2.04
Cr	83	67	31	36	39	40
Ni	76	57	56	90	107	295
V	114	53	67	66	58	101
Sc	24	7	12	12	9	20
Measured isotope ratios						
87Sr/86Sr	0.71643	0.71266			0.71384	
143Nd/144Nd	0.512228	0.512262			0.512245	
208Pb/204Pb	39.269	39.110				
207Pb/204Pb	15.711	15.701				
206Pb/204Pb	18.772	18.904				

Table 4.1. Chemical analyses of samples of sedimentary rocks from the Northeastern Indian Ocean from this study. Data in bold are from Ben Othman et al. (1989). See Appendix D and Figure 3.1 (Chapter 3) for the location of the samples.

Table 4.1 cont.

Sample	DSDP 22 213 13-4:91-93	DSDP 22 213 16-2:57-59	DSDP 27 261 2-2:33-38	DSDP 27 261 3-2:25-27	DSDP 27 261 4-1:99-101	DSDP 27 261 6-2:25-27
Lithology	Clay	Nanno Ooze	Clay	Nanno Ooze	Nanno Ooze	Clay
Age	Middle Miocene	Upper Paleocene	Quaternary	Lower Pliocene	Upper Miocene	Upper Cretaceous
SiO2	44.65	1.57	54.96	18.86	13.02	53.30
TiO2	0.81	0.01	0.68	0.23	0.17	1.05
Al2O3	14.46	0.53	15.58	6.62	4.94	16.68
Fe2O3	9.26	0.72	6.58	3.12	1.70	8.54
MnO	2.21	0.10	0.30	0.23	0.13	0.55
MgO	3.03	0.26	2.85	1.37	1.07	3.46
CaO	2.41	51.91	0.76	33.06	39.69	1.09
Na2O	3.44	0.58	4.19	1.52	1.15	2.04
K2O	2.62	0.31	1.95	1.14	0.65	3.39
P2O5	1.52	0.11	0.12	0.13	0.08	0.67
L.O.I.	15.29	43.37	11.77	34.00	37.22	9.77
Total	99.70	99.47	99.74	100.28	99.82	100.54
Rb	76	5	68	48	31	114
Ba	264	10	264	448	397	279
Sr	192	922	103	1150	1290	134
Pb	42	8	29	10	8	20
Cs	6.05	0.50	5.27	3.31	1.73	6.03
Zr	181	4	110	45	38	208
Hf	5.37	0.50	3.23	1.41	1.24	5.28
Nb	15	3	8	5	4	22
Ta	1.94	0.20	0.89	0.39	0.30	1.64
Y	247	14	22	16	15	92
Th	16.90	0.55	11.10	5.60	4.71	14.70
U						
La	152.0	19.4	25.9	15.1	12.2	70.7
Ce	252.0	10.2	58.7	25.5	20.1	232.0
Nd	197.0	11.1	25.2	11.9	13.6	84.5
Sm	42.2	2.0	6.0	2.6	2.8	18.6
Eu	10.30	0.46	1.47	0.57	0.40	4.23
Gd						
Tb	6.61	0.50	1.06	0.38	0.32	2.96
Dy						
Ho	8.42	0.52	1.05	0.50	0.50	3.20
Er						
Yb	21.40	0.93	2.91	1.20	1.11	7.00
Lu	3.37	0.14	0.41	0.21	0.19	1.05
Cr	39	22	23	57	62	83
Ni	374	19	59	28	30	197
V	149	33	50	9	22	129
Sc	28		3			39
Measured isotope ratios						
87Sr/86Sr	0.71237	0.70781		0.70981	0.70937	
143Nd/144Nd	0.512213	0.512207		0.511906	0.511964	
208Pb/204Pb	38.887	38.591		39.630	39.400	
207Pb/204Pb	15.670	15.652		15.776	15.782	
206Pb/204Pb	18.751	18.560		19.308	19.196	

Table 4.1 cont.

Sample	DSDP 27 261 8-5:20-22	DSDP 27 261 14-1:75-77	DSDP 27 261 22-5:21-24	DSDP 27 261 25-3:29-31	DSDP 27 261 29-2:29-31
Lithology	Clay	Claystone	Claystone	Claystone	Claystone
Age	Upper Cretaceous	Lower Cretaceous	Lower Cretaceous	Lower Cretaceous	Lower Cretaceous
SiO2	54.18	58.56	69.08	67.75	78.93
TiO2	1.12	0.74	0.65	0.47	0.37
Al2O3	15.36	10.96	7.13	6.28	5.13
Fe2O3	9.04	7.98	5.28	5.69	4.49
MnO	0.64	0.06	0.03	0.65	0.04
MgO	3.29	2.78	2.29	1.98	1.79
CaO	0.54	0.52	0.43	3.74	0.28
Na2O	2.22	1.99	1.39	1.15	0.97
K2O	3.54	2.24	2.04	1.48	1.56
P2O5	0.11	0.09	0.07	0.18	0.04
L.O.I.	9.40	13.97	11.25	10.30	5.87
Total	99.44	99.89	99.64	99.67	99.47
Rb	112	74	47	40	36
Ba	327	1423	596	3512	1063
Sr	146	89	53	130	51
Pb	20	28	14	19	15
Cs	5.82			1.57	0.96
Zr	204	143	104	82	100
Hf	5.13			2.12	2.69
Nb	22	14	12	7	11
Ta	0.99			0.58	0.73
Y	28	25	18	32	15
Th	11.40	9	6	6	5
U					
La	32.4			32.8	21.0
Ce	161.0			87.7	57.1
Nd	30.6			32.6	18.6
Sm	6.8			6.5	3.5
Eu	1.57			1.46	0.67
Gd					
Tb	1.34			0.97	0.40
Dy					
Ho	1.28			1.11	0.47
Er					
Yb	2.52			2.17	1.27
Lu	0.36			0.34	0.20
Cr	82	67	33	26	24
Ni	115	65	31	38	32
V	126	204	98	40	71
Sc	26	18	12	15	9
Measured isotope ratios					
87Sr/86Sr	0.71694	0.71710		0.71079	0.71522
143Nd/144Nd	0.512115	0.512215		0.512300	0.512240
208Pb/204Pb	39.393	38.813		38.919	38.752
207Pb/204Pb	15.767	15.656		15.682	15.646
206Pb/204Pb	18.891	18.572		18.673	18.576

Table 4.1 cont.

Sample	DSDP 27 261 31-4:26-28	DSDP 27 261 32-2:58-61	RC 14-67 103-107	V 28-341 115-118	V 28-343 63-67	V 28-343 325-326.5
Lithology	Claystone	Claystone	Volcanogenic	Biogenic	Peagic Clay	Diatom Clay
Age	Lower Cretaceous	Lower Cretaceous	Quaternary	Quaternary	Quaternary	Quaternary
SiO2	61.53	21.21	57.91	31.30	54.15	56.44
TiO2	0.79	0.42	0.58	0.40	0.67	0.56
Al2O3	11.98	4.47	18.30	11.18	16.05	13.31
Fe2O3	7.27	4.75	6.12	4.13	6.52	5.20
MnO	0.27	0.50	0.12	0.04	0.49	0.10
MgO	3.08	1.25	2.85	2.63	2.83	2.62
CaO	2.55	33.32	8.27	21.06	0.75	1.04
Na2O	1.49	0.69	3.19	1.42	3.77	4.47
K2O	2.47	1.16	0.76	0.93	2.23	1.95
P2O5	0.15	0.10	0.11	0.17	0.14	0.08
L.O.I.	7.97	32.26	2.04	26.30	12.13	14.19
Total	99.55	100.13	100.25	99.56	99.73	99.96
Rb	73	29	25	79.7	105	83
Ba	3064	49	246	1440	755	537
Sr	131	102	456	778	120	103
Pb	31	27	10	15	31	21
Cs	3.80			5.05	6.77	6.52
Zr	187	54	57	77	116	96
Hf	4.29			2.17	2.76	2.80
Nb	18	5	3	7	10	9
Ta	1.12			0.64	0.98	0.44
Y	38	24	15	19	24	19
Th	11.50	4	2	5	11.10	9.58
U					1.91	
La	39.3			19.8	25.6	22.7
Ce	120.0			39.3	59.4	51.4
Nd	42.0			17.3	28.6	22.8
Sm	9.1			3.4	5.2	4.8
Eu	1.83			0.74	0.87	1.06
Gd				2.99	4.40	
Tb	0.94				0.74	0.77
Dy				2.78	4.08	
Ho	1.16				0.98	0.87
Er				1.69	2.38	
Yb	2.88			1.66	2.48	2.13
Lu	0.46			0.248	0.39	0.35
Cr	56	22	16	84	72	45
Ni	76	42	11	58	78	77
V	113	46	106	109	118	90
Sc	22	22	18	18	17	9
Measured isotope ratios						
87Sr/86Sr		0.71079	0.70585	0.70996	0.71682	
143Nd/144Nd		0.512238	0.512734	0.512162	0.512163	
208Pb/204Pb		38.662	39.171	39.230	39.328	
207Pb/204Pb		15.651	15.674	15.697	15.741	
206Pb/204Pb		18.580	18.902	18.960	18.990	

Table 4.1 cont.

Sample	V 28-343 564-566	V 28-343 750-751.5	V 28-343 1050-1051.5	V 28-343 1142-1143.5	V 33-75 316-318
Lithology	Clay	Clay	Clay/Volcanogenic	Clay	Terrigenous/Biogenic
Age	Quaternary	Quaternary	Quaternary	Quaternary	Quaternary
SiO2	54.83	55.51	55.28	55.36	49.93
TiO2	0.59	0.61	0.80	0.60	0.73
Al2O3	15.05	15.09	15.38	14.83	17.77
Fe2O3	5.91	5.80	6.83	6.70	6.46
MnO	0.11	0.09	0.11	0.12	0.08
MgO	2.84	2.69	2.72	2.93	2.53
CaO	0.66	0.67	2.44	0.60	4.21
Na2O	4.53	3.81	4.30	4.31	2.91
K2O	2.10	2.28	1.91	2.20	1.45
P2O5	0.10	0.09	0.21	0.10	0.12
L.O.I.	13.74	12.79	10.06	12.61	13.83
Total	100.46	99.43	100.04	100.36	100.02
Rb	84	93	69	87	57
Ba	379	724	489	629	156
Sr	92	108	159	100	196
Pb	23	23	19	23	14
Cs	7.50	6.65	4.44	6.54	5.57
Zr	97	111	112	105	122
Hf	2.54	3.06	3.54	3.16	2.91
Nb	9	9	9	9	8
Ta	0.63	0.49	0.40	0.68	0.86
Y	20	20	24	23	20
Th	11.10	11.10	8.17	10.40	9.48
U					
La	25.1	25.2	21.8	24.2	17.5
Ce	58.5	59.8	40.1	55.2	38.0
Nd	30.5	31.2	19.4	25.9	17.0
Sm	5.3	5.3	4.5	5.3	3.6
Eu	1.10	1.03	1.26	1.31	0.90
Gd					3.37
Tb	0.91	1.00	0.74	0.63	
Dy					3.29
Ho	0.98	0.98	0.93	0.87	
Er					1.96
Yb	2.31	2.23	2.38	2.36	1.97
Lu	0.39	0.35	0.33	0.36	0.298
Cr	39	56	40	52	48
Ni	84	99	65	64	24
V	71	102	113	98	108
Sc	9	12	14	11	13
Measured isotope ratios					
87Sr/86Sr					0.70925
143Nd/144Nd					0.512481
208Pb/204Pb					39.170
207Pb/204Pb					15.712
206Pb/204Pb					18.818

Table 4.1 cont.

Sample	V 33-77 382-384	V 33-79 17-19	V 34-45 35-37	V 34-47 143-145.5	VM 28 RD 14-2 sediment
Lithology	Terrigenous/Biogenic	Terrigenous	Peagic Clay	Terrigenous	Sediment
Age	Quaternary	Quaternary	Quaternary	Quaternary	Quaternary
SiO2	54.95	48.41	53.21	49.95	47.29
TiO2	0.73	0.72	0.60	0.62	2.96
Al2O3	12.70	17.54	18.02	17.73	13.74
Fe2O3	6.52	8.36	6.44	6.82	10.47
MnO	0.09	0.10	0.99	0.70	0.26
MgO	2.27	2.57	4.07	3.39	2.74
CaO	9.25	3.22	0.91	0.56	1.66
Na2O	2.33	3.17	5.74	4.36	3.85
K2O	1.13	1.37	1.87	1.92	3.49
P2O5	0.12	0.11	0.32	0.20	0.48
L.O.I.	9.37	14.61	8.14	13.16	13.39
Total	99.46	100.18	100.31	99.41	100.33
Rb	36	46	58	85	72
Ba	130	129	1319	2342	175
Sr	432	160	128	111	206
Pb	12	17	40	37	7
Cs	2.14	3.73	3.65		
Zr	170	110	162	133	364
Hf	5.20	3.04	4.22	3.82	
Nb	6	6	9	10	87
Ta	0.45	0.47	0.68		
Y	19	18	78	49	23
Th	6.60	7.07	14.70	40.20	6
U	1.88	2.28	1.47	3.81	
La	14.0	12.9	46.4		
Ce	29.7	28.2	93.6		
Nd	13.8	13.4	59.6	39.9	
Sm	3.0	3.0	14.2	8.7	
Eu	0.81	0.84	3.38		
Gd	2.89	2.87			
Tb			2.50		
Dy	2.84	2.95			
Ho			3.03		
Er	1.74	1.75			
Yb	1.73	1.75	7.38		
Lu	0.261	0.273	1.10	0.588	
Cr	58	45	49	63	12
Ni	26	28	265	130	94
V	113	109	103	117	101
Sc	11	16	24	21	26
Measured isotope ratios					
87Sr/86Sr	0.70827	0.70802	0.71162	0.71326	
143Nd/144Nd	0.512492	0.512507	0.512278	0.512263	
208Pb/204Pb	38.867	38.950	38.800	39.083	
207Pb/204Pb	15.624	15.679	15.660	15.683	
206Pb/204Pb	18.738	18.670	18.850	18.885	

It is not necessary to describe here the new samples and major and trace element analytical results, as the same samples, or splits from the same cores, have been already analysed and the results discussed (references quoted in this chapter). As has been pointed out, the aim of this chapter is to provide a realistic estimate of average, representative compositions of oceanic sediments, and the new analytical data are provided to expand the qualitatively poor database, and to investigate Sr, Nd, and Pb isotope systematics in recent and old sediments with different chemical composition.

4.4 Variations in chemical composition of Northeastern Indian Ocean sediments

Principal component analysis (Le Maitre 1982) was used in this study to identify possible different populations within the mass of data, following an approach similar to that already successfully applied to Northeastern Indian Ocean sediments by Cook (1974). This approach is a useful approximation in this case, because sediments can easily be characterised - at least for the purposes of this discussion - by their chemical composition.

Table 4.2 shows the values of the eigenvectors for all the major and some trace elements using compositional data for those sediments for which full data are available; mainly data from Plank & Ludden (1992), and from this study, and including analytical data previously published by Ben Othman et al. (1989) and augmented here. The same relationships can be observed when the database is expanded to include the majority of analyses of Northeastern Indian Ocean sediments, although most are incomplete.

The first vector, which accounts for 52.8 % of the variance within the set of data, clearly shows that there is a very good positive correlation between Sr and CaO, and that these elements are negatively correlated with all the others. The first vector also reflects the similarities in behaviour of REEs and Y, and the mutual affinity of the ferro-magnesian elements expressed as Fe_2O_3, MnO, MgO, and Ni. The second vector shows again a positive correlation between CaO, REE, Y, MnO, P_2O_5, and Sr. Also, notice the anomalous behaviour of Ce compared with the other REEs, and the positive correlation between Rb and K_2O.

The first and second vectors, which together account for most (74 %) of the variance, clearly show the existence of two distinct populations: silicic-clastic sediments, and

	Vector 1	Vector 2	Vector 3	Vector 4
Rb	-0.15	-0.28	-0.11	-0.06
Ba	0.00	-0.08	0.07	0.87
Sr	0.16	0.20	-0.29	0.08
Pb	-0.20	0.06	0.27	0.19
Zr	-0.18	-0.20	-0.19	-0.02
Nb	-0.14	-0.20	-0.30	-0.05
Y	-0.22	0.21	-0.05	0.01
Th	-0.24	-0.08	0.11	-0.06
La	-0.23	0.17	-0.09	0.00
Ce	-0.24	0.03	-0.15	0.03
Nd	-0.23	0.18	-0.05	0.00
Sm	-0.23	0.18	-0.04	0.01
Eu	-0.23	0.19	-0.02	-0.01
Yb	-0.22	0.21	0.00	-0.02
Lu	-0.22	0.21	0.00	-0.02
Cr	-0.04	-0.21	-0.33	0.20
Ni	-0.22	0.16	0.04	0.09
V	-0.19	-0.14	-0.08	0.17
SiO2	-0.13	-0.25	0.31	0.04
TiO2	-0.17	-0.26	-0.17	-0.14
Al2O3	-0.17	-0.20	0.21	-0.13
Fe2O3	-0.22	-0.17	-0.06	-0.09
MnO	-0.20	0.22	0.03	0.04
MgO	-0.20	-0.17	0.03	0.19
CaO	0.17	0.23	-0.27	0.01
Na2O	-0.06	-0.01	0.50	-0.14
K2O	-0.18	-0.22	-0.17	-0.12
P2O5	-0.20	0.24	-0.09	-0.02

Variance proportion

Vector 1	0.528
Vector 2	0.212
Vector 3	0.116
Vector 4	0.042
Vector 5	0.027
Vector 6	0.021
Vector 7	0.014
Vector 8	0.012
Vector 9	0.008
Vector 10	0.005
Vector 11	0.005
Vector 12	0.004
Vector 13	0.002
Vector 14	0.002

Total variance	0.998
Total variance (first four vectors)	0.898

Table 4.2. Values of the first four eigenvectors, and variance proportion in a principal component analysis of sediments of the Northeastern Indian Ocean. Eigenvectors and variance were calculated using a StatView 512+™ software, and were extracted from a correlation matrix (see Le Maitre 1982, pages 106-121 for explanations).

Ca-Sr(-Mn-P-REEs-Y, and presumably U)-rich calcareous-organogenic sediments.

Further interpretation of these data is difficult, as already observed by Cook (1974), because the large differences in chemical composition between clastic and organogenic sediments mask the small differences within each group, and most elements have a complex behaviour, which, as will be discussed later in this chapter, depends strongly on the type of sediment and on the relative amounts of major elements.

Because the different behaviour of CaO (see Table 4.2) is responsible for many of the variations observed within the database, the two populations previously identified can be defined very well using CaO contents.

The histogram in Figure 4.1 shows the two CaO populations, one with a restricted CaO range with values up to approximately 5 %, and the other with most values in the range 30 % to 50 %, and the sediments can be subdivided into silicic-clastic sediments (SS) with CaO contents < 5-6% and calcareous-organogenic sediments (CS) with CaO contents > 5-6 %.

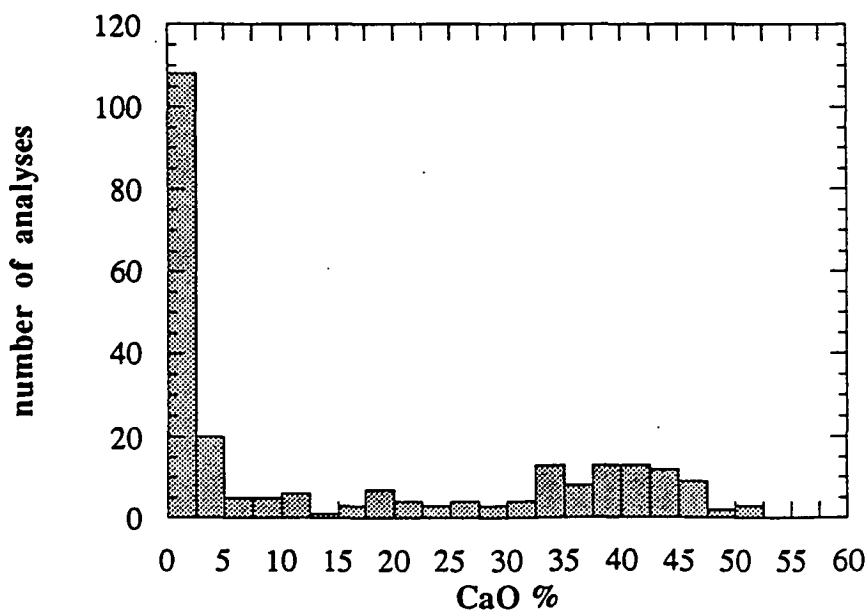

Figure 4.1. Histogram of CaO in sediments of the Northeastern Indian Ocean.

The placement of the boundary between the two populations at CaO = 5-6 % is arbitrary, because a considerable amount of data (approximately 18 % of the total) has CaO contents intermediate between the two groups (see Figure 4.1). However, the boundary was placed at CaO = 5-6 % for the following reasons:

1) unlike the CS, the SS show a very narrow and symmetrical distribution for CaO, suggesting a very homogeneous population with a very restricted compositional range;

2) the value of CaO = 5-6 % corresponds to the median (50 per cent value) in a cumulative curve (Figure 4.2), and the slope of the curve changes considerably for CaO > 5-6 %;

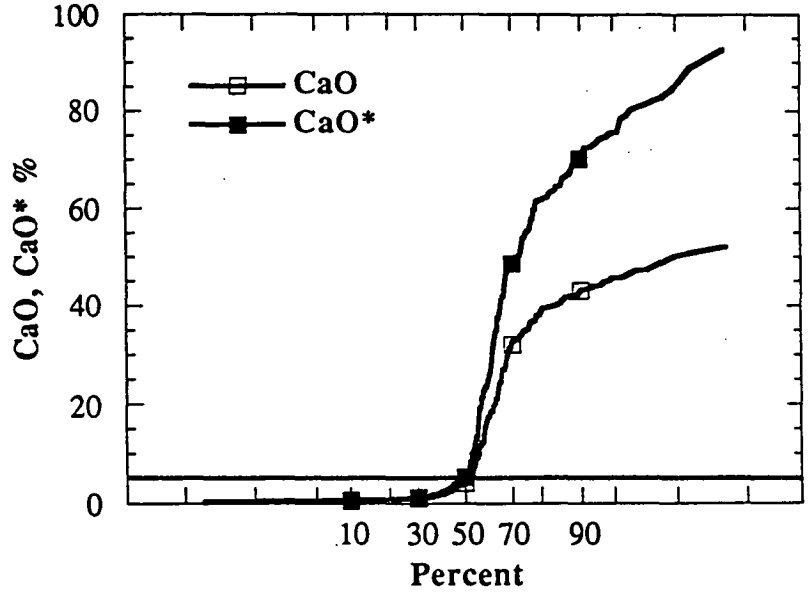

Figure 4.2. Cumulative curve of CaO in sediments of the Northeastern Indian Ocean. CaO is the actual measured CaO, whereas CaO* is the CaO value recalculated L.O.I.-free. The two values do not differ significantly for low Ca contents. The thick horizontal line marks the CaO content for the 50 % (median) value.

3) according to the lithological descriptions, relatively "pure" silicic-clastic sediments are common in the Northeastern Indian Ocean, while "pure" calcareous-organogenic sediments are rare, and usually contain variable amounts of silicic material - a "pelagic sediment" component.

4) the simple distinction into only two endmembers is appropriate, considering the amount and distribution of data, and the amount of samples relative to the extent of the area discussed. A further subdivision of the database into more populations could be numerically more accurate but would create statistically (and geologically) non representative groups.

The boundary at CaO = 5-6 %, therefore, defines a SS group with geochemical composition typical of a clay, with only a negligible CS component, whereas the CS group is not a "pure" endmember, but a more quantitatively realistic calcareous-organogenic sediment plus a certain amount of SS.

In Table 4.3 the calculated average composition of each group is reported, together with the composition of typical PAAS (Taylor & McLennan 1985), which will be used throughout this chapter as a reference composition for a terrigenous shale. As the database is dominated by data from Plank & Ludden (1992), the average composition of each group at sites 765 AND 261 (the only other site for which there is a reasonable amount of data), and for the database excluding site 765 (Table 4.4) were also calculated for comparison.

These tables show that no large, statistically significant differences exist among the single sites and the total averages. At site 261, Ba and Ce are similar to the average SS except for an anomalous sample with very high values which increase considerably the average Ba and Ce of the site. Also, Cs and Rb at site 261 are slightly low because many of the samples analysed for most trace elements are claystones, with low Cs and Rb contents (probably due to the loss of Cs and Rb during the early stages of compaction). Other minor differences appear when the amount of data is not statistically representative. The relatively large standard deviations indicate that a considerable scatter is present within each group, but for most elements within each endmember there is only one population, the median (50 % value) is reasonably close to the average value, and the distribution of the data within each endmember is nearly symmetrical with respect to the average composition.

The calculated average compositions are therefore sufficiently representative of the two endmembers, and because the set of data (which can be considered as a random sampling of the different types of sediments) covers all the observed compositions of sediments in the area, these two endmembers and their possible combinations can be used to describe from a geochemical point of view the sedimentary material in the

	Northeastern Indian Ocean Average Silicic sediments			Northeastern Indian Ocean Average Calcareous-organogenic sediments			PAAS
	#	(SS)	Std	#	(CS)	Std	Average
SiO2	140	59.06	9.25	116	22.96	15.09	60.08
TiO2	145	0.69	0.20	122	0.28	0.19	0.96
Al2O3	146	13.48	3.69	124	5.85	3.86	18.08
Fe2O3	138	7.02	2.02	121	2.69	1.77	6.84
MnO	140	0.39	0.51	119	0.13	0.14	0.11
MgO	145	2.90	0.89	124	2.37	1.72	2.10
CaO	146	1.62	1.36	124	31.91	12.37	1.24
Na2O	134	2.31	1.14	115	1.02	0.73	1.15
K2O	145	2.44	0.80	123	1.02	0.66	3.54
P2O5	136	0.18	0.12	118	0.11	0.05	0.15
LOI	138	9.62	3.90	118	31.00	9.03	5.74
Total		99.71			99.34		100.00
CaCO3 calc		2.13			56.80		
CO2 calc		0.94			24.99		
H2O calc		8.68			6.01		
Rb	65	83	30	48	40	21	160
Ba	132	856	815	107	294	233	650
Sr	136	160	89	121	1258	793	200
Pb	68	22	10	47	13	9	20
Cs	41	5.15	1.82	15	2.80	1.59	15
Zr	92	143	36	72	73	34	210
Hf	42	4.00	1.30	15	2.43	1.42	5
Nb	63	12	4	47	5	2	19
Ta	40	0.89	0.34	15	0.55	0.28	
Y	91	29	12	74	14	9	27
Th	44	10.40	3.00	17	4.90	2.50	14.6
U	21	1.29	0.49	11	1.21	0.59	3.1
La	39	34.80	13.70	15	20.00	9.20	38
Ce	63	82.60	33.20	47	24.40	17.50	80
Nd	38	31.90	11.60	15	16.70	8.00	32
Sm	38	6.97	2.73	15	3.60	1.90	5.6
Eu	37	1.48	0.61	15	0.76	0.41	1.1
Tb	35	0.94	0.33	13	0.53	0.25	0.77
Ho	16	1.11	0.36	3	0.51	0.01	1
Yb	36	2.85	0.95	15	1.73	0.74	2.8
Lu	37	0.45	0.15	15	0.27	0.11	0.43
Cr	95	64	32	75	41	24	110
Ni	136	85	55	120	33	28	55
V	99	118	38	79	57	35	150
Sc	71	16	6	39	8	6	16

Table 4.3. Calculated average compositions of silicic sediments (SS) and calcareous-organogenic sediments (CS). Also reported in the table is the number of analyses used to calculate the averages (#), the standard deviations (Std), and the average composition of PAAS (from Taylor & McLennan 1985). $CaCO_3$ contents are calculated from data by Plank & Ludden (1992), dividing their data set into two subsets (CaO < 3.7 and CaO > 6.2), and assuming the same $CaO/CaCO_3$ values measured by Plank & Ludden (1992) in the two subsets. CO_2 was calculated from $CaCO_3$, and H_2O is L.O.I.-CO_2. The average value of some elements is not reported because it is not statistically significant.

	1 Site 765 SS			2 Site 261 SS			3 All sites (excluding 765) SS		
	#		Std	#		Std	#		Std
SiO2	71	61.45	7.45	16	63.95	9.94	70	56.62	10.16
TiO2	71	0.77	0.18	16	0.63	0.25	75	0.62	0.20
Al2O3	71	14.45	3.53	16	10.38	4.41	75	12.56	3.62
Fe2O3	66	7.25	2.09	15	6.47	1.64	72	6.66	1.91
MnO	71	0.34	0.54	16	0.44	0.43	69	0.41	0.42
MgO	71	3.40	1.32	16	2.56	0.67	74	2.56	0.61
CaO	71	1.36	1.43	16	1.28	0.94	75	1.98	1.48
Na2O	71	1.83	0.77	16	2.17	1.05	63	2.79	1.26
K2O	70	2.65	0.90	16	2.24	0.74	75	2.24	0.63
P2O5	71	0.16	0.08	16	0.17	0.19	66	0.19	0.15
LOI	71	7.30	2.68	16	9.76	2.47	67	12.03	3.49
Total		100.96			100.05			98.66	
CaCO3 calc		1.79			1.69			2.61	
CO2 calc		0.79			0.74			1.15	
H2O calc		6.51			9.02			10.88	
Rb	40	89	32	8	70	30	24	73	25
Ba	70	969	1026	16	1347	1125	63	811	799
Sr	71	193	116	13	110	57	66	136	79
Pb				15	20	9	66	22	10
Cs	19	5.42	1.89	6	3.91	2.20	21	4.85	1.77
Zr	71	152	53	8	142	51	23	124	35
Hf	19	4.42	1.12	6	3.79	1.31	23	3.66	1.36
Nb	40	15	14	8	14	6	23	10	5
Ta	19	0.94	0.20	6	0.99	0.37	22	0.92	0.56
Y	71	30	12	8	34	25	24	36	26
Th	19	10.27	2.69	8	9.34	3.42	23	10.50	2.99
U	19	1.25	0.49				3	2.40	1.24
La	19	36.66	11.94	6	37.02	17.66	20	33.08	15.27
Ce	45	86.29	34.96	6	119.42	67.79	20	86.65	48.81
Nd	19	31.12	11.23	6	38.92	23.65	21	38.16	20.85
Sm	19	7.06	2.68	6	8.44	5.29	21	8.19	4.98
Eu	19	1.42	0.55	6	1.87	1.22	20	1.87	1.21
Tb	19	0.93	0.36	6	1.28	0.89	19	1.24	0.77
Ho				6	1.38	0.94	19	1.50	1.01
Yb	19	2.97	0.95	6	3.12	1.99	19	3.18	1.69
Lu	19	0.46	0.15	6	0.47	0.30	20	0.49	0.24
Cr	71	71	34	8	49	26	24	50	18
Ni	71	88	50	16	84	68	68	89	72
V	68	124	38	8	104	53	30	105	38
Sc	46	15	4	8	18	11	24	16	8

Table 4.4. Calculated compositions of SS at site 765, 261, and for the whole database excluding site 765 (column 1, 2, and 3 respectively), and of CS at site 765, 261, and for the whole database excluding site 765 (column 4, 5, and 6 respectively). See Table 4.3 for the recalculation of $CaCO_3$, CO_2, and H_2O.

Table 4.4 cont.

	4 Site 765 CS			5 Site 261 CS			6 All sites (excluding 765) CS		
	#		Std	#		Std	#		Std
SiO2	66	21.77	13.95	6	17.06	3.21	48	23.41	15.80
TiO2	66	0.27	0.16	6	0.24	0.09	54	0.28	0.21
Al2O3	66	5.37	3.27	6	5.02	1.39	56	6.14	4.26
Fe2O3	65	2.27	1.49	5	2.54	0.73	54	3.10	1.96
MnO	64	0.11	0.12	6	0.28	0.19	53	0.16	0.17
MgO	66	2.23	1.51	6	1.20	0.22	56	2.42	1.82
CaO	66	34.98	10.95	6	36.34	3.54	56	29.19	12.59
Na2O	66	0.57	0.37	6	1.19	0.43	47	1.63	0.67
K2O	66	0.90	0.57	6	0.92	0.27	55	1.12	0.72
P2O5	66	0.10	0.05	6	0.08	0.04	50	0.11	0.06
LOI	66	31.68	7.91	6	34.80	1.95	50	30.81	9.87
Total		100.25			99.67			98.37	
CaCO3 calc		61.99			64.69			51.96	
CO2 calc		27.28			28.46			22.86	
H2O calc		4.40			6.34			7.95	
Rb	40	41	21	3	36	10	7	36	23
Ba	63	371	456	6	314	211	43	325	237
Sr	65	1536	856	6	990	450	54	958	567
Pb				6	12	9	48	14	11
Cs	10	2.93	1.60	2	2.52	1.12	5	2.55	1.72
Zr	65	72	32	3	46	8	7	64	52
Hf	10	2.59	1.25	2	1.32	0.12	5	2.10	1.83
Nb	40	5	3	3	5	1	7	5	1
Ta	10	0.63	0.29	2	0.34	0.06	5	0.40	0.17
Y	65	13	8	3	18	5	7	17	3
Th	10	5.50	2.76	3	4.77	0.80	7	4.07	2.11
U	10	1.15	0.57				1	1.88	
La	10	21.95	10.66	2	13.65	2.05	5	16.10	3.36
Ce	42	24.37	18.27	2	22.80	3.82	5	24.96	10.84
Nd	10	18.22	9.45	2	12.75	1.20	5	13.54	2.39
Sm	10	4.03	2.22	2	2.68	0.14	5	2.76	0.50
Eu	10	0.85	0.47	2	0.48	0.12	5	0.60	0.18
Tb	10	0.57	0.27	2	0.35	0.04	3	0.40	0.09
Ho				2	0.50	0.00	3	0.51	0.01
Yb	10	1.94	0.81	2	1.15	0.06	5	1.33	0.35
Lu	10	0.29	0.12	2	0.20	0.01	5	0.21	0.05
Cr	65	39	22	3	47	22	8	48	25
Ni	65	29	25	6	27	9	53	37	31
V	65	50	29	3	26	19	13	88	45
Sc	34	6	4	1	22		4	17	5

Figure 4.3 shows that the SS have a REEs pattern similar to PAAS and are only slightly enriched in all the REEs compared with typical upper crust (average composition of upper crust, from Taylor & McLennan 1985), without any significant anomalies. On the other hand, CS have overall lower REEs values, similar to lower crust (average composition of lower crust, from Taylor & McLennan 1985), but without the positive Eu anomaly and with a significant negative Ce anomaly (the negative Ho anomaly is not statistically significant due to the small number of Ho analyses). CS also have overall trace element contents lower than SS (Figure 4.4), and define a trend parallel to the SS, except for the already mentioned Ce negative anomaly, and positive Sr and U anomalies. Compared with PAAS, both SS and CS are depleted in LILE - except Ba - and HFSE, and the SS closely resemble typical average upper crust, except for the lower U and the already mentioned higher REEs values.

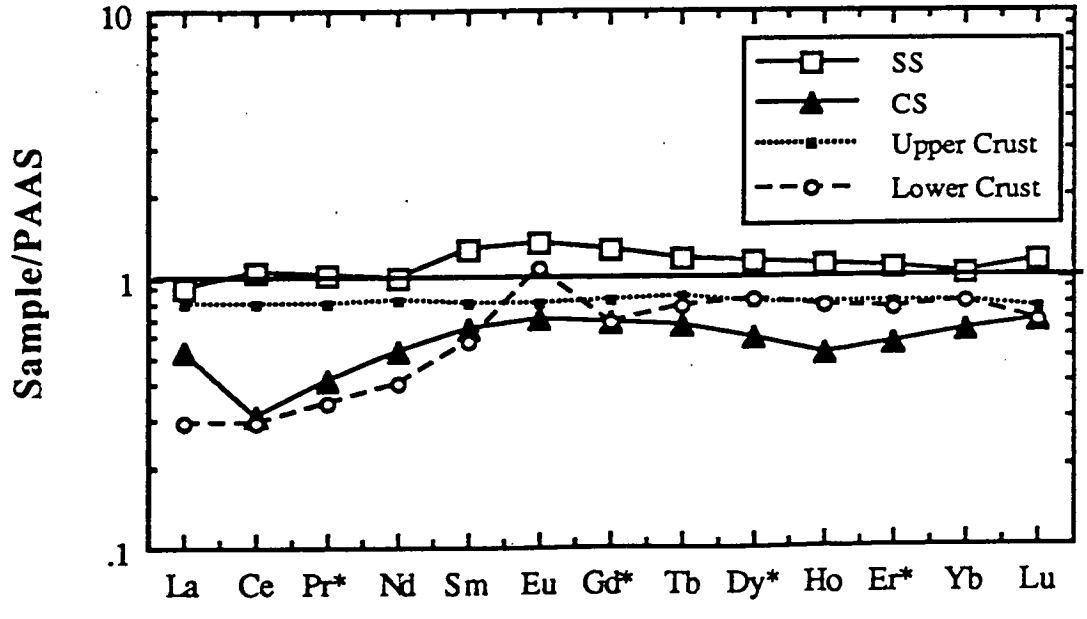

Figure 4.3. PAAS-normalised REE plot for CS and SS. PAAS, and upper and lower crust compositions (for comparison) are from Taylor & McLennan (1985). Pr*, Gd*, Dy*, and Er* in CS and SS are interpolated from the other REEs.

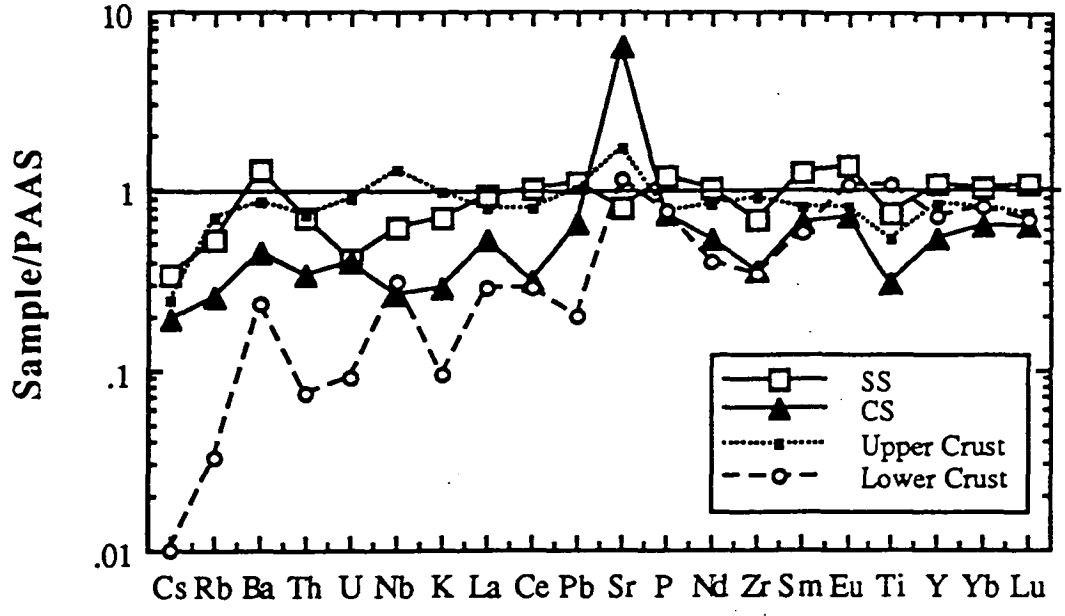

Figure 4.4. PAAS-normalised trace element plot for CS and SS. PAAS, and upper and lower crust compositions (for comparison) are from Taylor & McLennan (1985).

4.5 Origin of the difference between the two endmembers

As the trace element contents are higher in SS than in CS, to a first approximation and following the approach of Cook (1974) and Plank & Ludden (1992), it can be expected that CS are equivalent to SS diluted by $CaCO_3$. Furthermore, $CaCO_3$ can be seen as a pure diluent in CS, while excess SiO_2 (pure silica, i.e. Si that is not incorporated within the clay crystal structure but mainly present as detrital quartz and radiolarian-rich material) can be seen as a pure diluent within the field of the SS. It follows that the differences between SS and CS should disappear when they are normalised $CaCO_3$-free and excess Si-free.

In Table 4.5 are reported the results of these calculations. The average $CaCO_3$ content in SS was estimated from the $CaCO_3$ and CaO contents in clays reported by Plank & Ludden (1992), and the CO_2, and residual L.O.I. (L.O.I.* = L.O.I. - CO_2) and CaO

(CaO* = total CaO - CaO in $CaCO_3$) were calculated accordingly. For the CS, the average $CaCO_3$ calculated from data from Plank & Ludden (1992) was actually slightly too high for the CaO content in CS, and a lower $CaCO_3$ value was therefore estimated assuming that all the CaO in the CS goes into $CaCO_3$.

Estimation of the excess SiO_2 is more complex and model-dependent. In Table 4.5 the normalised major element compositions of SS and CS are similar except for the higher SiO_2 and lower L.O.I. in SS and higher MgO, P_2O_5, and L.O.I. in CS. The final "diluents"-free compositions of SS and CS (Table 4.5) were recalculated using the simplifying assumptions that the excess MgO in CS is due to the presence of magnesite and that the difference between SiO_2 in SS and CS is the excess SiO_2 in SS. The normalising factor required to take into account the SS dilution by excess SiO_2 was estimated to be approximately 1.1 (approximate ratio between SiO_2 in SS and SiO_2 in CS).

These simple calculations show that the differences in major element composition between SS and CS can be explained by dilution of SS by SiO_2 (and less importantly by $CaCO_3$), and by the strong dilution of CS by $CaCO_3$ (and less importantly by $MgCO_3$). The residual excess L.O.I. observed in the final calculated CS is probably due to minor amounts of carbonates, sulphates, and other hydrous phases which have not been taken into account in the calculation.

The recalculated trace element contents in Table 4.5 and Figures 4.5 and 4.6 show that:

1) even assuming that $MgCO_3$ is a pure diluent in CS, recalculated CS trace elements have systematically slightly higher REE and P than SS. As suggested by the principal component analysis (see also Plank & Ludden 1992), REEs are strongly correlated with P, and the higher REE values are probably due to the presence of P-rich phases which have not been taken into account in the calculations.

2) Sr is obviously concentrated in $CaCO_3$, and $CaCO_3$ does not appear to be a completely pure diluent for P and Pb in CS. The Sr and P enrichment in CS can be explained by the presence of Sr- and P-rich phases, most likely organogenic, associated with $CaCO_3$, whereas the Pb enrichment is probably a consequence of the geochemical affinity of Pb with U (in situ U decay?), which is strongly enriched in the CS.

	1	2		3	4	5	6		7	8
	SS					CS				
SiO2	59.06	60.49	SiO2	54.15	57.81	22.96	54.16	SiO2	54.16	57.29
TiO2	0.69	0.71	TiO2	0.71	0.76	0.28	0.66	TiO2	0.66	0.70
Al2O3	13.48	13.81	Al2O3	13.81	14.74	5.85	13.80	Al2O3	13.80	14.60
Fe2O3	7.02	7.19	Fe2O3	7.19	7.68	2.69	6.35	Fe2O3	6.35	6.72
MnO	0.39	0.40	MnO	0.40	0.43	0.13	0.31	MnO	0.31	0.33
MgO	2.90	2.97	MgO	2.97	3.17	2.37	5.59	MgO	2.97	3.14
CaO*	0.46	0.47	CaO*	0.47	0.50	0.00	0.00	CaO*	0.00	0.00
Na2O	2.31	2.37	Na2O	2.37	2.53	1.02	2.41	Na2O	2.41	2.55
K2O	2.44	2.50	K2O	2.50	2.67	1.02	2.41	K2O	2.41	2.55
P2O5	0.18	0.18	P2O5	0.18	0.19	0.11	0.26	P2O5	0.26	0.28
LOI*	8.71	8.92	LOI*	8.92	9.52	5.96	14.06	LOI*	11.20	11.85
Total	97.64	100.00	excess SiO2	6.33		42.39	100.00	MgCO3*	5.47	
			Total	100.00	100.00			Total	100.00	100.00
CaCO3 calc.	2.07					56.95				
CO2 calc	0.94					25.04				
NF	1.02					2.36				
Rb	83	85			93	40	94			
Ba	856	873			960	294	694			
Sr	160	163			180	1258	2969			
Pb	22	22			25	13	31			
Cs	5.15	5.25			5.78	2.80	6.61			
Zr	143	146			160	73	172			
Hf	4.00	4.08			4.49	2.43	5.73			
Nb	12	12			13	5	12			
Ta	0.89	0.91			1.00	0.55	1.30			
Y	29	30			33	14	33			
Th	10.4	10.6			11.7	4.9	11.6			
U	1.29	1.32			1.45	1.21	2.86			
La	34.8	35.5			39.0	20.0	47.2			
Ce	82.6	84.3			92.7	24.4	57.6			
Nd	31.9	32.5			35.8	16.7	39.4			
Sm	6.97	7.11			7.82	3.60	8.50			
Eu	1.48	1.51			1.66	0.76	1.79			
Tb	0.94	0.96			1.05	0.53	1.25			
Ho	1.11	1.13			1.25	0.51	1.20			
Yb	2.85	2.91			3.20	1.73	4.08			
Lu	0.45	0.46			0.50	0.27	0.64			
Cr	64	65			72	41	97			
Ni	85	87			95	33	78			
V	118	120			132	57	135			
Sc	16	16			18	8	18			

Table 4.5. Compositions of SS and CS recalculated $CaCO_3$-free and excess silica-free. See text for explanations. L.O.I.* = L.O.I. minus calculated CO_2; CaO* = total CaO minus CaO in calculated $CaCO_3$. Column 1 - SS as in Table 4.3 (L.O.I. value is slightly different because of approximations in the recalculations); NF - normalising factor used to recalculate the SS composition $CaCO_3$-free. Column 2 - SS normalised $CaCO_3$-free (and major elements recalculated to total = 100%). These values correspond to SS norm.1 in Figures 4.5 and 4.6. Column 3 - recalculated major element composition of SS including the estimated content of excess SiO_2. Column 4 - recalculated SS composition $CaCO_3$-free and excess SiO_2-free. Trace elements are recalculated assuming an approximate normalising factor (to account for the excess SiO_2) of 1.1. These values correspond to SS norm.2 in Figures 4.5 and 4.6. Column 5 - CS as in Table 4.3 (L.O.I. and CO_2 values are slightly different because of approximations in the recalculations); NF - normalising factor used to recalculate the CS composition $CaCO_3$-free. Column 6 - CS normalised $CaCO_3$-free (and major elements recalculated to total = 100%). These values correspond to CS norm in Figures 4.5 and 4.6. Compare the trace element values with those of Column 4. Column 7 - recalculated major element composition of CS including the estimated content of $MgCO_3$. Column 8 - recalculated CS composition $CaCO_3$-free and $MgCO_3$-free. Compare these values with those of Column 4.

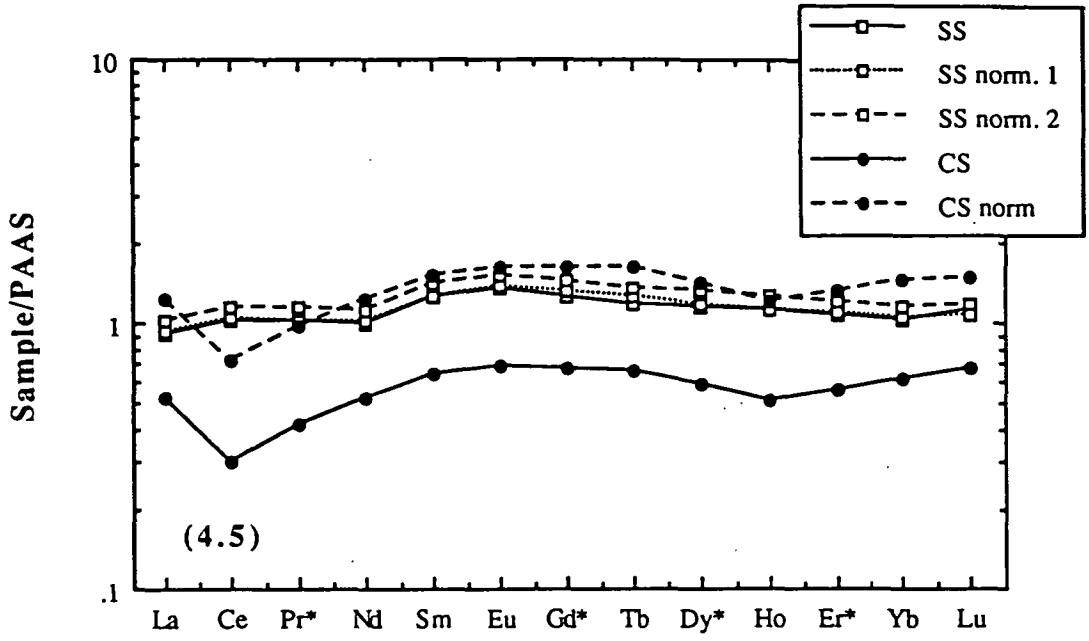

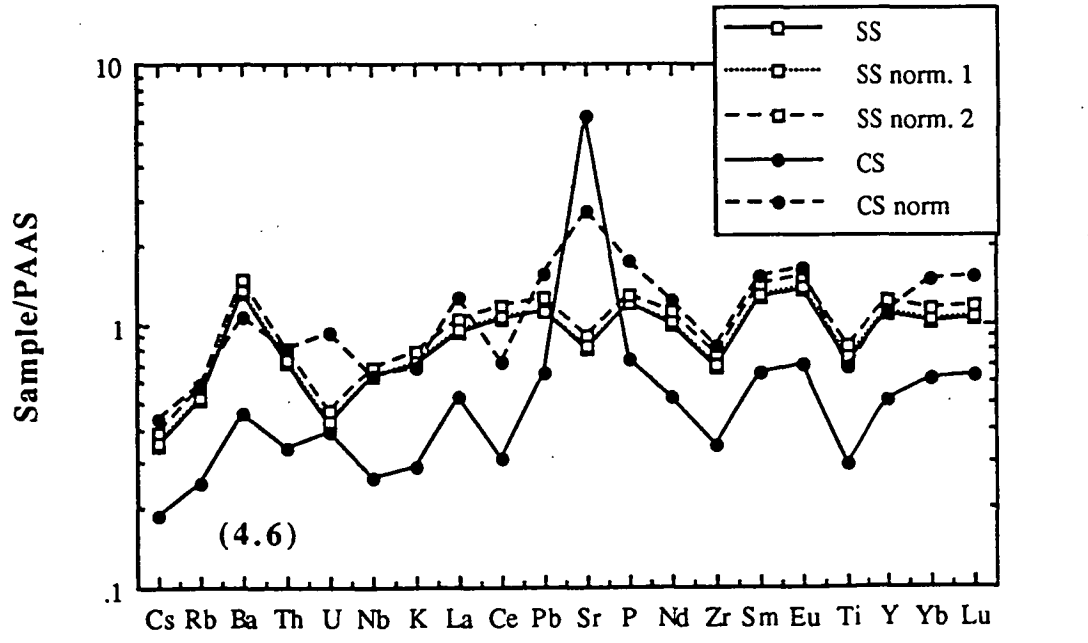

Figures 4.5 and 4.6. PAAS-normalised REE and trace element plots for CS and SS, CS and SS normalised $CaCO_3$-free (CS norm and SS norm.1), and SS further normalised excess silica-free (SS norm. 2). The Sr value in CS norm is actually the CS value divided by the normalising factor.

The seawater origin of Sr in CS has important implications for the Sr isotope systematics of CS. As the organogenic material is precipitated in equilibrium with seawater, the $^{87}Sr/^{86}Sr$ of CS should also be in equilibrium with that of the Sr in seawater. Due to the high Sr content, CS contamination can be very effective in increasing the $^{87}Sr/^{86}Sr$ value of the mixture, but this will never exceed that of seawater. Also, due to their very low Rb/Sr value, the $^{87}Sr/^{86}Sr$ value of CS will rise only slowly with time.

To the contrary, SS may not only have very high $^{87}Sr/^{86}Sr$ values inherited from their source rocks but also, due to their relatively high Rb/Sr values, their $^{87}Sr/^{86}Sr$ can be expected to increase relatively quickly with time. However, due to their relatively low Sr content, SS contamination is not as efficient in increasing the $^{87}Sr/^{86}Sr$ values of the resultant mixture. For these reasons, mixing between CS and SS will produce $^{87}Sr/^{86}Sr$ values similar to CS, excepting the case where there are very low amounts of CS in the mixture.

3) like Sr in $CaCO_3$, Ba in SS shows a positive correlation with the excess SiO_2, as Ba is enriched in radiolarian (SiO_2-rich) material.

4) if a negative Ce anomaly is typical of seawater (Elderfield & Greaves 1982), then these data suggest that the average SS retain their original REE signature, whereas the CS bear evidence for a strong sediment-seawater interaction, possibly for a high proportion of material precipitated from seawater. As a consequence, even when compared with chondritic values, only CS show a Ce negative anomaly.

The strong seawater signature of REEs in CS also has important implications for the Nd isotope systematics of CS. As with their $^{87}Sr/^{86}Sr$ systematics, the $^{143}Nd/^{144}Nd$ values of CS are likely to be similar to those of seawater, whereas the SS will again retain their original Nd isotope signature. However, unlike Sr concentrations in SS, Nd is relatively abundant, and therefore SS contamination will have a stronger influence on $^{143}Nd/^{144}Nd$ values. Due to the long half-life of ^{147}Sm and the relatively low Sm/Nd values, changes in $^{143}Nd/^{144}Nd$ values with time may be neglected for the sediments discussed here.

5) the conditions responsible for the oxidation of Ce (which produces the negative Ce anomaly) in the marine environment are associated with the formation of manganese nodules. Therefore, a negative Ce anomaly might be expected to be associated with low Mn concentrations. The Mn enrichment observed in CS shows that the Mn

concentrations are dependent on factors other than the precipitation of Mn-nodules. Although principal component analysis suggests that some correlation exists between Mn and the ferro-magnesian elements, the chemical behaviour of Mn is not well understood (see also Palmer 1985).

6) U is strongly concentrated in CS compared to SS. The geochemistry of U in a marine environment is also strongly dependent on the redox conditions of the depositional environment (Klinkhammer & Palmer 1991). Although it seems that U precipitates from seawater in the sediments as an inorganic compound (Langmuir 1978), the reaction seems to be initiated in an environment rich in organic material, and therefore the U enrichment is also strongly correlated with the organogenic $CaCO_3$. As for Nd, this might have important implications for the U-Th-Pb isotope systematics in SS and CS.

Therefore, bearing in mind that, for the reasons explained above, $CaCO_3$ and silica are not pure diluents for some elements, dilution processes will satisfactorily account for the important differences in element concentration between SS and CS. Minor differences exist, which are not due to different degrees of dilution, but which reflect the original characteristics of the source rocks of the sediments, but are very small and can only be detected when single samples are compared.

SiO_2 and $CaCO_3$ make up more than half of the composition in SS and CS, respectively, and therefore any major oxide plotted versus silica in clays and calcite in carbonates will have a negative slope. In other words, because silica and calcite are particularly abundant components, the differences in composition between CS and SS due to dilution by these components mask other differences related to the provenance of the sediments, when average compositions are compared. It is only possible to see whether an element is related to SiO_2 or $CaCO_3$ (see principal component analysis), but the relationships between one element and other major oxides are difficult to detect.

For example, samples 27 261/7-5:71-73 and 27 261/8-5:20-22 illustrate how important these relationships can be. These two clays have the same content of SiO_2 and Al_2O_3, and the content of calcite is likely to be negligible, if any. Nevertheless the values of many trace elements are different, and the different values of MnO, K_2O, TiO_2, Fe_2O_3 and MgO account for these differences. These relationships are virtually undetectable in the carbonates because of the strong dilution.

4.6 Effects of sediment contamination

It can be argued that the composition of the subducted sediment-derived material that eventually will contaminate the mantle is actually quite different from the measured composition of ocean-floor sediments, and despite the assumption that can be made about the ultimate composition of the "sediment-derived fluids" - based on the composition of rocks believed to represent previously subducted material (e.g. Reid et al. 1989; Barbey et al. 1990; Nelson 1991; Tilton et al. 1991) - the final estimates are always strongly model-dependent (e.g. Lin 1992). As White (1989, page 43) noted, "it is by no means clear that this process [recycling of continental crust into the mantle] is in fact responsible for all that it is called upon to account for", and Hart & Staudigel (1989, page 25) even concluded that "because of the myriad of possible processes operating in the subduction zone itself, which may short-circuit the long-term recycling process, and which may do so on a very element-specific basis [...] even a perfect knowledge of the composition of subducted oceanic crust and sediment will not help this situation".

Not only the element ratios, but also the absolute element abundances may be quite different in the "final product" compared with the initial sediment. The large amounts of CO_2, H_2O, and other volatile phases measured in sediments, where the "volatile" elements concentrate, are likely to be partly lost during the first stages of the subduction (e.g. Kay 1990; Moran et al. 1990; Peacock 1990; Pineau & Javoy 1990), leaving residues considerably depleted in LILE and LREE compared with the original sediments.

Despite the many reasonable assumptions that can be made, the selective loss of fluids with different compositions, and presumably with different relative element concentrations, dependent on the crystalline structure of the mineral phases that release these fluids, and on the thermodynamic and mechanical characteristics of the subducting slab, might create a very complex array of possible "sediment-derived fluids" (and melts).

However, if subducted sedimentary material is being recycled into arc magmas, then, unless the geochemically and lithologically different types of sediments are completely "homogenised" during the subduction/fluid extraction/mantle contamination process, spatial (and temporal, because the source, and therefore the composition of the sediments may change with time) variations in the composition of the subducted sediments should be mirrored by variations in the volcanic arc rocks,

provided that these variations are not due to other factors (e.g. variations in crustal thickness and composition, changes in the vertical and horizontal geometry of the subduction zone, variations in the composition of the mantle wedge). In other words, even if we cannot clearly identify the component derived from the subducted sediment and contributed to the arc magmatism, we might be able to detect variations in its composition.

This approach has been used already where Sr, Nd, and Pb isotope variations along a volcanic arc have been observed, for example in the North Luzon arc, where the observed variations in isotope geochemistry in the arc are believed to reflect those of sediments (McDermott et al. 1993), and in the Andes, where the spatial variations in the arc match variations in the underlying crust, and temporal variations in the arc are believed to reflect changes in crustal thickness (Hildreth & Moorbath 1988, 1991; Davidson et al.1990; Davidson & de Silva 1992).

As a corollary, the lack of spatial variations in the geochemistry of volcanic rocks from an arc which is being fed by geochemically different types of sediments, might suggest that sediment contamination is not the major source for the enrichment observed in the arc rocks.

Figures 4.5 and 4.6 show that the calculated SS has a composition very similar to that thought typical of the upper crust (average upper crust is from Taylor & McLennan 1985.

As was noted before, the REEs have similar relative abundances, and are only slightly more abundant in the SS than in average upper crust, whereas the SS have similar abundances of LREE, and only slightly lower HREE than the Sumatran granite. Other trace elements are also similar, especially the elements considered to be very "mobile", like Cs, Rb, Ba, K, Pb. On the other hand, CS have overall lower trace element concentrations (with the exception of Sr) but different element ratios (compared to crustal materials) only where U, Ce (and, of course, Sr), and less importantly Pb and P are involved.

These observations have two important implications. First, the commonly used trace element ratios (e.g. La/Ce, La/Sm, Ba/La, Cs/Rb, Rb/K, Pb/Ce) and LILE, LREE abundances - also commonly used as evidence for sediment contamination - cannot actually distinguish between SS and average upper crust. In other words, if the mantle/melt contamination was a simple bulk mixing process, then it would be

difficult to distinguish between sediment contamination of the mantle source and upper crustal contamination using major and trace elements, as bulk upper crust and bulk SS have a very similar composition. Second, only Sr, Ce, and U, and to a lesser extent P and Pb, can distinguish between CS and SS.

4.7 Sediment distribution and provenance

A study of the detrital fraction of non-carbonate sediments allowed Kolla (1974) and Kolla & Kidd (1982) to conclude that volcanic arc rocks have been a major source of sediments. In fact, according to Kolla (1974), basaltic volcanics have been the main source of sediments at least until the Middle Miocene, and continued to be important in the vicinity of the Sunda arc in later times (e.g. Kidd & Davies 1978, and references therein).

After the Miocene, three main different sources of sediments can be identified (Kolla 1974; Kolla & Kidd 1982): 1) the Ganges-Brahmaputra fluvial system, supplying mainly chlorite-illite-rich sediments; 2) the Indonesian volcanic arc, predominantly silicic, supplying smectites and volcanic ash; and 3) the aeolian transport of fine particles from Australia. These three sources define three different sediment provinces (Figure 4.7).

The results of this early work were later confirmed by Dia et al. (1992), who studied the $^{143}Nd/^{144}Nd$ variations in Quaternary sediments in the Indian Ocean and concluded that the Indonesian arc is the main source of sediments in the northeastern part of the Indian Ocean, whereas the Nd isotope systematics of the central Indian Ocean are consistent with the mixing between material coming from the erosion of the Indian shield and from the Indonesian arc. McLennan et al. (1990) also recognised an important component from an "old, upper crustal source" in turbidites sampled in the fore-arc in the proximity of the Sunda Strait. These studies have important implications.

First, the amount of volcanogenic material in the sediments of the Northeastern Indian Ocean has been grossly underestimated, because only the material that clearly shows textural evidence for a volcanogenic origin (ash-layers, glass shards, cumulates of heavy minerals, volcanic pebbles) has been recognised as "volcanogenic".

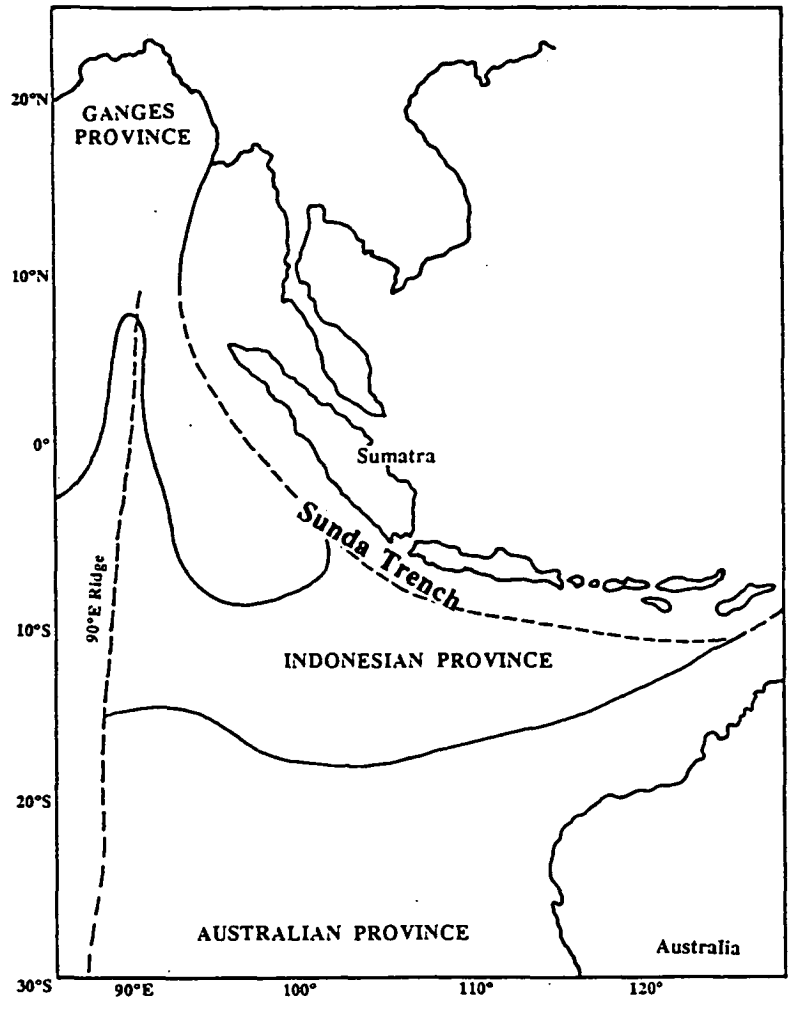

Figure 4.7. Sediment provinces in the Northeastern Indian Ocean, modified after Kolla (1974), Kolla & Kidd (1982), and Dia et al. (1992).

However, the particles eroded from volcanic material do lose their volcanic texture, mineralogy, and chemical composition, while retaining, to some extent, their original isotope signature.

Second, even though the material subducted along the Sunda arc might have a rather constant geochemical composition, its isotopic signature is variable.

Third, the isotopic signature of the sediment is dependent on its age, because the provenance of the sediments changed with time.

The effects of these three factors can easily be identified in Figures 4.8a, 4.9, and 4.10. In Mn-nodules Sr and Nd isotopes have been shown (e.g. Piepgras et al. 1979; Piepgras & Wasserburg 1980; Ben Othman et al. 1989) to reflect the composition of

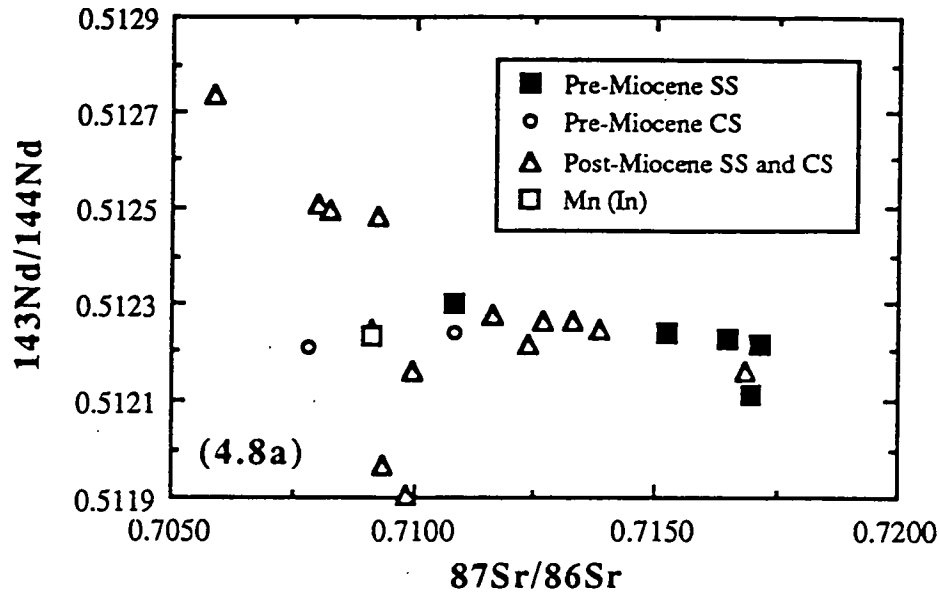

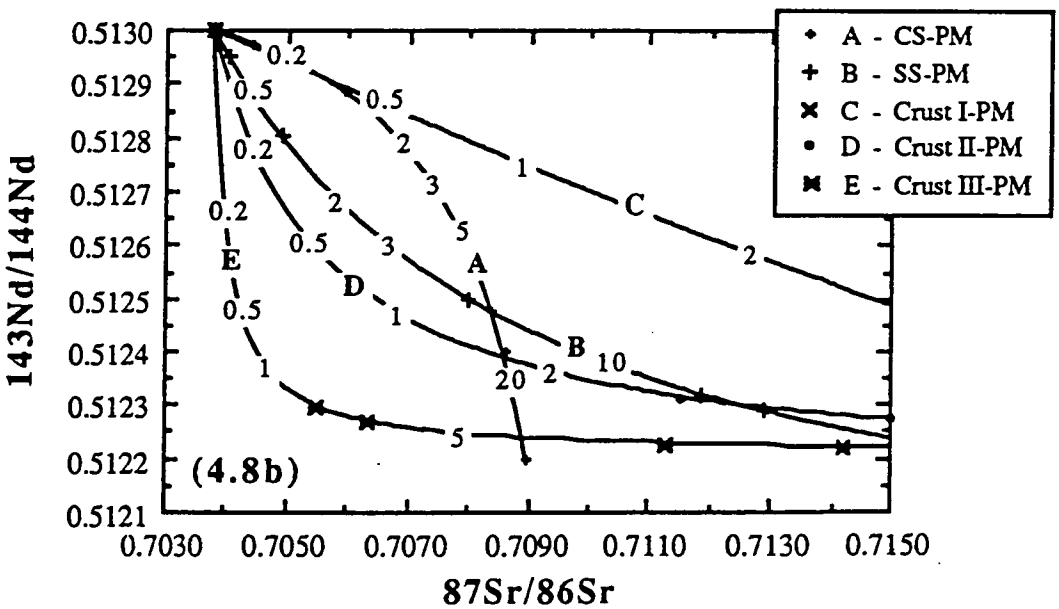

Figures 4.8a-b. Sr-Nd isotope diagram (Figure 4.8a) for sediments of the Northeastern Indian Ocean, and Sr-Nd isotope mixing curves (Figure 4.8b) between Northeastern Indian Ocean sediments, crust and mantle endmembers. Data from this study, O'Nions et al. (1978), Piepgras et al. (1979), Allegre & ben Othman (1980), Piepgras & Wasserburg (1980), Goldstein & O'Nions (1981), Ben Othman et al. (1989), France-Lanord et al. (1990), McLennan et al. (1989), Bouquillon et al. (1990), McLennan et al. (1990). In Figure 4.8b the marks along the mixing lines (curves A to E) are the percent of crustal/sedimentary material in the mixture (0.2, 0.5, 1, 2, 3, 5, 10, 15, 20 - some of the values are reported along the mixing curves). See text for explanation and composition of the endmembers (CS, SS, Crust I, Crust II, Crust III, and PM - primitive mantle). Mn(In) is the composition of an Indian Ocean manganese nodule.

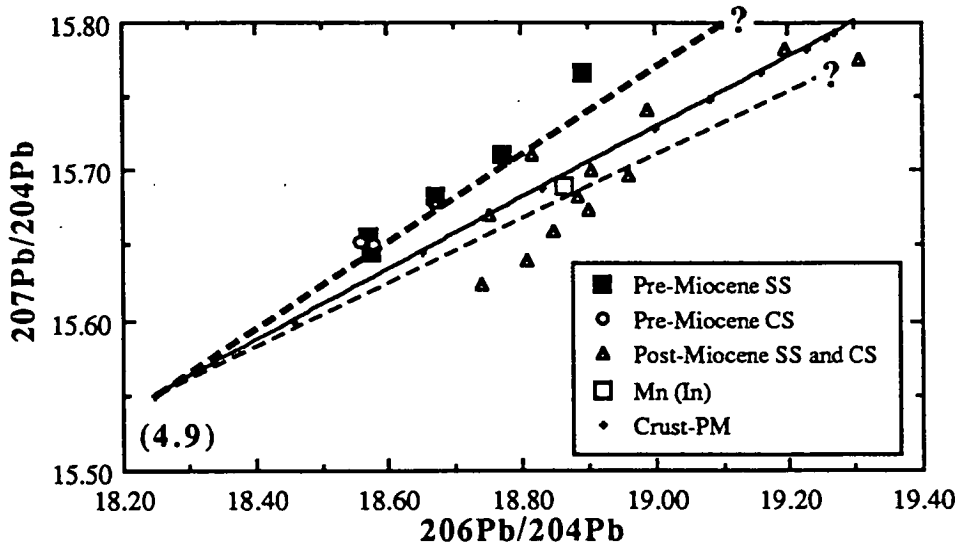

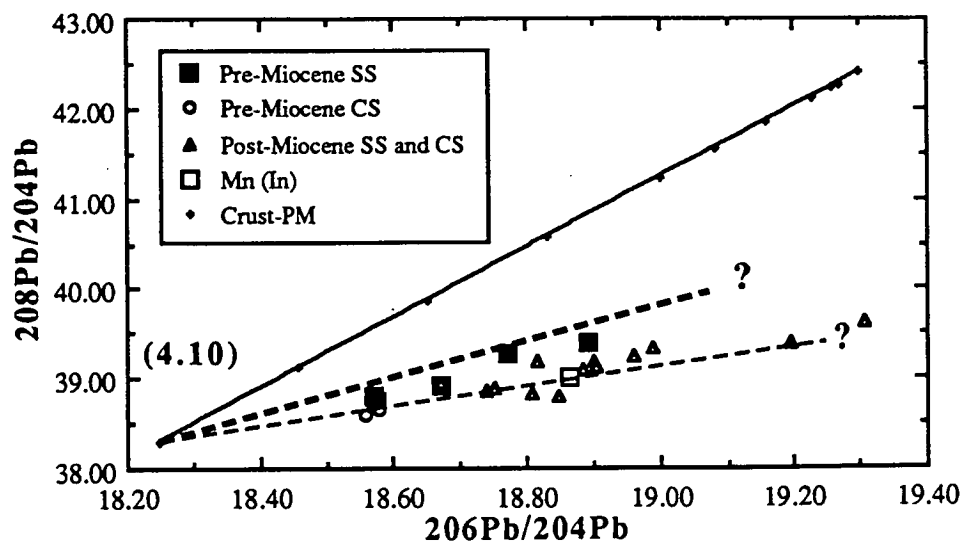

Figures 4.9 and 4.10. Pb isotope diagrams and mixing curves for sediments of the Northeastern Indian Ocean. Data sources as in Figures 4.8a-b. See text for explanation and composition of the endmembers and calculation of the mixing lines. Mn(In) is the composition of an Indian Ocean manganese nodule.

seawater, but while the $^{87}Sr/^{86}Sr$ value of seawater is rather constant in the different oceans (approximately 0.709), $^{143}Nd/^{144}Nd$ is variable, and this variation is reflected by the range in $^{143}Nd/^{144}Nd$ observed in Mn-nodules in the different oceans. In the Indian Ocean Mn-nodules have the same $^{87}Sr/^{86}Sr$ as is measured in seawater, but considerably higher $^{143}Nd/^{144}Nd$.

As would be expected, old CS (i.e. pre-Miocene, according to the distinction by Kolla 1974) have relatively low $^{87}Sr/^{86}Sr$, similar to the values measured in seawater and Mn-nodules, and systematically lower than in old SS, with the only exception of a single claystone (261 25-3) with anomalously high Ba content (>3500 ppm). No significant $^{143}Nd/^{144}Nd$ variations were observed, and both SS and CS have $^{143}Nd/^{144}Nd$ similar to those measured in Mn-nodules (approximately 0.5122). The same differences in $^{87}Sr/^{86}Sr$ between SS and CS exist in young sediments but, in general, old SS seem to have higher $^{87}Sr/^{86}Sr$ than young SS.

Among the young sediments, the only sample described as volcanogenic (Ben Othman 1989 - sample RC 14-67 103-107) has Sr and Nd isotopes similar to Sumatran arc andesites, with the slightly higher $^{87}Sr/^{86}Sr$ perhaps reflecting a minor organogenic component. Only three other samples (33-75, 33-77, and 33-79), described as terrigenous/biogenic, have considerably higher $^{143}Nd/^{144}Nd$ (0.5125), and are likely to be a mixture of arc material with more radiogenic sediments, as they were sampled in the Jawa fore-arc, where a strong volcanogenic component can be expected. In addition, their $^{87}Sr/^{86}Sr$ might have been slightly increased by a minor organogenic component, although the sample in which Ca and Sr are relatively high (33-77) does not show higher $^{87}Sr/^{86}Sr$. Relatively low $^{143}Nd/^{144}Nd$ values are shown only by two $CaCO_3$-rich samples (261 4-1, and 261 3-2).

In summary, young and old CS have relatively low $^{87}Sr/^{86}Sr$ values, similar to those of seawater, because they were formed in equilibrium with seawater and because the high content of organogenic Sr completely masks any minor contribution of more radiogenic Sr from the detrital component. Old SS generally have very high $^{87}Sr/^{86}Sr$ values, whereas the Sr isotope signature in young SS can be accounted for by mixing of relatively unradiogenic volcanic material with old crustal material. With a few exceptions, $^{143}Nd/^{144}Nd$ values vary little in young and old CS and SS, and only the sediments very rich in volcanogenic material have comparatively high $^{143}Nd/^{144}Nd$ values.

Ben Othman et al. (1989) have shown that mixing curves can be constructed between

"primitive mantle" and "sediment" endmembers which pass both through and outside the Sr-Nd isotopes mantle array, depending on the Sr/Nd value of the sediments used in the model.

Some possible mixing curves are plotted in Figure 4.8b. In all cases, the primitive mantle component is assumed to have Sr = 18 ppm and Nd = 1 ppm, as in the model by Ben Othman et al. (1989). These values give a Sr/Nd values for the mantle of 18, which is similar to that of E-MORB and OIB.

In Chapters 3 and 5 it is shown that mantle with higher $^{87}Sr/^{86}Sr$, $^{208}Pb/^{204}Pb$, $^{207}Pb/^{204}Pb$, $^{206}Pb/^{204}Pb$, and lower $^{143}Nd/^{144}Nd$ than Atlantic and Pacific mantles exists in the Northeastern Indian Ocean and in the mantle wedge of the Sunda arc, at least in south Sumatra. For these reasons, the values of $^{87}Sr/^{86}Sr = 0.7038$ and $^{143}Nd/^{144}Nd = 0.5130$ were adopted for the mantle, corresponding to the lowest $^{87}Sr/^{86}Sr$ and highest $^{143}Nd/^{144}Nd$ isotope values measured in the Sukadana basalts (see Chapter 5 and Chapter 6).

For the sediments, the calculated average Sr and Nd values reported in Table 4.3 were used, together with values for Nd and Sr isotopic ratios of $^{143}Nd/^{144}Nd = 0.5122$ for both CS and SS, $^{87}Sr/^{86}Sr = 0.709$ for CS (approximate value of seawater) and 0.717 (the highest measured value in SS) for SS. The Sr/Nd of SS and CS (respectively 5 and 74, from Table 4.3) is similar to the calculated average of the Sr/Nd values (5.5 ± 4 in SS and 72 ± 30 in CS).

Three possible crustal compositions were used in the modelling of the effects of crustal contamination. Crust 1 has the Sr and Nd values reported by Taylor & McLennan (1985) for the average upper crust, $^{87}Sr/^{86}Sr = 0.735$ and $^{143}Nd/^{144}Nd = 0.5118$ (typical values of Bengal Fan sediments and Himalayan old granitoids). Crust 2 has Sr = 192 ppm (average Sr content of the Central Province of Southeast Asian granitoids), Nd = 192 ppm (estimated from average Sm content of the Central Province of Southeast Asian granitoids), $^{87}Sr/^{86}Sr = 0.735$, and $^{143}Nd/^{144}Nd = 0.5122$ (average value of the two analyses of the Sumatran Granitoids of the Central Province - samples 78135 and 78136; see Chapter 2).

It should be noticed that Crust 1 and Crust 2 have similar Sr and Nd isotope ratios, but very different Sr/Nd values and Sr and Nd contents. Assuming that the granitoids of the Southeast Asian Central Province are representative of the composition of the upper crust, then Crust 2 represents the composition of upper crust in Sumatra.

It might be expected that these granitoids are considerably enriched in REE compared with their source, and therefore the Nd value in Crust 2 may therefore be a maximum value. Lower Nd contents would shift the Crust 2 - mantle mixing line towards the SS - mantle mixing line. Crust 3 has Sr and Nd contents and Sr and Nd isotope values typical of the Sumatran Granitoids of the Central Province (Palembang granitoids, samples 78135 and 78136; Sr = 51 ppm, Nd = 384 ppm, $^{87}Sr/^{86}Sr$ = 0.735, $^{143}Nd/^{144}Nd$ = 0.51221), and is an extreme case because these granitoids are strongly enriched in Nd (see Chapter 2).

Some important features can be seen in Figure 4.8b. First, CS and SS contamination can easily be distinguished in a Sr/Nd isotope plot due to their very different Sr/Nd values. Even taking into account the large standard deviation of Sr/Nd values, the CS - mantle mixing curve still maintains the same shape. Second, most sediments can be modelled as the result of mixing between a relatively "pure" detrital sediment and volcanogenic material. Third, contamination by upper crustal material similar in composition to the granitoids of the Southeast Asia Central Province is very similar to that by SS, but is likely to produce lower $^{143}Nd/^{144}Nd$ values without any significant changes in $^{87}Sr/^{86}Sr$ values (at least for low degrees of contamination). At the lower end of the observed Sr/Nd range (approximately 1) the SS - mantle mixing curve resembles that of Crust II - mantle. These results have important implication for the Sr and Nd isotope systematics of the Sunda arc rocks, and will be discussed in the next chapter.

Unlike Sr and Nd, Pb isotopes in Mn-nodules are very variable and believed to reflect the provenance of the Fe-Mg material in the nodules (O'Nions et al. 1978). As a consequence, it is difficult to estimate the isotopic composition of Pb in sedimentary material formed in equilibrium with seawater. Compared with old SS, old CS seem to have lower Pb isotopes, and Pb isotopes in old CS are also lower than in most Mn-nodules. In young sediments, variations in Pb isotope values do not seem to be related with the $CaCO_3$ content.

The most remarkable features of the Pb isotope distribution are the systematically higher $^{207}Pb/^{204}Pb$ (Figure 4.9) and $^{208}Pb/^{204}Pb$ (Figure 4.10) values in old sediments, with old and young sediments defining two subparallel trends (the only exceptions are two young sediments, 33-75 and 33-79, which, as was already observed, also show a strong arc component in their Sr-Nd isotope systematics) which mirror the difference in Pb isotope systematics between Atlantic-Pacific and Indian MORB. If, as suggested by Kolla (1974), old sediments in the Indian Ocean

mainly come from basaltic volcanics, these data suggest that old sediments retain the ^{207}Pb and ^{208}Pb enrichment typical of isotopically enriched basalts in the Indian Ocean.

It is difficult to calculate mixing lines for Pb isotopes as was done for Sr and Nd, because of the poor knowledge of the Pb-U-Th systematics of the possible endmembers (the Sumatran granitoids are enriched in Th and U and old, and therefore their Pb isotope systematics are presumably different from those of their source).

For the mixing line (crust-PM) in Figures 4.9 and 4.10, a Pb content in the mantle of 0.255 ppm was assumed, a value used by Ben Othman et al. (1989) for an OIB source, and Pb isotope values typical of the Sukadana basalts ($^{206}Pb/^{204}Pb$ = 18.25; $^{207}Pb/^{204}Pb$ = 15.55; $^{208}Pb/^{204}Pb$ = 38.3). The crustal endmember has Pb = 31.5 ppm (average Pb value of the Palembang granitoids) and Pb isotope systematics similar to those of the Palembang granite (sample 78136: $^{206}Pb/^{204}Pb$ = 19.3; $^{207}Pb/^{204}Pb$ = 15.8; $^{208}Pb/^{204}Pb$ = 42.4).

As was discussed in Chapter 2, the high Pb isotope values measured in the Palembang rocks are likely to be partly due to in-situ decay of the high U and Th contents fractionated into the granite during its formation, and therefore it might be that the crust from which the Palembang granite was formed has lower U and Th contents, and for this reason will probably possess lower present-day Pb isotope values.

Although with the available data it is not possible to calculate accurately the increase in Pb isotope values due to excess U-Th decay, it seems likely that present-day Sumatran crust has $^{207}Pb/^{204}Pb$ similar to that measured in the Palembang granite, but considerably lower $^{208}Pb/^{204}Pb$ and $^{206}Pb/^{204}Pb$, probably in the range $^{206}Pb/^{204}Pb$ = 19.1, and $^{208}Pb/^{204}Pb$ = 40, taking into consideration the approximate age and the relative U/Th and Pb isotope proportions of the two analysed granitoids, and assuming a common source (see Chapter 2).

Mixing between such a crustal component and the same mantle used for the Sr-Nd isotope calculations (thick broken line in Figures 4.9 and 4.10) can account for the Pb isotopes observed in the old sediments, whereas the young sediments would require a component which at this stage it is difficult to identify.

One possible explanation for the relatively high $^{206}Pb/^{204}Pb$ in young sediments is that these are enriched in a component which originally had high $^{238}U/^{204}Pb$ and low $^{232}Th/^{238}U$, that with time produced high $^{206}Pb/^{204}Pb$ and relatively low $^{208}Pb/^{204}Pb$. A possible mixing line between such a component and the mantle is plotted in Figures 4.9 and 4.10 (thin broken line).

Based on the available data (see Calvert & Price 1981; Zartman & Haines 1988; Ben Othman et al. 1989; Hart & Staudigel 1989; White 1989), the $^{238}U/^{204}Pb$ of different reservoirs is sufficiently well constrained and ranges from less than 1 in Mn-nodules, to 1 to 10 in pelagic clays, biogenic oozes, and hemipelagic sediments. Typical values of $^{238}U/^{204}Pb$ for primitive mantle, altered oceanic crust, and upper continental crust are respectively 8, 30, and 11, and extremely high values (up to several thousands) of the order of those necessary to explain the shift towards higher $^{206}Pb/^{204}Pb$ values in the young sediments in the Indian Ocean, have been measured only in organic carbon-rich sediments from continental shelves. Furthermore, due to the very high ^{238}U content, it can be expected that these organogenic sediments have low $^{232}Th/^{238}U$ values (much less than 1, compared to values greater than 3.5 in the other reservoirs, including the mantle and the continental crust).

It should be noted that, because pelagic and detrital sediments usually have low $^{238}U/^{204}Pb$ and high $^{232}Th/^{238}U$ values, in situ U-Th decay will produce two opposite Pb isotope signatures in the two types of sediments: relatively low $^{206}Pb/^{204}Pb$ and high $^{208}Pb/^{204}Pb$ in pelagic sediments, and relatively high $^{206}Pb/^{204}Pb$ and low $^{208}Pb/^{204}Pb$ in organogenic continental shelf sediments, with no differences in the $^{207}Pb/^{204}Pb$ values. The amount of ^{206}Pb and ^{208}Pb produced by in-situ decay will depend on the initial ^{238}U and ^{232}Th concentrations, and the effects that the addition of this ^{238}U-rich component to a pelagic sediment will produce on the final Pb isotopic ratios and element concentrations will depend on the U-Pb-Th concentrations and isotopic systematics in the two endmembers.

In a mixture between clastic and organogenic sediments, it can be expected that the ^{238}U-rich component will soon dominate the Pb isotope signature of the mixture, with only a slight increase in U, and possibly Sr, in the mixture relative to the U and Sr values in the clastic sediments, and presumably with little or no effects on the other elements, (with the possible exceptions of a slight increase in Sr and CaO values).

Continental shelves with abundant organogenic, ^{238}U-rich material, formed at the

same time as the onset of the Miocene volcanism in the Sunda arc (Hutchison 1982), and the ^{238}U-rich material, and more organogenic material from the Bengal Fan (Curray et al. 1982) mixed with the pelagic sediments to give the young sediments their peculiar Pb isotope signature, with no changes in Sr and Nd isotopes (possibly only a little depletion in ^{87}Sr, because this material has high Sr content and $^{87}Sr/^{86}Sr$ values similar to seawater and, in general, lower than clays).

Like for Sr and Nd isotopes, these results have important implications for the Pb isotopic characteristics of the Sunda arc rocks, and will be discussed in the next chapter.

4.8 Conclusions

1) Two sediment endmember components are identified in the Northeastern Indian Ocean: a siliceous-clastic sediment (SS) endmember component and a calcareous-organogenic sediment (CS) endmember component. Compared with previous calculations, these results are based on a considerably larger, both quantitatively and qualitatively, database, and are not restricted in their application to a specific geographical locality. Based on the available data, no other types of sediments are present in significant amounts, and the two endmembers and their mixture can adequately represent, from a geochemical point of view, the composition of sedimentary material in the Northeastern Indian Ocean.

2) Siliceous-clastic sediments (SS endmember) have major and trace element composition similar to post-Archaean average shales and average upper crust. Calcareous-organogenic sediments (CS endmember) can be regarded as SS diluted by organogenic material, mainly $CaCO_3$. $CaCO_3$ is a pure diluent for most elements, but not for those which are enriched in organogenic material associated with $CaCO_3$ (Sr, P, U, possibly Pb and Mn).

As is $CaCO_3$ in CS, organogenic and detrital silica ("excess silica") is a diluent in SS, but the effects of dilution are not as pronounced because this "excess silica" occurs in relatively lower amounts in SS compared with $CaCO_3$ in CS. "Excess silica" is a pure diluent for all the major end trace elements, except for Ba, which is highly concentrated in radiolarian-rich (and therefore SiO_2-rich) sediments.

Ce negative anomalies are only observed in CS, and this suggests that while the SS

retain the REE signature of the material of provenance, CS formed in equilibrium with seawater and that therefore their REE pattern is similar to that of seawater. The reasons for the difference in Mn content in SS and CS are not well understood, due to the complex behaviour of Mn in the marine environment.

These results are consistent with the present knowledge of the geochemical behaviour of elements in oceanic sediments, and with previous estimates of the composition of sediments in the Northeastern Indian Ocean.

3) Using element abundances and element ratios measured in sediments, it is not possible to distinguish between SS and "typical" upper crustal material. CS have considerably lower major and trace element concentrations (with the exceptions of $CaCO_3$-related elements), but only differ from SS in ratios with Sr, U, P, Ce and, to a minor extent, Pb.

4) Because the REE, U, and Sr in CS are concentrated in the organogenic component which precipitated in equilibrium with seawater, the Sr, Nd, and Pb isotope signature of CS is similar to that of seawater. On the contrary, SS maintain their original REE, U, and Sr content, and the Sr, Nd, and Pb isotope signature of their source-rocks.

5) Various types of sediments can be identified using their Sr, Nd, and Pb isotopic characteristics. Both old and young organogenic sediments have $^{87}Sr/^{86}Sr$ values similar to seawater, whereas detrital sediments have in general higher $^{87}Sr/^{86}Sr$ values, reflecting those of their source-rocks. No significant variations in $^{143}Nd/^{144}Nd$ values have been observed in the different types of sediments. On a $^{87}Sr/^{86}Sr$ - $^{143}Nd/^{144}Nd$ diagram the isotope composition of most sediments can be accounted for by mixing of variable amounts of two endmembers - Sumatran upper continental crust, and a magmatic source that has the same isotopic characteristics of the Indian Ocean mantle (mantle source of the Sukadana basalts - see Chapter 6).

Pb isotopes can distinguish between old and young sediments. Old sediments have relatively high $^{207}Pb/^{204}Pb$ and $^{208}Pb/^{204}Pb$ and, as for the Sr and Nd isotopes, plot on the mixing line between Sumatran upper continental crust and Indian Ocean mantle. Young sediments appear to have a component enriched in ^{238}U, probably organogenic material from a continental shelf.

6) Using Sr, Nd, and Pb isotopes, and the available information on the provenance and mineralogy of sediments, it is possible to identify different sedimentary

provinces in the Northeastern Indian Ocean. Pre-Miocene sediments are characterised by relatively high $^{207}Pb/^{204}Pb$ and $^{208}Pb/^{204}Pb$, consistent with their derivation from volcanic material with Pb isotopic values similar to those of Indian Ocean MORB. Post-Miocene sediments derive from three different sources - the Ganges-Brahmaputra fluvial system, the Sunda arc, and Australia - and define three sedimentary provinces. Post-Miocene sediments are characterised by relatively high $^{206}Pb/^{204}Pb$ values. As will be shown in the next chapter, the spatial and temporal distribution of these provinces can be used to test the importance of sediment contamination for the Sr, Nd, and Pb isotope systematics in the rocks of the Sunda arc.

CHAPTER 5

Isotopic variations along the Sunda arc: in search of a "deus ex machina"

5.1 Introduction

The enrichment of calcalkaline arc rocks in LILE and LREE, and their high $^{87}Sr/^{86}$ and $^{207}Pb/^{204}Pb$ and low $^{143}Nd/^{144}Nd$ values, compared with those of MORB, are commonly considered as evidence for the recycling of subducted lithospheric material into the source of arc magmatism.

In general, it is assumed that the process of recycling of sediments into the mantle resembles a metasomatizing process: fluids or small amounts of melt derived from the sediments and oceanic crust of the downgoing slab rise through the mantle wedge, where they induce partial melting (due to their high contents of water and other fluids) and change the composition of the mantle, enriching it in "volatile" elements, and modifying its isotopic signature. As it can be assumed that Sr, Nd, and Pb isotopic ratios are not fractionated during the subduction/fluid-melt extraction processes (provided that the process is not long enough to produce isotope differences due to element fractionation), the shapes of the mixing curves (e.g. in a $^{87}Sr/^{86}Sr$ - $^{143}Nd/^{144}Nd$ diagram) between fluids-melts and the mantle, or melts derived from the mantle, are only dependent on the Sr/Nd values (and not on the absolute Sr and Nd content), and the mixing can be modelled as bulk mixing. Only the relative proportions of the different components in the mixture are dependent on the absolute Sr and Nd contents of the endmembers.

Variations in element concentrations can be expected as a consequence of these fluid extraction/melting processes, but some trace element ratios between very "volatile" elements (like Cs/Rb) are believed not to be affected by these processes. Elements which have low partition coefficients in fluids and melts (most major elements, and MREE, HREE, and HFSE) are known to partition into the solid residue during fluid extraction/melting processes, and in fact they are often used to recognise and identify the "mantle component" in arc rocks. These elements should be taken into account only in a bulk mixing model.

Even if the mechanisms of the recycling and mixing process are not clearly

understood, it can be expected that similar types of sediments will suffer the same fluid extraction/melt processes in similar tectonic environments. In other words, if the amount and composition of sediments subducted along a trench remain constant, and the geometry of the subducting slab and physical and chemical conditions in the subduction zone remain constant along an arc, then it could be argued that *variations* in Sr, Nd, and Pb isotopic composition and LILE enrichment in the arc rocks are not a result of sediment contamination.

New data for the composition of the Sumatran continental crust, the sedimentary cover in the Northeastern Indian Ocean, and for the isotopic composition of the mantle wedge in south Sumatra are used in this chapter in an attempt to answer two important questions. First, can the effect of the mixing of subducted sediment with mantle material be distinguished from those produced by crustal contamination of melts derived from the unmetasomatised mantle wedge? Second, are the variations (or the lack of variations) in Sr, Nd, and Pb isotopes and LILE enrichment observed in Quaternary volcanics along the west Sunda arc consistent with the spatial variations observed in the crust and in the sediments subducted along the arc?

Recent models of the effects of crustal and sediment contamination on the O, He, Th/U, Be isotopes and B/Be values of arc rocks in the Sunda and Banda arcs will also be briefly reviewed.

5.2 Method of investigation and definition of the area of study

Wheller et al. (1987) noted that the Sunda-Banda arc can be subdivided into four sectors (i.e. West Jawa, Bali, Flores and Banda) based on geochemical and Sr isotope data characteristics. To these should be added the Sumatra sector, not discussed by Wheller et al. (1987) because of lack of data.

More recently, Hilton & Craig (1989), and Hilton et al. (1992), determined the isotopic composition of He from volcanic gases, hot springs and phenocrysts, and concluded that a transition from predominantly MORB-like $^{3}He/^{4}He$ values, which characterise the sector of the arc from Jawa to Flores, to very radiogenic $^{3}He/^{4}He$ values (from Flores to the Banda arc) occurs in a relatively narrow area along a volcanically inactive zone from central Flores to the island of Alor (east of Flores).

It should be noted that the boundaries between the sectors correspond with major

tectonic features: the Sunda Strait between Sumatra and west Jawa, transition from continental to transitional-oceanic crust between west Jawa and the Bali sector, the Sumba fracture between the Bali sector and the Flores sector, and the Pantar fracture between the Flores sector and the Banda arc (e.g. Audley-Charles 1975; Hamilton 1979; Hutchison 1989). In particular, the volcanic centres situated along and in the vicinity of the Sumba and Pantar fractures have variable geochemical and isotopic composition, and it is likely that the variability observed is somehow a consequence of the fractures themselves, rather than the result of along-arc variations, at least for some volcanic centres (Alzwar et al. 1981; Nishimura et al. 1981; Nishimura & Suparka 1986). Another complicating factor is the change from an ocean-arc subduction in Sumatra, Jawa, and the Bali sector, to a continental crust-arc collision system in east Flores and the Banda arc.

To avoid such complications, discussion will concentrate here on the along-arc isotope variations and some variations in LILE ratios from Sumatra to Lombok in the Bali sector, and only for centres situated above a depth to the Benioff zone of 100 to 200 km.

This portion of the arc is an ideal location to study the interactions between crust/sediments and mantle/melts, because along-arc variations occur in the composition and thickness of both crust beneath the arc (thick continental crust in Sumatra, transitional crust in Jawa, and oceanic crust in the Bali sector), and sediments subducted (see Chapter 4), and the geochemical and isotopic composition of crustal and oceanic sedimentary material have been estimated and discussed in Chapters 2 and 4. Only volcanic centres situated above a depth to the Benioff zone of 100 to 200 km are investigated because compositional variations between centres situated at different depths to the Benioff zone could be due to both vertical variations in the mantle source and differences in the mechanisms of magma generation and segregation. Important fracture zones (as the Sumba and the Pantar fracture zone) could affect the permeability of the crust and the underlying mantle wedge, and therefore their existence could have some effects on the mechanisms and depth of magma generation and segregation.

However, as was claimed by Furukawa (1993, page 8309), "temperature structure in the crust and the mantle wedge under arcs is insensitive to the angle and velocity of slab subduction, the temperature structure [as a function of its age] of the slab, and that of the back-arc region, and physical conditions such as temperature and pressure are similar under various arcs". Therefore, irrespective of the different velocity, age,

and angle of subduction of the slab from Sumatra to Lombok, variations in the composition of the primary magmas along the volcanic front (100 to 200 km above the depth to the Benioff zone), and where the crust and mantle wedge are not affected by tectonic activity, can only be due to 1) variable (horizontal variations) composition of mantle wedge materials; 2) different composition and flux rate of fluids from the subducted sediments (only sediments need to be considered in the discussion of the variations of Sr, Nd, and Pb isotopic ratios in arc volcanics, because fluids released from the altered oceanic basalts do not seem to be able to account for the variations in Sr, Nd, and Pb isotope systematics observed along the Sunda arc - see Chapter 3. In particular, fluids released from altered oceanic crust would have relatively high $^{143}Nd/^{144}Nd$ values, whereas the Sunda arc volcanics have relatively low $^{143}Nd/^{144}Nd$ values); and 3) different composition and extent of contamination of the underlying crust.

To minimise the effects of extreme degrees of crystal fractionation and possible crustal assimilation in the geochemically most evolved samples, and yet have a reasonable amount of data, samples with $SiO_2 > 57.9\%$ (mean chemical composition of andesites, from Le Maitre, 1976) and $MgO < 3\%$ have not been considered in the discussion of the LILE ratios, and, for reasons explained in the introduction, only variations in Sr, Nd, and Pb isotopes, and Sr, Nd, and U-Th-Pb contents will be investigated in detail. Only some parameters, namely Pb and Pb/Ce, Cs/Rb and Ba/Rb values, which are believed to be useful in testing the hypotheses of sediment contamination (Ben Othman et al. 1989), including new Pb/Ce, Cs/Rb and Ba/Rb data for Sumatra, will be discussed here.

5.3 Effects of sedimentary "cannibalism"

It has been pointed out (Ben Othman et al. 1989) that Pb isotopes are the most useful indicators of the presence of subducted material in the source of the arc magmatism. However, these authors also admitted that the "sediment signature" of the arc rocks in the West Sunda could simply exist because an important component of subducted sediments is volcanic material.

The possible existence of a volcanic component in the oceanic sediments has been discussed in Chapter 4, and it is reiterated that some of the sediments analysed by Ben Othman et al. (1989) were collected from the Sunda fore-arc, and therefore highly likely to contain an arc-derived (in fact, their sample RC 14-67 103-107 is described

as "volcanogenic") volcanic component, and indeed might account for their observation that $^{87}Sr/^{86}Sr$ values lower than seawater occur in some sediments.

If the Sr, Nd, and Pb isotope systematics in arc rocks are indeed similar to those of sediments primarily because the sediments have an important volcanic component, then the sediments might be expected to plot along a simple bulk mixing line between a relatively primitive arc component and silicic crustal material. As was observed by Ben Othman et al. (1989), reasonable amounts of volcanic material in the mixture can account for the $^{87}Sr/^{86}Sr$ values observed in the sediments, but not for the Pb isotopes. However, bulk mixing between an endmember with Sr, Nd, and Pb concentrations and Sr, Nd, and Pb isotopic compositions like those of the Crust 1 endmember discussed in Chapter 4, and 50 to 70% (in the mixture) of a relatively primitive arc rock (average composition of Rajabasa volcano in south Sumatra: $^{87}Sr/^{86}Sr = 0.70432$; $^{143}Nd/^{144}Nd = 0.512768$; $^{206}Pb/^{204}Pb = 18.593$; $^{207}Pb/^{204}Pb = 15.636$; $^{208}Pb/^{204}Pb = 38.786$; Sr = 492 ppm; Nd = 19.2 ppm; Pb = 5.5 ppm. See Appendix C) can account for the $^{87}Sr/^{86}Sr$ and $^{143}Nd/^{144}Nd$ values observed in most sediments, whereas 80 to 95% of the volcanic component are required in the mixture to account for the Pb isotopes in pre-Miocene sediments (post-Miocene sediments have higher $^{208}Pb/^{204}Pb$ values and plot outside a mixing curve between crustal and arc volcanic material as defined here - see Chapter 4). However, lower amounts of more evolved, Pb-rich volcanic rocks would be required in the mixture.

Therefore, although the estimates of the volcanic material present in the oceanic sediments based on the Sr, Nd, and Pb isotopic values are dependent on the choice of endmembers used in the mixing model, it seems obvious that a strong similarity in Sr, Nd, and Pb isotopic values between sediments and arc rocks can be expected, especially where, as in the Sunda arc, geological evidence suggests that volcanic material is the principal source of sediments.

5.4 Effects of sediment versus crustal contamination

Another alternative to contamination by subducted sediment of the source of the arc magmas is the assimilation of crustal material by magmas generated in the mantle wedge. These two processes have different effects on the Sr, Nd, and Pb isotope signature of the arc rocks, and these effects can be seen in Figures 5.1 to 5.3.

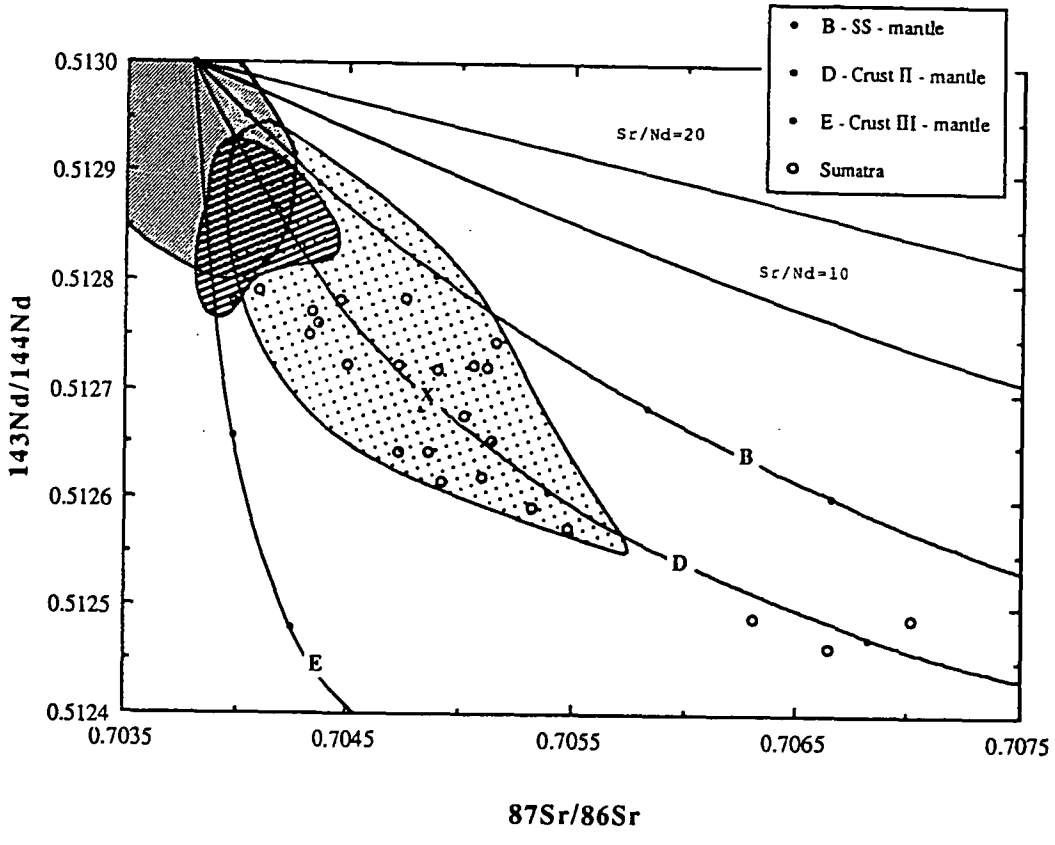

Figure 5.1. $^{87}Sr/^{86}Sr$ - $^{143}Nd/^{144}Nd$ diagram for Quaternary arc rocks from Sumatra, west Jawa (stippled area), and the Bali sector (heavily ruled area) excluding Sumbawa. Lightly ruled area (low $^{87}Sr/^{86}Sr$ and high $^{143}Nd/^{144}Nd$) is the field of basalts from Sukadana and Bukit Telor in south and central Sumatra (Chapter 6), Sumatran arc granitoids (Chapter 2) and pre-Miocene arc-related Sumatran volcanics (see Appendix C), and isotopically slightly "anomalous" basalts from the Northeastern Indian Ocean, including samples from the Ninetyeast Ridge, Christmas Island, tholeiites from Kerguelen, and two samples from the Investigator Ridge and the Cocos Plateau discussed in Chapter 3 (see also Chapter 3 for data sources).

Curves B, D, and E are sediment-mantle (curve B) and crust-mantle (curves D and E) mixing curves (see Chapter 4). Curves labelled Sr/Nd=10 and Sr/Nd=20 are hypothetical mixing curves between mantle and a sediment-derived fluid, for a fluid with the same $^{87}Sr/^{86}Sr$ and $^{143}Nd/^{144}N$ as for curve B, but different Sr and Nd contents and Sr/Nd values (respectively Sr=320 ppm, Nd=32 ppm; and Sr=1000 ppm, Nd=50 ppm).

Point X is the approximate composition of a mixture with 90% Sukadana high-Ti basalts and 10% crustal material, or 94% Sukadana high-Ti basalts and 6% melt produced by partial melting of crustal material. The mixing curve between Sukadana high-Ti basalts and crust or crust-derived melt overlaps curve D.

Data sources for rocks from west Jawa and the Bali sector are: Whitford (1975), Whitford et al. (1978), Foden (1979), Foden & Varne (1980), Foden & Varne (1981a,b), Whitford et al. (1981), Foden (1983), Varne & Foden (1986), Wheller (1986), Wheller et al. (1987), Vukadinovic & Nicholls (1989), Gerbe et al. (1992), Harmon & Gerbe (1992), Edwards et al. (1993), and unpublished data by J. Foden (Rinjani), U. Hartono (Wilis, Lawu), and D. Hilton (Agung, Talagabodas, and Galunggung).

Samples from Sumatra, and from the Jawa and Bali sectors (as defined by Wheller et al. 1987), excluding of Sumbawa, are plotted in Figure 5.1 together with three Sr-Nd isotopes mixing curves calculated in Chapter 4.

As has been pointed out in Chapter 4, silicic sediments like those of the Northeastern Indian Ocean have considerably higher Sr/Nd values than those of Sumatran crustal material, and bulk mixing of these sediments with a mantle source with $^{87}Sr/^{86}Sr$ and $^{143}Nd/^{144}Nd$ values respectively in the range 0.7038-0.7042 and 0.5130-0.5129, and Sr/Nd values of approximately 15-20, produces a bulk mixing curve (curve B in Figure 5.1) that plots outside the field of arc rocks from Sumatra, and the Jawa and Bali sectors: $^{143}Nd/^{144}Nd$ values are systematically high.

Fluids released by these sediments are likely to have higher Sr/Nd values, because of the lower incompatibility expected for Nd (lower Nd concentration) in these fluids and melts. For example, Lin (1992) calculated a Sr/Nd value of 103 for fluids derived from the slab beneath the Mariana arc, whereas sediments in the western Pacific have Sr/Nd values ranging from 1.2 (clays) to 43.1 (chalks), and, according to McCulloch & Gamble (1991) the "slab component" is relatively enriched in Sr compared with Nd.

Assuming that the sediment-derived fluids have the same $^{87}Sr/^{86}Sr$ and $^{143}Nd/^{144}Nd$ values as the sediment which yielded them, but higher Sr/Nd values, the mixing curve between this component and Indian Ocean mantle will plot outside the field of arc rocks in Sumatra, and the Jawa and Bali sectors, irrespective of the absolute Sr and Nd concentrations in the fluid or melt (curves Sr/Nd = 10, and Sr/Nd = 20 in Figure 5.1).

The most striking point illustrated in Figure 5.1 is that most volcanic rocks from Sumatra, and from the Jawa and Bali sectors plot along the mixing curve between Indian Ocean mantle and Sumatran crust calculated in Chapter 4 (curve D). However, as for the sediment-mantle mixing, it is unlikely that the crustal contamination occurs as a simple bulk mixing of crustal and mantle material.

Based on Sun & McDonough (1989), the Sr/Nd value is relatively constant in mantle-derived melts, and ranges from 12.3 in N-MORB, to 17.2 in E-MORB and OIB, to 15.6 in the primitive mantle itself. As will be shown in the next chapter, high-Ti basalts from Sukadana in south Sumatra have Sr and Nd contents and Sr/Nd values (average 17.3) similar to those of OIB. Although it might be argued that these

are not primary melts, it seems that the Sr/Nd values have not been modified by magmatic processes, and in fact Sr/Nd values are not strongly modified by crystal fractionation of olivine and clinopyroxene (e.g. Hart & Dunn 1993), the two phases which may have fractionated in the Sukadana basalts (see Chapter 6). It is therefore concluded that melts generated in the mantle wedge in south Sumatra will have a Sr/Nd value of approximately 17.

As these melts rise through the crust and start to crystallise, heat released will be sufficient to melt portions of the surrounding wall-rock, and the melts will possibly become contaminated by wall-rock material. If complete melting of the Sr and Nd-bearing phases occurs, then the contaminant will have a Sr/Nd value similar to that estimated for the source of the Sumatran granitoids in Chapter 4. If, as suggested by Rutter (1987) to explain the decoupling between LILE and LREE in Holocene Sardinian basalts, the quartzo-feldspathic crustal component is completely melted, leaving residual REE-rich phases (apatite, zircon, sphene, amphibole), the Sr/Nd value of the assimilated material can be expected to increase to values similar to those observed for sediment-derived fluids. On the other hand, if only partial melting occurs, feldspars will probably start melting before other Sr- and Nd-bearing phases, and as Nd is more incompatible than Sr in feldspars, it will concentrate in the melt fraction during partial melting of feldspars, and the Sr/Nd value of the assimilated material will probably decrease.

As a consequence, assimilation of Sumatran crustal material by a melt produced in the Sumatran mantle wedge can account for the range in Sr and Nd isotope composition observed in Quaternary arc rocks from Sumatra, and the Jawa and Bali sectors. The composition of the assimilated crustal material is similar to that observed in the Central Granitoid Province, and the melt produced in the mantle wedge has Sr and Nd isotope composition typical of Indian Ocean basalts, and Sr/Nd values typical of average OIB and Ti-rich OIB from south and central Sumatra.

If crustal assimilation can be modelled as a simple mixing between this melt (Sr=618 ppm, Nd=36 ppm, $^{87}Sr/^{86}Sr$=0.7038, and $^{143}Nd/^{144}Nd$=0.5130 - average Sr and Nd contents and lowest $^{87}Sr/^{86}Sr$ and highest $^{143}Nd/^{144}Nd$ values in Ti-rich OIB from south Sumatra) and crustal material with composition similar to that calculated in Chapter 4 (Crust 2), then approximately 10% of the crustal component in the mixture is required to produce the $^{87}Sr/^{86}Sr$ and $^{143}Nd/^{144}Nd$ values of most rocks in Sumatra and the Jawa sector, and less than 3% in the Bali sector. In fact, most samples from the Bali sector plot within the field of Indian Ocean basalts, and it is

generally agreed that the basalts of this sector do not carry any evidence for lithospheric contamination (see Chapter 1, and the discussion of other isotopic systems in this chapter).

The 10% value should be considered as a maximum value, because even if complete melting of the Sr and Nd-bearing phases occur, it is likely that a large proportion of the crustal material will remain in the solid residue. Estimates of the modal composition of crustal materials (Taylor & McLennan 1985) suggest that the Sr and Nd concentrations in the crustal melt might be up to 30-40% higher than those considered in this model. Without any changes in the slope of the mixing curves, less than 6% of this Sr and Nd-enriched component in the mixture would be required to produce the range in $^{87}Sr/^{86}Sr$ and $^{143}Nd/^{144}Nd$ values of most rocks in Sumatra and the Jawa sector.

As was anticipated in Chapter 4, estimation of the composition of the endmembers to be used in modelling Pb isotopic variations in arc volcanics is extremely difficult, partly because of difficulties in estimating the likely Pb contents and Pb isotope compositions of the endmembers, but mainly because of the poor understanding of the Pb-Th-U behaviour during melting and fluid extraction processes.

Despite these difficulties, Figures 5.2 and 5.3 clearly show that the arc volcanics in Sumatra and the Jawa sector have Pb isotope systematics similar to pre-Miocene sediments of the Northeastern Indian Ocean.

If the Pb isotope signature in these arc volcanics were the result of contamination of the mantle source by bulk sediment, or sediment-derived melt or fluid, we would expect the sediment to have overall more radiogenic or similar Pb isotope values compared with the arc rocks. This is not true. In fact, virtually all the arc rocks have Pb isotope values more radiogenic than the two analysed samples of pre-Miocene carbonaceous sediments, and some of the arc rocks have values even higher than the highest values measured in silicic sediments. Although, as observed by Ben Othman et al. (1989), a MORB magma source with as little as 2-3% of sediments in it will have Pb isotope values indistinguishable from those of sediments, it is unlikely that the present data set is not representative of the Pb isotope signature of sediments in the Northeastern Indian Ocean. Most sediments of the Northeastern Indian Ocean, including young and old sediments, have $^{207}Pb/^{204}Pb$ and $^{208}Pb/^{204}Pb$ in the range 15.65 - 15.72 and 38.6 - 39.3, respectively, and it seems that at least the Pb isotope systematics in arc rocks with $^{207}Pb/^{204}Pb$ and $^{208}Pb/^{204}Pb$ values higher than these

cannot be accounted for by sediment contamination of the mantle source.

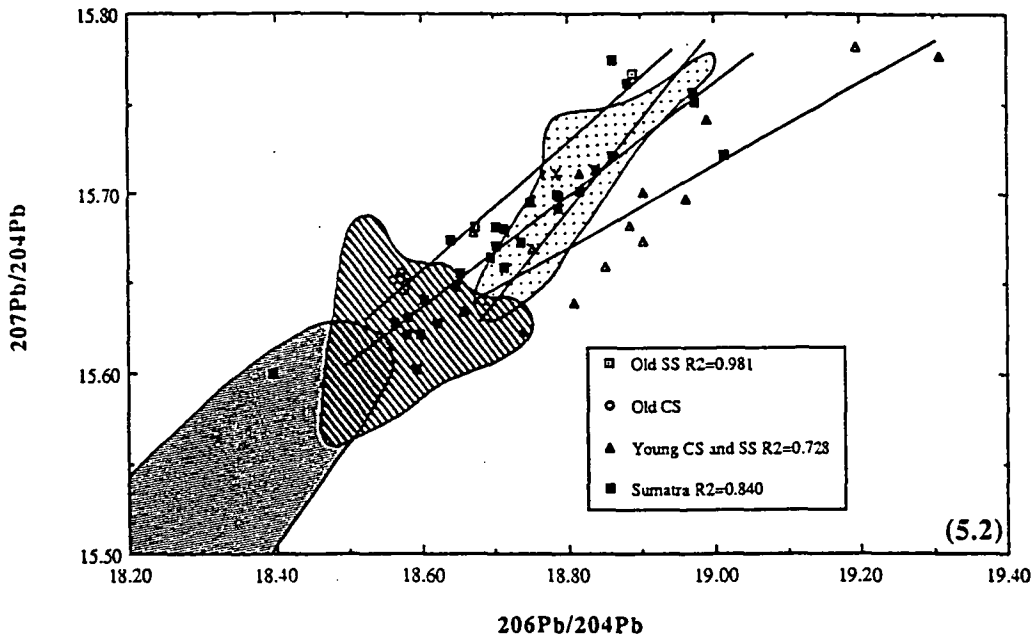

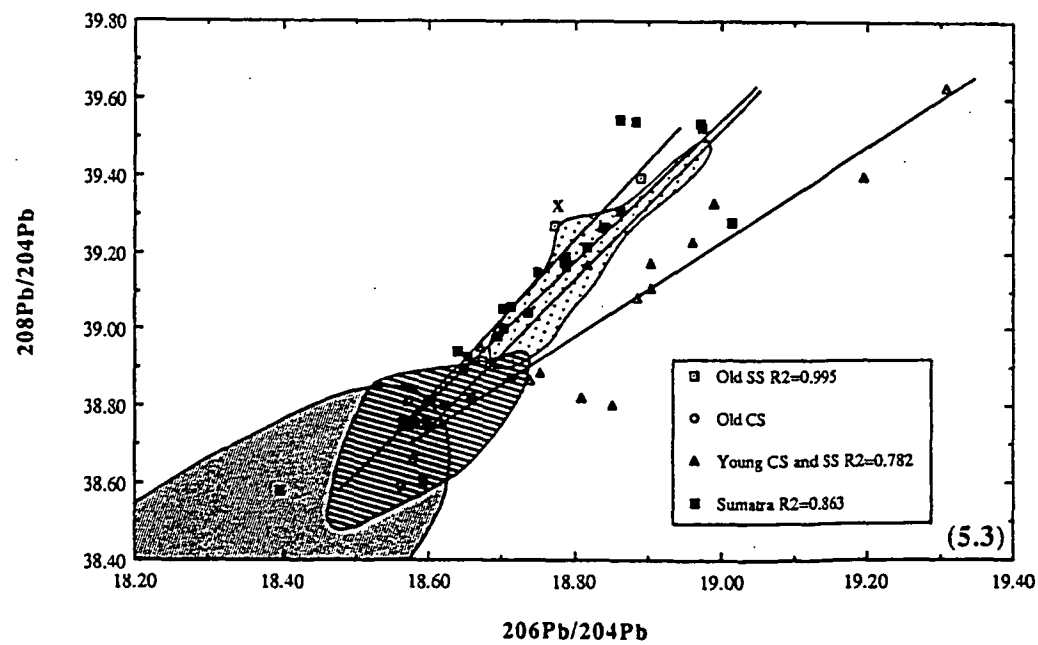

Figures 5.2 and 5.3. Pb isotopes diagrams for Quaternary arc rocks from Sumatra, west Jawa, and the Bali sector excluding Sumbawa. Fields and data sources as in Figure 5.1. Straight lines are the best fitting lines for four sets of samples (old silicic sediments - SS; Sumatran arc rocks; west Jawa arc rocks; and young sediments), and show that old sediments have Pb isotope values similar to those of Sumatran and west Jawanese volcanic rocks, whereas young sediments have higher $^{206}Pb/^{204}Pb$ values. Note the very good correlations (R^2 values reported in the legend). Point X as in Figure 5.1. See text for explanations.

In Chapter 4 it was shown that bulk mixing between the same endmembers used for the Sr-Nd isotopes mixing calculations can produce the Pb isotope values observed in pre - Miocene sediments. The same array is consistent with the mixing model discussed for Sr and Nd isotopes. Using the same Pb isotope values for the crust and the mantle source and Pb content in the crust discussed in Chapter 4, and a Pb content of 2 ppm (average Pb content in high-Ti basalts from south Sumatra), then approximately 10% (as for Sr and Nd isotopes) of the crustal component in the mixture is required to produce the Pb isotope values of most rocks in Sumatra and the Jawa sector. If a melt extracted from the crust will have higher Sr and Nd contents, then it will also be enriched in Pb, because, like Sr and Nd, Pb is also relatively concentrated in feldspars. Again, the assimilation of less than 6% of this Pb-enriched component in the mixture will produce the range in Pb isotope values observed in most arc rocks in Sumatra and the Jawa sector.

Another important point illustrated in Figures 5.2 and 5.3 is that, even if the radiogenic Pb isotope values observed in the arc rocks are due to subduction-related sediment contamination and not to crustal contamination, only pre-Miocene sediments seem to play a major role in the recycling process. As will be discussed later in this chapter, this is in agreement with $^{9}Be/^{10}Be$ data, that suggest that either young sediments are not recycled into Sunda arc magmatism, or that the recycling process occurs over a considerably long period of time (> 10 Ma).

5.5 Variation of the Sr, Nd, and Pb isotope composition in volcanic rocks along the west Sunda arc

In Figures 5.4 to 5.8, Sr, Nd, and Pb isotope ratios are plotted against distance along the arc (see figure caption). These data show that within each sector, samples that are geographically very close (1 degree of longitude) may show large differences in Sr isotopic ratios (normally up to 0.002, up to 0.004 in Sumatra). $^{87}Sr/^{86}Sr$ values of volcanic rocks in the Bali sector are generally lower. Note that values as low as 0.7040-0.7045 are found in all the sectors, and that very high $^{87}Sr/^{86}Sr$ values are found only in the volcanic rocks in the Toba area (see Chapter 2).

Rocks from west Jawa have Nd values lower than those of E Jawa and Bali, despite the similarities in $^{87}Sr/^{86}Sr$ values. Maximum $^{143}Nd/^{144}Nd$ values are in the range 0.51280 ± 5 except in the Bali sector, where values up to 0.5129 are common.

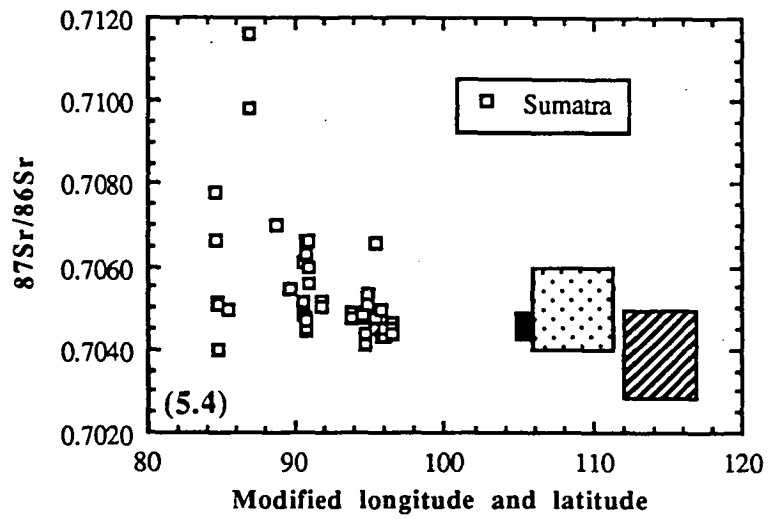

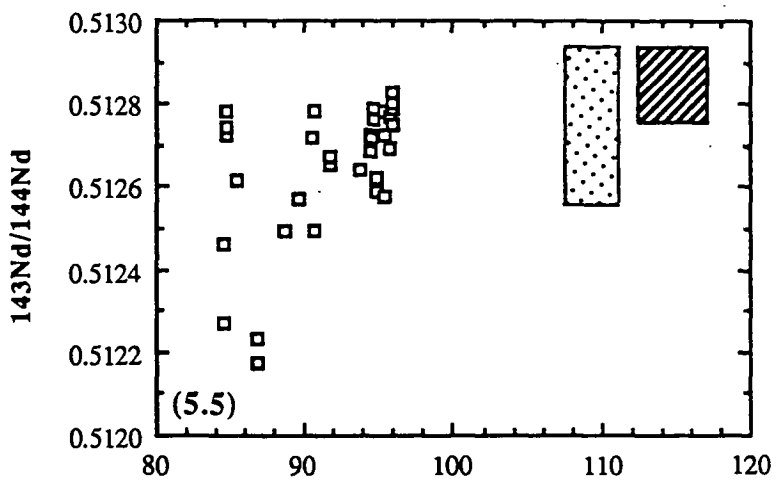

Figures 5.4 and 5.5. Along-arc variations of Sr and Nd isotopes in Quaternary arc rocks from Sumatra to Krakatau (black area), west Jawa (stippled area) and the Bali sector (ruled area) excluding Sumbawa. Distances along the x axis correspond to the location of the analysed samples, and are measured in degrees: longitude from Krakatau to Lombok (approximately from 105 °E to 117.°E), and latitude in Sumatra, measured from an arbitrary value of 100 and going from approximately 97 (south Sumatra) to 84 (north Sumatra). Data sources as in Figure 5.1.

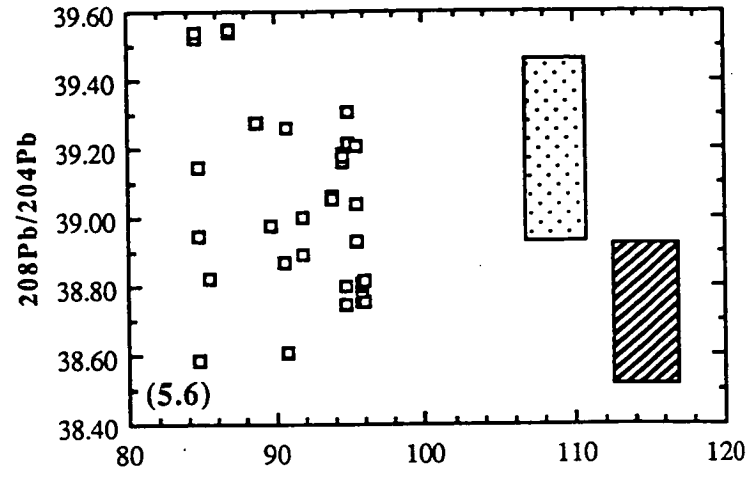

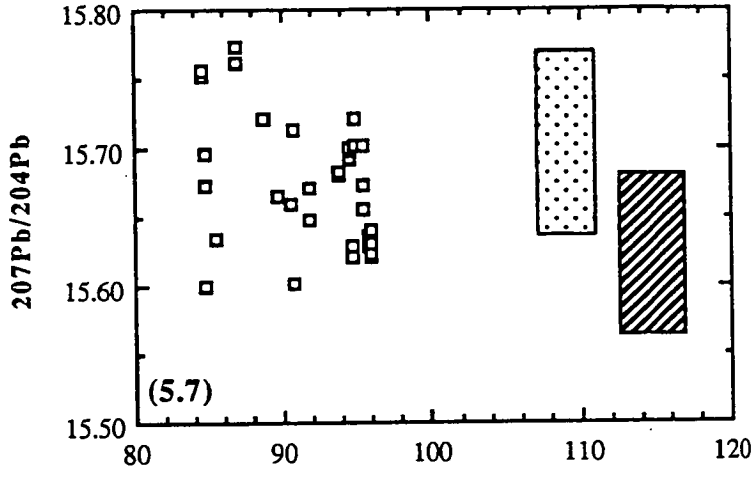

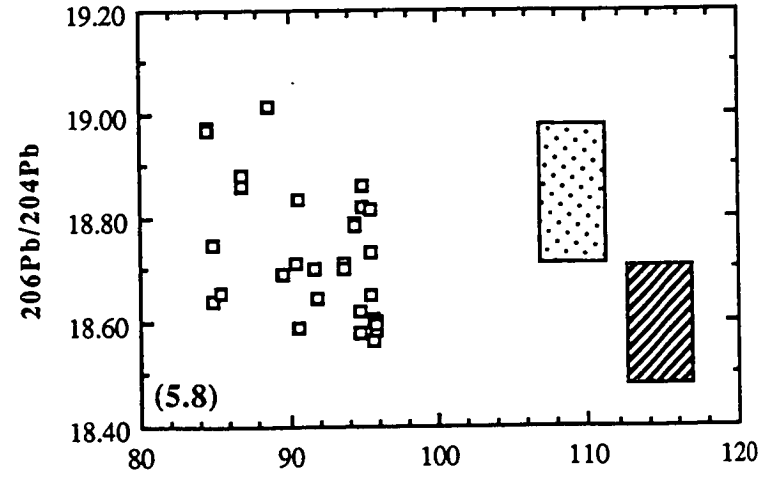

Figures 5.6 to 5.8. Along-arc variations of Pb isotopes in Quaternary arc rocks from Sumatra to west Jawa (stippled area) and the Bali sector (ruled area) excluding Sumbawa. Distances along the x axis correspond to the location of the analysed samples, and are measured in degrees: longitude from west Jawa to Lombok (approximately from 105 °E to 117 °E), and latitude in Sumatra, measured from an arbitrary value of 100 and going from approximately 97 (south Sumatra) to 84 (north Sumatra). Data sources as in Figure 5.1.

The variations in Pb isotopes are even more remarkable. Again, the lowest values are observed in the Bali sector, but many samples in Sumatra, especially in south Sumatra, also have relatively low Pb isotope values. As for Sr and Nd, Pb isotope variations within a sector are larger than among different sectors.

The important point is that rocks in the Bali sector have Sr, Nd, and Pb isotope systematics similar to those of "anomalous" Indian Ocean mantle (see next section), and the correspondence between low $^{87}Sr/^{86}Sr$ and Pb isotopes, and high $^{143}Nd/^{144}Nd$ values, and the lack of a continental crust in the Bali sector (e.g. Varne & Foden 1986; Hutchison 1989) is unlikely to be coincidental. Although sediment contamination of the source of the arc rocks can explain the Sr, Nd, and Pb isotope systematics of each sample in Sumatra and west Jawa, provided that the "right" sediment is used in the calculations, there are at least two reasons why it cannot explain the isotopic variations observed along the arc and within each sector.

First, it is difficult to understand how the large variations in isotopic ratios observed in a very small area can be produced by sediment contamination, where no variations in the composition of the sedimentary column, age and composition of the subducted crust, depth of the Benioff zone, and mechanical behaviour of the subducted slab are known or expected. In Chapter 2 it was pointed out that in Sumatra the volcanoes situated in the vicinity of large Quaternary calderas (Ranau, Maninjau, Toba) have considerably higher Sr and Pb and lower Nd isotopic ratios compared with volcanic centres situated far from these calderas, and the high Sr and Pb and low Nd isotopic ratios were interpreted as the result of significant contamination of the arc magmatism by Sumatran continental lithosphere. Therefore, it can be argued that, at least in Sumatra, sediment contamination in the source only produces a minor systematic increase in $^{87}Sr/^{86}Sr$ values and Pb isotopes, and decrease in $^{143}Nd/^{144}Nd$ values in the geochemically most primitive rocks, and the shift towards higher Sr and lower Nd isotopic ratios in centres located where there is a strong interaction of the magma with the crust - indicated by the formation of the calderas and large volume of silicic pyroclastic rocks - is caused by later crustal contamination of melts which had already suffered limited sediment contamination in the source. However, the isotopic values observed in the most isotopically and geochemically "primitive" samples in all the sectors of the west Sunda arc plot within the range of Indian Ocean basalts, and therefore no crustal nor sediment contamination is required to produce such values.

Second, this process does not explain the overall lower Sr and Pb and higher Nd isotopic ratios observed in the Bali sector compared with Sumatra and west Jawa.

Although it might be argued that the higher Sr and Pb and lower Nd isotopic ratios of Sumatra and west Jawa compared with those of the Bali sector are due to the fact that larger volumes of hemipelagic sediments and turbidites from the Ganges-Brahmaputra fluvial system are subducted beneath Sumatra and west Jawa, $^{9}Be/^{10}Be$ data, and $^{207}Pb/^{204}Pb$ and $^{208}Pb/^{204}Pb$ values in Sumatra and west Jawa, higher than those of post-Miocene sediments, all suggest that post-Miocene sediments (including the Ganges-Brahmaputra fluvial sediments) are not recycled into arc magmatism. This conclusion is also supported by the lack of along-arc variations in Sr, Nd, and Pb isotope systematics in the most primitive rocks from north Sumatra to west Jawa.

Plank (1993, and references therein) also concluded that only the pelagic sediments, but not the overlying turbidites, are subducted along Jawa, and assumed virtually constant composition and thickness of subducted sedimentary material from south Sumatra (DSDP site 211) to Sumbawa (DSDP site 261 and ODP site 765). A constant rate and composition of sediment supply from south Sumatra to Sumbawa cannot account for the variations in Sr, Nd, and Pb isotope systematics observed in relatively primitive volcanics from west Jawa to the Bali sector.

Furthermore, if the large volumes of post-Miocene sediments from the Ganges-Brahmaputra fluvial system were subducted and recycled into the magma source, we would expect to observe an increase in the "slab-derived" component in arc rocks from south to north Sumatra, corresponding to increasing volumes of subducted sediments, or at least a difference in Sr, Nd, and Pb isotopic values in arc rocks from Sumatra to west Jawa. It is not clear whether these Himalayan sediments are completely accreted rather than subducted, or simply, following the main argument of this chapter, do not have any pronounced effects on the source of arc magmatism. The key point is that no such along-arc differences in Sr, Nd, and Pb isotopic values are observed.

If only pre-Miocene sediments are subducted along the arc from Sumatra to the Bali sector, and if these sediments are responsible for the isotopic signature of the arc rocks, the overall lower Sr and Pb and higher Nd isotopic ratios in arc rocks in the Bali sector require that either sediments are not subducted or not recycled along the Bali sector. Alternatively, sediments subducted along this sector have overall lower Sr and Pb and higher Nd isotopic ratios compared with the sediments subducted along west Jawa and Sumatra. These requirements are actually in contrast with the known compositional characteristics and distribution of the sediments in the

Northeastern Indian Ocean.

5.6 Limitations of the model

In the previous paragraphs it was argued that the spatial variations and observed Sr, Nd, and Pb isotope systematics in the volcanics of the west Sunda arc, from Sumatra to west Jawa, can be modelled as the result of assimilation of crustal material by melts generated in the mantle wedge, but are not consistent with contamination of the source by subducted sediments or sediment-derived fluids. These conclusions are based on three assumptions.

First, it is assumed that only a mantle with the same Sr, Nd, and Pb isotope systematics observed in south Sumatra ("enriched" Indian Ocean mantle - see Chapter 6) exists in the mantle wedge along the arc from Sumatra to the Bali sector. This assumption is supported by two observations:

1) arc-related granitoids in Sumatra (see Chapter 2) have the same Sr, Nd, and Pb isotopic signature as the OIB basalts in south Sumatra (see Chapter 6), suggesting that the source that produced the OIB basalts exists in the mantle wedge at least from north to south Sumatra. Old, pre-Miocene volcanic rocks in Sumatra also have similar isotope systematics (Appendix C).

2) Varne & Foden (1986) and Stolz et al. (1990) suggested that isotopically non-MORB mantle exists beneath east Sunda, and ben Othman et al. (1989, page 14) observed that "*whether or not the subduction hypothesis is correct,* [Pb isotopic systematics in the Sunda arc] imply anomalous [i.e. non-MORB] mantle also exists beneath west Sunda, because an extrapolation of the west Sunda array intersects the radiogenic end of the Indian MORB array rather than average Indian MORB". This "radiogenic end of the Indian MORB field" also partially overlaps the field of basalts from the Bali sector and of the OIB basalts in south Sumatra (Figures 5.1 to 5.3). Furthermore, it was shown in Chapter 3 that basalts with similar Sr, Nd, and Pb isotope systematics appear to be relatively common in the Northeastern Indian Ocean. Interestingly, this isotopically "anomalous" mantle is capable of generating basalts with variable geochemical composition (from the "typical" OIB in south Sumatra, to the considerably more depleted basalts of the Ninetyeast Ridge - see Chapter 3).

Second, it is assumed that the pre-Miocene sediments discussed in this study are

representative of pre-Miocene sediments in the Northeastern Indian Ocean. Based on the available data this assumption is arbitrary, because the data only come from two sites (DSDP 22 211 and DSDP 27 261). If, as suggested by Kolla (1974) and Kolla & Kidd (1982), pre-Miocene sediments have a mainly volcanic origin, then it is reasonable to assume that these volcanic sources had Sr, Nd, and Pb isotope systematics similar to those of the anomalous mantle source discussed in the previous paragraph. The Ninetyeast Ridge volcanics and the pre-Miocene Sunda arc rocks (see Chapter 2 and Appendix C) have similar Sr, Nd, and Pb isotope systematics, and all must have been major sources of volcanogenic sedimentary material before the Miocene. Therefore the assumption that the pre-Miocene sediments discussed in this study are representative of pre-Miocene sediments in the Northeastern Indian Ocean is supported by all the existing data, and by geological evidence.

Third, although old Sumatran crust was used in the mixing calculations, it has not been shown that the same crust and continental basement found in Sumatra (SIBUMASU terrane - see Chapter 2) are present in west Jawa. However, according to Hutchison (1989), west Jawa, like Sumatra, has a continental pre-Mesozoic basement, and Sr, Nd, Pb concentrations and isotopic values similar to those estimated for the Sumatran crust can be expected.

5.7 Trace elements variations

According to Ben Othman et al. (1989), Cs/Rb, Ba/Rb, and Pb/Ce values can reveal the presence of subducted material in the source of arc rocks, because even though the absolute concentrations of these elements might change with magmatic processes (crystal fractionation and partial melting), in normal conditions their ratios remain virtually unchanged. Ben Othman et al. (1989) suggested that these ratios, and not other commonly used ratios (e.g. La/Sm, Ba/La), are unambiguous indicators of the presence of a slab derived component in the source of arc rocks, and their conclusions will be briefly commented on here.

Figure 5.9 shows that Cs is considerably enriched in sediments compared with crustal rocks, and that lower crustal rocks are relatively depleted in Rb (and Cs) compared with upper crustal rocks. The Cs/Rb and Ba/Rb values in crustal and sedimentary rocks reflect the extreme mobility of Cs in a fluid phase (fluid or fluid-rich melt). In fact, Cs is likely to be enriched relatively to Rb in any type of fluids and fluid-rich melts, including slab-derived and upper crustal material, and although high

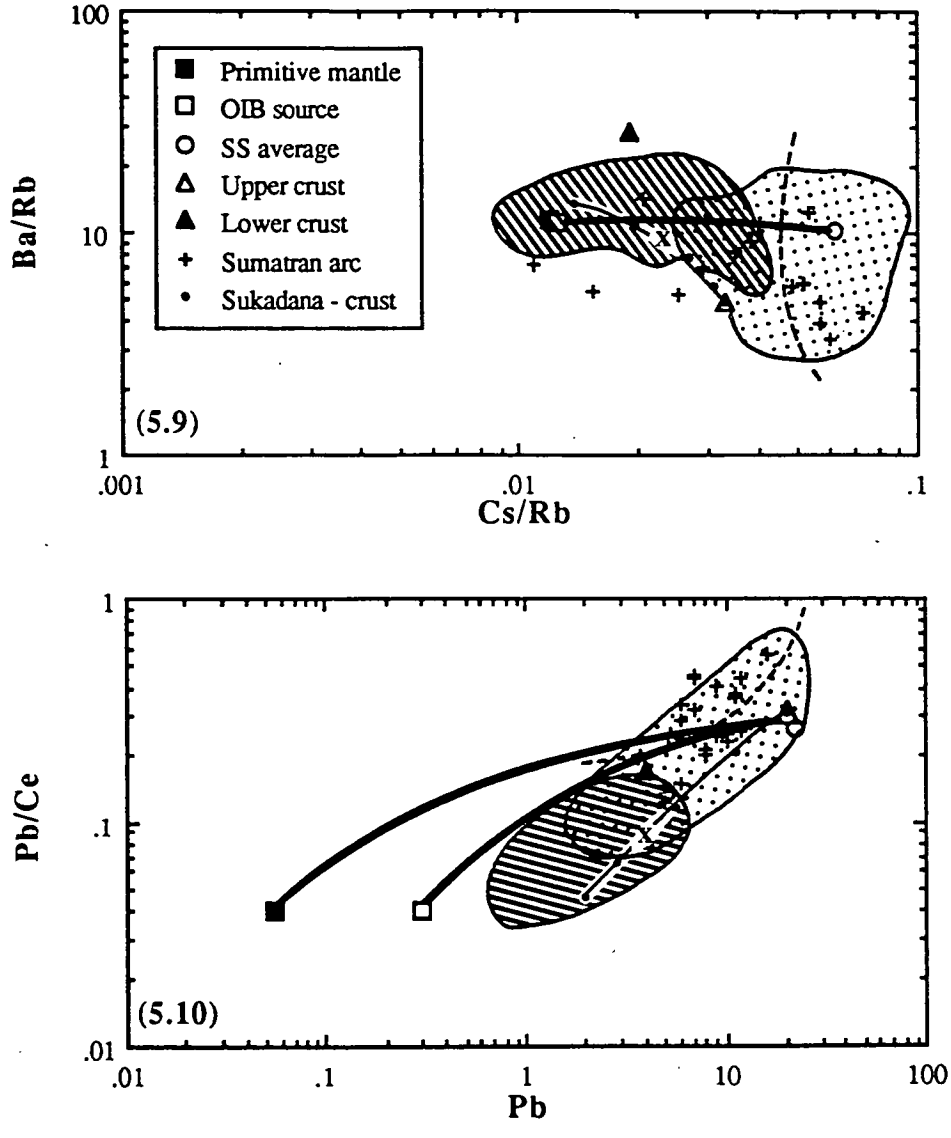

Figures 5.9 and 5.10. Cs/Rb versus Ba/Rb, and Pb versus Pb/Ce diagrams. Fields and data sources as in Figures 5.4 to 5.8. Field of rocks from the Bali sector includes the Sukadana basalts. Values of upper and lower crust are from Taylor & McLennan (1985). Primitive mantle and Cs/Rb and Ba/Rb for an OIB source (assuming that values in OIB = values in OIB source) are from Sun & McDonough (1989); Pb and Ce values for an OIB source are from Ben Othman et al. (1989). Thick lines are approximate mixing lines between mantle (OIB and primitive mantle) and silicic sediments (SS). Point X is 10% upper crustal material in a mixture between upper crust and Sukadana basalts (average values of high-Ti basalts). Sumatran rocks plotting right of (in the Cs/Rb - Ba/Rb diagram) and above (in the Pb - Pb/Ce diagram) the broken line are those situated in the proximity of large calderas and samples from Dempo.

Cs contents and Cs/Rb values unambiguously indicate that some enrichment occurred, they are not able to provide any indications of the nature of the enrichment process.

Silicic sediments and upper crustal material have similar Pb and Ce contents, and therefore plot virtually on the same point in a Pb/Ce - Pb diagram (Figure 5.10). As a consequence, as for Cs/Rb, high Pb and Pb/Ce values in arc rocks are evidence for some type of contamination, but they cannot distinguish between mantle source contamination and crustal assimilation.

A problem with these diagrams is that even relatively small analytical errors can produce large shifts in the position of the points. This is particularly evident for Pb, because 1 ppm is the precision of the methodology normally used (and also used in this study) to analyse Pb. Obviously these problems are bigger for elements that have low values close to detection limits, and where ratios have very small values (very large difference in absolute values, as for Cs and Rb). For these two reasons, Cs/Rb values are subject to very large errors.

Despite these limitations, four important points are illustrated in Figures 5.9 and 5.10.

First, neither bulk assimilation of crustal material (Cs/Rb values too low) by an OIB or MORB magma, nor bulk sediment (Ba/Rb values too high) mixing with a mantle source (irrespective of its composition) can account for most of the Cs/Rb and Ba/Rb values observed in Sumatra and west Jawa. On the other hand, both bulk assimilation of crustal material by an OIB or MORB magma and bulk sediment mixing with a mantle source could account for the Pb and Ce contents in some of the most geochemically primitive rocks in Sumatra and west Jawa. However, in either case the amount of Pb-rich material required to produce the Pb and Pb/Ce values observed in these arc rocks would be much greater than 10%.

Second, OIB basalts from south Sumatra have Cs/Rb, Ba/Rb, and Pb/Ce values indistinguishable from those of an OIB source (but different Cs, Rb, Ba, Ce, and Pb contents). Rocks from the Bali sector also have similar Cs/Rb, Ba/Rb, Pb/Ce and Pb values.

Third, a large spread in Cs/Rb, Pb/Ce, and Pb values is observed even in samples from the same volcano. For example, two samples from Sekincau in south Sumatra (samples 75232 and 75233 - see Appendix C) have very different Cs/Rb values, respectively 0.053 and 0.025. It is difficult to believe that the flux of sediment-derived material from the subducting slab was twice as high in the source of sample 75232 compared with the flux in the source of sample 75233, or that the source was

grossly heterogeneous in Cs/Rb values. More likely, these differences in Cs/Rb values occurred after the magma was formed.

Fourth, samples from volcanoes situated in the proximity of large pyroclastic deposits along the arc, from the lake Toba area, and from Dempo in south-central Sumatra, have not only higher $^{87}Sr/^{86}Sr$ and Pb isotope, and lower $^{143}Nd/^{144}Nd$ values, but also overall higher Cs/Rb and Pb/Ce values, and higher than the upper crustal values.

All these features confirm that most arc rocks in Sumatra and west Jawa suffered some contamination by Cs-rich and Pb-rich material (fluids or melts). However, Cs/Rb, Ba/Rb, Pb/Ce, and Pb values seem unable to distinguish between contamination of the mantle source by slab-derived Cs-rich and Pb-rich fluids and assimilation of Cs-rich and Pb-rich crustal material by mantle-derived melts. The variability in Cs/Rb and Pb/Ce values even in volcanics from the same centre and in different volcanoes from the same area suggest that the enrichment in Cs and Pb is not a systematic process, as might be expected for a contamination in the source, and is therefore not an essential part of the process that is producing the characteristic geochemistry of arc volcanics.

5.8 A "bulk sediment mixing" approach

It is generally believed that if sediments play a major role in the genesis of arc magmas, then either melts or fluids (or both) derived from the sediments, and not bulk sediments, mix with the mantle wedge to produce the LILE and LREE enrichment observed in arc volcanics. However, if only major and trace elements are used in the mixing models, it is difficult to estimate the bulk composition of the sediment-derived material which metasomatises the mantle wedge, and it is generally and implicitly assumed that a) this material has the same composition as the sediments sampled in the ocean floor, and b) the metasomatism can be described as a bulk mixing.

As was discussed early in this chapter, this approach is fundamentally incorrect (and hence the need for the use of isotopes for the understanding of sediment/mantle interactions), and yet it is still used by some authors. For example, Plank & Langmuir (1993) estimated the bulk composition of sediments subducted along eight volcanic arcs and suggested that, taking into account the effects of magmatic

processes (different degrees of partial melting and crystal fractionation), the LILE and LREE output in arc volcanics reflects the sediment input. These conclusions are based on a number of assumptions which will be briefly discussed here only for the Sunda arc.

First, in their calculations Plank & Langmuir (1993) used a convergence rate along Jawa of 8.1 cm/yr (Jarrard 1986), notably higher than the convergence rate of 6 to 7 cm/yr calculated in more recent studies (e.g. McCaffrey 1991), and the higher convergence rate results in higher estimated sediment fluxes.

Second, data from sites DSDP 261 and ODP 765 (and very few data from site DSDP 211), both situated off the east Sunda arc were used to estimate the bulk composition, water content, density, and sediment thickness of sediments off Jawa. Plank & Langmuir (1993) therefore assumed that the sediment flux is constant from south Sumatra (site DSDP 211) to Sumbawa (sites DSDP 261 and ODP 765), a distance of some 1700 km. Although, as was shown in Chapter 4, the major and trace element composition of the silicic and carbonaceous components of sediments in the Northeastern Indian Ocean do not seem to show variations along the Sunda arc, sediment thickness, water content, and bulk composition do vary. In particular, sediments off Jawa are believed to be less than 300 m thick (with the exception of the Roo Rise - see Udintsev et al. 1975), whereas in east Sunda (sites DSDP 261 and ODP 765) they are generally thicker than 500 m, and the water (and other fluids) content in the subducted sedimentary column is unlikely to be as high as 40% (see Chapter 4), as estimated by Plank & Langmuir (1993). Again, these values result in higher estimated sediment fluxes.

Third, and most important, Plank & Langmuir (1993) selected 6 volcanic centres from the volcanic front in west Jawa, out of the 35 active volcanoes of Jawa, to calculate the average basaltic composition of Jawanese volcanoes situated along the volcanic front (Tables 5.1a-b). As was shown by Wheller et al. (1987) (see also Table 5.1b, and discussion in paragraph 5.5), the K-group elements and LREE contents vary remarkably along the Sunda arc and from west to east Jawa, and the "average basaltic composition" of volcanoes of Jawa calculated by Plank & Langmuir (1993) does not represent any real composition (Table 5.1b). Therefore the "bulk sediment input - volcanic output" approach used by Plank & Langmuir (1993) to characterise the geochemical composition of Jawanese volcanics deliberately ignores and fails to account for the importance of along-arc geochemical variations, an important characteristic of the Sunda arc.

Arc	Guatemala	Mexico	Java	Tonga	East Aleutians	North Antilles	Vanuatu	Marianas
Convergence rate (cm yr^{-1})	6.4	6.5	8.1	12.2	5	3.7	8.6	7.7
Sediment thickness (m)	400	200	300	100	500	250	650	400
– / – (m)	100	50	100	50	100	50	100	100
Density (g cm^{-3})	1.62	1.37	1.65	1.29	1.71	1.66	1.6	1.93
Water (wt%)	49	59	40	64	38	37	38	23
Bulk compositions of sediment sections								
K_2O (wt%)	0.67	1.23	2.50	2.09	2.22	1.31	2.29	0.95
Ba (p.p.m.)	3,250	2,175	1,068	2,105	1,582	204		306
Sr (p.p.m.)	1,237	234	218	261	234	111	293	76.4
Rb (p.p.m.)	21.8	49.4	88	55.4	59.7	84	20	26.5
Cs (p.p.m.)	1.31	3.2	4.9	3.18	3.47	4.89		1.5
La (p.p.m.)	16.83	42.4	39.08	110.2	19.36	35.54		13.5
U (p.p.m.)			1.47	1.46	2.58	1.36		0.45
Th (p.p.m.)	1.42	8.6	9.8	9.57	5.92	12.1		2.23
Sediment fluxes (g yr^{-1} per cm arc length)								
K flux	1,176	746	4,960	983	4,885	1,454	10,542	3,610
Ba flux	687	159	255	119	419	20		140
Sr flux	261.6	17.1	52.1	14.8	62.0	10.7	162.5	35.0
Rb flux	4.61	3.61	21.03	3.14	15.82	8.13	11.09	12.13
Cs flux	0.28	0.23	1.17	0.18	0.92	0.47		0.69
La flux	3.56	3.10	9.34	6.24	5.13	3.44		6.18
U flux			0.35	0.08	0.68	0.13		0.21
Th flux	0.30	0.63	2.34	0.54	1.57	1.17		1.02
Average basaltic compositions								
K 6.0	0.71	1.02	1.01	0.35	0.77	0.53	0.95	0.61
Ba 6.0	397	302	269	122	298	108	206	163
Sr 6.0	539	526	340	195	460	360	584	310
Rb 6.0	11.9	13.2	21.4	4.2	12.6	5.4	16.9	9.5
Cs 6.0		0.56	0.94	0.20	0.51	0.16		0.32
La 6.0	6.7	10.8	11.6	1.2	8.2	5.4	7.5	4.9
U 6.0		0.42	0.64	0.12	0.63	0.41	0.41	0.24
Th 6.0	0.99	0.91	2.95	0.13	1.56	1.10	1.00	0.56
Na 6.0	2.90	3.87	2.98	1.57	2.87	2.76	2.53	2.39
Number of volcanoes	11	5	6	5	6	4	4	8

Table 5.1a Sediment fluxes into trenches and arc basalt composition (Table 1 of Plank & Langmuir 1993).

Volcano		Na6	Na#	K6	K#	Ba6	Ba#	Sr6	Sr#	Rb6	Rb#	Cs6	Cs#	La6	La#	U6	U#	Th6	Th#
Galunggung	low-K/Na	2.9	6	0.38	2	104	2	244	2	9	2	0.47	1	5.45	1	0.23	2	0.89	2
Guntur	low-K/Na	3	6	0.48	4	105	1	315	4	9.5	4	0.46	1	5.34	1	0.2	1	0.6	1
Slamet	medium-K/Na	3.2	6	1.15	6	246	1	294	6	22.9	6		0	17.4	1	0.87	1	3.46	1
Sumbing	medium-K/Na	2.95	6	1.24	1	336	1	310	1	30.3	1		0		0		0		0
Merapi	high-K/Na	2.9	6	1.45	1	409	1	496	1	29.8	1		0		0		0		0
Merbabu	high-K/Na	2.8	6	1.85	1	577	1	496	1	35.1	1	1.49	1	13.3	1	0.99	1		0
Ave*		**2.98**		**1.01**		**268**		**340**		**21.4**		**0.94**		**11.6**		**0.64**		**2.96**	

Table 5.1b Average basaltic composition of some low-K/Na (Galunggung and Guntur), medium-K/Na (Slamet and Sumbing), and high-K/Na (Merapi and Merbabu) Jawanese volcanoes. The six volcanoes listed here were chosen by Plank & Langmuir (1993) as representative of the low-K/Na, medium-K/Na, and high-K/Na volcanoes of Jawa, and the average basaltic composition (Ave*) of the Jawanese volcanoes is based on the relative abundances of low-K/Na, medium-K/Na, and high-K/Na volcanoes described by Whitford (1977). Na6, K6, Ba6 etc. are the calculated Na, K, Ba, etc. contents for MgO=6%, and Na#, K#, Ba#, etc. are the number of samples for each element used in the calculations. Na and K in weight percent, others in ppm. Note the very small number of samples: for example, no Cs values were available for the medium-K volcanoes, and these were probably estimated from the Cs contents in the high-K volcanoes. All data and calculations are from Plank (1993) and references therein.

It should be noted that the variations in LILE concentrations observed among different volcanic centres in Jawa are as large as those observed among different arcs. For example, the Ba content ranges from approximately 105 ppm (in the low-K/Na volcanoes Galunggung and Guntur) to more than 400 ppm in the high-K/Na volcano Merbabu (Table 5.1b), the same range observed in all the arcs studied by Plank & Langmuir (1993) (Table 5.1a). The same is true for the other LILE. Following the model of Plank & Langmuir (1993), this would imply large variations in sediment fluxes (and therefore composition and mass of subducted sediments) along Jawa, which is in contrast with one of the basic assumptions of the model.

Furthermore, large variations in element fluxes in different arcs do not always correspond with variations in basaltic compositions. For example, the calculated average K contents in Mexico and Jawa are similar, although the sediment K flux into the two arcs is very different, and the sediment K flux in Vanuatu is twice as high as in Jawa, but the two arcs have similar average K content.

Fourth, Plank & Langmuir (1993) seem to describe a bulk mixing between sediments and melts from a N-MORB source, although neither the mixing process nor the mechanisms of partial melting of the mantle source are sufficiently explained and discussed in their article. Furthermore, their partial melting trends are calculated assuming that clinopyroxene is the only melting phase, and it is not clear how the element concentrations corresponding to MgO=6% (only samples of arc volcanics with MgO>6% are discussed, to minimise the effects of melting and crustal differentiation) were calculated. Also, it should be noted that the Sc content in Indian Ocean sediments is relatively low (less than 20 ppm - see Chapter 4), and therefore bulk sediment contamination would produce low Sc contents in arc volcanics (see Figure 2 in Plank & Langmuir 1993).

Finally, and most important, Plank & Langmuir's (1993) model cannot distinguish between sediment contamination of the source and crustal contamination occurring during the early stages of crystallisation. In fact, the model implicitly assumes that the enrichment (compared with N-MORB) in LILE and LREE in arc volcanics is solely due to the sediment input (the possibility of crustal contamination of magma with MgO>6% is not discussed), and, based on this assumption, suitable compositions of arc volcanics, sediments, and sediment fluxes have been carefully selected.

For these reasons, Plank & Langmuir's (1993) model fails to explain the along-arc variations in K-group elements and LREE and, in particular, is inconsistent with the

geochemical and isotopic variations observed from west to east Jawa and the Bali sector.

5.9 Other isotope systems

The study of isotope systematics other than those of Sr, Nd, and Pb isotopes, has been applied to the Sunda-Banda arc volcanics only in a very limited number of articles, and those results are briefly discussed here.

5.9.1 O and He isotopes in the Banda arc and the Flores sector of the Sunda arc.

Oxygen isotope data for some andesites of the Banda arc were first presented by Magaritz et al. (1978), who pointed out that the high $\partial^{18}O$ values measured in most volcanics are primary features of the rocks and not the result of secondary post-eruptive alteration.

$\partial^{18}O$ values in MORB range from 5.35 to 6.04, according to Ito et al. (1987), and therefore all the volcanics in the Banda arc measured by Magaritz et al. (1978), with the exception of Manuk ($\partial^{18}O$ = 5.6) have values higher than the MORB values (Figure 5.11). The good correlation between $\partial^{18}O$ and $^{87}Sr/^{86}Sr$ led Magaritz et al. (1978) to believe that the high $\partial^{18}O$ values are not the result of magmatic processes, and other geochemical characteristics of the rocks ruled out some other possible origins (e.g. melting of subducted oceanic crust). The high $\partial^{18}O$ values were explained as the result of the mixing of mantle with up to 50% of a "sedimentary endmember", likely to be continent-derived crustal material (based on the $^{87}Sr/^{86}Sr$ values and on the Sr content) rather than non-terrigenous oceanic. Magaritz et al. (1978) also pointed out that a simple two-component bulk mixing model is likely to be an oversimplification of the real situation.

The nature and Nd and Pb isotopic composition of the mantle were not specified, and the possible existence of O and Sr isotope heterogeneities in the mantle was not investigated. However, based on the data published by Ito et al. (1987), Indian Ocean MORB have $\partial^{18}O$ values similar to those of Pacific and Atlantic MORB, so that if MORB mantle alone were involved in the source of the Banda volcanics, it would produce lower $\partial^{18}O$ values than those observed. The effects of crystal fractionation, to an extent consistent with the composition observed in the Banda rocks, would not increase the $\partial^{18}O$ to the values observed in most centres.

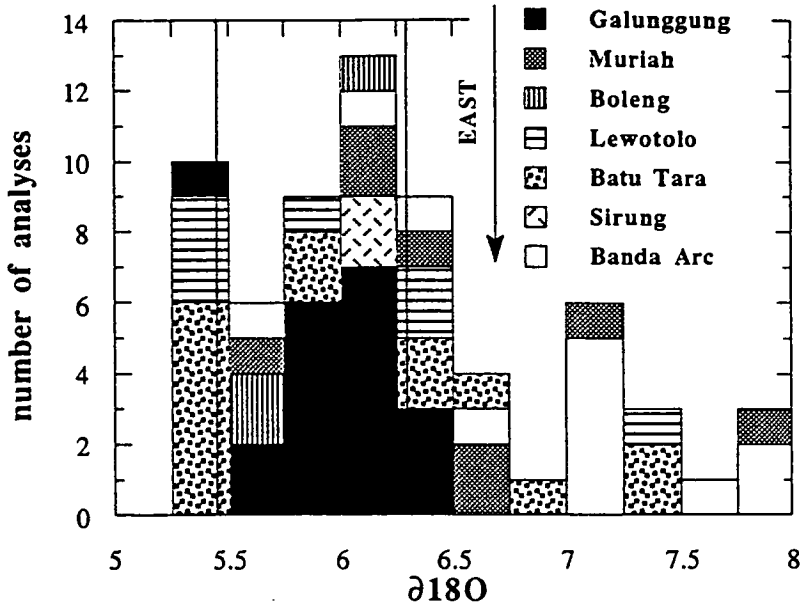

Figure 5.11. Oxygen isotope data histogram for the Sunda-Banda arc rocks, excluding the cordierite-bearing volcanics from Ambon ($\partial^{18}O$ = 14.1 to 16.7, in Magaritz et al. 1978) and the volcanics from Wetar ($\partial^{18}O$ variable from 6.2 to 18.1) described by McCulloch et al. (1983), but for which no $\partial^{18}O$ analyses were published. Data from references quoted in text. Volcanic centres are listed from west to east. The two parallel lines at $\partial^{18}O$ 5.4 and 6.3 mark the field of MORB basalts according to Ito et al. (1987).

Strong evidence for crustal contamination in the Banda arc is the existence of cordierite-bearing lavas in Ambon ("ambonites") with high $^{87}Sr/^{86}Sr$ and $\partial^{18}O$ values (respectively 0.716-0.717, and 14.1 to 16.7), and McCulloch et al. (1983) suggested that the trend towards high $^{87}Sr/^{86}Sr$ and $\partial^{18}O$ (respectively up to 0.72227 and 18.1) and low $^{143}Nd/^{144}Nd$ values observed in Wetar can be produced by "complex fractionation-assimilation processes operating within the arc crust".

Very low R/RA (R/RA is the ratio between the measured $^{3}He/^{4}He$ value in the sample, and atmospheric $^{3}He/^{4}He$ value) (1.31 to 1.69), among the lowest values measured in any island arc (Poreda & Craig 1989), were found in some Banda volcanoes where the volcanic rocks also have high $\partial^{18}O$ values and a broad correlation may exist between Sr, O, and He isotope ratios. For example, Banda island has the highest $^{3}He/^{4}He$, lowest $^{87}Sr/^{86}Sr$ values, and lowest $\partial^{18}O$ values of the Banda volcanoes, but $^{3}He/^{4}He$ of Serua is only slightly higher than that of Teun,

despite $\partial^{18}O$ and $^{87}Sr/^{86}Sr$ values which are considerably higher. However, few if any of the Banda samples which have been analysed for O and Sr isotopes are among those which have also been analysed for He isotopes, so any speculation about the causes of the apparent relationship is premature.

Even more complex are the O and He isotope systematics in the Flores sector, at the transition from the Banda sector of the arc, where the arc is colliding with the northward-migrating Australian margin, to the eastern Sunda sector, where Indian Ocean lithosphere is being subducted at the Jawa trench.

Not surprisingly, the most dramatic He and O isotopic variations are observed along and in the proximity of the Pantar Fracture, where $\partial^{18}O$ values range from MORB values in Boleng and Sirung (Varekamp et al. submitted for publication) to mainly MORB values, but up to approximately 7.5 for the Lewotolo and Batu Tara volcanoes (Stolz et al. 1988; Poorter et al. 1991; Varekamp et al. submitted for publication) (Figure 5.11), and R/RA values range from extremely low (0.0075 in Werung volcano in Lomblen) up to 4.5 in Batu Tara, 6 in Keli Mutu, and 7.3 - within the range of MORB values - in Sangeang Api (Sumbawa) (Hilton & Craig 1989; Hilton et al. 1992; Hilton, pers. comm.). Interestingly, Boleng and Sirung seem to have whole-rock $\partial^{18}O$ values (data reported in Varekamp et al. submitted for publication) well within the MORB range, but also very radiogenic $^{3}He/^{4}He$ values (R/RA respectively 1.43 and 1.01), with very small standard deviations, that were measured on clinopyroxene-olivine separates.

Hilton et al. (1992) presented some models of crustal and oceanic sediment contamination, and concluded, based on estimates of the He contents and $^{3}He/^{4}He$ values, that:

1) subducted continental crust (not sediments) is the principal source of radiogenic He in the Banda and east Sunda arc (at least as far west as Iya volcano in central Flores);

2) the extent of contamination decreases down-dip (i.e. for increasing depths of the Benioff zone) and away from the seismically inactive zone, from Alor to Romang. Hilton et al. (1992) did not consider the possible effects on $^{3}He/^{4}He$ values of the Pantar fracture, and concluded that the along-arc variations in He isotopic values in this sector of the Sunda arc are related only to the distance from the collision zone;

3) the decoupling of the He from the Sr isotope signature along the arc may be due either to different sources for He and Sr enrichment (e.g. He supplied by the crust, and Sr by the sediments), or of large differences in the He/Sr values in the endmembers (for a discussion of the reasons for the decoupling between $^3He/^4He$ and other isotope systems, see also Hilton et al. 1993).

5.9.2 Origin of He isotope variations in arc rocks

Taking into account the mineralogical composition and grain size of the Indian Ocean sediments, Hilton et al. (1992) estimated that unconsolidated oceanic sediments will lose all their He in a very short time. He loss will be faster for smaller particles and higher temperatures, so that increasing temperatures as the subduction zone is approached will increase the rate of loss. As a result, old sediments will have lost their He before approaching the subduction zone, whereas young sediments rich in He will lose it very quickly during the first phases of the subduction. In other words, He in sediments is very volatile, in fact too volatile to be subducted, so that the subducted sediments will have lost their He well before the slab reaches the depth of generation of the arc magmas. In support of this conclusion, recent $^3He/^4He$ analyses of old (Lower Cretaceous) claystones from DSDP site 261 (off Sumbawa) gave He concentrations of approximately 1 μcc STP/g (D. Hilton, pers. comm.), much lower than the values (approximately 0.007 to 0.0004 cc STP/g) estimated by Hilton et al. (1992) and used in their calculations, and the values estimated by Staudacher & Allègre (1988) for other oceanic sediments.

Hilton et al. (1992) conclude that "although sediments are unlikely to have supplied the radiogenic He, this is not necessarily the case for strontium or other elements". This may explain the observed decoupling between He and Sr isotopes, and also implies that He isotopes cannot, in general, be used to identify the presence of subducted sediments; only the involvement of consolidated crustal material in the source mantle can increase the ^4He content in the arc magmas. However, a few comments about the conclusions by Hilton et al. (1992) should be made.

In general, the temperature of the sea-floor will be close to 0-5 °C, and the temperature of the sedimentary column is likely to be in the same range, even for very thick columns. Under these conditions, even relatively small grains (5-10 μm) of minerals with high He retentivity (like hornblende, which was used by Hilton et al. 1992 to estimate the He retentivity, and other minerals with activation energies similar to that of hornblende and that have been found in most DSDP cores in the

Northeastern Indian Ocean, such as augite and sulphates; see Lippolt & Weigel 1988) will retain most of their He even as long as 140 Ma, the approximate maximum age of sediments in site DSDP 27 261).

During the early stages of subduction, when He will be lost due to the increase in temperature, both He and Sr (and the other "volatile" elements) will partition into the fluid phase, and although the He might effectively escape from the host mineral grains, it might remain in the slab-derived fluids and be carried down. In this case, only if He exsolves from the fluid phase, leaving behind the other incompatible elements, before the fluid reaches the depth of generation of the arc rocks, will He - Sr decoupling occur. Although this might be thermodynamically possible, it is difficult to believe that the slab is permeable enough to allow the systematic loss of He but not of the other fluid/gaseous phases. Therefore high $^{3}He/^{4}He$ values in arc rocks will be considered as evidence for the lack of contamination by crustal *and* sedimentary material.

The problem of the loss of He as a function of mineralogy, grain size, age, and temperature is one aspect of the more general question of the compositional changes that might occur to subducted sediments during the various stages of subduction, a consequence of the selective mass transport of various elements. Evaluation of the flux of various slab-derived elements entering the trench during the subduction process is relatively easy compared with the evaluation of the amounts of this flux into the trench that goes on to be subducted into the deep mantle, as opposed to the amounts which are either retained in the arc crust within the accretionary prism, or returned to the arc crust through involvement in arc magmatism, or fixed in the mantle wedge.

Although it might be argued (e.g. Reid et al. 1989; Leeman et al. 1992) that some elements which have high concentrations in arc rocks (e.g. Cs, U, B) are depleted (compared with their original concentrations in the pre-metamorphosed rocks) in the residual rocks that have undergone metamorphism in a subduction environment (with the implication that, for mass balance, the fluids derived from these rocks must be enriched), the exact mass transfer processes are poorly understood, and are usually only deduced from the composition of arc rocks (e.g. Plank & Langmuir 1993).

This is actually a good example of sophistry applied to geology, which gives rise to another problem, as was observed by Leeman et al. (1990; see also Peacock 1990 for a review of the ideas on the mechanical behaviour of the sedimentary column during

subduction): if some elements are very soluble in the dehydration fluid phase at shallow depths (« 100 km), how can they be carried down to the depth of generation of the arc magmas, and not be released through the accretionary prism during the early stages of the subduction before the fluids metasomatise the mantle wedge at the depth of generation of the arc rocks? The behaviour of volatiles in subduction zones is a function of the thermal gradient and fluid composition, itself a function of P-T conditions. As the fluids must be efficiently trapped in the slab to be carried to depth, the geometry and mechanical behaviour of the sedimentary column are also likely to be, like the grain size, important variables. The understanding and quantification of these processes and variables will continue to be one of the most challenging problems in geochemistry and isotope geochemistry for the next few years at least.

5.9.3 B/Be and Be isotopes in the Sunda arc

Two elements, B (B/Be values) and Be (Be isotopes), which are potentially useful for the solution of these problems have been studied in the Sunda arc. Be isotopes and B/Be systematics in the Sunda arc have been briefly reviewed in Chapter 1, where appropriate references are also cited, but a further comment on Edwards et al. (1993) is appropriate here. Edwards et al. (1993) make the following points:

1) MORB and OIB, even the HIMU and EMII types, have low and indistinguishable B/Be values of 3-5, and therefore "B/Be in arc volcanics are insensitive to the pre-existing composition of the mantle wedge and are strongly controlled by the subduction zone component";

2) Be and B have "similar bulk distribution coefficients in arc lavas", and their ratio is "largely unaffected by partial melting and fractional crystallisation", although "enhanced solubility of B relative to Be in hydrous fluids is expected, and could produce variations in the ratios. The high ratios in arc lavas seem to require preferential extraction of B from the slab relative to Be, probably by a hydrous fluid".

3) The estimated residence time of B in the sub-arc mantle is ≤ 5 Ma, and therefore "only lavas derived from mantle which has been modified recently by subduction will have high B/Be values, and older subduction will produce lavas with B/Be values similar to MORB and OIB".

4) The different Sr, Nd, and Pb isotope systematics are interpreted as evidence for the existence of a heterogeneous mantle, and the high B/Be values in calcalkaline

volcanics are related to a "high B/Be subduction component", which will not produce "pronounced Sr and Nd isotope signatures". However, the calcalkaline and tholeiitic volcanics seem to "record greater extremes of mantle isotopic composition than do the smaller volume alkaline lavas".

5) The new ^{10}Be data are similar to those reported by Tera et al. (1986), and "low ^{10}Be concentrations in the Indonesian lavas require only that any subducted sediment involved in magma genesis be too old to contain ^{10}Be".

The evidence for point 1) is very weak. Very few basalts have been analysed both for B and Be, and more data are required to confirm that OIB and MORB have systematically low B/Be values in the range 3 to 5. Other very sensitive indicators of the presence of a subducted component show very large variations in MORB and in various types of OIB (e.g. R/RA values range from 5 to 30). Although the existence of B/Be variations in different types of OIB is not necessary for the following discussion, the possibility of mantle heterogeneities with respect to B/Be should be taken into account. At least the samples with B/Be < 3 (some samples of Watukubu and Ringgit Beser discussed by Edwards et al. 1993) require either B/Be fractionation or the existence of reservoirs with B/Be different from those measured so far.

The higher solubility in hydrous fluids of B relative to Be is consistent with the preferential extraction of B from the slab relative to Be, but the B concentration also increases in the melt during magmatic differentiation. Ryan & Langmuir (1993) observed that solid/melt partition coefficient of B approximates that of K during melting in the mantle, low-pressure crystallisation, and differentiation processes in arc volcanics. A good positive correlation can therefore be expected between B/Be values and any index of differentiation (e.g. SiO2) during magmatic differentiation.

A good correlation between SiO_2 and B in volcanics from several arcs was observed by Ryan & Langmuir (1993), and a positive correlation between B/Be values and SiO_2 can be observed in four of the five calcalkaline volcanoes studied by Edwards et al. (1993) (Figure 5.12). Excluding one sample from Seram with B/Be = 7, Seram and Guntur show the same, almost perfect, positive correlation between B/Be and SiO_2. An extrapolation of the trend towards SiO_2 contents of about 48% suggests that less evolved compositions would be expected to have B/Be values within the range observed in MORB and OIB. The same extrapolation indicates similar SiO_2 and B/Be values for Keli Mutu, whereas the calcalkaline rocks of Ringgit Beser

indicate lower SiO_2 (similar to the SiO_2 values in the alkaline volcanics) for B/Be values within the MORB-OIB range.

If the high B/Be values were the result of a contamination of the mantle source, as suggested by Edwards et al. (1993) and Ryan & Langmuir (1993), then we would expect to see high B/Be values even in the most primitive basalts. The positive SiO_2 - B/Be correlation, and the low B/Be inferred for primitive compositions, suggest that

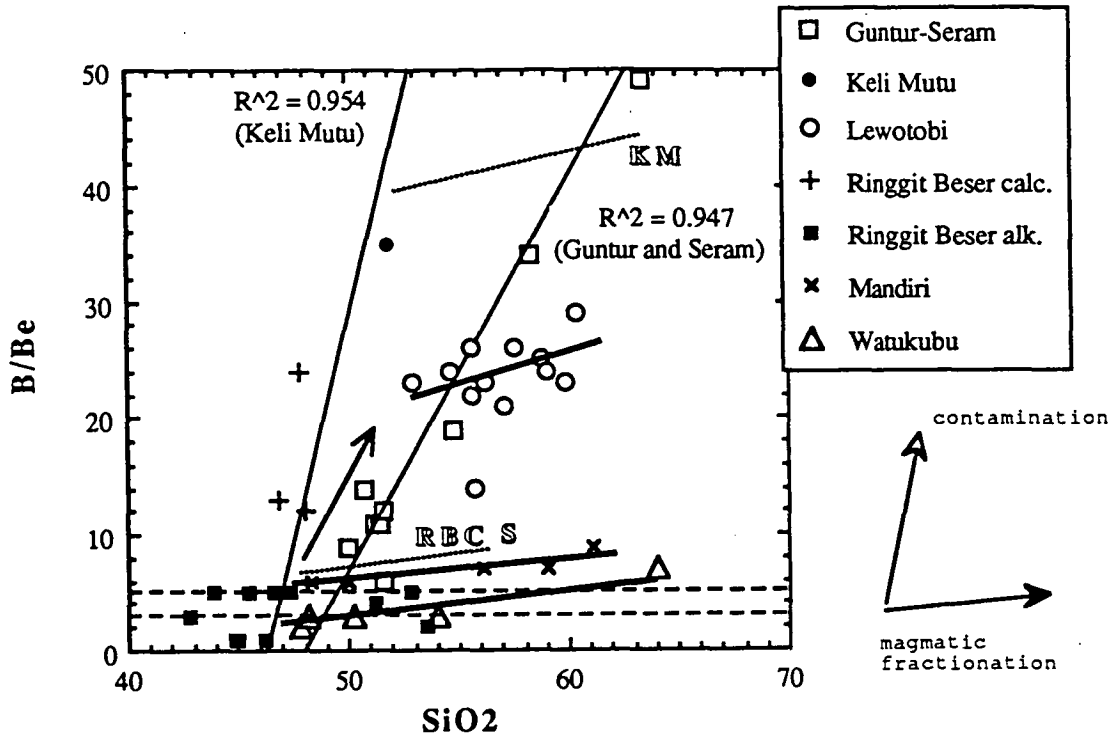

Figure 5.12. SiO_2 versus B/Be diagram for the rocks of the Sunda arc, according to the data published by Edwards et al. (1993). The two parallel broken lines at B/Be 3 and 5 mark the field of B/Be values for MORB and OIB. The two thin lines are the best fitting lines (number are the regression values) respectively for Keli Mutu and the Jawanese calcalkaline volcanoes (Guntur and Seram). Samples with B/Be higher than 50 are not shown in the plot but have been taken into account for the calculation of the best fitting lines.

Thick lines are the best fitting lines for Lewotobi, Mandiri, and Watukubu, and are interpreted as the B/Be (and SiO_2) evolution trend in an essentially closed system, mainly by magmatic fractionation. Compared with the other two centres, Lewotobi has a slightly steeper slope, which indicates that the system might have been relatively more open. The arrows is an estimate of the first stage of evolution of the Lewotobi rocks in an open system (like Guntur, Seram, and Keli Mutu). KM, RBC, and S are the three samples from respectively Keli Mutu, Ringgit Beser calcalkaline, and Seram with relatively low B/Be for high SiO_2 values. Contrary to the other samples from these centres, which evolved in an open system, these samples probably evolved in a relatively closed system, and the dotted lines represent possible evolutionary trends.

the high B/Be values are not the result of contamination of the mantle source, but that they arise after the formation of the magma from which the andesites crystallised, and are mainly a function of magmatic differentiation at a later stage, and possibly of the introduction of crustal fluids (probably also shallow meteoric fluids) and crustal material during differentiation. The slope of the SiO_2 - B/Be correlation is therefore dependent on two factors: 1) the degree of evolution of the sample as a function of its content in fluid phases; and 2) whether or not the system is open, and the amount of crustal (solid + fluid) input.

If this interpretation of the B/Be data is adopted, the differences in B/Be values between alkaline and calcalkaline rocks are not surprising. The alkaline rocks are much less differentiated, may therefore not reside at shallow levels before eruption, and may have insufficient time to a) fractionate B through magmatic processes, and b) be contaminated by crustal fluids. Both these processes might generally occur in the magma chambers where the andesitic rocks formed.

The fact that some samples of calcalkaline volcanics with high SiO_2 have relatively low B/Be (samples Ca15 in Seram, R30 in Ringgit Beser, and K33 in Keli Mutu) suggests that the increase in B/Be values caused by magmatic differentiation is small compared with that caused by crustal contamination. This effect can also be seen in the more evolved alkaline volcanics: assuming that the increase in B/Be in Mandiri is only caused by magmatic differentiation, an increase in SiO_2 from 48 to 61% corresponds to a B/Be variation of only 3 units. Interestingly, the SiO_2 - B/Be slope observed in Mandiri is the same as that inferred to be due to magmatic differentiation alone in calcalkaline volcanics. In calcalkaline rocks the effects of crustal contamination are more pronounced in the more evolved compositions, consistent with a longer time of residence of the magma at shallow levels and higher fluid contents.

The most primitive samples analysed in Lewotobi have B/Be values similar to those of the samples from Guntur and Seram with comparable SiO_2 values. The basalts in Lewotobi, which have not been sampled by Edwards et al. (1993), might have followed the same trend shown by Guntur and Seram, but the magmatic system became closed (or at least less open) in Lewotobi after the melt reached a composition of $SiO_2 \approx 52$-53 %, and the B/Be values were no longer (or less strongly) affected by crustal input.

The "unusual" Sr, Nd, and Pb isotope systematics (see point 4 of Edwards et al.

1993) are consistent with the interpretations of Stolz et al. (1990) and Hilton et al. (1992) and with the different Sr, Nd, and Pb systematics of Indian Ocean MORB and OIB (see Chapters 3 and 6) (Figures 5.13a-b). According to Stolz et al. (1990), the source of low-K tholeiites and (in part) of the medium- to high-K calcalkaline rocks (Seram, Guntur, Keli Mutu, Lewotobi, and the calcalkaline rocks in Ringgit Beser are all low-K tholeiites and calcalkaline) "were probably formed by relatively large degrees of melting of depleted MORB-source mantle", whereas the K-rich volcanics (like Mandiri, Watukubu, and the alkaline rocks in Ringgit Beser) derived from an OIB source.

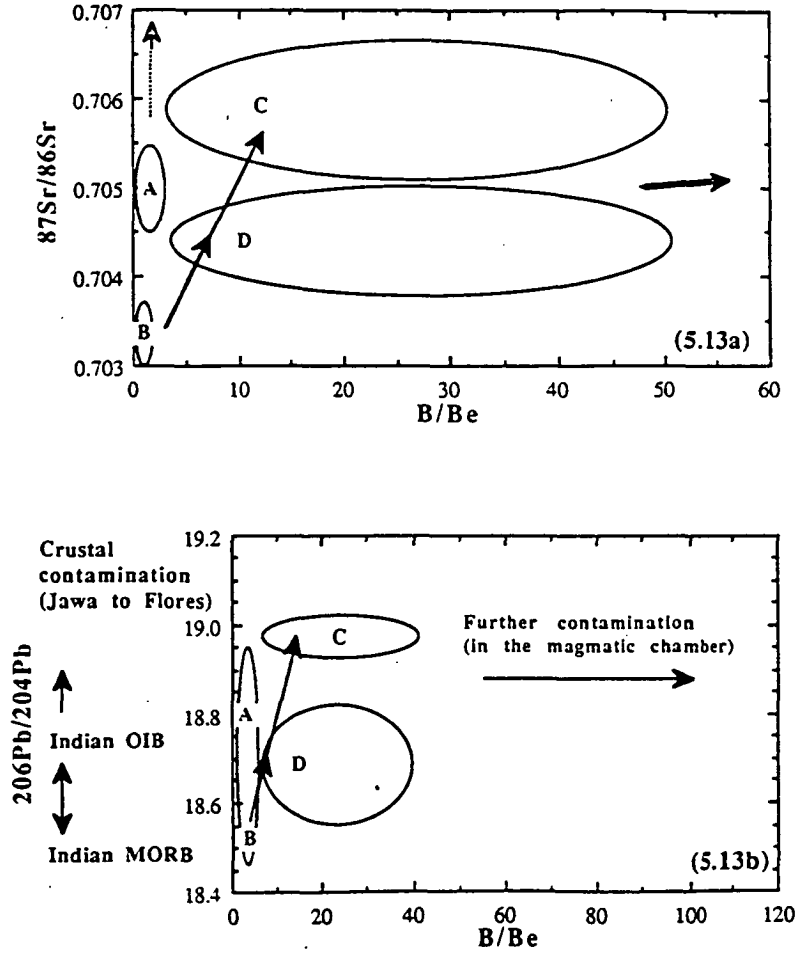

Figures 5.13a-b. Sketch model for the B/Be - $^{87}Sr/^{86}Sr$ and B/Be - $^{206}Pb/^{204}Pb$ evolution of the Sunda arc rocks. Data from Edwards et al. (1993) and references quoted in the text for Indian Ocean MORB $^{87}Sr/^{86}Sr$ and $^{206}Pb/^{204}Pb$ values. Fields are: A) Alkaline rocks from Jawa and Flores; B) Indian Ocean MORB; C) Calcalkaline rocks from Flores; D) Calcalkaline rocks from Jawa.

The diagram shows that alkaline rocks in both Flores and Jawa might have a common Indian Ocean OIB-type source, although some centres in Flores might have been further enriched by crustal contamination (dotted arrow) (see also Hilton et al. 1992). On the other hand, calcalkaline rocks in both Flores and Jawa might have a common Indian Ocean MORB source, and the rocks in Flores are more enriched possibly because of an overall greater extent of crustal contamination. Nd isotope data are also consistent with this model, whereas the A and B fields for Pb isotopes largely overlap and the distinction is not so clear.

In the Indian Ocean, MORB and OIB with an "enriched" mantle component (see Chapter 3) differ strongly in their Nd and Sr isotope values, and MORB sources have considerably lower Sr and higher Nd isotopic ratios, but Pb isotopic ratios are rather scattered and the two fields largely overlap. The alkaline and calcalkaline rocks in Jawa analysed by Edwards et al. (1993) have similar $^{206}Pb/^{204}Pb$ and $^{207}Pb/^{204}Pb$ values, but the alkaline rocks seem to have considerably higher $^{87}Sr/^{86}Sr$ and $^{208}Pb/^{204}Pb$ values and overall lower $^{143}Nd/^{144}Nd$ values, and these differences are generally consistent with the derivation of the alkaline rocks from a source with an "enriched" OIB component. The calcalkaline rocks probably had even less radiogenic Sr and more radiogenic Nd isotopic ratios, but these were slightly modified by secondary crustal contamination (as suggested by the relatively high B/Be values).

The isotope systematics in Flores require a different explanation. According to Hilton et al. (1992) a strong crustal He signature can be recognised as far west as Iya volcano in central Flores, and therefore all the Flores centres studied by Edwards et al. (1993) should show a crustal signature superimposed on the original OIB (or mixture of OIB and MORB) composition of the mantle wedge. In fact, all the rocks in Flores, especially those with calcalkaline affinity, have relatively (compared with Jawa) low $^{143}Nd/^{144}Nd$, and high $^{87}Sr/^{86}Sr$, and high Pb isotopic ratios, as a result of a stronger crustal contamination.

In summary, the shift towards higher $^{87}Sr/^{86}Sr$ values and Pb isotopic ratios, and lower $^{143}Nd/^{144}Nd$ values in the alkaline rocks from Jawa to Flores might be consistent with 1) relatively stronger crustal contamination in the Flores sector (or absence of crustal contamination in the Jawa sector), and 2) at least for some centres, original differences in the composition of the mantle source, with an overall stronger influence of an OIB source beneath Flores. The higher $^{87}Sr/^{86}Sr$ values and Pb isotopic ratios, and lower $^{143}Nd/^{144}Nd$ values in calcalkaline rocks compared with Indian MORB values in each sector may be a consequence of contamination suffered by the calcalkaline melts during their residence in (shallow) crustal magma chambers.

Edwards et al. (1993) already pointed out that the homogeneity of the subduction component implied by their conclusions is in contrast with most of the $^{3}He/^{4}He$ values of the volcanoes in Flores. The only volcano in Flores for which both B/Be and $^{3}He/^{4}He$ values are available, Keli Mutu, has the highest, most mantle-like $^{3}He/^{4}He$ (Hilton & Craig 1989; Hilton et al. 1992) value and relatively (compared with the other volcanoes in Flores analysed by Edwards et al. 1993) low Pb and high Nd isotopic ratios. Contrary to the expectations, Keli Mutu also has the highest B/Be

measured in the region and relatively high $^{87}Sr/^{86}Sr$. Contamination of the source of Keli Mutu would probably produce high $^{87}Sr/^{86}Sr$ and B/Be values, but also high $^{208}Pb/^{204}Pb$, $^{207}Pb/^{204}Pb$, $^{206}Pb/^{204}Pb$ values, and low $^{3}He/^{4}He$ and $^{143}Nd/^{144}Nd$ values. On the contrary, secondary magmatic and metasomatizing processes would probably increase the B/Be and $^{87}Sr/^{86}Sr$ values of the Keli Mutu volcanics, due to the relatively high "mobility" of Sr and B, leaving the Pb, Nd, and He isotopic values unchanged, and therefore producing the observed isotope systematics.

However, too little is known about the behaviour of B, Be, and He in fluids and magmatic processes, and some of the discrepancies observed could actually be a sampling problem: there is no rock in the Sunda arc that has been analysed as yet for Sr, Nd, Pb, He isotopes, B and Be. Analysed samples have been compared without taking into due account their different magmatic histories and degrees of evolution.

The timing of the subduction and metasomatism of the mantle wedge is another problem for the model discussed by Edwards et al. (1993). According to Morris et al. (1990), the residence time of B in the sub-arc mantle is ≤ 5 Ma. The 5 Ma includes the time for a sediment to be subducted and for the metasomatism of the mantle wedge, the time of formation of a magma, and the time of residence of this magma in a magma chamber before the eruption.

If the high B/Be values observed in the Sunda arc are the result of mantle contamination by subducted crustal material, then the sediments (or sediment-derived fluids) responsible for the B/Be anomalies started their subduction ≤ 5 Ma ago. High ^{10}Be values in arc volcanics also require that "sediments must be subducted and recycled in less than 10 Ma" (Tera et al. 1986), but only very low ^{10}Be values, similar to those measured in non-arc environments, have been found in the Sunda arc (Tera et al. 1986; Edwards et al. 1993). These low ^{10}Be values imply a subduction and recycling time longer than 10 Ma, and are inconsistent with high B/Be values, which require a subduction and recycling time shorter than 5 Ma.

Although the ^{10}Be content in sediments in the Northeastern Indian Ocean is not known, ^{10}Be has an atmospheric origin, and is therefore not dependent on the composition of sediment. There is no reason to expect a ^{10}Be depletion in the sediments of the Indian Ocean compared with other sediments elsewhere in the world. It might also be argued that the uppermost ^{10}Be-rich layers of sediments could be accreted and not subducted. However, B also tends to concentrate in the uppermost layers of the sediments (Edwards et al. 1993, and references therein; see

also Ishikawa & Nakamura 1993, and Bebout et al. 1993), and therefore this process would produce both low ^{10}Be and low B/Be values.

As B is more soluble than Be in hydrous fluids (Edwards et al. 1993, and references therein), this could cause high B/Be values, but the rocks that suffered contamination by these fluids should still carry a distinct ^{10}Be enrichment because of the short subduction and recycling time of B compared with the time necessary for ^{10}Be to decay to "normal" (non-arc) values. Only if all the ^{10}Be were to fractionate into the solid residue would we expect to see low ^{10}Be and high B/Be values, but there is no evidence for such an extreme fractionation and, in fact, the existing data are against it.

Finally, Morris et al. (1990) clearly showed that the subducted B is not stored in the sub-arc mantle, and therefore the high B/Be and low ^{10}Be values cannot be the consequence of extraction from the mantle of B accumulated over a long enough period for ^{10}Be to decay to very low levels. Furthermore, according to Edwards et al. (1993), B and Be have similar partition coefficients in arc magmas, and their ratio is only slightly affected by magmatic processes. This is consistent with the observed variations in B/Be values with fractionation.

In summary, based on the knowledge of the behaviour of B and Be in the processes that lead to the generation of arc magmas, the existing B, Be, and ^{10}Be data for Jawa and Flores in the Sunda arc rule against the involvement of recently subducted sediments, irrespective of their volume, age, and composition, in the genesis of any of the different types of volcanics in the Sunda arc. On the contrary, contamination by old (>10 Ma) continental crust, including the continental sedimentary cover, can produce the observed low ^{10}Be coupled with high B/Be values.

5.9.4 He isotopes in the Sunda arc

In Bali, two analyses of olivines from Batur gave R/RA values of, respectively, 8.8 and 7.41, and clinopyroxenes from Agung gave a value of 8.52 (Hilton & Craig 1989; Hilton, pers. comm.). Including a value of 7.87 measured for a hot spring in Batur (Hilton, pers. comm.), the average of the R/RA values measured in Bali is 8.15 ± 0.54, which is both within the standard deviation for each single analysis, and within the field of MORB basalts as defined by Poreda & Craig (1989).

In Jawa, geochemically similar calcalkaline volcanic centres are characterised by both high B/Be values and by rather high $^{3}He/^{4}He$ values. The only He isotope analysis of

a mineral separate in Jawa is a 7.32 value (R/RA) measured in olivines from the 1982-83 basalt flow of Galunggung, in central Jawa; other analyses of hot springs and fumaroles in closely spaced centres (Galunggung, Guntur, Talagabodas, Papandajan, Tangkuban Prahu) gave R/RA values ranging from 8.17 to 6.62. Only the summit fumaroles of Merapi gave considerably lower values - 5.4 to 5.7. (all data from Hilton & Craig 1989; D. Hilton, pers. comm.). If Merapi is excluded, the remaining values yield an average of 7.29 ± 0.57, i.e. similar to the value measured in olivine separates from Galunggung, and still within the MORB range. However, the large range observed, from 8.17 in Tangkuban Prahu to 6.62 in Papandajan, requires a more careful analysis.

Hilton & Craig (1989) and Hilton et al. (1992) pointed out that, on large volcanoes, flank fumaroles tend to have lower $^3He/^4He$ values than summit fumaroles. Olivines picked from the recent volcanics of Kerinci volcano in Sumatra gave a R/RA value of 7.55 ± 0.6, whereas hot springs believed to be part of the plumbing system of the same volcano have much lower (approximately 2.1) values (Hilton, pers. comm.), suggesting either that those waters belong to a different system, or that they are strongly diluted by a non-atmospheric contaminant rich in radiogenic He. The ^4He contribution given by juvenile meteoric waters can be easily detected during the He isotope analysis, but deeper and older crust-derived fluids can very efficiently increase the ^4He content. Summit fumaroles are more likely to sample only the juvenile magmatic material and to circulate entirely within it, whereas hot springs and flank fumaroles, even if they originate from the same juvenile magmatic material, are likely to travel for longer distances and times, and through different types of rocks.

Irrespective of their composition, these rocks at the base of the volcanic edifice will in general be older than the juvenile magmatic material, and therefore relatively more or less strongly enriched in radiogenic He. Obviously, the actual distance of a fumarole or hot spring from the volcanic vent is not indicative of the distance travelled by the water/gases, and the final ^4He enrichment will mainly depend on the timing and geometry of the subsurface drainage system.

As a consequence, and because all the crustal materials have considerably lower $^3He/^4He$ than any mantle source, high $^3He/^4He$ values are an unambiguous indicator of an unmodified mantle source for He. Relatively low $^3He/^4He$ values might be the result of 1) metasomatism of the mantle at the source 2) later modification of the melt during its rise to the surface through the continental (in Jawa) crust and residence in the magma chamber (bulk mixing with crustal material, degassing, isotopic

fractionation). The fluid phase derived from the juvenile material in the magma chamber might suffer further contamination due to its residence in the shallow crust and sediments before coming to the surface.

It might be argued that mineral separates of the most primitive phases are the best indicators of the He isotope composition of the mantle source. Although it is true that mineral separates will not, in general, suffer the extreme contamination that might be experienced by hot springs and gases, only mineral phases which are in equilibrium with mantle compositions, and more evolved phases which evolved in a geochemically closed system (in terms of mass transfer) will have He isotope values representative of their mantle source. Neither of these conditions seem to be generally applicable to the great majority of rocks in the Sunda arc, where olivine and pyroxene crystals are in general strongly evolved compared with the "mantle array".

If a melt crystallised in a closed system, then we would expect to see the same He isotope values throughout the crystallisation sequence. It is unlikely that crystallisation would occur over a period of time long enough to produce ^{4}He by radioactive decay, and the effect of degassing on He isotope systematics is also negligible, unless large amounts of He are lost (Trull & Kurz 1993). It is likely, however, that if the melt interacts with the crust during its rise to the surface then its He isotope signature will probably change. During crystallisation, the magma in the magma chamber may record a progressive fall in ^{3}He/^{4}He values. For example, an olivine crystal with Fo = 85 will have lower ^{4}He than an olivine crystal with Fo = 75 precipitated when more of the melt had crystallised, and after it had assimilated (or was metasomatised by) material/fluids from the crust surrounding the magma chamber, unless the ^{3}He/^{4}He values in the more "primitive" crystals re-equilibrated with those of the melt (see discussion in Trull & Kurz 1993).

To date, the effects of crustal contamination on the ^{4}He content in phenocryst phases during crystallisation have not been investigated in detail (but see Hilton et al. (1993). However, it should be noted that all He isotope analyses of the relatively most primitive olivine and clinopyroxene separates in Jawa, Bali, and Sumatra gave high R/RA values in the range 7.32 to 8.81, with an average of 7.84 ± 0.67 (Hilton, pers. comm.), all well within the typical He isotope range in MORB.

If ^{4}He enrichment were a characteristic of the source, produced as a result of the addition of radiogenic He from subducted material, we would expect to see ^{4}He enrichment even in the products of crystallisation of the most primitive melts. Based

on the existing data, the lack of a ^4He anomaly in the most primitive phases indicates that 1) the subducted material did not modify the He isotope systematics in the mantle source of the arc volcanics in Bali, Jawa, and Sumatra (or if it did, the ^4He enrichment was very small and statistically not significant), and 2) the ^4He enrichment does not occur in the source, but is a consequence of processes which affect the melt after its generation in the mantle and mainly at a shallow depth within the magma chamber.

Assuming that the high $^3He/^4He$ values found in Bali (Agung and Batur), Jawa (Galunggung and the acid springs in Tangkuban Prahu), and Sumatra (Sukadana, Bukit Mapas, Bukit Telor, and Kerinci) are representative of the mantle source, the existing data also show that, on a large scale, the mantle source of the arc rocks in Bali, Jawa, and Sumatra is fairly homogeneous in terms of He isotopes. Based on these assumptions, He isotope systematics in OIB basalts with an "enriched" mantle signature (Bukit Telor, Sukadana - see Chapter 6) do not differ from those in rocks with a clear Sr-Nd-Pb isotopic and geochemical arc affinity, like Kerinci and Sekincau in Sumatra, and Galunggung in Jawa.

The basalts of the 1982-83 flow in Galunggung are considered to be the most primitive found in Jawa, and likely to be representative of a primary magma (Nicholls & Whitford 1976; Gerbe et al. 1992; Harmon & Gerbe 1992). Their major and trace element composition is typical of arc rocks, with high Sr and Pb isotopic ratios, and low Nd isotopic ratios, but with He and O isotopes within the MORB range. Harmon & Gerbe (1992) suggested that the MORB-like $\partial^{18}O$ values coupled with higher $^{87}Sr/^{86}Sr$ and lower $^{143}Nd/^{144}Nd$, when compared with Pacific MORB, in the basalts can be explained in terms of contamination of the mantle wedge by very minor amounts of subducted sediment. However, this explanation is inconsistent with the Indian MORB affinity, rather than Pacific or Atlantic MORB, of the sub-arc mantle beneath the Sunda arc, and the existence of isotopically more enriched "pockets" of OIB mantle with a more or less strong "enriched" mantle component. Other isotopic variations in more evolved samples occurred at a later stage during the residence of the melt in the magma chamber.

In principle, the He - Sr/Nd/Pb isotope decoupling indicates that either 1) mantle reservoirs with different Sr, Nd, and Pb systematics can have the same He isotope values, or 2) the measured Sr, Nd, and Pb isotopes, which are measured on the whole rocks, are the result of processes which modified the original isotope systematics not in the source, but after the crystallisation of the most primitive

phases. However, as for B and Be, little is known about the behaviour of He in the processes that lead to the generation of arc magmas, and other mechanisms, in part discussed by Hilton et al. (1992, 1993) and Trull & Kurz (1993, and references therein), could be responsible for the observed decoupling between He and other isotopes. Nevertheless, the fact that olivine phenocrysts from the most primitive centres in Sumatra with a geochemical and isotopic OIB signature (Sukadana, Bukit Telor) have He isotopes that do not differ from those measured in olivines of isotopically and geochemically typical arc volcanics (Kerinci, Bukit Mapas) is very remarkable, because it might indicate a strong link between an OIB source and the source of arc volcanics in the mantle wedge of the Sunda arc, at least in south Sumatra. This "link" will be discussed in detail in the next chapter.

5.9.5 Th-U disequilibrium data in the Sunda arc

U series disequilibrium geochemistry could be another powerful aid to the detection of crustal material in the source of arc rocks. In young volcanics, and assuming that ^{230}Th and ^{238}U are in equilibrium in the magma source at the time of formation of the melt, the measured $^{230}Th/^{232}Th$ in melts reflects the Th/U values of the source, as it is not affected by crystal fractionation processes. Because of the very short half-life of ^{230}Th, the main limitation of this system is that the sample must be young compared with the time of formation in the source, not relatively to the time of eruption. In other words, a sample which originally had a ^{238}U - ^{230}Th disequilibrium, erupted recently but after a long residence in the crust since its formation (as is likely for many andesites), would no longer show a U - Th disequilibrium and the original $^{230}Th/^{232}Th$ value (e.g. Gill & Condomines 1992).

The U-Th isotope characteristics of volcanic rocks from the Sunda arc were discussed by Tanzer (1985), Hemond (1986), Wheller (1986), Rubin et al. (1989), Gill & Williams (1990) and McDermott & Hawkesworth (1991). Wheller et al. (submitted for publication), provide a recent review of U series disequilibrium systematics from Krakatau to Flores.

In general, Wheller et al. (submitted for publication) concluded that $^{230}Th/^{232}Th$ values for Holocene low-K, to high-K basalts to andesites in the Sunda arc range from 0.68 to 0.83, similar to values measured in the Philippines, and OIB from Samoa, Tristan da Cuña and Heard Island. These values correspond to bulk U/Th values in the mantle source of approximately 4, typical of primitive mantle and OIB. ^{230}Th - ^{238}U are generally in equilibrium, and $^{230}Th/^{232}Th$ values are less than 1.4,

typical of rocks associated with continental or thick arc lithosphere.

In summary, the low $^{230}Th/^{232}Th$ values are indicative of an OIB source, and the lack of U enrichment suggests that the mantle source was not metasomatised by slab-derived, presumably U-rich fluids. Interestingly, there is no correlation between $^{230}Th/^{232}Th$ and $^{87}Sr/^{86}Sr$, and it was suggested that the higher $^{87}Sr/^{86}Sr$ values are associated with areas where the continental lithosphere is present. Wheller et al. (submitted for publication) ascribed the trend from relatively low $^{87}Sr/^{86}Sr$ to higher $^{87}Sr/^{86}Sr$ at similar $^{230}Th/^{232}Th$ as one due to crustal interaction, whereas the trend at $^{87}Sr/^{86}Sr$ values of about 0.704 from high $^{230}Th/^{232}Th$ to low $^{230}Th/^{232}Th$ was ascribed to intra-mantle fractionation processes.

In the final model by Wheller et al. (submitted for publication) the mantle wedge beneath the Sunda arc, source of the arc magmas, is a mixture of Indian MORB and OIB mantle. The low-degree melts produced in the mantle wedge as the result of subduction are LILE- (including Th and U) and LREE-enriched because of the low degrees of melting and not because of the LILE - LREE transfer into the mantle wedge from subduction-derived fluids. The range in Sr, Nd, and Pb isotopes partly reflects the presence in the mantle wedge both of a "normal" Indian Ocean MORB-source and an isotopically enriched plume-related source. Thus the observed isotope systematics (but not the Th isotope ratios) are a primary characteristic of an isotopically composite mantle wedge, apart from minor variations due to Rb/Sr, Sm/Nd, U/Pb, and Th/U fractionation during the magmatic processes, and minor crustal (or subducted slab) contamination.

5.10 Conclusions

Sr, Nd, and Pb isotope systematics in the Sumatran mantle wedge and continental crust, and in Northeastern Indian Ocean sediments were used to model the effects of crustal versus sediment contamination in the Quaternary volcanics of the west Sunda arc, from north Sumatra to Lombok.

The data suggest that neither contamination of the mantle source by bulk sediment nor bulk assimilation of crustal material by an uprising melt can satisfactorily account for the Sr, Nd, and Pb isotope systematics observed in most arc rocks in the west Sunda arc.

Based on the present knowledge of the behaviour of Sr, Nd, and Pb in a fluid phase, fluids released from the subducted sediments do not seem to be able to reproduce the range and spatial distribution of $^{87}Sr/^{86}Sr$ - $^{143}Nd/^{144}Nd$ values observed in the west Sunda volcanic rocks. Pb isotopic values and their variations along the arc also suggest that subducted sediments did not have any effects on the Pb systematics of the west Sunda volcanic rocks.

Calculations to test the proposition that the Sr, Nd, and Pb isotopic compositions of the arc rocks are due to contamination of the mantle source by sediment-derived metasomatizing fluids are successful only when "ad hoc" and unrepresentative sediment and mantle endmembers are used and implausible models adopted.

On the contrary, assimilation of partial melts of crustal material, up to a maximum of approximately 6% in the mixture, probably less than 3-4% for most arc volcanics in Sumatra and west Jawa, and very little or none in the Bali sector, by uprising magmas can account for the Sr, Nd, and Pb isotope systematics in arc rocks and is consistent with the spatial distribution of Sr, Nd, and Pb isotope values observed from north Sumatra to Lombok. The prerequisites for this model are 1) the presence of Indian Ocean OIB-like mantle as well as MORB mantle in the mantle wedge; 2) the existence of pre-Mesozoic continental crust in Sumatra and west Jawa, but its absence in the Bali sector from east Jawa to Lombok.

High Cs and Pb contents in arc rocks are unambiguous indicators of contamination by lithospheric material. However, it seems that LILE ratios, like Cs/Rb, Rb/Ba, and Pb/Ce, cannot distinguish between contamination of the mantle source by sediment-derived fluids and assimilation of crustal material by uprising magmas.

Relatively low $^{3}He/^{4}He$, and high B/Be and $\partial^{18}O$ values in rocks and mineral phases in the west Sunda volcanics are rare, and are best explained by processes occurring at shallow levels (degassing of the magma, percolation of meteoric fluids, assimilation of crustal material), in the magma chamber or at near-surface levels. $^{230}Th/^{232}Th$ values in Holocene rocks are indicative of an OIB source, and there is no evidence for ^{230}Th - ^{238}U disequilibrium and metasomatism of the mantle source by slab-derived fluids.

In summary, $^{3}He/^{4}He$, B/Be, $^{230}Th/^{232}Th$, and $\partial^{18}O$ values also suggest that crustal contamination, and not subducted sediment-derived metasomatizing fluids, is responsible for the isotopic characteristics of Quaternary volcanics in the west Sunda

arc. The effects of crustal contamination on the major and trace element, and isotopic composition of a particular suite of rocks in south Sumatra will be examined in detail in the next chapter.

CHAPTER 6

Olivine-phyric and intraplate basalts in Sumatra, and other occurrences in Indonesia

6.1 Introduction

In 1949, van Bemmelen published a monumental work on the geology of Indonesia, with a comprehensive summary and review of the studies on the Indonesian geology and volcanism, and a wealth and accuracy of information and ideas unmatched by present-day works. Since van Bemmelen's work, several authors have described the volcanic activity of the Sunda arc (see Chapter 1) and tried to understand the complex mechanisms of genesis and evolution of volcanic rocks in a subduction environment, and the Sunda arc itself is now regarded as a stereotype of subduction-related volcanism. However, only the most spectacular, accessible, potentially dangerous, and compositionally unusual volcanoes, like Krakatau in the Sunda Strait, the active volcanoes of densely populated Jawa, and Muriah in central Jawa, have received the due attention from the scientific community. Also, alteration is often a big problem in tropical areas, and collecting fresh samples from inactive volcanoes often requires time, patience, and luck.

For all these reasons, volcanism in Sumatra has been virtually neglected by the scientific community. Rainfall and temperature in Sumatra are higher than in the other islands of the arc, and the rate of alteration is often spectacular, even in extremely young samples. Furthermore, most of the active volcanoes in Sumatra produced only very small amounts of consolidated juvenile material in recent times, and some of the most interesting centres became extinct not a long time ago, but enough for alteration and erosion to take place, and turn the geologist's enthusiasm into frustration. The other problem of Sumatra is its accessibility. A relatively good road, the so-called "Trans-Sumatra Highway", running from south to north parallel to the volcanic arc was completed only a few years ago, and air, road, and river transport to some of the most scarcely populated and remote areas where most of the volcanic centres are situated may be a problem. Field work in Sumatra can still be a risky and time consuming, but romantically exciting and extremely rewarding activity.

In his work, van Bemmelen pointed out the existence in Sumatra of olivine-phyric basalts, and related their existence to the "tensional stresses and major fissures along

the edges of the Sunda land" caused by "the bending of the consolidated crust due to the downwarp of marginal troughs" (van Bemmelen 1949, vol.1, page 253). These basalts were recognised as petrographically different from the rare olivine-bearing, relatively primitive basalts found in other areas along the arc, and they clearly occupy a back-arc position. Also, they outcrop in Sumatra, which is built on continental crust, whereas the other islands of the arc where olivine-bearing basalts are found, are made of younger and thinner transitional or oceanic crust.

The aims of this chapter are twofold. First, the Sumatran olivine-bearing basalts are investigated with the principal objective of defining their source characteristics. Compared with arc andesites, which are usually geochemically evolved and modified by a number of volcanic processes that make the recognition of their original source problematic, the olivine-bearing basalts are relatively primitive, so can potentially yield information about the composition of the source from which they were generated. The second aim of this chapter is to test, investigate and understand the relationship between the olivine-bearing basalts in Sumatra, and those reported from other localities in Indonesia: are they geochemically and isotopically similar? and, what is the relationship between their spatial and temporal distribution and the tectonic framework of the Indonesian region?

Only the Sumatran occurrences of olivine-phyric basalts will be discussed in detail in this chapter. The other occurrences will be briefly described and discussed only as a comparison with those of Sumatra.

6.2 General tectonic setting of Sumatra

The island of Sumatra (Figures 6.1 and 6.2), the sixth largest in the world, runs parallel to the westernmost section of the Sunda Trench, from which is separated by a well developed fore-arc (Mentawai Archipelago) and an outer arc basin, from about 6° S 105° E to 6° N 95° E. The Australian-Indian Ocean Plate is currently subducted under Southeast Asia at a fairly constant rate of 6 to 7 cm/year, in a N3E direction (McCaffrey 1991). Therefore the direction of convergence varies from about 0° off Jawa (i.e. perpendicular to the trench), to N25E off south Sumatra, to N31E off north Sumatra (Newcomb & McCann 1987).

Subduction along the Sunda Trench has been active at least since the Permian (Cameron et al. 1980), and the age of the subducted Indian Ocean crust (based on

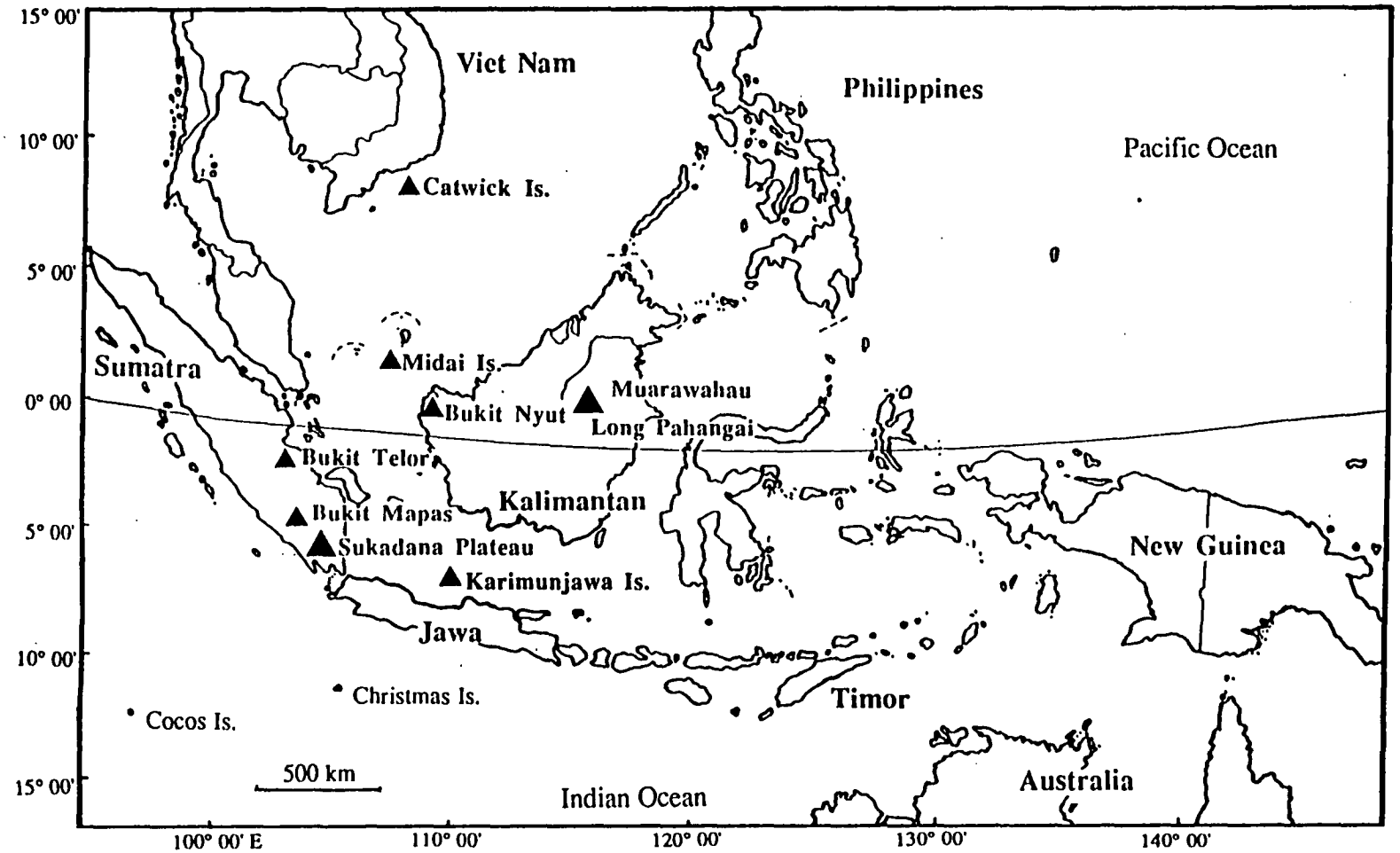

Figure 6.1. Location of the olivine-bearing basalts in the Indonesian region (according to van Bemmelen 1949, and Westerveld 1952): Bukit Telor, Bukit Mapas and Sukadana Plateau (Sumatra), Karimunjawa Islands (off north Jawa), Bukit Nyut, Muarawahau and Long Pahangai volcanic centres (central Kalimantan), Midai Island (Natuna Islands), Catwick Islands (off Viet Nam).

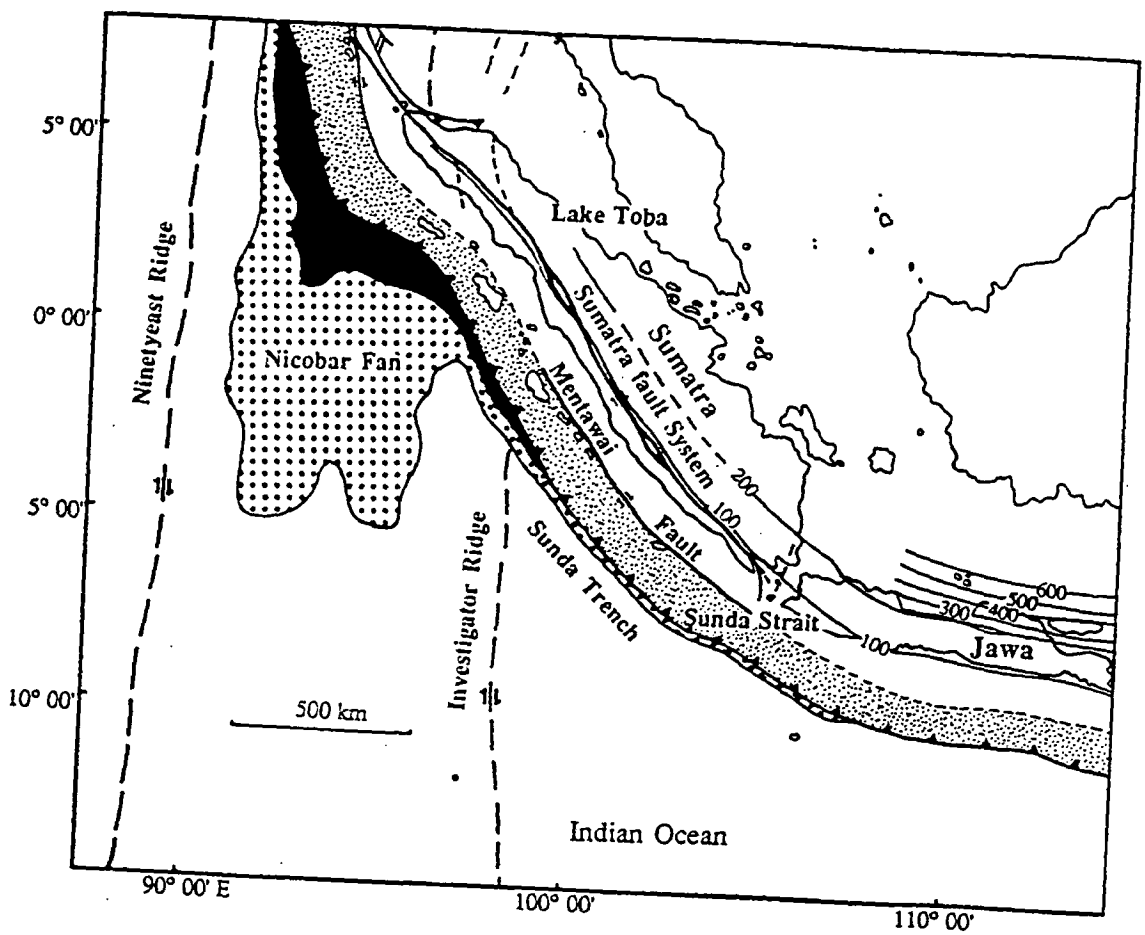

Figure 6.2. Tectonic sketch map of Jawa, Sumatra and the northeastern portion of the Indian Ocean.

TRANSFORM FAULT

SUMATRA AND MENTAWAI FAULT SYSTEMS

OTHER FAULTS (OBSERVED OR POSTULATED)

ACCRETIONARY PRISM

TRENCH

ACTIVE SPREADING RIDGE (ANDAMAN SEA)

THICKNESS OF SEDIMENTS:
> 1 km

> 2 km

DEPTH OF THE BENIOFF ZONE (in km)

paleomagnetic anomalies) varies from about 80 Ma in the Sunda Strait to less than 60 Ma in north Sumatra (Liu et al. 1983). An important consequence of the different angle of subduction is the difference in intensity and depth of earthquakes in Sumatra and Jawa. Large interplate earthquakes are common off Sumatra, and define a Benioff zone dipping at low angles. In contrast, foci of earthquakes in Jawa reach a maximum depth of about 650 km, and define a much steeper Benioff zone (Hamilton 1979; Newcomb & McCann 1987).

The Sumatran fore-arc (Mentawai Archipelago) is made of a complex sequence of pre-Miocene mélanges and Neogene successions, and lithologies from the Indian Ocean, the Nicobar Fan and Sumatra have been recognised (Harbury & Kallagher 1991). The nature of the crust at the base of the fore-arc is still a matter of debate (see e.g. Karig et al. 1980; Newcomb & McCann 1987; Liu et al. 1989; McCaffrey 1991; Diament et al. 1992), and this discussion goes beyond the aims of this thesis. However, the most recent data seem to suggest that the fore-arc is not a single rigid plate. Diament et al. (1992) recognised the existence of a "long linear structure, parallel to the Sumatra fault zone, on the western flank of the fore-arc basin, from the southernmost part of Sumatra to north of Siberut", and interpreted it as a strike slip dextral fault system, similar and complementary to the Sumatra Fault System, that marks the boundary between the fore-arc ridge and the fore-arc basin (corresponding with the continent-ocean boundary).

Based on the seismic record of the region in the last 300 years, Newcomb & McCann (1987) identified a number of structures that control the distribution of earthquakes. One of these structures, the Investigator Ridge (see Chapter 3), is an oceanic dextral fracture zone that may extend into the fore-arc and underneath the continental margin: the Lake Toba caldera is situated on the continuation of the ridge, and its activity might be more closely related to it than to the Sumatran Fault System, which runs west of the caldera. Also, the distribution of the Quaternary volcanic centres changes dramatically north of the intersection of the extrapolated ridge crest with the island, and the ridge acted as an effective barrier to the sediments from the Ganges-Brahmaputra fluvial system (Figure 6.2).

Such N-S trending fractures (and a fossil ridge, the Wharton Ridge, that became extinct approximately 45 Ma ago - see Liu et al. 1983) characterise the western portion of the Northeastern Indian Ocean from the Investigator Ridge to the Ninetyeast Ridge. Only one of the many oceanic plateaux situated south of the trench from 90° E to 115° E, the Roo Rise, is believed to continue into the trench and interact

with the fore-arc off central Jawa (Newcomb & McCann 1987).

The main tectonic feature of mainland Sumatra is the Sumatra Fault System (or Semangko Fault), a strike-slip dextral fault system that extends for the whole length of the island from the Sunda Strait to the Andaman Sea, where it links with a series of transform faults which continue further north. In south and central Sumatra all the Quaternary volcanic centres are situated within 50 km of the fault, and, as in Jawa (Hamilton 1979), it seems that the Tertiary volcanics lie slightly closer to the south coast, suggesting that the Tertiary volcanic axis was closer to the Sunda Trench than the Quaternary (Rock et al. 1982). The importance of the Semangko fault as a tectonic and basement boundary was discussed in Chapter 2.

North of Lake Toba the fault separates older, mainly Tertiary, volcanic and plutonic units to the south from Quaternary volcanoes to the north. Page et al. (1979) suggested that the offset of the active volcanic arc to the north is the result of a change of the angle of subduction corresponding with the point where the Investigator Ridge intersects the trench.

Curray et al. (1982) proposed the existence of a SSE dipping subduction zone, active since the Pleistocene, located 20 to 25 km off the coast of north Sumatra (Aceh Province), which may be a consequence of the opening of the Andaman Sea, and, according to Rock et al. (1982), some of the Quaternary volcanoes (Olim volcanics; Bennett et al. 1981a) situated N of Lake Toba could actually be related to this younger subduction rather than to the subduction along the Sunda Trench.

The main tectonic trends in Sumatra run parallel to the Sumatra Fault System. There is general agreement in considering this fault system as a consequence of the oblique subduction, but estimates of the SE-NW offset are highly variable, ranging from about 100 km (Posavec et al. 1973) to up to 500 km since the Oligocene (Wajzer et al. 1991). This variability is related to the complexity of the fore-arc, as it is not clear how much of the strain is accommodated by the fore-arc itself.

It is generally agreed that Sumatra is made mostly of continental crust. Paleozoic sedimentary rocks (van Bemmelen 1949) are known, and granitic bodies similar to those observed in peninsular Malaysia are widespread (Clarke & Beddoe-Stephens 1987; Hutchison 1989; Gasparon & Varne, submitted for publication; see also Chapter 2). Silicic pyroclastic rocks are far more abundant than andesitic and basaltic volcanics (Westerveld 1952).

The Sunda Strait marks the transition from a frontal to an oblique subduction, and is interpreted as an area of extension resulting from the northwestward motion of the fore-arc slivers situated between the trench and the Sumatra Fault System (Huchon & Le Pichon 1984). The area is tectonically and topographically very complex as a result of the compressional stress regime due to the oblique subduction, and the stress regime can be resolved into two interacting forces: the above mentioned transcurrent NW-SE force, and a compressional N-S force related to the subduction of the Indian Ocean plate. According to Ninkovich (1976) the opening of the strait is the result of "a clockwise rotation of Sumatra of about 20° about an axis located in or near the Sunda Strait" since the Late Miocene. His early conclusions, mainly based on the geometry of the arc, have received partial support from Nishimura et al. (1986), who summarised a number of paleomagnetic declination values of Quaternary rocks from west Jawa and south Sumatra and concluded that the existing data are consistent with a clockwise rotation of Sumatra in relation to Jawa of about 5° to 10° per Ma since at least 2 Ma. More detailed recent studies (Harjono et al. 1991) supported the early conclusions by Huchon & Le Pichon (1984), and confirmed that the Sunda Strait is an area of extensional regime.

An important consequence of the extensional regime may have been the eruption in recent times of large volumes of acid pyroclastic rocks and subordinate andesites and basalts within and at the margins of the strait. Nishimura et al. (1986) identified two large low gravity anomalies in south Sumatra, and an even larger one just off the coast of Jawa, and suggested that these may be the sources of the thick Quaternary ignimbrites that cover large areas in south Sumatra (Lampung and Tarahan Formations, and pyroclastic deposits of the Semangko Valley) and west Jawa (Malingping and Banten Tuffs). According to their calculations, the large low gravity anomaly off west Jawa is consistent with the existence of a caldera with a diameter of about 26 km, that erupted about 110 billions of tonnes of crustal material in the last 0.1 Ma. Their estimates were based on a calculated (from gravity anomalies data) crustal density of about 2.4 g/cm^3 - similar to the density of Tertiary sediments - in west Jawa, compared with a higher density of 2.6 g/cm^3 - consistent with the existence of Paleozoic gneisses and granites - in south Sumatra.

Both Nishimura et al. (1986) and Harjono et al. (1991) suggested that a N35E trending fracture zone runs from Panaitan Island to Krakatau and on to Sebesi and Sebuku Islands, to Mt Rajabasa in mainland Sumatra, and to the Sukadana Plateau. However, there is as yet no evidence that volcanism evolved in time and composition along this fracture, as suggested by Nishimura et al. (1986) and Harjono et al.

(1991), who based their interpretation only on the location of these volcanic centres. The available age (Soeria-Atmadja et al. 1985; Nishimura et al. 1986; Simkin & Fiske 1983) and geochemical (see further discussion) data seem to suggest that these structures formed virtually at the same time, and that there are no systematic relationships between age and composition, and location along the fracture zone.

The fracture zone is clearly identified by a cluster of shallow earthquakes, and is an important tectonic boundary (perhaps the southernmost margin of the SIBUMASU terrane; see Chapter 2) between the eastern part of the Sunda Strait - a relatively flat and shallow area filled with up to more than 3000 m of Quaternary to Upper Pliocene marine sediments and interpreted as a rapidly subsiding trough (Noujaim 1976), and the western part, characterised by a 1800 m deep N-S trending graben believed to be the continuation of the Sumatran Fault System (Nishimura et al. 1986; Harjono et al. 1991).

6.3 Previous studies

Olivine-phyric basalts in Sumatra (Figure 6.1) were first recognised by Dutch geologists in the early 30's (cited by van Bemmelen 1949) during the geological surveys of the island. In his comprehensive work, van Bemmelen (1949) discussed the occurrence of olivine bearing basalts in Sumatra, and considered them to be "basaltic effusions in the post-orogenic stage". According to van Bemmelen (1949), to this stage belong the Sukadana and the Bukit Telor basalts in Sumatra and rare basalts found in other small areas in SE Asia: the Karimunjawa Islands north of central Jawa, Bukit Nyut in west Kalimantan and some Quaternary volcanoes in central Kalimantan, Midai Island in the Natuna Islands group, and the Isle des Cendres and Cecir de Mer (now Catwick Islands), two small islets off the southern coast of Viet Nam (see Figure 6.1). No other occurrences of this type of basalts, apart from the Bukit Mapas basalts reported by Westerveld (1952), have been recognised in Indonesia since van Bemmelen's work.

More recently, Westerveld (1952) reported some analyses of basalts from the Sukadana Plateau and from Bukit Mapas, made by Dutch analysts in 1929 and 1931. In his geological sketch map of south Sumatra, the basalts from Sukadana and Bukit Mapas are recognised as different from (and contemporaneous with) the other basalts related with the mainly andesitic centres forming the volcanic arc, although, based on major elements chemistry, they were interpreted as genetically related to the arc

andesites.

Finally, Soeria-Atmadja et al. (1985) analysed and dated some samples from the Karimunjawa Islands and the Sukadana plateau, and compared the Karimunjawa and the Sukadana basalts with the Sumatran arc andesites, pointing out some of their peculiar intra-plate and back-arc characteristics. The petrography and geochemistry of the Karimunjawa basalts, described by Soeria-Atmadja et al. (1985) will be discussed in this chapter along with the new data.

Nishimura et al. (1986) in their study of volcanism in the Sunda Strait, reported a K-Ar age of 0.8 Ma and some trace element data for a sample from Sukadana. Dosso et al. (1987), and Romeur et al. (1990) also studied the basalts of Sukadana and other basalts in a back-arc position in the Sunda arc. These authors described the Sukadana basalts as relatively primitive tholeiitic basalts, with 8-9% MgO, 250-350 ppm Cr, and 150-200 ppm Ni, high but variable concentrations of hygromagmaphile elements, and with $^{87}Sr/^{86}Sr$ values and εNd values in the range 0.7037 - 0.7045 and +1.6 - +6.5 respectively (Dosso et al. 1987), intermediate between MORB and OIB. A correlation observed between εNd and Th/Ta was interpreted as evidence for variations in source(s) compositions involved in the genesis of these magmas, and subducted sediments were proposed as a most likely endmember. However, no data were published in support of these conclusions.

The small outcrops of Bukit Telor (also known as Bukit Ibul), Midai and the Catwick Islands, and Bukit Nyut and the other Quaternary volcanoes in central Kalimantan have never been previously investigated in detail, and no information was found in the literature on these centres. The volcanic rocks of Kalimantan have been recently mapped as part of the joint Indonesian-Australian geological mapping program, and according to Harahap (1990) "a detailed geochemical study has been made of the volcanic rocks of West Kalimantan". However, it seems that no analyses of the Quaternary centres of Kalimantan have been published.

Midai and the Catwick Islands were not visited during this work, nor was it possible to acquire samples from these localities for study.

6.4 Arc-related volcanic rocks of Sumatra

Volcanic rocks associated with the active volcanic arc outcrop extensively in Sumatra (see Appendix C) and range in composition from rare basalts to abundant andesites and dacites. Virtually all the active and extinct volcanoes of south and central Sumatra were visited and described by Dutch geologists during the period 1910-1940, and whole-rock major element analyses performed during this period were collected and published by Westerveld (1952). Neumann van Padang (1951) also published a few major element analyses of volcanic rocks from some of the active volcanoes. More recently, Kusumadinata (1979) reviewed the volcanic activity in the Indonesian arc, and reported more major element analyses from the same centres.

The part of the island north of Lake Toba, the Aceh Special Province, remained virtually geologically unexplored until the mid seventies, when the "North Sumatran Project" was undertaken by the Indonesian and British Governments. A description of the geology of north Sumatra can be found in Page et al. (1979), Bennett et al. (1981a,b), and Cameron et al. (1983). Analyses of Permian to Quaternary volcanic rocks from north Sumatra were published by Rock et al. (1982).

It is clear, from the available data and descriptions, that the volcanic rocks of the Quaternary Sumatran arc include calcalkaline basalts, andesites, and dacites, "typical" of a volcanic arc built on continental crust. Little is known, however, about their trace element and isotope geochemistry. Isotope data are particularly rare. A few Rb/Sr, $^{87}Sr/^{86}Sr$ and K/Ar values for intrusive units in north Sumatra have been reported by Bennett et al. (1981a,b), and $^{87}Sr/^{86}Sr$ values for samples of arc andesites and associated tuffs were reported by Leo et al. (1980) for the Padang area, and by Whitford (1975) for the nearby Marapi volcano and for the tuffs of Lake Toba (see Chapter 2). No complete sets of Sr, Pb and Nd isotope data have been published for rocks from the Quaternary Sumatran arc.

Reconnaissance sampling and a major and trace element, and Sr, Nd and Pb isotope study of the Sumatran Quaternary arc volcanics was carried out during this study, and the analyses and a brief description of the samples are reported in Appendix C. These data are not discussed in detail in this thesis, and their chemical and isotopic composition are used mainly for comparative purposes.

6.5 Geological setting of the olivine-phyric basalts in Sumatra

6.5.1 Sukadana plateau

The Sukadana basaltic plateau (Figure 6.3) is situated in SE Sumatra (Lampung Province), about 30 to 40 km NNE of the capital city of the province, Tanjungkarang. It covers an area of approximately 1000 square kilometres, and is made of several basaltic flows up to two-three metres thick, erupted along fissures trending NW-SE, parallel to the Semangko Fault. The average height of the plateau above the surrounding area is only 30 to 40 m, but several hills - that probably represent the eruptive centres - are more than 200 m (above sea level) high, and although the basaltic pile might locally be up to 200 m thick, no outcrops thicker than about 10 metres have been observed. Most of the area is covered by up to 2 metres of lateritic soil, and outcrops are only found occasionally along river scarps, quarries, and on top of the youngest, best preserved eruptive centres. The exposed flows may show columnar jointing, and where the base of the pile is visible, it overlays Quaternary tuffaceous deposits of the Lampung Formation.

Samples from several localities have been dated by Soeria-Atmadja et al. (1985) and Nishimura et al. (1986), and their K/Ar ages range from 1.15 ± 0.17 Ma to 0.44 ± 0.13 Ma for the oldest samples (first cycle of Soeria-Atmadja et al. 1985), to less than 0.01 Ma (second cycle) for the youngest ones from well preserved flows and spatter cones.

Despite its clearly back-arc position, the axis of the Sukadana plateau is situated only less than 50 km away from two coeval andesitic centres (Mt. Rajabasa and Mt. Ratai) that are part of the Quaternary Sumatran volcanic arc, and it overlays pyroclastic products (Lampung and Tarahan Formations) emitted by centres within the volcanic arc.

6.5.2 Bukit Telor

Bukit Telor (also known as Bukit Ibul) is an isolated hill made of basaltic material and only 38 meters high, situated about 40 km NNE of Jambi (Jambi Province), more than 200 km behind the axis of the Quaternary Sumatran volcanic arc. The hill is surrounded by Holocene alluvium and swamp deposits, Pliocene to Pleistocene tuffaceous sandstones and claystones (Kasai and Muaraenim Formations), and Miocene sandstones and claystones (Airbenakat Formation), which are folded into

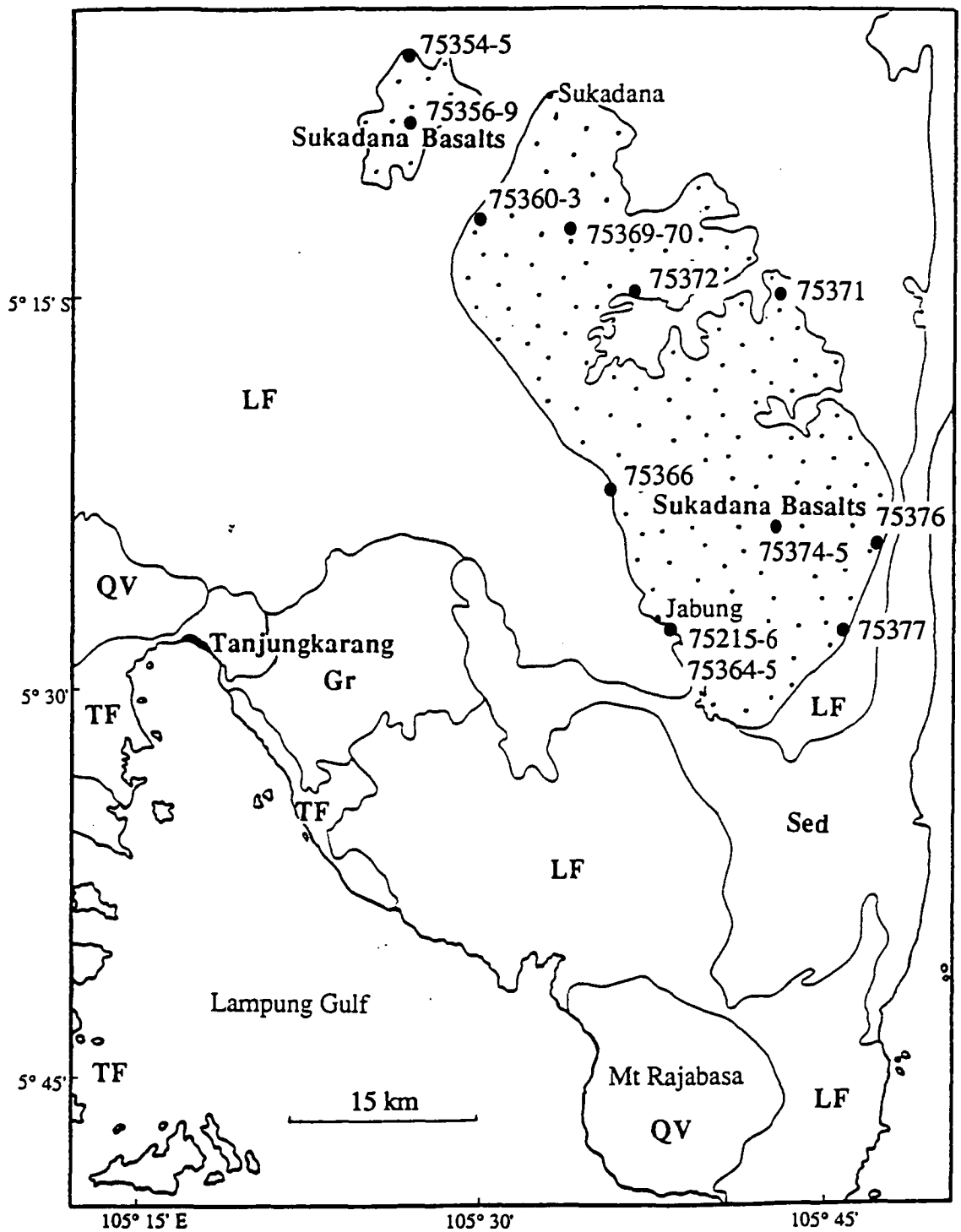

Figure 6.3. Geological sketch map of the Sukadana - Lampung Gulf area (simplified from Mannga et al. 1986). Light stippled areas: Sukadana Basalts; QV: Quaternary andesitic centers; LF: Lampung Formation; TF: Tarahan Formation; Gr: Tertiary granites; Sed: Quaternary fluvial sediments. Dots and sample numbers mark the location of samples collected during this study.

closely spaced and gently dipping synclines and anticlines with axes trending parallel to the Semangko fault zone.

The area of the Bukit Telor outcrop is less than 4 square kilometres, and fresh rock can only be found under several tens of centimetres of soil. Fluvial deposits bearing basaltic fragments and olivine crystals - presumably from Bukit Telor - have been found nearby, at Kampung Rano. The stratigraphic age of these basalts is clearly Quaternary, and this has been recently confirmed by a K/Ar age of 1.25 ± 0.19 my (Syachrir and Kardana, Indonesian Geological Research Centre, personal communication, 1991).

6.5.3 Bukit Mapas

Bukit Mapas is a basaltic-andesitic central volcano situated within the arc, and less than 50 km northeast of the Semangko Fault.

The volcanic complex, which covers an area of about 100 square kilometres a few kilometres south of the town of Martapura (South Sumatra Province), and rises about 150 metres above the surrounding area, is associated with 12 smaller lava domes (van Bemmelen 1949). The samples discussed here were collected from a quarry at the base of one of the hills (Pematang Bedil).

The radiometric age of these products is not known, but stratigraphic relationships, the morphology of the structure and the freshness of the lava flows suggest that they are not older than Pleistocene, and therefore contemporaneous with the Sukadana basalts. At the base of the structure, Oligocene to mainly Pliocene and Pleistocene sedimentary (Kasai and Muaraenim Formations) as well as Plio-Pleistocene volcanic sequences (Ranau Formation) have been observed.

Several other older igneous units outcrop in the vicinity of these basaltic centres, including some of the oldest basalts found in Sumatra (Trias-Jurassic Basalt Complex - Pardede & Gafoer 1986; see samples 75243, 75244, and 75245 in Appendix C) and Late Cretaceous granites (Garba Granites - Pardede & Gafoer 1986), and several andesitic centres of the volcanic arc.

6.6 Petrography

Andesites and andesitic basalts in the Indonesian arc are usually highly porphyritic, with up to 30% phenocrysts of plagioclase, orthopyroxene and clinopyroxene, and titanomagnetite, and occasionally olivine, and hornblende in the most evolved rocks.

The rocks from the localities described here are all olivine-phyric, but with variable paragenesis and texture.

A general petrographic description of these rocks is given below. Microprobe analyses of phenocryst phases and inclusions are listed in Appendix F, and will be discussed later in this chapter.

6.6.1 Sukadana plateau

All the samples from the Sukadana plateau (Figures 6.4a-d) are basaltic lavas, and differ considerably from the arc andesites in both texture and paragenesis.

Most of the basalts are porphyritic with micro- to cryptocrystalline groundmass, with rare patches of glass. The only almost ubiquitous phenocryst phase is olivine, normally less than 5% of the rock, but ranging from almost 0% to about 7-8%, which usually occurs in euhedral to subhedral crystals up to 3 mm long, often with thin iddingsitic rims in the low-Ti samples, and which normally contains abundant Cr-spinel inclusions. The groundmasses are usually made up of euhedral plagioclase laths (labradorite core and andesine to oligoclase rim - optical determination), with intergranular augite and olivine, and variable amounts (up to a few percent) of spinel and accessory apatite. Spinel and augite in the groundmass, and olivine phenocrysts are considerably more abundant in the high-Ti samples. Also, olivine phenocrysts are bigger in the high-Ti samples. Olivine (and rarely plagioclase) is sometime present as microphenocryst.

Most of the basalts are moderately vesicular (rarely as much as 5 to 10% by volume), with some cavities partly in-filled by mamillary glass, and rarely zeolites in the slightly altered samples. Fe-Ti oxides coat vesicles in the most vesiculated parts of the flows.

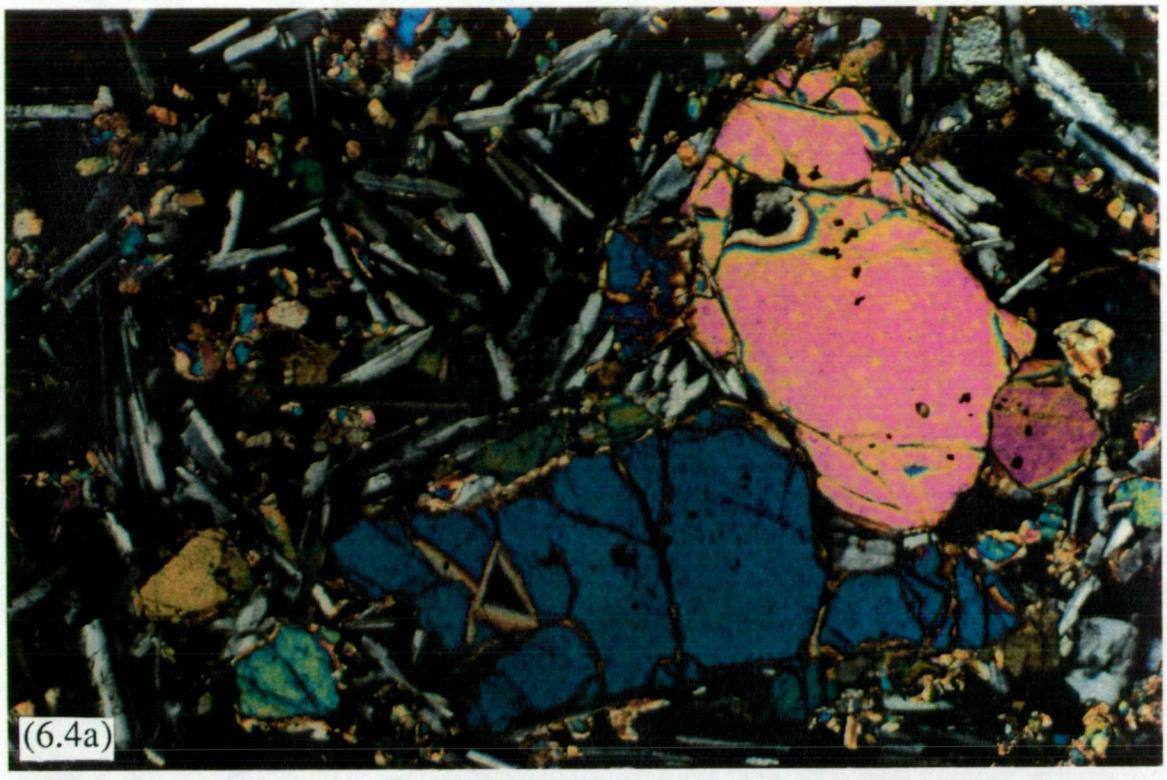

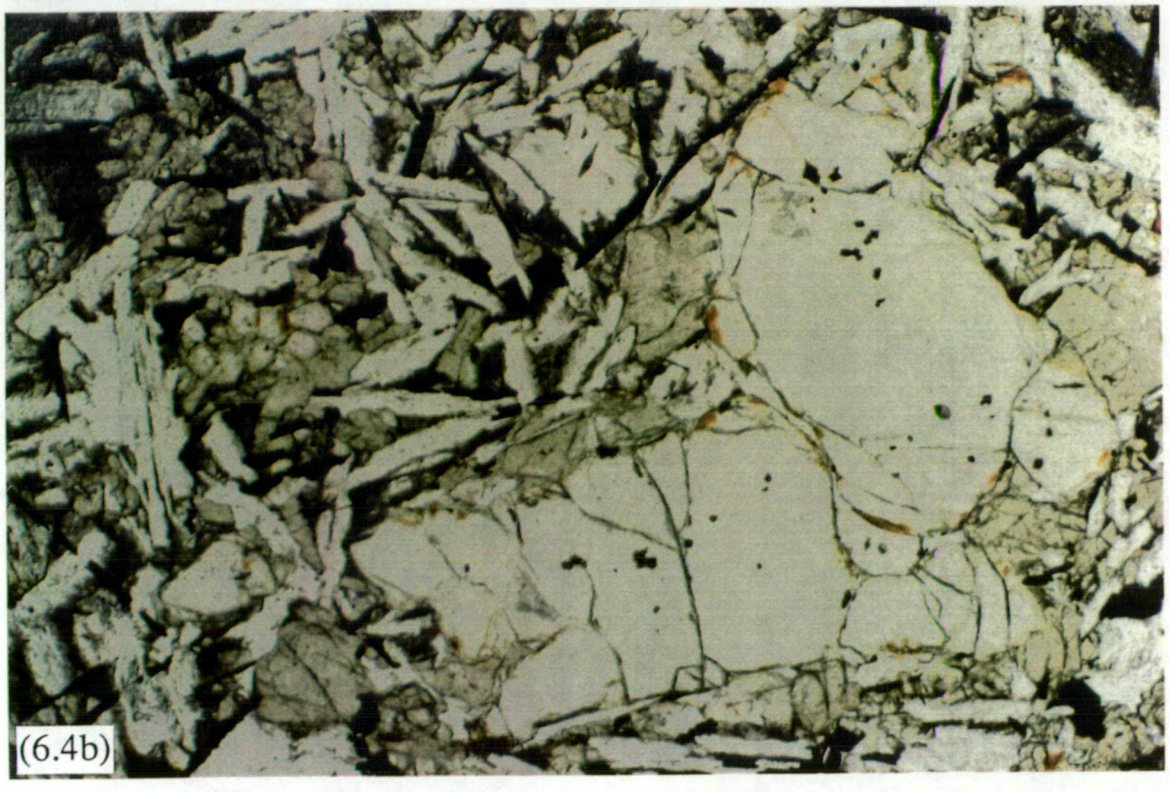

Figures 6.4a-b. Photomicrographs of high-Ti basalts of Sukadana, showing olivine phenocrysts and minerals in the groundmass. Figure 6.4a - crossed nicols, 5x; 6.4b - parallel nicols, 5x.

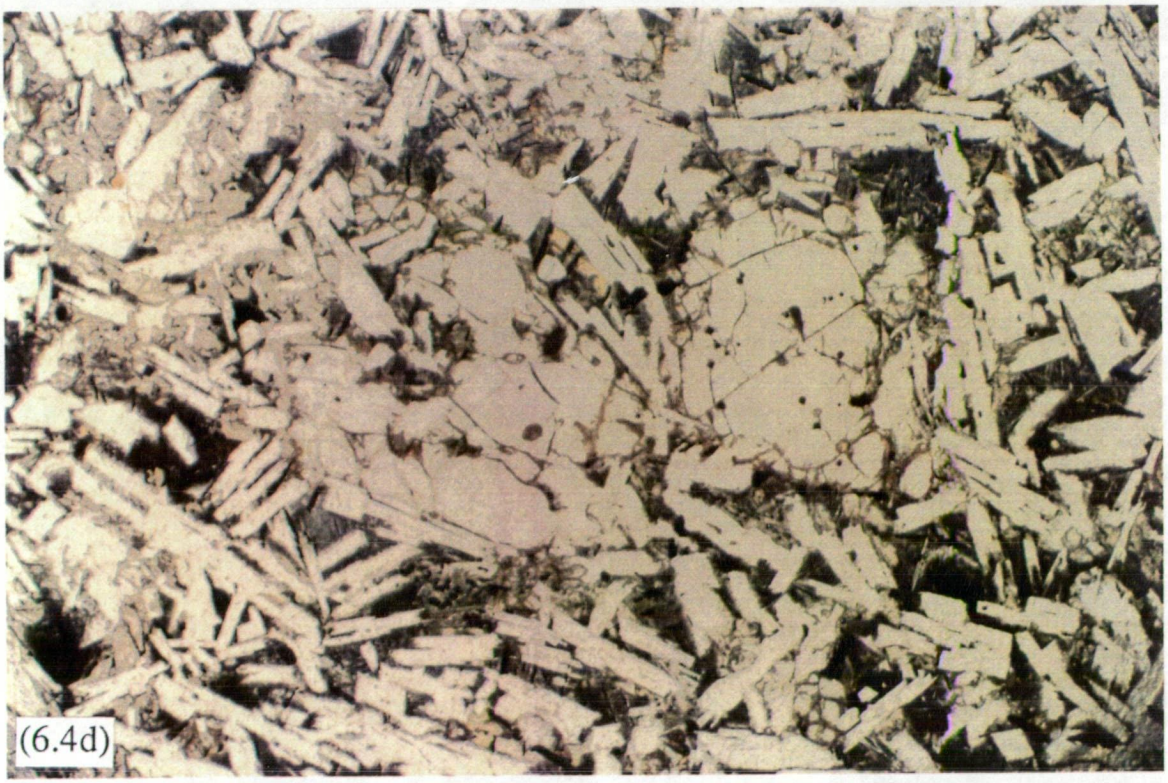

Figures 6.4c-d. Photomicrographs of low-Ti basalts of Sukadana, showing olivine phenocrysts and minerals in the groundmass. Figure 6.4c - crossed nicols, 5x; 6.4d - parallel nicols, 5x.

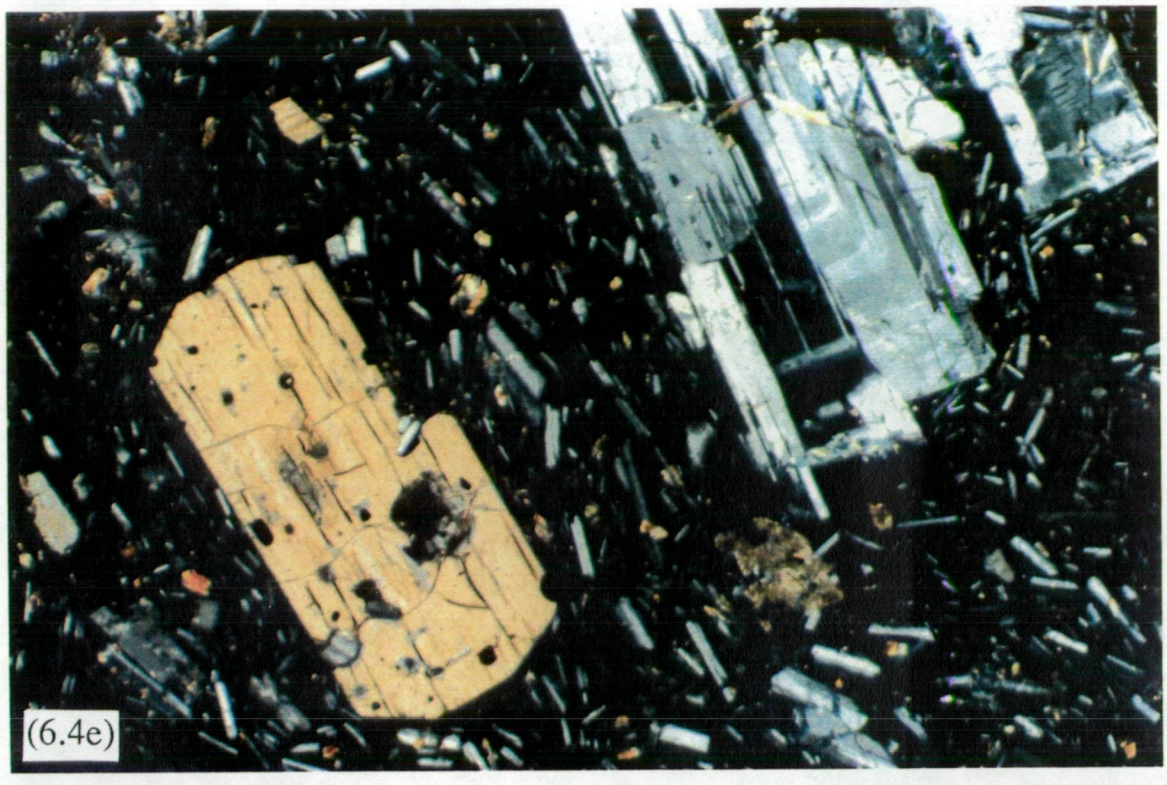

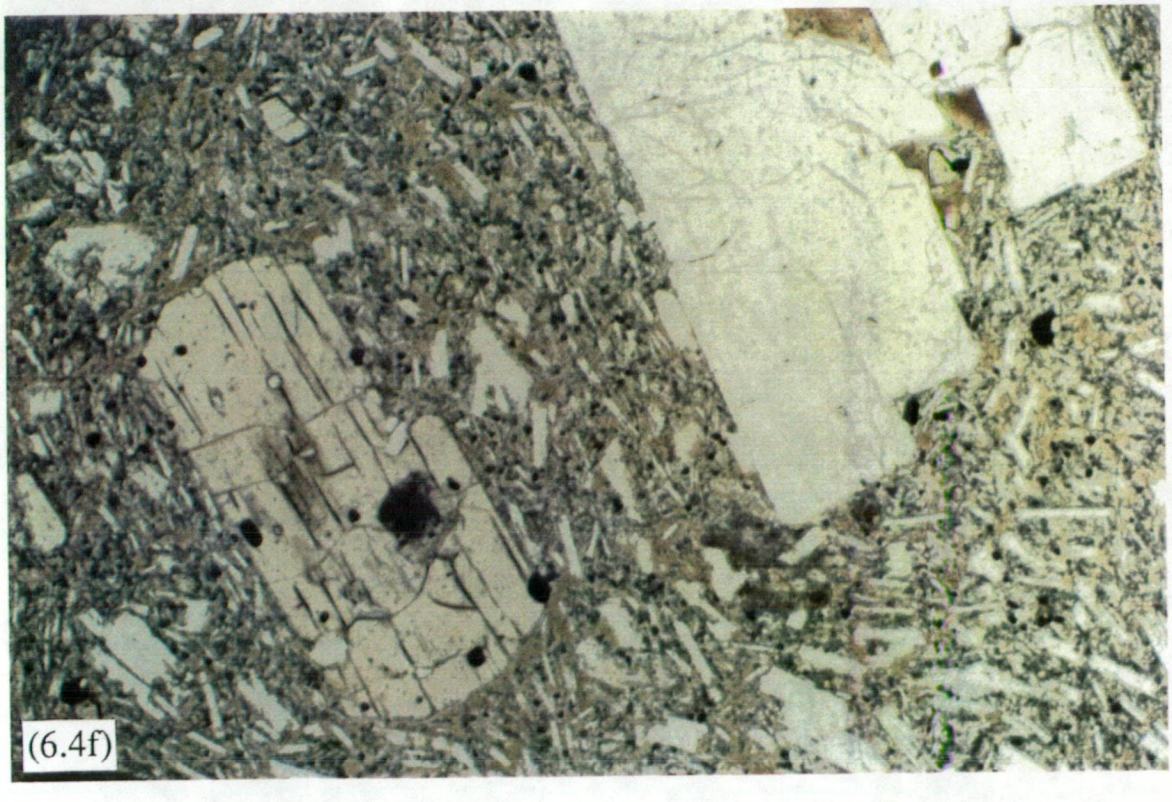

Figures 6.4e-f. Photomicrographs of Kalimantan basalts (Group 1), showing large hypersthene and plagioclase phenocrysts. Figure 6.4e - crossed nicols, 5x; 6.4f - parallel nicols, 5x.

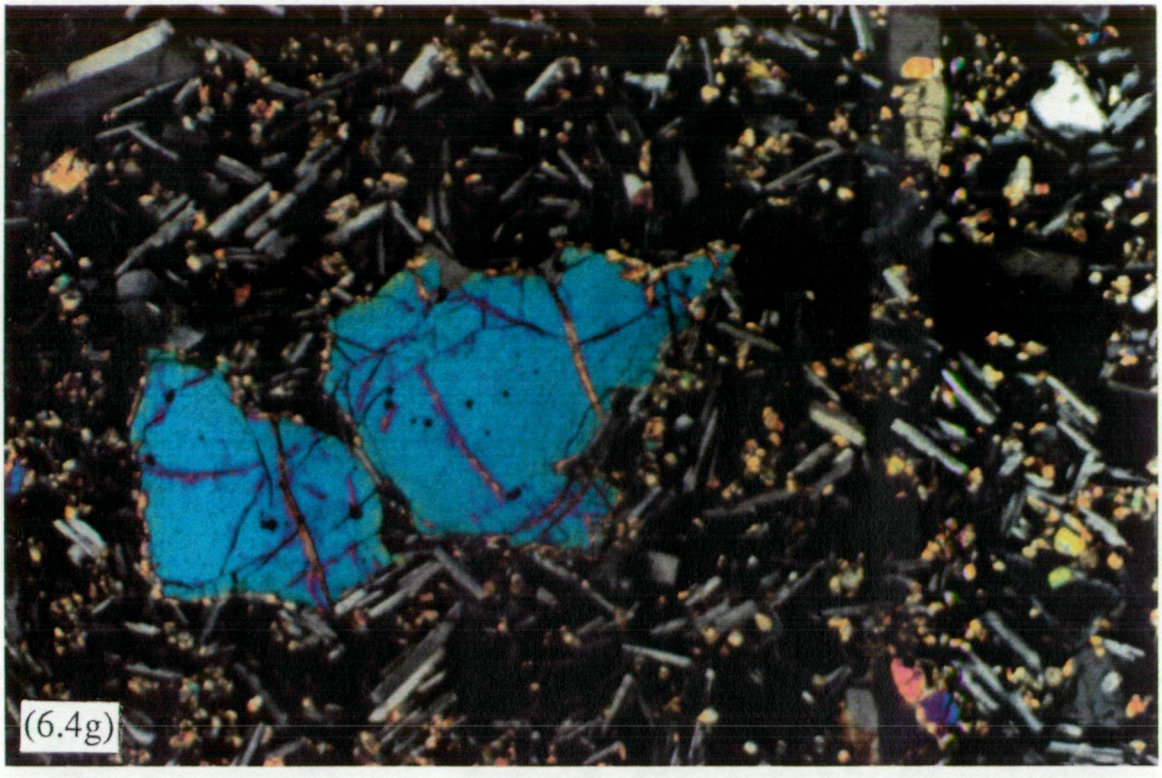

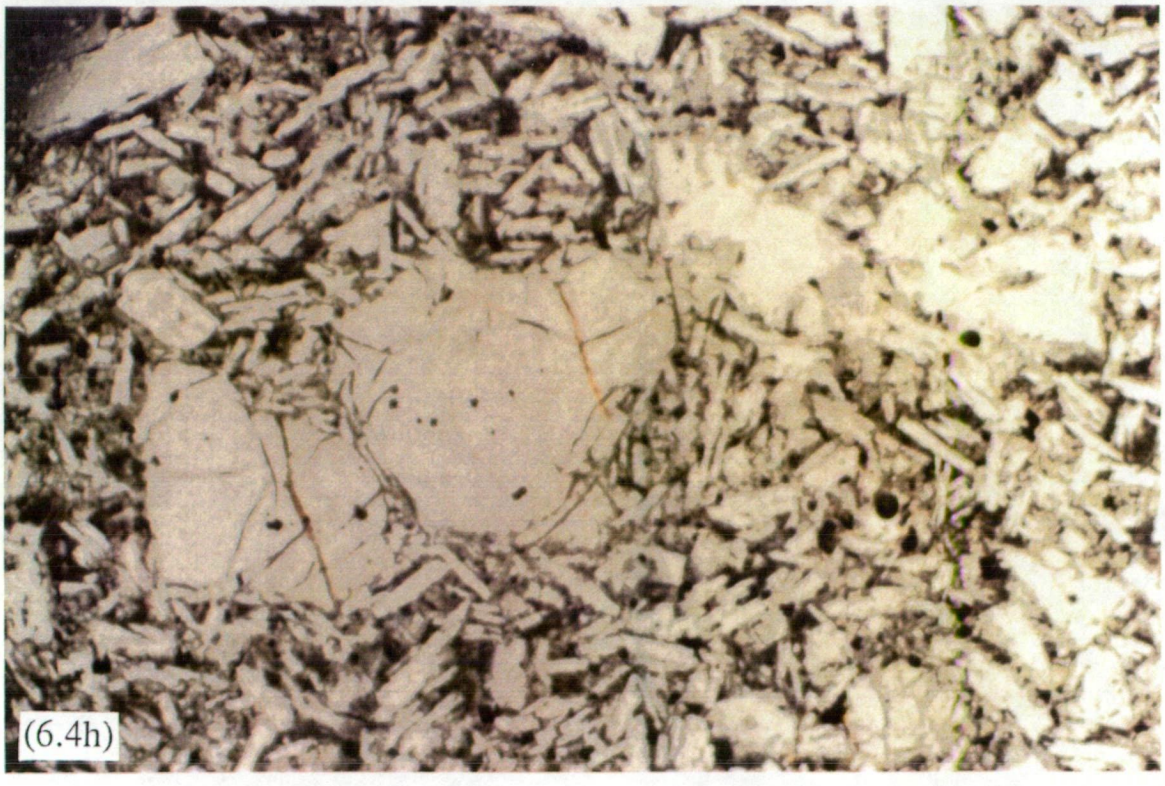

Figures 6.4g-h. Photomicrographs of Kalimantan basalts (Group 2), showing olivine phenocrysts and minerals in the groundmass. Figure 6.4g - crossed nicols, 5x; 6.4h - parallel nicols, 5x.

6.6.2 Bukit Telor

The three samples from Bukit Telor (75378, 75379, and 75389) have different textures. 75389 is holocrystalline (Figure 6.5a-b); olivine microphenocrysts are euhedral, commonly forming glomeroporphyritic clusters, and are set in a groundmass with intergranular, almost equigranular, texture composed of plagioclase, augite, spinel and accessory apatite, with texture and mineral proportions and compositions similar to some of the Sukadana plateau lavas, but overall higher content in mafics. No chromite inclusions occur in the olivines, unlike those of Sukadana. 75378-9 are both nearly aphyric: abundant olivine and augite microphenocrysts occur in glassy to cryptocrystalline groundmasses. 75379 is xenolith bearing but slightly altered: large (up to 5 mm long) olivine crystals (Figure 6.5c) are common, and some small lherzolite xenoliths occur (Figure 6.5d), made of olivine, clinopyroxene and orthopyroxene. All the olivine crystals are inclusion-free.

6.6.3 Bukit Mapas

Two different lithological types were recognised in the field - aphyric and an olivine-phyric. Microphenocrysts are seriate and make about 15-20% of the total volume of the rock, and include euhedral plagioclase (10%), strongly zoned euhedral ortho- and clinopyroxene, some resorbed, rare olivine, and rare, skeletal black amphibole. Groundmasses are glassy, with microliths of plagioclase? and tiny crystals of magnetite.

Olivine and pyroxene microphenocrysts are more abundant in the olivine-phyric samples, where the olivine phenocrysts make up to about 5-7% of the volume of the rock. Some glomerocrysts with olivine and pyroxenes have also been observed. Phenocrysts are euhedral olivine (Figure 6.6a) and clinopyroxene in variable amounts, rare, smaller resorbed plagioclase, and quartz (Figure 6.6b) and titanomagnetite (xenocrysts) with zircon and apatite inclusions. Vesicles make up less than 5% of the rock.

Basalts from Bukit Mapas differ from those of Sukadana and Bukit Telor in having abundant plagioclase phenocrysts, larger olivine phenocrysts with abundant spinel inclusions, both clinopyroxene and orthopyroxene, no ilmenite, glassy groundmass and some up to 4-5 mm large quartz and magnetite fragments. Apart from their unusually high content in large olivine phenocrysts, their texture and paragenesis, and mineral composition are typical of the Indonesian arc andesites.

Figures 6.5a-b. Photomicrographs of Bukit Telor basalts (sample 75389), showing olivine microphenocrysts and minerals in the groundmass. Figure 6.5a - crossed nicols, 5x; 6.5b - parallel nicols, 5x.

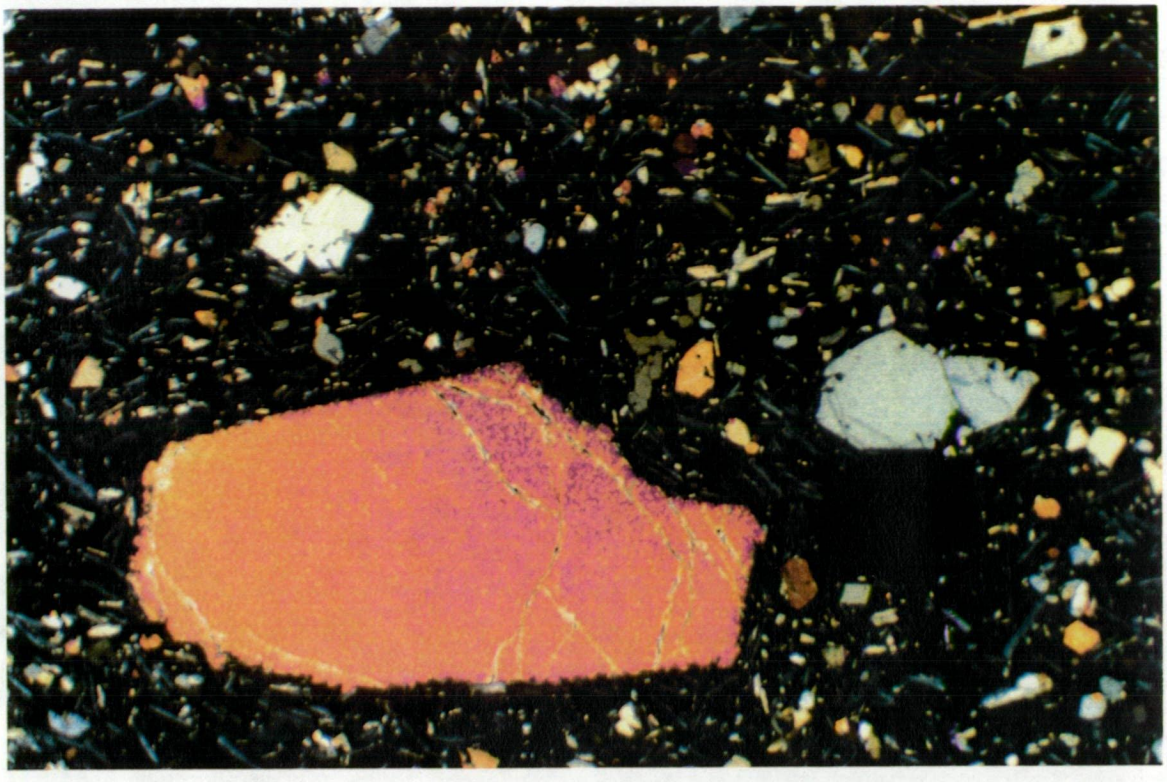

Figure 6.5c. Photomicrograph of Bukit Telor basalts (sample 75379), showing a large olivine crystal. Note the lack of mineral and fluid inclusions. Crossed nicols, 2.5x.

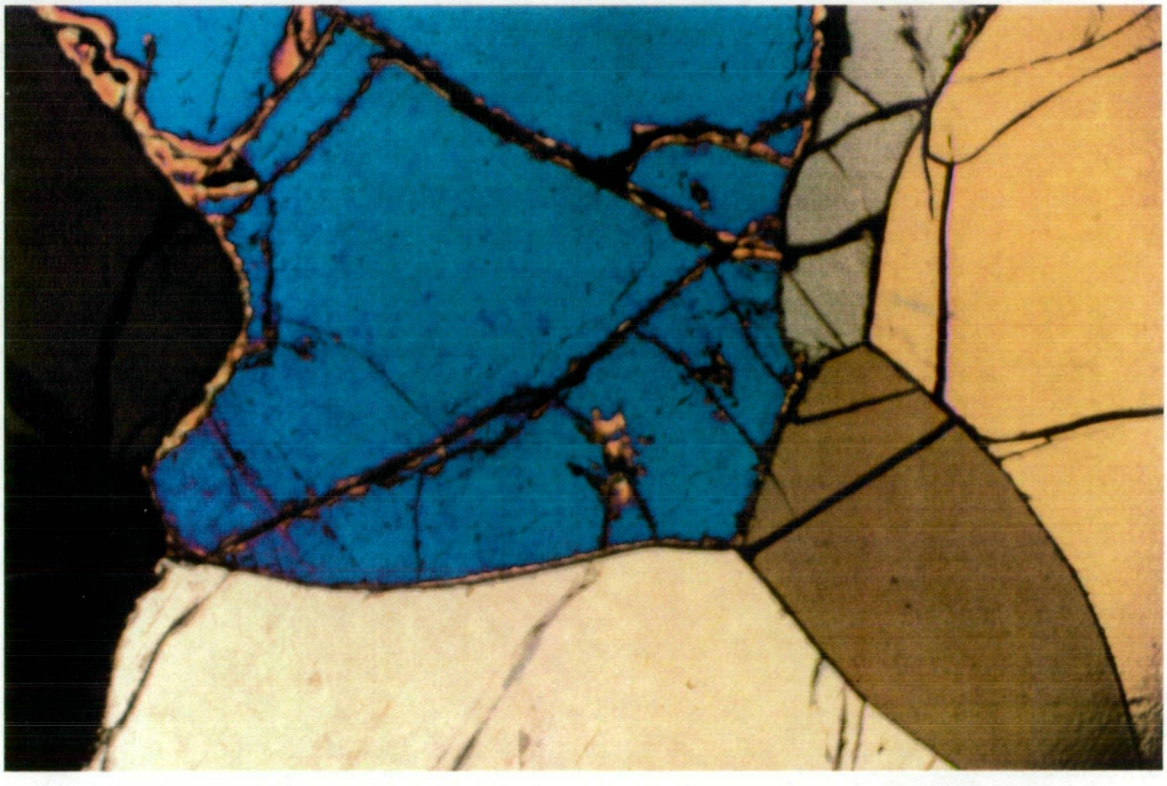

Figure 6.5d. Photomicrograph of a xenolith in Bukit Telor basalts (sample 75389), with crystals of olivine and orthopyroxene. Crossed nicols, 5x.

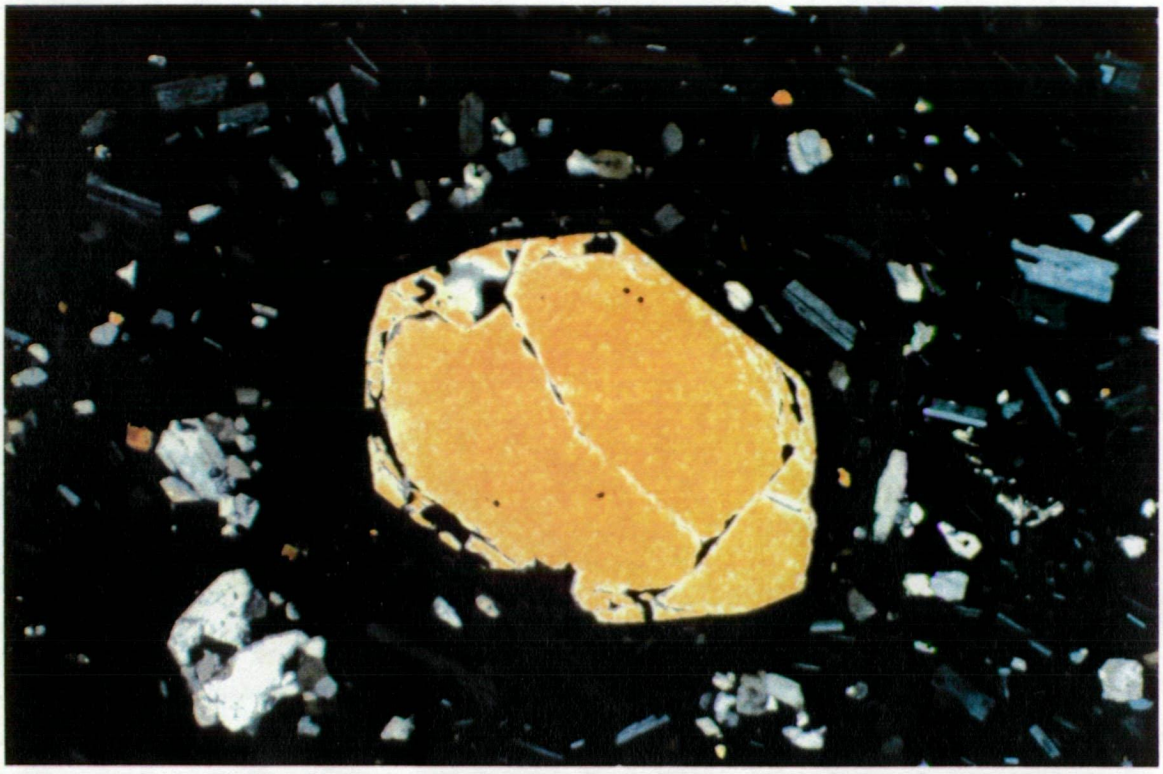

Figure 6.6a. Photomicrograph of Bukit Mapas volcanics, showing a large olivine phenocryst. Crossed nicols, 5x.

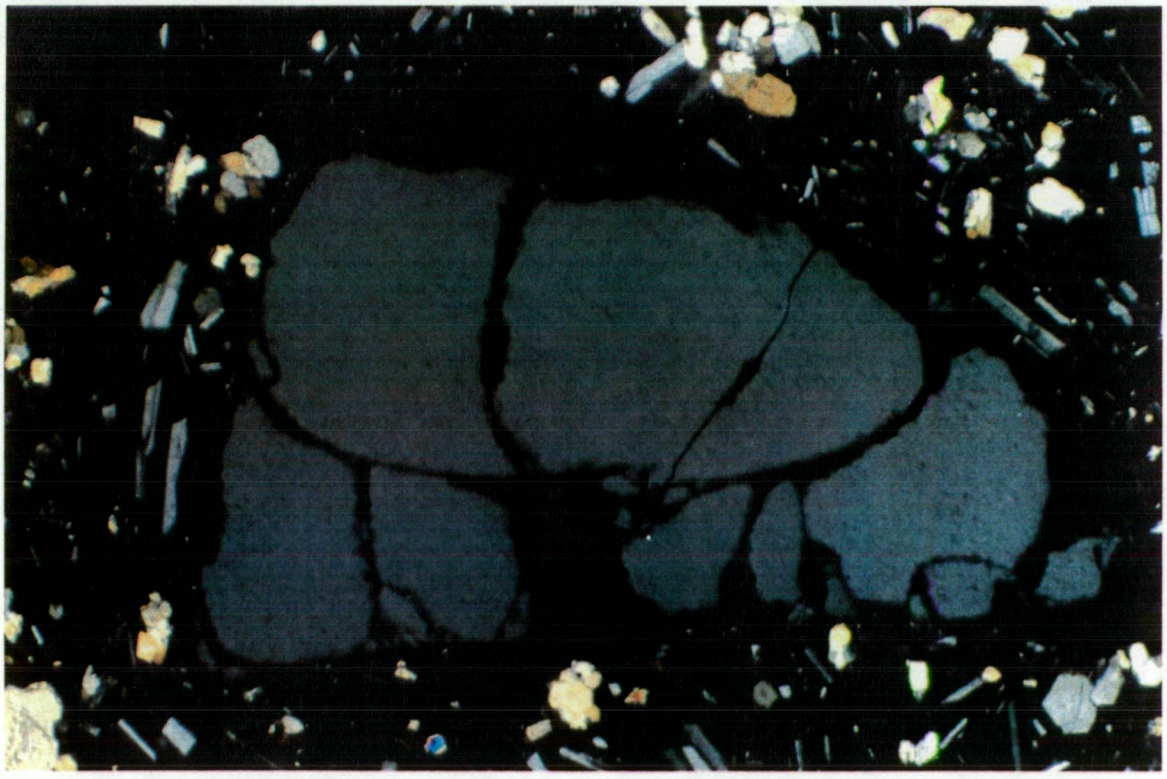

Figure 6.6b. Photomicrograph of Bukit Mapas volcanics, showing a large quartz xenocryst. Crossed nicols, 5x.

6.7 Analytical results for the rocks of Bukit Telor, Bukit Mapas, and the Sukadana plateau

6.7.1 Classification and major and trace element composition

6.7.1.1 Bukit Telor

The Bukit Telor basalts (Table 6.1) are slightly alkaline (based on the total alkalis/SiO_2 values - Figure 6.7), olivine-and hypersthene-normative, with high normative olivine values (7 to 20%), and relatively high TiO_2, K_2O and P_2O_5 contents, respectively about 2.5, 1.8 and 0.70%. The high contents of MgO and lower SiO_2, Al_2O_3 and CaO contents in 75378-9 reflect richness in olivine phenocrysts (approximately 7%) compared with 75389. In diagrams (Figures 6.8 and 6.9) used to discriminate the tectonic environments (Pearce & Cann 1973; Wood et al. 1979; Wood 1980), they plot in the field of within-plate basalts. Al_2O_3/CaO values are in the range 1.6 - 1.7.

The three Bukit Telor samples have composition very close to Sun & McDonough's (1989) average OIB, although 75378, which contains lherzolite xenoliths and is olivine-rich, is slightly more alkaline and richer in most incompatible trace elements, and Cr and Ni. All the samples show a marked enrichment in both LILE and HFSE, although LREE, particularly La and Ce contents, are comparatively low, and Nb, Ta and P contents are different in the three samples (Figures 6.10a and 6.11a).

6.7.1.2 Sukadana

The Sukadana plateau basalts (Tables 6.1 and 6.2) range in composition from slightly oversaturated, quartz tholeiites, to more abundant olivine tholeiites and slightly alkaline olivine basalts (all hypersthene and olivine normative); on a TAS diagram (Figure 6.7) they cluster around the basalts/basaltic andesites boundary, and could be collectively described as "transitional basalts".

The more alkaline samples (75215, 75216, 75364, 75365, 75360 -hereafter high-Ti basalts) have relatively low SiO_2 and Al_2O_3 values (respectively about 50% and 14.5%), and TiO_2 and P_2O_5 values up to twice as high as in the other samples (hereafter low-Ti basalts). No samples have been found with TiO_2 in the range 1.6 to 2.3%, and there seems to be no correlation between Mg# and TiO_2 content within the low-Ti group, although the low-Ti basalts seem to have overall slightly higher Mg#

	Sukadana high-Ti					Sukadana low-Ti				
Catalogue #	75215	75216	75360	75364	75365	75354	75355	75361	75362	75363
Sample name	SMG6	SMG7	SMG137	SMG141	SMG142	SMG131	SMG132	SMG138	SMG139	SMG140
Locality	Jabung	Jabung	Negerikaton	Jabung	Jabung	Bumijawa	Bumijawa	Negerikaton	Negerikaton	Negerikaton
Longitude	105°39'E	105°39'E	105°30'E	105°39'E	105°39'E	105°28'E	105°28'E	105°30'E	105°30'E	105°30'E
Latitude	5°26'S	5°26'S	5°10'S	5°26'S	5°26'S	5°02'S	5°02'S	5°10'S	5°10'S	5°10'S
SiO2	50.34	49.58	49.63	49.87	50.33	53.33	52.9	51.65	49.19	52.6
TiO2	2.97	2.88	2.36	2.85	2.76	1.27	1.31	1.31	1.43	1.25
Al2O3	14.57	14.53	14.54	14.69	14.3	15.86	15.89	16.17	15.35	15.99
Fe2O3	10.77	10.65	10.12	10.63	10.5	8.77	9.03	10.47	10.45	9.54
MnO	0.15	0.15	0.14	0.14	0.14	0.13	0.13	0.14	0.15	0.13
MgO	7.96	7.81	9.18	8.1	8.19	7.63	7.78	7.34	8.36	7.37
CaO	8.8	8.85	8.34	8.77	8.77	7.84	8.02	8.55	7.86	8.31
Na2O	3.34	3.47	3.39	3.22	3.3	3.36	3.83	3.78	2.95	3.35
K2O	1.1	1.09	1.29	0.97	1.06	0.95	0.95	0.79	1.19	0.8
P2O5	0.57	0.52	0.51	0.56	0.56	0.27	0.22	0.21	0.3	0.19
LOI	-0.43	-0.13	-0.08	-0.3	-0.28	0.19	0.2	-0.27	2.61	-0.03
Total	100.14	99.4	99.42	99.5	99.63	99.6	100.26	100.14	99.84	99.5
Mg#	63.26	63.08	67.88	63.97	64.50	66.96	66.75	62.03	65.08	64.28
Rb	16	13	14	14	12	14	16	12	14	13
Ba	187	183	244	189	183	157	177	119	168	124
Sr	613	638	661	606	613	545	551	409	549	473
Pb	2	2	2	2	2	1	2	2	3	1
Cs	0.19		0.24			0.69		0.19		
Zr	266	258	218	252	249	87	93	63	99	72
Hf	5.06		4.09			1.7		1.49		
Nb	37	36	36	36	34	13	13	10	19	10
Ta	2.61		2.15			0.86		0.89		
Y	33	31	30	30	39	17	18	15	21	17
Th	1.86	3	2.09	2	2	2.23		1.49	2	2
La	17.1	17	17.5	17	17	8.58		6.39	11	6
Ce	40.1	44	43	44	46	18.2		14.1	20	11
Nd	30.1	37	29.7	37	40	14		10.2	14	10
Sm	8.62		7.97			3.6		2.99		
Eu	2.88		2.59			1.2		1.1		
Tb	1.12		0.97			0.57		0.54		
Ho	1.05		0.91			0.63		0.54		
Yb	1.91		1.79			1.12		1.06		
Lu	0.25		0.25			0.15		0.13		
Cr	349	353	411	352	371	312	325	294	362	309
Ni	165	162	199	172	170	186	204	149	197	143
V	210	205	200	204	200	165	166	212	182	186
Sc	21	22	20	21	22	19	19	21	20	21
87Sr/86Sr	0.70391		0.70390			0.70410		0.70407		
143Nd/144Nd	0.512981		0.512969			0.512855		0.512869		
208Pb/204Pb	38.506					38.327		38.456		
207Pb/204Pb	15.591					15.561		15.598		
206Pb/204Pb	18.418					18.344		18.396		

Table 6.1. Chemical analyses of samples from Sukadana (high-Ti and low-Ti basalts) and Bukit Telor.

Table 6.1 cont.

Sukadana low-Ti (cont.)

Catalogue #	75366	75369	75370	75371	75372	75374	75375	75376	75377
Sample name	SMG143	SMG146	SMG147	SMG148	SMG149	SMG150	SMG151	SMG152	SMG153
Locality	close to Jabung	G. Mirah	G. Mirah	close to Djepara	close to Djepara	G. Wana	G. Wana	G. Samang	close to Labuhanmaringgai
Longitude	105°35'E	105°35'E	105°35'E	105°43'E	105°40'E	105°45'E	105°45'E	105°46'E	105°45'E
Latitude	5°22'S	5°08'S	5°08'S	5°13'S	5°13'S	5°20'S	5°20'S	5°21'S	5°25'S
SiO2	52.46	52.34	51.44	52.02	51.56	51.66	51.46	50.37	50.07
TiO2	1.26	1.38	1.37	1.35	1.23	1.36	1.35	1.26	1.43
Al2O3	15.75	16.06	15.81	16.19	15.36	15.82	15.64	15.49	15.72
Fe2O3	9.45	9.51	9.33	9.59	10.58	9.47	9.46	9.21	9.76
MnO	0.16	0.15	0.13	0.14	0.53	0.15	0.14	0.15	0.15
MgO	7.43	7.05	6.76	7.25	5.19	8.11	8.42	7.95	9.28
CaO	8.32	7.91	8.26	8.25	7.9	8.56	8.23	7.86	8.84
Na2O	3.45	3.76	3.8	4.05	3.49	3.52	3.54	3.29	3.07
K2O	0.92	1.19	1.19	0.95	0.76	1.32	1.19	1.15	1.3
P2O5	0.24	0.28	0.31	0.28	0.22	0.32	0.31	0.26	0.34
LOI	0.08	0.06	1.25	-0.24	2.83	-0.14	-0.24	2.8	-0.15
Total	99.52	99.69	99.65	99.83	99.65	100.15	99.5	99.79	99.81
Mg#	64.69	63.33	62.80	63.79	53.33	66.61	67.47	66.79	68.90
Rb	13	21	18	12	13	16	17	15	16
Ba	105	183	174	139	113	205	172	175	270
Sr	450	543	542	524	446	509	482	472	642
Pb	1	3	2	3	1	3	2	2	4
Cs		0.23				0.45			0.19
Zr	82	100	101	86	73	105	100	100	125
Hf		2.09				2.29			2.38
Nb	12	15	15	15	10	20	17	16	24
Ta		0.96				1.5			1.52
Y	16	17	17	16	20	23	17	19	21
Th	2	2.25	4		3	2.36	3		2.58
La	6	9.38	11		8	13.4	10		12.2
Ce	13	20.4	21		17	28.1	26		26.5
Nd	11	11.2	15		9	17.2	15		15
Sm		3.35				4.15			4.06
Eu		1.19				1.31			1.31
Tb		0.63				0.57			0.63
Ho		0.65				0.7			0.73
Yb		1.27				1.51			1.4
Lu		0.15				0.2			0.18
Cr	308	265	253	304	261	397	364	341	410
Ni	180	164	156	177	147	179	181	161	235
V	177	175	163	175	168	187	175	170	176
Sc	21	18	19	20	19	24	21	20	22
Co									
87Sr/86Sr		0.70412				0.70382			0.70393
143Nd/144Nd		0.512837				0.512895			0.512929
208Pb/204Pb		38.548				38.396			38.264
207Pb/204Pb		15.600				15.577			15.557
206Pb/204Pb		18.468				18.327			18.267

Table 6.1 cont.

	Sukadana low-Ti (Gunung Tiga)				Bukit Telor		
Catalogue #	75356	75357	75358	75359	75378	75379	75389
Sample name	SMG133	SMG134	SMG135	SMG136	SMG153B1	SMG153B2	BDNG2
Locality	G. Tiga	G. Tiga	G. Tiga	G. Tiga	Bt. Telor	Bt. Telor	Bt. Telor
Longitude	105°28'E	105°28'E	105°28'E	105°28'E	103°45'E	103°45'E	103°45'E
Latitude	5°05'S	5°05'S	5°05'S	5°05'S	1°17'S	1°17'S	1°17'S
SiO2	52.71	52.85	52.43	52.24	47.75	47.09	49.98
TiO2	1.5	1.5	1.52	1.59	2.44	2.54	2.6
Al2O3	16.26	15.9	16.03	16.62	12.93	13.8	14.3
Fe2O3	8.85	8.79	8.84	9.1	10.58	11.23	10.55
MnO	0.14	0.13	0.13	0.14	0.15	0.16	0.15
MgO	6.49	6.8	6.65	6.62	11.6	11.03	8.38
CaO	8.4	8.46	8.43	8.72	7.74	6.34	8.14
Na2O	3.43	3.43	3.59	3.68	3.19	2.58	3.45
K2O	1.22	1.18	1.24	1.25	1.84	1.87	1.75
P2O5	0.32	0.32	0.32	0.29	0.79	0.85	0.58
LOI	0.47	0.18	0.23	0.22	0.46	2.8	0.03
Total	99.79	99.54	99.41	100.47	99.47	100.29	99.91
Mg#	63.08	64.32	63.67	62.89	71.87	69.59	64.92
Rb	20	18	19	17	31	30	32
Ba	202	246	208	203	397	469	392
Sr	563	583	582	587	697	482	543
Pb	2	1	2	2	5	6	4
Cs			0.26		0.64		0.3
Zr	113	120	118	119	257	279	222
Hf			2.45		5.23		4.75
Nb	19	19	20	19	71	74	54
Ta			1.48		3.87		3.17
Y	24	19	32	20	28	38	27
Th	3	3		3	5.17		4.2
La	16	12	16.4	13	27.5		21.2
Ce	29	25	34.1	29	60.6		44.2
Nd	19	16	21.4	18	33.8		25.4
Sm			5.4		7.56		6.71
Eu			1.87		2.34		2.15
Tb			0.96		0.9		1.05
Ho			1.12		0.87		1.16
Yb			2.13		1.75		1.77
Lu			0.3		0.25		0.22
Cr	265	303	287	270	505	532	313
Ni	115	130	112	114	383	355	205
V	192	186	207	206	162	168	180
Sc	24	22	24	25	18	21	21
Co							
87Sr/86Sr			0.70402		0.70403		0.70430
143Nd/144Nd			0.512898		0.512891		0.512882
208Pb/204Pb			38.367		38.706		38.609
207Pb/204Pb			15.569		15.626		15.634
206Pb/204Pb			18.353		18.429		18.382

	Sukadana Westerveld (1952)							
Sample name	W47	W48	W49	W50	W51	W52	W53	W54
Longitude	105°40'E	105°35'E	105°35'E	105°40'E	105°40'E	105°43'E	105°28'E	105°40'E
Latitude	5°15'S	5°08'S	5°08'S	5°22'S	5°15'S	5°18'S	5°05'S	5°15'S
SiO2	50.13	50.23	50.34	51.42	51.81	51.55	53.28	55.44
TiO2	1.45	1.54	1.29	1.45	1.37	1.34	1.54	1.05
Al2O3	16.27	16.03	16.41	16.04	16.41	15.94	16.19	19.45
Fe2O3	2.39	2.64	2.61	2.55	2.00	2.68	3.01	2.71
FeO	7.38	6.70	6.67	6.42	7.41	6.41	5.42	4.14
MnO	0.13	0.12	0.11	0.12	0.12	0.11	0.12	0.12
MgO	8.57	8.45	8.43	8.23	7.27	7.45	6.58	2.66
CaO	8.30	8.63	8.63	8.36	8.54	8.48	8.49	8.20
Na2O	3.43	3.29	3.19	3.47	3.25	3.12	3.64	3.03
K2O	1.08	1.68	1.65	1.28	0.80	1.05	1.23	1.93
P2O5	0.13	0.22	0.17	0.14	0.13	0.18	0.25	0.20
LOI	0.57	0.38	0.43	0.54	0.75	1.20	0.51	1.08
H2O-	0.28	0.19	0.29	0.29	0.29	0.75	0.19	0.31
Total	100.14	100.10	100.22	100.35	100.19	100.26	100.47	100.32
Mg# *	67.42	69.21	69.25	69.55	63.61	67.44	68.39	53.38
Mg# (Fe2O3/FeO=0.15)	65.34	66.12	66.21	66.44	62.33	63.91	62.92	45.88
Cr	205			274	274		137	

	Sukadana Soeria-Atmadja et al. (1985)			Karimunjawa Soeria-Atmadja et al. (1985)			
Sample name	BK26A	WL16	GT17A	KG6 (Genting)	KG9 (Genting)	KP13 (Parang)	KP20 (Parang)
SiO2	50.32	50.78	52.95	48.50	48.30	50.50	47.50
TiO2	2.86	1.27	1.37	1.57	1.59	1.99	2.18
Al2O3	14.05	16.75	15.50	14.51	13.27	13.83	13.27
Fe2O3	10.93	10.71	9.03	10.70	11.22	11.18	11.74
MnO	0.14	0.14	0.12	0.17	0.18	0.17	0.16
MgO	8.63	7.46	8.01	8.58	11.43	8.20	8.54
CaO	9.03	8.77	8.05	10.17	9.02	8.49	8.88
Na2O	3.05	3.62	3.61	3.01	3.05	3.12	2.72
K2O	1.01	0.57	1.06	1.55	0.82	1.49	2.00
P2O5	0.40	0.14	0.24	0.45	0.40	0.45	0.50
LOI	0.30	0.33	0.21	0.79	0.43	1.08	2.12
Total	100.72	100.54	100.15	100.00	99.71	100.50	99.61
Mg# (Fe2O3/FeO=0.15)	64.78	61.87	67.39	65.14	70.36	63.08	62.89

Table 6.2. Chemical analyses of samples from Sukadana and the Karimunjawa Islands reported by Westerveld (1952) and Soeria-Atmadja et al. (1985). In the analyses reported by Westerveld (1952), Mg# is calculated based on the measured FeO content, and these values was not considered in the following discussion and diagrams. Based on these values, the Fe_2O_3/FeO value in the Sukadana basalts ranges from 0.85 to 0.80, the same range observed in the melt inclusions (see following discussion).

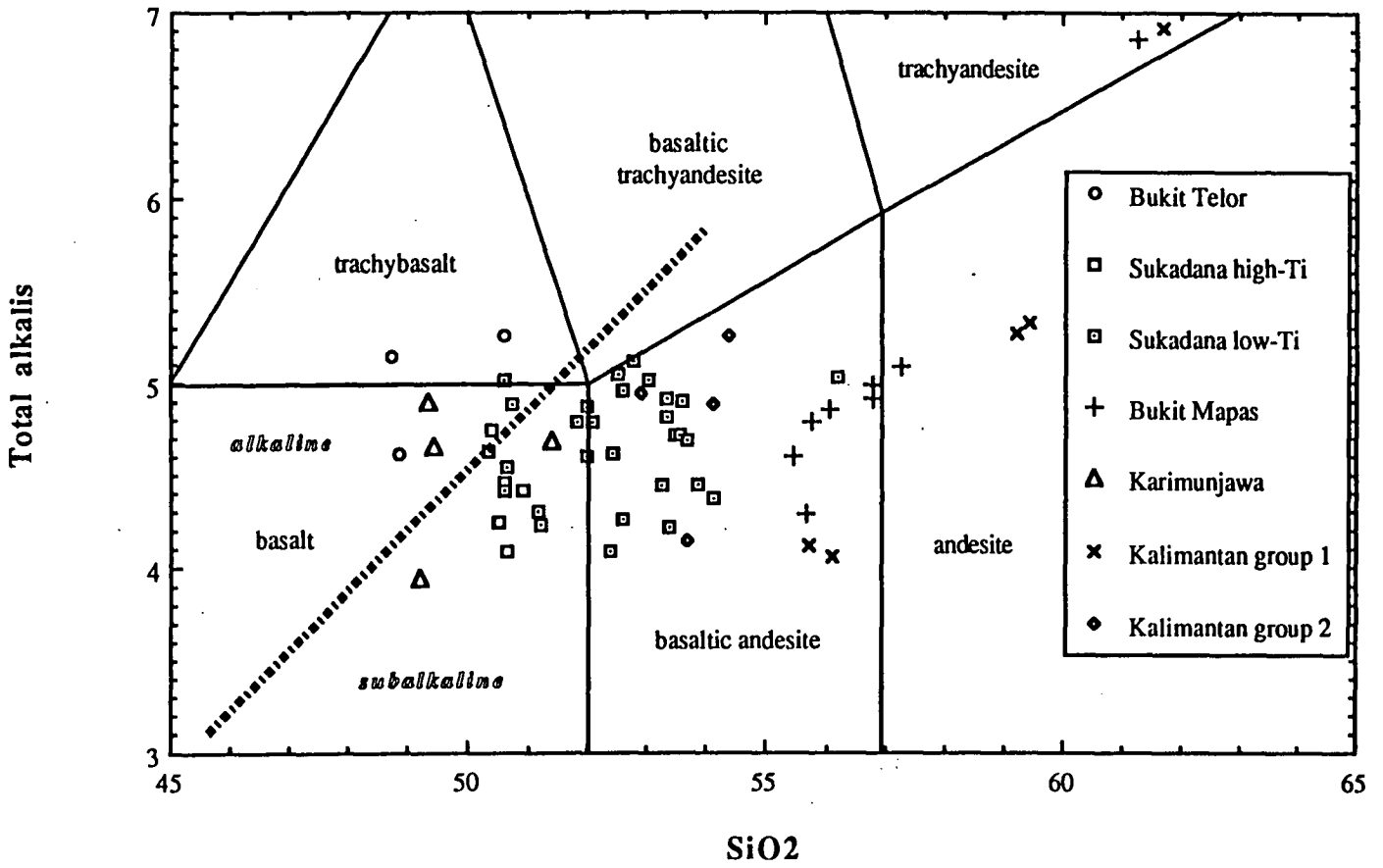

Figure 6.7. Total alkali-SiO_2 classification diagram (after Le Bas et al. 1992; alkaline-subalkaline field dividing line after Irvine & Baragar 1971) for the basaltic rocks of Sukadana, Bukit Telor, Karimunjawa, Kalimantan, and Bukit Mapas. Data from this study, and Westerveld (1952), and Soeria-Atmadja et al.(1985).

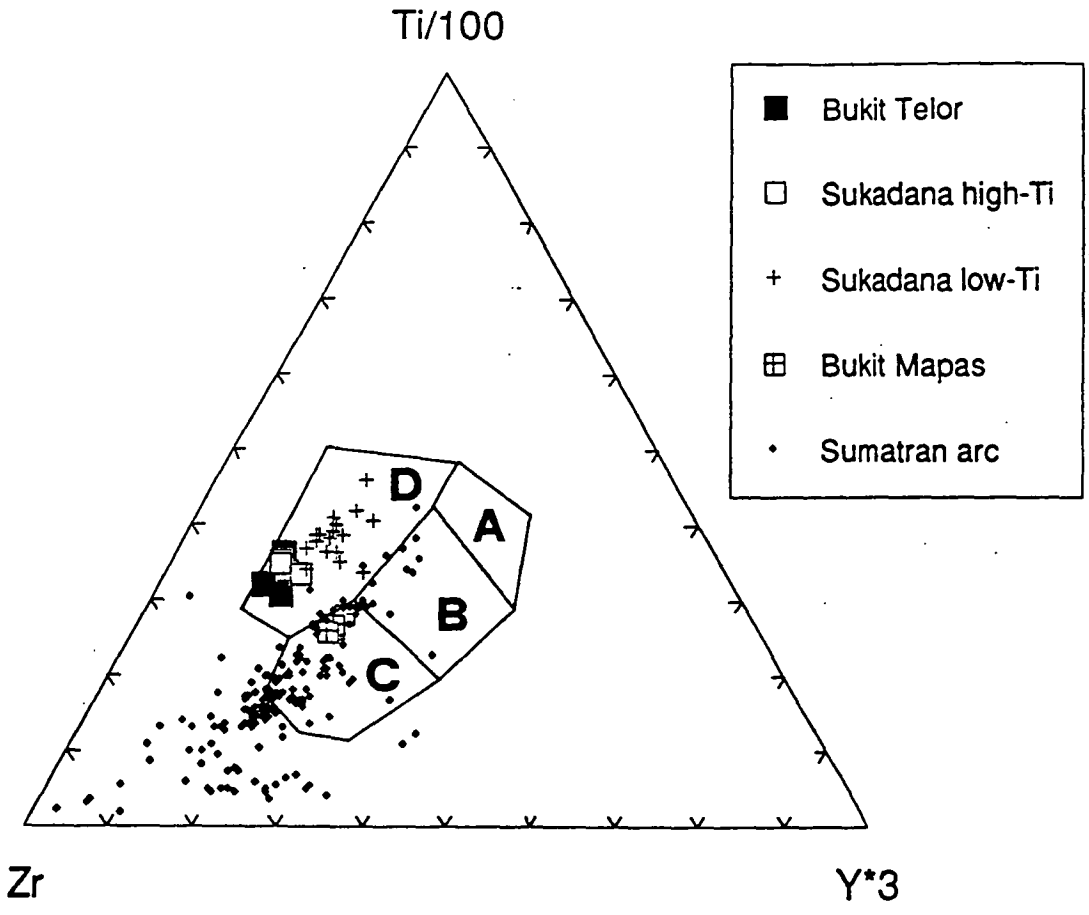

Figure 6.8. Ti/Zr/Y tectonic environment discrimination diagram (after Pearce & Cann 1973) for the Sukadana and Bukit Telor rocks. Fields are: A, B - island arc; B - ocean floor; B, C - calc-alkaline; D - within-plate. A main trend of increasing Zr for increasing degree of alkalinity can be recognized, alongside less defined trends of increasing Y values, starting from the transitional and tholeiitic fields.

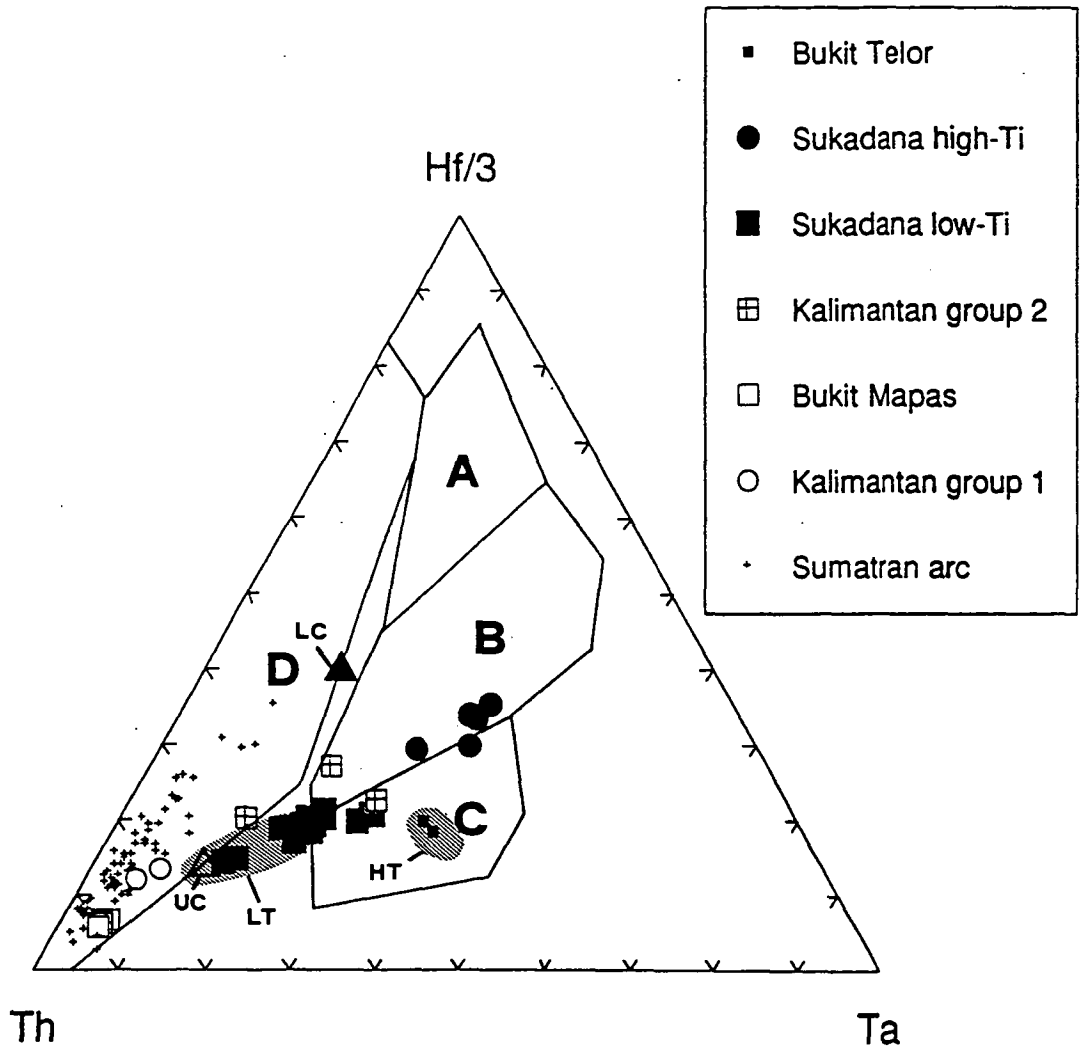

Figure 6.9. Th/Ta/Hf tectonic environment discrimination diagram (after Wood et al. 1979; Wood 1980). Fields of Karimunjawa (LT - low-Ti; HT - high-Ti) basalts are from Soeria-Atmadja et al. (1985). Fields are: A - N-MORB; B - E-MORB, and tholeiitic within-plate basalts; C - alkaline within-plate basalts; D - arc rocks. Also shown are average composition of upper (UC) and lower (LC) crust, from Taylor & McLennan (1985).

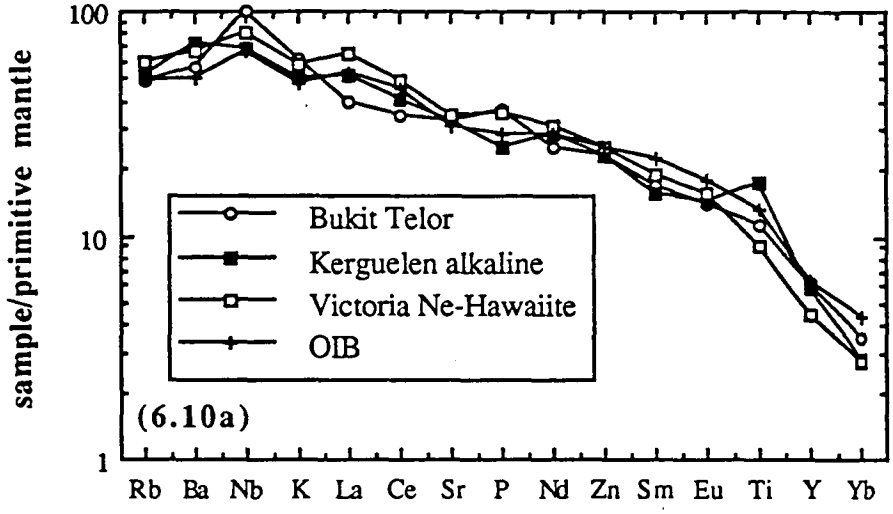

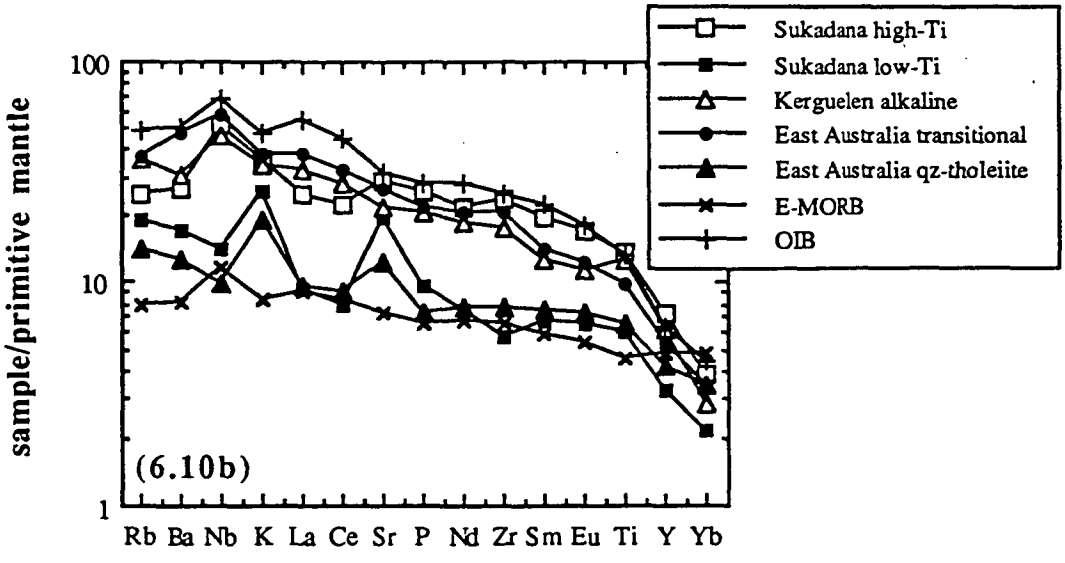

Figures 6.10a-b. Trace element values normalised to primitive mantle values (from Sun & Mc Donough 1989 - also E-MORB and OIB values) for representative samples from Bukit Telor (Figure 6.10a) and Sukadana (Figure 6.10b). Data for Kerguelen are from Gautier et al. (1990) and Storey et al. (1988). Data for the Australian volcanics are from Ewart et al. (1988).

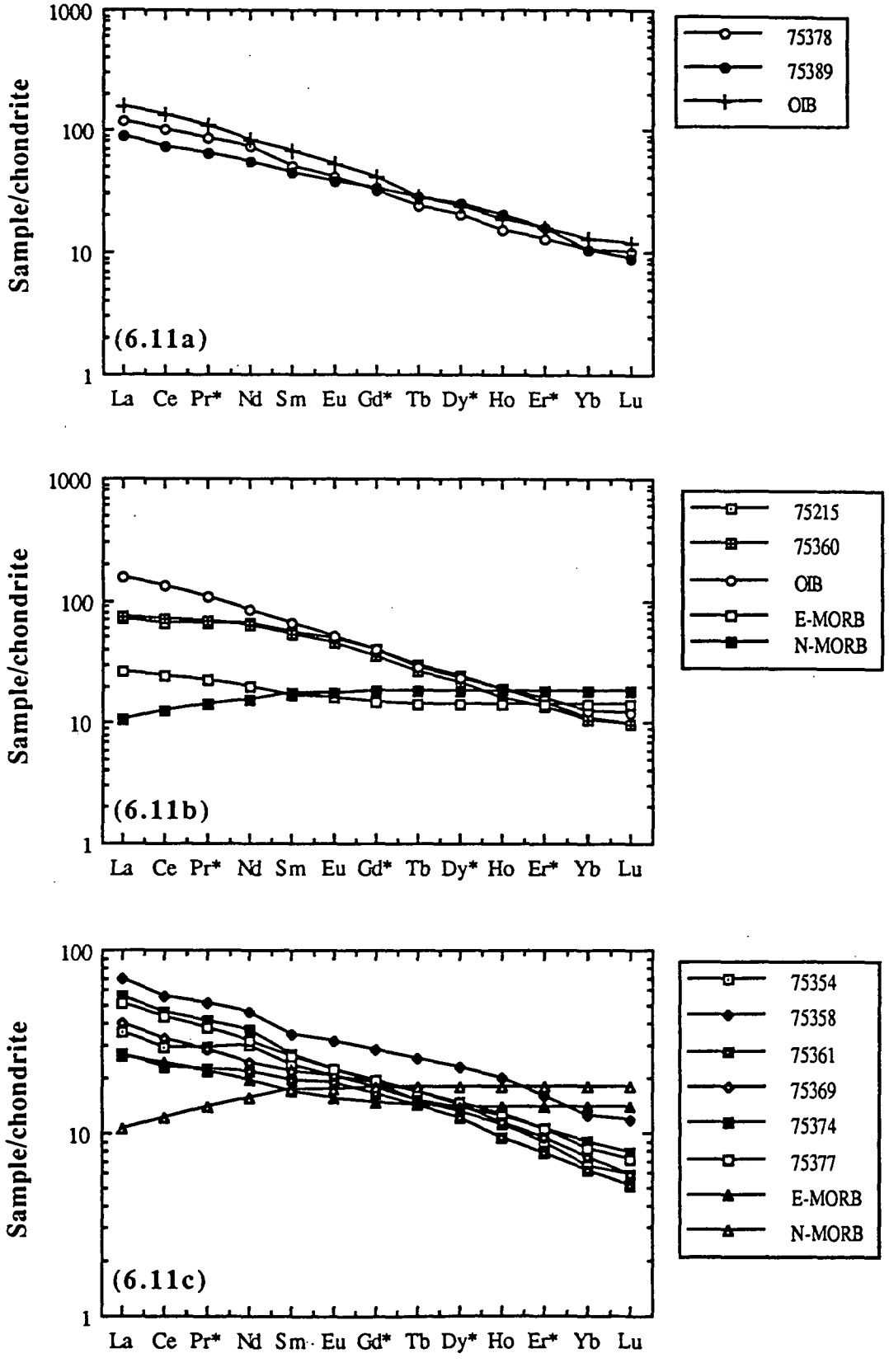

Figures 6.11a-c. REE values normalised to chondrite values (from Sun & Mc Donough 1989 - also E-MORB and OIB values) for representative samples from Bukit Telor (Figure 6.11a), and Sukadana high-Ti (Figure 6.11b), and low-Ti (Figure 6.11c) basalts. The values of some REE (marked with an asterisk) have been interpolated from the other REE.

values (Figure 6.12). Apart from the considerably lower K_2O content, the major element composition of the high-Ti samples does not differ from that of the olivine-poor alkaline basalts from Bukit Telor (sample 75389). Other small variations in major element compositions within the two groups are mainly due to differing amounts of phenocrysts (olivine and clinopyroxene, and plagioclase in the more tholeiitic samples) in the rocks. The Al_2O_3/CaO values range from about 1.6 - 1.7 in the high-Ti basalts (same values as in Bukit Telor), to 1.9 - 2.0 in the low-Ti basalts. Some samples (75362, 75372, 75376) show incipient alteration.

The differences between the high-Ti and low-Ti basalts are also evident when the samples are plotted on a Th/Hf/Ta diagram (Figure 6.9). The high-Ti basalts fall in the field of alkaline within plate basalts (like the basalts from Bukit Telor), at the boundary with the field of E-MORB and tholeiitic within-plate basalts, whereas the low-Ti basalts are relatively enriched in Th and seem to tend towards a more arc-type affinity. This distinction can also be seen in a Ti/Zr/Y diagram (Figure 6.8), where the Zr content gradually increases with the increasing alkalinity, and the low-Ti samples relatively enriched in Th are also slightly enriched in Y, and trend towards the field of calcalkaline basalts.

The trace element compositions of the high-Ti basalts are remarkably constant and OIB-like (Figures 6.10b and 6.11b), although somewhat depleted in La and Ce contents, as are the Bukit Telor basalts, and in Cs, Rb, Ba, Th and Pb contents. At the other end of the compositional range, the low-Ti basalts have rather variable compositions (Figures 6.10b and 6.11c). The most "enriched" samples have trace element contents considerably lower than in the high-Ti basalts, and the most "depleted" samples have progressively lower trace element content, with LREE values as low as in E-MORB, negative Nb, Ta, Zr and Hf peaks, and small positive K and Sr peaks.

All the samples from Bukit Telor and Sukadana are slightly depleted in La and Ce, but all have parallel chondrite-normalised REE patterns: basalts from Bukit Telor have the highest REE and HFSE contents, high-Ti and low-Ti basalts from Sukadana are progressively more depleted.

Ni and Cr contents within and between the high-Ti and low-Ti groups vary with the content of clinopyroxene and olivine crystals. Within the group of the low-Ti basalts ($1.2 < TiO_2 < 1.6$) the concentrations of all the analysed trace elements increase systematically with TiO_2 content, but only the HFSE show an almost linear increase

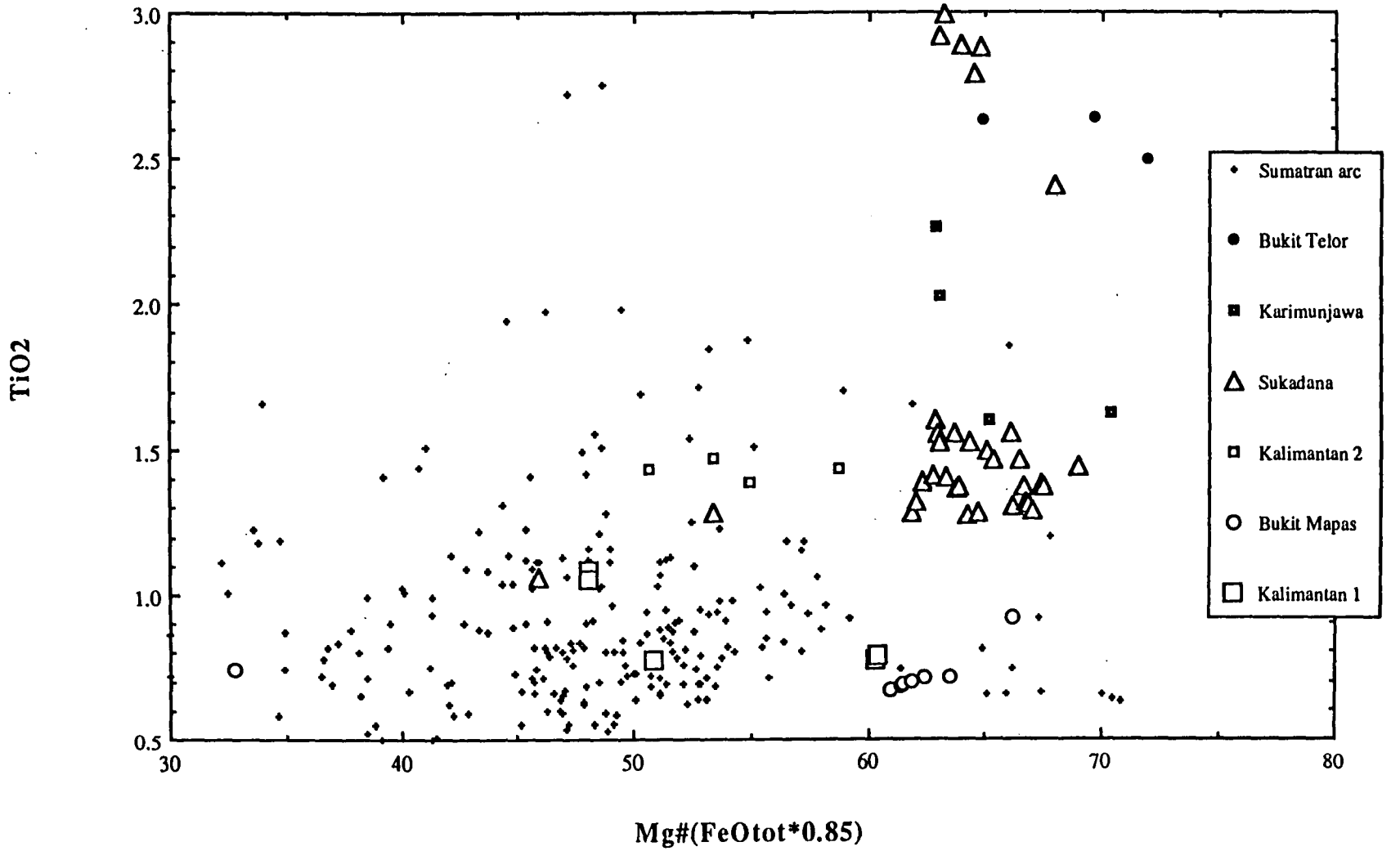

Figure 6.12. Mg# (calculated assuming $FeO/Fe_2O_3=0.85$) versus TiO_2 content in olivine-phyric rocks of Sumatra, Karimunjawa, Kalimantan, and the Sumatran Quaternary arc. Data from this study and references quoted in the text (see Appendix C)

in abundance from low-Ti to high-Ti basalts (Figures 6.13, 6.14 and 6.15). LILE and REE contents increase linearly with TiO_2 within the group of low-Ti basalts, but low-Ti basalts have virtually the same LILE and only slightly lower REE contents than do the high-Ti basalts. Hence, all the samples from Sukadana have very similar HFSE ratios, but very different LILE/HFSE and only slightly different REE/HFSE values (Table 6.3).

The only high-Ti basalt dated by Soeria-Atmadja et al. (1985) (sample BK26A) is virtually non-radiogenic (0.01 Ma), and it might be that the high-Ti basalts are systematically younger than the low-Ti basalts, but more K/Ar data are needed to confirm this hypothesis. Within the group of the low-Ti basalts, there seems to be no correlation between composition, age and locality. For example, 75372 was collected at the contact with the Lampung Formation in the inner part of the plateau, and may represent the base of one of the flows of the first cycle (older basalts) of Soeria-Atmadja et al. (1985); 75362 and 75376 show some signs of weak deformation and are also slightly altered, which may suggest they belong with the older flows. Apart from minor differences due to alteration, these samples are chemically indistinguishable from those collected high in the succession.

In summary, the basalts from the Sukadana plateau range in composition from rare quartz-tholeiites to slightly alkaline basalts, and show a clear within plate affinity, in agreement with the previously published data (Westerveld 1952; Soeria-Atmadja et al. 1985), but with a clear trend towards compositions typical of the calcalkaline basalts and andesites of the Sumatran volcanic arc. Basalts from Bukit Telor also have a distinctive within-plate affinity, and are the most alkaline rocks discussed in this study. Based on petrography, Mg#, MgO, Cr, Ni, and Al_2O_3/CaO values, only the xenolith-bearing basalt from Bukit Telor might represent a primary - or slightly differentiated - magma, whereas all the other samples from Bukit Telor and the Sukadana plateau must have suffered variable degrees of differentiation (see discussion).

6.7.1.3 Bukit Mapas

The Bukit Mapas volcanics (Table 6.4) have a distinctive calcalkaline affinity, and are more evolved than the Sukadana basalts, plotting in the field of basaltic andesites (Figure 6.7), and in the field of arc volcanics in tectonic environment discrimination diagrams (Figures 6.8 and 6.9). Yet, compared with the other arc-related basaltic andesites, they have higher MgO contents (and Mg# values), consistent with their

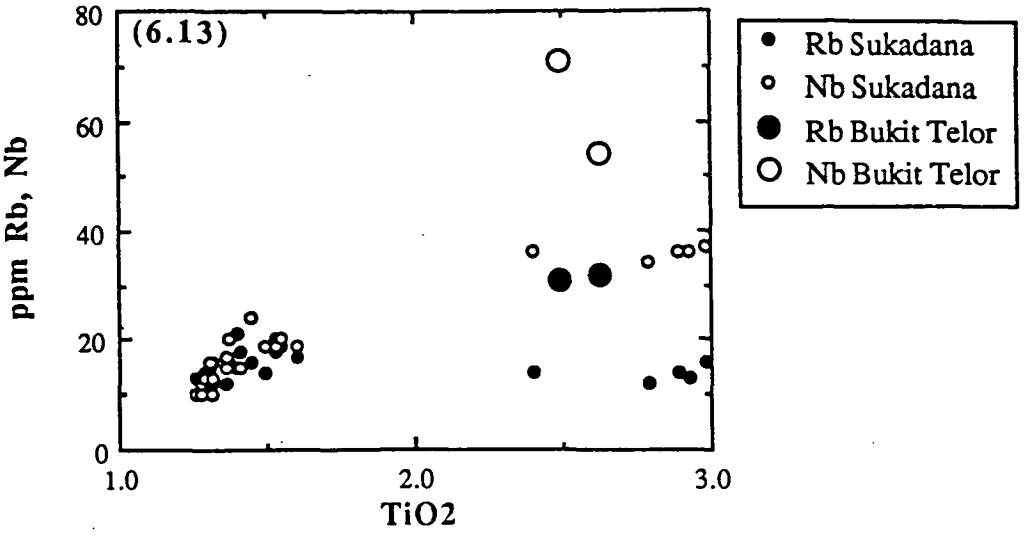

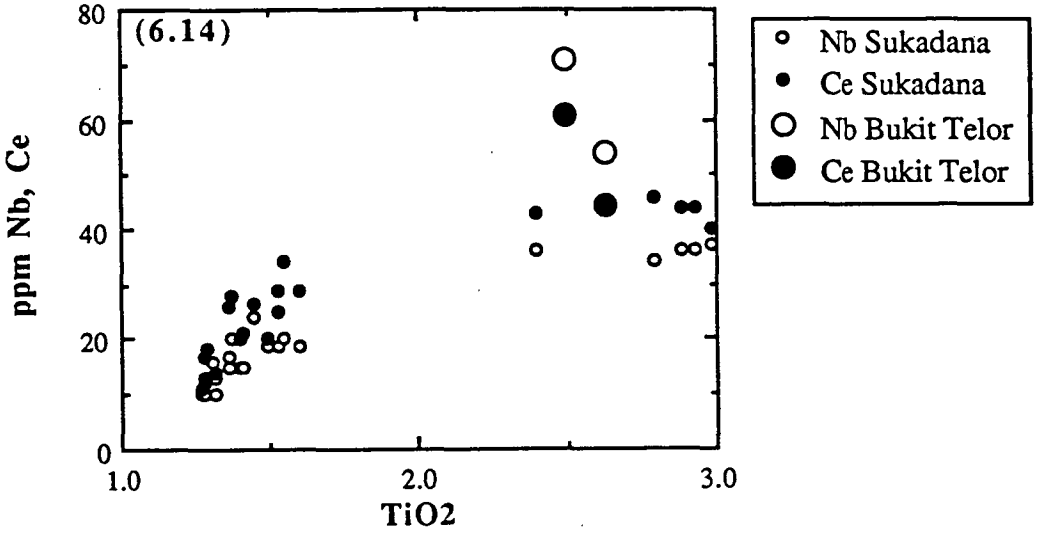

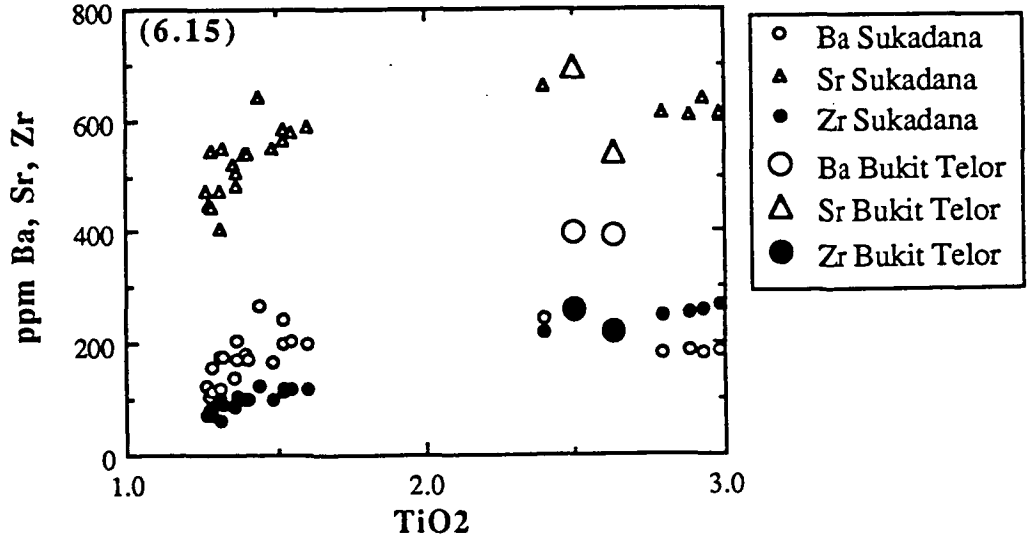

Figures 6.13, 6.14, 6.15. TiO_2 versus HFSE, REE and LILE plots for low-Ti and high-Ti basalts of Sukadana and Bukit Telor.

	LILE/HFSE					LREE/HFSE			HFSE/HFSE	
	Th/Nb	Rb/Nb	Ba/Nb	K/Nb	Ba/Zr	La/Nb	Ce/Nb	Ce/Zr	Ti/Zr	Zr/Nb
High-Ti group	0.05±.00	0.4±.0	5.5±.6	256±24	0.8±.2	0.5±.0	1.2±.1	0.17±.02	67±1	6.9±.5
Low-Ti group	0.14±.02	1.0±.2	11.1±1.3	580±62	1.8±.2	0.7±.1	1.4±.2	0.22±.04	86±13	6.3±.6
Bukit Telor	0.08±.00	0.5±.1	6.4±.7	231±27	1.7±.1	0.4±.0	0.8±.0	0.22±.02	61±7	3.8±.2
OIB	0.083	0.646	7.29	250	1.25	0.78	1.67	0.29	61	5.8
E-MORB	0.072	0.607	6.87	253	0.78	0.76	1.81	0.20	82	8.8

	Ba/Th	Ba/Ce	Ba/La	Th/La
High-Ti group	109±8	4.5±.6	11.5±1.2	0.11±.01
Low-Ti group	85±11	8.2±1.4	17.1±2.8	0.22±.03
Bukit Telor	85±8	7.7±1.2	16.5±2.0	0.19±.01
OIB	88	4.4	9.5	0.11
E-MORB	95	3.8	9.1	0.10

Table 6.3. Significative trace element ratios (average values and standard deviations) of low-Ti and high-Ti basalts of Sukadana and Bukit Telor. Data for typical OIB and E-MORB are from Sun & McDonough (1989).

	Bukit Mapas						Bukit Mapas Westerveld (1952)	
Catalogue #	78129	78130	78131	78132	78133	78134		
Sample name	SMG 161	SMG 162	SMG 163	SMG 164	SMG 165	SMG 166	W58	W59
Longitude	104°19'E	104°19'E	104°19'E	104°19'E	104°19'E	104°19'E	104°19'E	104°19'E
Latitude	4°30'S	4°30'S	4°30'S	4°30'S	4°30'S	4°30'S	4°29'S	4°29'S
SiO2	54.90	55.29	56.51	56.18	55.98	55.00	55.52	60.72
TiO2	0.70	0.69	0.66	0.67	0.68	0.70	0.92	0.73
Al2O3	16.06	16.30	16.38	16.27	16.25	16.27	14.76	17.82
Fe2O3	7.74	7.52	7.08	7.28	7.31	7.62	3.1	5.82
FeO							4.68	0.58
MnO	0.15	0.15	0.14	0.14	0.14	0.15	0.1	0.09
MgO	5.85	5.29	4.79	5.02	5.05	5.49	6.96	1.35
CaO	9.59	9.12	8.59	8.90	8.84	9.19	9.55	5.72
Na2O	2.74	2.95	3.01	2.97	2.95	2.81	2.43	3.83
K2O	1.82	1.83	2.01	1.97	1.89	1.91	1.84	2.96
P2O5	0.18	0.19	0.17	0.17	0.17	0.19	0.15	0.08
LOI	0.23	0.35	0.66	0.43	0.54	0.39	0.26	0.52
H2O-							0.06	0.08
Total	99.96	99.68	100.00	100.00	99.80	99.72	100.33	100.30
Mg# (measured Fe2O3/FeO)							72.60	80.57
Mg# (Fe2O3/FeO=0.15)	63.78	62.11	61.18	61.64	61.68	62.67	66.14	32.73
Rb	50	53	61	58	60	52		
Ba	315	335	383	377	371	337		
Sr	515	519	495	515	505	513		
Pb	8	7	7	8	8	8		
Zr	73	78	80	78	78	73		
Nb	7	8	7	8	8	7		
Y	18	18	18	18	18	18		
Th	8	8	9	9	9	9		
U	2	2	3	2	1	1		
La	16	15	18	16	18	16		
Ce	32	34	36	36	37	32		
Nd	15	16	15	14	14	13		
Cr	220	208	99	109	108	212		
Ni	50	47	21	22	22	52		
V	211	200	176	194	186	202		
Sc	30	27	25	27	25	27		
87Sr/86Sr			0.70436			0.70409		
143Nd/144Nd			0.512760			0.512790		
208Pb/204Pb			38.801			38.749		
207Pb/204Pb			15.628			15.621		
206Pb/204Pb			18.620			18.579		

Table 6.4. Chemical analyses of samples from Bukit Mapas, including data from Westerveld (1952).

high content in olivine phenocrysts. Apart from the MgO content, their major element compositions do not differ from those of nearby (e.g. G. Dempo, G. Sekincau and Lake Ranau area) basaltic andesitic and andesitic volcanoes of the Quaternary arc (see Appendix C), and the higher Al_2O_3 (and Na_2O), and lower MgO (and CaO) contents in the arc andesites only reflect their high content in andesine-oligoclase plagioclase phenocrysts, and lack of olivine phenocrysts. As a consequence, Al_2O_3/CaO values in Bukit Mapas are considerably lower than in the arc andesites, ranging from about 1.65 to 1.9.

All the samples analysed have similar trace element composition, apart from the different Cr and Ni contents which are consistent with the variable MgO contents. Also, the relatively MgO-poor and olivine- and clinopyroxene-poor samples seem to be slightly but systematically enriched in incompatible element, and depleted in Sc and V, compared with the other samples.

Westerveld (1952) published two analyses of rocks from Bukit Mapas. One of them is a basaltic andesite with composition similar to those reported here, whereas the other is a trachyandesite with composition indistinguishable from that of the other trachyandesites of the volcanic arc, with typically low MgO content and high Al_2O_3/CaO values. Therefore, Westerveld's data also suggest a strong genetic link between the arc andesites and the Bukit Mapas volcanics.

In summary, the texture, paragenesis, and major and trace element composition of the Bukit Mapas volcanics are similar to those of the most primitive basaltic andesites of the Sumatran volcanic arc (Figure 6.16c), but the rocks of Bukit Mapas are considerably primitive, with fairly high contents of olivine phenocrysts and Mg# values, and do not show the enrichment in plagioclase phenocrysts typical of arc rocks with similar composition.

6.7.2 Isotopic composition

In Figures 6.17, 6.18, and 6.19, Sr, Nd and Pb isotopic ratios of samples from Bukit Telor, Sukadana and Bukit Mapas are plotted together with samples from the Sumatran arc and central Kalimantan. Six low-Ti basalts from Sukadana have $^{87}Sr/^{86}Sr$ values ranging from about 0.70382 to 0.70412, and $^{143}Nd/^{144}Nd$ in the range 0.512837 to 0.512929. Two high-Ti basalts have $^{87}Sr/^{86}Sr$ values of 0.70390 and 0.70391, within the range of values of the low-Ti basalts, and higher $^{143}Nd/^{144}Nd$, respectively 0.512969 and 0.512981. The two groups define a trend

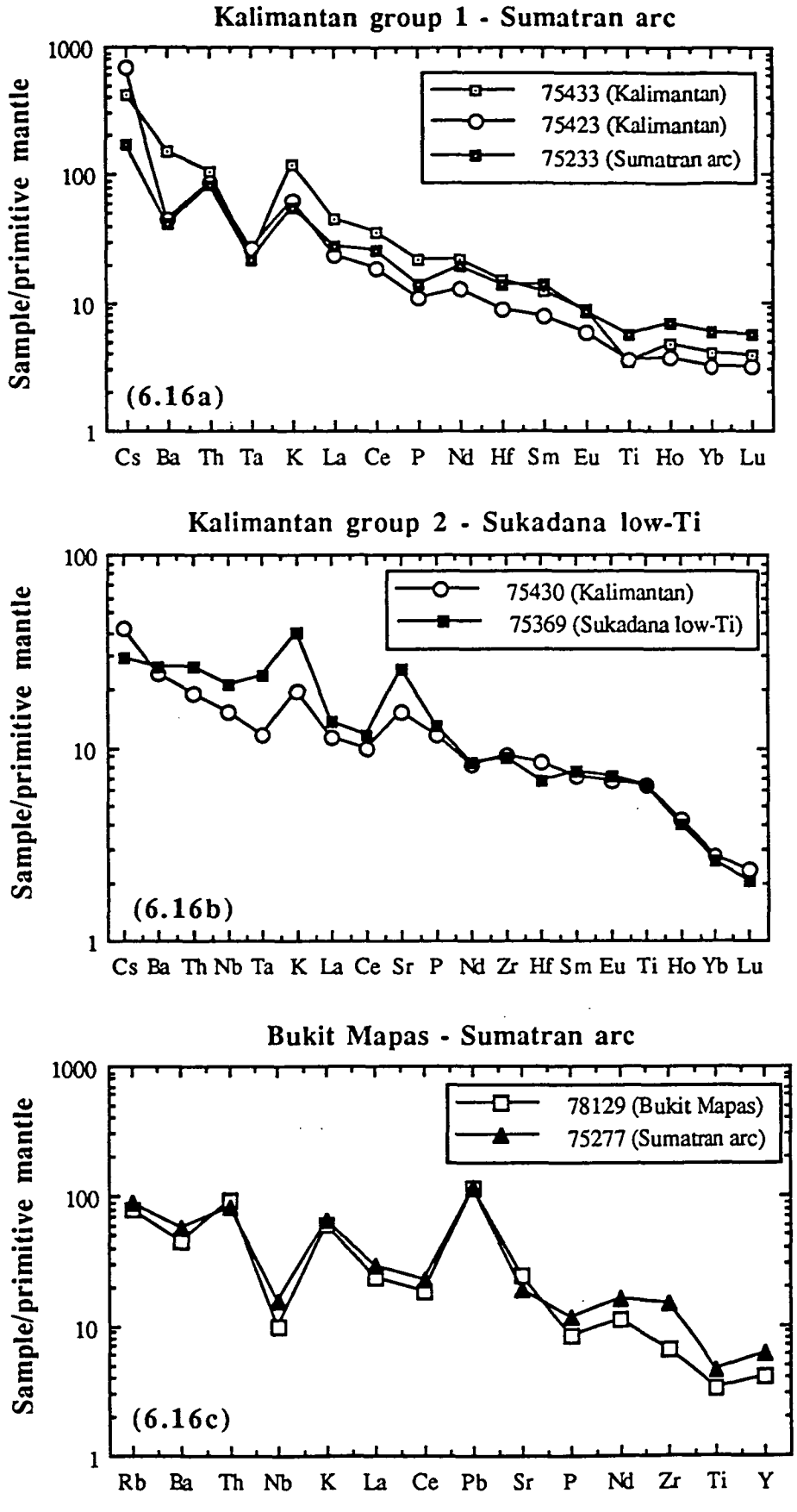

Figures 6.16a-c. Trace element values normalised to primitive mantle values (from Sun & Mc Donough 1989) for representative samples from Sukadana (75369) and the Sumatran arc (75233, and 75277), compared with arc rocks of Kalimantan (75433 and 75423 - Figure 6.16a) and low-Ti basalts (75430 - Figure 6.16b) of Kalimantan, and basaltic andesites of Bukit Mapas (78129 - Figure 6.16c).

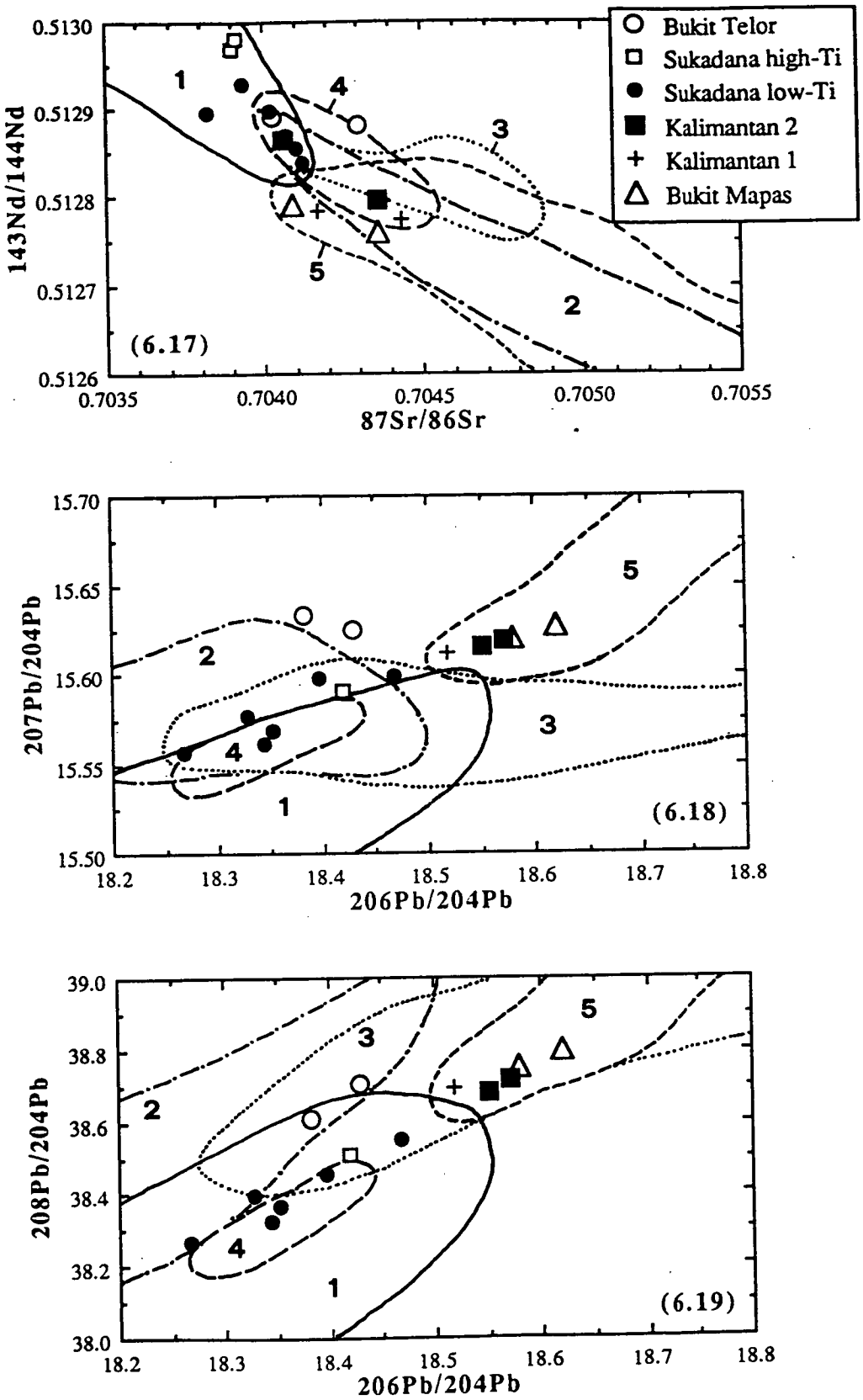

Figures 6.17, 6.18, 6.19. Sr, Nd, and Pb isotope diagrams for basalts of Bukit Telor, Sukadana, Bukit Mapas, Kalimantan, and the Sumatran arc (for comparison). Also shown are the fields of Indian Ocean MORB and OIB. Fields are: 1 - Indian Ocean MORB (see Chapter 3); 2 - Kerguelen (see Chapter 3); 3 - Ninetyeast Ridge (see Chapter 3); 4 - Sumatran arc granitoids (see Chapter 2); 5 - Sumatran Quaternary volcanics (see Appendix C).

that goes from the low $^{87}Sr/^{86}Sr$ and high $^{143}Nd/^{144}Nd$ values of the high-Ti basalts to the high $^{87}Sr/^{86}Sr$ and low $^{143}Nd/^{144}Nd$ values of the low-Ti basalts. The two samples of basalts from Bukit Telor have $^{87}Sr/^{86}Sr$ values in the range 0.70403 - 0.70430, and $^{143}Nd/^{144}Nd$ values of respectively 0.512891 and 0.512882.

The Pb isotopic values of high-Ti basalts of Sukadana plot within the field of the low-Ti basalts (Figures 6.18 and 6.19). Among the analysed low-Ti basalts, 75369 is the one with higher Sr, lower Nd and more radiogenic Pb isotopic values, 75361 has intermediate values, and 75354, 75358, and 75374 have overall higher $^{143}Nd/^{144}Nd$ values and lower $^{87}Sr/^{86}Sr$ values and Pb isotopic ratios. Sample 75377, which has minor but significant peculiarities in its chemical composition (high Mg#, Cr and Ni content, and a relatively low Al_2O_3/CaO value), has Sr and Nd isotopic ratios similar to those of the high-Ti basalts, but very low Pb isotopic ratios. Compared with the high-Ti basalts of Sukadana, basalts of Bukit Telor have slightly but consistently higher $^{208}Pb/^{204}Pb$ and $^{207}Pb/^{204}Pb$ values, and lower $^{143}Nd/^{144}Nd$ values, and do not fall on the trend defined by the high-Ti and low-Ti basalts.

Figures 6.20a-c show that a good correlation exists in Sukadana between $^{143}Nd/^{144}Nd$ values and incompatible element ratios, with increasing LREE/HFSE and LILE/HFSE values for decreasing $^{143}Nd/^{144}Nd$ (and $^{87}Sr/^{86}Sr$ values slightly increase for increasing LREE/HFSE and LILE/HFSE values), suggesting that low-Ti and high-Ti basalts of Sukadana are genetically related and at the same time different from the more alkaline basalts of Bukit Telor.

Overall, the Sukadana and Bukit Telor basalts overlap the field of the arc-related Sumatran granitoids (see Chapter 2) that outcrop along the Sumatran arc (Figure 6.17, 6.18, and 6.19). All the Quaternary arc volcanics of Sumatra, including the basaltic andesites of Bukit Mapas, which are isotopically similar to the least enriched basaltic andesites and andesites of the Sumatran arc, have systematically higher $^{87}Sr/^{86}Sr$ values and Pb isotopic ratios, and lower $^{143}Nd/^{144}Nd$ values.

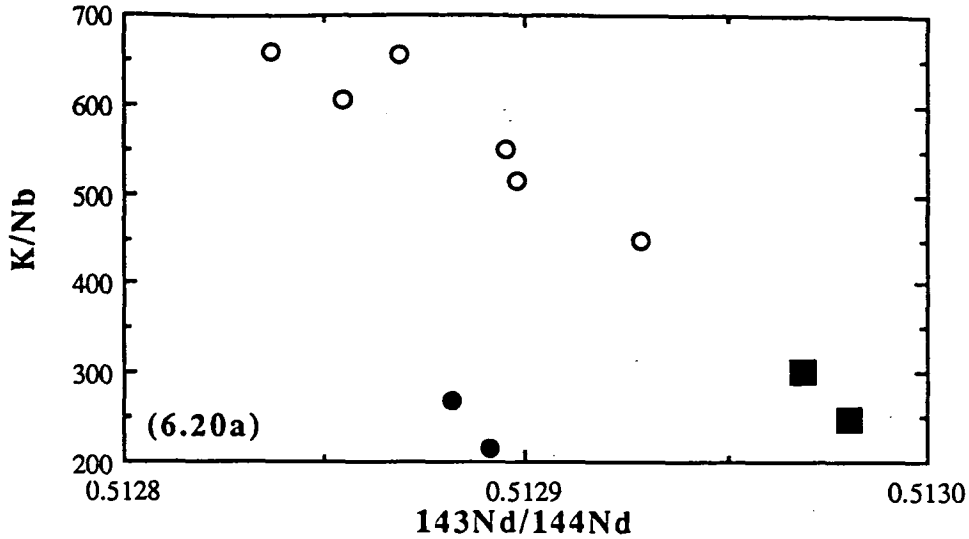

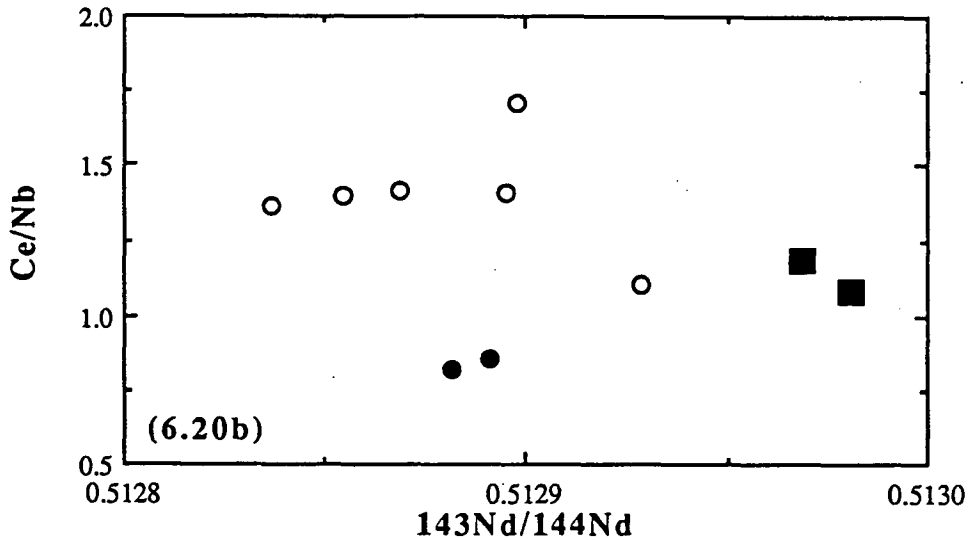

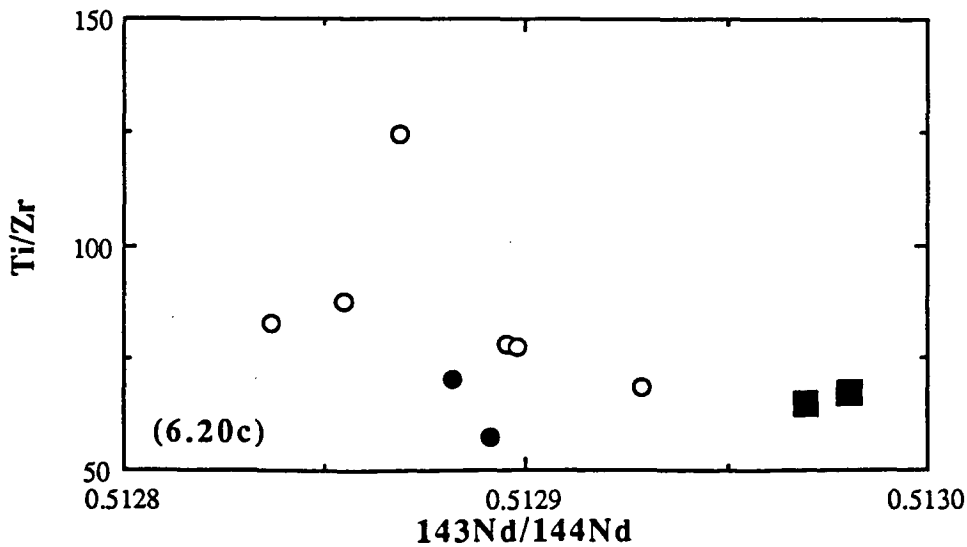

Figures 6.20a-c. Representative LILE/HFSE, LREE/HFSE and HFSE/HFSE values plotted versus $^{143}Nd/^{144}Nd$ values for the Sukadana and Bukit Telor samples. Open cirles - Sukadana low-Ti; Filled circles - Bukit Telor; Filled squares - Sukadana high-Ti.

6.8 Other known occurrences of olivine-phyric basalts in Indonesia: the Karimunjawa Islands and the Quaternary volcanoes of central Kalimantan

6.8.1 Karimunjawa Islands

6.8.1.1 Geological setting

The Karimunjawa archipelago is a group of 27 islands situated less than 100 km off the coast of central Jawa (Figure 6.1), where the Benioff zone is at a depth of approximately 550 km. The islands are essentially made up of pre-Tertiary recrystallised slates, quartzites, quartz conglomerates and granites (Marks 1931), and are extensively quarried for granitic rocks. The basaltic lava flows show columnar jointing and are often cut by swarms of dykes and usually covered in lateritic soil, but outcrops of fresh basalts can be observed in many of the islands. Soeria-Atmadja et al. (1985) dated four samples from two of the islands (Parang and Genting), and obtained a range of ages from 1.82 ± 0.27 to 6.51 ± 0.33 Ma.

6.8.1.2 Geochemistry

According to the description by Soeria-Atmadja et al. (1985), the basalts from the Karimunjawa Islands are petrographically similar to the basalts from the Sukadana plateau, although more porphyritic (about 15-30%), and with more anorthitic plagioclase phenocrysts. Compositionally they are similar to the basalts of Bukit Telor and to the high-Ti basalts from the Sukadana plateau (Table 6.2), with only one of the samples reported being slightly more alkaline, with about 1% normative nepheline. This slightly more alkaline affinity is also indicated by the presence in the groundmass of some samples of "minor amounts of interstitial soda-sanidine and/or anorthoclase", not observed in the samples from Bukit Telor and the Sukadana plateau. Plotted on a Th/Ta/Hf diagram (Figure 6.9) they fall either in the same field (older Parang basalts) as the Bukit Telor rocks, or have a more "orogenic" signature (Quaternary Genting basalts), similar to the most Th-rich basalts of the Sukadana low-Ti group.

Although the trace element composition of the Karimunjawa basalts was discussed by Soeria-Atmadja et al. (1985), no trace element data were published and no isotope data are available, and therefore the conclusions reached by those authors cannot be evaluated. From the available data, it seems that these rocks have a within-plate rather

than a back-arc affinity, as suggested by Soeria-Atmadja et al. (1985) for both the Karimunjawa and the Sukadana basalts. K_2O and P_2O_5 values are higher than those normally found in back-arc basin basalts, and the most alkaline Parang basalts have Hf/Ta/Th values similar to those of Bukit Telor and typical of within-plate alkaline basalts. As in the basalts from the Sukadana plateau, a trend towards a more "orogenic" affinity for the tholeiitic (or less alkaline) samples can be observed in a Hf/Ta/Th diagram. This trend and its significance for the Sukadana basalts will be discussed later in this chapter.

6.8.2 The Quaternary volcanoes of central Kalimantan

6.8.2.1 Geological setting

The samples of basalts from central Kalimantan discussed in this study come from some unnamed volcanic centres in the upper Mahakam river region (Long Pahangai and Muara Wahau 1:250 000 geological maps - Abidin et al. 1989; Supriatna 1990). The volcanic unit from which the samples were collected was described by Pieters & Supriatna (1990) as "Mio-Pliocene basalt to andesite lava, breccia, tuff, agglomerate, laharic breccia; dykes, plugs and stocks of diorite, meladiorite, porphyritic andesite, basalt.", and it overlies mainly Upper Cretaceous to Eocene turbidite basin sediments and Upper Eocene foreland basin sediments, although Upper Jurassic to Lower Cretaceous oceanic basement rocks and overlying sediments, continental arc-related Cretaceous granites and basement rocks are found in the area.

These rocks do not seem to be associated with any active trench. The Northwest Borneo Trench, running parallel to the northern coast of northeastern Borneo, and approximately 500 km away from the Quaternary volcanoes of central Kalimantan, is inactive and probably became so in the Late Miocene (Hamilton 1979).

6.8.2.2 Petrography

The samples of the Quaternary volcanoes from central Kalimantan have variable texture and composition (Figures 6.4e-h), and two very different lithologies have been recognised.

Samples 75433, and 75422-3-4-5, (hereafter called group 1) are porphyritic with a seriate texture, with plagioclase and clinopyroxene microliths in the cryptocrystalline groundmass. Eu- to subhedral plagioclase is ubiquitous as a microphenocryst, and

makes up to 25% of the volume of the rock. Strongly zoned plagioclase phenocrysts are less abundant (up to 10%). Sample 75433, 75423, and 75424 are the only ones with hypersthene, in very small amounts (<2%) in the groundmass with augite in sample 75433, and as eu- to subhedral, seriate crystals (up to 5%) and in the groundmass of samples 75423 and 75424. Oxyhornblende microphenocrysts and phenocrysts (up to 10% of volume) with black rims and partially resorbed at the centre have been observed in sample 75433, and rare (2-3%), completely altered microphenocrysts of green amphibole have been found in samples 75423 and 75424. Olivine microphenocrysts and phenocrysts with iddingsitic rims have been found usually in very small amounts (up to 5% microphenocrysts, less than 1-2% phenocrysts) in samples 75422 (up to 10%, with corona texture and resorbed), 75423, 75424, and 75425 (in very small amounts, euhedral to skeletal, always in disequilibrium, often altered).

In summary, samples 75433, 75423 and 75424 have textures and paragenesis typical of arc andesites (Figures 6.4e-f): they are highly porphyritic, with abundant, strongly zoned plagioclase phenocrysts and microphenocrysts + augite + hypersthene + hornblende. Samples 75425 and 75422 are slightly more primitive, but still closely resemble the basaltic andesites found in the arc.

The samples described above have been selected for XRF analysis, and are relatively fresh and homogeneous. However, in other samples with the same texture and paragenesis, large fragments of orthoclase, quartz, plagioclase and muscovite, presumably from the disgregation of granitoid rocks, and nodules of sandstone and clayey material, ranging in size from less than a centimetre to tens of centimetres, are common. This is a strong petrographic evidence for the assimilation of shallow crustal material (Cretaceous granites, and turbidite basin sediments) by the andesitic magmas.

Samples 75434, 75430, 75426, and 75427, (hereafter called group 2) are porphyritic with micro- to cryptocrystalline groundmasses, and rare (less than 2-3% of the total volume of the rock) olivine phenocrysts, eu- to subhedral, with abundant Cr-spinel inclusions, and thin iddingsitic rims, and olivine and plagioclase microphenocrysts (less than 2-3%). The groundmasses are composed of euhedral plagioclase (about 50%, with labradorite cores and andesine to oligoclase rims) laths, with intergranular augite (20-30%) and olivine (about 5%), smaller spinel, and interstitial yellowish, rarely blackish glass and glassy patches (about 10%).

In thin section, these rocks closely resemble the olivine-poor, low-Ti basalts of the Sukadana plateau (Figures 6.4g-h).

6.8.2.3 Geochemistry

The very different texture and paragenesis of the two groups is clearly reflected in their geochemical composition (Table 6.5).

Samples 75423 and 75424, in agreement with their petrographic characteristics, have very similar chemical compositions, and are readily classifiable as andesites in a TAS diagram (Figure 6.7). Sample 75433, the petrographically most evolved and hornblende-rich, has a very similar, but slightly more evolved composition, and falls at the boundary between andesites and trachyandesites. The other two samples of group 1 where no hydrous phases were noticed in thin section are geochemically more primitive, and plot within the field of the basaltic andesites.

Compositional characteristics of the rocks of group 1, which are generally typical of Sumatran arc andesites, include the high Al_2O_3/CaO values (ranging from 2.3 to 2.9 in the most evolved sample), the rather low MgO contents (about 4 to 2.5%) and Ni and Cr contents, and the typical enrichment in LILE and LREE, and depletion in Ti and Nb (Figure 6.16a). These andesites from central Kalimantan plot with the Sumatran arc rocks in a Th/Hf/Ta diagram (Figure 6.9), and follow a typical calcalkaline differentiation trend, indistinguishable from that shown by the Quaternary Sumatran volcanic centres (see e.g. the data from Rajabasa, Sekincau, Dempo, Kerinci, and Marapi - Appendix C).

The samples of group 2 have a very restricted composition, with SiO_2 and Al_2O_3 values ranging respectively from 52 to 54%, and from 15.5 to 16.5%, constant TiO_2 (about 1.4%) and Al_2O_3/CaO (about 2) values. The rocks of this group are basaltic andesites (Figure 6.7), with Mg# similar to those of the andesites of group 1 (Mg# approximately 50-60%) (Figure 6.12), but with considerably higher Fe, Mg, Ni, and Cr contents. Also, compared with group 1, they have systematically higher TiO_2 (and Nb and Ta), and P_2O_5, and plot in the field of within-plate basalts in a Th/Hf/Ta diagram (Figure 6.9).

Apart from their systematically lower MgO, Cr, Ni, and V contents, the rocks of group 2 have a trace element chemical composition very similar to the low-Ti basalts of the Sukadana plateau (Figures 6.16b and 6.21).

	Kalimantan - Group I					Kalimantan - Group II			
Catalogue #	75433	75422	75423	75424	75425	75434	75430	75426	75427
Sample name	86SK2D	89SS25A	89SS25B	89SS25D	89SS25E	86AM63A	86SS12C	89SS25F	89SS28A
SiO2	60.33	54.02	57.39	57.63	54.52	52.03	51.98	53.84	52.30
TiO2	0.75	1.04	0.77	0.75	1.03	1.37	1.38	1.38	1.45
Al2O3	16.20	19.08	16.90	17.03	18.58	15.30	15.42	16.67	16.35
Fe2O3	5.64	7.40	6.00	5.85	8.73	11.20	10.35	9.75	11.19
MnO	0.12	0.14	0.12	0.11	0.15	0.15	0.13	0.15	0.18
MgO	2.52	2.97	3.96	3.85	3.50	4.98	6.38	5.16	5.56
CaO	5.52	8.28	6.94	6.92	7.90	7.14	7.87	7.43	7.70
Na2O	3.16	2.62	3.26	3.32	3.16	3.54	3.43	3.88	3.85
K2O	3.61	1.29	1.84	1.85	0.86	1.16	0.58	1.32	1.03
P2O5	0.46	0.14	0.23	0.18	0.21	0.26	0.25	0.35	0.28
LOI	1.14	2.52	2.72	2.28	0.97	2.60	1.69	0.30	-0.32
Total	99.85	99.50	100.13	99.77	99.61	99.73	99.46	100.23	99.57
Mg#	51.00	48.32	60.59	60.53	48.30	50.88	58.95	55.22	53.65
Ba	1050	246	317	312	245	197	171	237	160
Pb						5		4	4
Cs	3.39		5.94				0.33		0.52
Hf	4.67		2.75				2.61		2.69
Ta	0.9		1.07				0.47		1.15
Th	9.1		7.33			3	1.63	5	1.92
La	30.5	15	15.8	20	14	15	7.78	22	11.2
Ce	62.7	31	32.8	35	32	30	17.4	45	23.7
Nd	29.4	17	16.8	15	17	16	11.1	22	15.6
Sm	5.43		3.42				3.16		3.92
Eu	1.45		0.97				1.13		1.35
Tb	0.61		0.47				0.57		0.74
Ho	0.77		0.61				0.7		0.9
Yb	2		1.56				1.35		1.87
Lu	0.28		0.23				0.17		0.24
Cr	27	36	43	40	8	176	221	133	143
Ni	11	13	27	25	6	85	112	60	87
V	134	109	135	129	156	150	139	146	151
Sc	16	27	20	19	30	21	21	20	22
87Sr/86Sr	0.70443		0.70417				0.70406		0.70436
143Nd/144Nd	0.512778		0.512788				0.512869		0.512801
208Pb/204Pb			38.639				38.715		38.678
207Pb/204Pb			15.612				15.619		15.616
206Pb/204Pb			18.519				18.57		18.551

Table 6.5. Chemical analyses of samples from Kalimantan.

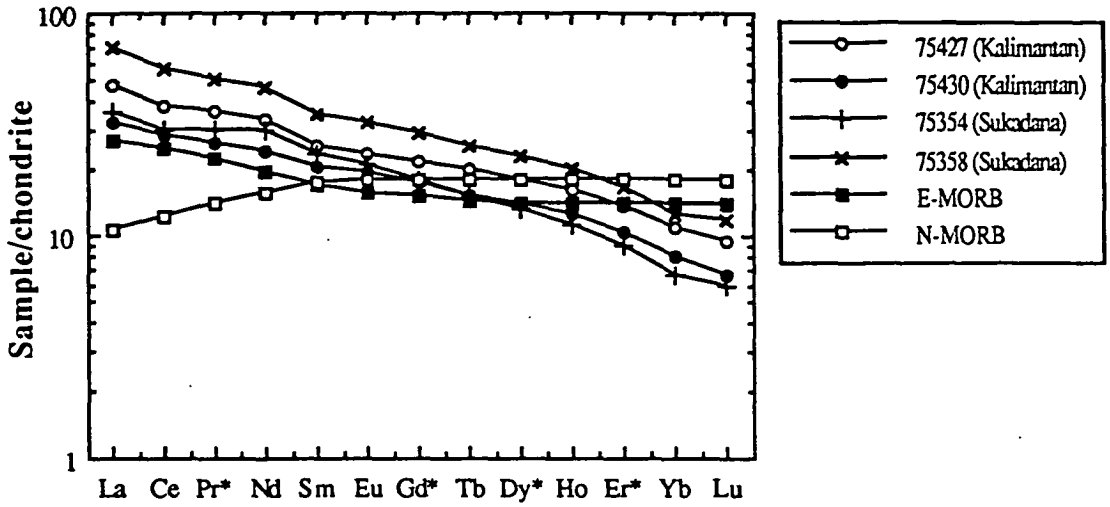

Figure 6.21. REE values normalised to chondrite values (from Sun & McDonough 1989 - also E-MORB and OIB values) for representative samples from central Kalimantan (group 2 - 75427 and 75430), and Sukadana low-Ti (75354 and 75358) basalts. Some REE (marked with an asterisk) have been interpolated from the other REE.

6.8.2.4 Isotopic composition

Two samples from each group were selected for Pb, Sr, and Nd isotope analysis (but only Sr and Nd for sample 75433) (Figures 6.17, 6.18, and 6.19).

Sample 75423 is one of the two most primitive in group 1, and has Sr, Nd, and Pb isotopic values typical of some among the most primitive Sumatran arc volcanics (e.g. Rajabasa, Marapi). Sample 75433, geochemically more evolved, also has slightly higher Sr and lower Nd isotopic ratios.

In group 2, samples 75430 and 75427 have very similar Pb isotopic composition, but the latter has higher $^{87}Sr/^{86}Sr$ and lower $^{143}Nd/^{144}Nd$. The significant difference in $^{143}Nd/^{144}Nd$ values accompanies a slight enrichment in K_2O and LREE, a lower MgO and olivine content, and the presence of a few phenocrysts of plagioclase in the sample with lower $^{143}Nd/^{144}Nd$ (and higher $^{87}Sr/^{86}Sr$) values - 75427.

In summary, the two groups seem to have very similar Pb isotopic compositions, systematically slightly higher than those of the basalts of the Sukadana plateau, and similar to those of the most primitive Sumatran arc volcanics and Bukit Mapas. Sr and Nd isotopic values of samples in group 1 are also similar to those of the Sumatran volcanic arc, whereas those of group 2 are intermediate between the Sumatran volcanic arc and the Sukadana low-Ti basalts.

6.9 Mineral chemistry of spinel and melt inclusions in olivine phenocrysts from Bukit Telor, Sukadana, and Bukit Mapas

Spinel precipitates early from mafic magmas and it remains in the liquidus until the complete solidification of the melt. In this study of olivine-bearing basalts from Sumatra, spinels are the earliest precipitating-phase present in the rocks, and many of the spinels are enclosed by olivine phenocrysts. These olivine phenocrysts also contain melt inclusions, and investigations of the compositions of the spinels and of the phases in the melt inclusions together provide important insights into the early history of the basalts in which they occur.

The melt inclusions consist of quenched glass, crystalline phases and gas bubbles, and were originally a small portion of melt trapped by growing crystals, that later solidified during cooling. A "shrinkage bubble" (a vacuum) is usually observed in the melt inclusions, as the volume of the solidified melt inclusion is smaller than the volume of the melt. Melt inclusions can be primary, i.e. trapped during the growth of the crystal and indirectly reflecting the composition of the melt from which the host mineral crystallised, and secondary, i.e. trapped at a later stage within the cracks of the crystal.

Only primary inclusions were analysed in this study. Melt inclusions completely enclosed in the host mineral and free of secondary cracks were heated up to their temperatures of homogenisation (see Sobolev et al. 1980, 1991) and then rapidly quenched: the composition of the inclusion at this stage should be the same as the original composition of the trapped melt, and the temperature of homogenisation should be the same as the original temperature of trapping.

Four major problems can arise during the heating experiments. First, the heating experiments are done under visual control, and it is often difficult to detect the disappearance of all the phases, so that the measured liquidus temperature may be different from the real liquidus temperature.

Second, the temperature of homogenisation measured during the experiment may be considerably different (higher) from the real temperature of trapping, as a result of kinetic factors. In other

words, some phases inside the inclusions may not homogenise due to their refractory nature, (e.g. spinels) or due to changes in the pressure and pH_2O conditions (e.g. gas bubbles); as a result, the inclusion is overheated in an attempt to homogenise these phases, and part of the host mineral is melted and added to a melt which has the composition of the original trapped melt (minus the phases that did not homogenise during the experiment).

Third, any H_2O which might have originally been present in the inclusion may dissociate and hydrogen can easily diffuse through the host mineral, thus changing the oxygen fugacity and pressure conditions inside the inclusion.

Fourth, it may be that the melt already contained some crystalline phases at the time of trapping. In this case, to obtain the real composition of the original melt, these phases should not be homogenised during the experiment. It could also be that not all phases were in equilibrium with the melt.

For these reasons kinetic experiments were carried out to determine the homogenisation temperature and the "behaviour" of the melt inclusion.

During this study of inclusions in olivines from Sukadana and Bukit Mapas, it was never possible to homogenise the shrinkage bubble found in all the inclusions, and therefore the homogenisation temperature was considered as the temperature of disappearance of all the phases believed to be in equilibrium with the melt. Of the crystalline phases in the inclusions, the rare Al-spinels in Bukit Mapas and some of the Cr-spinels in Sukadana could not be homogenised. In some experiments the He atmosphere in the sample chamber was often not pure enough, and the samples were oxidised during the experiment. Most melt inclusions were very small (less than 50 μm across), and the melt/host olivine interactions might have been very strong.

All these factors indicate that H_2O dissociation, H_2 diffusion, and possibly other chemical reactions between the melt inclusion and the host olivine crystal might have occurred, thus modifying the homogenisation temperature and the chemical composition of the melt inclusion. For these reasons, the results presented here should be regarded as preliminary and qualitative only, and only to be used as a support to the geochemical and mineral chemistry data to further emphasise the relative differences among the studied samples.

Olivine phenocrysts are the earliest silicate to crystallise from the volcanic rocks discussed in this section. Spinel and melt inclusions in olivine phenocrysts will therefore not only closely reflect the composition of the melt from which they crystallised, but this melt composition should also be close to the original liquidus composition the magma. For these reasons, this study concentrated on

spinel and melt inclusions in olivine phenocrysts.

Approximately 50 to 200 olivine grains for each sample (less than 50 for some olivine-poor samples from Kalimantan and the Sumatran arc) were hand picked to avoid "sampling" problems: faster separation techniques using heavy-liquids or magnetic separators would also separate heavy (Fe-rich) olivines from light (Fe-poor) olivines, and olivines with spinel inclusions from those without. A statistically representative number of grains was analysed at random. The spot of the electron microprobe analysis was located next to the spinel inclusion(s), or in the core of the crystal in those cases where no spinel inclusions were exposed on the surface of the analysed grain. The composition of all the other mounted grains that were not analysed was visually checked and estimated, based on the EDS (Energy Dispersive Spectrum). This method gives an estimate of the olivine composition to approximately ± 1 Fo. Normally, all spinel inclusions found on the surface of olivine grains mounted for the analysis were analysed.

Grains containing melt inclusions were then selected and extracted from the epoxy mounts and polished on two sides to create the best conditions for the observation in transmitted light during the heating stage experiment. After the experiment, grains were polished again to bring the melt inclusion to the surface. Several melt inclusions can be lost during the preparation or the experiment for three reasons: 1) they can be exposed before the experiment because of an excessive polishing, and therefore part of the melt can escape during the experiment; 2) they can "explode" during the experiment, or cracks can form in the host mineral and material from the melt inclusion can escape through the cracks; 3) they can be polished away after the experiment in an attempt to bring them to the surface.

During this study, approximately 0 to 5% of the grains (up to 10% in a few samples) were suitable for melt inclusion study, and approximately 10% of these were lost during the preparation or the experiment.

Only the samples from Bukit Telor, Sukadana, and Bukit Mapas are considered for a detailed spinel and melt inclusions study. Additional data from the Quaternary volcanoes of the Sumatran arc and Galunggung in West Jawa will be used for comparative purposes only.

The mineral chemistry data discussed in this section, and some microphotographs and electron microscope photographs of representative mineral grains, are reported in Appendix E.

6.9.1 Bukit Telor

Olivine crystals in Bukit Telor (sample 75379) are eu- to subhedral, very light green

to almost colourless, and range in size from 2 to 3 mm, occasionally up to 5 mm. Light green/brown orthopyroxene and bright green clinopyroxene crystals from the lherzolite xenoliths are similar in size to the olivines. The xenoliths are too rare and small to allow an estimate of the relative proportions of olivine, clinopyroxene and orthopyroxene. All phases in the xenoliths and all the olivine crystals are free of spinel and primary melt inclusions.

Olivine crystals have a very constant composition, with Mg# = 89.6 ± 0.4 (Figure 6.22a) in the disaggregated crystals and 89.9 ± 0.2 in the xenoliths, low CaO (0.05 to 0.10%) and MnO (0.10 to 0.15%), and high NiO (0.4 to 0.5%) contents. There are no differences between the crystals in the xenoliths and those in the rock.

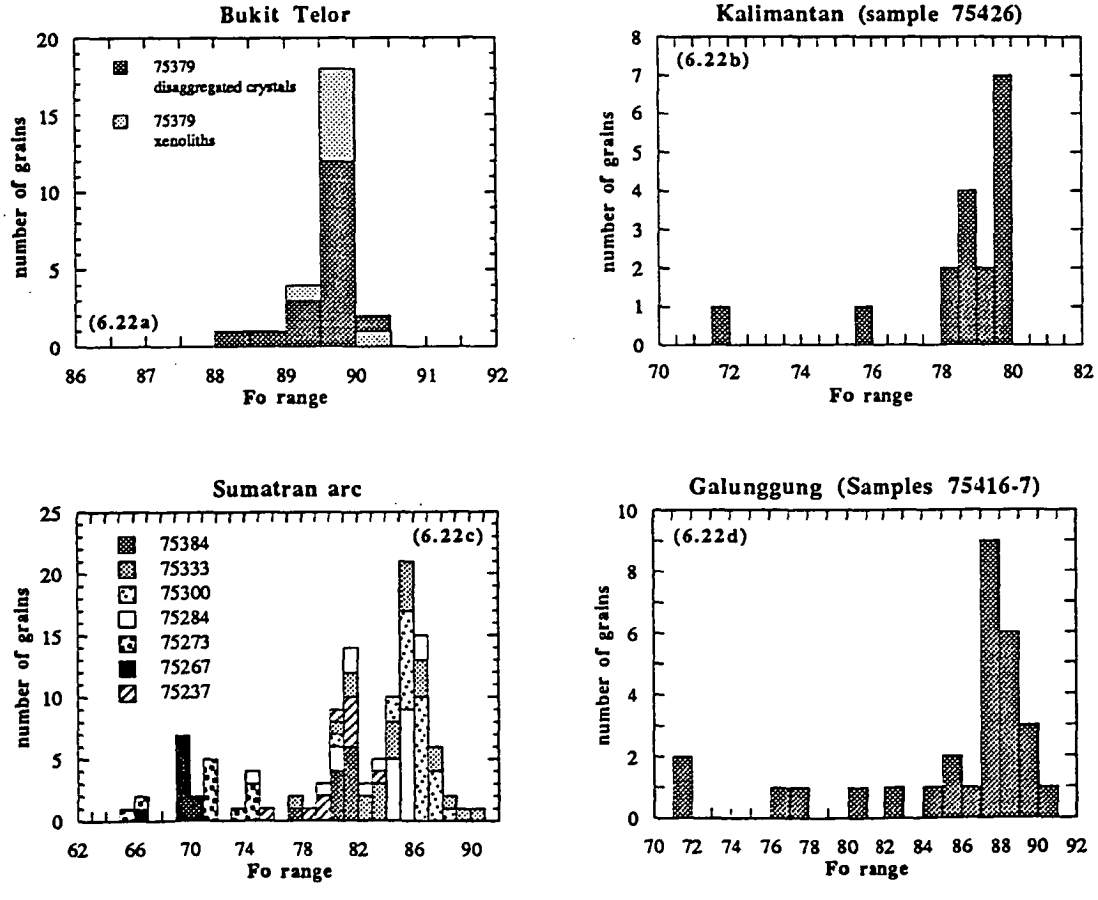

Figures 6.22a-d. Stack histograms showing the range in Fo values in olivine phenocrysts of Bukit Telor (Figure 6.22a), sample 75426 (group 2) of Kalimantan (Figure 6.22b), samples of the Sumatran Quaternary arc (Figure 6.22c) and Galunggung in west Jawa (Figure 6.22d).

Clinopyroxenes and orthopyroxenes in the xenoliths also have constant composition and Mg# (respectively 90.1 ± 0.2 and 90.2 ± 0.2) similar to the olivines, and relatively high Al_2O_3 content (respectively >7% and >5%).

6.9.2 Sukadana

Olivine phenocrysts in the high-Ti basalts are light green, euhedral, and range in size from approximately 0.5 mm to 1 mm, with most grains in the 0.8 mm to 1 mm range. Cr-spinel inclusions are euhedral, 10 to 40 μm. Some grains are spinel-free, others have up to several tens of spinel inclusions randomly distributed within the grain. Small (< 2 μm) secondary melt inclusions are common. Primary melt inclusions up to 100 μm across are filled with crystalline and fluid phases and glass: most of these inclusions are rounded, but more rarely are elongated and irregular in shape. Fluid inclusions up to 50 μm are less common. Two fluid inclusions 10 μm across were found in an olivine grain in sample 75365, and the temperature of their transformation into liquid was estimated to be about 25 °C, which indicates a CO_2 density of about 0.77 g/cm^3, assuming that the inclusion is pure CO_2 or a pure H_2O-CO_2 mixture. For a measured homogenisation (trapping) temperature of about 1200 °C, this corresponds to a pressure of crystallisation of less than 5 kbar (Angus et al. 1976; Bergman 1982), typical of magmatic chambers in continental crust.

Olivines in sample 75216 have yellowish altered rims. Olivines in sample 75360 are generally smaller (0.3 to 0.8 mm), and richer in smaller (5 to 20 μm) spinel inclusions, up to several hundreds in some grains, and secondary melt inclusions. However, some olivine grains are similar to those observed in the other high-Ti basalts. Primary melt inclusions in 75360 are particularly scarce, and not suitable for melt inclusion study.

Olivine grains in the low-Ti basalts are usually smaller and considerably less abundant than in the high-Ti basalts, with the exception of sample 75377. The amount, size and shape of the Cr-spinel, melt and fluid inclusions are rather variable within each sample, but there seems to be no systematic variation among the different samples. Many grains are slightly fractured, and yellow/red altered rims (iddingsite) are common.

A single olivine grain was found in sample 75362. It is inclusion-free, with low CaO and high NiO contents, and its Fo content is slightly lower than those of the olivines from Bukit Telor. Apart from this single olivine grain and a few other altered crystals

which may have been similar, this sample is aphyric.

Olivine grains in basalts from Gunung Tiga (75356 to 75359) are very densely fractured and altered, and tiny secondary melt inclusions are particularly abundant. Cr-spinel inclusions are surrounded by thin (≤ 3 μm) rims of melt, too small to be analysed. Olivine grains in sample 75359 are extremely fractured and filled with spinel and secondary melt inclusions, and are virtually black in transmitted light. All the spinel inclusions in this sample are surrounded by a thick reaction rim.

Olivine phenocrysts in the high-Ti basalts in Sukadana have a fairly constant composition (Figures 6.23a-d, 6.25a), with Fo values showing an asymmetric distribution with a peak at approximately Fo 86-85, gradually decreasing to 80.

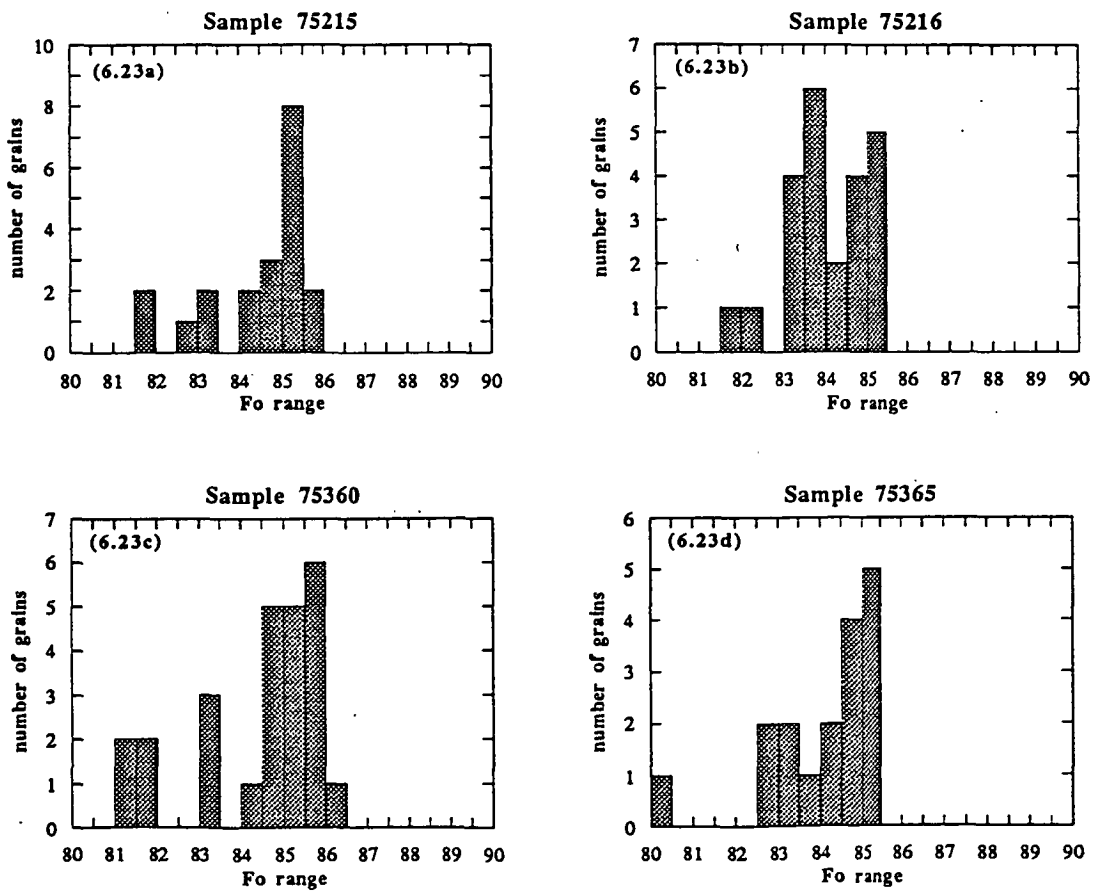

Figures 6.23a-d. Stack histograms showing the range in Fo values in olivine phenocrysts of the Sukadana high-Ti basalts.

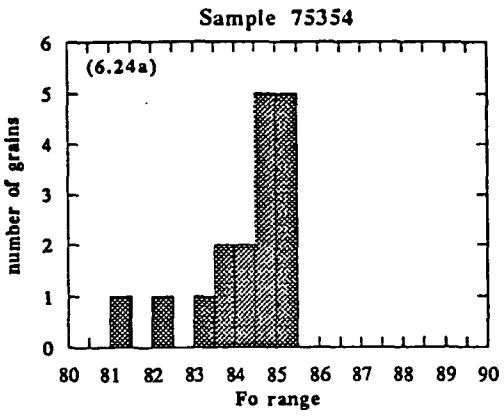

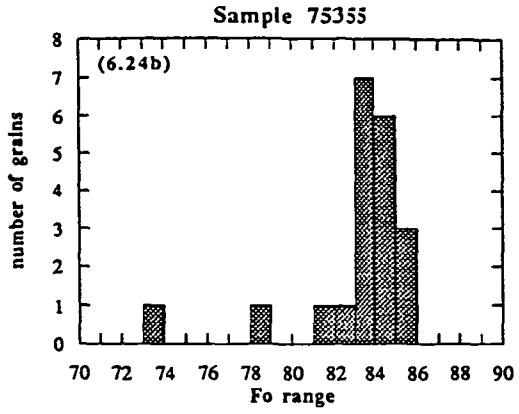

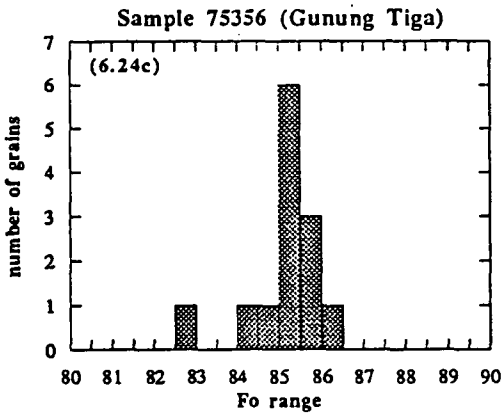

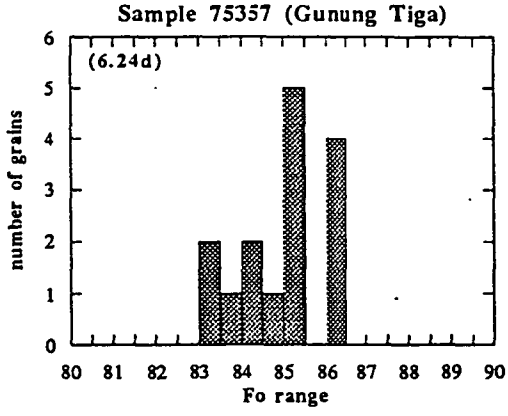

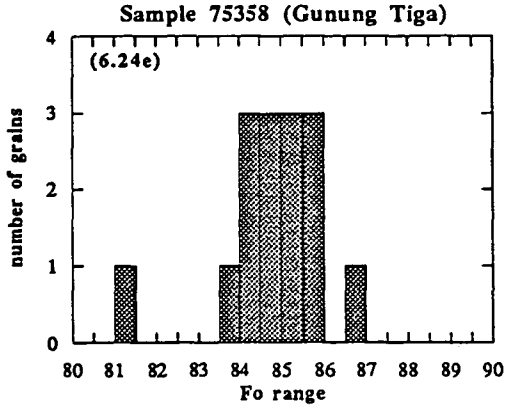

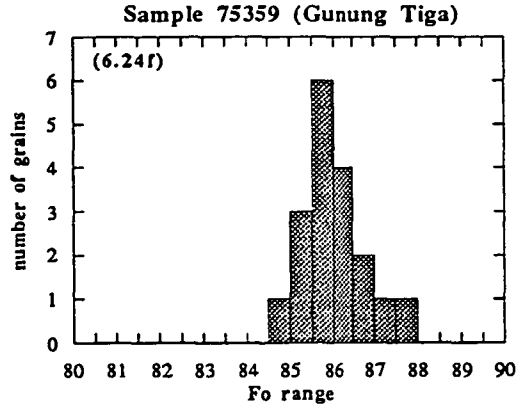

Figures 6.24a-f. Stack histograms showing the range in Fo values in olivine phenocrysts of the Sukadana low-Ti basalts.

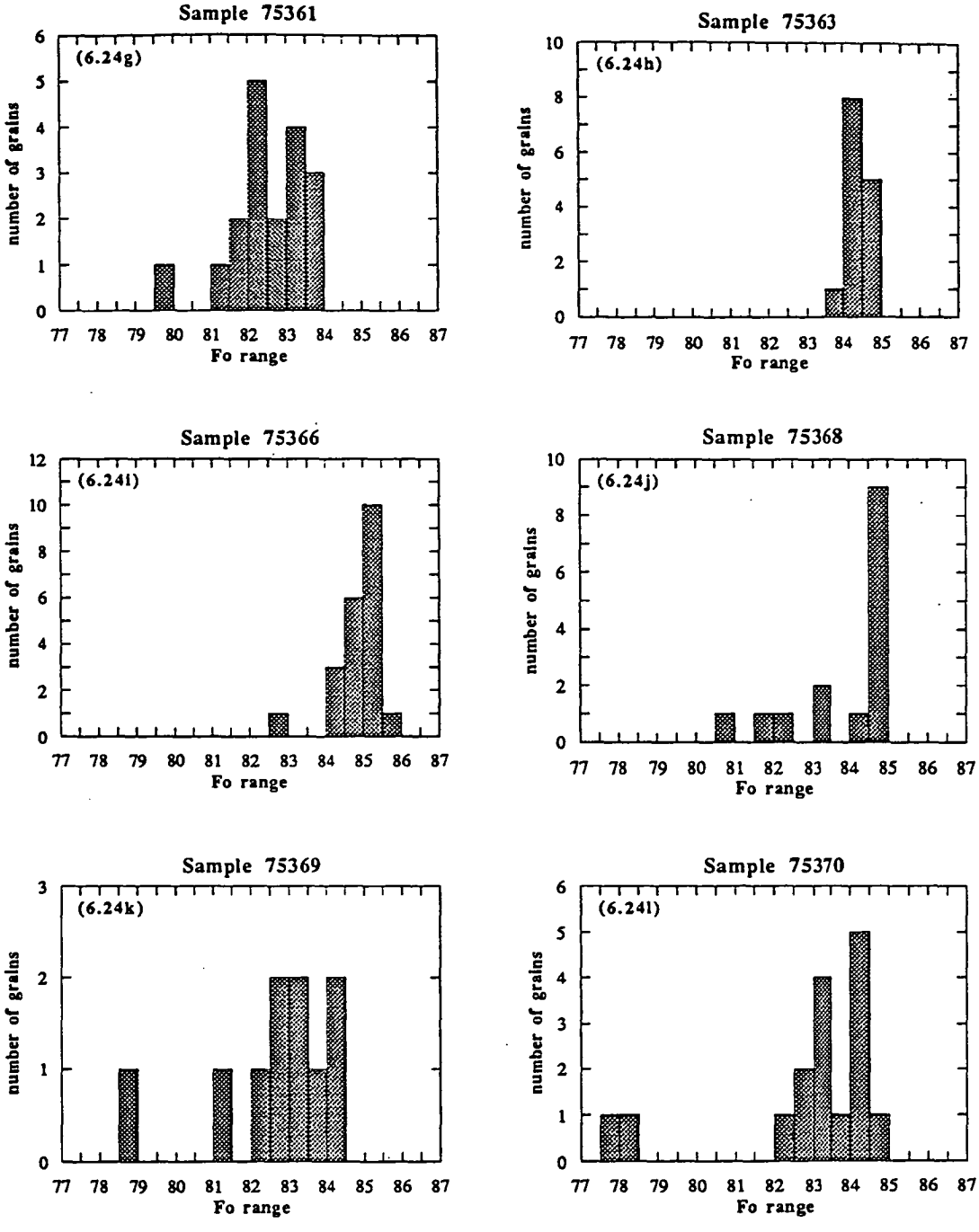

Figures 6.24g-l (cont.). Stack histograms showing the range in Fo values in olivine phenocrysts of the Sukadana low-Ti basalts.

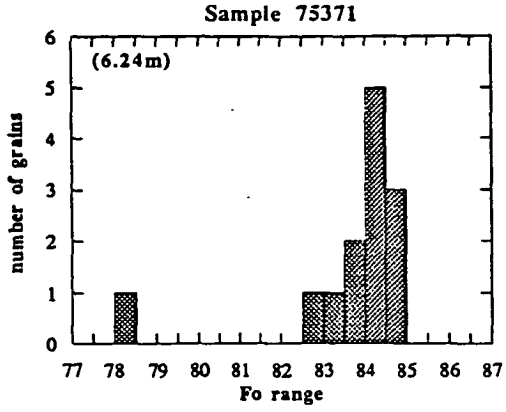

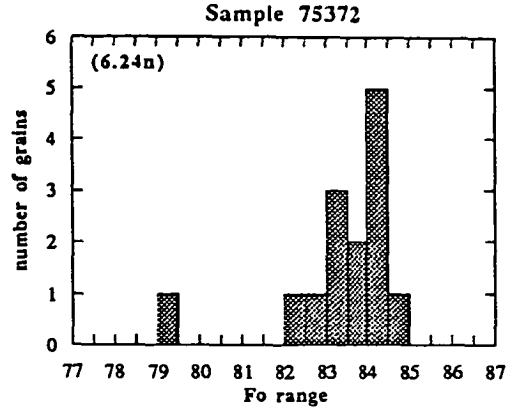

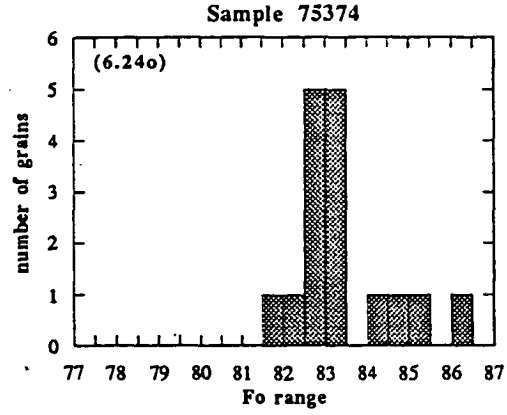

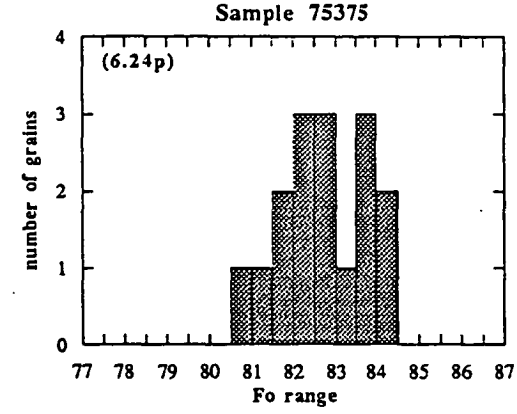

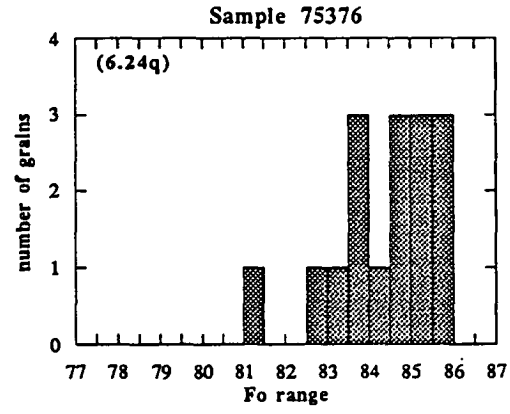

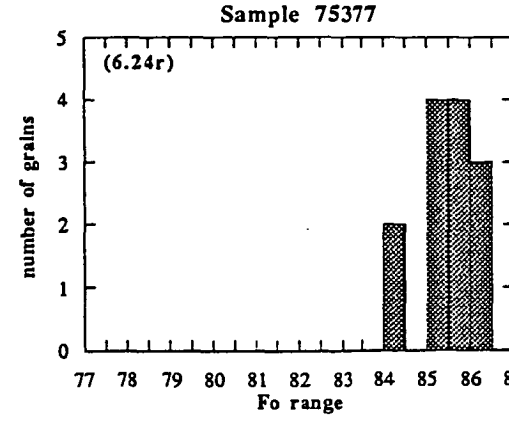

Figures 6.24m-r (cont.). Stack histograms showing the range in Fo values in olivine phenocrysts of the Sukadana low-Ti basalts.

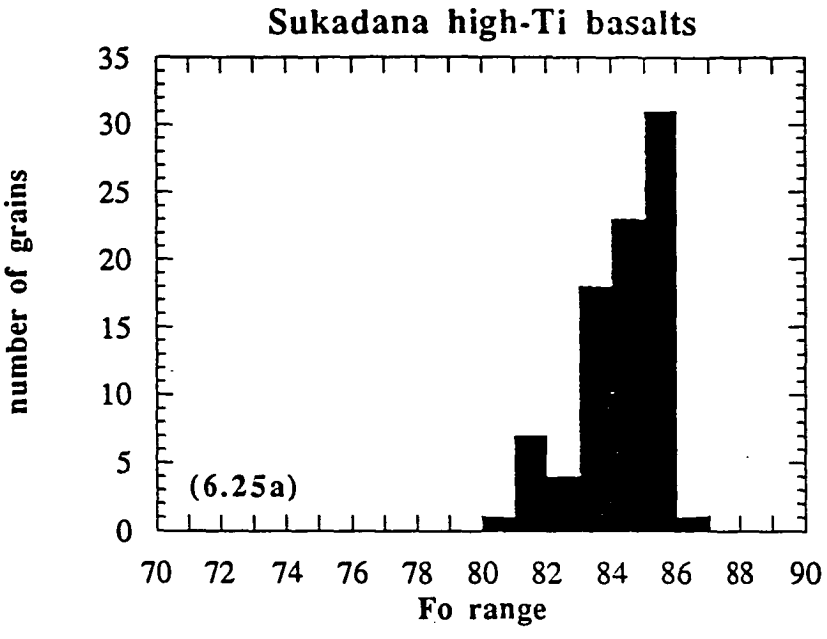

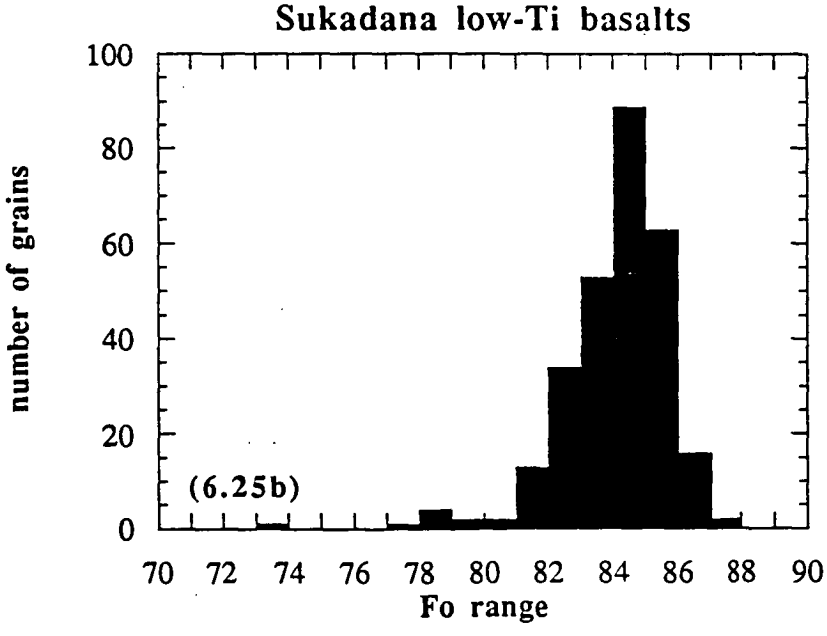

Figures 6.25a-b. Cumulative histograms showing the range in Fo values in olivine phenocrysts of the Sukadana high-Ti (Figure 6.25a) and low-Ti (Figure 6.25b) basalts.

Only one highly vesicular sample (75216) seems to have slightly lower Fo values overall. The olivine phenocrysts in the low-Ti basalts show a different Fo distribution but a similar range (Figures 6.24a-r, 6.25b), with a more symmetrical distribution around Fo values slightly lower (85-84) than those of the olivine phenocrysts of the high-Ti basalts, and significant differences among the different samples (e.g. 75374 - average Fo ≈ 83, and 75377 - average Fo ≈ 86). However, olivines with Fo>86 appear to be more common in the low-Ti basalts. No significant differences between the two groups of basalts have been noticed in the trace element (CaO, MnO, NiO) contents of olivine phenocrysts.

The differences in whole-rock composition between the two groups of basalts are reflected by the composition of their respective spinel inclusions in olivine phenocrysts: high-Ti basalts have high-Ti spinel inclusions, and low-Ti basalts have low-Ti spinel inclusions (Appendix F).

The two groups of spinels follow different parallel positive trends in Fo/Mg#, Fo/MgO, and MgO/FeO diagrams (Figures 6.26, 6.27, and 6.28). The low-Ti group has higher Mg# and MgO and lower FeO contents for a given Fo value of the host olivine. For a Fo range of 86-82 in the host olivine, Mg# values for the low-Ti and the high-Ti groups range respectively from 0.65 to 0.50, and from 0.58 to 0.45. The samples from Gunung Tiga (75356 to 75359) have lower MgO and Mg# values, and slightly lower than in the high-Ti group. Sample 75359 has considerably lower MgO and Mg# values. Among the low-Ti samples, 75360 is the one with the highest MgO and Mg#, with some spinels plotting within the field of the low-Ti group.

Cr# and Al_2O_3 values (Figures 6.29, 6.30, and 6.31) respectively increase and decrease for decreasing Mg# in the spinel and Fo values in the host olivine, and the high-Ti group has overall higher Cr# and lower Al_2O_3. Samples from Gunung Tiga have intermediate Cr# and Al_2O_3 values. Again, some spinels of 75360 plot within the field of the low-Ti group.

The TiO_2 content (Figures 6.32 and 6.33) is considerably higher and very variable (from about 4% to as low as 1.5% in 75360) in the high-Ti group, and is negatively correlated with Mg# in the spinel and the Fo value in the host olivine. In the low-Ti group the TiO_2 content is rather constant, about 1.2% ± 0.3. All the samples from Gunung Tiga, including 75359, have constant TiO_2 values and are similar to the low-Ti group.

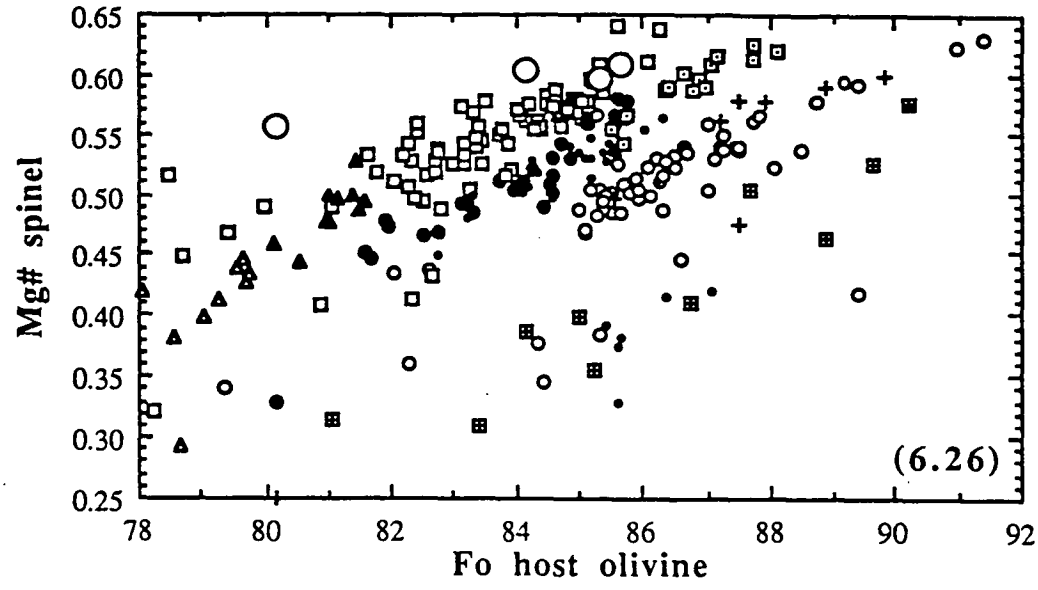

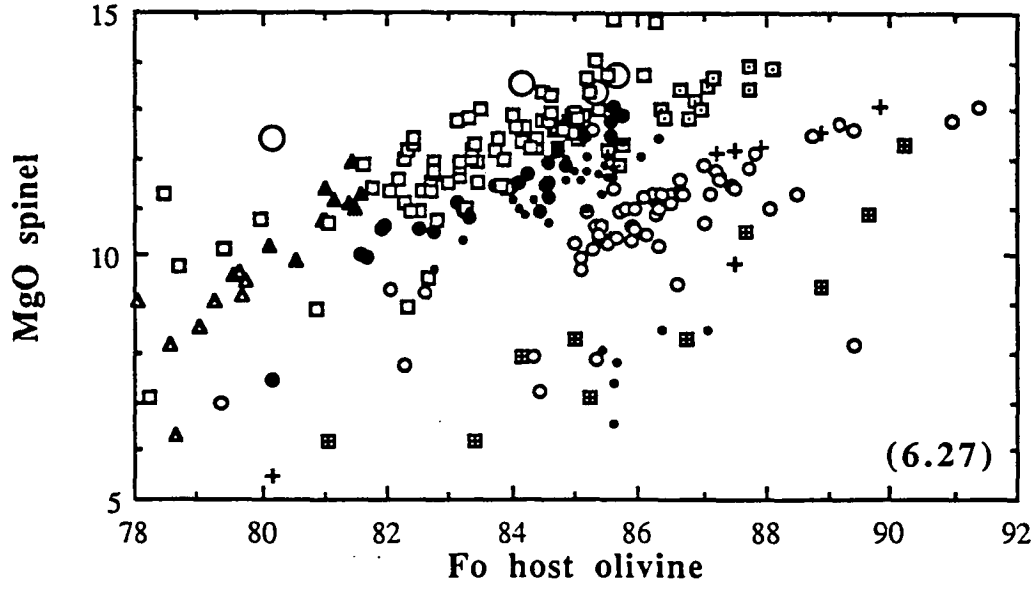

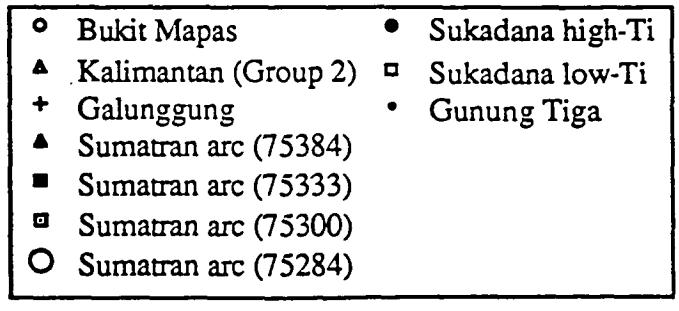

Figures 6.26 and 6.27. Variations of Fo $[Mg^{2+}/(Mg^{2+} + Fe^{2+})]$ values in host olivine versus Mg# $[Mg^{2+}/(Mg^{2+} + Fe^{2+})]$ values (Figure 6.26) and MgO contents (Figure 6.27) in spinel inclusions in olivine phenocrysts in low-Ti and high-Ti basalts of Sukadana, low-Ti basalts of Kalimantan, and arc rocks of Sumatra (including Bukit Mapas) and Jawa (Galunggung). For Bukit Mapas, only the Cr-rich spinels have been plotted in these diagrams. Same symbols for both diagrams.

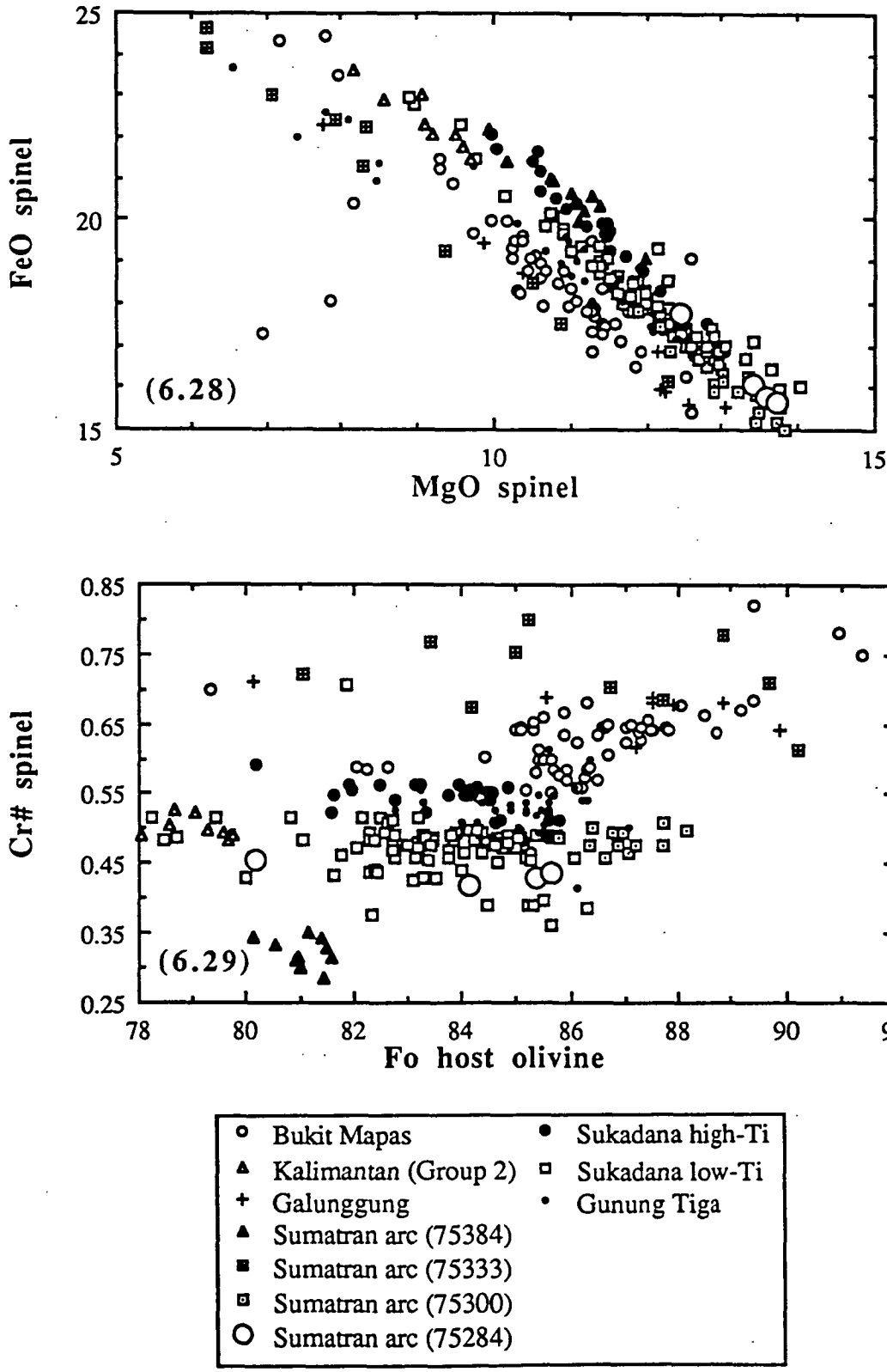

Figures 6.28 and 6.29. Variations of MgO versus FeO contents (Figure 6.28) in spinel inclusions, and Fo [$Mg^{2+}/(Mg^{2+} + Fe^{2+})$] values in host olivine versus Cr# [Cr/(Cr + Al)] values (Figure 6.29) in spinel inclusions in olivine phenocrysts in low-Ti and high-Ti basalts of Sukadana, low-Ti basalts of Kalimantan, and arc rocks of Sumatra (including Bukit Mapas) and Jawa (Galunggung). For Bukit Mapas, only the Cr-rich spinels have been plotted in these diagrams. Same symbols for both diagrams.

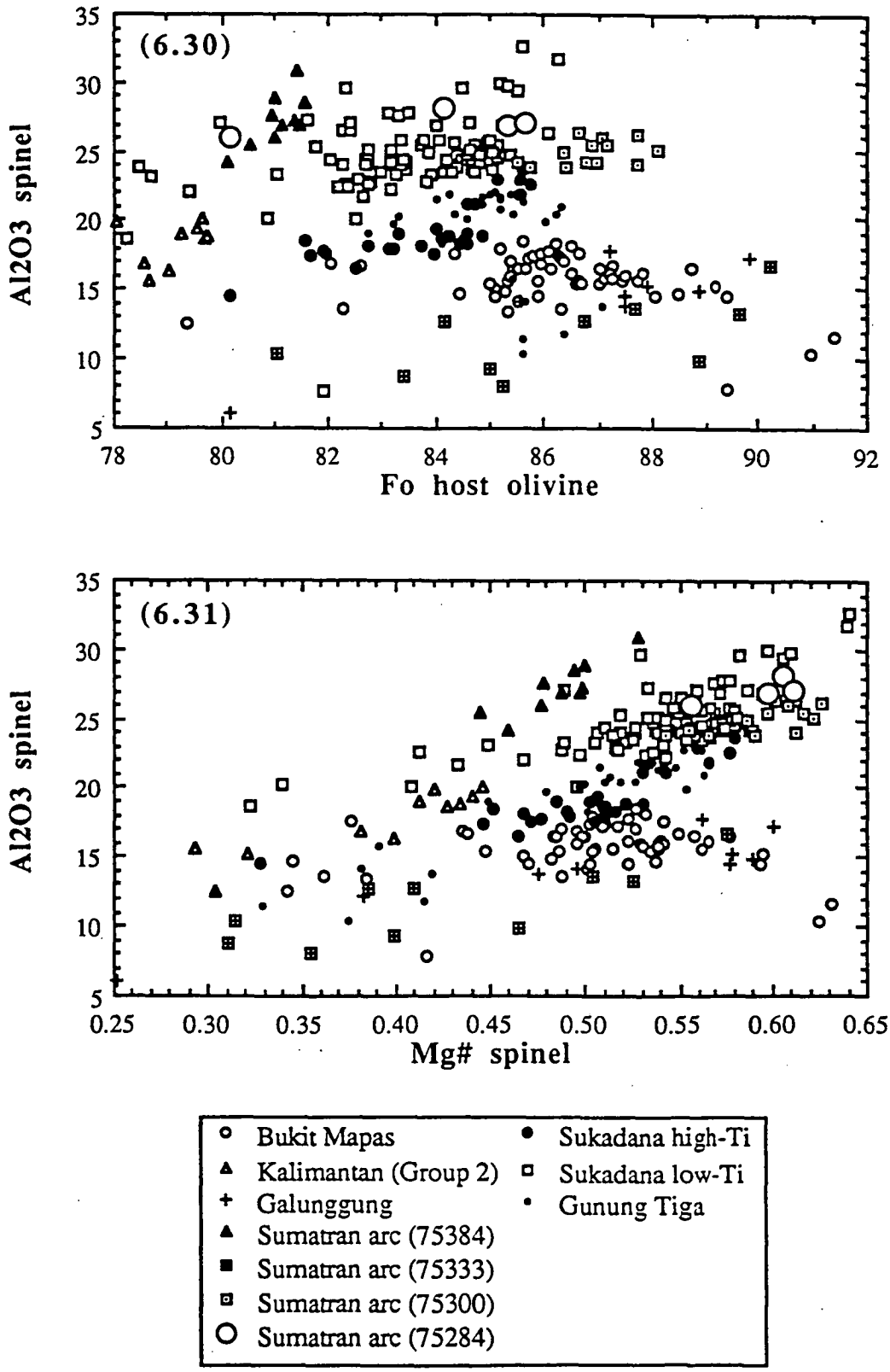

Figures 6.30 and 6.31. Variations of Fo $[Mg^{2+}/(Mg^{2+} + Fe^{2+})]$ values in host olivine versus Al_2O_3 (Figure 6.30) contents in spinel inclusions, and Mg# $[Mg^{2+}/(Mg^{2+} + Fe^{2+})]$ values in spinel inclusions versus Al_2O_3 contents (Figure 6.31) in spinel inclusions in olivine phenocrysts in low-Ti and high-Ti basalts of Sukadana, low-Ti basalts of Kalimantan, and arc rocks of Sumatra (including Bukit Mapas) and Jawa (Galunggung). For Bukit Mapas, only the Cr-rich spinels have been plotted in these diagrams. Same symbols for both diagrams.

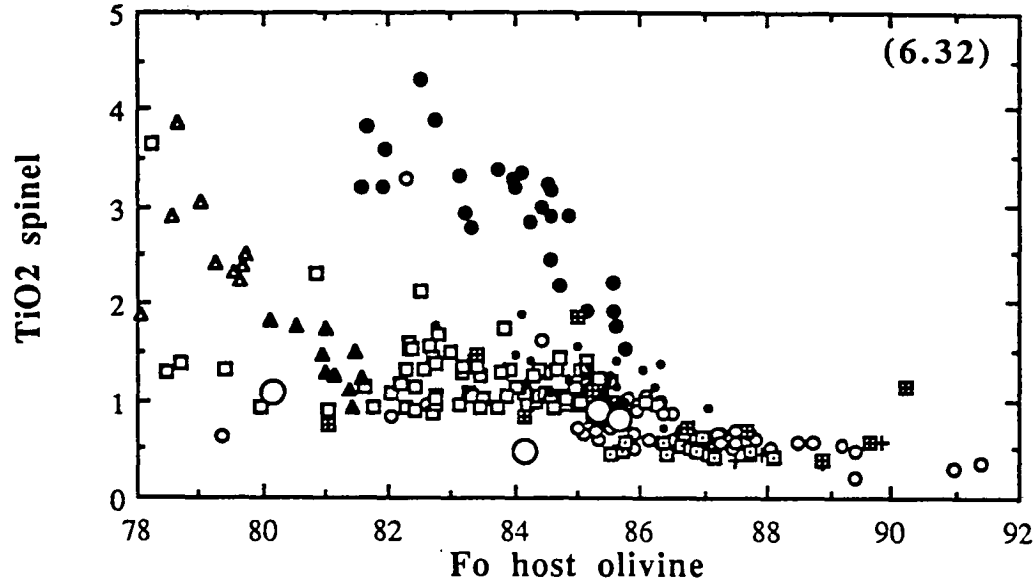

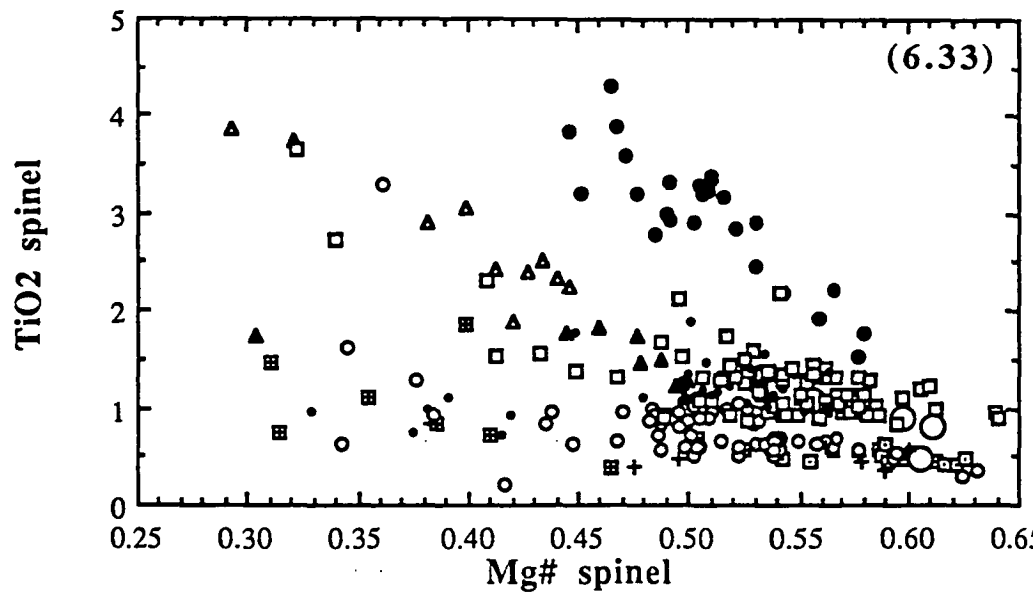

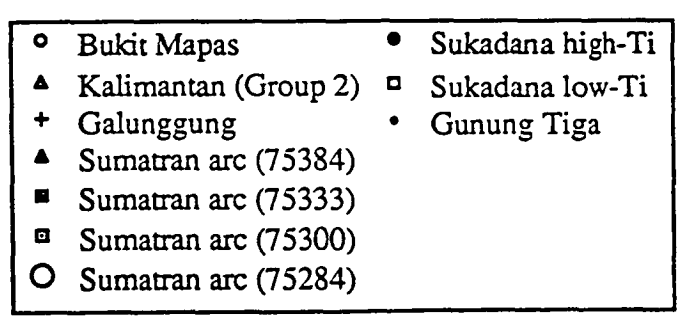

Figures 6.32 and 6.33. Variations of Fo [$Mg^{2+}/(Mg^{2+} + Fe^{2+})$] values in host olivine versus TiO_2 (Figure 6.32) contents in spinel inclusions, and Mg# [$Mg^{2+}/(Mg^{2+} + Fe^{2+})$] values in spinel inclusions versus TiO_2 contents (Figure 6.33) in spinel inclusions in olivine phenocrysts in low-Ti and high-Ti basalts of Sukadana, low-Ti basalts of Kalimantan, and arc rocks of Sumatra (including Bukit Mapas) and Jawa (Galunggung). For Bukit Mapas, only the Cr-rich spinels have been plotted in these diagrams. Same symbols for both diagrams.

The Fe^{2+}/Fe^{3+} values (Figure 6.34), taken as an indicator of the oxidation conditions during crystallisation, seem to be independent of the Mg# value, and are very variable in both groups, and are generally higher in the low-Ti spinels, 2.4 to 1.5, compared with more constant values in the high-Ti group (2 to 1.5). Samples from Gunung Tiga overlap the field of the two groups, while 75359 has extremely low values (less than 1).

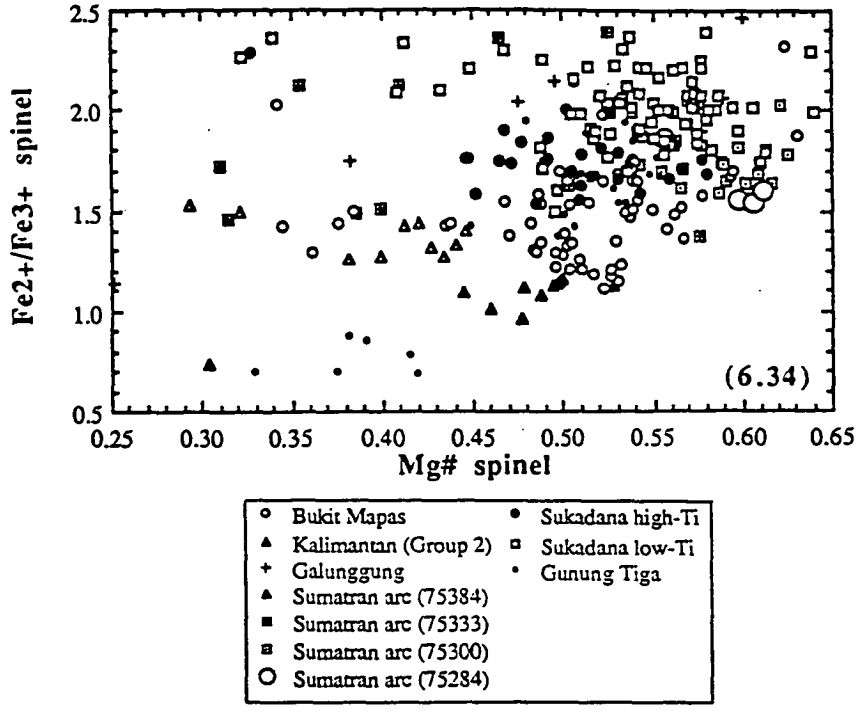

Figure 6.34. Variations of Mg# [$Mg^{2+}/(Mg^{2+} + Fe^{2+})$] values in spinel inclusions versus Fe^{2+}/Fe^{3+} values in spinel inclusions in olivine phenocrysts in low-Ti and high-Ti basalts of Sukadana, low-Ti basalts of Kalimantan, and arc rocks of Sumatra (including Bukit Mapas) and Jawa (Galunggung). For Bukit Mapas, only the Cr-rich spinels have been plotted in these diagrams.

The differences observed in whole-rock and spinel compositions between low-Ti and high-Ti rocks are maintained in the melt inclusions (Table 6.6). Compared with the whole-rock composition (Figures 6.35a-j), all melt inclusions have similar Mg# (Table 6.6). Consistent with the host whole-rock composition, melt inclusions in olivines of 75377 are the most primitive among the low-Ti basalts. Melt inclusions from Gunung Tiga are unusual in having high Mg# (but low MgO and FeO contents) and high alkalis. As was also observed for the spinel inclusions, there is a continuum between high-Ti and low-Ti compositions, with some melt inclusions in olivines from low-Ti samples (75366) ranging in their TiO_2 contents from 1.4 to 3.2.

Homogenisation temperatures of melt inclusions show little variation, consistent with the small Fo range of the host olivines (Table 6.6).

Table 6.6. List of melt inclusions analyzed in samples of Sukadana and Bukit Mapas. In the table are listed (from the top):
1) composition of host olivine, analyzed next to the melt inclusion, and Fo value;
2) composition of the melt inclusion;
3) temperature of homogenization or partial homogenization (see text for explaination);
4) composition of the melt inclusion recalculated to 100%;
5) Mg# of the melt inclusion, calculated assuming that Fe_2O_3=0;
6) corresponding Fo value of olivine in equilibrium with such a melt (Roeder & Emslie 1970);
7) FeO/Fe_2O_3 value of the melt inclusion, calculated from the average FeO/Fe_2O_3 of spinel inclusions in each sample using the relationship between FeO/Fe_2O_3 in spinel and coexisting melt described by Maurel & Maurel (1983), and assuming equilibrium between melt and spinel inclusions in olivine phenocrysts;
8) corresponding Mg# of the melt inclusion;
9) corresponding Fo value of olivine in equilibrium with such a melt (Roeder & Emslie 1970);
10) approximate amount (in weight percent) of host olivine accidentally added during the homogenization of the melt inclusion (overheating), estimated from the difference between the observed Fo value in the host olivine, and the Fo value of olivine in equilibrium with the Mg# of the melt calculated in 5). Negative numbers indicate that the melt inclusion was not homogenized (that is, part of the glass crystallized from the melt inclusion on the walls of the melt inclusion was not homogenized);
11) recalculated composition of the melt inclusion, after subtraction of the excess olivine estimated in 10). The Fo value of the olivine (13) in equilibrium with the melt (12) is now similar to the Fo value measured in the host olivine (1).
14) same as steps 10 to 13, but calculating the FeO/Fe_2O_3 in the melt as in 7). These values have been plotted in Figures 6.35a-j.

Melt inclusions which require the subtraction of more than 5-6% olivine indicate excessive overheating during the homogenization, and have not been taken into account in the discussion. Note that very small amounts of olivine subtracted from the melt strongly modify the MgO content in the melt. Because the temperature of homogenization is only approximately known, and MgO-FeO exchange and gradients can be expected at the boundary between the melt inclusion and the host olivine, the amount of olivine subtracted (steps 10 and 14) might be excessive, as it is suggested by the very low MgO contents in melt inclusions, systematically lower than in the whole-rock. Therefore, the measured compositions of the melt inclusions are likely to be better estimates of the "real" composition. If this is true, then the composition of the melt inclusions is very similar to that of the whole-rock, when the effects of Fe-Mg diffusion (and possibly of crystal fractionation) are taken into account.

Sukadana

1	Olivine	75215-0	75215-1	75215-2	75215-4	75215-5	75215-6	75215-7	75216	75365-1	75365-2	75365-3	75377-1	75377-3
	SiO2	39.18	39.83	39.82	39.77	38.75	39.78	40.47	39.68	39.20	39.79	40.04	39.09	39.49
	FeO	14.21	14.90	14.92	14.64	14.55	14.68	16.07	14.18	14.96	14.93	14.31	13.43	13.08
	MgO	45.01	45.10	45.22	44.86	44.96	45.78	45.93	45.46	44.60	44.89	45.76	45.22	45.56
	CaO	0.22	0.38	0.34	0.31	0.28	0.33	0.38	0.21	0.31	0.38	0.30	0.23	0.27
	MnO	0.17	0.20	0.08	0.15	0.23	0.18	0.20	0.16	0.19	0.17	0.12	0.20	0.21
	NiO	0.40	0.28	0.28	0.28	0.33	0.28	0.25	0.50	0.32	0.24	0.28	0.37	0.42
	Total	99.20	100.68	100.67	100.03	99.09	101.03	103.29	100.19	99.58	100.39	100.81	98.55	99.04
	Fo	84.95	84.36	84.38	84.52	84.63	84.75	83.59	85.10	84.16	84.27	85.07	85.71	86.12
2	Melt	75215-0	75215-1	75215-2	75215-4	75215-5	75215-6	75215-7	75216	75365-1	75365-2	75365-3	75377-1	75377-3
	SiO2	50.90	52.70	50.40	49.32	47.54	52.19	53.10	47.90	53.26	52.42	53.66	51.77	50.95
	TiO2	3.08	3.12	3.26	2.46	1.67	3.79	3.08	2.87	2.62	3.39	3.46	1.58	1.75
	Al2O3	16.49	18.02	16.16	12.72	9.41	17.17	16.87	11.05	16.50	17.16	16.49	17.91	18.65
	FeO	5.67	5.52	5.50	9.73	9.20	5.90	7.06	7.68	5.40	5.88	5.89	6.18	4.55
	MnO	0.09	0.03	0.00	0.24	0.17	0.16	0.09	0.00	0.16	0.27	0.04	0.13	0.00
	MgO	6.57	6.00	7.57	13.70	25.67	6.51	6.71	17.45	6.09	6.19	5.93	5.93	5.98
	CaO	8.81	9.54	10.05	7.18	5.30	9.50	9.44	4.81	8.27	9.65	8.61	8.45	9.63
	Na2O	3.80	4.09	3.66	2.79	2.21	3.76	3.94	3.18	4.08	3.83	4.04	4.42	4.34
	K2O	1.12	1.21	1.08	0.79	0.61	1.06	1.12	0.89	1.19	1.25	1.14	1.75	1.82
	P2O5	0.34	0.45	0.35	0.27	0.28	0.32	0.39	0.33	0.31	0.36	0.38	0.31	0.28
	Total	96.86	100.67	98.04	99.20	102.07	100.37	101.80	96.17	97.88	100.41	99.65	98.42	97.96
3	T homogenization (°C)	1180	1185	1350	1360	1185*	1185*	1184	1190	1180	1185	1195	1200	1200

* melted for more than 5 minutes

4	Melt composition	(recalculated to 100 %)												
		75215-0	75215-1	75215-2	75215-4	75215-5	75215-6	75215-7	75216	75365-1	75365-2	75365-3	75377-1	75377-3
	SiO2	52.55	52.34	51.41	49.72	46.58	52.00	52.16	49.82	54.41	52.21	53.85	52.60	52.01
	TiO2	3.18	3.10	3.33	2.48	1.64	3.78	3.02	2.98	2.68	3.37	3.48	1.60	1.78
	Al2O3	17.02	17.90	16.49	12.82	9.22	17.10	16.58	11.49	16.85	17.09	16.55	18.20	19.04
	FeO	5.86	5.48	5.61	9.81	9.01	5.88	6.93	7.98	5.51	5.86	5.91	6.28	4.64
	MnO	0.09	0.03	0.00	0.24	0.17	0.16	0.08	0.00	0.16	0.27	0.04	0.13	0.00
	MgO	6.78	5.96	7.73	13.81	25.15	6.49	6.59	18.14	6.22	6.17	5.95	6.03	6.11
	CaO	9.09	9.48	10.25	7.24	5.19	9.47	9.28	5.00	8.45	9.61	8.64	8.59	9.83
	Na2O	3.92	4.07	3.74	2.81	2.16	3.75	3.87	3.31	4.17	3.82	4.06	4.49	4.44
	K2O	1.16	1.20	1.10	0.80	0.60	1.05	1.11	0.93	1.22	1.24	1.15	1.78	1.86
	P2O5	0.35	0.45	0.36	0.27	0.27	0.32	0.38	0.35	0.32	0.36	0.38	0.31	0.28
	Total	100.00	100.00	100.00	100.00	100.00	100.00	100.00	100.00	100.00	100.00	100.00	100.00	100.00
	Al2O3/CaO	1.87	1.89	1.61	1.77	1.78	1.81	1.79	2.30	1.99	1.78	1.92	2.12	1.94
5	Mg#(100% FeO)	67.35	65.96	71.05	71.51	83.25	66.29	62.87	80.19	66.79	65.22	64.19	63.11	70.09
6	Fo equilibrium	87.30	86.59	89.11	89.33	94.31	86.76	84.95	93.10	87.02	86.21	85.66	85.08	88.65
7	calculated % FeO	0.81	0.81	0.81	0.81	0.81	0.81	0.81	0.81	0.81	0.81	0.81	0.84	0.84
8	corresponding Mg#	71.80	70.52	75.19	75.61	85.99	70.83	67.64	83.33	71.29	69.83	68.88	67.07	73.61
9	Fo equilibrium	89.46	88.86	90.99	91.17	95.34	89.00	87.45	94.34	89.22	88.53	88.06	87.16	90.29
10	% olivine added assuming 100% FeO	2.50	2.00	5.50	11.00	55.00	2.00	1.50	26.00	2.50	2.00	0.50	-0.50	2.50
11	SiO2	53.07	52.74	52.47	51.53	55.01	52.39	52.47	54.86	55.01	52.60	53.96	52.50	52.49
	TiO2	3.30	3.19	3.63	2.93	3.48	3.90	3.10	4.46	2.79	3.48	3.50	1.59	1.85
	Al2O3	17.70	18.46	17.97	15.15	19.62	17.64	16.97	17.17	17.52	17.62	16.67	18.06	19.79
	FeO	5.52	5.19	4.78	8.93	2.62	5.61	6.73	4.93	5.13	5.58	5.85	6.33	4.31
	MnO	0.09	0.02	-0.01	0.26	0.10	0.16	0.08	-0.08	0.16	0.27	0.04	0.13	-0.01
	MgO	5.24	4.75	4.39	8.18	2.36	5.27	5.69	4.68	4.69	4.97	5.64	6.33	4.53
	CaO	9.45	9.76	11.14	8.49	10.72	9.75	9.49	7.37	8.77	9.90	8.70	8.52	10.21
	Na2O	4.08	4.19	4.07	3.32	4.60	3.87	3.97	4.95	4.34	3.94	4.09	4.45	4.61
	K2O	1.20	1.24	1.20	0.95	1.28	1.09	1.13	1.39	1.27	1.28	1.16	1.76	1.94
	P2O5	0.36	0.46	0.39	0.32	0.58	0.33	0.39	0.52	0.33	0.37	0.39	0.31	0.29
	Total	100.00	100.00	100.00	100.00	100.00	100.00	100.00	100.00	100.00	100.00	100.00	100.00	100.00
12	Mg#	62.84	61.99	62.05	62.01	61.54	62.62	60.12	62.85	61.95	61.33	63.22	64.05	65.23
13	Fo equilibrium	84.93	84.46	84.50	84.47	84.21	84.81	83.40	84.94	84.44	84.10	85.14	85.59	86.21
14	% olivine added assuming x % FeO	4.50	4.00	7.00	14.00	56.00	4.00	3.50	27.50	4.50	3.50	2.50	1.50	4.00
	SiO2	53.50	53.15	52.77	52.06	55.22	52.80	52.88	55.21	55.50	52.90	54.40	52.90	52.78
	TiO2	3.41	3.29	3.71	3.06	3.53	4.02	3.19	4.56	2.88	3.56	3.61	1.64	1.90
	Al2O3	18.26	19.03	18.39	15.84	19.88	18.19	17.50	17.56	18.07	18.03	17.20	18.62	20.25
	FeO	5.24	4.89	4.55	8.67	2.46	5.33	6.45	4.72	4.82	5.37	5.59	6.11	4.10
	MnO	0.09	0.02	-0.01	0.27	0.09	0.16	0.08	-0.08	0.16	0.28	0.04	0.13	-0.01
	MgO	3.97	3.52	3.44	6.51	1.78	4.03	4.48	3.75	3.43	4.05	4.39	5.10	3.57
	CaO	9.74	10.05	11.39	8.86	10.86	10.05	9.77	7.54	9.04	10.12	8.97	8.78	10.44
	Na2O	4.21	4.32	4.17	3.47	4.66	3.99	4.09	5.06	4.47	4.03	4.22	4.59	4.72
	K2O	1.24	1.28	1.23	0.99	1.30	1.12	1.17	1.42	1.30	1.31	1.19	1.82	1.98
	P2O5	0.37	0.47	0.40	0.34	0.59	0.34	0.40	0.53	0.34	0.38	0.40	0.32	0.30
	Total	100.00	100.00	100.00	100.00	100.00	100.00	100.00	100.00	100.00	100.00	100.00	100.00	100.00
	Mg#	62.49	61.25	62.46	62.30	61.43	62.45	60.41	63.61	61.03	62.42	63.36	63.92	64.87
	Fo equilibrium	84.74	84.05	84.72	84.63	84.15	84.72	83.57	85.35	83.92	84.70	85.22	85.52	86.02

		Sidradoca								Butzi Mapas					
1	Olivine	75354	75357-1	75357-2	75361-1	75361-4	75361-6	75366-1	75366-2	78129-1	78129-2	78129-2/2	78129-3	78129-3/2	78129-3-3
	SiO2	39.44	39.44	39.53	39.34	39.18	39.44	39.68	38.72	40.13	40.18		40.40		
	FeO	14.39	13.67	13.83	14.86	15.49	15.27	14.61	13.59	12.57	12.18		10.44		
	MgO	45.24	46.07	46.10	44.16	44.55	44.64	44.74	44.73	47.11	46.82		48.36		
	CaO	0.28	0.30	0.30	0.23	0.34	0.31	0.23	0.20	0.21	0.24		0.20		
	MnO	0.24	0.20	0.16	0.16	0.15	0.14	0.24	0.23	0.18	0.23		0.21		
	NiO	0.31	0.38	0.32	0.54	0.28	0.29	0.36	0.57	0.13	0.17		0.31		
	Total	99.91	100.05	100.23	99.29	100.00	100.09	99.86	98.03	100.33	99.81		99.91		
	Fo	84.85	85.72	85.59	84.11	83.67	83.90	84.52	85.44	86.97	87.26	87.26	89.19	89.19	89.19
2	Melt	75354	75357-1	75357-2	75361-1	75361-4	75361-6	75366-1	75366-1/2	75366-2	78129-1	78129-2	78129-2/2	78129-3	78129-3/2	78129-3-3
	SiO2	55.89	56.02	58.37	52.96	55.10	55.99	55.35	52.45	52.79	41.32	44.87	44.47	44.40	44.28	42.69
	TiO2	2.22	1.99	1.75	1.36	1.32	1.23	1.30	2.96	1.72	1.11	1.18	1.11	1.04	1.10	1.02
	Al2O3	17.98	18.53	18.25	17.99	18.80	18.76	18.78	17.54	18.49	14.75	16.11	16.17	16.42	16.46	16.21
	FeO	4.68	3.88	3.44	5.91	5.18	6.04	4.82	4.97	4.57	13.37	8.49	8.08	8.49	8.44	8.45
	MnO	0.00	0.00	0.30	0.08	0.16	0.11	0.20	0.13	0.07	0.18	0.02	0.00	0.24	0.03	0.20
	MgO	5.20	4.87	3.97	6.97	5.51	5.83	5.40	5.09	5.89	10.84	9.64	9.56	9.60	9.43	9.56
	CaO	7.58	7.83	6.89	8.71	8.96	9.04	9.11	8.02	9.26	14.07	16.78	16.64	16.82	16.81	16.98
	Na2O	4.54	4.80	5.21	3.92	4.10	4.05	4.12	4.41	3.97	2.53	2.84	2.81	2.73	2.81	2.71
	K2O	1.51	1.47	1.65	0.71	0.87	0.77	0.94	2.03	0.93	0.58	0.65	0.63	0.62	0.59	0.61
	P2O5	0.25	0.30	0.27	0.17	0.20	0.18	0.16	0.22	0.22	0.48	0.55	0.53	0.47	0.56	0.52
	Total	99.86	99.70	100.10	98.77	100.20	102.00	100.18	97.82	97.91	99.23	101.13	100.00	100.83	100.51	98.95
3	T homogenization (°C)	1180	1174	1170	1200	1180	1180	1177	1177	1190	1248	1240	1240	1241	1241	1241
4	Melt composition	(recalculated to 100 %)														
		75354	75357-1	75357-2	75361-1	75361-4	75361-6	75366-1	75366-1/2	75366-2	78129-1	78129-2	78129-2/2	78129-3	78129-3/2	78129-3-3
	SiO2	55.96	56.19	58.31	53.62	54.99	54.89	55.25	53.62	53.92	41.64	44.37	44.47	44.03	44.06	43.14
	TiO2	2.22	1.99	1.74	1.37	1.32	1.20	1.30	3.03	1.76	1.12	1.17	1.11	1.03	1.09	1.03
	Al2O3	18.01	18.59	18.23	18.21	18.76	18.40	18.75	17.93	18.89	14.86	15.93	16.17	16.28	16.38	16.38
	FeO	4.69	3.89	3.44	5.99	5.17	5.93	4.81	5.09	4.67	13.47	8.40	8.08	8.42	8.40	8.54
	MnO	0.00	0.00	0.30	0.08	0.16	0.11	0.20	0.13	0.07	0.18	0.02	0.00	0.24	0.03	0.20
	MgO	5.21	4.88	3.97	7.05	5.50	5.71	5.39	5.20	6.02	10.92	9.53	9.56	9.52	9.38	9.66
	CaO	7.60	7.86	6.88	8.82	8.94	8.86	9.09	8.19	9.46	14.18	16.59	16.64	16.68	16.72	17.16
	Na2O	4.55	4.82	5.21	3.97	4.10	3.97	4.11	4.50	4.06	2.55	2.81	2.81	2.71	2.80	2.74
	K2O	1.51	1.48	1.65	0.71	0.87	0.75	0.94	2.08	0.95	0.58	0.64	0.63	0.61	0.59	0.62
	P2O5	0.25	0.30	0.27	0.17	0.20	0.17	0.16	0.23	0.22	0.48	0.54	0.53	0.47	0.56	0.53
	Total	100.00	100.00	100.00	100.00	100.00	100.00	100.00	100.00	100.00	100.00	100.00	100.00	100.00	100.00	100.00
	Al2O3/CaO	2.37	2.37	2.65	2.07	2.10	2.08	2.06	2.19	2.00	1.05	0.96	0.97	0.98	0.98	0.95
5	Mg#(100% FeO)	66.44	69.08	67.28	67.74	65.49	63.21	66.63	64.57	69.68	59.10	66.92	67.83	66.83	66.57	66.84
6	Fo equilibrium	86.84	88.16	87.27	87.50	86.35	85.14	86.94	85.87	88.45	82.81	87.09	87.54	87.04	86.91	87.05
7	calculated % FeO	0.84	0.81	0.81	0.84	0.84	0.84	0.84	0.81	0.84	0.65	0.65	0.65	0.65	0.65	0.65
8	corresponding Mg#	70.21	73.40	71.74	71.43	69.31	67.16	70.39	69.23	73.23	68.97	75.69	76.44	75.61	75.39	75.62
9	Fo equilibrium	88.71	90.19	89.43	89.29	88.28	87.21	88.80	88.24	90.12	88.11	91.21	91.53	91.18	91.08	91.18
10	% olivine added assuming 100% FeO	1.50	2.00	1.00	3.50	2.00	1.00	2.00	1.00	3.00	-8.00	-0.50	0.50	-4.00	-4.00	-4.00
11	SiO2	56.35	56.71	58.61	54.39	55.48	55.13	55.73	53.84	54.60	41.44	44.34	44.50	43.82	43.84	42.98
	TiO2	2.27	2.06	1.77	1.45	1.36	1.22	1.34	3.08	1.84	0.99	1.16	1.12	0.97	1.03	0.97
	Al2O3	18.43	19.17	18.51	19.22	19.34	18.68	19.33	18.21	19.77	13.09	15.81	16.29	15.31	15.40	15.39
	FeO	4.46	3.59	3.28	5.49	4.85	5.78	4.51	4.93	4.24	13.36	8.42	8.05	8.54	8.52	8.66
	MnO	-0.01	-0.01	0.30	0.08	0.16	0.11	0.19	0.13	0.06	0.18	0.02	0.00	0.24	0.04	0.20
	MgO	4.28	3.60	3.31	4.99	4.29	5.12	4.17	4.58	4.16	15.22	9.82	9.27	11.84	11.72	12.02
	CaO	7.77	8.09	6.98	9.29	9.21	8.99	9.37	8.32	9.90	12.51	16.47	16.77	15.70	15.73	16.13
	Na2O	4.66	4.97	5.29	4.19	4.22	4.03	4.24	4.57	4.25	2.25	2.79	2.83	2.55	2.63	2.57
	K2O	1.55	1.53	1.68	0.75	0.89	0.76	0.97	2.11	1.00	0.51	0.64	0.63	0.58	0.55	0.58
	P2O5	0.26	0.31	0.27	0.18	0.21	0.18	0.17	0.23	0.23	0.43	0.54	0.53	0.44	0.52	0.49
	Total	100.00	100.00	100.00	100.00	100.00	100.00	100.00	100.00	100.00	100.00	100.00	100.00	100.00	100.00	100.00
12	Mg#	63.07	64.11	64.32	61.83	61.20	61.22	62.24	62.30	63.62	66.99	67.49	67.25	71.19	71.02	71.21
13	Fo equilibrium	85.06	85.62	85.73	84.37	84.02	84.03	84.60	84.63	85.36	87.12	87.38	87.25	89.17	89.10	89.18
14	% olivine added assuming x % FeO	3.00	3.00	2.00	5.00	3.50	2.50	3.50	2.50	4.50	2.00	6.00	6.50	3.00	3.00	3.00
	SiO2	56.74	56.98	58.90	54.73	55.85	55.48	56.10	54.17	54.94	41.69	44.76	44.91	44.20	44.22	43.27
	TiO2	2.33	2.09	1.80	1.48	1.39	1.25	1.37	3.15	1.88	1.15	1.28	1.22	1.08	1.15	1.08
	Al2O3	18.85	19.46	18.80	19.66	19.79	19.10	19.77	18.64	20.23	15.33	17.43	17.84	17.04	17.14	17.16
	FeO	4.23	3.43	3.11	5.27	4.60	5.57	4.27	4.71	4.01	13.50	8.04	7.65	8.33	8.30	8.45
	MnO	-0.01	-0.01	0.30	0.07	0.16	0.11	0.19	0.13	0.06	0.18	0.00	-0.02	0.24	0.02	0.20
	MgO	3.33	2.94	2.66	4.08	3.36	4.23	3.23	3.62	3.20	9.79	6.02	5.70	7.71	7.56	7.83
	CaO	7.94	8.21	7.09	9.50	9.41	9.19	9.58	8.51	10.12	14.62	18.13	18.34	17.45	17.50	17.96
	Na2O	4.76	5.04	5.37	4.28	4.32	4.13	4.34	4.68	4.34	2.63	3.07	3.10	2.83	2.93	2.87
	K2O	1.59	1.55	1.70	0.77	0.92	0.78	0.99	2.16	1.02	0.60	0.70	0.70	0.64	0.61	0.65
	P2O5	0.26	0.32	0.28	0.18	0.21	0.18	0.17	0.23	0.24	0.50	0.59	0.58	0.49	0.58	0.55
	Total	100.00	100.00	100.00	100.00	100.00	100.00	100.00	100.00	100.00	100.00	100.00	100.00	100.00	100.00	100.00
	Mg#	62.52	65.36	65.24	62.15	60.79	61.69	61.62	62.88	62.87	66.53	67.24	67.12	71.75	71.41	71.75
	Fo equilibrium	84.76	86.28	86.22	84.55	83.79	84.29	84.26	84.96	84.95	86.89	87.25	87.18	89.44	89.28	89.43

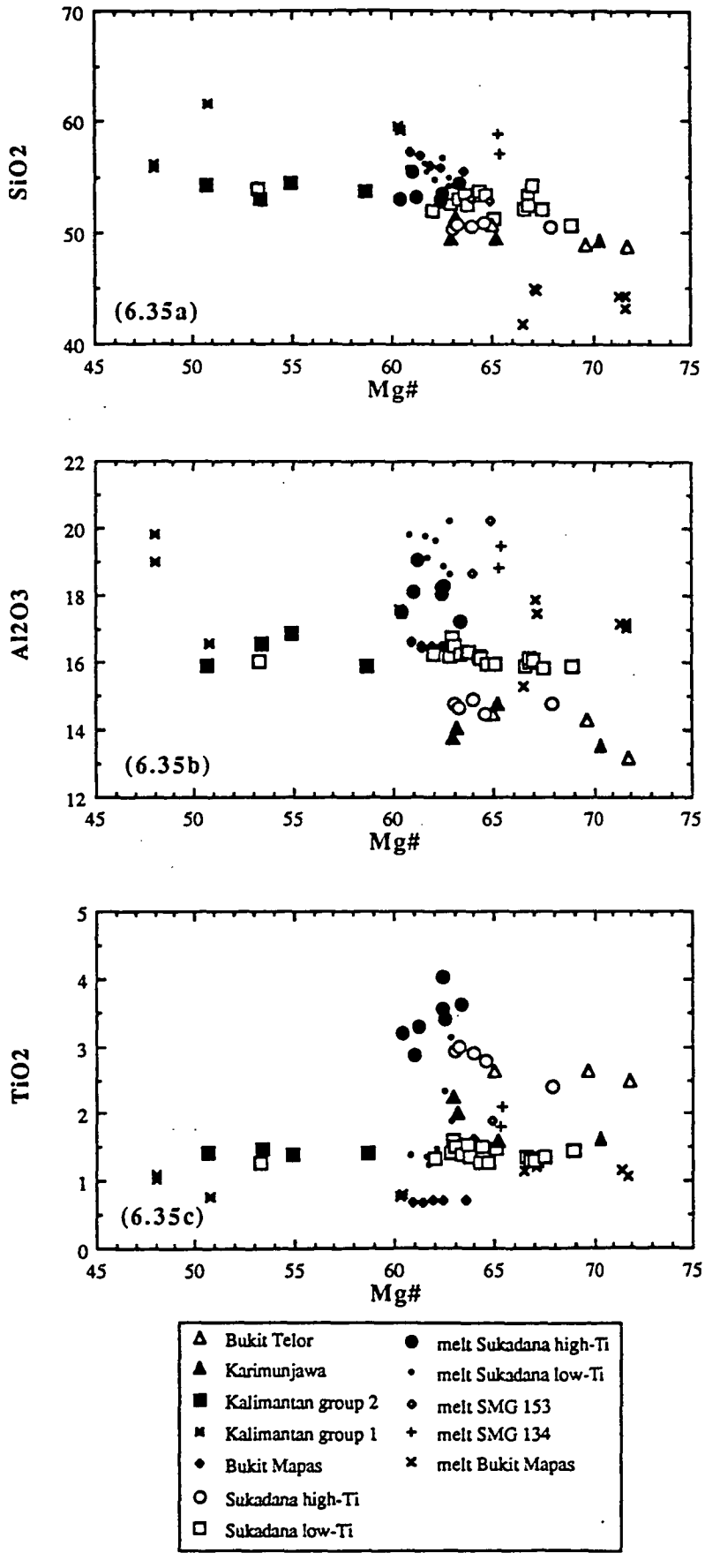

Figures 6.35a-c. Comparison between variations of Mg# values versus major element oxides in whole-rock and recalculated (see Table 6.6) melt inclusions in olivine phenocrysts. Whole-rock composition of Karimunjawa basalts is from Soeria-Atmadja et al. (1985).

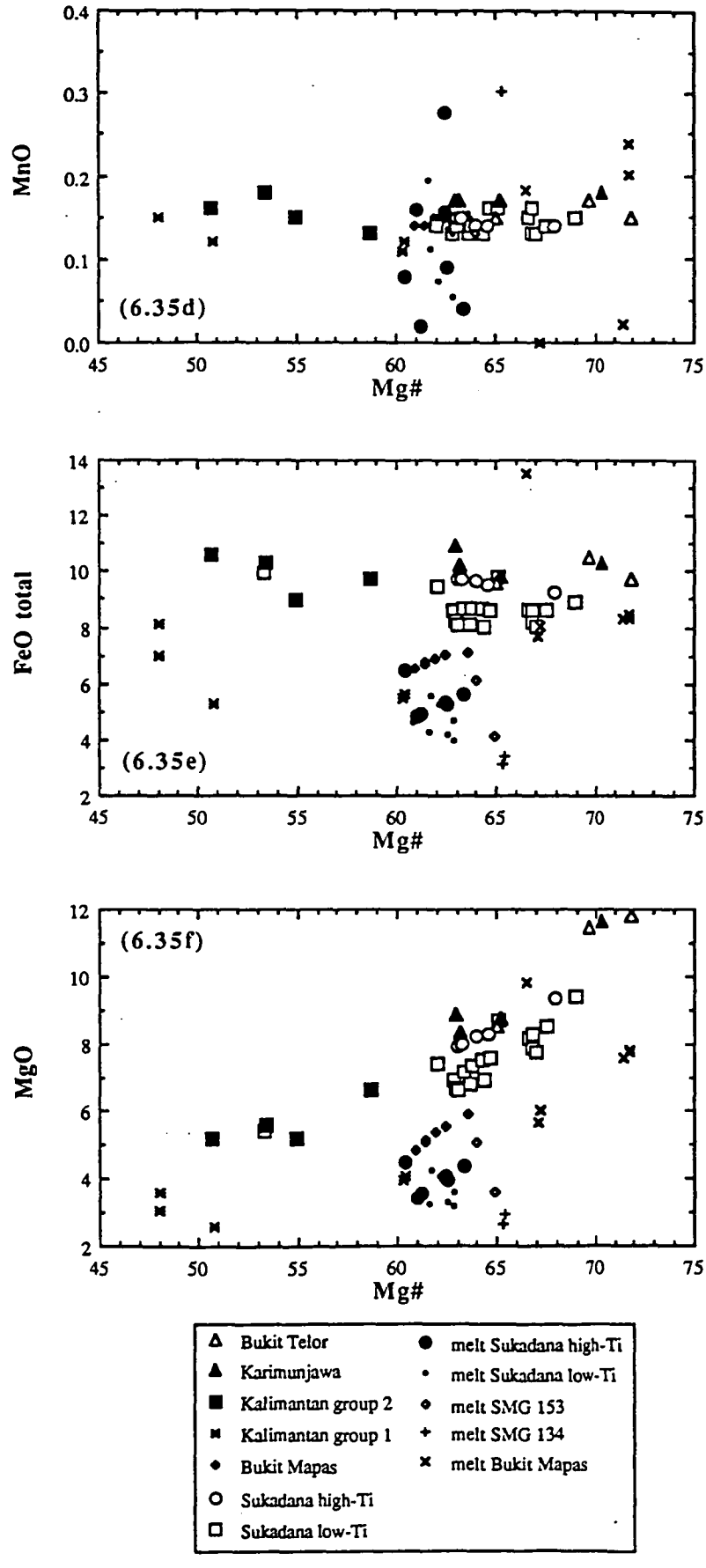

Figures 6.35d-f (cont.). Comparison between variations of Mg# values versus major element oxides in whole-rock and recalculated (see Table 6.6) melt inclusions in olivine phenocrysts. Whole-rock composition of Karimunjawa basalts is from Soeria-Atmadja et al. (1985).

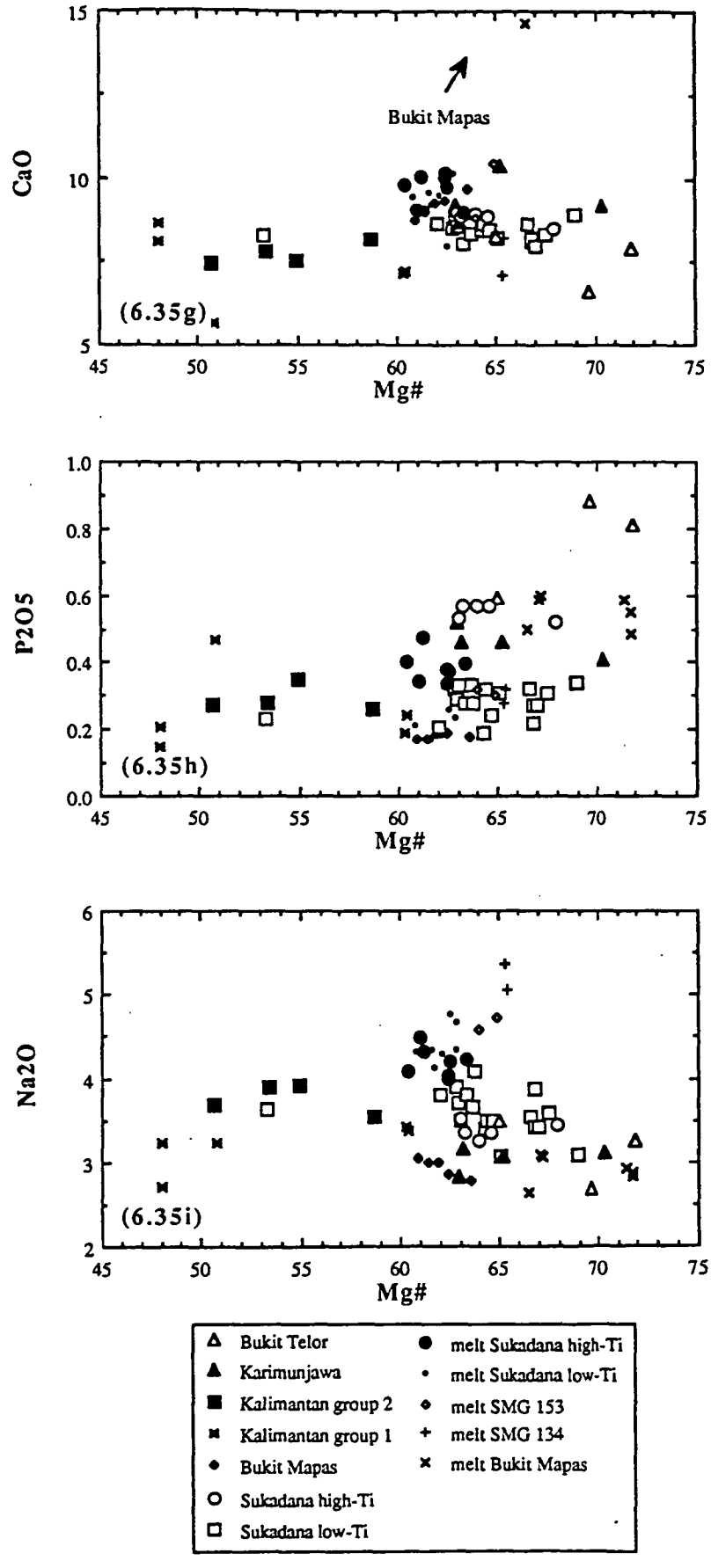

Figures 6.35g-i (cont.). Comparison between variations of Mg# values versus major element oxides in whole-rock and recalculated (see Table 6.6) melt inclusions in olivine phenocrysts. Whole-rock composition of Karimunjawa basalts is from Soeria-Atmadja et al. (1985).

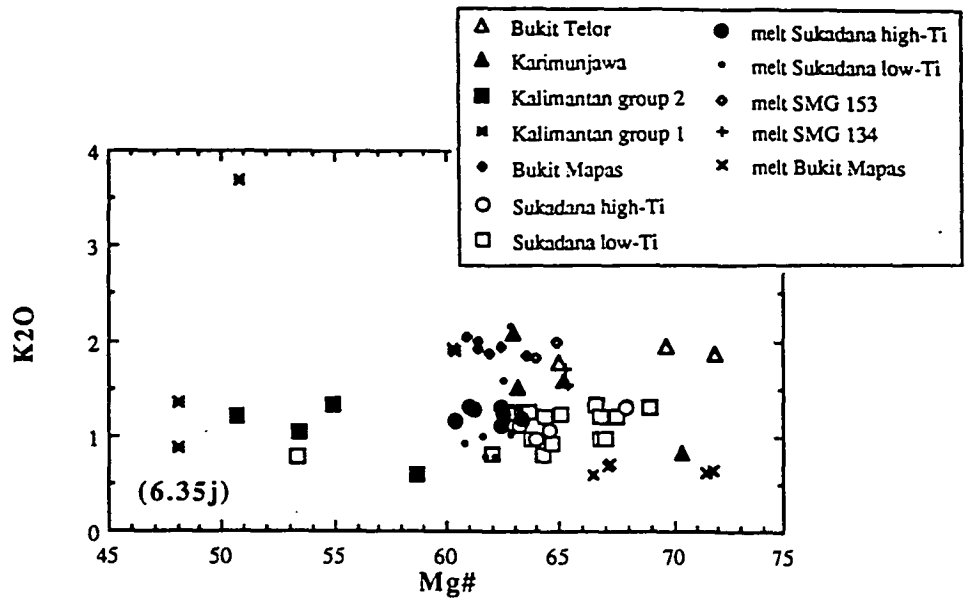

Figure 6.35j (cont.). Comparison between variations of Mg# values versus P_2O_5 in whole-rock and recalculated (see Table 6.6) melt inclusions in olivine phenocrysts. Whole-rock composition of Karimunjawa basalts is from Soeria-Atmadja et al. (1985).

6.9.3 Bukit Mapas

Clinopyroxene phenocrysts are euhedral bright green crystals, and range in size from 0.1 to 1 mm. Primary and secondary elongated melt inclusions are abundant, but too small to be analysed (all are < 5 μm, except one inclusion approximately 20 μm across, which is cracked). No spinel inclusions were found in clinopyroxene phenocrysts.

Olivine phenocrysts are euhedral, of similar size to the clinopyroxenes, and usually contain inclusions containing various combinations of melt, fluid and mineral. High-Mg grains (Fo > 90) are colourless, and can easily be recognised in transmitted light. Mineral inclusions are of Cr- and Al-rich spinel and rounded clinopyroxene, up to 200 μm across. Melt inclusions are both silicates (spinel, clinopyroxene, interstitial glass and shrinkage bubbles) and sulphides (mainly pyrrhotite? - EDS visual estimation), occurring as individual globules up to 60 μm across, always in olivines with Al-rich spinel inclusions. Fluid inclusions are mainly CO_2, with a distinct boundary between the fluid and the gaseous phase. Tiny fluid inclusions (less than 1 μm across) have been observed next to all the mineral inclusions, and also as secondary inclusions in cracks in olivine phenocrysts, often associated with Al-rich

spinels. As for some fluid inclusions in the high-Ti basalts of Sukadana, the temperature of transformation into liquid for the fluid inclusions was estimated at approximately 25 °C, which indicates a CO_2 density of about 0.77 g/cm^3, assuming that the inclusion is pure CO_2 or a pure H_2O-CO_2 mixture. For a measured trapping temperature of 1250 °C, this corresponds to a pressure of less than 5 kbar (Angus et al. 1976; Bergman 1982).

Spinels account for more than 90% of all the inclusions, while sulphide, fluid and clinopyroxene inclusions are rare (about 2%).

6.9.3.1 Spinel inclusions in olivine phenocrysts in Bukit Mapas volcanics

The most interesting and unusual characteristic of the Bukit Mapas volcanics is the occurrence of Al-rich spinels which coexist with the more typical and common Cr-rich spinels as inclusions in olivine phenocrysts. Two different spinel extreme compositions have been recognised. Cr-rich spinels are very abundant (more than 90% of the spinel inclusions in olivines) as reddish-brown (in transmitted light) euhedral inclusions, and range in size from about 5 μm to more than 100 μm. Al-rich spinels are dull green, euhedral or slightly rounded, and the same size as the Cr-rich spinels.

Chromium-rich spinel (Cr_2O_3 in the range 17-70%) is the most common spinel-type in ultramafic and basaltic volcanic rocks, but Al-rich and Cr-poor (Cr_2O_3 less than 5%) spinel, belonging to the $Mg(Al, Fe^{3+})_2O_4$ - $Fe(Al, Fe^{3+})_2O_4$ series is considered to be extremely rare in volcanic assemblages, and in an arc environment it has only previously been described in the basanitoids of Grenada Island in the Lesser Antilles (Arculus 1974, 1978; Arculus & Wills 1980), in island-arc, high-Al primitive basalts from Akutan Island (Hot Springs Bay Volcanics) in the Aleutian arc (Romick et al. 1990), and in cumulate gabbroic inclusions dredged from the caldera of Epi, Vanuatu (Crawford et al. 1988).

In Bukit Mapas, the crystal inclusions in olivines occur both as individual grains and in clusters of two to several tens of grains, and they are usually randomly distributed, although both the Cr- and the Al-spinels may form a regular pattern following the olivine shape.

Al-rich rims on Cr-spinels, similar to those observed in Bukit Mapas, were described in metamorphosed mafic-ultramafic rocks from Panton sill (East Kimberley Region,

Western Australia) by Hamlyn (1975).

6.9.3.2 Spinel crystals in melt inclusions in Bukit Mapas olivine phenocrysts

In addition to the spinel inclusions, most olivine phenocrysts contain primary melt inclusions composed of crystalline and fluid phases, and residual, interstitial glass. Their size ranges from a few up to a few hundred microns, usually with rounded isometric shape, less commonly elongated or irregular.

The crystalline phases observed are clinopyroxene and Cr- and Al-spinel. Clinopyroxene, usually as a euhedral single crystal, makes more than 50% of the volume of the inclusion. Spinels are always found at the margins of the inclusion, and in many cases are partly enclosed by the host olivine. Al-spinel can occur as single crystals, like the Cr-spinels, or as a number of tiny grains (up to 10), and as an overgrowth on a Cr-spinel crystal. The proportion between the Cr-rich and the Al-rich parts of these aggregates is variable, and is not dependent on the size of the melt inclusion.

6.9.3.3 Mineral chemistry of Bukit Mapas volcanics

The results of the systematic microprobe study of olivine and clinopyroxene phenocrysts, and spinel, clinopyroxene and melt inclusions in olivine phenocrysts in Bukit Mapas volcanics, are reported in Appendix F. These results show that:

1) olivine phenocrysts with composition Fo 86 ± 2 are the most common in all analysed samples (Figures 6.36a-f, 6.37), but the distribution is not unimodal, and Fo values range from ≈ 93 to 82. The compositions of olivine phenocrysts in all the rocks seem to have similar Fo ranges and distribution, although rare olivines with Fo > 90 are restricted to two samples only. CaO contents of olivines in all the samples range from approximately 0.15 to 0.25%, with a negative correlation with Fo (Figure 6.38).

2) clinopyroxene phenocrysts have a fairly constant composition, similar to that of the clinopyroxene solid inclusions in olivines, and are augites with Mg# ranging from approximately 89 to 86.

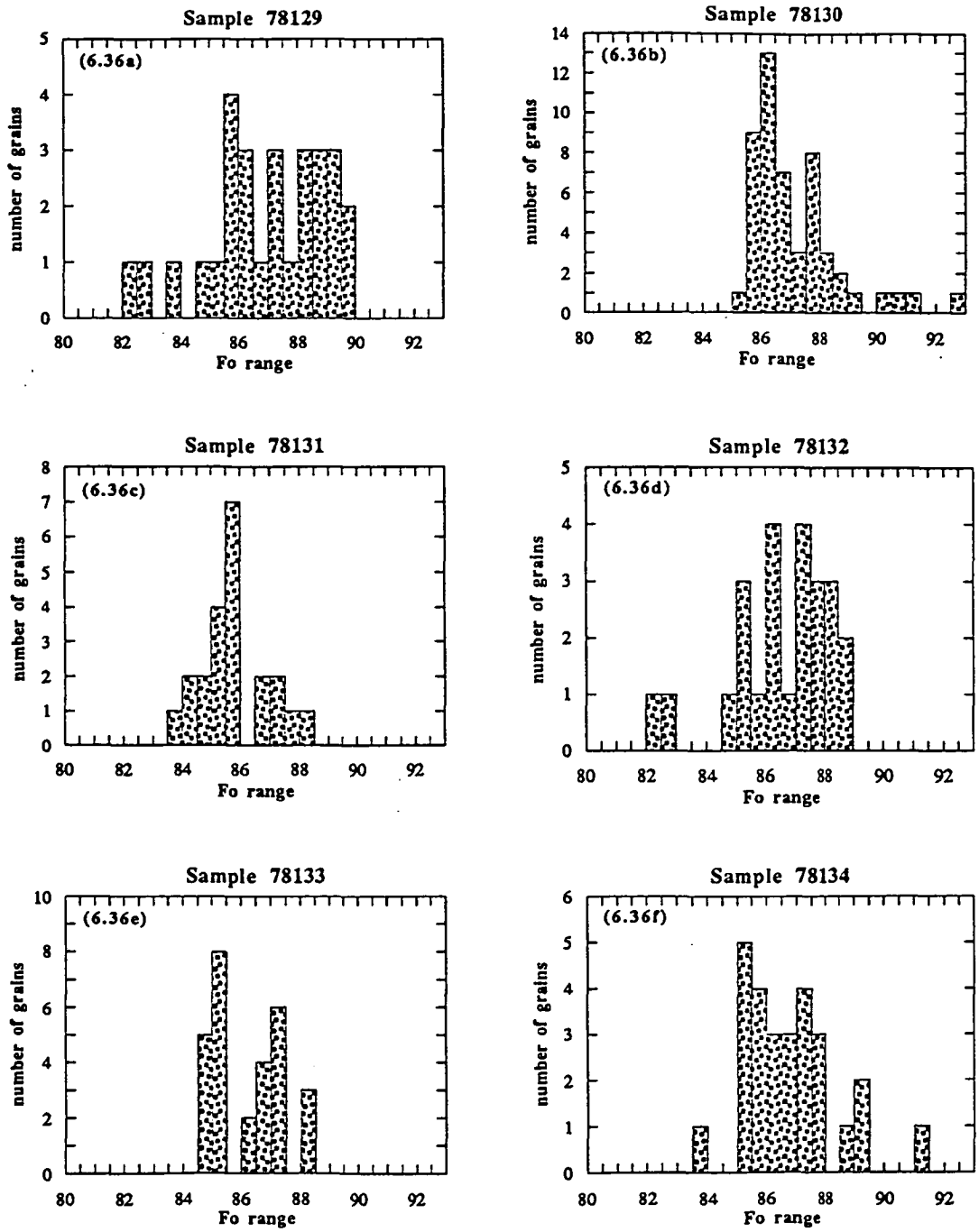

Figures 6.36a-f. Stack histograms showing the range in Fo values in olivine phenocrysts of the Bukit Mapas basalts.

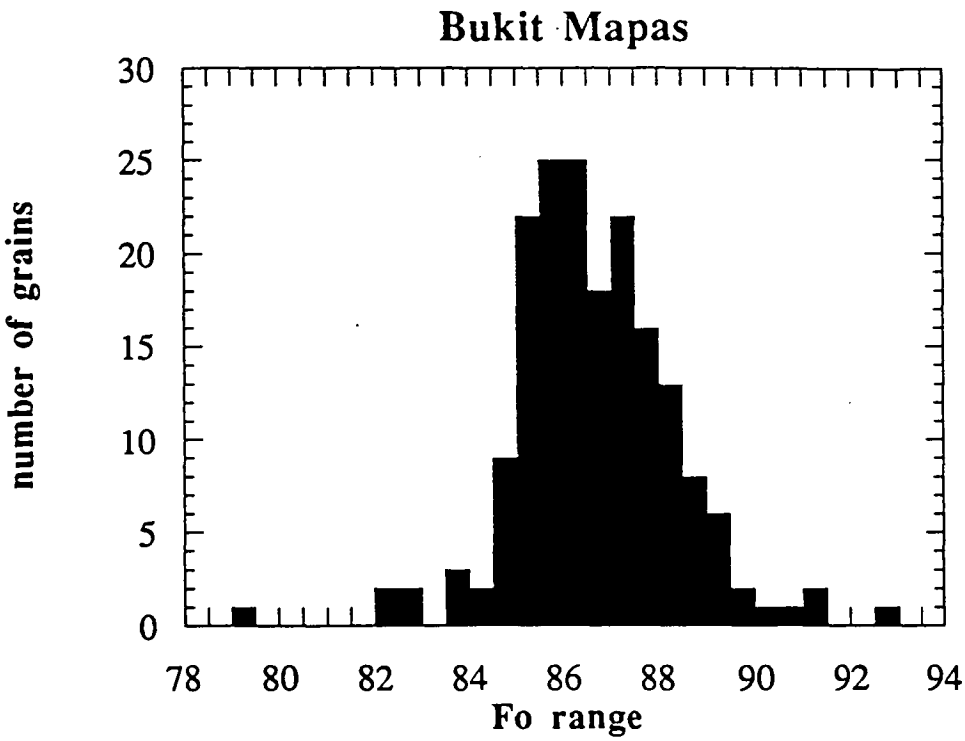

Figure 6.37. Cumulative histogram showing the range in Fo values in olivine phenocrysts of the Bukit Mapas basalts.

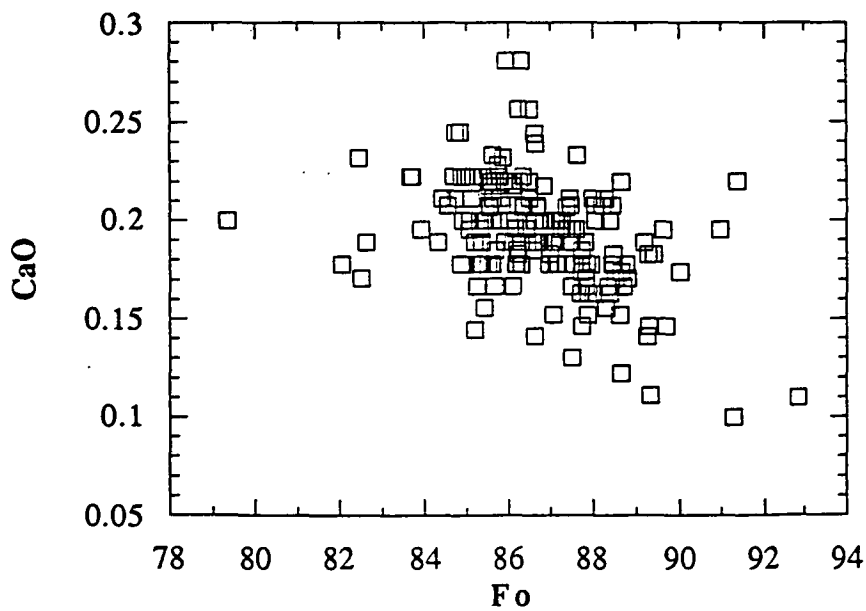

Figure 6.38. Variations of Fo values versus CaO content in olivine phenocrysts of the Bukit Mapas basalts.

3) Based on their Al_2O_3 contents, three different groups of spinel inclusions were recognised: Al-spinel (Al_2O_3 > 50%), Cr-spinel (Al_2O_3 < 25%), and spinel with intermediate Al-Cr composition (Al-Cr spinel) (Figure 6.39). These correspond respectively to a Cr# of 0-10, 50-80, and 10-25 mol%, and to a Mg# of 70-90, 40-65, and 60-70 mol% (Figures 6.40 and 6.41). This relationship between Cr# and Mg# is consistent with that described by Dick & Bullen (1984).

4) Al- and Cr-spinel inclusions are associated with host olivine phenocrysts with Fo 92-82. There is a strong positive correlation between Fo in the host olivine and Mg# in the spinel (Figure 6.41), and the NiO content in the host olivine is also strongly positively correlated with the Mg# in the spinel within each group (Figure 6.42), and the host olivines for the Al- and Cr-spinel have the same range of NiO values (0.05-0.40 wt%). Al-Cr spinel is restricted to a host olivine composition of Fo 86.5-85. Minor element contents in host olivines (Mn, Ca, Ni, and Cr) are not correlated to the type of spinel inclusion.

5) Cr-spinel inclusions have systematically higher Fe^{2+}/Fe^{3+} (Figure 6.43) and TiO_2 (Figure 6.44) values compared with Al-spinel inclusions, and within each of the two groups there is a negative correlation between Mg# and TiO_2. Spinel solid inclusions in high-Mg olivines (Fo > 89) have low TiO_2 (0.2 to 0.4%), high Mg# (approximately 0.62 to 0.63) and high Cr# (0.75 to 0.85).

6) Spinel solid inclusions in olivine phenocrysts have the same composition as spinels in melt inclusions, and follow the same crystallisation trends. The only difference is that the olivine phenocrysts in which melt inclusions contain Al-spinels include the more magnesian olivines (Fo 91-85), whereas the Al-spinel solid inclusions are restricted to olivines with Fo contents in the range 86.5-83.

7) Clinopyroxene inclusions in olivine (Figures 6.45a-c), whether solid inclusions or crystals in melt inclusions, have a very wide compositional range, with exceptionally high Al_2O_3 (up to 15%) contents, complementary to SiO_2 contents as low as 40%. Clinopyroxene solid inclusions have the same composition as the phenocrysts in the rock, and are overall more magnesian than those found in the melt inclusions. Clinopyroxene crystals in the melt inclusions are similar to those described by Arculus (1978) and Romick et al. (1990).

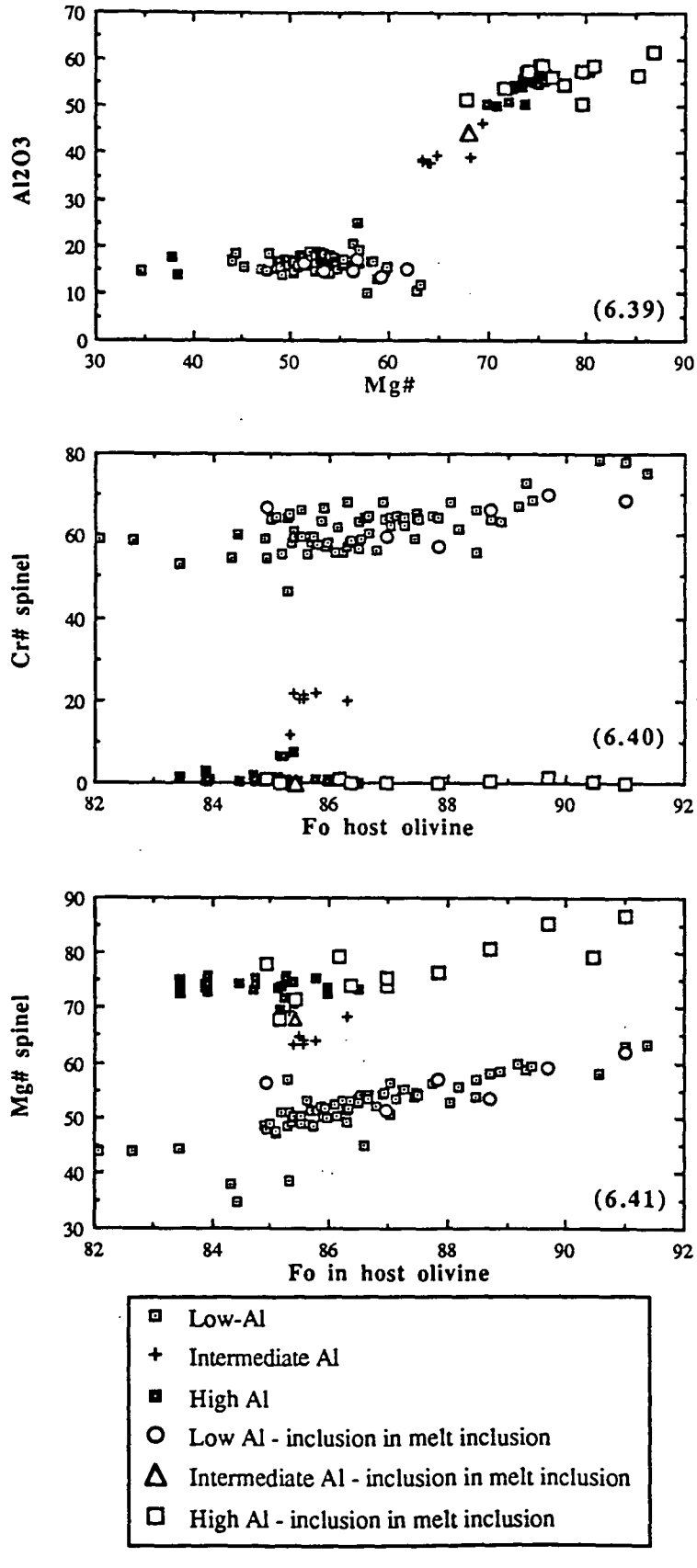

Figures 6.39, 6.40, and 6.41. Compositional variations in spinel inclusions in olivine phenocrysts in basaltic andesites of Bukit Mapas. Figure 6.39 - Mg# [$Mg^{2+}/(Mg^{2+} + Fe^{2+})$] value in spinel inclusion versus Al_2O_3 content in spinel inclusion; Figure 6.40 - Fo [$Mg^{2+}/(Mg^{2+} + Fe^{2+})$] value in host olivine versus Cr# [Cr/(Cr + Al)] value in spinel inclusion; Figure 6.41 - Fo [$Mg^{2+}/(Mg^{2+} + Fe^{2+})$] value in host olivine versus Mg# [$Mg^{2+}/(Mg^{2+} + Fe^{2+})$] value in spinel inclusion. Same symbols for all the diagrams.

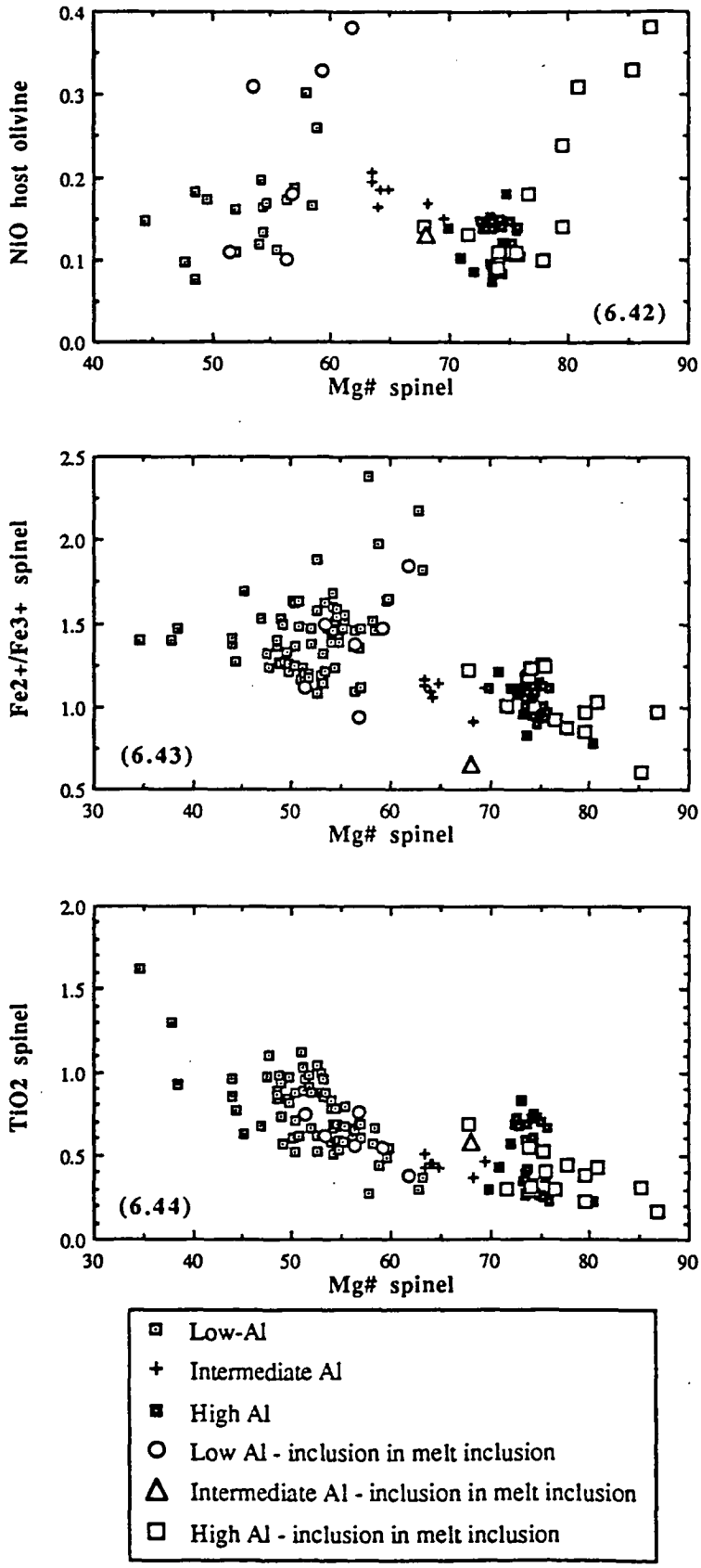

Figures 6.42, 6.43, and 6.44. Compositional variations in spinel inclusions in olivine phenocrysts in basaltic andesites of Bukit Mapas. Figure 6.42 - Mg# [$Mg^{2+}/(Mg^{2+} + Fe^{2+})$] value in spinel inclusion versus NiO content in host olivine; Figure 6.43 - Mg# [$Mg^{2+}/(Mg^{2+} + Fe^{2+})$] value in spinel inclusion versus Fe^{2+}/Fe^{3+} value in spinel inclusion; Figure 6.44 - Mg# [$Mg^{2+}/(Mg^{2+} + Fe^{2+})$] value in spinel inclusion versus TiO_2 content in spinel inclusion. Same symbols for all the diagrams.

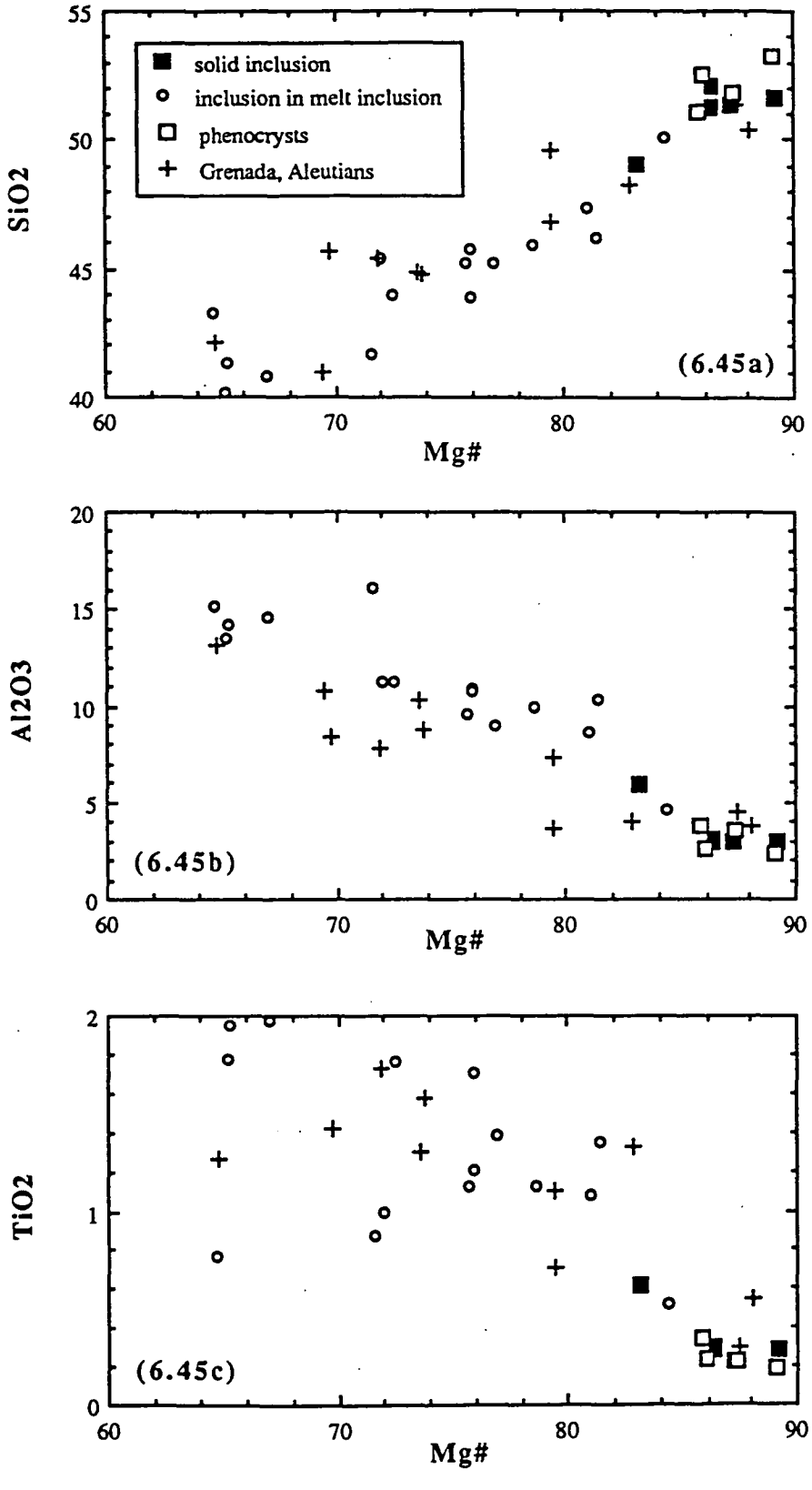

Figures 6.45a-c. Variations of Mg# [$Mg^{2+}/(Mg^{2+} + Fe^{2+})$] values versus SiO_2 (Figure 6.45a), Al_2O_3 (Figure 6.45b), and TiO_2 (Figure 6.45c) contents in clinopyroxene phenocrysts, clinopyroxene inclusions in olivine phenocrysts, and clinopyroxene inclusions in melt inclusions in olivine phenocrysts in basaltic andesites of Bukit Mapas. Clinopyroxene inclusions in olivine phenocrysts in rocks from Grenada and the Aleutians are respectively from Arculus (1978) and Romick et al. (1990).

8) Al-spinels were found in all the melt inclusions, and did not melt during the heating experiments. The measured temperature of homogenisation (Table 6.6) was always very high (about 1250 °C), and the recalculated composition of the melt inclusion is rather unusual, with very low SiO_2 and high CaO and Mg#, and notably different from the typical andesitic whole-rock composition (Figures 6.35a-j).

6.9.4 Kalimantan

Only one sample among those from central Kalimantan, 75426 (belonging to group 2 as defined in a previous paragraph) was suitable for olivine-spinel pairs study.

In this sample, olivine phenocrysts are euhedral, and range in size from usually 0.5 up to 1 mm. Euhedral Cr-spinel inclusions, up to 50 μm but usually 10 to 30 μm across, are abundant in the olivine phenocrysts. Primary and secondary melt and fluid inclusions are common, but primary melt inclusions are unsuitable for melt inclusions study (too small or opened by secondary cracks in the host olivine).

The compositional distribution of olivine phenocrysts is unimodal, with Fo values in the range 79 ± 1 (Figure 6.22b), much lower than in Sukadana and Bukit Mapas. Spinel inclusions (Figures 6.26 to 6.34) also have low Mg# values (0.45 to 0.35) and Al_2O_3 contents (20 to 15%), and follow the trend of the low-Ti spinels from Sukadana. TiO_2 values are also similar to those in the most evolved samples of the low-Ti group in Sukadana. However, Fe^{2+}/Fe^{3+} values are lower than those of spinel inclusions in Sukadana and fairly constant (1.35 ± 0.15).

6.9.5 Olivine phenocrysts and spinel inclusions in olivine phenocrysts in "typical", relatively primitive volcanics from the Sunda arc : data from the Sumatran volcanoes and Galunggung (West Jawa)

The distinctive compositions of the spinels in the volcanic rocks described here from Sukadana, Kalimantan and Bukit Mapas are most easily displayed by comparing them with examples of spinels from other better-known magmatic associations. However, only relatively few analyses of spinels from arc volcanics have been published, reflecting the scarcity of relatively primitive arc rocks.

Data from the Sunda arc are particularly scarce, and come mainly from relatively evolved rocks (Wheller 1986), or from high-K volcanics and coarse-grained ultramafic and mafic xenoliths (Foden 1979; F.N. Della Pasqua, U. Hartono, V.S.

Kamenetsky, pers. comm. 1993). An exception is Galunggung in West Jawa, a calcalkaline volcano which in 1982-83 erupted volcanics with compositions ranging from "typical" continental-arc andesite to primitive, olivine-rich high-Mg basalts containing abundant Cr-spinels, recently studied in detail by Gerbe (1989), Gerbe et al. (1992), and Harmon & Gerbe (1992). From the similarities between the andesites of the Sumatran volcanoes and those of Galunggung, it might be assumed that the abundant Cr-spinels in the primitive basalts of Galunggung could reflect the composition of the parental melt in the continental-arc sector of the Sunda arc.

Olivine-spinel pairs in all the available, sufficiently olivine-phyric, samples from the Sumatran arc have been analysed during this study, and a brief petrographic description, and major and trace element, isotope, and mineral chemistry data for the samples of Sumatran arc volcanics and for Galunggung are reported in Appendices C and F.

6.9.5.1 Galunggung

The only sample from Galunggung analysed during this study, which was collected from a large bomb on the crater rim, is petrographically and geochemically indistinguishable (Appendix C) from the 1982-83 basalts reported by Gerbe (1992); in fact, this sample alone shows the whole compositional range of the mineral phases described in that study for a rather large number of samples.

Most olivine phenocrysts have Fo values in the range 90 to 87, but crystals with Fo as low as 70, typical of basaltic andesites, also occur (Figure 6.22d). The olivine phenocrysts are euhedral, 0.5 to 1 mm, with abundant Cr-spinel inclusions (10 to 30 μm) and small melt inclusions (usually less than 10 μm). In Fo-poor olivines, melt inclusions are more abundant, and titanomagnetite (not analysed) is the only solid inclusion. In one grain (analysis # 51; Fo 77) some sulphide globules were found; these were too small to be analysed (less than 3 μm), but an EDS scan revealed only peaks for S and Fe.

Cr-spinel in the most magnesian olivines (Fo 90-85) have high Mg# and Cr# (Figures 6.26 and 6.29), like the Cr-spinels in Bukit Mapas. Other element distributions in spinel inclusions in Galunggung also resemble Bukit Mapas (Figures 6.27, 6.28, and 6.30 to 6.33), and the two localities only seem to differ in their Fe^{2+}/Fe^{3+} values (Figure 6.34), which are slightly higher in Galunggung and similar to the low-Ti basalts from Sukadana.

6.9.5.2 Sumatran arc

Only seven samples among those collected in the Sumatran arc were rich enough in olivine crystals for a mineral chemistry study (Figure 6.22c). 75333 is a mafic block in an andesitic breccia, and 75300 is a small andesitic flow in a tuffaceous deposit. The other samples were collected as loose blocks and are presumably from lava flows (75237 and 75384), blocks (75273), and scoriaceous lava flows (75267 and 75284). Chemical analyses are reported in Appendix C.

Olivine phenocrysts in 75267 and 75273 are small (respectively up to 0.8 mm and less than 0.5 mm), rare, and have very low Fo values (75 to 65), with rare titanomagnetite inclusions (respectively up to 50 μm and 20-30 μm). 75237 has small (up to 0.5 mm), more magnesian olivines (Fo 84 to 76), very rare and small (less than 10 μm) titanomagnetite inclusions. No Cr-spinel inclusions suitable for analysis were found in these three samples, and all the olivine phenocrysts have slightly altered rims, and abundant cracks and secondary melt and fluid inclusions.

Olivines in 75284 and 75384 are euhedral, slightly bigger (respectively 0.5 to 1 mm, and 0.5 to 0.7 mm) than those of samples 75267, 75273, and 75237 , but with very rare Cr-spinel (20 to 30 μm across) and melt (up to 50 μm across) inclusions, and very abundant secondary melt inclusions. Fo values of olivines from 75284 range from 86 to 74, and no Cr-spinels were found in olivines with Fo < 80. In 75384 the olivines are less magnesian, with Fo in the range 82 to 77.

Olivine phenocrysts in 75333 range in composition from Fo 91 to Fo 77, and the grains, 0.7 to 1 mm across, have altered rims and are cloudy because of the secondary inclusions and cracks. Spinel inclusions (20-40 μm across) are very rare.

75300 is the only among the samples from the Sumatran arc with clear, fresh magnesian (Fo 89 to 84, mainly 86 ± 1) olivine crystals (0.5 to 1 mm) and abundant (up to more than a hundred in some grains), small (usually less than 20 μm across) Cr-spinel inclusions, and rare, small (less than 20 μm across) melt inclusions.

The composition of the spinel inclusions in olivines covers a very large compositional range. With the exception of 75333, Mg# values show the same positive correlation with Fo in the host olivine (Figure 6.26) and are in the range 0.68-0.54 (75300), 0.61-0.56 (75284) 0.53-0.44 (75384); MgO and FeO values vary accordingly (Figures 6.27 and 6.28). Interestingly, these spinels follow the trends of the low-Ti

spinels of low-Ti basalts in Sukadana, and not the trend of other arc rocks (Bukit Mapas, Galunggung). Al_2O_3 contents and Cr# values (Figures 6.30, 6.31, and 6.29) of spinels are more variable: 75284 and 75300 still follow the trend of the low-Ti spinels of low-Ti basalts in Sukadana, whereas 75384 has higher Al_2O_3 and FeO contents, and therefore lower Cr# values. A lower FeO content in 75384 is complementary to a lower Fe^{2+}/Fe^{3+} value; on the other hand, 75284 and 75300 have Fe^{2+}/Fe^{3+} values intermediate between those of the Sukadana and the Bukit Mapas spinels (Figure 6.34).

However, despite the similarities with the low-Ti spinels of the low-Ti basalts in Sukadana, TiO_2 contents in 75300 (Figures 6.32 and 6.33) are as low as in Bukit Mapas and Galunggung, and just slightly higher in 75284. TiO_2 contents in spinels in 75384 range from approximately 1 to 2%, but the high TiO_2 contents in this sample are due to crystal fractionation (note the low Mg# value of the spinel and the low Fo content of the host olivine) and do not represent the TiO_2 content of the primary melt.

Spinel inclusions in 75333 have a rather unusual composition, being strongly depleted in MgO and Al_2O_3, and also slightly depleted in FeO, and therefore having Mg# and Cr# respectively lower and higher than any other samples of this study, and MgO, FeO and Al_2O_3 contents similar to those of some spinels in Bukit Mapas and 75359, but higher Fe^{2+}/Fe^{3+} values. TiO_2 contents range from values similar to those of spinel inclusions in the most magnesian olivines in arc rocks of Sumatra, to slightly higher values for the most evolved samples.

6.9.6 Spinel in volcanic rocks as an indicator of their tectonic environment

Arai (1992) collected a large number of data from the literature and proposed a spinel classification diagram based on the TiO_2 contents and Fe^{3+}# [= $Fe^{3+}/(Cr + Al + Fe^{3+})$] values in spinel, and showed that such a classification based on the composition of spinel inclusions can successfully distinguish arc basalts from OIB and MORB (Figure 6.46). In addition, it will be shown here that the TiO_2 and Al_2O_3 content in spinels (Figure 6.47) can also help in the discrimination of their original tectonic setting.

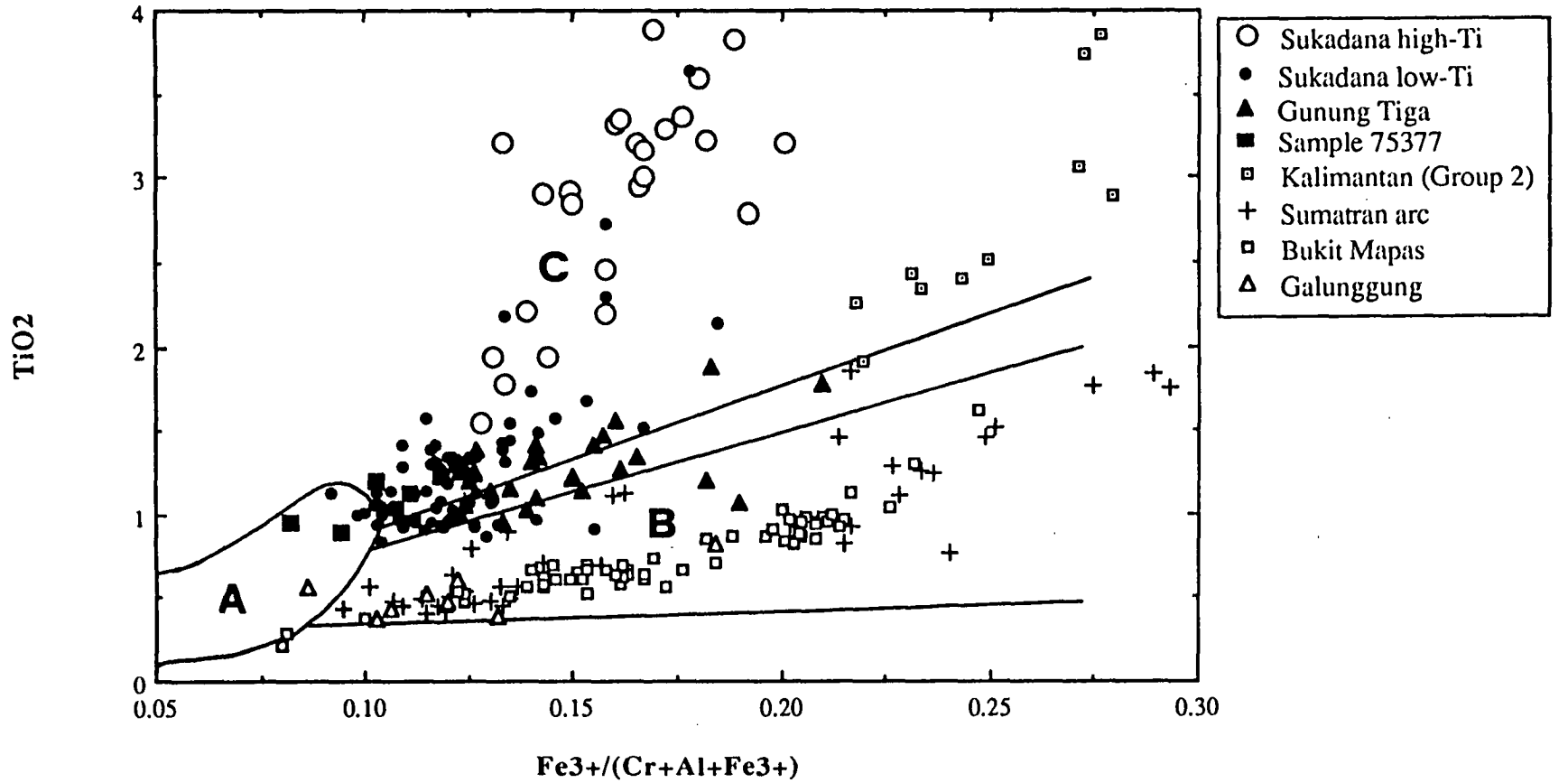

Figure 6.46. Classification diagram for spinels of different tectonic environments (Arai 1992). Fields are: A - spinels of MORB; B - spinels of arc environments; C - spinels of intra-plate basalts. Data sources for the definition of the fields are listed in Arai (1992).

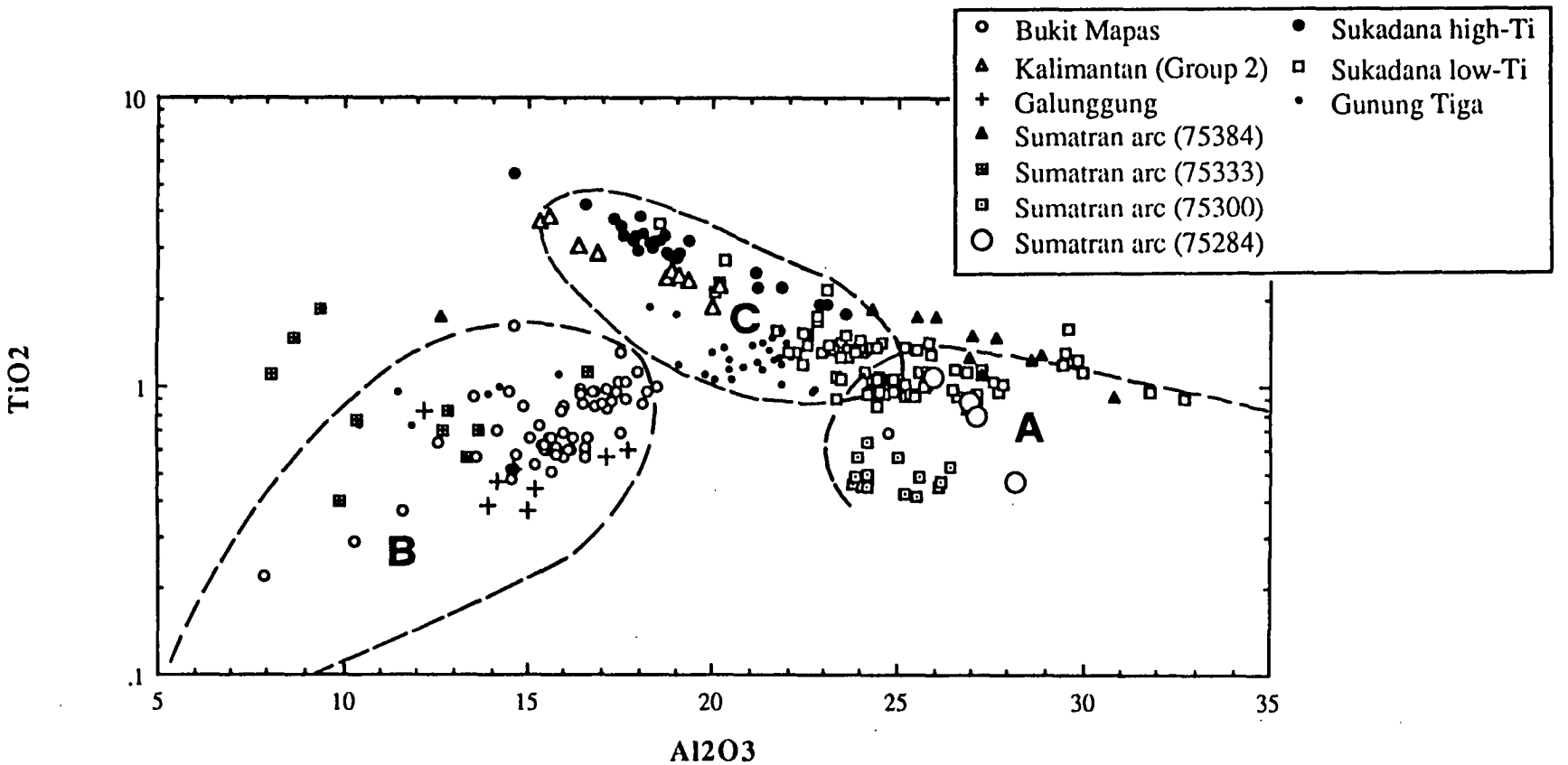

Figure 6.47. Diagram showing the variations of Al_2O_3 content versus TiO_2 content in spinel inclusions, used as a classification diagram. Fields are: A - spinels of MORB; B - spinels of arc environments; C - spinels of intra-plate basalts. The fields were defined using mainly unpublished data (V.S. Kamenetsky, I.A. Sigurdsson, U. Hartono, S.Eggins pers. comm.) from several localities, including Christmas Island, Hawaii, Hunter Ridge and Hunter Fracture zone, FAMOUS area, Greenland, Macquarie Island, central Jawa, Lau Basin, Kamchatka, Vanuatu

As pointed out by Scowen et al. (1991), spinel inclusions in olivine can change their original composition by interaction with the host olivine in particular circumstances, but the TiO_2 content is not affected by such secondary reactions because of the very low diffusivity of Ti in olivine. Al also has a relatively low (lower than Mg and Fe^{2+}, but higher than Ti) diffusivity in olivine, and Al_2O_3 should be a sufficiently reliable indicator of the original composition in cases where the original fO_2 conditions have been modified by secondary processes (variations in fO_2 would strongly affect the Fe^{3+}# parameter used by Arai 1992).

Despite all the differences observed in the previous diagrams, most spinel inclusions in volcanics from the Sumatran arc, Galunggung and Bukit Mapas fall within the field of spinels of arc rocks defined by Arai (1992), and only a few spinels of 75284 and 75333 plot at the boundary between the field of arc spinels and that of intraplate spinels. Apart from these exceptions, all the arc spinels studied here follow a single trend from low-Ti and low-Fe^{3+}# primitive (high-Mg and high-Fo in the host olivine) spinels to higher Ti and Fe^{3+}# values for the most evolved spinels. The low-Ti and low-Al, high-Mg spinels found in olivines with Fo > 90 have a very low Fe^{3+}# value, and plot at the boundary with the field of MORB spinels.

On the other hand, almost all the spinels in Sukadana and Kalimantan (group 2) basalts plot within the field of intraplate spinels. The spinels of 75377, the basalt with the highest Mg# in the low-Ti basalt group in Sukadana, have the lowest Fe^{3+}# values, and some fall within the field of MORB spinels. The other spinels of the low-Ti group of Sukadana define a positive TiO_2/Fe^{3+}# trend with a slope similar to that of the arc spinels, but with higher TiO_2 values, and reaching the highest TiO_2 and Fe^{3+}# values in the most evolved spinels in Kalimantan. Spinels in olivines of Gunung Tiga, with the exception of those of sample 75359, follow the same trend but have higher TiO_2 and Fe^{3+}# relative to their Mg# and to the Fo of the host olivine, and some of them fall within the field of arc spinels. 75359 has the same TiO_2 content as the other samples from Gunung Tiga, but has very high Fe^{3+}# values (0.35 to 0.50, out of the range of the diagram), like one unusual spinel analysed in sample 75384.

High-Ti spinels of high-Ti basalts of Sukadana also fall within the field of intraplate spinels, partially overlap the field of the low-Ti spinels for low TiO_2 and Fe^{3+}# values, and define a positive TiO_2/Fe^{3+}# correlation with a steeper slope.

In summary, not only can the TiO_2 - Fe^{3+}# diagram successfully distinguish the

spinels of arc rocks (Bukit Mapas, Galunggung, and some samples of the Sumatran arc) from those of intraplate settings (Sukadana high-Ti and low-Ti), but it can also provide some useful information about the evolution and differentiation of the spinels, since TiO_2 contents and Fe^{3+}# values are negatively correlated with the Mg# values in the spinels.

It seems that the classification diagram based on the TiO_2 and Al_2O_3 contents in spinel inclusions (Figure 6.47) is only partly successful in discriminating spinels from the various tectonic environments. Spinels of Bukit Mapas, Galunggung and 75333 still fall within the field of spinels of arc rocks, but those from the other arc rocks of Sumatra (75284, 75300, 75384) plot within the field of E-MORB spinels, and partially overlap the field of the low-Ti spinels of low-Ti basalts from Sukadana, which plot at the boundary between the E-MORB and OIB fields. As in the other classification diagram, spinels of 75377 are those among the spinels of low-Ti basalts with the strongest MORB "affinity". Spinels of Kalimantan and high-Ti basalts of Sukadana fall within the field of OIB spinels and partially overlap with the low-Ti spinels. Interestingly, the low-Ti and high-Ti spinels of Sukadana define negative TiO_2 - Al_2O_3 correlations (with a steeper slope for the high-Ti spinels), whereas the arc spinels (Bukit Mapas, Galunggung) have a strong positive TiO_2 - Al_2O_3 correlation. Spinels from Gunung Tiga have lower Al_2O_3 and seem to trend towards the field of the arc spinels, with 75359 definitely plotting within it.

In summary, and despite its apparent limitations as a classification diagram, the TiO_2 - Al_2O_3 diagram can provide useful information about the origin and differentiation of Cr-spinels in different tectonic environments, the significance of which will be investigated in the following discussion.

6.10 Discussion

6.10.1 Bukit Mapas

Major and trace element, mineral chemistry, petrography, and Sr, Nd, and Pb isotope data, all indicate that the basaltic andesites of Bukit Mapas are indistinguishable from the other calcalkaline rocks of the Quaternary Sumatran arc, and are unrelated to the intra-plate basalts of Bukit Telor and Sukadana. However, despite their affinities with the arc andesites, the basaltic andesites of Bukit Mapas are characterised by having unusually abundant high-MgO olivines, and by the occurrence in the olivines of Al-

spinel as well as Cr-spinel inclusions.

Primitive basalts with very MgO-rich olivines and Cr-spinels similar to those of Bukit Mapas are rare in the west Sunda arc, possibly because they are erupted only during the last stage of very long magmatic eruptions (Gerbe et al. 1992). However, olivines with Cr-spinel inclusions similar to those of Bukit Mapas have been found elsewhere in primitive basalts in Indonesia, and have been described in some detail from Galunggung (Gerbe et al. 1992; this study). As in Bukit Mapas, where both the mineral chemistry of spinel inclusions in olivine, and the whole-rock chemistry indicate an arc affinity, these other Indonesian basalts also seem to be genetically related to the more abundant arc andesites and dacites. However, unlike Galunggung, where the chemical variations observed from basalts to andesites are believed to be a result of crystal fractionation and magma mixing within the magma chamber (Gerbe et al. 1992), the basaltic andesites of Bukit Mapas show textural evidence for crustal contamination.

Forsteritic olivines with inclusions of Cr-spinel and Al-spinel have also been described from tholeiites and ankaramites in Vanuatu, and high-K shoshonitic ankaramites of the Ulakan Formation in Bali (Della Pasqua et al. submitted for publication), and have been reported from several localities in other arcs (see Della Pasqua et al. submitted for publication, for a review). The peculiarity of the olivines in Bukit Mapas is that their Fo content is in disequilibrium with the host rock, suggesting that the olivines have a xenocrystal origin. Other textural evidence for complex mixing/assimilation processes includes the occurrence of fragments of quartz, magnetite, and strongly resorbed plagioclase (bytownite) crystals. Further evidence for disequilibrium is the coexistence of Cr- and Al-spinel inclusions in olivine, and the difference in composition between melt inclusions in olivine phenocrysts and host rock.

These forsteritic olivines in basaltic andesites may have crystallised from a primitive magma which later mixed with more evolved melts from the same batch within the magma chamber, and were then brought to the surface during the eruption.

In Bukit Mapas it seems that two different episodes of magma mixing were involved: the first is responsible for the formation of the high-Al spinel and operated during the early stages of the crystallisation; the second, which seems to be a very common process, given the similarity in major and trace elements between the Bukit Mapas rocks and most basaltic andesites in the Sumatran arc, affected the melt at a much

later stage of its evolution.

The origin of the rare high-Al spinel inclusions in Bukit Mapas volcanics is problematic. Possible explanations for the origin of high-Al spinels include 1) a xenocrystal origin (assimilation of material containing crystals of Al-rich spinel - e.g. Arculus 1978), 2) a product of exsolution or breakdown of Al-bearing minerals (e.g. plagioclase, Al-pyroxene, garnet) and trapping of these phases by olivine crystals (e.g. Weibe 1986; Obata 1980; Griffin et al. 1984), 3) crystallisation at high pressure and later trapping at lower pressure (e.g. Irvine 1967; Fisk & Bence 1980), and 4) breakdown of amphibole inclusions in olivine (e.g. Lykins & Jenkins 1992). Finally, if the existence of high-Al spinel is to be explained by direct crystallisation from an Al-rich melt then we have to assume that "pockets" of high-Al melt coexisted in the magma chamber with "normal" Cr-bearing melt, because co-crystallisation of high-Al and high-Cr spinel from the same melt does not seem to be possible (e.g. Maurel & Maurel 1982), despite their coexistence in, for example, volcanics from Bukit Mapas.

Textural evidence led Della Pasqua et al. (submitted for publication) to believe that processes 1), 2), and 3) are unlikely explanations for the occurrence of high-Al spinels in Bukit Mapas, and a magmatic origin was suggested. However, it is not clear whether the high-Al melt from which these spinels crystallised was produced by assimilation of crustal Al-rich material (probably lower crustal gabbroic xenoliths) or assimilation of amphibole-rich cumulates in the magma chamber.

It is notable that olivine crystals of Bukit Mapas have high, mantle-like $^{3}He/^{4}He$ values, approximately R/RA 7.8 ± 0.7 (D. Hilton, pers. comm.), within the range also observed in Sukadana, Bukit Telor, and Bali (Hilton & Craig 1989; D. Hilton, pers. comm.), and yet, as in Galunggung, the chemical composition of spinel inclusions and whole-rock Sr, Nd, and Pb isotopes indicate an arc affinity for these rocks. If both the composition of spinel inclusions in primitive olivines and the $^{3}He/^{4}He$ values in primitive olivines reflect the composition of their mantle source, then these data suggest that an apparently rather homogeneous source in terms of He isotopes is capable of generating melts with arc and intraplate affinities, in other words that an arc and an intraplate source cannot be distinguished, in the west Sunda arc, using He isotopes.

Despite the similarities in $^{3}He/^{4}He$ in olivine phenocrysts in arc and intra-plate rocks, the host rock have different Sr, Nd, and Pb isotopic values. According to Hilton et al. (1992; 1993) a possible explanation for the decoupling observed between He and

other isotope systematics is that subducted sediments lose their He before entering the subduction zone or during the early stages of the subduction, whereas Sr and other elements are efficiently carried down to the depth of generation of arc magmas. Not only this conclusion is questionable (see discussion in Chapter 5), but also it was shown in Chapter 5 that mantle source contamination by sediments, a process which, according to Hilton et al. (1992; 1993) would produce a Sr, Nd, and Pb arc signature in the arc rocks leaving the He isotope signature of the source unchanged, does not satisfactorily account for the Sr, Nd, and Pb isotopic values observed in the Sumatran and west Jawanese rocks.

An alternative explanation for the decoupling between He and Sr-Nd-Pb isotopes in arc rocks can be deduced from the results of Hilton et al. (1993), who observed increasingly lower $^3He/^4He$ values for more evolved glasses in the Lau Basin, and explained these variations as the result of increasing assimilation of crustal material by the more evolved rocks.

It should also be noted that the negative correlation between SiO_2 and $^3He/^4He$ values observed by Hilton et al. (1993) in the Lau Basin is consistent with the positive correlation between SiO_2 and B/Be values observed in the Sunda arc and discussed in Chapter 5.

Because the olivines in Bukit Mapas are forsteritic, they may represent the first products of crystallisation of a melt which had just been emplaced in the magma chamber and had had little or no interaction with the surrounding crust. Increasingly SiO_2-rich melts could have evolved from this magma within the magmatic chamber while it was crystallising. The heat released by the hot magma (the temperature of homogenisation of melt inclusions was determined experimentally, and estimated to be approximately 1250 ± 50 °C - see Table 6.6) during the crystallisation may have been sufficient to partially melt the host rock, and this assimilation may have caused an increase in Sr and Pb and decrease in Nd and He isotopic ratios. Only the very first-formed and most primitive crystals (olivine phenocrysts) were not affected by crustal contamination, and these are the crystals from which He was extracted and its isotopic ratios measured, whereas Sr, Nd, and Pb isotopic ratios are measured on the geochemically and isotopically evolved whole-rock.

If this process occurred, then only the most primitive olivine phenocrysts would retain their original $^3He/^4He$ signature (unless their He content and isotopic composition re-equilibrate with those of the melt: see Trull & Kurz 1993), because

the assimilation would be very efficient, especially during the first stages of the crystallisation, due to the high temperature of the magma and the large amounts of heat released during crystallisation. More evolved olivines will later crystallise from this contaminated melt and any He trapped as they crystallised could have lower $^{3}He/^{4}He$ values.

It might be argued that this model can explain the decoupling between He and Sr-Nd-Pb isotopes where there is geochemical and textural evidence for crustal contamination, as in Bukit Mapas, but not in Galunggung where, according to Gerbe et al. (1992) and Harmon & Gerbe (1992) crustal contamination was insignificant. Although the lack of evidence for crustal contamination during fractionation does not imply that the magma did not suffer crustal contamination at an early stage of its evolution, the most primitive samples of Galunggung seem to have an unmodified mantle source in terms of O, He, and Th-U isotopes.

Even if the explanation proposed by Hilton et al. (1992) for the decoupling between He and Sr-Nd-Pb isotopes is accepted, it should be noted that if the presence of sediment-derived material in the source was responsible for the high $^{87}Sr/^{86}Sr$ and Pb isotopic ratios and low $^{143}Nd/^{144}Nd$ values, then the same material would have modified the O and Th-U isotope systematics. The mantle values of O, He, and Th-U isotopes in Galunggung suggest that its Sr, Nd, and Pb isotope signature is also a primary characteristic of its mantle source, implying that the mantle wedge beneath the west Sunda arc is rather homogeneous in its He isotope signature, but heterogeneous for Sr, Nd, and Pb isotopes.

6.10.2 Bukit Telor

The basalts of Bukit Telor closely resemble transitional alkaline basalts from east Australia and Kerguelen (see also McDonough et al. 1985) both in their major and trace element compositions. According to calculations of Frey et al. (1978), east Australian volcanic rocks with similar compositions could be the result of partial melting (5 to 7% for olivine-nephelinite and basanite, and up to 11 to 15% for alkali olivine basalts) of a source pyrolite mantle relatively enriched in LILE and LREE (see also Ewart et al. 1988).

Green (1970) and Irving & Green (1976) suggested that basalts with Mg#>68 can be considered to be primary mantle liquids derived from an upper mantle peridotite with Mg# of approximately 88-89. Another evidence for the "primary" character of melts

is the occurrence of mantle xenoliths. Xenoliths do occur in Bukit Telor, and the high Mg# of the mineral phases in the xenoliths, and the absence of crystal, fluid, and melt inclusions, and the low CaO content in olivine phenocrysts (Simkin & Smith 1970), all indicate that these xenoliths are true mantle xenoliths.

However, it is difficult to decide whether the high Mg# in two of the basalts of Bukit Telor is a primary characteristic or a result of olivine accumulation. Trace element data show that the sample with higher MgO and olivine content (75378) also has higher incompatible trace element abundances than the olivine phenocryst-free sample (75389). However, relatively high Al_2O_3/CaO, similar to those of more evolved rocks (olivine basalts; see e.g. McDonough et al. 1985) suggest that either the melting process left residual clinopyroxene in the source, or that low pressure fractionation of clinopyroxene occurred, which would normally imply that olivine may also have crystallised and been fractionated (see discussion in Frey et al. 1978).

Interestingly, basalts from Bukit Telor do not show such pronounced LILE and LREE enrichment as was observed by Frey et al. (1978) in the east Australian basalts, nor is there textural evidence in the xenoliths for the presence of a metasomatizing fluid. In particular, LREE, Rb, and Ba are generally lower in Bukit Telor than in the east Australian volcanics, and LILE/HFSE and LREE/HFSE values are either similar or lower than those of typical OIB (Table 6.3).

In summary, the olivine phenocryst-free basalt from Bukit Telor (sample 75389) has major and trace element chemistry similar to olivine basalts from the Newer Volcanic Province (McDonough et al. 1985), and the relatively low Mg# and high Al_2O_3/CaO suggest that fractionation of clinopyroxene and olivine occurred. Frey et al. (1978) estimated that approximately 13 to 17% melting of a mantle-derived parental magma that fractionated 10% olivine can produce similar liquids (cf. sample 2152 in Frey et al. 1978).

On the other hand, the olivine-rich samples from Bukit Telor are unlikely to represent primary melts, despite their relatively high Mg#, and probably have fractionated clinopyroxene and accumulated olivine. However, trace element abundances and the presence of mantle xenoliths suggest that these rocks are relatively primitive. Based on the study of Frey et al. (1978), basalts in east Australia similar to those of Bukit Telor can be produced by lower degrees of melting of the same source that produced the east Australian olivine tholeiites.

Despite minor variations in degrees of partial melting and crystal fractionation, these basalts have overall major and trace element content and "immobile" and "mobile" element relative abundances typical of OIB, and do not bear any textural nor geochemical evidence for lithospheric contamination. Therefore it can be concluded that the Sr, Nd, Pb, and He isotopes signature of these rocks is representative of their mantle source.

6.10.3 Sukadana high-Ti basalt

Like the basalts of Bukit Telor, the high-Ti basalts of Sukadana have major and trace element composition typical of intra-plate basalts, and closely resemble similarly evolved rocks from Kerguelen and east Australia. This conclusion is also supported by mineral chemistry data, as spinel inclusions in olivines of Sukadana high-Ti basalts were shown to have typical intra-plate composition.

An interesting feature of these basalts, already noted for Bukit Telor, is their depletion in LREE compared with other intra-plate rocks at similar Mg#. In fact, compared with olivine tholeiites in east Australia and the South China Sea, high-Ti basalts of Sukadana have similar HFSE and lower LREE and LILE contents, resulting in relatively lower LILE/HFSE and LREE/HFSE values (Table 6.3). As for Bukit Telor, the low LREE and LILE values suggest that the "enrichment" or "metasomatizing" process believed to have affected the east Australian and South China Sea basalts (Frey et al. 1978; Flower et al. 1992; Tu et al. 1992) did not modify the source of the Sukadana basalts, despite the fact that an active subduction zone exists beneath the Sukadana basalts. However, irrespective of their lack of LILE and LREE enrichment, the Sukadana basalts have relatively high Th/Ce values (Figure 6.48) and Ba contents, indicative of a EM-type OIB (e.g. Saunders et al. 1988; Weaver 1991).

Not only are LILE/HFSE and LREE/HFSE values lower than in basalts believed to derive from "metasomatised" mantle sources, but they are also slightly lower than "typical" OIB values (Table 6.3). In other words, the high-Ti Sukadana basalts seem to be relatively depleted in LILE and LREE compared with other intra-plate basalts not associated with arc volcanism, and the LILE and LREE depletion in the Sukadana (and Bukit Telor) basalts mirror the LILE and LREE enrichment and HFSE depletion in arc rocks, and a slight enrichment in HFSE in Sukadana is suggested by the relatively high (compared with Hawaiian basalts with similar composition) TiO_2 contents in Cr-spinel inclusions in olivine phenocrysts.

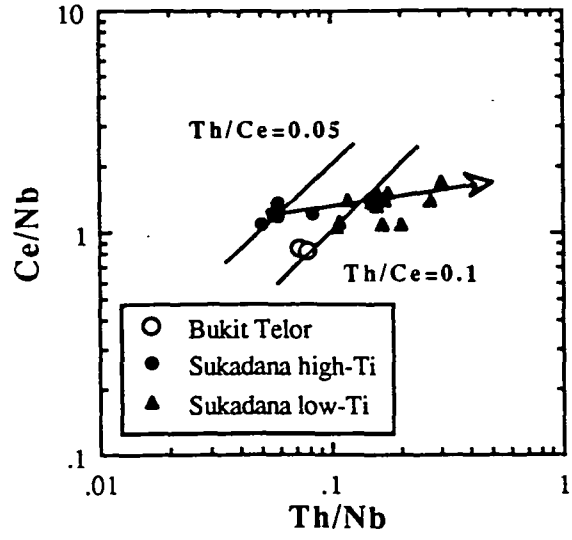

Figure 6.48. Th/Nb versus Ce/Nb diagram for basalts of Bukit Telor and Sukadana.The two subparallel lines are Th/Ce=0.05 and 0.1. The arrow indicates the trend of magmatic fractionation.

The existence of an OIB-type mantle source in arcs has been suggested by several authors to explain the major and trace element and isotopic composition of some arc volcanics (see Chapter 1), and a mantle reservoir with OIB-like, plume-related Sr, Nd, and Pb isotope systematics has been shown to exist at least in the east Sunda arc (Varne & Foden 1986; Stolz et al. 1990; Edwards et al. 1993; Wheller et al. submitted for publication). However, OIB sources are relatively enriched in HFSE compared with MORB, and, to account for the low content in HFSE in arc volcanics, the generation of arc rocks from an OIB source may require the existence of a HFSE-rich residual phase, and the existence of such a phase in an arc environment is extremely controversial (see discussion in Chapter 1).

According to Woodhead et al. (1993), melting of an OIB source would be expected to produce melts with high HFSE contents and low Ti/Zr and V/Ti, and these melts would be therefore similar to the Sukadana basalts in terms of HFSE contents, but would probably have relatively (compared with the Sukadana basalts) undepleted LILE and LREE values. However, Woodhead et al. (1993) pointed out that the parameters used in their discussion (Ti/Zr, V/Ti, and Sc/Y values versus Zr contents) cannot distinguish between different degrees of partial melting and melting of sources with different degrees of depletion, and therefore it could be expected that both an OIB and a MORB melt could be produced by a MORB source, or, conversely, that both a MORB and an OIB source can ultimately produce OIB-like melts (in terms of their HFSE contents), and that the distinction between a MORB and an OIB source loses its significance.

On the other hand, residues of the extraction of arc melts from a depleted "primitive mantle" source (i.e. a source that can produce MORB and, for lower degrees of partial melting, OIB, and which suffered previous episodes of melt extraction) can be expected to be relatively enriched in HFSE and depleted in LILE and LREE, and would have relatively high Ti/Zr and low V/Ti values. Very low degrees of melting of these residues could, in principle, reproduce the relative HFSE enrichment (Figures 6.49 to 6.52) and LILE, LREE depletion observed in the Sukadana basalts. In other words, the mantle wedge in south Sumatra could resemble a "primitive mantle" source, depleted after the extraction of MORB (first stage of depletion) melts. Partial melting of this depleted mantle source would then produce arc melts (second stage of depletion) , enriched in LILE and LREE and depleted in HFSE and with high Ti/Zr, V/Ti, and Sc/Y values, leaving a residue relatively depleted in LREE and LILE, enriched in HFSE, and with relatively low Ti/Zr, V/Ti, and Sc/Y. Small degrees of partial melting of this residue would produce a melt with relatively higher (compared to the residue itself) LILE, LREE, and HFSE concentrations, and lower Ti/Zr, V/Ti, and Sc/Y, similar to that observed in Sukadana.

The "residual" character of the high-Ti basalts source is also evident when these basalts are compared with the basalts of Bukit Telor, which are more distant from the arc and therefore can be expected to have suffered only a minor depletion: basalts of Bukit Telor have overall slightly lower LILE/HFSE values (Table 6.3). However, similar dramatic variations in LILE/HFSE and LREE/HFSE values occur in other intraplate provinces (e.g. Kerguelen, Newer Volcanic Province - Johnson 1989; Gautier et al. 1990), and discussing the East Australian basalts, Frey et al. (1978) showed that relatively small differences in the degree of partial melting of a common source can produce such differences.

According to this model, the OIB basalts of Sukadana do not need to be plume-derived, and might simply be the result of several stages of melt extraction from a depleted primitive mantle. Following this interpretation, it can be argued that both the low-Ti and the high-Ti basalts closely resemble back-arc basalts, and that their high HFSE content and low Ti/Zr, V/Ti, and Sc/Y compared with most back-arc basalts are simply due to lower degrees of partial melting, maybe as a consequence of the intracontinental setting of these rocks, compared with the intraoceanic setting of other back-arcs.

However, it is difficult to believe that the Sukadana basalts might represent lower degrees of melting in a "typical" back-arc basalts suite for at least two reasons.

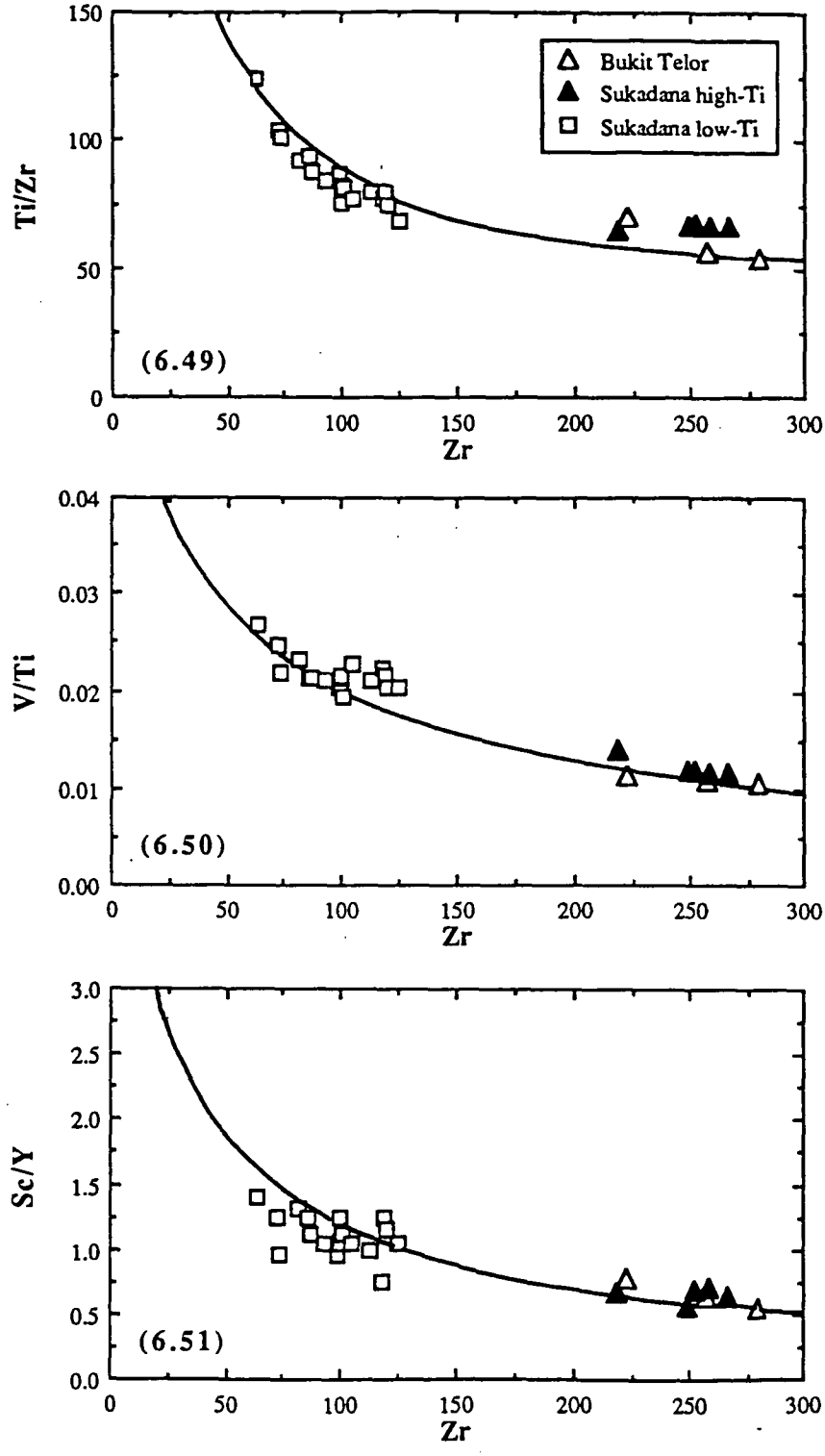

Figures 6.49, 6.50, and 6.51. Zr versus Ti/Zr (Figure 6.49), Sc/Y (Figure 6.50), and V/Ti (Figure 6.51) values of basalts of Sukadana and Bukit Telor. As Zr is strongly incompatible and more incompatible than Ti during upper mantle melting (Woodhead et al. 1993, and references therein), increasing degrees of partial melting (as it can be observed from the high-Ti to the low-Ti basalts), or melting of a more depleted source, produces low Zr contents and high Zr/Ti, V/Ti, and Sc/Y (Ti and Y are respectively more incompatible than V and Sc) values. The curve in the diagram approximates the trend of fractional melting calculated by Woodhead et al. (1993), starting from a "double"-depleted residue (see text). Note that melting of an amphibole-bearing source would produce lower Ti/Zr and higher V/Ti values (Woodhead et al. 1993), inconsistent with the values observed in Sukadana.

In Figure 6.50 the kink in V/Ti values for Zr=110 ppm might be due to the crystallization of more Ti-rich spinel in the more differentiated samples.

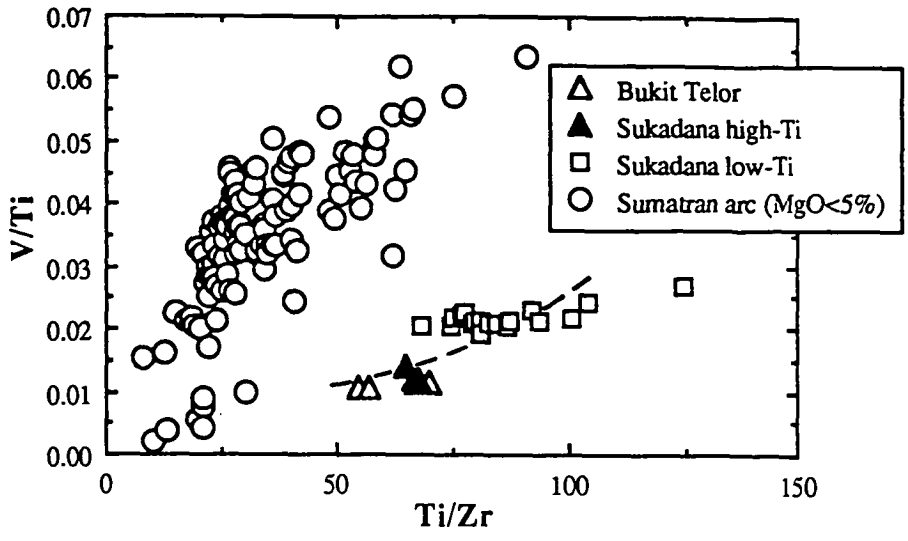

Figure 6.52. Ti/Zr versus V/Ti values of basalts of Sukadana and Bukit Telor. Residues from extraction of arc melts have Ti/Zr and V/Ti values higher than those observed in Sukadana and Bukit Telor (outside the field of the diagram), and melting of such residues will produce melts which might resemble the Sukadana and Bukit Telor basalts. However, this diagram cannot distinguish between this process and the melting of very small (5 to 1% for the low-Ti basalts, and less than 1% fot the Bukit Telor and Sukadana high-Ti basalts - broken line in the diagram) degrees of a "N-MORB source" (see Woodhead et al. 1993).

First, back-arc basalts are normally enriched in H_2O compared with MORB (e.g. Hochstaedter et al. 1990a; Muenow et al. 1990), and even when the H_2O content is low they still have characteristically high H_2O/K_2O values (e.g. Aggrey et al. 1988; Hochstaedter et al. 1990b; Danyushevsky et al. 1993). In contrast, the Sukadana basalts seem to have low H_2O contents, normally less than 0.6-0.7% in the whole-rock (values estimated assuming that L.O.I.=H_2O, and taking into account the Fe oxidation during ignition), and H_2O/K_2O values always lower than 1.

Second, while back-arc basalts normally require an additional "enriched" component in their source, the Sr, Nd, and Pb isotope signature of the high-Ti basalts of Sukadana is a characteristic of their source and has not been modified by recent fluxing from the subducted slab.

Therefore, and despite the direct and indirect evidence for the depletion of the mantle source of arc magmas (e.g. Dick & Fisher 1984; Bonatti & Michael 1989; Barsdell & Berry 1990; Maury et al. 1992), it is not clear whether only a MORB source, and not

an OIB source, can ultimately become sufficiently depleted to be the source of arc magmatism, and different models to account for the observed depletion in HFSE in arc volcanics, and which do not specifically require that the mantle source be a MORB source, have been developed (e.g. Navon & Stolper 1987; Kelemen et al. 1990).

In summary, high-Ti basalts of Sukadana have major and trace element composition similar to typical OIB, do not show the LILE and LREE enrichment observed in basalts which suffered metasomatism of their mantle source, and in fact have slightly lower LILE and LREE and higher HFSE contents compared with typical OIB. Melting of the source that produced these basalts is unlikely to produce arc magmas, but the high-Ti Sukadana basalts could represent the product of small degrees of partial melting of a residue after the extraction of arc magmas from a depleted source.

Although it is not clear whether the source of the arc magmas had a MORB or a plume-related isotopic composition, the lack of LILE and LREE enrichment suggests that the Sr, Nd, and Pb isotope characteristics of these basalts are those of their mantle source, apparently unmodified by recent (i.e. more recent than, or contemporaneous with the extraction of arc melts) metasomatic processes, and their relatively "enriched" isotope signature is consistent with their high Th/Ce values and Ba contents, indicative of a EM-type OIB, and with the existence of similar Sr, Nd, and Pb isotopic values in rocks which are not related to recent subduction/arc magmatism.

6.10.4 Origin of the low-Ti basalts (excluding Gunung Tiga)

Increasing degrees of partial melting (see e.g. Frey et al. 1978; McDonough et al. 1985; Ewart et al. 1988 for examples in east Australian rocks) of a common source will produce magmas progressively depleted in incompatible elements and with a stronger tholeiitic affinity. The effects on major elements of the variations of the degrees of partial melting for the range of compositions observed in Sukadana (transitional basalts) will be an increase in the most "compatible" (SiO_2, Al_2O_3) elements and Mg# values, and a decrease in the most "incompatible" (TiO_2, FeO, K_2O, P_2O_5, LILE, REE, HFSE) elements. In fact, spinel inclusions (representative of the composition of the melt) in low-Ti basalts have overall higher Al_2O_3 (and Mg#, as a result of their lower FeO and higher MgO contents), and lower TiO_2 than do spinel inclusions in high-Ti basalts.

The trend from OIB to E-MORB spinels in a TiO_2-Al_2O_3 diagram is therefore compatible with the compositional trend expected in spinels which have crystallised from a series of liquids derived by increasing partial melting of a common source.

The importance of the increase in the degree of partial melting as a cause for the variations observed from high-Ti to low-Ti basalts is also supported by the range in incompatible versus strongly incompatible elements (e.g. Ti/Zr, V/Ti; see Figures 6.49 to 6.52).

As suggested by the relatively low Mg# values and Cr, Ni contents, and high Al_2O_3/CaO values in high-Ti and low-Ti basalts, and by the increasing Al_2O_3/CaO values for the more evolved samples, fractionation of olivine and clinopyroxene - and also plagioclase (and possibly magnetite?) in the most evolved samples - is likely to have occurred, as it was also shown by Frey & Green (1978) for similar basalts in East Australia.

Although the analogies with quartz tholeiites and transitional basalts from east Australia and Kerguelen suggest that these rocks can be modelled as the result of increasing degrees of partial melting of a source similar to that which yielded the Sukadana high-Ti and Bukit Telor basalts, it might be argued that the low-Ti basalts are the result of mixing between an OIB melt (like the high-Ti basalts) and a MORB melt, or that they may derive from a MORB source.

The most "depleted" low-Ti basalts have LREE and LILE contents similar to E-MORB, and also have incompatible element ratios intermediate between OIB and E-MORB. Spinel inclusions in olivines in low-Ti basalts fall mostly within the field of E-MORB spinels, and define an OIB - E-MORB mixing trend with spinel inclusions in high-Ti basalts. However, all the low-Ti samples are depleted in HREE compared with MORB, and the samples with the lowest LREE values also have the lowest HREE values. The depletion in HREE is strong evidence against a MORB source for these rocks, unless the mineralogy, but not the chemical composition of the source differed from that of MORB, and mixing between OIB melts and MORB melts would produce increasingly high HREE for increasingly low LREE, contrary to what is observed.

6.10.5 Effects of crustal (vs. sediment) contamination

Although variations in trace element ratios, especially LILE/HFSE, are not definite

indicators of lithosphere contamination, and although variations in Sr, Nd, and Pb isotope values might reflect isotopic heterogeneities in the mantle source, low HFSE contents combined with high LILE/HFSE values and low $^{143}Nd/^{144}Nd$ and high $^{87}Sr/^{86}Sr$ and Pb isotopes are viewed as a reliable indication of lithosphere contamination.

An indication that the Sukadana low-Ti basalts have suffered some contamination is illustrated by their relative Th, Ta, and Hf contents in Figure 6.9, where the low-Ti basalts are clearly relatively enriched in Th compared with the high-Ti basalts and trend towards compositions typical of arc rocks. Importantly, this diagram can also distinguish between upper and lower crustal bulk contamination, as the upper crust is relatively enriched in Th, and the lower crust is overall more depleted, but relatively enriched in Ta and Hf (Taylor & McLennan 1985), although it may be expected that melts extracted from both the lower and the upper crust will be enriched in Th and depleted in Ta and Hf compared with bulk crustal material.

Based on the mixing model discussed in Chapter 5, mixing of basaltic magmas with the chemical and isotopic composition of the high-Ti basalts of Sukadana with Sumatran crustal material would produce large variations in $^{143}Nd/^{144}Nd$ but only small variations in $^{87}Sr/^{86}Sr$, due to the low Sr/Nd value of the contaminant crust (bulk crust and crustal melt) and the high Sr content of the high-Ti Sukadana basalts. In fact, compared with the low-Ti basalts, the high-Ti basalts have higher $^{143}Nd/^{144}Nd$, but similar $^{87}Sr/^{86}Sr$ values.

Crustal contamination would also increase the Pb isotopic values in the low-Ti basalts, but the low-Ti basalts have Pb isotopic values similar to, or lower than, those of the high-Ti basalts. It could be argued that low Pb isotopic values of most low-Ti basalts reflect a stronger MORB affinity, as Indian Ocean MORB have overall lower Pb isotope systematics compared with high-Ti basalts of Sukadana, but this is in contrast with 1) the depleted HREE patterns, and 2) the higher $^{87}Sr^{86}Sr$ and lower $^{143}Nd/^{144}Nd$ in the low-Ti basalts. The important point is that the variability in Sr, Nd, and Pb isotopic values is not caused by a stronger OIB affinity in the high-Ti basalts, because they actually have lower $^{87}Sr/^{86}Sr$ and higher $^{143}Nd/^{144}Nd$, whereas they should have higher $^{87}Sr/^{86}Sr$ and lower $^{143}Nd/^{144}Nd$, if their OIB geochemical signature was coupled with a plume isotopic signature.

The simplest explanation for the differences between Sr-Nd and Pb isotopes in the low-Ti and high-Ti basalts is the existence of small-scale Pb isotopes heterogeneities

in their mantle source. Because low-Ti and high-Ti were produced by different degrees of partial melting, it is not surprising that they might derive from slightly isotopically different sources. Also, the range in Pb isotopic values is fairly small: the Sukadana basalts plot in a very restricted Pb isotope range compared with other volcanic provinces with similar isotope signatures, and both low-Ti and high-Ti basalts plot within the field of basalts with an EM component.

If this interpretation is correct, then the high Pb isotopic ratios in the high-Ti basalts might be a characteristic of their source, whereas the high Pb and Sr and low Nd isotopes in the low-Ti basalts are due to crustal contamination. In support of this interpretation, the geochemically most primitive low-Ti basalt (75377) has the lowest Pb isotopic values and also the lowest $^{87}Sr/^{86}Sr$ and highest $^{143}Nd/^{144}Nd$ values among the low-Ti basalts.

Therefore, the high Sr and Pb and low Nd isotopic values in low-Ti basalts are not due to the presence of an "enriched" component (a plume component), but might simply be the effect of crustal contamination.

The good correlation between LILE/HFSE (e.g. K/Nb, Rb/Nb) values and $^{143}Nd/^{144}Nd$ (and, to a lesser extent, $^{87}Sr/^{86}Sr$) seems good evidence for crustal contamination (see Figures 6.20a-f). LREE/HFSE (e.g. Ce/Nb) values also show a negative correlation with $^{143}Nd/^{144}Nd$, but the increase in LREE/HFSE is not so dramatic because, in general, LREE can be expected to be less mobile than LILE during crustal contamination. Once again, it is worth pointing out that a subduction-derived fluid would be relatively enriched in Sr, and if this fluid was the reason for the high LILE/HFSE values, a strong variation in $^{87}Sr/^{86}Sr$ values should be observed, and no, or little, correlation with $^{143}Nd/^{144}Nd$ should be expected.

Because the Ti/Zr values increase with increasing degrees of partial melting (e.g. Woodhead et al. 1993), the negative correlation between Ti/Zr and $^{143}Nd/^{144}Nd$ (and the positive correlation with $^{87}Sr/^{86}Sr$) isotopes is an indication that the effects of contamination are stronger for higher degrees of partial melting: tholeiites appear to be more contaminated than alkali basalts, possibly because the most alkaline basalts are relatively primitive and were emplaced in a relatively short time, whereas the tholeiites are more fractionated (higher Al_2O_3/CaO values and lower MgO, Ni, Cr contents) and probably resided for a longer time in the magma chamber.

Finally, the effects of crustal contamination on major element chemistry are to

decrease FeO and TiO_2, and to increase SiO_2 and K_2O (e.g. Cox & Hawkesworth 1984, 1985). Therefore the depletion in TiO_2 and FeO and enrichment in SiO_2 in the low-Ti basalts (and in spinel inclusions in olivines in the low-Ti basalts) is probably the result of two concomitant processes, namely higher degrees of partial melting and crustal contamination, whereas the K_2O content is regulated by two opposite processes (decrease of K_2O content for higher degrees of partial melting, and increase for stronger crustal contamination).

In summary, high-Ti basalts of Sukadana and Bukit Telor have major and trace element typical of intra-plate basalts. The relatively low LILE and LREE contents are evidence for a depleted mantle source, which was not metasomatised by recent subduction-derived fluids, and the depletion was probably the result of previous episodes of melt extraction. Isotopically, these basalts resemble the most "enriched" Indian Ocean MORB and the most "depleted" Indian Ocean volcanics with a DUPAL component in their source.

There is no evidence for the derivation of the low-Ti basalts from a MORB source, or from mixing between a MORB and an OIB melt. Increasing degrees of partial melting of the same OIB source that generated the high-Ti basalts can produce some of the major and trace element systematics observed in the low-Ti basalts, but the high LILE/HFSE values coupled with low $^{143}Nd/^{144}Nd$ suggest that crustal contamination, as modelled in Chapter 5, also occurred in the low-Ti basalts.

6.10.6 Relationship between arc melts and Sukadana melts

In general, increasing degrees of partial melting will produce a suite of rocks progressively depleted in incompatible elements. Because crust-derived melts are enriched in LILE, LREE, and SiO_2, and depleted in HFSE, HREE, and FeO (e.g. Cox & Hawkesworth 1984, 1985; Thompson et al. 1984), the effects of crustal contamination on rocks produced by a relatively large degree of partial melting, like the low-Ti basalts of Sukadana, will be a further decrease in HFSE and HREE, but an increase in LILE and LREE values. Increasing degrees of crustal contamination, coupled with fractionation in the magma chamber of olivine, clinopyroxene, plagioclase, and spinel (from Cr-spinel to progressively more Ti-rich titanomagnetite) - all the phases observed in the Sukadana basalts - can therefore, in principle, be expected to produce the trace element patterns observed in the Sumatran arc basalts, and progressively higher Sr and Pb, and lower Nd isotopic ratios.

The four low-Ti Sukadana basalts from Gunung Tiga (75356 to 75359) have whole-rock major and trace element and isotope systematics similar to those of the other low-Ti basalts, but very different olivine, spinel, and melt inclusion compositions. Olivine crystals are overall slightly more forsteritic than in all the other low-Ti basalts, and olivine phenocrysts and spinel inclusions bear strong textural evidence for disequilibrium. Melt inclusions, analysed only in one sample (75357), appear to have slightly higher SiO_2, Na_2O, and K_2O contents, and lower CaO, FeO, and MgO contents than other melt inclusions in low-Ti basalts. Also, the composition of melt inclusions in other low-Ti basalts is (within the error due to the calculation of the Mg# in melt inclusions - see Table 6.6) similar to that of the whole-rock, suggesting equilibrium between whole-rock and melt inclusion composition. To the contrary, melt inclusions in 75357 have systematically higher alkalis and lower FeO and MgO contents than in the whole-rock analysis.

Because spinel inclusions in the samples of Gunung Tiga are in disequilibrium with the host olivine, especially those of sample 75359, it is difficult to understand whether the difference in spinel composition between the basalts of Gunung Tiga and the other low-Ti basalts reflects compositional differences in the source, or secondary re-equilibration of the spinel with olivine and with the melt through olivine. Scowen et al. (1991) showed that Mg and Fe^{2+} can easily diffuse through olivine, and therefore they are not good indicators of the source when textural disequilibrium is evident. On the other hand, the diffusivities of Al and Ti (especially Ti) are much lower, and it can be expected that spinels retain, to some extent, their original Al and Ti content even after re-equilibration.

A particularly remarkable characteristic of the spinel inclusions in olivine phenocrysts in the basalts from Gunung Tiga is their relatively low Al_2O_3 and TiO_2 contents. In an Al_2O_3-TiO_2 plot, all the spinels from high-Ti and low-Ti basalts plot along a trend that goes from OIB spinels towards more Al-rich and Ti-poor composition, whereas the spinels of Gunung Tiga have low Al_2O_3 and TiO_2 contents, and seem to trend towards the field of arc spinels, and the spinels of one of the samples (75359) clearly plot within the field of arc spinels.

The interpretation of this trend is difficult, partly because of the low amount of data (and of the large uncertainties in the calculation of the composition of the melt inclusions), and because it is not clear to what extent the original compositions of spinel and melt inclusions and olivine phenocrysts were modified by secondary processes. One possibility is that the spinels crystallised from slightly more evolved

and contaminated melts, compared with the "normal" spinels in low-Ti basalts. These melts would be enriched in SiO_2 and alkalis, and depleted in MgO and FeO as a result of fractionation, and further depleted in FeO and enriched in alkalis because of crustal contamination, and such melts have been observed as melt inclusions in the olivine phenocrysts. Therefore, according to this interpretation, it might be possible to produce arc melts by increasing the degree of partial melting, crystal fractionation, and crustal contamination of high-Ti basalts like those of Sukadana.

An interesting implication of this interpretation is that a residual melt after the extraction of arc melts ("normal" low-Ti melts, like those of the Quaternary Sumatran arc) can still produce melts with composition similar to that of arc melts, if it is sufficiently contaminated and fractionated. In Sukadana, it seems that these more evolved melts were trapped by less fractionated and contaminated melts, similar to the "normal" low-Ti melts, because there are no differences in whole-rock composition between the basalts from Gunung Tiga and the other low-Ti basalts.

Another interesting point that suggests a strong link between arc rocks and the Sukadana basalts, but not necessarily the derivation of the arc rocks from the Sukadana basalts, is that the composition of spinel inclusions in olivine phenocrysts in some arc volcanics (75284, 75300, and 75384, three out of the four samples where spinel inclusions were analysed) is unusual for "typical" arc spinels, and more similar to that of the spinels from the low-Ti basalts of Sukadana. It is possible, therefore, that these spinels, which are found in different localities in Sumatra, actually crystallised from a melt like that of the low-Ti basalts, and then were trapped by arc melts (the arc rocks where these spinels are found are always more evolved than the spinels). However, little is known about the composition of spinel inclusions in olivines in relatively evolved arc rocks, and other explanations can be put forward but cannot, at this stage, be adequately tested.

Finally, the differences observed between spinel and whole-rock composition are indicative of the timing of the contamination observed in the low-Ti basalts. Even when the rock (whole-rock) appears to be contaminated - like the low-Ti basalts - spinel inclusions in olivines, that represent the most primitive melt from which the rock crystallised, still have a non-arc signature (with the exception of the most "evolved" spinels of Gunung Tiga), suggesting, in agreement with isotopic evidence (see Chapter 5), that the contamination occurred late in the evolution of the rock (within the crust) and not when the melt was formed in the mantle.

6.10.7 Comparison between the Sr, Nd, and Pb isotope systematics in basalts of Sukadana and Bukit Telor and intraplate basalts from nearby areas

Perhaps the most interesting feature of the basalts from Sukadana and Bukit Telor is their high Pb isotopic ratios compared with most MORB: all the samples analysed have higher $^{87}Sr/^{86}Sr$ values and Pb isotopic ratios, and lower $^{143}Nd/^{144}Nd$ values than those of typical Indian Ocean MORB, and plotting within the field of the basalts from the Investigator Ridge and of basalts from Kerguelen and the Ninetyeast Ridge with relatively low $^{87}Sr/^{86}Sr$ values and high $^{143}Nd/^{144}Nd$ values. The range in trace element composition observed in the Sukadana and Bukit Telor basalts is similar to that shown by tholeiitic to mildly alkaline basalts in Kerguelen and in the East Australian volcanic province, the only difference being the slightly but systematically lower LILE and LREE content in the Sumatran basalts.

Although both the East Australian volcanic province and the Kerguelen plateau are overall more alkaline than the Sumatran basalts, tholeiites with high $^{143}Nd/^{144}Nd$ and low $^{87}Sr/^{86}Sr$ values - like those observed in Sukadana and Bukit Telor - do exist in these localities (Watkins et al. 1974; White & Hofmann 1982; Ewart et al. 1988). The available data from the Indian Ocean basalts show that oceanic basalts have rather variable Pb isotopic values that partially overlap the Kerguelen values, but very different Sr and Nd isotopic ratios. Therefore, the mixing of the most alkaline basalts from Kerguelen with typical Indian Ocean MORB would produce a range of rocks with relatively similar Pb isotopic ratios, but very different $^{143}Nd/^{144}Nd$ and $^{87}Sr/^{86}Sr$ values.

However, even the most alkaline basalts in Sukadana and Bukit Telor have relatively low $^{87}Sr/^{86}Sr$ and high $^{143}Nd/^{144}Nd$ values compared with transitional and slightly alkaline basalts in Kerguelen, and therefore the models proposed to explain the evolution from low $^{87}Sr/^{86}Sr$, high $^{143}Nd/^{144}Nd$ tholeiites to high $^{87}Sr/^{86}Sr$, low $^{143}Nd/^{144}Nd$ transitional and alkaline basalts in Kerguelen (Gautier et al. 1990) seem not to be applicable to the Sumatran basalts. In contrast, most basalts from the East Australian Volcanic Province (Ewart et al. 1988) have the isotope systematics similar to those shown by the Sukadana and Bukit Telor basalts, without significant variations and anomalies in Sr and Nd isotopic values.

It is important to notice that the isotopic composition of the Sukadana and Bukit Telor basalts is not found only in continental areas and in (so far) identified plume-related localities. Some basalts from the Ninetyeast Ridge, and rocks from a submarine

volcano (DODO 232) from the Northeastern Indian Ocean (see Chapter 3) closely resemble the low-Ti basalts of Sukadana (Figure 6.53), apart from the undepleted HREE values in the Indian Ocean rocks, indicative of a MORB affinity. On the other hand, the dolerite sill from site DSDP 22 211 has OIB-like composition similar to that of the Sukadana and Bukit Telor basalts (Figure 6.53), but different isotope systematics, typical of Kerguelen alkaline basalts (see Chapter 3).

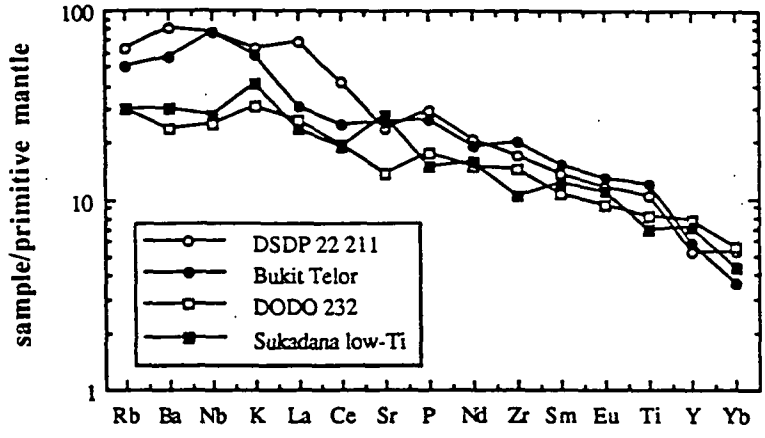

Figure 6.53. Trace element values normalised to primitive mantle values (from Sun & Mc Donough 1989) showing the similarities between the Sukadana and Bukit Telor basalts and rocks from the Northeastern Indian Ocean (samples DSDP 22 211 and DODO 232 - see Chapter 3).

Similar isotopic and geochemical compositions are observed in basalts from east Australia (mainly in north and central Queensland) and the South China Basin (see also Figures 6.54a-b).

In summary, the increasing alkalinity in the Sukadana basalts is not correlated with increasing $^{87}Sr/^{86}Sr$ and decreasing $^{143}Nd/^{144}Nd$, as it would be expected if the increase in alkalinity was produced by a higher amount of plume-related component with high $^{87}Sr/^{86}Sr$ and low $^{143}Nd/^{144}Nd$ values in the source. However, the Pb isotopic values, which are generally higher than those of Pacific and Atlantic MORB, are clear evidence that Indian Ocean-type mantle, isotopically similar to the source of the least "enriched" plume-related basalts in the Indian Ocean (Ninetyeast and Investigator Ridges; tholeiitic basalts of Kerguelen), exists in the mantle wedge of Sumatra. In fact, this type of mantle is extremely common not only in the Indian Ocean, but also in east Australia and, in the northern hemisphere, in the South China Sea, and is only slightly "enriched" in a EM2 component compared with "typical" PREMA (PREvalent MAntle; see e.g. Hart & Zindler 1989).

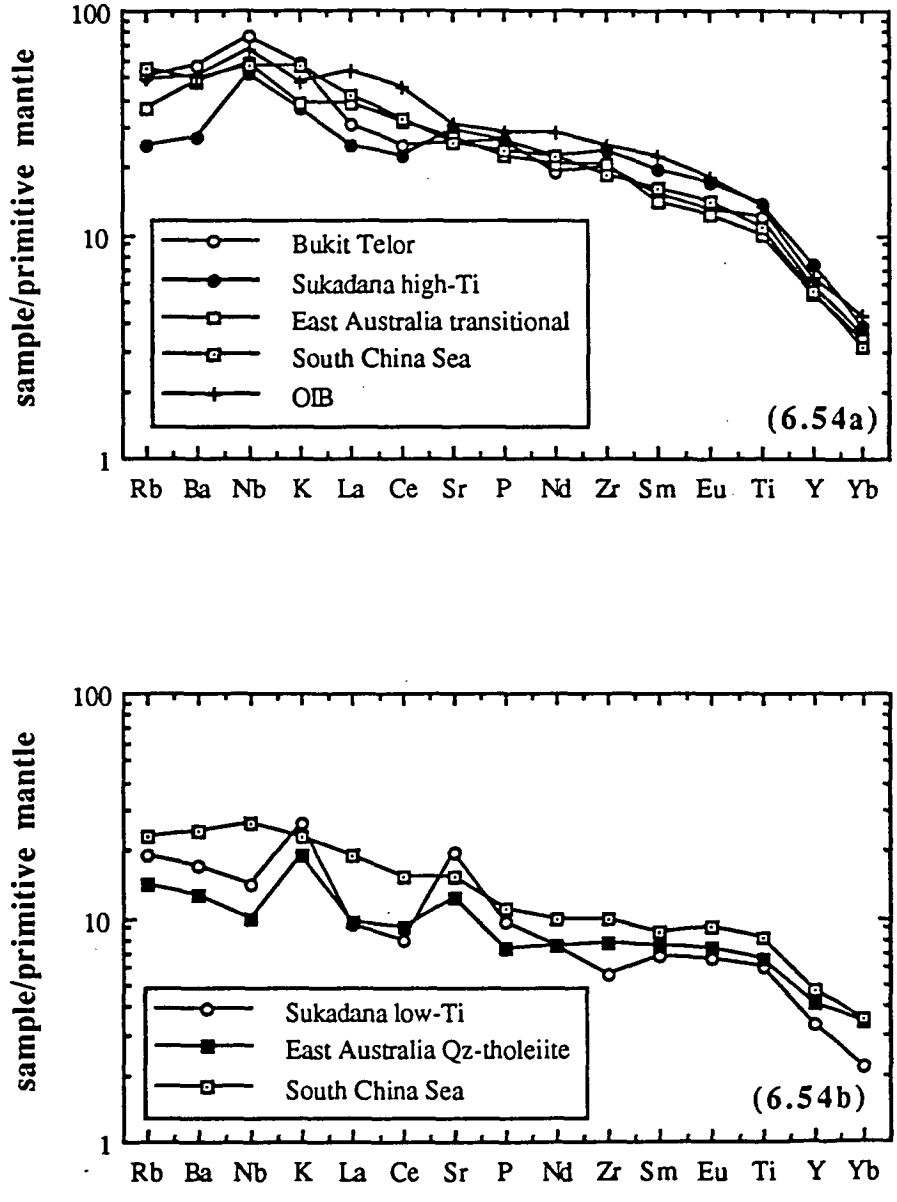

Figure 6.54a-b. Trace element values normalised to primitive mantle values (from Sun & Mc Donough 1989) showing the similarities between the Sukadana and Bukit Telor basalts and rocks from east Australia (data from Ewart et al. 1988) and Hainan (South China Sea - data from Flower et al. 1992).

6.10.8 Karimunjawa and Kalimantan

Based on the data discussed by Soeria-Atmadja et al. (1985), the low-Ti and high-Ti basalts of Karimunjawa closely resemble the basalts of Sukadana and Bukit Telor in their major and trace element compositions (particularly in their Th-Hf-Ta systematics), and the model discussed before for the origin and evolution of the Sukadana basalts may apply to the Karimunjawa basalts as well. However, as no isotope data are available, it is not clear whether the source of the Karimunjawa basalts is "enriched" in a EM2 component, like in Sukadana, or is a "normal" Indian Ocean mantle source.

Like in Sukadana and Karimunjawa, the low-Ti basalts of Kalimantan appear to be temporally and spatially associated with arc rocks, although there is no active subduction in Kalimantan. Therefore, the low-Ti basalts in Sukadana and in Kalimantan could have been produced by a mantle source that suffered the same type and extent of "depletion". Furthermore, an Early Mesozoic continental basement, similar in age and possibly in composition to the basement of Sumatra (see Chapter 2) outcrops in the vicinity of the Quaternary volcanoes in Kalimantan and, like in Sumatra, the location of the arc in central Kalimantan might correspond with a major tectonic boundary (Hamilton 1979; Pieters & Supriatna 1990). However, the interpretation of the low-Ti basalts of Kalimantan is problematic, mainly because of the high degree of evolution of these rocks, and partly because of the textural evidence of shallow level contamination.

The relatively high, compared with those of Group 1, TiO_2 (both in the rocks and in spinel inclusions) and HFSE contents of the Kalimantan Group 2 basalts are similar to those of the low-Ti basalts of Sukadana. Although the high TiO_2 values of spinel inclusions may be partly due to the fact that the host olivines are fairly evolved (when titanomagnetite begins to crystallise in relatively low-Mg melts, the spinel inclusions in olivine become TiO_2-rich. Titanomagnetite has been observed in the groundmasses of these rocks, and the crystallisation of titanomagnetite is consistent with the relatively low Fe^{2+}/Fe^{3+} - high oxygen fugacity - in these spinels), Figure 6.46 shows that the Kalimantan spinels still plot within the field of spinels in intra-plate basalts. Other major element variations in spinel inclusions and major and trace element in whole-rock are consistent with higher degrees of fractionation from rocks similar to the low-Ti basalts of Sukadana. In fact, the Kalimantan low-Ti basalts have major and trace element composition similar to that of the most evolved low-Ti basalt in Sukadana discussed in this study - 75372.

If this interpretation is correct, then the Sr, Nd, and Pb isotope systematics of the low-Ti basalts of Kalimantan, which are generally similar to those of arc rocks of Kalimantan and Sumatra, simply reflect a higher degree of crustal contamination of progressively more evolved melts, and the low-Ti basalts of Kalimantan fill the previously discussed gap between Sumatran arc rocks and the low-Ti basalts of Sukadana.

In summary, all the available data seem to indicate that the basalts of Karimunjawa and central Kalimantan are similar to those of Sukadana and compositionally (but not necessarily genetically) different from arc-related volcanics, thus supporting van Bemmelen's (1949) early suggestions. Apart from this, little can be said at this stage about their source and magmatic evolution, partly because of the lack of data (in Karimunjawa) and because crystal fractionation and crustal contamination modified the original composition of these rocks (in the low-Ti basalts of central Kalimantan). In particular, it is not clear whether the source of these rocks (Karimunjawa and central Kalimantan) was isotopically similar to the source of the Sukadana basalts. However, all the available data suggest that the basalts of Sukadana, Bukit Telor, Karimunjawa, and central Kalimantan might have been subjected to basically the same type and sequence of magmatic processes.

6.11 Conclusions

The results of the study of the origin and evolution of basalts of Bukit Telor, Bukit Mapas, Sukadana, central Kalimantan, and Karimunjawa, have been described during the discussion, and those results are briefly summarised in this section.

6.11.1 Bukit Telor

The basalts of Bukit Telor are slightly alkaline and olivine-rich, and, despite minor variations in degrees of partial melting and crystal fractionation, have overall major and trace element content and "immobile" and "mobile" element relative abundances typical of OIB, except for a slight depletion in LREE which may be a characteristic of their source. These basalts and their mantle xenoliths probably represent the composition of the unmetasomatised mantle wedge at some distance from the volcanic arc, and do not bear any textural nor geochemical evidence for lithospheric contamination.

These basalts are unlikely to represent primary melts, despite their relatively high Mg#, and probably have fractionated clinopyroxene and olivine. However, trace element abundances and the presence of lherzolitic xenoliths suggest that these rocks are relatively primitive.

Their Sr, Nd, Pb, and He isotopes signature is similar to that of Indian Ocean basalts "enriched" in a EM component (Ninetyeast Ridge, and some Indian Ocean MORB). The OIB-type geochemical composition coupled with relatively un-enriched isotopic ratios suggests that they are not derived from hot spot volcanic activity, and that they might represent small degrees of partial melting of an isotopically slightly enriched Indian Ocean mantle source.

6.11.2 Sukadana

The Sukadana basalts range in composition from slightly oversaturated, quartz tholeiites, to more abundant olivine tholeiites and slightly alkaline olivine basalts, and can be subdivided into two groups: high-Ti ($TiO_2 > 2.3\%$) and low-Ti ($TiO_2 < 1.6\%$) basalts.

The more alkaline, olivine-rich high-Ti basalts have major and trace element composition similar to that of OIB, but are relatively depleted in LILE and LREE, whereas the low-Ti basalts show variable degrees of depletion and enrichment in LILE and HFSE, without significant variations in Mg#.

The increasing alkalinity in the Sukadana basalts is not correlated with increasing $^{87}Sr/^{86}Sr$ and decreasing $^{143}Nd/^{144}Nd$, as it would be expected if the increase in alkalinity was produced by a higher amount of plume-related component with high $^{87}Sr/^{86}Sr$ and low $^{143}Nd/^{144}Nd$ values in the source. However, the Pb isotopic signature of the Sukadana basalts are clear evidence that Indian Ocean-type mantle, isotopically similar to the source of the least "enriched" plume-related basalts in the Indian Ocean (Ninetyeast and Investigator Ridges; tholeiitic basalts of Kerguelen), exists in the mantle wedge of Sumatra.

The depletion in LREE and LILE in the high-Ti Sukadana basalts is unusual, because in such a tectonic environment we would expect to see an enrichment in LILE and LREE, due to the flux of these elements from the subducting slab. The depletion in LILE and LREE is likely to be a characteristic of the source, and may be due to the previous extraction of melts enriched in LILE and LREE and depleted in HFSE, like

arc melts. This conclusion is strongly supported by the fact that these rocks are spatially and temporally associated with arc rocks, and that arc-related granitoids in Sumatra derived from an isotopically similar source.

Therefore the high-Ti basalts of Sukadana do not need to be plume-derived, and might simply be the result of several stages of melt extraction from a depleted primitive mantle. Relatively high degrees of partial melting of the same source that produced the high-Ti basalts yielded less alkaline basalts with low HFSE, and low LILE and LREE. These basalts then suffered varying degrees of crustal contamination, which produced an array of LILE and LREE contents for almost constant HFSE contents, and high LILE/HFSE values coupled with low $^{143}Nd/^{144}Nd$. Mineral chemistry and Sr, Nd, and Pb isotope data indicate that contamination occurred at relatively shallow level in the crust, and not in the source, and that relatively large degrees of crustal contamination can create melts geochemically and isotopically similar to arc melts.

6.11.3 Bukit Mapas

Major and trace element, mineral chemistry, petrography, and Sr, Nd, and Pb isotope data, all indicate that the basaltic andesites of Bukit Mapas are indistinguishable from the other calcalkaline rocks of the Quaternary Sumatran arc, and are unrelated to the intra-plate basalts of Bukit Telor and Sukadana. However, despite their affinities with the arc andesites, the basaltic andesites of Bukit Mapas are characterised by having unusually abundant, high-MgO olivines, and by the occurrence in the olivines of Al-spinel as well as Cr-spinel inclusions. The origin of the Al-rich spinels is not clear, but textural and geochemical evidence suggest that they crystallised from an Al-rich melt, possibly formed by melting of crustal material.

6.11.4 Karimunjawa and Kalimantan

Very little is known about these two localities. The Karimunjawa basalts are petrographically similar to those of Sukadana, and the most alkaline basalts have Hf/Ta/Th values similar to those of Bukit Telor and typical of within-plate alkaline basalts, whereas the low-Ti basalts have a more "orogenic" affinity, like the low-Ti basalts of Sukadana.

Two different groups of rocks have been found in central Kalimantan. One group has textures and paragenesis, and geochemical and isotopic composition typical of arc

andesites, and similar to the Sumatran andesites. The other group closely resembles the olivine-poor, low-Ti basalts of the Sukadana plateau, but appears to have been strongly contaminated by crustal material.

Like in Sukadana and Karimunjawa, the low-Ti basalts of Kalimantan seem to be temporally and spatially associated with arc rocks, and the low-Ti basalts in Sukadana and in Kalimantan may have been produced by a mantle source that suffered the same type and extent of "depletion".

References

Abbott M.J., Chamalaun F.H. (1981)
Geochronology of some Banda arc volcanics.
in: "Geology and tectonics of eastern Indonesia" (A.J. Barber & Wiryosujono S. Eds.) GRDC Spec. Publ. 2, 253-268

Abidin H.Z., Pieters P.E., Sudana D. (1989)
1:250,000 Preliminary geologic map of the Long Pahangai quadrangle, Kalimantan.
Geological Research and Development Centre, Bandung, Indonesia

Aggrey K.E., Muenow D.W., Sinton J.M. (1988)
Volatile abundances in submarine glasses from the North Fiji and Lau back-arc basins.
Geoch. Cosmoch. Acta 52, 2501-2506

Albarède F., Michard A. (1989)
Hydrothermal alteration of the oceanic crust.
in "Crust/mantle recycling at convergence zones" by Hart & Gülen (Eds), 29-36 NATO ASI Series (Series C)

Allègre C.J., ben Othman D. (1980)
Nd-Sr isotopic relationship in granitoid rocks and continental crust development: a chemical approach to orogenesis.
Nature 286, 335-342

Alzwar M., Barberi F., Bizouard H., Boriani A., Cavallin A., Eva C., Gelmini R., Giorgetti F., Iaccarino S., Innocenti F., Marinelli G., Sudradjat A. (1981)
A structural discontinuity with associated potassic volcanism in the Indonesian island arc: first results of the CNR-CNRS-VSI mission to the island of Sumbawa.
Rend. Soc. Geol. It. 4, 275-288

Amin T.C., Santosa S., Gunawan W. (1988)
1:250,000 Geologic map of the Kotaagung quadrangle, Sumatra.
Geological Research and Development Centre, Bandung, Indonesia

Angus S., Armstrong B., deReuck K.M., Altunin V.V., Gadetskii O.G., Chapela G.A., Rowlinson J.S. (1976)
International thermodynamic tables of the fluid state. Vol.3 - Carbon dioxide.
Pergamon Press, Oxford, 385 pp.

Arai S. (1992)
Chemistry of chromian spinel in volcanic rocks as a potential guide to magma chemistry.
Min. Mag. 56, 173-184

Arculus R.J. (1974)
Solid solution characteristics of spinels: pleonaste-chromite-magnetite compositions in some island-arc basalts.
Carnegie Inst. Wash. Year Book 73, 322-327

Arculus R.J. (1978)
Mineralogy and petrology of Grenada, Lesser Antilles island arc.
Contrib. Mineral. Petrol. 65, 413-424

Arculus R.J., Wills K.J.A. (1980)
The petrology of plutonic blocks and inclusions from the Lesser Antilles island arc. Jour. Petrol. 21, 743-799

Arculus R.J., Powell R. (1986)
Source component mixing in the regions of arc magma generation.
Jour. Geophys. Res. 91(B6), 5913-5926

Asnachinda P. (1978)
Tin mineralization in the Burmese-Malayan peninsula - a plate tectonic model.
in "Third regional conference on geology and mineral resources of Southeast Asia" (P. Nutalaya Ed.), Wiley, N.Y., 293-299

Aspden J.A., Kartawa W., Aldiss D.T., Djunuddin A., Whandoyo R., Diatma D., Clarke M.C.G., Harahap P. (1982)
1:250,000 Geologic map of the Padangsidempuan and Sibolga quadrangle, Sumatra.
Geological Research and Development Centre, Bandung, Indonesia

Audley-Charles M.G., Carter D.J., Milsom J.S. (1972)
Tectonic development of eastern Indonesia in relation to Gondwanaland dispersal.
Nature Phys. Sci. 39, 35-39

Audley-Charles M.G. (1975)
The Sumba fracture: a major discontinuity between eastern and western Indonesia.
Tectonophysics 26, 213-228

Audley-Charles M.G., Carter D.J., Barber A.J., Norvick M.S., Tjokrosapoetro S. (1979)
Reinterpretation of the geology of Seram: implications for the Banda arcs and northern Australia.
Jour. Geol. Soc. London 136, 547-566

Audley-Charles M.G. (1981)
Geometrical problems and implications of large-scale over-thrusting in the Banda arc-Australian margin collision.
in: "Thrust and nappe tectonics" (K. McClay & N. Price Eds.) Geol. Soc. London Spec. Publ. 9, 407-416

Audley-Charles M.G. (1988)
Evolution of the southern margin of Tethys (North Australia Region) from Early Permian to Late Cretaceous.
in "Gondwana and Tethys", Geol. Soc. Spec. Publ. 37, Geol. Soc. London (M. Audley-Charles and H. Hallam Eds.), 79-100

Baksi A.K., Barman T.R., Paul D.K., Farrar E. (1987)
Widespread Early Cretaceous flood basalt volcanism in eastern India: geochemical data from the Rajmahal - Bengal - Sylhet traps.
Chem. Geol. 63 (1-2), 133-141

Barber A.J., Audley-Charles M.G. (1976)
The significance of the metamorphic rocks of Timor in the development of the Banda arc, eastern Indonesia.
Tectonophysics 30, 119-128

Barber A.J. (1981)
Structural interpretations of the island of Timor, eastern Indonesia.
in: "Geology and tectonics of eastern Indonesia" (A.J. Barber & Wiryosujono S. Eds.) GRDC Spec. Publ. 2, 183-197

Barbey P., Macaudiere J., Nzenti J.P. (1990)
High-pressure dehydration melting of metapelites:evidence from the migmatites of Yaoundé (Cameroon).
Jour. Petrol. 31(2), 401-427

Barsdell M., Berry R. (1990)
Origin and evolution of primitive island arc ankaramites from Western Epi, Vanuatu.
Jour. Petrol. 31, 747-777

Batiza R. (1984)
Inverse relationship between Sr isotope diversity and rate of oceanic volcanism has implications for mantle heterogeneity.
Nature 309, 440-441

Bebout G.E., Ryan J.G., Leeman W.P. (1993)
B-Be systematics in subduction-related metamorphic rocks: characterization of the subducted component.
Geoch. Cosmoch. Acta 57, 2227-2237

Beckinsale R.D., Suensilpong S., Nakapadungrat S., Walsh J.N. (1979)
Geochronology and geochemistry of granite magmatism in Thailand in relation to a plate tectonic model.
Jour. Geol. Soc. London 136, 529-540

Ben Avraham Z., Emery K.O. (1973)
Structural framework of Sunda Shelf.
Amer. Assoc. Petrol. Geol. Bull. 57, 2323-2366

Bennett J.D., Bridge D.McC., Cameron N.R., Djunuddin A., Ghazali S.A., Jeffery D.H., Kartawa W., Keats W., Rock N.M.S., Thompson S.J., Whandoyo R. (1981a)
1:250,000 Geologic map of the Banda Aceh quadrangle, Sumatra.
Geological Research and Development Centre of Indonesia Directorate General of Mines Ministry of Mines and Energy

Bennett J.D., Bridge D.McC., Cameron N.R., Djunuddin A., Ghazali S.A., Jeffery D.H., Kartawa W., Keats W., Rock N.M.S., Thompson S.J., Whandoyo R. (1981b)
1:250,000 Geologic map of the Calang quadrangle, Sumatra.
Geological Research and Development Centre of Indonesia Directorate General of Mines Ministry of Mines and Energy

Ben Othman D., White W.M., Patchett J. (1989)
The geochemistry of marine sediments, island arc magma genesis, and crust-mantle recycling.
Earth Plan. Sci. Lett. 94, 1-21

Bergman S.C. (1982)
Petrogenetic aspects of the alkali basaltic lavas and included megacrysts and nodules from the Lunar Crater volcanic field, Nevada, USA.
Unpubl. PhD thesis, Princeton University, Princeton, NJ, USA.

Berry R.F., Grady A.E. (1981)
The age of the major orogenesis in Timor.
in: "Geology and tectonics of eastern Indonesia" (A.J. Barber & Wiryosujono S. Eds.) GRDC Spec. Publ. 2, 171-181

Bonatti E., Michael P.J. (1989)
Mantle peridotites from continental rifts to ocean basins to subduction zones.
Earth Plan. Sci. Lett. 91, 297-311

Bouquillon A., France-Lanord C., Michard A., Tiercelin J.-J. (1990)
Sedimentology and isotopic chemistry of the Bengal Fan sediments: the denudation of the Himalaya.
ODP Scientific Results vol. 116, 43-58

Bowin C., Purdy G.M., Johnston C., Shor G., Lawver L., Hartono H.M.S., Jezek P. (1980)
Arc-continent collision in the Banda Sea region.
Bull. Amer. Assoc. Petrol. Geol. 64, 868-915

Bunopas S. (1981)
Paleogeographic history of Western Thailand and adjacent parts of Southeast Asia - a plate tectonics interpretation.
Geol. Surv. Thailand Pap. 5, 1-810

Burgess I.R. (1978)
Unpubl. BSc Hon. thesis, University Western Australia, Australia

Burrett C. (1974)
Plate tectonics and the fusion of Asia.
Earth Plan. Sci. Lett. 21, 181-189

Burrett C., Stait B. (1985)
South East Asia as a part of an Ordovician Gondwanaland - a palaeobiogeographic test of a tectonic hypothesis.
Earth Plan. Sci. Lett. 75, 184-190

Burollet P.F., Salle C. (1981)
Tectonic framework of eastern Indonesia.
in: "Geology and tectonics of eastern Indonesia" (A.J. Barber & Wiryosujono S. Eds.) GRDC Spec. Publ. 2, 49-52

Calanchi N., Lucchini F., Rossi P.L. (1983)
Considerazioni sui rapporti tra le serie alte in K e l'arco vulcanico indonesiano alla luce dei vulcani Muriah e Lasem (Giava).
Miner. Petrogr. Acta 27, 15-34

Calvert S.E., Price N.B. (1981)
Geochemistry of Namibian shelf sediments.
in "Coastal upwelling: its sedimentary record, Part A: responses of the sedimentary regime to present coastal upwelling." (E. Suess & J. Thiede Eds.) Plenum Press, New York N.Y., pp. 337-376

Cameron N.R., Clarke M.C.G., Aldiss D.T., Aspden J.A., Djunuddin A. (1980)
The geological evolution of Northern Sumatera.
Proc. 9th Ann. Conv. Indon. Petrol. Ass., 149-187

Cameron N.R., Bennett J.D., Bridge D.McC., Clarke M.C.G., Djunuddin A., Ghazali S.A., Harahap H., Jeffery D.H., Kartawa W., Keats W., Ngabito H., Rock N.M.S., Thompson S.J. (1983)
1:250,000 Geologic map of the Takengon quadrangle, Sumatra.
Geological Research and Development Centre of Indonesia Directorate General of Mines Ministry of Mines and Energy

Cardwell R.K., Isacks B.L. (1978)
Geometry of the subducted lithosphere beneath the Banda Sea in eastern Indonesia from seismicity and fault plane solutions.
Jour. Geophys. Res. 83, 2825-2838

Cardwell R.K., Isacks B.L., Karig D.E. (1980)
The spatial distribution of earthquakes, focal mechanism solutions and subducted lithosphere in the Philippines and northeastern Indonesian islands.
in "Tectonic/geologic evolution of southeast Asia" (D.E. Hayes Ed.) AGU Monograph 23, 1-35.

Cardwell R.K., Isacks B.L. (1981)
A review of the configuration of the lithosphere subducted beneath the eastern Indonesian and Philippine islands.
in: "Geology and tectonics of eastern Indonesia" (A.J. Barber & Wiryosujono S. Eds.) GRDC Spec. Publ. 2, 31-47

Carey S.W. (1976)
Tectonic evolution of southeast Asia.
Proc. 4th Ann. Conv. Indones. Petrol. Ass. Jakarta, 1975, 17-48

Carter D.J., Audley-Charles M.G., Barber A.J. (1976)
Stratigraphycal analysis of island arc-continental margin collision in eastern Indonesia.
Jour. Geol. Soc. London 132, 179-198

Chappell B.W., White A.J.R., Hine R. (1988)
Granite provinces and basement terranes in the Lachlan Fold belt, southeastern Australia.
Austr. Jour. Earth Sci. 35, 505-521

Charlton T.R. (1986)
A plate tectonic model of the eastern Indonesia collision zone.
Nature 319, 394-396

Charlton T.R. (1991)
Postcollision extension in arc-continent collision zones, eastern Indonesia.
Geology 19, 28-31

Chesner C.A., Rose W.I., Deino A., Drake R., Westgate J.A. (1991)
Eruptive history of Earth's largest Quaternary caldera (Toba, Indonesia) clarified.
Geology 19, 200-203

Chesner C.A., Rose W.I. (1991)
Stratigraphy of the Toba Tuffs and the evolution of the Toba Caldera Complex, Sumatra, Indonesia.
Bull. Volc. 53, 343-356

Clarke M.C.G., Beddoe-Stephens B. (1987)
Geochemistry, mineralogy and plate tectonic setting of a Late Cretaceous Sn-W granite from Sumatra, Indonesia.
Min. Mag. 51, 371-387

Class C., Goldstein S.L., Galer S.J.G., Weis D. (1993)
Young formation age of a mantle plume source.
Nature 362, 715-721

Cloetingh S., Stein C., Reemst P., Gradstein F., Williamson P., Exon N., von Rad U. (1992)
Continental margin stratigraphy, deformation, and intraplate stresses for the Indo-Australian region.
ODP Scientific Results vol. 123, 671-713

Cobbing E.J., Mallick D.I.J., Pitfield P.E.J., Teoh L.H. (1986)
The granites of the Southeast Asian tin belt.
Jour. Geol. Soc. London 143, 537-550

Coleman P.J., Michael P.J., Mutter J.C. (1982)
The origin of the Naturaliste Plateau, SE Indian Ocean: implications from dredged basalts.
Jour. Geol. Soc. Australia 29, 457-468

Cook P.J. (1974)
Major and trace element geochemistry of sediments from DSDP leg 27, sites 259-263, Eastern Indian Ocean.
Initial Reports of the Deep Sea Drilling Project Volume 27, 481-497 National Science Foundation

Cox K.G., Hawkesworth C.J. (1984)
Relative contribution of crust and mantle to flood basalt magmatism, Mahabaleshwar area, Deccan Traps.
Phil. Trans. R. Soc. London A310, 627-641

Cox K.G., Hawkesworth C.J. (1985)
Geochemical stratigraphy of the Deccan Traps at Mahabaleshwar, Western Ghats, India, with implication for open system magmatic processes.
Jour. Petrol. 26(2), 355-377

Crawford A.J., Greene H.G., Neville F.E. (1988)
Geology, petrology and geochemistry of submarine volcanoes around Epi Island, New Hebrides island arc.
in "Geology and offshore resources of Pacific island arcs-Vanuatu region, Circum-Pacific council for energy and mineral resources earth sciences series." (H.G. Greene and F.L. Wong Eds.) 8, 301-327

Crostella A.A. (1977)
Geosynclines and plate tectonics in Banda arcs, eastern Indonesia.
Bull. Amer. Assoc. Petrol. Geol. 61(12), 2063-2081

Curray J.R., Shor Jr G.G., Raitt W.W., Henry M. (1977)
Seismic refraction and reflection studies of crustal structure of the eastern Sunda and western Banda arcs.
Jour. Geophys. Res. 82, 2479-2489

Curray J.R., Emmel F.J., Moore D.G., Raitt R.W. (1982)
Structure, tectonics, and geological history of the Northeastern Indian Ocean.
in "The ocean basins and margins. vol. 6: The Indian Ocean" (A.E.M. Nairn & F.G. Stehli eds.) 399-450 Plenum Press

Curray J.R., Munasinghe T. (1991)
Origin of the Rajmahal Traps and the 85° E Ridge: preliminary reconstruction of the trace of the Crozet hotspot.
Geology 19, 1237-1240

Danyushevsky L.V., Falloon T.J., Sobolev A.V., Crawford A.J., Carroll M., Price R.C. (1993)
The H_2O content of basalt glasses from Southwest Pacific back-arc basins.
Earth Plan. Sci. Lett. 117, 347-362

Davidson J.P., McMillan N.J., Moorbath S., Worner G., Harmon R.S., Lopez-Escobar L. (1990)
The Nevados de Payachata volcanic region (18°S, 69°W, N. Chile) II. Evidence for widespread crustal involvement in Andean magmatism.
Contrib. Mineral. Petrol. 105, 412-432

Davidson J.P., de Silva S.L. (1992)
Volcanic rocks from the Bolivian Altiplano: insights into crustal structure, contamination, and magma genesis in the Central Andes.
Geology 20, 1127-1130

Davies H.L., Sun S.-s., Frey F.A., Gautier I., McCulloch M.T., Price R.C., Bassias Y., Klootwijk C.T., Leclaire L. (1989)
Basalt basement from the Kerguelen Plateau and the trail of a DUPAL plume.
Contrib. Mineral. Petrol. 103, 457-469

Debon F., Le Fort P. (1983)
A chemical-mineralogical classification of common plutonic rocks and associations.
Trans. Royal Soc. Edinburgh: Earth Sciences, 73, 135-149

Debon F., Le Fort P. (1988)
A cationic classification of common plutonic rocks and their magmatic associations: principles, method, applications.
Bull. Mineral. 111, 493-510

Dia A., Dupré B., Allègre C.J. (1992)
Nd isotopes in Indian Ocean sediments used as a tracer of supply to the ocean and circulation paths.
Mar. Geol. 103, 349-359

Diament M., Harjono H., Karta K., Deplus C., Dahrin D., Zen M.T.Jr., Gérard M., Lassal O., Martin A., Malod J. (1992)
Mentawai fault zone off Sumatra: a new key to the geodynamics of western Indonesia.
Geology 20, 259-262

Dick H.J.B., Bullen T. (1984)
Chromiun spinel as a petrogenetic indicator in abyssal and alpine-type peridotites and spatially associated lavas.
Contrib. Mineral. Petrol. 86, 54-76

Dick H.J.B., Fisher R.L. (1984)
Mineralogic studies of the residues of mantle melting: abyssal and alpine-type peridotites.
in "Kimberlites II: the mantle and crust-mantle relationships" (Developments in petrology, vol. 11B, J. Kornprobst Ed.) Elsevier, Amsterdam, 295-308

Dickinson W.R., Hatherton T. (1967)
Andesitic volcanism and seismicity around the Pacific.
Science 157, 801-803

Dosso L., Joron J.-L., Maury R., Bougault H. (1987)
Isotopic (Sr, Nd) and trace element study of back-arc basalts behind the Sunda arc.
Terra Cognita 7, 398

Dosso L., Bougault H., Beuzart P., Calvez J.-Y., Joron J.-L. (1988)
The geochemical structure of the South-East Indian Ridge.
Earth Plan. Sci. Lett. 88, 47-59

Duncan R.A. (1981)
Hotspots in the southern oceans - an absolute frame of reference for motion of the Gondwana continents.
Tectonophysics 74, 29-42

Duncan R.A., Hargraves R.B. (1990)
40Ar/39Ar geochronology of basement rocks from the Mascarene Plateau, Chagos Bank, and the Maldives Ridge.
ODP Scientific Results vol. 115, 43-51

Duncan R.A. (1991)
Age distribution of volcanism along seismic ridges in the eastern Indian Ocean.
ODP Scientific Results vol. 121, 507-517

Dupre' B., Allegre C.J. (1983)
Pb-Sr isotope variation in Indian Ocean basalts and mixing phenomena.
Nature 303, 142-146

Edwards C., Menzies M., Thirlwall M. (1991)
Evidence from Muriah, Indonesia, for the interplay of supra-subduction zone and intraplate processes in the genesis of potassic alkaline magmas.
Jour. Petrol. 32, 3, 555-592

Edwards C.M.H., Morris J.D., Thirlwall M.F. (1993)
Separating mantle from slab signatures in arc lavas using B/Be and radiogenic isotope systematics.
Nature, 362, 530-533

Elderfield H., Greaves M.J. (1982)
The rare earth element in seawater.
Nature 296, 214-219

Engel C.G., Fisher R.L., Engel A.E.J. (1965)
Igneous rocks of the Indian Ocean floor.
Science 150, 605-610

Eva C., Cattaneo M., Merlanti F. (1988)
Seismotectonics of the central segment of the Indonesian arc.
Tectonophysics 146, 241-259

Ewart A., Chappell B.W., Menzies M.A. (1988)
An overview of the geochemical and isotopic characteristics of the eastern Australian Cainozoic volcanic provinces.
Jour. Petrol. Special Lithosphere Issue, 225-273

Falloon T.J., Varne R., Hart S.R., Duncan R.A.
The age and petrogenesis of alkaline volcanic rocks from Christmas Island and Vening Meinesz seamounts, NE Indian Ocean.
submitted for publication

Ferrara G., Lucchini F., Rossi P.L., Tonarini S. (1981)
Dati geologici, petrochimici e isotopici sul vulcano Muriah (Central Java, Indonesia).
Rend. Soc. Geol. It. 4, 289-299

Finger L.W. (1972)
The uncertainty in the calculated ferric iron content of a microprobe analysis.
Carnegie Inst. Wash. Year Book 71, 600-603

Fisk M.R., Bence A.E. (1980)
Experimental crystallization of chrome spinel in FAMOUS basalt 527-1-1.
Earth Plan. Sci. Lett. 48, 111-12

Fitch T.J. (1970)
Earthquake mechanisms and island arc tectonics in the Indonesian-Philippine region.
Bull. Seismol. Soc. Amer. 60, 565-591

Fitch T.J. (1972)
Plate convergence, transcurrent faults and internal deformation adjacent to southeast Asia and the western Pacific.
Jour. Geophys. Res. 77, 4432-4460

Fitch T.J., Molnar P. (1970)
Focal mechanisms along inclined earthquake zones in the Indonesian-Philippine region.
Jour. Geophys. Res. 75, 1431-1444

Flower M.F.J., Zhang M., Chen C.-Y., Tu K., Xie G. (1992)
Magmatism in the South China Basin: 2. Post-spreading Quaternary basalts from Hainan Island, South China.
Chem. Geol. 97, 65-87

Foden J.D. (1979)
The petrology of some young volcanic rocks from Lombok and Sumbawa, Lesser Sunda Islands.
Unpubl. PhD thesis, University of Tasmania, Australia

Foden J.D., Varne R. (1980)
The petrology and tectonic setting of Quaternary-recent volcanic centres of Lombok and Sumbawa, Sunda arc.
Chem. Geol. 30, 201-226

Foden J.D., Varne R. (1981)
The geochemistry and petrology of the basalt-andesite-dacite suite from Rinjani volcano, Lombok: implications for the petrogenesis of island arc, calcalkaline magmas.
in: "Geology and tectonics of eastern Indonesia" (A.J. Barber & Wiryosujono S. Eds.) GRDC Spec. Publ. 2, 115-134

Foden J.D., Varne R. (1981)
Petrogenetic and tectonic implications of near coeval calc-alkaline to highly alkaline volcanism on Lombok and Sumbawa islands in the eastern Sunda arc.
in: "Geology and tectonics of eastern Indonesia" (A.J. Barber & Wiryosujono S. Eds.) GRDC Spec. Publ. 2, 135-152

Foden J.D. (1983)
The petrology of the calcalkaline lavas of Rindjani volcano, east Sunda arc: a model for island arc petrogenesis.
Jour. Petrol. 24, 98-130

Foden J.D. (1986)
The petrology of Tambora volcano, Indonesia: a model for the 1815 eruption.
Jour. Volc. Geoth. Res. 27, 1-41

Foley S.F., Wheller G.E. (1990)
Parallels in the origin of the geochemical signatures of island arc volcanics and continental potassic igneous rocks: the role of residual titanates.
Chem. Geol. 85, 1-18

France-Lanord C., Michard A., Bouquillon A., Tiercelin J.-J. (1990)
Isotopic chemistry and sedimentology of the Bengal Fan sediments: the denudation of the Himalaya.
Chem. Geol. 84, 368-370

Frey F.A., Dickey J.S. Jr. (1977)
Eastern Indian Ocean DSDP sites: correlations between petrography, geochemistry and tectonic setting.
in "Indian Ocean geology and biostratigraphy" by Heirtzler et al. (Eds), 189-257 American Geophysical Union

Frey F.A., Green D.H., Roy S.D. (1978)
Integrated models of basalt petrogenesis: a study of quartz tholeiites to olivine melilitites from south eastern Australia utilizing geochemical and experimental petrological data.
Jour. Petrol. 19(3), 463-513

Frey F.A., Jones W.B., Davies H., Weis D. (1991)
Geochemical and petrologic data for basalts from sites 756, 757, and 758: implications for the origin and evolution of the Ninetyeast Ridge.
ODP Scientific Results vol. 121, 611-659

Furukawa Y. (1993)
Magmatic processes under arcs and formation of the volcanic front.
Jour. Geophys. Res. 98 (B5), 8309-8319

Gatinsky Y., Hutchison C.S., Minh N., Tri T.V. (1984)
Tectonic evolution of South East Asia.
in "Tectonics of Asia" (A.L. Yanshin Ed.), 27th Int. Geol. Congress, Colloquium 5, 225-240, Nauka, Moscow

Gautier I., Weis D., Mennessier J.-P., Vidal P., Giret A., Loubet M. (1990)
Petrology and geochemistry of the Kerguelen Archipelago basalts (South Indian Ocean): evolution of the mantle sources from ridge to intraplate position.
Earth Plan. Sci. Lett. 100, 59-76

Gerbe M.C. (1989)
Evolution d'une chambre magmatique zonée en système dos: exemple de l'éruption de 1982-83 du Galunggung (Java, Indonesia).
Unpubl. PhD thesis, Université Blaise Pascal, Clermont-Ferrand, France.

Gerbe M.-C., Gourgaud A., Sigmarsson O., Harmon R.S., Joron J.-L., Provost A. (1992)
Mineralogical and geochemical evolution of the 1982-1983 Galunggung eruption (Indonesia).
Bull. Volc. 54, 284-298

Gill J.B., Williams R.W. (1990)
Th isotope and U-series studies of subduction-related volcanic rocks.
Geoch. Cosmoch. Acta 54, 1427-1442

Gill J., Condomines M. (1992)
Short-lived radioactivity and magma genesis.
Science 257, 1368-1376

Goldstein S.L., O'Nions R.K. (1981)
Nd and Sr isotopic relationships in pelagic clays and ferromanganese deposits.
Nature 292, 324-327

Green D.H. (1970)
The origin of basaltic and nephelinitic magmas.
Trans. Leicester Lit. Phil. Soc. 64, 28-54

Green R., Adkins J.S., Harrington H.J., Untung M. (1979)
Bouguer gravity anomaly map of Indonesia, with marginal text.
Univ. of New England, Armidale, N.S.W., Australia.

Green T.H. (1981)
Experimental evidence for the role of accessory phases in magma genesis.
Jour. Volc. Geoth. Res. 10, 405-422

Griffin W.L., Wass S.Y., Hollis J.D. (1984)
Ultramafic xenoliths from Bullenmerri and Gnotuk maars, Victoria: petrology of a subcontinental crust-mantle transition.
Jour. Petrol. 25, 53-87

Hadikusumo D. (1961)
Bullettin of the Volcanological Survey of Indonesia for the period 1950-1957.
Republik Indonesia Dept. Perindustrian Dasar/Pertambangan Djawatan Geologi, Bandung, 122 pp.

Haile N.S. (1981)
Palaeomagnetic evidence and the geotectonic history and palaeogeography of eastern Indonesia.
in: "Geology and tectonics of eastern Indonesia" (A.J. Barber & Wiryosujono S. Eds.) GRDC Spec. Publ. 2, 81-87

Hamelin B., Allègre C.J. (1985)
Large-scale regional units in the depleted upper mantle revealed by an isotope study of the South-West Indian Ridge.
Nature 315, 196-199

Hamelin B., Dupré B., Allègre C.J. (1985-86)
Pb-Sr-Nd isotopic data of Indian Ocean ridges: new evidence of large-scale mapping of mantle heterogeneities.
Earth Plan. Sci. Lett. 76, 288-298

Hamilton W.B. (1970)
Tectonic map of the Indonesian region, a progress report.
U.S. Geol. Surv. Open File Report, 29 pp.

Hamilton W.B. (1972)
Preliminary tectonic map of the Indonesian region.
U.S. Geol. Surv. Open File Report, 3 sheets.

Hamilton W.B. (1973)
Tectonics of the Indonesian region.
Bull. Geol. Soc. Malaysia 6, 3-10

Hamilton W.B. (1976)
Subduction in the Indonesian region.
Proc. 5th Ann. Conv. Indones. Petrol. Ass. Jakarta, 1976, II, 3-23

Hamilton W.B. (1977)
Subduction in the Indonesian region.
in: "Island arcs, deep sea trenches and backarc basins." Amer. Geophys. Union (Maurice Ewing Series 1), 15-31

Hamilton W.B. (1978)
Tectonic map of the Indonesian region 1:5,000,000.
Map 1-875-D US Geol. Surv.

Hamilton W.B. (1979)
Tectonics of the Indonesian region.
U.S. Geol. Surv. Prof. Pap. 1078, 345 pp.

Hamilton W.B. (1981)
Plate motions in eastern Indonesia and surrounding regions.
in: "Geology and tectonics of eastern Indonesia" (A.J. Barber & Wiryosujono S. Eds.) GRDC Spec. Publ. 2, 29

Hamilton W.B. (1988)
Plate tectonics and island arcs.
Bull. Geol. Soc. Amer. 100, 1503-1527

Hamilton W.B. (1989)
Convergent plate tectonics viewed from the Indonesian region.
in "Tectonic evolution of the Tethyan Region" (Sengor A.M.C. editor et al.) NATO Advanced Study Institutes Series - Series C; Mathematical and Physical Sciences 655-698

Hamlyn P.R. (1975)
Chromite alteration in the Panton Sill, East Kimberley region, Western Australia.
Min. Mag. 40, 181-192

Harahap B.H. (1990)
Magmatism in West Kalimantan.
Jour. Southeast Asian Earth Sci. 4(1), 76

Harbury N.A., Kallagher H.J. (1991)
The Sunda outer-arc ridge, North Sumatra, Indonesia.
Jour. Southeast Asian Earth Sci. 6 (3/4), 463-476

Harjono H., Diament M., Dubois J., Larue M., Zen M.T. (1991)
Seismicity of the Sunda Strait: evidence for crustal extension and volcanological implications.
Tectonics 10, 1, 17-30

Harmon R.S., Gerbe M.-C. (1992)
The 1982-83 eruption at Galunggung volcano, Java (Indonesia): oxygen isotope geochemistry of a chemically zoned magma chamber.
Jour. Petrol. 33(3), 585-609

Hart S.R. (1984)
A large scale isotope anomaly in the Southern Hemisphere mantle.
Nature 309, 753-757

Hart S.R., Staudigel H. (1986)
Ocean crust vein mineral deposition: Rb/Sr ages, U-Th-Pb geochemistry, and duration of circulation at DSDP sites 261, 462 and 516.
Geoch. Cosmoch. Acta 50, 2751-2761

Hart S.R. (1988)
Heterogeneous mantle domains: signatures, genesis and mixing chronologies.
Earth Plan. Sci. Lett. 90(3), 273-296

Hart S.R., Staudigel H. (1989)
Isotopic characterization and identification of recycled components.
in "Crust/mantle recycling at convergence zones" by Hart & Gülen (Eds), 15-28 NATO ASI Series (Series C)

Hart S.R., Zindler A. (1989)
Constraints on the nature and development of chemical heterogeneities in the mantle.
in "Mantle convection - Plate tectonics and global dynamics." (W.R. Peltier Ed.) pp. 261-387

Hart S.R., Hauri E.H., Oschmann L.A., Whitehead J.A. (1992)
Mantle plumes and entrainment: isotopic evidence.
Science 256, 517-520

Hart S.R., Dunn T. (1993)
Experimental cpx/melt partitioning of 24 trace elements.
Contrib. Mineral. Petrol. 113, 1-8

Hatherton T., Dickinson W.R. (1969)
The relationship between andesite volcanism and seismicity in Indonesia, the Lesser Antilles, and other island arcs.
Jour. Geophys. Res. 74, 5301-5310

Heezen B.C., Lynde P.R. Jr., Fornari D.J. (1977)
Geological map of the Indian Ocean.
in "Indian Ocean geology and biostratigraphy" by Heirtzler et al. (Eds), American Geophysical Union

Hehuwat F. (1976)
Isotopic age determinations in Indonesia: the state of the art.
Proceedings of the Seminar on Isotopic Dating (CCOP/TP .3), 135-157

Hekinian R. (1968)
Rocks from the Mid-Oceanic Ridge in the Indian Ocean.
Deep Sea Res. 15, 195-213

Hekinian R. (1974)
Petrology of igneous rocks from leg 22 in the northeastern Indian Ocean.
Initial Reports of the Deep Sea Drilling Project Volume 22, 413-447 National Science Foundation

Hémond C. (1986)
Unpubl. Thèse 3eme Cycle, Université Paris VII, France

Hildreth W., Moorbath S. (1988)
Crustal contributions to arc magmatism in the Andes of Central Chile.
Contrib. Mineral. Petrol. 98, 455-489

Hildreth W., Moorbath S. (1991)
Reply to comment on "Crustal contributions to arc magmatism in the Andes of Central Chile".
Contrib. Mineral. Petrol. 108, 247-252

Hilton D.R., Craig H. (1989)
A helium isotope transect along the Indonesian archipelago.
Nature 342, 906-908

Hilton D.R., Hoogewerff J.A., van Bergen M.J., Hammerschmidt K. (1992)
Mapping magma sources in the east Sunda-Banda arcs, Indonesia: constraints from helium isotopes.
Geoch. Cosmoch. Acta 56, 851-859

Hilton D.R., Hammerschmidt K., Loock G., Friedrichsen H. (1993)
Helium and argon isotope systematics of the central Lau Basin and Valu Fa Ridge: evidence of crust/mantle interactions in a back-arc basin.
Geoch. Cosmoch. Acta 57, 2819-2841

Hochstaedter A.G., Gill J.B., Kusakabe M., Newman S., Pringle M., Taylor B., Fryer P. (1990a)
Volcanism in the Sumisu Rift, I. Major element, volatile, and stable isotope geochemistry.
Earth Plan. Sci. Lett. 100, 179-194

Hochstaedter A.G., Gill J.B., Morris J.D. (1990b)
Volcanism in the Sumisu Rift, II. Subduction and non-subduction related components.
Earth Plan. Sci. Lett. 100, 195-209

Hofmann A.W. (1988)
Chemical differentiation of the Earth: the relationship between mantle, continental crust, and oceanic crust.
Earth Plan. Sci. Lett. 90, 297-314

Hoffmann A.W. (1990)
Volatile or melt transfer of Nb, Ta, and Pb during subduction?
abstract in "V.M. Goldschmidt conference", 2-4/5/1990

Holcombe C.J. (1977)
Earthquake foci distribution in the Sunda arc and rotation of the back arc area.
Tectonophysics 43, 169-180

Holcombe C.J. (1977)
How rigid are the lithospheric plates? Fault and shear rotations in southeast Asia.
Jour. Geol. Soc. London 134, 325-342

Holness M.B., Richter F.M. (1989)
Possible effects of spreading rate on MORB isotopic and rare earth composition arising from melting of a heterogeneous source.
Jour. Geology 97, 247-260

Huchon P., Le Pichon X. (1984)
Sunda Strait and central Sumatra fault.
Geology 12, 668-672

Hutchison C.S. (1973)
Tectonic evolution of Sundaland: a Phanerozoic synthesis.
Bull. Geol. Soc. Malaysia 6, 61-86

Hutchison C.S. (1975)
Correlation of Indonesian active volcanic geochemistry with Benioff zone depth.
Geologie en Mijnbouw 54, 157-168

Hutchison C.S. (1976)
Indonesian active volcanic arc: K, Sr, and Rb variation with depth to the Benioff zone.
Geology 4, 407-408

Hutchison C.S. (1977)
Granite emplacement and tectonic subdivision of Peninsular Malaysia.
Bull. Geol. Soc. Malaysia 9, 187-207

Hutchison C.S. (1978)
Southeast Asian tin granitoids of contrasting tectonic setting.
Physics of the Earth 26 (supp.) S221-S232

Hutchison C.S., Taylor D. (1978)
Metallogenesis in S.E. Asia.
Jour. Geol. Soc. London 135, 407-428

Hutchison C.S. (1981)
Review of the Indonesian volcanic arc.
in: "Geology and tectonics of eastern Indonesia" (A.J. Barber & Wiryosujono S. Eds.) GRDC Spec. Publ. 2, 65-80

Hutchison C.S. (1982)
Southeast Asia.
in "The ocean basins and margins. Vol. 6 - The Indian Ocean" (A.E.M. Nairn & F.G. Stehli Eds.) pp. 451-512

Hutchison C.S. (1983)
Multiple Mesozoic Sn-W-Sb granitoids of southeast Asia.
Mem. Geol. Soc. Am. 159, 35-60

Hutchison C.S. (1989)
Geological evolution of South-east Asia.
Oxford Monographs on Geology and Geophysics 13, pp. 368

Iddings J.P., Morley E.W. (1915)
Contribution to the petrography of Java and Celebes.
Jour. Geol. 23, 231-245

Irvine T.N. (1967)
Chromian spinel as a petrogenetic indicator, Part 2: Petrologic applications.
Can. Jour. Earth Sci. 4, 71-103

Invine T.N., Baragar W.R.A. (1971)
A guide to the chemical classification of the common volcanic rocks.
Can. Jour. Earth Sci. 8(5), 523-548

Irving A.J., Green D.H. (1981)
Geochemistry and petrogenesis of the Newer basalts of Victoria and South Australia.
Jour. Geol. Soc. Australia. 23, 45-66

Ishikawa T., Nakamura E. (1993)
Boron isotope systematics of marine sediments.
Earth Plan. Sci. Lett. 117, 567-580

Ishiwatari A. (1992)
Petrology, geochemistry, and mineralogy of the Early Cretaceous evolved N-MORB from sites 765 and 766, Eastern Indian Ocean.
ODP Scientific Results vol. 123, 201-213

Ito E., White W.M., Göpel C. (1987)
The O, Sr, Nd, and Pb isotope geochemistry of MORB.
Chem. Geol. 62, 157-176

Jacobson R.S., Shor Jr G.G., Kieckhefer R.M., Purdy G.M. (1979)
Seismic refraction and reflection studies in the Timor-Aru Trough system and Australian continental shelf.
in: "Geological and geophysical investigation of the continental margins" (J. Watkins et al. Eds.), Amer. Assoc. Petrol. Geol. Mem. 29, 209-222

Jarosewich E.J., Nelen J.A., Norberg J.A. (1980)
Reference samples for electron microprobe analysis.
Geostandards Newsletter 4, 43-47

Jarrard R.D. (1986)
Relations among subduction parameters.
Rev. Geophys. 24(2), 217-284

Jezek P.A., Hutchison C.S. (1978)
Banda arc of eastern Indonesia: petrology and geochemistry of the volcanic rocks.
Bull. Volc. 41, 586-608

Jochum K.P., McDonough W.F., Palme H., Spettel B. (1989)
Compositional constraints on the continental lithospheric mantle from trace elements in spinel peridotite xenoliths.
Nature 340, 548-550

Johnson R.W.(1989)
Intraplate volcanism in eastern Australia and New Zealand.
Cambridge University Press 408 pp.

Johnston C.R. (1981)
A review of Timor tectonics, with implications for the development of the Banda arc.
in: "Geology and tectonics of eastern Indonesia" (A.J. Barber & Wiryosujono S. Eds.) GRDC Spec. Publ. 2, 199-216

Jones M.T., Reed B.L., Doe B.R., Lanphere M.A. (1977)
Age of tin mineralization and plumbotectonics, Belitung, Indonesia.
Econ. Geol. 72(5), 745-752

Karig D.E., Lawrence M.B., Moore G.F., Curray J.R. (1980)
Structural framework of the fore-arc basin, NW Sumatra.
Jour. Geol. Soc. London 137, 77-91

Karig D.E., Barber A.J., Charlton T.R., Klemperer S., Hussong D.M. (1987)
Nature and distribution of deformation across the Banda arc-Australian collision zone at Timor.
Bull. Geol. Soc. Am. 98, 18-32

Katili J.A. (1971)
A review of the geotectonic theories and tectonic maps of Indonesia.
Earth Sci. Rev. 7, 143-163

Katili J.A. (1973)
Geochemistry of west Indonesia and its implications for plate tectonics.
Tectonophysics 19, 195-212

Katili J.A. (1975)
Volcanism and plate tectonics in the Indonesian island arc.
Tectonophysics 26, 165-188

Kay R.W. (1990)
Subduction zone fluids: fact and fiction.
abstract in "V.M. Goldschmidt conference", 2-4/5/1990

Kelemen P.B., Johnson K.T.M., Kinzler R.J., Irving A.J. (1990)
High-field-strength element depletions in arc basalts due to mantle-magma interactions.
Nature 345, 521-524

Kempe D.R.C. (1975)
Normative mineralogy and differentiation patterns of some drilled and dredged oceanic basalts.
Contrib. Mineral. Petrol. 50(4), 305-320

Kidd R.B., Davies T.A. (1978)
Indian Ocean sediment distribution since the Late Jurassic.
Mar. Geol. 26, 49-70

Kieckhefer R.M., Shor Jr G.G., Curray J.R., Sugiarta W., Hehuwat F. (1980)
Seismic refraction studies of of the Sunda Trench and forearc basin.
Jour. Geophys. Res. 85, 863-889

Klinkhammer G.P., Palmer M.R. (1991)
Uranium in the oceans: where it goes and why.
Geoch. Cosmoch. Acta 55, 1799-1806

Knight M.D., Walker G.L., Ellwood B.B., Diehl J.F. (1986)
Stratigraphy, paleomagnetism, and magnetic fabric of the Toba tuffs: constraints on the sources and eruptive styles.
Jour. Geophys. Res. 91, 10355-10382

Kolla V. (1974)
Mineralogical data from sites 211, 212, 213, 214 and 215 of DSDP Leg 22 and origin of noncarbonate sediments in the equatorial Indian Ocean.
DSDP Initial Reports vol. 22, 489-501

Kolla V., Kidd R.B. (1982)
Sedimentation and sedimentary processes in the Indian Ocean.
in "The ocean basins and margins. Vol. 6 - The Indian Ocean" (A.E.M. Nairn & F.G. Stehli Eds.) pp. 1-50

Kuno H. (1959)
Origin of Cenozoic petrographic provinces in Japan and surrounding areas.
Bull. Volc. II, 20, 37-76

Kusumadinata K. (1979)
Data dasar gunungapi Indonesia.
Volcanological Survey of Indonesia, 820 pp.

Langmuir D. (1978)
Uranium solution-mineral equilibria at low temperature with application to sedimentary ore deposits.
Geoch. Cosmoch. Acta 42, 547-569

Lavrentev Y.G., Pospelova L.N., Sobolev N.V. (1974)
Rock-forming mineral compositions determination by X-ray microanalysis.
Zavodskaya Laboratoria 40, 657-666

Le Bas M.J., Le Maitre R.W., Woolley A.R. (1992)
The construction of the total alkali-silica chemical classification of volcanic rocks.
Mineralogy and Petrology 46, 1-22

Lee C.S., McCabe R. (1986)
The Banda-Celebes-Sulu basin - a trapped piece of Cretaceous-Eocene oceanic crust?
Nature 322, 51-54

Leeman W.P. (1990)
The utility of boron as a tracer of subducted processes: slab contribution to arc magmatism and implications for recycling of lithospheric material into the deep mantle.
abstract in "V.M. Goldschmidt conference", 2-4/5/1990

Le Maitre R.W. (1976)
Chemical variability of some common igneous rocks.
Jour. Petrol. 17, 589-637

Le Maitre R.W. (1982)
Numerical petrology.
Elsevier, Amsterdam 281 pp.

Leo G.W., Hedge C.E., Marvin R.F. (1980)
Geochemistry, strontium isotope data, and potassium-argon ages of the andesite-rhyolite association in the Padang area, West Sumatra.
Jour. Volc. Geoth. Res. 7, 139-156

Le Roex A.P., Dick H.J.B., Erlank A.J., Reid A.M., Frey F.A., Hart R. (1983)
Geochemistry, mineralogy and petrogenesis of lavas erupted along the Southwest Indian Ridge between the Bouvet triple junction and 11 degrees east.
Jour. Petrol. 24, 3, 267-318

Le Roex A.P. (1985)
Geochemistry, mineralogy and magmatic evolution of the basaltic and trachytic lavas from Gough Island, South Atlantic.
Jour. Petrol. 26, 149-186

Le Roex A.P., Dick H.J.B., Fisher R.L. (1989)
Petrology and geochemistry of MORB from 25° E to 46° E along the Southwest Indian Ridge: evidence for contrasting styles of mantle enrichment.
Jour. Petrol. 30, 4, 947-986

Lin P.-N. (1992)
Trace element and isotopic characteristics of Western Pacific pelagic sediments: implications for the petrogenesis of Mariana arc magmas.
Geoch. Cosmoch. Acta 56, 1641-1654

Lippolt H.J., Weigel E. (1988)
4He diffusion in 40Ar-retentive minerals.
Geoch. Cosmoch. Acta 52, 1449-1458

Liu C.S., Curray J.R., McDonald J.M. (1983)
New constraints on the tectonic evolution of the eastern Indian Ocean.
Earth Plan. Sci. Lett. 65, 331-342

Liu C.S., Curray J.R., Shor G.G.Jr (1989)
Structure and nature of the fore-arc basin off West Central Sumatra.
EOS Trans. (abs) 70 (20), 603

Ludden J.N. (1992)
Radiometric age determinations for basement from sited 765 and 766, Argo Abyssal Plain and northwestern Australian margin.
ODP Scientific Results vol. 123, 557-559

Ludden J.N., Dionne B. (1992)
The geochemistry of oceanic crust at the onset of rifting in the Indian Ocean.
ODP Scientific Results vol. 123, 791-799

Luyendyk B.P. (1974)
Gondwanaland dispersal and the early formation of the Indian Ocean.
DSDP Initial Reports vol. 26, 945-952

Luyendyk B.P. (1977)
Deep sea drilling in the Ninetyeast Ridge: synthesis and a tectonic model.
in "Indian Ocean geology and biostratigraphy" by Heirtzler et al. (Eds), 165-187 American Geophysical Union

Lykins R.L., Jenkins D.M. (1992)
Experimental determination of pargasite stability relations in the presence of orthopyroxene.
Contrib. Mineral. Petrol. 112, 405-413

Magaritz M., Whitford D.J., James D.E. (1977)
Oxygen and strontium isotope variation and the origin of andesites.
Geol. Soc. Amer. Abs. with Progs. 9, 7, 1082

Magaritz M., Whitford D.J., James D.E. (1978)
Oxygen isotopes and the origin of high-87Sr/86Sr andesites.
Earth Plan. Sci. Lett. 40, 220-230

Mahoney J.J., Macdougall J.D., Lugmair G.W., Gopalan K. (1983)
Kerguelen hotspot source for Rajmahal Traps and Ninetyeast Ridge?
Nature 303, 385-389

Mahoney J., Le Roex A.P., Peng Z., Fisher R.L., Natland J.H. (1992)
Southwestern limits of Indian Ocean Ridge mantle and the origin of low 206Pb/204Pb Mid-Ocean Ridge basalts: isotope systematics of the central Southwest Indian Ridge (17° - 50° E).
Jour. Geophys. Res. 97(B13), 19771-19790

Mangga A.S., Gafoer S., Suwarti T., Amiruddin (1986)
1:250,000 Geologic map of the Tanjungkarang quadrangle, Sumatra.
Geological Research and Development Centre, Bandung, Indonesia

Marks P. (1931)
Stratigraphic lexicon of Indonesia.
Publikasi Keilmuan No. 31 Seri Geologi, 231 pp.

Masson D.G. (1988)
Active margin tectonics in eastern Indonesia: a study with GLORIA and underway geophysics.
Wormley, U.K. Institute of Oceanographic Sciences, Cruise Rep. 202, 20 pp.

Masson D.G., Parson L.M., Milsom J., Nichols G., Sikumbang N., Dwiyanto B., Kallagher H. (1990)
Subduction of seamounts at the Java Trench: a view with long-range sidescan sonar.
Tectonophysics 185, 51-65

Maurel C., Maurel P. (1982)
Etude experimentale de la distribution de l'aluminium entre bain silicate basique et spinelle chromifere. Implications petrogenetiques: teneur en chrome des spinelles.
Bull. Mineral. 105, 197-202

Maurel C., Maurel P. (1983)
Influence du fer ferrique sur la distribution de l'aluminium entre bain silicaté basique et spinelle chromifère.
Bull. Mineral. 106, 623-624

Maury R.C., Defant M.J., Joron J.-L. (1992)
Metasomatism of the sub-arc mantle inferred from trace elements in Philippine xenoliths.
Nature 360, 661-663

McBride J.H., Karig D.E. (1987)
Crustal structure of the outer Banda arc: new free-air gravity evidence.
Tectonophysics 140, 265-273

McCaffrey R., Silver E.A., Raitt R.W. (1980)
Crustal structure of the Molucca Sea collision zone, Indonesia.
Amer. Geophys. Union Geophys. Monograph 23, 161-178

McCaffrey R. (1981)
Evidence for lateral segmentation of the subducted Australian-Indian plate beneath the Banda arc near western Timor.
EOS Trans. AGU 62, 949

McCaffrey R., Silver E.A., Raitt R.W. (1981)
Crustal structure of the Molucca Sea collision zone, Indonesia.
in: "Geology and tectonics of eastern Indonesia" (A.J. Barber & Wiryosujono S. Eds.) GRDC Spec. Publ. 2, 341

McCaffrey R. (1982)
Lithospheric deformation within the Molucca Sea arc-arc collision - evidence from shallow and intermediate earthquake activity.
Jour. Geophys. Res. 87, 3663-3678

McCaffrey R., Molnar P., Roecker S.W., Joyodiwiryo Y.S. (1985)
Microearthquake seismicity and fault plane solutions related to arc-continent collision in the eastern Sunda arc, Indonesia.
Jour. Geophys. Res. 90(B6), 4511-4528

McCaffrey R., Nabelek J. (1984a)
The geometry of backarc thrusting along the eastern Sunda arc, Indonesia: constraints from earthquake and gravity data.
Jour. Geophys. Res. 89, 6171-6179

McCaffrey R., Nabelek J. (1984b)
Depths and source mechanisms of earthquakes from the eastern Sunda arc, Indonesia.
EOS Trans. AGU 65, 997

McCaffrey R. (1988)
Active tectonics of the eastern Sunda and Banda arcs.
Jour. Geophys. Res. 93, 15163-15182

McCaffrey R. (1991)
Slip vectors and stretching of the Sumatran fore arc.
Geology 19, 881-884

McCulloch M.T., Compston W., Abbott M., Chivas A. (1983)
Neodymium, strontium, lead and oxygen isotopic and trace element constraints on magma genesis in the Banda island-arc, Wetar.
Sixth Australian Geological Convention, Canberra 1983, Abs. 9, 152-153

McCulloch M.T., Gamble J.A. (1991)
Geochemical and geodynamical constraints on subduction zone magmatism.
Earth Plan. Sci. Lett. 102, 358-374

McDermott F., Hawkesworth C. (1991)
Th, Pb and Sr isotope variations in young island arc volcanics and oceanic sediments.
Earth Plan. Sci. Lett. 104, 1-15

McDermott F., Defant M.J., Hawkesworth C.J., Maury R.C., Joron J.-L. (1993)
Isotope and trace element evidence for three component mixing in the genesis of the North Luzon arc lavas (Philippines).
Contrib. Mineral. Petrol. 113, 9-23

McDonough W.F., McCulloch M.T., Sun S.S. (1985)
Isotopic and geochemical systematics in Tertiary-Recent basalts from southeastern Australia and implications for the evolution of the sub-continental lithosphere.
Geoch. Cosmoch. Acta 49, 2051-2067

McDougall I. (1974)
Potassium-argon ages on basaltic rocks recovered from DSDP, leg 22, Indian Ocean.
Initial Reports of the Deep Sea Drilling Project Volume 22, 377-379 National Science Foundation

McLennan S.M., McCulloch M.T., Taylor S.R., Maynard J.B. (1989)
Effects of sedimentary sorting on neodymium isotopes in deep-sea turbidites.
Nature 337, 547-549

McLennan S.M., Taylor S.R., McCulloch M.T., Maynard J.B. (1990)
Geochemical and Nd-Sr isotopic composition of deep-sea turbidites: crustal evolution and plate tectonic associations.
Geoch. Cosmoch. Acta 54, 2015-2050

McMillan N.J., Davidson J.P., Wörner G., Harmon R.S., Moorbath S., Lopez-Escobar L. (1993)
Influence of crustal thickening on arc magmatism: Nevados de Payachata volcanic region, northern Chile.
Geology 21, 467-470

Metcalfe I. (1984)
Late Palaeozoic palaeogeography of southeast Asia: some stratigraphical, palaeontological and palaeomagnetic constraints.
5th Regional Congress Geology and Mineral Resources of S.E. Asia, Kuala Lumpur, Abs. 20

Metcalfe I. (1988)
Origin and assembly of South-East Asian continental terranes.
in "Gondwana and Tethys", Geol. Soc. Spec. Publ. 37, Geol. Soc. London (M. Audley-Charles and H. Hallam Eds.), 101-118

Michard A., Montigny R., Schlich R. (1986)
Geochemistry of the mantle beneath the Rodriguez triple junction and the South-East Indian Ridge.
Earth Plan. Sci. Lett. 78, 104-114

Middlemost E.A.K., Paul D.K., Fletcher I.R. (1988)
Geochemistry and mineralogy of the minette-lamproite association from the Indian Gondwanas.
Lithos 22, 31-42

Mitchell A.H.G. (1977)
Tectonic settings for emplacement of Southeast Asian tin granites.
Bull. Geol. Soc. Malaysia 9, 123-140

Molnar P., Tapponnier P. (1975)
Tectonics of Asia: consequences and implications of a continental collision.
Science 189, 419-426

Moore G.F., Curray J.R., Moore D.J., Karig D.E. (1980)
Variations in geologic structures along the Sunda fore arc, northeastern Indian Ocean.
Amer. Geophys. Union Geophys. Monograph 23, 145-160

Moore G.F., Silver E.A. (1982)
Collision processes in the northern Molucca Sea.
Amer. Geophys. Union Geophys. Monograph 27, 360-372

Moran A.E., Sisson V.B., Leeman W.P. (1990)
The fate of boron in subducted oceanic slab: effects of burial, metamorphism, and chemical processing.
abstract in "V.M. Goldschmidt conference", 2-4/5/1990

Morris J.D., Hart S.R. (1980)
Lead isotopic geochemistry of the Banda arc.
EOS Trans. 61(46), 1157

Morris J.D., Hart S.R. (1983)
Isotopic and incompatible element constraints on the genesis of island arc volcanics from Cold Bay and Amak Islands, Aleutians, and implications for mantle structure.
Geoch. Cosmoch. Acta 47, 2015-2030

Morris J.D., Leeman W.P., Tera F. (1990)
The subducted component in island arc lavas: constraints from Be isotopes and B-Be systematics.
Nature 344, 31-36

Muenow D.W., Garcia M.O., Aggrey K.E., Bednarz U., Schmincke H.U. (1990)
Volatiles in submarine glasses as a discriminant of tectonic origin: application to the Troodos ophiolite.
Nature 343, 159-161

Müller R.D., Royer J.-Y., Lawver L.A. (1993)
Revised plate motions relative to the hotspots from combined Atlantic and Indian Ocean hotspot tracks.
Geology 21, 275-278

Navon O., Stolper E. (1987)
Geochemical consequences of melt percolation: the upper mantle as a chromatographic column.
Jour. Geol. 95, 285-307

Nelson B.K. (1991)
Sediment-derived fluids in subduction zones: isotopic evidence from veins in blueschist and eclogite of the Franciscan Complex, California.
Geology 19, 1033-1036

Neumann van Padang M. (1951)
Catalogue of the active volcanoes of the world including solfatara fields. Part 1: Indonesia.
International Volcanological Association, Napoli, 271 pp.

Newcomb K.R., McCann W.R. (1987)
Seismic history and seismotectonics of the Sunda Arc.
Jour. Geophys. Res. 92, B1, 421-439

Nicholls I.A., Whitford D.J. (1976)
Primary magmas associated with Quaternary volcanism in the western Sunda arc, Indonesia.
in: "Volcanism in Australasia" (R.W. Johnson Ed.), 77-90

Nicholls I.A., Whitford D.J., Harris K.L., Taylor S.R. (1980)
Variation in the geochemistry of mantle sources for tholeiitic and calc-alkaline mafic magmas, western Sunda volcanic arc, Indonesia.
Chem. Geol. 30, 177-199

Nicholls I.A., Whitford D.J. (1983)
Potassium rich volcanic rocks of the Muriah complex, Jawa, Indonesia: products of multiple magma sources?
Jour. Volc. Geoth. Res. 18, 337-359

Nielson D.R., Stoiber R.E. (1973)
Relationship of potassium content in andesitic lavas and depth to the seismic zone.
Jour. Geophys. Res. 78, 6887-6892

Ninkovich D., Hays J.D. (1972)
Mediterranean island arcs and origin of high potash volcanoes.
Earth Plan. Sci. Lett. 16, 331-345

Ninkovich D. (1976)
Late Cenozoic clockwise rotation of Sumatra.
Earth Plan. Sci. Lett. 29, 269-275

Ninkovich D., Shackleton N.J., Abdel-Monem A.A., Obradovich J.D., Izett G. (1978a)
K-Ar age of the Pleistocene eruption of Toba, North Sumatra.
Nature 276, 574-577

Ninkovich D., Sparks R.S.J., Ledbetter M.T. (1978b)
The exceptional magnitude and intensity of the Toba eruption, Sumatra: an example of the use of deep-sea tephra layers as a geological tool.
Bull. Volc. 41-3, 286-298

Nishimura S. (1980)
Geochemistry of volcanic rocks at Krakatau, Indonesia.
in "Physical geology of the Indonesian island arcs" (Ed. S. Nishimura), 109-113

Nishimura S., Otofuji Y., Ikeda T., Abe E., Yokoyama T., Kobayashi Y., Hadiwisastra S., Sophaluwakan J., Hehuwat F. (1981)
Physical geology of the Sumba, Sumbawa and Flores islands.
in: "Geology and tectonics of eastern Indonesia" (A.J. Barber & Wiryosujono S. Eds.) GRDC Spec. Publ. 2, 105-113

Nishimura S., Abe E., Nishida J., Yokoyama T., Hehanussa P., Hehuwat F. (1984)
A gravity and volcanostratigraphic interpretation of the Lake Toba region, North Sumatra, Indonesia.
Tectonophysics 109, 253-272

Nishimura S., Nishida J., Yokoyama T., Hehuwat F. (1986)
Neo-tectonics of the Strait of Sunda, Indonesia.
Jour. Southeast. Asian Earth Sci. 1(2), 81-91

Nishimura S., Suparka S. (1986)
Tectonic development of east Indonesia.
Jour. Southeast Asian Earth Sci. 1, 45-57

Norvick M.S. (1979)
The tectonic history of the Banda arcs, eastern Indonesia: a review.
Jour. Geol. Soc. London 136, 519-527

Norrish K., Chappell B.W. (1977)
X-ray fluorescence spectrography.
in "Physical methods in determinative mineralogy." (J. Zussman Ed.) Academic Press, 161-214

Norrish K., Hutton J.T. (1969)
An accurate X-ray spectrographic method for the analysis of a wide range of geological samples.
Geoch. Cosmoch. Acta 33, 431-455

Noujaim A.K. (1976)
Drilling in high temperature and over-pressured area, Pertamina/Amin Oil Well C-1-SX, Sunda Strait, Indonesia.
Jakarta, 27 pp.

Obata M. (1980)
The Ronda peridotite: garnet-, spinel-, and plagioclase-lherzolite facies and the P-T trajectories of a high-temperature mantle intrusion.
Jour. Petrol. 21, 533-572

O'Nions R.K., Carter S.R., Cohen R.S., Evensen N.M., Hamilton P.J. (1978)
Pb, Nd, and Sr isotopes in oceanic ferromanganese deposits and ocean floor basalts.
Nature 273, 435-438

Page B.G.N., Bennett J.D., Cameron N.R., Bridge D.McC., Jeffery D.H., Keats W., Thaib J. (1979)
A review of the main structural and magmatic features of northern Sumatra.
Jour. Geol. Soc. London 136, 569-579

Palacios C.M., Oyarzun R.M. (1975)
Relationship between depth to Benioff zone and K and Sr concentrations in volcanic rocks of Chile.
Geology 3, 595-596

Palmer M.R. (1985)
Rare earth elements in foraminifera tests.
Earth Plan. Sci. Lett. 73, 285-298

Pardede R., Gafoer S. (1986)
1:250,000 Geologic map of the Baturaja (Kotabumi) quadrangle, Sumatra.
Geological Research and Development Centre, Bandung, Indonesia

Paul D.K., Potts P.J. (1981)
Rare-earth abundances and origin of some Indian lamprophyres.
Geol. Mag. 118, 393-399

Peacock S.M. (1990)
Fluid processes in subduction zones.
Science 248, 329-337

Pearce J.A., Cann J.R. (1973)
Tectonic setting of basic volcanic rocks determined using trace element analyses.
Earth Plan. Sci. Lett. 19, 290-300

Pearce J.A., Norry M.J. (1979)
Petrogenetic implications of Ti, Zr, Y, and Nb variations in volcanic rocks.
Contrib. Mineral. Petrol. 69, 33-47

Pearce J.A., Harris N.G.W., Tindle A.J. (1984)
Trace element discrimination diagrams for the tectonic interpretation of granitic rocks.
Jour. Petrol. 25, 956-983

Piepgras D.J., Wasserburg G.J., Dasch E.J. (1979)
The isotopic composition of Nd in different ocean masses.
Earth Plan. Sci. Lett. 45, 223-236

Piepgras D.J., Wasserburg G.J. (1980)
Neodymium isotopic variations in seawater.
Earth Plan. Sci. Lett. 50, 128-138

Pieters P.E., Supriatna S. (1990)
1:1,000,000 Geologic map of the West, Central and East Kalimantan area.
Geological Research and Development Centre, Bandung, Indonesia

Pigram C.J., Panggabean H. (1983)
Age of the Banda Sea, eastern Indonesia.
Nature 301, 231-234

Pineau F., Javoy M. (1990)
Carbon isotope geochemistry at convergent margins and fluid exchanges at mantle-crust boundaries.
abstract in "V.M. Goldschmidt conference", 2-4/5/1990

Plank T., Ludden J.N. (1992)
Geochemistry of sediments in the Argo abyssal plain at site 765: a continental margin reference section for sediment recycling in subduction zones.
ODP Scientific Results 123, 167-189

Plank T. (1993)
Unpubl. PhD thesis, Columbia University, USA

Plank T., Langmuir C.H. (1993)
Tracing trace elements from sediment input to volcanic output at subduction zones.
Nature 362, 739-743

Poorter R.P.E., Varekamp J.C., Poreda R.J., van Bergen M.J., Kreulen R. (1991)
Chemical and isotopic compositions of volcanic gases from the east Sunda and Banda arcs, Indonesia.
Geoch. Cosmoch. Acta 55, 3795-3807

Poreda R., Craig H. (1989)
Helium isotope ratios in circum-Pacific volcanic arcs.
Nature 338, 473-478

Posavec M., Taylor D., van Leeuwen T., Spector A. (1973)
Tectonic control of volcanism and complex movements along the Sumatran fault system.
Geol. Soc. of Malaysia Bull. 6, 43-60

Price R.C., Kennedy A.K., Riggs-Sneeringer M., Frey F.A. (1986)
Geochemistry of basalts from the Indian Ocean triple junction: implications for the generation and evolution of Indian Ocean ridge basalts.
Earth Plan. Sci. Lett. 78, 379-396

Priem H.N.A., Boelrijk N.A.I.M., Born E.H. (1975)
Isotope geochronology in the Indonesian tin belt.
Geologie en Mijnbouw 54, 61-70

Purdy G.M., Detrick R., Shor Jr G.G. (1977)
Crustal structure of the Banda Sea and Weber Deep.
EOS Trans. Amer. Geophys. Union 58(6), 509

Putthapiban P., Gray C.M. (1983)
Age and tin-tungsten mineralization of the Phuket granites, Thailand.
Proceedings of the Conference on Geology and Mineral Resources of Thailand, DMR Bangkok, 1-10

Raitt R.W. (1967)
Marine seismic refraction studies of the Indonesian island arc.
EOS Trans. Amer. Geophys. Union 48, 217

Reagan M.K., Gill J.B. (1989)
Coexisting calcalkaline and high-niobium basalts from Turrialba volcano, Costa Rica: implications for residual titanates in arc magma sources.
Jour. Geophys. Res. 94(B4), 4619-4633

Reed D.L., Silver E.A., Prasetyo H., Meyer A.W. (1986)
Deformation and sedimentation along a developing terrane suture - eastern Sunda forearc, Indonesia.
Geology 14, 1000-1003

Reid M.R., Hart S.R., Padovani E.R., Wandless G.A. (1989)
Contribution of metapelitic sediments to the composition, heat production, and seismic velocity of the lower crust of southern New Mexico, USA.
Earth Plan. Sci. Lett. 95, 367-381

Rittman A. (1953)
Magmatic character and tectonic position of the Indonesian volcanoes.
Bull. Volc. II, 14, 45-58

Robinson P.T., Whitford D.J. (1974)
Basalts from the eastern Indian Ocean, DSDP leg 27
Initial Reports of the Deep Sea Drilling Project Volume 27, 551-559 National Science Foundation

Rock N.M.S., Syah H.H., Davis A.E., Hutchison D., Styles M.T., Lena R. (1982)
Permian to recent volcanism in Northern Sumatra, Indonesia: a preliminary study of its distribution, chemistry and peculiarities.
Bull. Volc. 45-2, 127-152

Roeder P.L., Emslie J.C. (1970)
Olivine-liquid equilibrium.
Contrib. Mineral. Petrol. 29, 275-289

Romeur M., Dosso L., Maury R., Bougault H., Joron J.-L. (1990)
Arc and back-arc geochemical features of the Sunda arc: trace element and isotopic (Sr, Nd, Pb) data from South Sumatra, Central and East Java.
EOS Trans. 71(43), 1700

Romick J.D., Perfit M.R., Swanson S.E., Shuster R.D. (1990)
Magmatism in the eastern Aleutian Arc: temporal characteristic of igneous activity on Akutan Island.
Contrib. Mineral. Petrol. 104, 700-721

Royer J.-Y, Peirce J.W., Weissel J.K. (1991)
Tectonic constraints on the hot-spot formation of the Ninetyeast Ridge.
ODP Scientific results vol. 121, 763-775

Rubin K.H., Wheller G.E., Tanzer M.O., MacDougall J.D., Varne R., Finkel R. (1989)
238U decay series systematics of young lavas from Batur volcano, Sunda Arc.
Jour. Volc. Geoth. Res. 38, 215-226

Rutter M.J. (1987)
Evidence for crustal assimilation by turbulently convecting, mafic alkaline magmas: geochemistry of mantle xenolith-bearing lavas from northern Sardinia.
Jour. Volc. Geoth. Res. 32, 343-354

Ryan J.G., Langmuir C.H. (1993)
The systematics of boron abundances in young volcanic rocks.
Geoch. Cosmoch. Acta 57, 1489-1498

Ryerson F.J., Watson E.B. (1987)
Rutile saturation in magmas: implications for Ti-Nb-Ta depletion in island-arc basalts.
Earth Plan. Sci. Lett. 86, 225-239

Sager W.W., Fullerton L.G., Buffler R.T., Handschumacher D.W. (1992)
Argo Abyssal Plain magnetic lineations revisited: implications for the onset of seafloor spreading and tectonic evolution of the eastern Indian Ocean.
ODP Scientific Results vol. 123, 659-669

Saunders A.D., Norry M.J., Tarney J. (1988)
Origin of MORB and chemically-depleted mantle reservoirs: trace element constraints.
Jour. Petrol. Spec. Vol., 415-445

Salters V.J.M., Shimizu N. (1988)
World-wide occurrence of HFSE-depleted mantle.
Geoch. Cosmoch. Acta 52, 2177-2182

Salters V.J.M., Storey M., Sevigny J.H., Whitechurch H. (1992)
Trace element and isotopic characteristics of Kerguelen-Heard plateau basalts.
ODP Scientific Results vol. 120, 55-62

Sarkar A., Paul D.K., Balasubrahmanyan M.N., Sengupta N.R. (1980)
Lamprophyres from Indian Gondwanas; K/Ar ages and chemistry.
Geol. Soc. India J. 21 (4), 188-193

Sato K. (1991)
K-Ar ages of granitoids in central Sumatra, Indonesia.
Bull. Geol. Survey of Japan 42(3), 111-123

Saunders A.D., Storey M., Gibson I.L., Leat P., Hergt J., Thompson R.N. (1991)
Chemical and isotopic constraints on the origin of basalts from Ninetyeast Ridge, Indian Ocean: results from DSDP Legs 22 and 26 and ODP Leg 121.
ODP Scientific Results vol. 121, 559-590

Schlich R. (1982)
The Indian Ocean: aseismic ridges, spreading centres, and oceanic basins.
in "The ocean basins and margins. vol. 6: The Indian Ocean" (A.E.M. Nairn & F.G. Stehli eds.) 51-147 Plenum Press

Sclater J.G., Fisher R.L. (1974)
Evolution of the east central Indian Ocean with emphasis on the tectonic setting of the Ninetyeast Ridge.
Geol. Soc. Am. Bull. 85, 683-702

Scowen P.A.H., Roeder P.L., Helz R.T. (1991)
Reequilibration of chromite within Kilauea Iki lava lake, Hawaii.
Contrib. Mineral. Petrol. 107, 8-20

Sengor A.M.C., Altiner D., Cin A., Ustaomer T, Hsu K.J. (1988)
Origin and assembly of the Tethyside orogenic collage at the expense of Gondwanaland.
in "Gondwana and Tethys", Geol. Soc. Spec. Publ. 37, Geol. Soc. London (M. Audley-Charles and H. Hallam Eds.), 119-181

Sengupta S., Ray K.K., Acharyya S.K., de Smeth J.B. (1990)
Nature of ophiolite occurrences along the eastern margin of the Indian Plate and their tectonic significance.
Geology 18, 439-442

Sheraton J.W. (1983)
Geochemistry of mafic igneous rocks of the northern Prince Charles Mountains, Antarctica.
Jour. Geol. Soc. Australia 30 (3), 295-304

the Shipboard Scientific Party (1974)
Initial Reports of the Deep Sea Drilling Project Volume 22
National Science Foundation

the Shipboard Scientific Party (1974)
Initial Reports of the Deep Sea Drilling Project Volume 26
National Science Foundation

the Shipboard Scientific Party (1974)
Initial Reports of the Deep Sea Drilling Project Volume 27
National Science Foundation

the Shipboard Scientific Party (1989)
Initial Reports of the Deep Ocean Drilling Program Volume 118
National Science Foundation

the Shipboard Scientific Party (1989)
Initial Reports of the Deep Ocean Drilling Program Volume 119
National Science Foundation

the Shipboard Scientific Party (1989)
Initial Reports of the Deep Ocean Drilling Program Volume 120
National Science Foundation

the Shipboard Scientific Party (1989)
Initial Reports of the Deep Ocean Drilling Program Volume 121
National Science Foundation

the Shipboard Scientific Party (1990)
Initial Reports of the Deep Ocean Drilling Program Volume 122
National Science Foundation

the Shipboard Scientific Party (1990)
Initial Reports of the Deep Ocean Drilling Program Volume 123
National Science Foundation

the Shipboard Scientific Party (R.P. von Herzen, J. Fox, A. Palmer-Julson, P.T. Robinson Eds.) (1991)
Scientific Results of the Deep Ocean Drilling Program Volume 118
National Science Foundation

the Shipboard Scientific Party (J. Barron, J. Anderson, J.G. Baldauf, B. Larsen Eds.) (1991)
Scientific Results of the Deep Ocean Drilling Program Volume 119
National Science Foundation

the Shipboard Scientific Party (S.W. Wise Jr, A. Palmer-Julson, R. Schlich, E. Thomas) (1991)
Scientific Results of the Deep Ocean Drilling Program Volume 120
National Science Foundation

the Shipboard Scientific Party (J. Weissel, J. Alt, J. Peirce, E. Taylor Eds.) (1991)
Scientific Results of the Deep Ocean Drilling Program Volume 121
National Science Foundation

the Shipboard Scientific Party (U. von Rad, B. Ul Haq, R.B. Kidd, S. O'Connell Eds.) (1992)
Scientific Results of the Deep Ocean Drilling Program Volume 122
National Science Foundation

the Shipboard Scientific Party (F.M. Gradstein, A.C. Adamson, J.N. Ludden, W. Poag Eds.) (1992)
Scientific Results of the Deep Ocean Drilling Program Volume 123
National Science Foundation

Silver E.A., Moore J.C. (1978)
The Molucca Sea collision zone, Indonesia.
Jour. Geophys. Res. 83, 1681-1689

Silver E.A., Reed D., McCaffrey R. Joyodiwiryo Y.S. (1983)
Back arc thrusting in the eastern Sunda arc, Indonesia: a consequence of arc-continent collision.
Jour. Geophys. Res. 88 (B9), 7429-7448

Silver E.A., Gill J.B., Schwartz D., Prasetyo H., Duncan R.A. (1985)
Evidence for a submerged and displaced continental borderland, north Banda Sea, Indonesia.
Geology 13, 687-691

Simkin T., Fiske R.S. (1983)
Krakatau 1883.
Smithsonian Inst. Press, Washington D.C. 463 pp.

Simkin T., Smith J.V. (1970)
Minor element distribution in olivines.
Jour. Geol. 78, 304-325

Sobolev A.V., Dmitriev L.V., Barsukov V.L., Nevsorov V.N., Slutsky A.B. (1980)
The formation conditions of the high-magnesium olivines from monomineralic fraction of Luna 24 regolith.
Proc. Lunar Planet. Sc. Conf. 11th Pergamon Press 105-116

Sobolev A.V., Dmitriev L.V., Tsameryan O.P., Kononkova N.N., Robinson P.T. (1991)
A possible primary melt composition for the ultramafic lavas of the Margi area, Troodos ophiolite, Cyprus.
Geol. Surv. Canada Paper 90-20 - "Cyprus crustal study project: initial report, holes CY-1 and 1a" (I.L. Gibson, J. Malpas, P.T. Robinson, and C. Xenophontos Eds.), 203-216

Soeria-Atmadja R., Maury R.C., Bellon H., Joron J.L., Cyrille Y., Bougault H., Hasanuddin (1985)
The occurrence of back-arc basalts in western Indonesia.
Proceedings PIT XIV Ikatan Ahli Geologi Indonesia, Jakarta 10-11 Desember 1985

Staudacher T., Allegre C.J. (1988)
Recycling of oceanic crust and sediments: the noble gas subduction barrier.
Earth Plan. Sci. Lett. 89, 173-183

Stolz A.J., Varne R., Wheller G.E., Foden J.D., Abbott M.J. (1988)
The geochemistry and petrogenesis of K-rich alkaline volcanics from the Batu Tara volcano, eastern Sunda arc.
Contrib. Mineral. Petrol. 98, 374-389

Stolz A.J., Varne R., Davies G.R., Wheller G.E., Foden J.D. (1990)
Magma source components in an arc-continent collision zone: the Flores-Lembata sector, Sunda arc, Indonesia.
Contrib. Mineral. Petrol. 105, 585-601

Storey M., Saunders A.D., Tarney J., Leat P., Thirlwall M.F., Thompson R.N., Menzies M.A., Marriner G.F. (1988)
Geochemical evidence for plume-mantle interactions beneath Kerguelen and Heard Islands, Indian Ocean.
Nature 336, 371-374

Storey M., Saunders A.D., Tarney J., Gibson I.L., Norry M.J., Thirlwall M.F., Leat P., Thompson R.N., Menzies M.A. (1989)
Contamination of Indian Ocean asthenosphere by the Kerguelen-Heard mantle plume.
Nature 338, 574-576

Storey M., Kent R.W., Saunders A.D., Salters V.J., Hergt J., Whitechurch H., Sevigny J.H., Thirlwall M.F., Leat P., Ghose N.C., Gifford M. (1992)
Lower Cretaceous volcanic rocks on continental margins and their relationship to the Kerguelen Plateau.
ODP Scientific Results vol. 120, 33-53

Subbarao K.V., Hekinian R., Chandrasekharam D. (1977)
Large ion lithophile elements and Sr and Pb isotopic variation in volcanic rocks from the Indian Ocean.
in "Indian Ocean geology and biostratigraphy" by Heirtzler et al. (Eds), 259-278 American Geophysical Union

Subbarao K.V., Kempe D.R.C., Reddy V.V., Reddy G.R., Hékinian R. (1979)
Review of the geochemistry of Indian and other oceanic rocks.
Phys. Chem. Earth 11, 367-399

Suensilpong S., Putthapiban P., Mantajit N. (1983)
Some aspects of tin granite and its relationship to tectonic setting.
Mem. Geol. Soc. Am. 159, 77-85

Sugimura A. (1960)
Zonal arrangement of some geophysical and petrological features in Japan and its environs.
Jour. Fac. Sci. Tokyo Univ. II, 12, 133-153

Sun S.-s., McDonough W.F. (1989)
Chemical and isotopic systematics of oceanic basalts: implications for mantle composition and processes.
in Saunders A.D. & Norry M.J. (eds) "Magmatism in the Ocean Basins", Geol. Soc. Special Publication No 42, 315-345

Supriatna S. (1990)
1:250,000 Preliminary geologic map of the Muarawahau quadrangle, Kalimantan.
Geological Research and Development Centre, Bandung, Indonesia

Tanzer M.O. (1985)
Unpubl. MSc thesis, University of California (San Diego), USA

Tatsumi Y., Hamilton D.L., Nesbitt R.W. (1986)
Chemical characteristics of fluid phase released from a subducted lithosphere and origin of arc magmas: evidence from high-pressure experiments and natural rocks.
Jour. Volc. Geoth. Res. 29, 293-309

Taylor S.R., McLennan S.M. (1985)
The continental crust: its composition and evolution.
Blackwell, Oxford

Tera F., Brown L., Morris J., Sacks I.S., Klein J., Middleton R. (1986)
Sediment incorporation in island-arc magmas: inferences from 10Be.
Geoch. Cosmoch. Acta 50, 535-550

Thompson G., Bryan W.B., Frey F.A., Dickey Jr. J.S. (1978)
Basalts and related rocks from deep-sea drilling sites in the central and eastern Indian Ocean.
Mar. Geol. 26, 119-138

Thompson R.N., Morrison M.A., Hendry G.L., Parry S.J. (1984)
An assessment of the relative roles of crust and mantle in magma genesis: an elemental approach.
Phil. Trans. R. Soc. London A310, 549-590

Tilton G.R., Schreyer W., Schertl H.-P. (1991)
Pb-Sr-Nd behavior of deeply subducted crustal rocks from the Dora Maira Massif, Western Alps, Italy -II: what is the age of the ultrahigh-pressure metamorphism?
Contrib. Mineral. Petrol. 108, 22-33

Tjia H.D., Fujii S., Kigoshi K., Sugimura A. (1974)
Late Quaternary uplift in eastern Indonesia.
Tectonophysics 23, 427-433

Trull T.W., Kurz M.D. (1993)
Experimental measurements of 3He and 4He mobility in olivine and clinopyroxene at magmatic temperatures.
Geoch. Cosmoch. Acta 57, 1313-1324

Tu K., Flower M.F.J., Carlson R.W., Xie G., Chen C.-Y., Zhang M. (1992)
Magmatism in the South China Basin: 1. Isotopic and trace-element evidence for an endogenous Dupal mantle component.
Chem. Geol. 97, 47-63

Udintsev G.B. (Chief Editor) (1975)
Geological-geophysical atlas of the Indian Ocean.
Acad. of Science of the U.S.S.R., Moscow

Untung M., Sato Y. (1978)
Gravity and geological studies in Jawa, Indonesia.
Geol. Survey of Indonesia Spec. Publ. 6, 207 pp.

Untung M., Barlow B.C. (1981)
The gravity field in eastern Indonesia.
in: "Geology and tectonics of eastern Indonesia" (A.J. Barber & Wiryosujono S. Eds.) GRDC Spec. Publ. 2, 53-63

van Bemmelen R.W. (1949)
The geology of Indonesia.
Government Printing Office, The Hague, 3 vol.

van Bergen M.J., Erfan R.D., Sriwana T., Suharyono K., Poorter R.P.E., Varekamp J.C., Vroon P.Z., Wirakusumah A.D. (1989)
Spatial geochemical variations of arc volcanism around the Banda Sea.
Netherlands Jour. Sea Res. 24 (2/3), 313-322

van Gool M., Huson W.J., Prawirasasra R., Owen T.R. (1987)
Heat flow and seismic observations in the northwestern Banda arc.
Jour. Geophys. Res. 92, 2581-2586

Varekamp J.C., van Bergen M.J., Vroon P.Z., Poorter R.P.E., Wirakusumah A.D., Erfan R., Sriwana T., Suharyono K.
The nature of potassic volcanism in the Sunda Arc, Indonesia.
submitted for publication to Jour. Geophys. Res.

Varekamp J.C., van Bergen M.J., Vroon P.Z., Poorter R.P.E., Wirakusumah A.D., Erfan R., Suharyono K., Sriwana T. (1989)
Volcanism and tectonics in the Eastern Sunda Arc, Indonesia.
Netherlands Jour. Sea Res. 24 (2/3), 303-312

Varne R. (1985)
Ancient subcontinental mantle: a source for K-rich orogenic volcanics.
Geology 13, 405-408

Varne R., Foden J.D. (1986)
Geochemical and isotopic systematics of eastern Sunda arc volcanics: implications for mantle sources and mantle mixing processes.
in "The origin of arcs" (F.C. Wezel Ed.), 159-189

Veevers J.J. (1977)
Models of the evolution of the Eastern Indian Ocean.
in "Indian Ocean geology and biostratigraphy" by Heirtzler et al. (Eds), 151-163 American Geophysical Union

Vening Meinesz F.A. (1954)
Indonesian archipelago - a geophysical study.
Geol. Soc. Amer. Bull. 65, 143-164

Verma S.P. (1992)
Seawater alteration effects on REE, K, Rb, Cs, Sr, U, Th, Pb and Sr-Nd-Pb isotope systematics of Mid-Ocean Ridge Basalts.
Geochem. Jour. 26, 159-177

Vinogradov A.P., Udintsev G.B., Dmitriev L.V., Kanaev V.F., Neprochnov Y.P., Petrova G.N., Rikunov L.N. (1969)
The structure of the mid-oceanic rift zone of the Indian Ocean and its place in the world rift system.
Tectonophysics 8, 377-401

Viswanatha Reddy V., Subbarao K.V., Reddy G.R., Matsuda J., Hekinian R. (1978)
Geochemistry of volcanics from the Ninetyeast Ridge and its vicinity in the Indian Ocean.
Mar. Geol. 26, 99-117

von der Borch C.C. (1979)
Continent-island arc collision in the Banda arc.
Tectonophysics 54, 169-193

Vukadinovic D., Sukhyar R., Nicholls I.A. (1988)
Strontium isotope and trace element evidence for involvement of "slab generated fluids" in Quaternary basalts from central Java.
Chem. Geol. 70, 54

Vukadinovic D., Nicholls I.A. (1989)
The petrogenesis of island arc basalts from Gunung Slamet volcano, Indonesia: trace element and 87Sr/86Sr constraints.
Geoch. Cosmoch. Acta 53, 2349-2363

Wajzer M.R., Barber A.J., Hidayat S., Suharsono (1991)
Accretion, collision and strike-slip faulting: the Woyla Group as a key to the tectonic evolution of North Sumatra.
Jour. Southeast Asian Earth Sci. 6 (3/4), 447-461

Watkins N.D., Gunn B.M., Nougier J., Baksi A.K. (1974)
Kerguelen: continental fragment or oceanic island?
Geol. Soc. Am. Bull. 85, 201-212

Weaver B.L. (1991)
The origin of ocean island basalt end-member compositions: trace element and isotopic constraints.
Earth Plan. Sci. Lett. 104, 381-397

Weibe R.A. (1986)
Lower crustal cumulate nodules in proterozoic dikes of the Nain Complex: evidence for the origin of Proterozoic anorthosites.
Jour. Petrol. 27, 1253-1275

Weis D., Bassias Y., Gautier I., Mennessier J.-P. (1989)
DUPAL anomaly in existence 115 Ma ago: evidence from isotopic study of the Kerguelen Plateau (South Indian Ocean).
Geoch. Cosmoch. Acta 53, 2125-2131

Weis D., Frey F.A., Saunders A., Gibson I., Leg 121 Scientific Shipboard Party (1991)
Ninetyeast Ridge (Indian Ocean): a 5000 km record of a DUPAL mantle plume.
Geology 19, 99-102

Weis D., Frey F.A. (1991)
Isotope geochemistry of the Ninetyeast Ridge basement basalts: Sr, Nd, and Pb evidence for involvement of the Kerguelen hot spot.
ODP Scientific Results vol. 121, 591-610

Weis D., Frey F.A., Leyrit H., Gautier I. (1993)
Kerguelen archipelago revisited: geochemical and isotopic study of the Southeast Province lavas.
Earth Plan. Sci. Lett. 118, 101-119

Westerveld J. (1952)
Quaternary volcanism in Sumatra.
Bull. Geol. Soc. Am. 63, 561-594

Wheller G.E. (1986)
Petrogenesis of Batur Caldera, Bali, and the geochemistry of Sunda-Banda arc basalts.
Unpubl. PhD thesis, University of Tasmania, Australia

Wheller G.E., Varne R. (1986)
Genesis of dacitic magmatism at Batur volcano, Bali, Indonesia: implications for the origins of stratovolcano calderas.
Jour. Volc. Geoth. Res. 28, 363-378

Wheller G.E., Varne R., Foden J.D., Abbott M.J. (1987)
Geochemistry of Quaternary volcanism in the Sunda-Banda arc, Indonesia, and three-component genesis of island-arc basaltic magmas.
Jour. Volc. Geoth. Res. 32, 137-160

Wheller G.E., Varne R., Stolz A.J.
Uranium and thorium radionuclides in Sunda Arc volcanics and the enrichment of arc magma sources.
submitted for publication to Geoch. Cosmoch. Acta

White W.M., Hofmann A.W. (1982)
Sr and Nd isotope geochemistry of oceanic basalts and mantle evolution.
Nature 296, 821-825

White W.M. (1989)
Geochemical evidence for crust-to-mantle recycling in subduction zones.
in "Crust/mantle recycling at convergence zones" by Hart & Gülen (Eds), 43-58 NATO ASI Series (Series C)

Whitford D.J. (1975)
Strontium isotopic studies of the volcanic rocks of the Sunda arc, Indonesia, and their petrogenetic implications.
Geoch. Cosmoch. Acta, 39, 1287-1302

Whitford D.J., Nicholls I.A. (1976)
Potassium variation in lavas across the Sunda arc in Jawa and Bali.
in: "Volcanism in Australasia" (R.W. Johnson Ed.), 63-75

Whitford D.J., Compston W., Nicholls I.A., Abbott M.J. (1977)
Geochemistry of Late Cenozoic lavas from eastern Indonesia: role of subducted sediments in petrogenesis.
Geology 5, 571-575

Whitford D.J., Foden J.D., Varne R. (1978)
Sr isotope geochemistry of calc-alkaline and alkaline lavas from the Sunda arc in Lombok and Sumbawa, Indonesia.
Carnegie Inst. Wash. Year Book 77, 613-620

Whitford D.J., Jezek P.A. (1979)
Origin of Late Cenozoic lavas from the Banda arc, Indonesia: trace elements and Sr isotope evidence.
Contrib. Mineral. Petrol. 68, 141-150

Whitford D.J., Nicholls I.A., Taylor S.R. (1979)
Spatial variations in the geochemistry of Quaternary lavas across the Sunda arc in Jawa and Bali.
Contrib. Mineral. Petrol. 70, 341-356

Whitford D.J., White W.M., Jezek P.A. (1981)
Neodymium isotopic composition of Quaternary island arc lavas from Indonesia.
Geoch. Cosmoch. Acta 45, 989-995

Whitford D.J., Jezek P.A. (1982)
Isotopic constraints on the role of subducted sialic material in Indonesian island-arc magmatism.
Bull. Geol. Soc. Amer. 93, 504-513

Wikarno U., Suyatna D.A.D., Sukardi S. (1988)
Granitoids of Sumatra and the tin islands.
in "Geology of tin deposits in Asia and the Pacific; mineral concentrations and hydrocarbon accumulations in the ESCAP region." (Hutchison C.S. editor) Springer-Verlag, New York, N.Y. USA, 3, 571-589

Williams R.W., Gill J.B., Bruland K.W. (1983)
Th and U decay series nuclides in historic arc lavas from Java, Japan and Mt. St Helens.
EOS Trans. Amer. geophys. Union 64, 906

Williams S. (1992)
Unpubl. BSc Hon. thesis, Australian National University, Australia

Windom H.L. (1975)
Eolian contributions to marine sediments.
Jour. Sedim. Petrol. 45, 2, 520-529

Wood D.A., Joron J.-L., Treuil M. (1979)
A re-appraisal of the use of trace elements to classify and discriminate between magma series erupted in different tectonic settings.
Earth Plan. Sci. Lett. 45, 326-336

Wood D.A. (1980)
The aplication of a Th-Hf-Ta diagram to problems of tectonomagmatic classification and to establishing the nature of crustal contamination of basaltic lavas of the British Tertiary volcanic province.
Earth Plan. Sci. Lett. 50, 11-30

Woodhead J., Eggins S., Gamble J. (1993)
High field strength and transition element systematics in island arc and back-arc basin basalts: evidence for mutli-phase melt extraction and a depleted mantle wedge.
Earth Plan. Sci. Lett. 114, 491-504

Zartman R., Haines S.M. (1988)
The plumbotectonic model for Pb isotopic systematics among major terrestrial reservoirs - a case for bi-directional transport.
Geoch. Cosmoch. Acta 52, 1327-1340

Zindler A., Hart S.R. (1986)
Chemical geodynamics.
Annu. Rev. Earth Planet. Sci. 14, 493-571

Appendix A

Analytical techniques

A1 Whole-rock analyses

Approximately 1 to 2 kg of fresh rock samples were crushed in a steel jaw-crusher. Only the fresh 1 to 3 cm fragments were hand-picked, and 50 to 100 g (only 10 to 20 g were available for most sediments and oceanic basalts) of rock chips were crushed to approximately 325 mesh in a tungsten carbide shatterbox. This powder fraction was used for all the whole-rock and isotope analyses.

Major and most trace elements, respectively as fused glass disks (Norrish & Hutton 1969) and as pressed powder pellets cased in boric acid (Norrish & Chappell 1977) were analysed by XRF spectrometry at the Department of Geology of the University of Tasmania, using an automated Philips PW 1410 spectrometer. Instrumental conditions are listed in Table A1. Trace element concentrations were determined using mass absorption coefficients calculated from major element analyses. Results were corrected using a number of international and secondary standards used at the University of Tasmania (Table A2), and specpure silica blanks. L.O.I. is the sum of H_2O^+ and H_2O^- (and other gaseous phases) measured on approximately 1 g of powder left at 1000 °C for about 12 hours (the powders had been kept in a desiccator for several hours before weighing). Negative L.O.I. values indicate that the gain in weight during the ignition because of the oxidation of FeO to Fe_2O_3 was larger than the loss in volatiles. In general, 2-3 standards and blanks, and one (chemistry) duplicate were run every 6-7 samples.

Ta, Hf and Cs, and some REEs (where LREE, MREE, and HREE are reported) and Th (where at least one decimal digit is reported) were analysed by INAA at the Becquerel Laboratories, Lucas Heights Research Laboratories, NSW (Dr Helen Waldron analyst). Detection limits are listed in Table A3. Several standards and duplicates indicate a precision within the detection limits. The Ta contamination from the shatterbox has been estimated to be approximately 0.4 ppm for the samples of volcanic rocks, and 0.2 ppm for the sediments (Figure A1). The Ta values reported in the tables are not corrected, but the contamination has been taken into account in the figures and discussion.

Unless otherwise specified, Fe_2O_3 is the total Fe as Fe_2O_3, Mg# is $(Mg^{2+}/(Mg^{2+} + Fe^{2+}))*100$, and Fe^{2+} was calculated assuming $Fe_2O_3/FeO = 0.15$.

A2 Isotope analyses

Sr and Nd for isotopic concentration analyses on whole-rock powders were separated at the Department of Geology of the University of Tasmania, using a three-stage ion separation technique, with Amberlite CG 120 (first and second stage) and HDEHP/teflon powder (third stage) columns. 0.1 g of sample powder was dissolved in a teflon beaker using HNO_3, HF, and HCl. The Rb fraction was discarded, and then the Sr and REE fractions were collected. The Sr fraction was put through the columns again, to obtain a very pure Sr fraction. In the second stage Ba was completely separated from the REE fraction, and in the third stage Nd was collected. Different solutions of double-distilled H_2O, HCl, and HNO_3 were used for the separations.

BCR-1 was used as an international standard for both Sr and Nd, and the Sr and Nd fractions were separated from the powder using the same technique used for the samples. Solutions of "NBS 987" and "La Jolla" international standards were also used respectively for Sr and Nd.

Sr was analysed on a single Ta filament configuration on a Finnigan MAT 261 single collector mass spectrometer at the Department of Geology of the University of Adelaide, and on a double Re filament configuration on a multiple collector Finnigan MAT 261 mass spectrometer at the Department of Geochemistry of the Freie Universität of Berlin. A diluted HNO_3 loading solution was used in both cases.

Nd was analysed on the Ta filament of a double Ta-Re filament configuration (Adelaide), and on a double Re filament configuration (Berlin) on the same mass spectrometers. A diluted HNO_3 loading solution was used in both cases.

"Common Pb" was separated and analysed at the Department of Geochemistry of the Freie Universität of Berlin, using a single Re filament configuration on a multiple collector Finnigan MAT 261 mass spectrometer. 0.1 g of powder sample was dissolved in a teflon beaker using HF, HNO_3, HCl, and HBr. Different dissolution techniques and acids (e.g. simple leaching with HCl at different temperatures and concentrations for variable amounts of time, followed by dissolution) tested on sediments and granite samples gave the same results as the "standard" dissolution technique. Samples were dried in teflon bombs in N_2 atmosphere. Pb was separated in teflon columns with Bio-Rad AG 1-x 8 anion exchange resin, using HCl and HBr. Three-times distilled H_2O, HCl, and HBr were used for the separation.

Analyses of international and internal standards, details of the analytical conditions, and the corrected values and standard deviations of the samples analysed are listed in Table A4.

A3 Mineral chemistry analyses

Samples for mineral chemistry were hand crushed, sieved, and olivine (and clinopyroxene) crystals were hand picked from the size fractions 0.3-1 mm. Grains were mounted in epoxy and analysed using a fully automated three spectrometers Cameca SX 50 electron microprobe (University of Tasmania) calibrated with natural mineral standards (PAP data reduction). Olivine (USNM 111312/444), basaltic glass (USNM 111240/52) and clinopyroxene (USNM 122142) (Jarosewich et al. 1980), and spinel (UV 126) (Lavrentev et al. 1974) were used as secondary standards (Table A5). The standards were analysed at least twice during each probe session (5 to 7 hours). For most grains a shorter program for the analysis of olivine crystals was used to reduce the time of the analysis. Analytical conditions were 15 kV accelerating voltage, 20 nA (minerals) and 10 nA (glasses) beam current, and 1-2 μm (minerals) and 10-20 μm (glasses) beam size.

Spinel, olivine, and pyroxene crystals were analysed together with the coexisting host olivine, and spinel analyses were recalculated assuming a stoichiometric composition (Finger 1972).

Melt inclusions were heated using the heating-stage technique under visual control described by Sobolev et al. (1980) up to the temperature of melting of the crystalline phases, and quenched for the determination of the melt composition. The heating-stage apparatus at the Department of Geology of the University of Tasmania was used for the heating-stage experiments.

Table A1. INSTRUMENTAL CONDITIONS FOR MAJOR AND TRACE ELEMENT ANALYSIS
ROUTINE XRF AUTOMATED ANALYSIS

X-Ray tube is operated at 60 kV and 40 mA, except for Ba, Sc, La, Ce and Nd where 50 kV and 50 mA are used.
Detection limits are 3 sigma (99 %) confidence levels.

Major elements.

Oxide	Line	Tube	Crystal	Counter	Collimator	Vacuum	Time (sec)	
SiO2	K alpha	Rh	PE	Flow	Coarse	YES	100	
TiO2	K alpha	Rh	LiF200	Flow	Coarse	YES	20	
Al2O3	K alpha	Rh	PE	Flow	Coarse	YES	100	
Fe2O3	K alpha	Rh	LiF200	Flow	Fine	YES	20	
MnO	K alpha	Rh	LiF200	Flow	Fine	YES	40	
MgO	K alpha	Rh	TLAP	Flow	Coarse	YES	100	
CaO	K alpha	Rh	LiF200	Flow	Fine	YES	20	
Na2O	K alpha	Rh	TLAP	Flow	Coarse	YES	100+100	(two counts)
K2O	K alpha	Rh	PE	Flow	Coarse	YES	20	
P2O5	K alpha	Rh	GE	Flow	Coarse	YES	40	

Trace elements.

Element	Line	Tube	Crystal	Counter	Collimator	Vacuum	Detection limit (ppm)	Precision
Sc	K alpha	Cr	LiF200	Flow	Coarse	YES	1	10±1, 30±1
V	K alpha	Au	LiF220	Flow	Fine	YES	3	30±2, 100±1
Cr	K alpha	Au	LiF200	Flow	Fine	YES	2	10±2, 400±4
Ni	K alpha	Au	LiF200	Flow	Fine	YES	1	3±0.5, 20±0.5, 200±2
Rb	K alpha	Rh	LiF220	Scintillation	Fine	NO	2	10±1, 70±1, 170±2
Sr	K alpha	Rh	LiF220	Scintillation	Fine	NO	2	10±1, 200±2, 500±5
Y	K alpha	Rh	LiF220	Scintillation	Fine	NO	1.5	10±2, 20±1, 100±2
Zr	K alpha	Rh	LiF220	Scintillation	Fine	NO	1	100±2, 250±4, 500±10
Nb	K alpha	Rh	LiF220	Scintillation	Fine	NO	1	10±0.5, 20±1
Ba	L alpha	Cr	LiF200	Flow	Fine	YES	3	500±5, 1200±5
La	L alpha	Au	LiF220	Flow	Coarse	YES	2.5	20±1, 40±2, 100±2
Ce	L beta	Au	LiF220	Flow	Coarse	YES	5	30±2, 80±3, 150±1
Nd	L alpha	Au	LiF220	Flow	Coarse	YES	3	15±1, 30±2, 50±2
Pb	L beta	Mo	LiF200	Scintillation	Fine	NO	3	20±1, 50±1
Th	L alpha	Mo	LiF220	Scintillation	Fine	NO	2	25±1, 100±2
U	L alpha	Mo	LiF220	Scintillation	Fine	NO	2	5±1, 40±1

Figure A1. Ta-Nb correlation

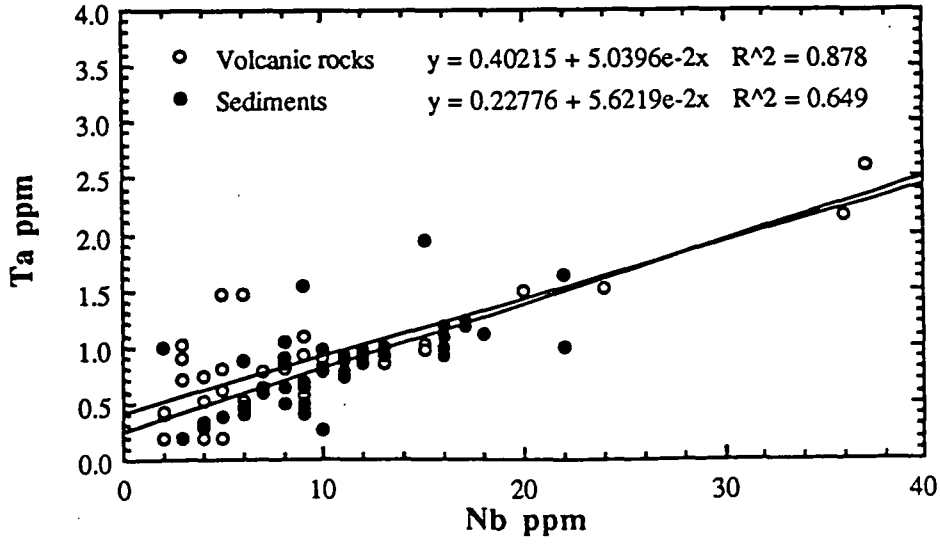

Table A2. CHEMICAL COMPOSITION OF
TASBAS AND TASGRAN INTERNAL STANDARDS

	TASBAS			TASGRAN		
		± 1 sigma	% sigma		± 1 sigma	% sigma
SiO2	44.56	0.23	0.5	72.6	0.17	0.2
TiO2	2.31	0.04	1.7	0.29	0.01	3.4
Al2O3	14.14	0.10	0.7	13.65	0.08	0.6
Fe2O3	12.65	0.09	0.8	2.29	0.03	1.3
MnO	0.17	0.01	5.1	0.04	0.003	7.5
MgO	8.16	0.11	1.3	0.59	0.04	6.8
CaO	7.81	0.06	0.8	1.87	0.02	1.1
Na2O	5.43	0.12	2.1	2.82	0.1	3.5
K2O	1.86	0.03	1.6	4.61	0.04	0.9
P2O5	0.97	0.03	2.6	0.12	0.002	1.7
LOI	1.56	0.02	1.3	0.86	0.02	2.3
Total	99.62			99.74		
Ba	204	3.0	1.5	462	4.5	1.0
Rb	16.5	0.7	4.2	259	3.0	1.2
Nb	61.4	1.2	2.0	17	0.5	2.9
La	43.4	1.4	3.2	38.8	1.0	2.6
Ce	89	3.4	3.9	86.9	3.2	3.7
Sr	1025	11.2	1.1	152	1.5	1.0
Nd	41.2	2.4	5.8	37.4	1.8	4.8
Zr	260	4.3	1.7	157	2.5	1.6
Y	23.1	0.6	2.6	35	1.0	2.9
Sc	13.1	0.5	3.8	6.7	0.3	4.5
V	163	2.3	1.4	25.4	1.0	3.9
Cr	198	4.1	2.1	10	0.5	5.0
Ni	154	2.0	1.3	3.4	0.2	5.9
Pb	5.9	0.8	13.6	18.8	0.5	2.7
Th	4.7	0.4	8.5	26.8	1.3	4.9
U	1.5	0.5	33.3	4.1	0.7	17.1

Table A3. DETECTION LIMITS
FOR INAA ANALYSIS (in ppm)

La	0.1
Ce	1
Nd	2
Sm	0.05
Eu	0.2
Tb	0.5
Ho	0.5
Yb	0.1
Lu	0.05
Cs	0.5
Hf	0.5
Ta	0.2
Th	0.2

Table A4.1. Sr and Nd data of samples analyzed in Adelaide, August to December 1992

International standard used BCR-1 for both Sr and Nd
Internal standard used TASBAS for both Sr and Nd
The TASBAS values were normalized using the BCR-1 values.

Average measured BCR-1 values (August-December 1992)
corrected for mass fractionation using

88Sr/86Sr	8.375209		
146Nd/144Nd	0.721903		
		2 sigma	BCR-1 recommended values
87Sr/86Sr	0.70488	0.00001	0.70495
143Nd/144Nd	0.512614	0.000001	0.512664

The 2 sigma values are for chemistry duplicates (external precision).

Average TASBAS values (August-December 1992)
normalized to BCR-1 values

		2 sigma	Berlin average values (normalized to the international standards)
87Sr/86Sr	0.70352	0.00001	0.70350
143Nd/144Nd	0.512962	0.000010	0.512943

The 2 sigma values are for chemistry duplicates (external precision).

Sample name	87Sr/86Sr	2 sigma on 5 blocks*
75212	0.70453	0.000109
75354	0.70410	0.000081
75358	0.70402	0.000027
75360	0.70390	0.000150
75361	0.70407	0.000051
75369	0.70412	0.000139
75374	0.70382	0.000145
75377	0.70393	0.000096
75378	0.70403	0.000065
75389	0.70430	0.000079
78131	0.70436	0.000146
78134	0.70409	0.000036
78135	0.74036	0.000168
78136	0.73290	0.000092

Sample Name	143Nd/144Nd	2 sigma on 20 blocks*
DSDP 27 261 3-2 25-27	0.511906	0.000018
DSDP 27 261 4-1 99-101	0.511964	0.000040
DSDP 27 261 8-5 20-22	0.512115	0.000018
DSDP 27 261 25-3 29-31	0.512300	0.000014
75210	0.512786	0.000046
75212	0.512804	0.000028
75213	0.512829	0.000067
75215	0.512981	0.000062
75227	0.512771	0.000040
75232	0.512783	0.000042
75237	0.512619	0.000043
75238	0.512592	0.000033
75254	0.512684	0.000029
75256	0.512718	0.000059
75257	0.512723	0.000041
75267	0.512652	0.000039
75268	0.512491	0.000054
75300	0.512721	0.000042

Table A4.1 cont.

Sample Name	143Nd/144Nd	2 sigma on 20 blocks*
75310	0.512491	0.000042
75354	0.512855	0.000036
75358	0.512898	0.000025
75360	0.512969	0.000023
75361	0.512869	0.000041
75369	0.512837	0.000048
75374	0.512895	0.000035
75377	0.512929	0.000058
75378	0.512891	0.000040
75389	0.512882	0.000049
75416	0.512899	0.000066
78131	0.512760	0.000015
78134	0.512790	0.000025
78135	0.512210	0.000044
78136	0.512219	0.000019

* 1 block = 20 analyses (Sr) and 11 analyses (Nd)
The actual 2 sigma can be estimated at about 1/10
of the values reported here.

Table A4.2. Sr analyses data Berlin Jan-May 1992

International reference standard NBS 987 (87Sr/86Sr 0.71014)
Internal standard - TASBAS (Adelaide average value corrected for fractionation and using BCR-1 as an international standard 0.70352) - average value 0.70350
Corrections were not necessary as the average of 15 measured NBS 987 was 0.710178 (2s 0.000054)
Where necessary, results were corrected for Rb interference
Data corrected for mass fractionation using 88Sr/86Sr 8.375209
Average TASBAS recommended value 0.70351 (2s 0.00001)

Internal precision based on 11 duplicates was 0.000003 to 0.000050 (average 0.000018) (excluding the values for the NBS 987 standard 0.000054 for 15 runs,
External precision based on three chemistry duplicates of TASBAS was 0.000038

NBS 987 measured value	Date	Number of analyses	88Sr/86Sr initial	88Sr/86Sr final	87Sr/86Sr	2 sigma
NBS 987	13/2/92	98	8.3285067	8.3285344	0.71021	0.00001
NBS 987	16/2/92	98	8.3620770	8.3657856	0.71023	0.00002
NBS 987	16/2/92	98	8.3004237	8.3050138	0.71017	0.00002
NBS 987	16/2/92	98	8.3158386	8.3230362	0.71017	0.00002
NBS 987	19/2/92	100	8.3593193	8.3680704	0.71019	0.00002
NBS 987	9/3/92	97	8.3768881	8.3687048	0.71013	0.00002
NBS 987	9/3/92	98	8.3681783	8.3528484	0.71018	0.00002
NBS 987	7/3/92	99	8.3726045	8.3858830	0.71017	0.00002
NBS 987	6/3/92	98	8.3379446	8.3326082	0.71008	0.00002
NBS 987	7/3/92	212	8.3531066	8.3719187	0.71019	0.00001
NBS 987	9/3/92	98	8.3642985	8.3763571	0.71019	0.00002
NBS 987	9/3/92	99	8.3894459	8.3762516	0.71025	0.00002
NBS 987	11/3/92	98	8.3612276	8.3627708	0.71020	0.00002
NBS 987	14/3/92	98	8.3480658	8.3611481	0.71006	0.00002
NBS 987	23/3/92	20	8.5214736	8.5214736	0.71025	0.00013
Average NBS 987					0.71018	0.00005
TASBAS measured values						
TASBAS 1	13/2/92	96	8.2913959	8.2924671	0.70350	0.00002
TASBAS 3	13/2/92	97	8.2843728	8.2880041	0.70353	0.00001
TASBAS 1	16/2/92	96	8.3554409	8.3584710	0.70353	0.00002
TASBAS 1	19/2/92	98	8.3748849	8.3932485	0.70352	0.00002
TASBAS 2	8/3/92	99	8.3040184	8.3091262	0.70345	0.00002
TASBAS 3	22/3/92	98	8.3513898	8.3550633	0.70354	0.00002
Average TASBAS (average of three samples)					0.70350	0.00004

Sample name	87/86 corr	2 sigma
22 211 12-1 125-127	0.70567	0.00002
22 211 13-1 10-12	0.71643	0.00002
22 213 1-3 30-32	0.71266	0.00005
22 213 7-5 71-73	0.71384	0.00002
22 213 13-4 91-93	0.71237	0.00003
22 213 16-2 57-59	0.70781	0.00004
22 213 18-2 115-117	0.70321	0.00002
27 261 3-2 25-27	0.70981	0.00003
27 261 4-1 99-101	0.70937	0.00002
27 261 8-5 20-22	0.71694	0.00005
27 261 14-1 75-77	0.71710	0.00004
27 261 25-3 29-31	0.71079	0.00002
27 261 29-2 29-31	0.71522	0.00002

Table A4.2 cont

Sample name	87/86 corr	2 sigma
27 261 32-2 58-61	0.71079	0.00003
27 261 34-2 100-102	0.70409	0.00003
DODO 232 N	0.70398	0.00002
V 28 14 A	0.70415	0.00006
75211	0.70432	0.00001
75215	0.70391	0.00002
75221	0.70494	0.00003
75222	0.70495	0.00002
75227	0.70433	0.00002
75231	0.70652	0.00006
75232	0.70476	0.00002
75233	0.70450	0.00003
75237	0.70510	0.00002
75238	0.70532	0.00004
75244	0.70389	0.00004
75248	0.70560	0.00001
75250	0.70537	0.00002
75251	0.70555	0.00003
75254	0.70483	0.00002
75256	0.70490	0.00007
75257	0.70473	0.00004
75264	0.70502	0.00002
75267	0.70514	0.00003
75268	0.70630	0.00003
75277	0.70446	0.00003
75286	0.70406	0.00002
75289	0.70473	0.00002
75300	0.70512	0.00003
75302	0.70548	0.00002
75310	0.70702	0.00001
75318	0.70983	0.00002
75324	0.71162	0.00003
75332	0.70492	0.00002
75333	0.70398	0.00004
75335	0.70506	0.00006
75342	0.70516	0.00003
75343	0.70776	0.00003
75346	0.70664	0.00002
75381	0.70486	0.00003
75384	0.70473	0.00007
75391	0.70466	0.00002
75400	0.70412	0.00003
75403	0.70418	0.00002
75406	0.70435	0.00002
75410	0.71026	0.00002
75413	0.70477	0.00002
75416	0.70443	0.00003
75423	0.70417	0.00002
75427	0.70436	0.00003
75430	0.70406	0.00003
75433	0.70443	0.00002
78136	0.73287	0.00006

Table A4.3. Nd data Berlin April/May 1992

International reference standard - La Jolla Nd Standard (143Nd/144Nd 0.511860)
Internal standard - Tasbas (Adelaide average value corrected for fractionation
and using BCR-1 as an international standard 0.512962) - average uncorrected value 0.512938

Correction factor based on La Jolla standard 1.000008987
Corrected Tasbas value 0.512943
Average Tasbas recommended value 0.512953 (2s 0.000010)

Data corrected for mass fractionation using 146Nd/144Nd 0.721903
Internal precision based on 10 duplicates was 0.000000 to 0.000009 (average 0.0000042)
(excluding the values for the La Jolla standard 0.000012 for 5 runs)
External precision based on three chemistry duplicates of TASBAS was 0.000007

"La Jolla" measured values	Date	Number of analyses	146Nd/144Nd initial	146Nd/144Nd final	143Nd/144Nd	2 sigma
LA JOLLA	1/5/92	194	0.7217525	0.7232641	0.511872	0.000006
LA JOLLA	2/5/92	196	0.7200407	0.7220821	0.511864	0.000007
LA JOLLA	4/5/92	196	0.7216708	0.7236891	0.511853	0.000005
LA JOLLA	13/5/92	195	0.7233509	0.7235351	0.511850	0.000006
LA JOLLA	12/5/92	195	0.7221414	0.7241613	0.511838	0.000007
Average "LA JOLLA"					0.511855	0.000006
TASBAS 96	28/4/92	198	0.7219821	0.7230543	0.512952	0.000004
TASBAS 96	29/4/92	95	0.7208056	0.7218524	0.512946	0.000006
TASBAS 96	29/4/92	195	0.7230600	0.7234523	0.512943	0.000005
TASBAS 96	30/4/92	192	0.7205919	0.7214645	0.512944	0.000005
TASBAS 96	30/4/92	196	0.7221855	0.7228195	0.512949	0.000003
TASBAS 116	29/4/92	196	0.7213730	0.7218369	0.512928	0.000003
TASBAS 116	29/4/92	196	0.7219416	0.7215584	0.512933	0.000004
TASBAS 116	30/4/92	194	0.7212268	0.7222871	0.512950	0.000003
TASBAS 84	5/5/92	189	0.7216058	0.7227262	0.512932	0.000003
TASBAS 84	12/5/92	178	0.7209428	0.7231718	0.512928	0.000004
Average measured TASBAS values						
TASBAS 84					0.512930	0.000004
TASBAS 96					0.512947	0.000006
TASBAS 116					0.512937	0.000004
Average corrected TASBAS values						
TASBAS 84					0.512935	0.000004
TASBAS 96					0.512952	0.000006
TASBAS 116					0.512942	0.000004

Sample Name	Measured143Nd/144Nd	2s	Corrected values
22 211 12-1 125-127	0.512688	0.000007	0.512693
22 211 13-1 10-12	0.512223	0.000006	0.512228
22 213 1-3 30-32	0.512257	0.000002	0.512262
22 213 7-5 71-73	0.512240	0.000004	0.512245
22 213 13-4 91-93	0.512208	0.000003	0.512213
22 213 16-2 57-59	0.512202	0.000003	0.512207
22 213 18-2 115-117	0.512989	0.000004	0.512994
27 261 14-1 75-77	0.512210	0.000003	0.512215
27 261 29-2 29-31	0.512235	0.000003	0.512240
27 261 32-2 58-61	0.512233	0.000007	0.512238
27 261 34-2 100-102	0.513073	0.000005	0.513078
DODO 232N	0.512843	0.000003	0.512848
V 28 14A	0.512842	0.000003	0.512847
75211	0.512745	0.000005	0.512750
75221	0.512686	0.000004	0.512691
75222	0.512685	0.000003	0.512690
75231	0.512570	0.000005	0.512575
75233	0.512718	0.000007	0.512723
75244	0.512916	0.000004	0.512921
75248	0.512763	0.000004	0.512768
75250	0.512727	0.000004	0.512732
75251	0.512721	0.000006	0.512726
75264	0.512670	0.000004	0.512675
75277	0.512777	0.000004	0.512782
75286	0.512926	0.000007	0.512931
75289	0.512746	0.000003	0.512751
75302	0.512568	0.000003	0.512573

Table A4.3 cont.

Sample Name	Measured143Nd/144Nd	2s	Corrected values
75318	0.512225	0.000007	0.512230
75324	0.512168	0.000003	0.512173
75332	0.512609	0.000003	0.512614
75333	0.512774	0.000007	0.512779
75335	0.512717	0.000006	0.512722
75342	0.512738	0.000005	0.512743
75343	0.512264	0.000003	0.512269
75346	0.512458	0.000004	0.512463
75381	0.512638	0.000003	0.512643
75384	0.512638	0.000004	0.512643
75391	0.512855	0.000003	0.512860
75400	0.512830	0.000003	0.512835
75403	0.512844	0.000003	0.512849
75406	0.512833	0.000004	0.512838
75410	0.512476	0.000004	0.512481
75413	0.512741	0.000007	0.512746
75415	0.5127	0.000041	0.5127
75423	0.512783	0.000003	0.512788
75427	0.512796	0.000004	0.512801
75430	0.512864	0.000004	0.512869
75433	0.512773	0.000006	0.512778

Table A4.4. Pb Isotope data Berlin Jan-March 1992
In the following table only the corrected values are reported

International reference standard NBS 981 (208Pb/206Pb 2.1681)
Internal standards were not used
Average measured 208Pb/206Pb NBS 981 value (13 values) 2.1606320
Correction Factor x mass unit 1.00155

Internal precision based on 11 duplicates was:
208Pb/204Pb 0.11 to 1.45 per mil (average 0.65)
207Pb/204Pb 0.03 to 1.09 per mil (average 0.45)
206Pb/204Pb 0.14 to 0.73 per mil (average 0.40)

External precision based on 10 chemistry duplicates was:
208Pb/204Pb 0.33 to 1.55 per mil (average 1.02)
207Pb/204Pb 0.02 to 1.09 per mil (average 0.71)
206Pb/204Pb 0.21 to 0.87 per mil (average 0.48)

NBS 981 measured values	Date	Number of analyses	208/204 VALUE	2 sigma	207/204 VALUE	2 sigma	206/204 VALUE	2 sigma	208/206 VALUE	2 sigma	207/206 VALUE	2 sigma	204/206 VALUE	2 sigma
NBS 981	20/1/92	193/195/194	36.5141200	0.0067484	15.4311206	0.0026408	16.8941724	0.0027587	2.1612980	0.0001094	0.9133784	0.0000249	0.0591921	0.0000097
NBS 981	26/1/92	187/186/186	36.4603026	0.0079785	15.4121418	0.0034355	16.8778806	0.0037008	2.1601963	0.0000486	0.9131836	0.0000209	0.0592493	0.0000130
NBS 981	28/1/92	188/191/188	36.5146358	0.0031293	15.4315450	0.0010634	16.8935841	0.0010064	2.1614551	0.0000750	0.9134534	0.0000138	0.0591942	0.0000035
NBS 981	2/2/92	190/189/190	36.4937105	0.0052662	15.4244712	0.0022039	16.8897167	0.0024194	2.1607006	0.0000498	0.9132351	0.0000153	0.0592077	0.0000085
NBS 981	2/5/92	189/190/190	36.4987902	0.0039055	15.4271693	0.0016139	16.8914094	0.0016922	2.1607822	0.0000667	0.9133233	0.0000155	0.0592017	0.0000059
NBS 981	2/10/92	192/192/190	36.5086209	0.0054394	15.4296480	0.0020590	16.8938438	0.0020972	2.1610519	0.0000840	0.9133305	0.0000170	0.0591932	0.0000074
NBS 981	2/11/92	192/193/190	36.4885091	0.0069207	15.4237659	0.0028949	16.8886306	0.0031277	2.1605229	0.0000521	0.9132458	0.0000193	0.0592123	0.0000111
NBS 981	22/2/92	188/190/190	36.4802013	0.0042684	15.4195345	0.0018347	16.8824140	0.0019902	2.1607992	0.0000299	0.9133485	0.0000133	0.0592336	0.0000070
NBS 981	25/2/92	193/195/193	36.4682408	0.0065730	15.4155996	0.0027398	16.8820085	0.0029484	2.1601925	0.0000572	0.9131578	0.0000186	0.0592347	0.0000103
NBS 981	29/2/92	193/190/189	36.4758658	0.0027566	15.4196277	0.0011435	16.8850771	0.0013181	2.1602460	0.0000350	0.9132095	0.0000122	0.0592239	0.0000046
NBS 981	3/2/92	192/192/194	36.4590170	0.0074875	15.4134259	0.0032514	16.8792829	0.0035936	2.1599258	0.0000543	0.9131371	0.0000220	0.0592444	0.0000126
NBS 981	25/3/92	189/188/190	36.4833364	0.0054317	15.4218141	0.0022555	16.8867949	0.0025293	2.1605590	0.0000278	0.9132550	0.0000132	0.0592179	0.0000089
NBS 981	26/3/92	194/192/195	36.4805461	0.0032102	15.4203879	0.0013076	16.8852538	0.0013808	2.1604868	0.0000501	0.9132468	0.0000132	0.0592233	0.0000048
Average uncorrected NBS 981			36.487	0.019	15.422	0.006	16.887	0.006						

Table A4.4 cont.

Sample name	208/204 VALUE	2 sigma	207/204 VALUE	2 sigma	206/204 VALUE	2 sigma
22 211 12-1 125-127	38.710	0.004	15.578	0.001	18.445	0.002
22 211 13-1 10-12	39.269	0.002	15.711	0.001	18.772	0.001
22 213 1-3 30-32	39.110	0.002	15.701	0.001	18.904	0.001
22 213 13-4 91-93	38.887	0.002	15.670	0.001	18.751	0.001
22 213 16-2 57-59	38.591	0.005	15.652	0.001	18.560	0.001
27 261 3-2 25-27	39.630	0.006	15.776	0.002	19.308	0.002
27 261 4-1 99-101	39.400	0.006	15.782	0.002	19.196	0.002
27 261 8-5 20-22	39.393	0.002	15.767	0.001	18.891	0.001
27 261 14-1 75-77	38.813	0.007	15.656	0.004	18.572	0.004
27 261 25-3 29-31	38.919	0.003	15.682	0.001	18.673	0.001
27 261 29-2 29-31	38.752	0.002	15.646	0.001	18.576	0.001
27 261 32-2 58-61	38.662	0.003	15.651	0.001	18.580	0.001
27 261 34-2 100-102	37.438	0.005	15.509	0.002	18.145	0.002
DODO 232N	38.499	0.004	15.561	0.001	18.269	0.001
V 28 14 A	39.513	0.003	15.633	0.001	19.376	0.001
75210	38.814	0.006	15.641	0.002	18.602	0.002
75211	38.757	0.004	15.631	0.001	18.583	0.002
75212	38.757	0.002	15.623	0.001	18.596	0.001
75213	38.756	0.002	15.622	0.001	18.598	0.001
75215	38.506	0.007	15.591	0.003	18.418	0.003
75221	38.770	0.003	15.630	0.001	18.598	0.001
75222	38.805	0.002	15.636	0.001	18.605	0.001
75227	38.755	0.006	15.628	0.002	18.564	0.002
75231	39.204	0.003	15.701	0.001	18.817	0.001
75232	39.041	0.004	15.673	0.002	18.735	0.002
75233	38.927	0.003	15.656	0.001	18.651	0.001
75237	39.214	0.002	15.702	0.001	18.818	0.001
75238	39.306	0.005	15.721	0.002	18.861	0.002
75244	38.291	0.005	15.539	0.002	18.447	0.002
75248	38.801	0.004	15.622	0.001	18.688	0.001
75250	38.913	0.003	15.650	0.001	18.681	0.001
75251	38.803	0.003	15.617	0.001	18.673	0.001
75254	39.176	0.003	15.700	0.001	18.785	0.001
75256	39.187	0.003	15.699	0.001	18.789	0.002
75257	39.164	0.003	15.692	0.001	18.787	0.002
75264	38.896	0.002	15.648	0.001	18.647	0.001
75267	39.001	0.003	15.671	0.001	18.701	0.001
75268	39.265	0.002	15.714	0.001	18.837	0.001
75277	38.607	0.006	15.602	0.002	18.591	0.002
75286	38.071	0.002	15.520	0.001	18.193	0.001
75289	38.482	0.004	15.577	0.002	18.447	0.002
75300	38.873	0.002	15.659	0.001	18.713	0.001
75302	38.980	0.003	15.665	0.001	18.694	0.001
75310	39.280	0.002	15.721	0.001	19.014	0.001
75318	39.545	0.005	15.774	0.002	18.861	0.002
75324	39.539	0.002	15.761	0.001	18.882	0.001
75332	38.820	0.002	15.634	0.001	18.658	0.001
75333	38.581	0.005	15.600	0.002	18.396	0.002
75335	39.146	0.005	15.696	0.002	18.750	0.002
75342	38.944	0.005	15.674	0.002	18.639	0.002
75343	39.535	0.003	15.756	0.001	18.970	0.001
75346	39.526	0.005	15.751	0.002	18.974	0.002
75354	38.327	0.004	15.561	0.002	18.344	0.002
75358	38.367	0.004	15.569	0.002	18.353	0.002
75361	38.456	0.006	15.598	0.002	18.396	0.003
75369	38.548	0.009	15.600	0.003	18.468	0.004
75374	38.396	0.004	15.577	0.001	18.327	0.002
75377	38.264	0.006	15.557	0.002	18.267	0.003
75378	38.706	0.004	15.626	0.001	18.429	0.001
75381	39.058	0.002	15.681	0.001	18.712	0.001
75384	39.052	0.003	15.682	0.001	18.703	0.001
75389	38.609	0.003	15.634	0.001	18.382	0.001
75391	38.282	0.003	15.563	0.001	18.292	0.001
75400	38.614	0.003	15.608	0.001	18.458	0.001
75403	38.175	0.005	15.539	0.002	18.286	0.002
75406	38.299	0.002	15.562	0.001	18.329	0.001
75410	39.114	0.002	15.695	0.001	19.047	0.001
75413	38.421	0.002	15.580	0.001	18.417	0.001
75415	38.545	0.002	15.614	0.001	19.108	0.001
75416	39.189	0.004	15.700	0.001	18.800	0.001

Table A4.4 cont.

Sample name	208/204 VALUE	2 sigma	207/204 VALUE	2 sigma	206/204 VALUE	2 sigma
75423	38.639	0.002	15.612	0.001	18.519	0.001
75427	38.678	0.005	15.616	0.002	18.551	0.003
75430	38.715	0.006	15.619	0.002	18.570	0.003
78131	38.801	0.003	15.628	0.001	18.620	0.001
78134	38.749	0.003	15.621	0.001	18.579	0.001
78135	44.815	0.002	15.812	0.001	19.765	0.001
78136	42.427	0.001	15.788	0.000	19.289	0.001

Table A4.5. Pb, Sr, and Nd total blanks

During the period of the analyses, Pb total blanks measured in Berlin were in the range 244 to 1018 pg (average of 12 blanks 558 ±195 pg), corresponding to a Pb contamination of the samples of 1 per mil to 3 per mil.
Sr (Berlin chemistry) and Nd (Hobart chemistry) total blanks measured in Berlin were always < 0.6 ng (usually < 0.4).
This contamination is negligible in this study for these samples.

Sr blanks for samples prepared in Hobart and measured in Adelaide and Berlin were in the range 3 to 6 ng.
Two laboratory blanks gave a $^{87}Sr/^{86}Sr$ value of 0.706420 and 0.705618 respectively.
Given the high Sr content of the samples analyzed, and the fact that the $^{87}Sr/^{86}Sr$ values of the laboratory blanks are not dissimilar from the $^{87}Sr/^{86}Sr$ values of the samples, this contamination is negligible in this study for these samples.

Table A5. Microprobe standards - June-December 1992

Olivine SC-OL (USNM 111312/444)	# analyses	Average	2 sigma	Recommended values
SiO2	31	40.58	0.26	40.81
FeO	31	9.48	0.31	9.55
MnO	8	0.14	0.03	0.14
MgO	31	48.71	0.33	49.42
CaO	31	0.09	0.02	< 0.10
NiO	8	0.35	0.05	0.37
Total		99.35		100.39

Spinel UV-126	# analyses	average	2 sigma	
SiO2	24	0.33	0.03	0.30
TiO2	24	4.83	0.09	4.61
Al2O3	24	8.88	0.12	8.79
FeO	24	27.07	0.46	26.30
MnO	24	0.25	0.07	0.29
MgO	24	14.29	0.19	14.10
Cr2O3	24	45.30	0.39	44.80
NiO	24	0.25	0.06	0.32
Total		101.20		99.51

Clinopyroxene KA (USNM 122142)	# analyses	average	2 sigma	
SiO2	2	50.70	0.00	50.73
TiO2	2	0.83	0.01	0.74
Al2O3	2	8.82	0.08	8.73
FeO	2	6.66	0.01	6.37
MnO	2	0.18	0.03	0.13
MgO	2	16.73	0.14	16.65
CaO	2	15.78	0.05	15.82
Na2O	2	1.28	0.04	1.27
Total		100.98		100.44

Glass VG-2 (USNM 111240/52)	# analyses	average	2 sigma	
SiO2	2	50.39	0.87	50.81
TiO2	2	1.94	0.02	1.85
Al2O3	2	13.94	0.11	14.06
FeO	2	12.74	0.14	11.84
MnO	2	0.16	0.01	0.22
MgO	2	6.66	0.02	6.71
CaO	2	11.34	0.15	11.12
Na2O	2	2.61	0.02	2.62
K2O	2	0.20	0.00	0.19
P2O5	2	0.41	0.02	0.20
Total		100.39		99.62

Appendix B

List of samples of Sumatran intrusive and fragmental rocks from this study, with a brief petrographic description

Samples are listed from south to north. For each sample are reported:
1) sample number (University of Tasmania catalogue number)
2) approximate location and name of the quadrant of the 1:250,000 geologic map
3) name of the formation or volcanic unit to which the sample belongs, and approximate stratigraphic (and absolute, if available) age (based on the information published in the 1:250,000 geologic maps)
4) approximate location in degrees and minutes (based on the latest published 1:250,000 topographic maps of Sumatra. The coordinates reported here may not coincide with previously published maps)
5) brief macroscopic description of the sample. The type of rock, indicated for the intrusive samples, is based solely on the Q-P cationic classification of Debon & Le Fort (1988)
6) brief petrographic description of consolidated samples

Samples 75412 to 75415, and 75409, 75410, 75411, 75391, 75398, 75402, and 75403 were donated by Dr Rab Sukamto (Geological Research and Development Centre, Bandung, Indonesia). All the other samples were collected in the field during this study.

75212
N of Bakauheni (Tanjungkarang)
Lampung fm. (Pliocene-Pleistocene)
105 43'E 5 50'S
Scoriaceous light gray aphyric tuff.
Cryptocrystalline tuff, with small flat vesicles (20-30%) and rare sanidine microliths.

75220
close to Tanjungkarang (Tanjungkarang)
Mapped as Tarahan fm. (Paleocene-Eocene). Possibly still Lampung fm. (Pliocene-Pleistocene)
105 15'E 5 28'S
Light gray loose sandy deposit, possibly a pyroclastic surge, with white pumice fragments and biotite crystals.

75221
close to Tanjungkarang (Tanjungkarang)
Mapped as Tarahan fm. (Paleocene-Eocene). Possibly still Lampung fm. (Pliocene-Pleistocene)
105 15'E 5 28'S
Block in pyroclastic flow (same unit as the surge 75220). Aphyric, fairly massive white welded tuff, with abundant angular microlithics.
Glassy vesicular (10%) volcanic rock (possibly a welded ignimbrite), with fresh glassy groundmass and tiny crystals of quartz and plagioclase (<5%) and rare (<1%) green amphibole.

75222
close to Tanjungkarang (Tanjungkarang)
Mapped as Tarahan fm. (Paleocene-Eocene). Possibly still Lampung fm. (Pliocene-Pleistocene)
105 15'E 5 28'S
Block in pyroclastic flow (same unit as the surge 75220). Light gray, massive banded volcanic rock, very fine grained with rare sanidine and mafic crystals.
Glassy/cryptocrystalline rock, with oriented sanidine microliths and rare (<1%) plagioclase and sanidine fragments and biotite crystals.

75223
close to Tanjungkarang (Tanjungkarang)
Mapped as Tarahan fm. (Paleocene-Eocene). Possibly still Lampung fm. (Pliocene-Pleistocene)
105 15'E 5 28'S
Block in pyroclastic flow (same unit as the surge 75220). Light to dark gray, banded volcanic rock, vesicular, aphyric.
Glassy rock, slightly vesicular, with oriented sanidine microliths and rare (<1%) plagioclase and sanidine fragments and biotite crystals.

75224
close to Tanjungkarang (Tanjungkarang)
Mapped as Tarahan fm. (Paleocene-Eocene). Possibly still Lampung fm. (Pliocene-Pleistocene)
105 15'E 5 28'S
Block in pyroclastic flow (same unit as the surge 75220). Brown, strongly vesicular, almost aphyric volcanic rock, with rare feldspar phenocrysts.
Porphyritic seriate glassy/cryptocrystalline brownish rock, vesicular (15%), with abundant plagioclase tiny microliths and very rare (<1%) small euhedral plagioclase phenocrysts.

75225
close to Tanjungkarang (Tanjungkarang)
Mapped as Tarahan fm. (Paleocene-Eocene). Possibly still Lampung fm. (Pliocene-Pleistocene)
105 15'E 5 28'S
Block in pyroclastic flow (same unit as the surge 75220). White, fairly massive tuff, with abundant angular and rounded, compositionally heterogeneous lithics.
Fine grained glassy tuff, vesicular (10%), with small crystals of quartz and plagioclase (<5%) and rounded blobs of fresh and altered rhyolite (<10%).

75226
close to Tanjungkarang (Tanjungkarang)
Mapped as Tarahan fm. (Paleocene-Eocene). Possibly still Lampung fm. (Pliocene-Pleistocene)
105 15'E 5 28'S
Block in pyroclastic flow (same unit as the surge 75220). Banded, massive, white to pink volcanic rock, aphyric with rare small plagioclase crystals.
Glassy/cryptocrystalline layered rock, with rare (<2%) seriate euhedral plagioclase and quartz.

75218
close to Tanjungkarang (Tanjungkarang)
Tarahan fm. (Paleocene-Eocene)
105 18'E 5 27'S
Whitish aphyric tuff, possibly an ash fall, slightly altered (red veins and alteration patches).
Microcrystalline aggregate of quartz (60-70%) and muscovite crystals.

75219
close to Tanjungkarang (Tanjungkarang)
Tarahan fm. (Paleocene-Eocene)
105 19'E 5 27'S
Altered massive tuff, aphyric, with some lithics.
Similar to 75218, but more compact, and slightly altered.

75415
close to Wai Tatayan (Kotaagung)
Seputih granite (Lower Tertiary)
104 51'E 5 07'S
Very fine grained pink granodiorite, possibly slightly altered (patches).
Intergranular microcrystalline quartz (40-45%), cloudy plagioclase (30-35%) and orthoclase (20%), and rare interstitial chloritized biotite (1-2%). Accessory apatite and rare opaques.

75412
close to Wai Anda (Kotaagung)
Seputih granite (Lower Tertiary)
104 43'E 5 05'S
Medium grained granodiorite, with white and pink feldspar, quartz and hornblende crystals.
Intergranular strongly zoned euhedral plagioclase (30%) up to several mm long, orthoclase (20%) and quartz (30%), some myrmekites. Abundant (15-20%) amphiboles (some euhedral), chlorite replacing amphiboles, biotite and opaques.

75413
close to Wai Pengubuan (Kotaagung)
Seputih granite (Lower Tertiary)
104 43'E 5 03'S
Medium grained monzodiorite, with pink and white feldspar, quartz and hornblende crystals.
Intergranular microperthite (70-80%), often cloudy, quartz (10%) with strongly undulate extinction, and chlorite (15%), both primary and replacing amphiboles.

75414
close to Wai Pengubuan (Kotaagung)
Seputih granite (Lower Tertiary)
104 43'E 5 03'S
Fine grained tonalite, with white feldspar, quartz and hornblende.
Similar to 75415, but with less quartz (30%) and poorer in mafics.

75230
close to lake Ranau (Kotaagung)
Ranau fm. (Pliocene-Pleistocene)
104 17'E 5 02'S
Light brown, loose sandy deposit with small pumice fragments and biotite crystals.

75231
close to lake Ranau (Kotaagung)
Ranau fm. (Pliocene-Pleistocene)
104 17'E 5 02'S
Pumice in pyroclastic deposit (75230). White pumice, with abundant quartz and biotite crystals.
Glassy, vesicular pumice, with rare (<2-3%) embayed quartz and rounded plagioclase, and fragmented biotite.

75241
Lake Ranau (Baturaja)
Ranau fm. (Pliocene-Pleistocene)
104 00'E 4 50'S
Yellowish loose clayey deposit, possibly a pyroclastic surge, with white pumice fragments up to 1.5 cm big, and biotite crystals.

75242
Lake Ranau (Baturaja)
Ranau fm. (Pliocene-Pleistocene)
104 01'E 4 50'S
Pumice block in tuff. White, highly vesicular pumice, with oriented flat vescicles. Some quartz, feldspar and biotite crystals up to 3 mm big. Rare yellowish-red alteration patches.
Highly vesicular (40%) pumice, with subangular fragments of plagioclase, sanidine and quartz, and biotite crystals (total <5%).

75246
close to Baturaja (Baturaja)
Kikim fm. (Paleocene-Oligocene)
104 12'E 4 29'S
Violet massive tuff, with abundant rounded milky feldspar phenocrysts, and rare tiny laths of dark brown mafics.
Massive cryptocrystalline tuff, with altered clayey matrix and some euhedral crystals of sanidine and rare plagioclase (<5%) and altered mafics (possibly clinopyroxene, <2%).

75247
close to Tanjungsakti (Manna)
Hulusimpang fm. (Lower Miocene)
103 03'E 4 13'S
Dark gray reddish massive tuff, very fine grained with small feldspar microphenocrysts.
Massive tuff, slightly altered, with rare sanidine (2-3%) and altered mafics (<2%) microphenocrysts.

75248
close to Tanjungsakti (Manna)
Hulusimpang fm. (Lower Miocene)
103 03'E 4 13'S
Greenish medium grained quartz diorite.
Very fine grained intergranular quartz, chlorite and orthoclase in variable amounts, and some (<2%) opaques. Some areas with several mm large anhedral poikiloblasts of perthite with chlorite.

75249
close to Tanjungsakti (Manna)
Granite (Middle Miocene)
103 03'E 4 13'S
White-reddish adamellite, coarse grained.
Intergranular cryptoperthitic feldspar (80%) and quartz (15%), and interstitial blueish-green chlorite and opaques.

75250
close to Tanjungsakti (Manna)
Granite (Middle Miocene)
103 03'E 4 13'S
White-greenish quartz diorite, coarse grained.
Intergranular cryptoperthite (40%) and oligoclase (40%), with some quartz (5%) and yellow-green anhedral, intergranular clinoamphibole, often with chlorite rims. Rare opaques and secondary minerals.

75251
close to Tanjungsakti (Manna)
Granite (Middle Miocene)
103 03'E 4 13'S
Very coarse grained gabbro, with greenish and white feldspars, some alteration veins and altered interstitial mafics.
Very coarse grained, intergranular (in places microperthitic) orthoclase (75%), quartz (10-15%) and chlorite, rare resorbed plagioclase and muscovite. Some fine grained areas with intergranular quartz and plagioclase in equal amounts, and anhedral chloritized interstitial clinopyroxene.

76100
Bukit Batu (Tulung Selapan)
Granite (Jurassic)
105 07'E 3 06'S
Medium grained dark green quartz syenite, with green feldspar and black amphibole.
Intergranular orthoclase (80%), amphibole and chlorite (15%), and rare quartz.

76101
Bukit Batu (Tulung Selapan)
Granite (Jurassic)
105 07'E 3 06'S
Fine to medium grained white quartz syenite, with feldspar, quartz and interstitial biotite.
Intergranular orthoclase (70 to 80%) and variable amounts of quartz (up to 30%) and interstitial biotite.

75290
close to Sicincin (Padang)
Pumiceous tuff (Quaternary)
100 15'E 0 33'S
Block in pumice tuff. White banded pumice, rather heavy, with some quartz crystals up to 2 mm large.
White pumice, with subangular fragments of plagioclase, sanidine and large quartz crystals (total <5%).

75291
close to Sicincin (Padang)
Pumiceous tuff (Quaternary)
100 15'E 0 33'S
Block in pumice tuff. Gray, massive aphyric volcanic rock.
Porphyritic holocrystalline rock. Cryptocrystalline groundmass, with small, extremely abundant, randomly oriented plagioclases and microliths, and tiny opaques. The rare (<5%) pheno- and microphenocrysts are of eu- to subhedral plagioclase, zoned and commonly resorbed in the centre, eu- to anhedral hypersthene, some with augite rims, and subhedral augite (phenocrysts only).

75292
close to Sicincin (Padang)
Pumiceous tuff (Quaternary)
100 15'E 0 33'S
Block in pumice tuff. Gray, massive fine grained volcanic rock, with some slightly altered feldspar phenocrysts.
Porphyritic seriate rock. Oriented plagioclase microliths and opaques set in a glassy groundmass. Microphenocrysts are abundant euhedral plagioclase always resorbed in the core (20%), and rare hypersthene (<3%). Rare (2-3%) plagioclase phenocrysts, euhedral but almost totally resorbed, some in glomerocrysts with hypersthene and opaques.

75293
close to Sicincin (Padang)
Pumiceous tuff (Quaternary)
100 15'E 0 33'S
Block in pumice tuff. Fine grained, reddish, slightly vesicular volcanic rock, with abundant slightly altered feldspar phenocrysts, and rare, tiny mafics.
Porphyritic seriate rock, slightly vesicular (<5%). Crypto/microcrystalline reddish groundmass. Eu- to subhedral plagioclase (15%) zoned and usually resorbed at the centre, rarely skeletal; rare sub- to euhedral augite (2-3%) and hypersthene (<1%), both with black rims.

75286
Sicincin (Padang)
Granite (Tertiary?)
100 20'E 0 29'S
White mid-grained granodiorite, with abundant greenish-black mafics.
Intergranular quartz (40%), microcline (15%) and perthite (10%), plagioclase (15-20%), and rare interstitial chlorite. Common accessory apatite.

75287
Sicincin (Padang)
Granite (Tertiary?)
100 20'E 0 29'S
Light gray mid-grained tonalite, more abundant greenish-black mafics, and gray feldspars.
Similar to 75286, but with more abundant chlorite (10-15%).

75289
G. Tandikat (Padang)
Mapped at the contact between "Quaternary volcanics" and "Tertiary Granites"
100 20'E 0 29'S
Mid to coarse grained massive hornblende-rich volcanic rock, sampled at the contact between the granites 75286-75287 and the andesites from Tandikat volcano.
Porphyritic gabbro. Fine grained plagioclase and rare quartz gabbroid aggregate, with very abundant (40%) seriate euhedral basaltic hornblende crystals, up to 4-5 mm long. The cores of plagioclase in the matrix are almost totally replaced by secondary minerals: these make up, together with interstitial and patchy chlorite and minor calcite, about 50% of the matrix. Most hornblende crystals are optically zoned, with variable pleochroism and rims of chlorite.
This sample was collected at the contact between Tertiary granites and Quaternary andesites, and it is probably a hornblende-rich cumulate related to the Quaternary andesites, rather than a mafic enclave within the Tertiary granites.

75306
close to Tarutung (Pangururan)
Toba tuff (Quaternary)
98 58'E 2 02'N
Light brown loose sandy deposit, possibly a pyroclastic surge, with fragments of white pumice up to 2 cm across, and biotite crystals.

75307
close to Tarutung (Pangururan)
Toba tuff (Quaternary)
98 58'E 2 02'N
White welded ignimbrite, with abundant biotite and some sanidine and hornblende phenocrysts.
Glassy volcanic rock, probably a welded ignimbrite, with fresh glassy groundmass and quartz and sanidine (<5%), and rare (<2%) green amphibole phenocrysts.

75308
close to Prapat (Pangururan)
Toba tuff (Quaternary)
98 59'E 2 37'N
Block in pumice tuff. White pumice, with abundant sanidine and biotite phenocrysts.
White pumice, with abundant fragments of sanidine, quartz and biotite (total <15%).

75309
Prapat (Pangururan)
Toba granodiorite (Quaternary)
98 58'E 2 38'N
Medium grained granodiorite, with white feldspar, green hornblende and rare biotite.
Intergranular orthoclase and plagioclase (30% each) and quartz (20%), green hornblende and rare biotite.

75411
close to Tapaktuan (Tapaktuan)
Samadua granite (Lower Miocene)
97 10'E 3 20'N
Medium grained adamellite, with white and pink feldspar, and interstitial hornblende and biotite crystals up to 3 mm big.
Intergranular perthite (35%), altered plagioclase (25%), and quartz (15%), and equal amounts of biotite and chlorite (as alteration of biotite, rarely primary) and muscovite. Abundant accessory apatite, opaques and sphene.

75409
close to Blang Pidie (Tapaktuan)
Susoh intrusive (Lower Miocene)
96 40'E 3 45'N
Mid to coarse grained adamellite, with pink and white feldspar, quartz and hornblende.
Intergranular quartz (30%), often with undulate extinction, perthite (30-35%) and zoned plagioclase (25-30%) often totally replaced; also some biotite (5%), and accessory opaques and apatite.

75410
close to Blang Pidie (Tapaktuan)
Kluet fm. (Jurassic-Cretaceous)
96 40'E 3 45'N
Coarse grained granite, with pink feldspar, quartz and hornblende crystals up to 2 cm big.
Intergranular quartz (50-60%) with undulate extinction, totally sericitized plagioclase (30%) and rare orthoclase, muscovite and chlorite.

75403
close to Calang (Calang)
Sikuleh batolith - younger complex (Lower Cretaceous to Paleocene? K-Ar age of 97.7 0.7 Ma - Bennett et al. 1981b)
95 34'E 4 47'N
Medium grained granodiorite, with white feldspar and quartz, and minor hornblende.
Intergranular orthoclase and plagioclase (35% each) and quartz (15%), and equal amounts of green hornblende and biotite, partly chloritized.

75402
close to Calang (Calang)
Sikuleh batolith - younger complex (Lower Cretaceous to Paleocene? K-Ar age of 97.7 0.7 Ma - Bennett et al. 1981b)
95 35'E 4 48'N
Fine grained pinkish granodiorite, with white feldspar and quartz, slightly altered.
Intergranular quartz (30-40%) and orthoclase (60-70%) often interdigitating, radiated or micrographic. Rare and small green hornblende, magnetite and muscovite.

75398
N of Calang (Banda Aceh)
Unga diorite (Miocene)
95 28'E 5 02'N
Medium to fine grained gray diorite.
Hypoabyssal, chloritized and sericitized diorite. Originally with plagioclase phenocrysts (20%) in a coarse grained plagioclase and clinopyroxene? groundmass, with abundant opaques (2-3%). Rare (2-3%) anhedral clinopyroxene phenocrysts and microphenocrysts.

75391
S of Banda Aceh (Banda Aceh)
Geunteut granodiorite (Middle Miocene. K-Ar age of 14.3 0.5 Ma - Bennett et al. 1981a)
95 17'E 5 15'N
Mid grained tonalite, with interstitial hornblende in white-yellowish feldspar and quartz. Hornblende granodiorite and subsidiary diorite.
Intergranular plagioclase (70%) and quartz (15-20%) with oriented microfractures, and slightly chloritized augite usually in small euhedral crystals.

Appendix C

Table C1 - List of Indonesian volcanic rocks

Figure C1 - Location of samples of Sumatran volcanic rocks

Table C2 - Whole-rock analyses of Indonesian Quaternary volcanics

Table C3 - Whole-rock analyses of Sumatran pre-Pliocene volcanics

Table C1. List of Indonesian samples.

Catalogue #	Field #	Volcano/Locality	Formation - Age	Quadrant (1:250,000 map)	Longitude (degrees and minutes)	Latitude
Sumatra						
75210	SMG1	G. Rajabasa	Quaternary volcanics	Tanjungkarang	105.35E	5.45S
75211	SMG2	G. Rajabasa	Quaternary volcanics	Tanjungkarang	105.35E	5.45S
75212	SMG3	N of Bakauheni	Lampung fm. (base of Sukadana bas.) (Plioc-Pleistoc)	Tanjungkarang	105.43E	5.50S
75213	SMG4	N of Bakauheni	Andesite (Plioc)	Tanjungkarang	105.42E	5.47S
75214	SMG5	G. Rajabasa	Quaternary volcanics	Tanjungkarang	105.38E	5.45S
75215	SMG6	Jabung	Sukadana basalts (Quat)	Tanjungkarang	105.39E	5.26S
75216	SMG7	Jabung	Sukadana basalts (Quat)	Tanjungkarang	105.39E	5.26S
75217	SMG8	Jabung	Sukadana basalts (Quat)	Tanjungkarang	105.39E	5.26S
75218	SMG9	close to Tanjungkarang	Tarahan fm. (Paleoc-Eoc)	Tanjungkarang	105.18E	5.27S
75219	SMG9B	close to Tanjungkarang	Tarahan fm. (Paleoc-Eoc)	Tanjungkarang	105.19E	5.27S
75220	SMG10	close to Tanjungkarang	Tarahan fm. (Paleoc-Eoc)	Tanjungkarang	105.15E	5.28S
75221	SMG11A	close to Tanjungkarang	Tarahan fm. (Paleoc-Eoc) (xeno)	Tanjungkarang	105.15E	5.28S
75222	SMG11B	close to Tanjungkarang	Tarahan fm. (Paleoc-Eoc) (xeno)	Tanjungkarang	105.15E	5.28S
75223	SMG11C	close to Tanjungkarang	Tarahan fm. (Paleoc-Eoc) (xeno)	Tanjungkarang	105.15E	5.28S
75224	SMG11D	close to Tanjungkarang	Tarahan fm. (Paleoc-Eoc) (xeno)	Tanjungkarang	105.15E	5.28S
75225	SMG11E	close to Tanjungkarang	Tarahan fm. (Paleoc-Eoc) (xeno)	Tanjungkarang	105.15E	5.28S
75226	SMG11F	close to Tanjungkarang	Tarahan fm. (Paleoc-Eoc) (xeno)	Tanjungkarang	105.15E	5.28S
75227	SMG12	G. Ratai	Quaternary volcanics	Tanjungkarang	105.02E	5.32S
75228	SMG13	close to Ulubelu	Quaternary volcanics	Kotaagung	104.41E	5.21S
75229	SMG14	Bt. Sulanalah	Quaternary volcanics	Kotaagung	104.18E	5.03S
75230	SMG15	close to D. Ranau	Quaternary volcanics	Kotaagung	104.17E	5.02S
75231	SMG16	close to D. Ranau	Quaternary volcanics	Kotaagung	104.17E	5.02S
75232	SMG17	G. Sekincau	Quaternary volcanics	Kotaagung	104.17E	5.07S
75233	SMG18	G. Sekincau	Quaternary volcanics	Kotaagung	104.20E	5.04S
75234	SMG19	D. Ranau	Quaternary volcanics	Baturaja	103.58E	4.53S
75235	SMG20	G. Seminung	Quaternary volcanics	Baturaja	103.59E	4.53S
75236	SMG21	G. Seminung	Quaternary volcanics	Baturaja	103.59E	4.53S
75237	SMG22	D. Ranau	Quaternary volcanics	Baturaja	104.00E	4.51S
75238	SMG23	D. Ranau	Quaternary volcanics	Baturaja	103.53E	4.51S
75239	SMG24	D. Ranau	Quaternary volcanics	Baturaja	103.53E	4.51S
75240	SMG25	D. Ranau	Quaternary volcanics	Baturaja	103.55E	4.49S
75241	SMG26	D. Ranau	Ranau fm. (Plioc-Pleistoc)	Baturaja	104.00E	4.50S
75242	SMG27	D. Ranau	Ranau fm. (Plioc-Pleistoc)	Baturaja	104.01E	4.50S
75243	SMG28A	close to Muaradua	Basalt complex (Trias-Jura?)	Baturaja	104.09E	4.31S
75244	SMG28B	close to Muaradua	Basalt complex (Trias-Jura?)	Baturaja	104.09E	4.31S
75245	SMG29	close to Baturaja	Basalt complex (Trias-Jura?)	Baturaja	104.11E	4.30S
75246	SMG30	close to Baturaja	Kikim fm. (Paleoc-Oligoc)	Baturaja	104.12E	4.29S
75247	SMG31	close to Tanjungsakti	Hulusimpang fm. (Early Mioc)	Manna	103.03E	4.13S
75248	SMG32	close to Tanjungsakti	Hulusimpang fm. (Early Mioc)	Manna	103.03E	4.13S
75249	SMG33	close to Tanjungsakti	Granite (Mid Mioc)	Manna	103.03E	4.13S
75250	SMG34	close to Tanjungsakti	Granite (Mid Mioc)	Manna	103.03E	4.13S
75251	SMG35	close to Tanjungsakti	Granite (Mid Mioc)	Manna	103.03E	4.13S
75252	SMG36	G. Dempo	Quaternary volcanics	Manna	103.04E	4.07S
75253	SMG37	G. Dempo	Quaternary volcanics	Manna	103.04E	4.07S
75254	SMG38	G. Dempo	Quaternary volcanics	Manna	103.05E	4.06S
75255	SMG39	G. Dempo	Quaternary volcanics	Manna	103.06E	4.05S
75256	SMG40	G. Dempo	Quaternary volcanics	Manna	103.06E	4.04S
75257	SMG41	G. Dempo	Quaternary volcanics	Manna	103.07E	4.02S
75258	SMG42	G. Dempo	Quaternary volcanics	Manna	103.07E	4.03S
75259	SMG43	G. Dempo	Quaternary volcanics	Manna	103.07E	4.03S
75260	SMG44	G. Dempo	Quaternary volcanics	Manna	103.14E	4.02S
75261	SMG45	G. Dempo	Quaternary volcanics	Manna	103.12E	4.04S
75262	SMG46	G. Dempo	Quaternary volcanics	Manna	103.12E	4.04S
75263	SMG47	close to G. Besar	Quaternary volcanics (?)	Bengkulu	103.18E	3.58S
75264	SMG48	G. Kerinci	Quaternary volcanics	Painan	101.18E	1.43S
75265	SMG49	G. Kerinci	Quaternary volcanics	Painan	101.18E	1.43S
75266	SMG50	G. Kerinci	Quaternary volcanics	Painan	101.18E	1.43S
75267	SMG51	G. Kerinci	Quaternary volcanics	Painan	101.18E	1.39S
75268	SMG52	G. Tandikat	Quaternary volcanics (Plioc?)	Padang	100.20E	0.30S
75269	SMG53	D. Maninjau	Quaternary volcanics (Plioc?)	Padang	100.15E	0.18S
75270	SMG54A	D. Maninjau	Quaternary volcanics (Plioc?)	Padang	100.15E	0.18S
75271	SMG54B	D. Maninjau	Quaternary volcanics (Plioc?)	Padang	100.15E	0.18S
75272	SMG55	close to D. Maninjau	Quaternary volcanics	Padang	100.18E	0.17S
75273	SMG56	G. Marapi	Quaternary volcanics	Padang	100.28E	0.22S
75274	SMG57	G. Marapi	Quaternary volcanics	Padang	100.28E	0.22S
75275	SMG58	G. Marapi	Quaternary volcanics	Padang	100.28E	0.22S
75276	SMG59	G. Marapi	Quaternary volcanics	Padang	100.28E	0.22S
75277	SMG60	G. Marapi	Quaternary volcanics	Padang	100.28E	0.22S
75278	SMG61	G. Marapi	Quaternary volcanics (xeno in block)	Padang	100.28E	0.22S
75279	SMG62	G. Marapi	Quaternary volcanics	Padang	100.28E	0.22S
75280	SMG63	G. Marapi	Quaternary volcanics	Padang	100.28E	0.22S
75281	SMG64	G. Marapi	Quaternary volcanics	Padang	100.28E	0.22S
75282	SMG65A	G. Marapi	Quaternary volcanics	Padang	100.28E	0.22S
75283	SMG65B	G. Marapi	Quaternary volcanics	Padang	100.28E	0.22S
75284	SMG66	G. Marapi	Quaternary volcanics	Padang	100.27E	0.22S
75285	SMG67	G. Marapi	Quaternary volcanics	Padang	100.27E	0.22S
75286	SMG68A	Sicincin	Granite (Tertiary?)	Padang	100.20E	0.29S
75287	SMG68B	Sicincin	Granite (Tertiary?)	Padang	100.20E	0.29S
75288	SMG69	G. Tandikat	Quaternary volcanics (Plioc?)	Padang	100.20E	0.29S
75289	SMG70	G. Tandikat	Basic cumulate (Tertiary?)	Padang	100.20E	0.29S
75290	SMG71A	close to Sicincin	Quaternary volcanics (xeno)	Padang	100.15E	0.33S

Table C1 cont. List of Indonesian samples.

Catalogue #	Field #	Volcano/Locality	Formation - Age	Quadrant (1:250,000 map)	Longitude (degrees and minutes)	Latitude
Sumatra						
75291	SMG71B	close to Sicincin	Quaternary volcanics (xeno)	Padang	100.15E	0.33S
75292	SMG71C	close to Sicincin	Quaternary volcanics (xeno)	Padang	100.15E	0.33S
75293	SMG71D	close to Sicincin	Quaternary volcanics (xeno)	Padang	100.15E	0.33S
75294	SMG72	G. Tandikat	Quaternary volcanics (Plioc?)	Padang	100.16E	0.26S
75295	SMG73	G. Singgalang	Quaternary volcanics (Plioc?)	Padang	100.17E	0.25S
75296	SMG74	close to G. Singgalang	Quaternary volcanics (Plioc?) (plug)	Padang	100.18E	0.23S
75297	SMG75	G. Sirabungan	Quaternary volcanics (Paleoc?-Quat)	Padang	100.14E	0.03S
75298	SMG76	Bt. Batastinjaulaut	Quaternary volcanics (Paleoc?-Quat)	Padang	100.10E	0.04S
75299	SMG77	close to Kumpulan	Quaternary volcanics (Paleoc?-Quat)	Padang	100.11E	0.04S
75300	SMG78	close to Kumpulan	Quaternary volcanics (Paleoc?-Quat)	Padang	100.11E	0.04S
75301	SMG79	close to Kumpulan	Quaternary volcanics (Paleoc?-Quat)	Padang	100.12E	0.04S
75302	SMG80	Sorik Marapi	Quaternary volcanics	Natal	99.32E	0.40N
75303	SMG81	Sorik Marapi	Quaternary volcanics (mud)	Natal	99.32E	0.41N
75304	SMG82	Sorik Marapi	Quaternary volcanics (mud)	Natal	99.32E	0.41N
75305	SMG83	Sorik Marapi	Quaternary volcanics	Natal	99.32E	0.41N
75306	SMG84	close to Tarutung	Toba tuff (Piloc.?-Quat)	Pangururan	98.58E	2.02N
75307	SMG85	close to Tarutung	Toba tuff (Piloc.?-Quat)	Pangururan	98.58E	2.02N
75308	SMG86	close to Prapat	Toba tuff (Piloc.?-Quat)	Pangururan	98.59E	2.37N
75309	SMG87	Prapat	Toba granodiorite (Plioc?-Quat)	Pangururan	98.58E	2.38N
75310	SMG88	Bual Buali	Quaternary volcanics	Padangsidempuan	99.15E	1.34N
75311	SMG89	G. Sibayak	Quaternary volcanics	Medan	98.29E	3.15N
75312	SMG90	G. Sibayak	Quaternary volcanics	Medan	98.30E	3.15N
75313	SMG91	G. Sibayak	Quaternary volcanics	Medan	98.30E	3.15N
75314	SMG92	G. Sinabung	Quaternary volcanics	Medan	98.23E	3.10N
75315	SMG93	G. Sinabung	Quaternary volcanics	Medan	98.23E	3.10N
75316	SMG94	G. Sinabung	Quaternary volcanics	Medan	98.23E	3.10N
75317	SMG95	G. Sinabung	Quaternary volcanics	Medan	98.23E	3.10N
75318	SMG96	G. Sinabung	Quaternary volcanics	Medan	98.23E	3.10N
75319	SMG97	G. Sinabung	Quaternary volcanics	Medan	98.23E	3.10N
75320	SMG98	G. Sinabung	Quaternary volcanics	Medan	98.23E	3.10N
75321	SMG99	G. Sibayak	Quaternary volcanics	Medan	98.28E	3.12N
75322	SMG100	G. Sibayak	Quaternary volcanics	Medan	98.28E	3.12N
75323	SMG101	G. Sibayak	Quaternary volcanics	Medan	98.29E	3.11N
75324	SMG102	G. Sibayak	Quaternary volcanics	Medan	98.29E	3.11N
75325	SMG103	close to Takengon	Quaternary volcanics	Takengon	96.47E	4.36N
75326	SMG104	close to Takengon	Quaternary volcanics	Takengon	96.47E	4.36N
75327	SMG105	close to Takengon	Quaternary volcanics	Takengon	96.47E	4.36N
75328	SMG106	close to Takengon	Quaternary volcanics	Takengon	96.47E	4.36N
75329	SMG107	G. Geureudong	Quaternary volcanics	Takengon	96.46E	4.44N
75330	SMG108	G. Geureudong	Quaternary volcanics	Takengon	96.48E	4.45N
75331	SMG109	G. Geureudong	Quaternary volcanics	Takengon	96.48E	4.45N
75332	SMG110	close to Bireuen	Quaternary volcanics	Takengon	96.44E	4.57N
75333	SMG111	close to Sare	Quaternary volcanics	Banda Aceh	95.48E	5.23N
75334	SMG112	G. Seulemium	Quaternary volcanics	Banda Aceh	95.41E	5.22N
75335	SMG113	G. Seulemium	Quaternary volcanics (xeno)	Banda Aceh	95.41E	5.22N
75336	SMG114	G. Seulemium	Quaternary volcanics (xeno)	Banda Aceh	95.41E	5.22N
75337	SMG115	G. Seulemium	Quaternary volcanics	Banda Aceh	95.41E	5.22N
75338	SMG116	G. Seulemium	Quaternary volcanics (xeno)	Banda Aceh	95.41E	5.22N
75339	SMG117	G. Seulemium	Quaternary volcanics (xeno)	Banda Aceh	95.41E	5.22N
75340	SMG118	G. Seulemium	Quaternary volcanics (xeno)	Banda Aceh	95.41E	5.22N
75341	SMG119	G. Seulemium	Quaternary volcanics (xeno)	Banda Aceh	95.41E	5.22N
75342	SMG120	G. Seulemium	Quaternary volcanics	Banda Aceh	95.41E	5.22N
75343	SMG121	P. Weh	Quaternary volcanics	Banda Aceh	95.18E	5.47N
75344	SMG122	P. Weh	Quaternary volcanics	Banda Aceh	95.18E	5.47N
75345	SMG123	P. Weh	Quaternary volcanics	Banda Aceh	95.19E	5.48N
75346	SMG124	P. Weh	Quaternary volcanics	Banda Aceh	95.18E	5.50N
75347	SMG124B	P. Weh	Quaternary volcanics	Banda Aceh	95.19E	5.48N
75348	SMG125	P. Weh	Quaternary volcanics	Banda Aceh	95.18E	5.46N
75349	SMG126	P. Weh	Quaternary volcanics	Banda Aceh	95.18E	5.46N
75350	SMG127	P. Weh	Quaternary volcanics	Banda Aceh	95.18E	5.46N
75351	SMG128	P. Weh	Quaternary volcanics	Banda Aceh	95.18E	5.46N
75352	SMG129	P. Weh	Quaternary volcanics	Banda Aceh	95.15E	5.49N
75353	SMG130	P. Weh	Quaternary volcanics	Banda Aceh	95.15E	5.49N
75354	SMG131	Bumijawa	Sukadana basalts (Quat)	Tanjungkarang	105.28E	5.02S
75355	SMG132	Bumijawa	Sukadana basalts (Quat)	Tanjungkarang	105.28E	5.02S
75356	SMG133	G. Tiga	Sukadana basalts (Quat)	Tanjungkarang	105.28E	5.05S
75357	SMG134	G. Tiga	Sukadana basalts (Quat)	Tanjungkarang	105.28E	5.05S
75358	SMG135	G. Tiga	Sukadana basalts (Quat)	Tanjungkarang	105.28E	5.05S
75359	SMG136	G. Tiga	Sukadana basalts (Quat)	Tanjungkarang	105.28E	5.05S
75360	SMG137	Negerikaton	Sukadana basalts (Quat)	Tanjungkarang	105.30E	5.10S
75361	SMG138	Negerikaton	Sukadana basalts (Quat)	Tanjungkarang	105.30E	5.10S
75362	SMG139	Negerikaton	Sukadana basalts (Quat)	Tanjungkarang	105.30E	5.10S
75363	SMG140	Negerikaton	Sukadana basalts (Quat)	Tanjungkarang	105.30E	5.10S
75364	SMG141	Jabung	Sukadana basalts (Quat)	Tanjungkarang	105.39E	5.26S
75365	SMG142	Jabung	Sukadana basalts (Quat)	Tanjungkarang	105.39E	5.26S
75366	SMG143	close to Sukadana	Sukadana basalts (Quat)	Tanjungkarang	105.35E	5.22S
75367	SMG144	close to Sukadana	Sukadana basalts (Quat)	Tanjungkarang	105.35E	5.22S
75368	SMG145	close to Sukadana	Sukadana basalts (Quat)	Tanjungkarang	105.35E	5.22S
75369	SMG146	G. Mirah	Sukadana basalts (Quat)	Tanjungkarang	105.35E	5.08S
75370	SMG147	G. Mirah	Sukadana basalts (Quat)	Tanjungkarang	105.35E	5.08S
75371	SMG148	close to Djepara	Sukadana basalts (Quat)	Tanjungkarang	105.43E	5.13S

Table C1 cont. List of Indonesian samples.

Catalogue #	Field #	Volcano/Locality	Formation - Age	Quadrant (1:250,000 map)	Longitude (degrees and minutes)	Latitude
Sumatra						
75372	SMG149	close to Djepara	Sukadana basalts (Quat)	Tanjungkarang	105.40E	5.13S
75373	SMG149B	G.Emas	Sukadana basalts (Quat)	Tanjungkarang	105.41E	5.18S
75374	SMG150	G. Wana	Sukadana basalts (Quat)	Tanjungkarang	105.45E	5.20S
75375	SMG151	G. Wana	Sukadana basalts (Quat)	Tanjungkarang	105.45E	5.20S
75376	SMG152	G. Samang	Sukadana basalts (Quat)	Tanjungkarang	105.46E	5.21S
75377	SMG153	close to Labuhanmaringgai	Sukadana basalts (Quat)	Tanjungkarang	105.45E	5.25S
75378	SMG153B1	Bt. Telor	Sukadana basalts (Jambi) (Quat)	Jambi	103.45E	1.17S
75379	SMG153B2	Bt. Telor	Sukadana basalts (Jambi) (Quat)	Jambi	103.45E	1.17S
75380	SMG154	G. Kaba	Quaternary volcanics	Bengkulu	102.37E	3.31S
75381	SMG155	G. Kaba	Quaternary volcanics	Bengkulu	102.37E	3.31S
75382	SMG156	G. Kaba	Quaternary volcanics	Bengkulu	102.37E	3.31S
75383	SMG157	G. Kaba	Quaternary volcanics	Bengkulu	102.37E	3.31S
75384	SMG158	G. Kaba	Quaternary volcanics	Bengkulu	102.37E	3.31S
75385	SMG159	G. Kaba	Quaternary volcanics	Bengkulu	102.37E	3.31S
75386	SMG160	G. Kaba	Quaternary volcanics	Bengkulu	102.37E	3.31S
75387	SMG160A	G. Kaba	Quaternary volcanics	Bengkulu	102.37E	3.31S
75388	BDNG1	Kampung Rano	Sukadana basalts (Jambi) (Quat)	Jambi	103.46E	1.13S
75389	BDNG2	Bt. Telor	Sukadana basalts (Jambi) (Quat)	Jambi	103.45E	1.17S
75390	BA1	SW of Banda Aceh	Bentaro fm. (Jura-Creta)	Banda Aceh	95.15E	5.20N
75391	BA7	S of Banda Aceh	Geunteut granodiorite (Eoc-Oligoc)	Banda Aceh	95.17E	5.15N
75392	BA8	SW of Banda Aceh	Bentaro fm. (Jura-Creta)	Banda Aceh	95.19E	5.13N
75393	BA9	SW of Banda Aceh	Bentaro fm. (Jura-Creta)	Banda Aceh	95.19E	5.11N
75394	BA10	SW of Banda Aceh	Bentaro fm. (Jura-Creta)	Banda Aceh	95.18E	5.04N
75395	BA12	SW of Banda Aceh	Bentaro fm. (Jura-Creta)	Banda Aceh	95.18E	5.07N
75396	BA16	SW of Banda Aceh	Bentaro fm. (Jura-Creta)	Banda Aceh	95.18E	5.09N
75397	BA20	N of Calang	Calang fm. (Mid Mioc)	Banda Aceh	95.20E	5.03N
75398	BA21	N of Calang	Unga diorite (Late Mioc)	Banda Aceh	95.28E	5.02N
75399	BA23	N of Calang	Calang fm. (Mid Mioc)	Calang	95.24E	4.56N
75400	BA24	N of Calang	Calang fm. (Mid Mioc)	Calang	95.24E	4.56N
75401	BA27	close to Calang	Tangla fm. (Early Mioc)	Calang	95.25E	4.52N
75402	BA29	close to Calang	Sikuleh batolith (Creta)	Calang	95.35E	4.48N
75403	BA31	close to Calang	Sikuleh batolith (Creta)	Calang	95.34E	4.47N
75404	BA32	close to Calang	within Sikuleh batolith (xeno)	Calang	95.45E	4.43N
75405	BA32B	close to Calang	within Sikuleh batolith (xeno)	Calang	95.45E	4.43N
75406	BA33A	close to Calang	within Sikuleh batolith (xeno)	Calang	95.45E	4.43N
75407	BA35A	Calang	Calang fm. (Mid Mioc)	Calang	95.34E	4.38N
75408	BA35B	Calang	Calang fm. (Mid Mioc)	Calang	95.34E	4.38N
75409	BP3	close to Blang Pidie	Susoh intrusive (Early Mioc)	Tapaktuan	96.40E	3.45N
75410	BP5	close to Blang Pidie	Kluet fm. (Jura-Creta)	Tapaktuan	96.40E	3.45N
75411	TT2	close to Tapaktuan	Samadua granite (Early Mioc)	Tapaktuan	97.10E	3.20N
75412	SU105/1	close to Wai Anda	Seputih granite (Early Tertiary)	Kotaagung	104.43E	5.05S
75413	SU125/1	close to Wai Pengubuan	Seputih granite (Early Tertiary)	Kotaagung	104.43E	5.03S
75414	SU125/2	close to Wai Pengubuan	Seputih granite (Early Tertiary)	Kotaagung	104.43E	5.03S
75415	SU129	close to Wai Tatayan	Seputih granite (Early Tertiary)	Kotaagung	104.51E	5.07S
78129	SMG 161	Bukit Mapas	Quaternary volcanics (Mapas)	Baturaja	104°19' E	4°30' S
78130	SMG 162	Bukit Mapas	Quaternary volcanics (Mapas)	Baturaja	104°19' E	4°30' S
78131	SMG 163	Bukit Mapas	Quaternary volcanics (Mapas)	Baturaja	104°19' E	4°30' S
78132	SMG 164	Bukit Mapas	Quaternary volcanics (Mapas)	Baturaja	104°19' E	4°30' S
78133	SMG 165	Bukit Mapas	Quaternary volcanics (Mapas)	Baturaja	104°19' E	4°30' S
78134	SMG 166	Bukit Mapas	Quaternary volcanics (Mapas)	Baturaja	104°19' E	4°30' S
78135	Pal GB	Bukit Batu	Granite (Jura)	Tulung Selapan	105°07' E	3°06' S
78136	Pal GR	Bukit Batu	Granite (Jura)	Tulung Selapan	105°07' E	3°06' S
Jawa						
75416	GG1	G. Galunggung	Quaternary volcanics	Jawa Barat	Exact location unknown	
75417	GG2	G. Galunggung	Quaternary volcanics	Jawa Barat	Exact location unknown	
75418	TAL	G. Talagabodas	Quaternary volcanics	Jawa Barat	Exact location unknown	
Kalimantan						
75419	89SS21B	unknown	Quaternary volcanics	Muara Wahau	Exact location unknown	
75420	89SS22A	unknown	Quaternary volcanics	Muara Wahau	Exact location unknown	
75421	89SS23D	unknown	Quaternary volcanics	Muara Wahau	Exact location unknown	
75422	89SS25A	unknown	Quaternary volcanics	Muara Wahau	Exact location unknown	
75423	89SS25B	unknown	Quaternary volcanics	Muara Wahau	Exact location unknown	
75424	89SS25D	unknown	Quaternary volcanics	Muara Wahau	Exact location unknown	
75425	89SS25E	unknown	Quaternary volcanics	Muara Wahau	Exact location unknown	
75426	89SS25F	unknown	Quaternary volcanics	Muara Wahau	Exact location unknown	
75427	89SS28A	unknown	Quaternary volcanics	Muara Wahau	Exact location unknown	
75428	89SS43G	unknown	Quaternary volcanics	Muara Wahau	Exact location unknown	
75429	89SS43H	unknown	Quaternary volcanics	Muara Wahau	Exact location unknown	
75430	86SS12C	unknown	Quaternary volcanics	Long Pahangai	Exact location unknown	
75431	86SS21A	unknown	Quaternary volcanics	Long Pahangai	Exact location unknown	
75432	86SM19A	unknown	Quaternary volcanics	Long Pahangai	Exact location unknown	
75433	86SK2D	unknown	Quaternary volcanics	Long Pahangai	Exact location unknown	
75434	86AM63A	unknown	Quaternary volcanics	Long Pahangai	Exact location unknown	

Thin sections are available for all the samples.
Whole-rock and mineral analyses are reported in Chapters 2 and 6, and Appendices C and F

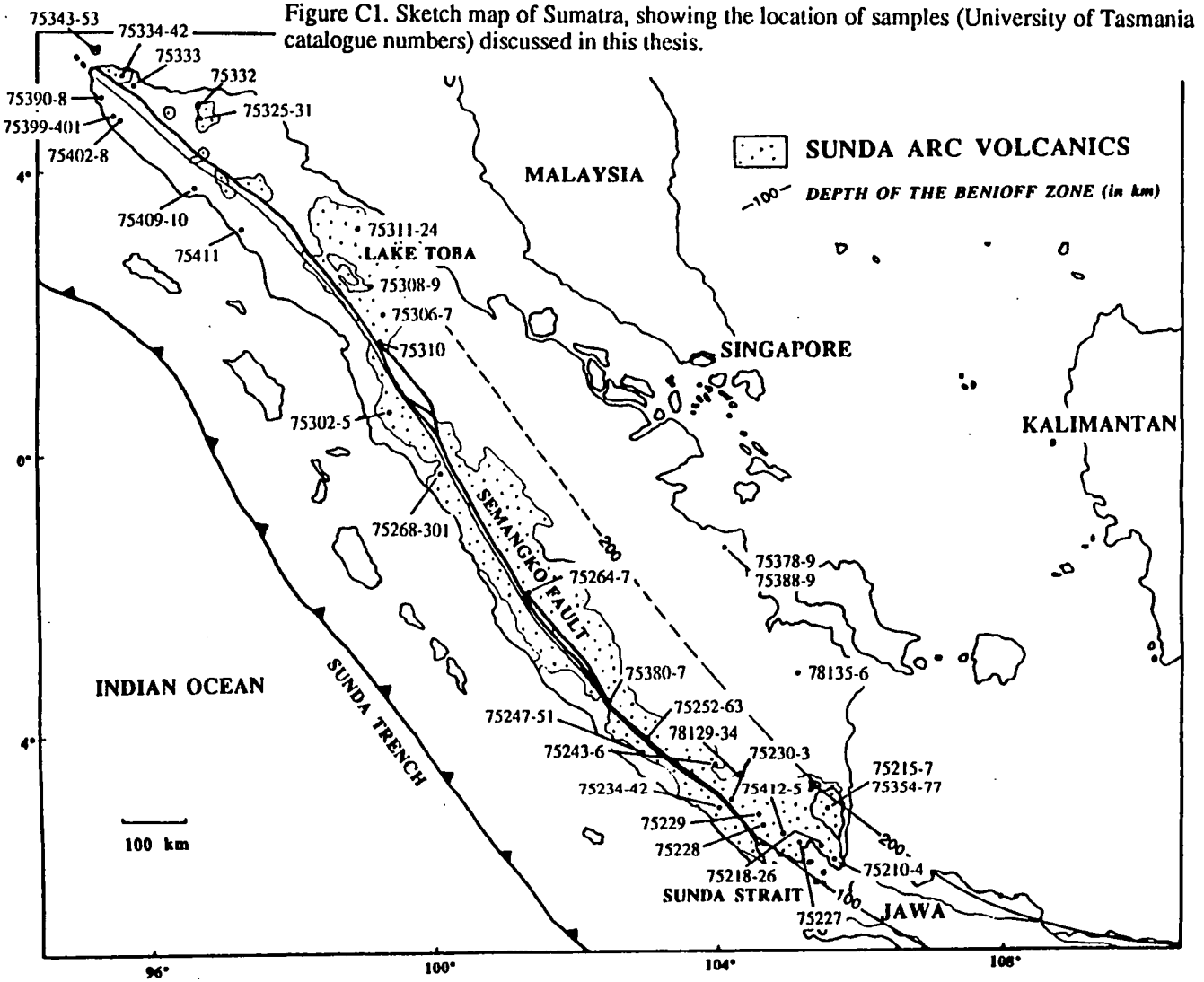

Figure C1. Sketch map of Sumatra, showing the location of samples (University of Tasmania catalogue numbers) discussed in this thesis.

Table C2. Whole-rock analyses of Indonesian Quaternary volcanics

	Jawa		Sumatra				
Catalogue #	75416	75417	75210	75211	75213	75214	75227
Field #	GG1	GG2	SMG1	SMG2	SMG4	SMG5	SMG12
Volcano	Galunggung	Galunggung	Rajabasa	Rajabasa	North of Bakauheni	Rajabasa	Ratai
Longitude	108°05'E	108°05'E	105°35'E	105°35'E	105°42'E	105°38'E	105°02'E
Latitude	7°15'S	7°15'S	5°45'S	5°45'S	5°47'S	5°45'S	5°32'S
SiO2	49.30	49.11	53.25	55.41	65.41	56.66	56.56
TiO2	0.80	0.81	0.93	0.85	0.49	0.74	0.81
Al2O3	15.95	16.11	17.87	17.76	15.83	17.67	17.64
Fe2O3	9.89	9.85	9.30	8.59	4.04	7.73	8.42
MnO	0.17	0.17	0.17	0.17	0.08	0.15	0.24
MgO	10.36	10.14	4.22	3.76	1.23	3.83	3.10
CaO	11.28	11.34	8.38	7.64	3.64	7.46	6.91
Na2O	2.33	2.33	3.13	3.42	3.96	3.31	3.82
K2O	0.35	0.35	1.55	1.60	2.59	1.98	1.52
P2O5	0.11	0.09	0.23	0.22	0.12	0.20	0.32
LOI	-0.52	-0.54	0.62	0.08	2.18	0.27	0.64
Total	100.02	99.76	99.65	99.50	99.57	100.00	99.98
Mg#	70.93	70.57	51.39	50.49	41.50	53.58	46.17
Rb			49	45	92	66	42
Ba			271	312	363	339	305
Sr			491	538	244	448	633
Pb			5		9	6	5
Cs			0.75	1.31	1.44		0.46
Zr			104	123	201	117	144
Hf			2.32	2.68	4.34		3.42
Nb			4	4	6	3	5
Ta			0.51	0.19	0.53		0.81
Y			23	23	24	22	26
Th			6.59	6.22	11.74	10	4.76
La			14.62	17	21.1	22	17.7
Ce			34.2	35.9	40.4	40	40.4
Nd			18.2	19.3	20.1	20	23.3
Sm			4.4	4.32	4.1		5.19
Eu			1.36	1.19	0.92		1.5
Tb			0.67	0.61	0.62		0.78
Ho			0.85	0.88	0.87		1.02
Yb			1.99	2.02	2.29		2.28
Lu			0.27	0.28	0.32		0.33
Cr			11	9	20	17	1
Ni			13	13	13	15	5
V			245	213	68	197	143
Sc			27	23	13	25	16
87Sr/86Sr	0.70443			0.70432			0.70433
143Nd/144Nd	0.512899		0.512786	0.512750	0.512829		0.512771
208Pb/204Pb	39.189		38.814	38.757	38.756		38.755
207Pb/204Pb	15.700		15.641	15.631	15.622		15.628
206Pb/204Pb	18.800		18.602	18.583	18.598		18.564

Table C2 cont. Whole-rock analyses of Indonesian Quaternary volcanics

	Sumatra							
Catalogue #	75228	75229	75232	75233	75234	75235	75236	75237
Field #	SMG13	SMG14	SMG17	SMG18	SMG19	SMG20	SMG21	SMG22
Volcano	Close to Ulubelu	Sulanalah	Sekincau	Sekincau	By Lake Ranau	Seminung	Seminung	By Lake Ranau
Longitude	104°41'E	104°18'E	104°17'E	104°20'E	103°58'E	103°59'E	103°59'E	104°00'E
Latitude	5°21'S	5°03'S	5°07'S	5°04'S	4°53'S	4°53'S	4°53'S	4°51'S
SiO2	61.46	55.08	53.21	54.71	63.53	60.22	63.83	53.43
TiO2	0.73	1.20	1.01	1.21	0.63	0.73	0.68	0.90
Al2O3	16.31	16.35	18.60	16.37	16.47	16.92	17.10	18.43
Fe2O3	6.94	10.95	9.42	10.32	5.07	6.50	4.80	9.02
MnO	0.14	0.18	0.17	0.18	0.10	0.12	0.10	0.14
MgO	2.52	3.60	3.82	3.68	1.92	3.10	1.49	4.54
CaO	6.31	7.39	9.08	7.88	5.14	6.65	5.11	9.16
Na2O	3.46	3.38	3.16	3.21	4.15	3.44	4.10	2.71
K2O	1.55	1.02	0.69	1.68	2.22	1.87	2.20	1.17
P2O5	0.15	0.31	0.20	0.30	0.19	0.14	0.21	0.12
LOI	0.65	0.54	1.17	-0.03	0.15	0.00	0.20	0.04
Total	100.22	100.00	100.53	99.51	99.57	99.69	99.82	99.66
Mg#	45.83	43.37	48.58	45.38	46.87	52.63	41.97	53.97
Rb	46	26	12	55	96	77	87	48
Ba	304	207	151	291	350	276	356	190
Sr	312	343	400	427	309	328	318	386
Pb		8	6			13	19	9
Cs			0.64	1.39				2.69
Zr	114	129	94	183	159	151	171	93
Hf			2.24	4.25				2.42
Nb	3	4	2	6	4	2	5	2
Ta			0.41	0.88				0.42
Y	30	60	32	35	26	24	25	21
Th		3	2.23	7.08				5.35
La		30	9.81	19.2				10.1
Ce		38	21.2	45.5				22.4
Nd		40	13.6	25.2				13
Sm			3.51	5.99				3.36
Eu			1.24	1.43				1.02
Tb			0.67	0.9				0.54
Ho			0.87	1.11				0.73
Yb			2.29	2.84				1.84
Lu			0.35	0.41				0.27
Cr	6	9	23	14	9	27	6	29
Ni	8	14	15	12	7	14	5	24
V	170	312	276	289	103	159	87	273
Sc	24	37	35	35	17	23	16	31
87Sr/86Sr			0.70476	0.70450				0.70510
143Nd/144Nd			0.512783	0.512723				0.512619
208Pb/204Pb			39.041	38.927				39.214
207Pb/204Pb			15.673	15.656				15.702
206Pb/204Pb			18.735	18.651				18.818

Table C2 cont. Whole-rock analyses of Indonesian Quaternary volcanics

	Sumatra							
Catalogue #	75238	75239	75240	75252	75253	75254	75256	75257
Field #	SMG23	SMG24	SMG25	SMG36	SMG37	SMG38	SMG40	SMG41
Volcano	By Lake Ranau	By Lake Ranau	By Lake Ranau	Dempo	Dempo	Dempo	Dempo	Dempo
Longitude	103°53'E	103°53'E	103°55'E	103°04'E	103°04'E	103°05'E	103°06'E	103°07'E
Latitude	4°51'S	4°51'S	4°49'S	4°07'S	4°07'S	4°06'S	4°04'S	4°02'S
SiO2	55.73	55.23	55.48	73.34	61.60	53.10	53.63	54.63
TiO2	0.82	0.79	0.81	0.25	0.98	1.05	1.01	1.13
Al2O3	17.39	17.37	17.56	13.07	16.85	18.34	18.03	18.54
Fe2O3	7.88	7.91	8.05	2.17	6.00	9.36	9.24	9.47
MnO	0.13	0.15	0.14	0.07	0.12	0.17	0.16	0.16
MgO	4.38	4.52	4.31	0.65	1.61	4.20	4.12	3.60
CaO	8.07	8.44	8.44	1.95	4.46	8.22	8.30	8.53
Na2O	3.01	2.92	2.82	3.87	4.70	3.26	3.05	3.24
K2O	1.62	1.74	1.62	2.61	2.54	1.20	1.27	1.13
P2O5	0.11	0.14	0.14	0.06	0.36	0.22	0.22	0.21
LOI	0.70	0.80	0.86	1.83	0.62	0.70	0.64	-0.31
Total	99.84	100.01	100.23	99.87	99.84	99.82	99.67	100.33
Mg#	56.43	57.11	55.50	41.10	38.47	51.11	50.95	46.97
Rb	69	69	67	108	94	41	49	39
Ba	232	233	232	385	402	240	213	192
Sr	375	377	380	145	375	434	392	401
Pb	12	13	13	20	13	11	11	6
Cs	4.16					1.99	3.59	2.20
Zr	129	121	123	140	197	126	121	108
Hf	2.74					2.87	3.04	2.68
Nb	3	2	2	3	4	3	5	4
Ta	0.90					0.71	0.19	0.73
Y	26	23	23	21	43	26	24	26
Th	7.22					5.69	6.02	4.31
La	12.2					12.3	12.6	11
Ce	27.2					29.8	29.1	25.3
Nd	16.6					17.8	17.5	16.2
Sm	3.78					4.38	4.4	4.11
Eu	0.92					1.29	1.22	1.25
Tb	0.67					0.63	0.69	0.65
Ho	0.76					0.84	0.93	0.81
Yb	1.84					2.17	2.36	2.18
Lu	0.27					0.3	0.32	0.29
Cr	96	89	61	4	3	15	15	9
Ni	33	27	25	3	5	10	13	8
V	223	222	232	24	59	263	253	284
Sc	28	28	30	7	20	32	31	33
87Sr/86Sr	0.70532					0.70483	0.70490	0.70473
143Nd/144Nd	0.512592					0.512684	0.512718	0.512723
208Pb/204Pb	39.306					39.176	39.187	39.164
207Pb/204Pb	15.721					15.700	15.699	15.692
206Pb/204Pb	18.861					18.785	18.789	18.787

Table C2 cont. Whole-rock analyses of Indonesian Quaternary volcanics

	Sumatra							
Catalogue #	75258	75259	75260	75261	75262	75264	75265	75266
Field #	SMG42	SMG43	SMG44	SMG45	SMG46	SMG48	SMG49	SMG50
Volcano	Dempo	Dempo	Dempo	Dempo	Dempo	Kerinci	Kerinci	Kerinci
Longitude	103°07'E	103°07'E	103°14'E	103°12'E	103°12'E	101°18'E	101°18'E	101°18'E
Latitude	4°03'S	4°03'S	4°02'S	4°04'S	4°04'S	1°43'S	1°43'S	1°43'S
SiO2	55.49	66.30	54.63	62.96	56.56	60.96	59.96	52.55
TiO2	0.88	0.50	0.93	0.85	0.76	1.00	1.01	1.10
Al2O3	20.45	16.30	18.60	22.03	20.01	16.94	17.10	18.77
Fe2O3	6.53	3.88	8.91	2.32	5.19	6.37	6.91	9.65
MnO	0.11	0.15	0.16	0.04	0.17	0.17	0.17	0.17
MgO	1.83	1.07	4.35	1.15	1.32	1.83	1.98	3.97
CaO	7.73	3.31	8.34	0.44	2.60	4.47	4.74	8.10
Na2O	3.97	4.78	3.06	0.23	4.07	5.18	4.88	4.05
K2O	1.53	3.05	1.17	0.09	1.40	2.35	2.35	1.35
P2O5	0.26	0.22	0.21	0.07	0.27	0.48	0.54	0.27
LOI	0.76	0.04	0.10	9.90	7.47	-0.14	-0.03	-0.23
Total	99.54	99.60	100.46	100.08	99.82	99.61	99.61	99.75
Mg#	39.50	39.12	53.22	53.59	37.21	40.10	40.03	48.94
Rb	65	128	42	4	17	69	66	31
Ba	290	449	191	34	519	465	476	285
Sr	489	328	402	36	287	421	442	544
Pb	10	23						
Cs						2.82		
Zr	132	229	116	258	239	307	290	134
Hf						6.96		
Nb	3	5	3	6	8	10	10	5
Ta						0.84		
Y	34	29	24	102	46	48	46	27
Th						8.41		
La						32.3		
Ce						77		
Nd						43.7		
Sm						9.63		
Eu						2.16		
Tb						1.46		
Ho						1.88		
Yb						4.35		
Lu						0.62		
Cr	2	1	11	1	2	2	2	10
Ni	4	2	13	1	3	4	4	14
V	129	12	216	96	21	34	54	248
Sc	21	8	28	22	11	19	19	29
87Sr/86Sr						0.70502		
143Nd/144Nd						0.512675		
208Pb/204Pb						38.896		
207Pb/204Pb						15.648		
206Pb/204Pb						18.647		

Table C2 cont. Whole-rock analyses of Indonesian Quaternary volcanics

	Sumatra							
Catalogue #	75267	75268	75269	75270	75271	75272	75273	75274
Field #	SMG51	SMG52	SMG53	SMG54A	SMG54B	SMG55	SMG56	SMG57
Volcano	Kerinci	Tandikat	By Lake Maninjau	By Lake Maninjau	By Lake Maninjau	By Lake Maninjau	Marapi	Marapi
Longitude	101°18'E	100°20'E	100°15'E	100°15'E	100°15'E	100°18'E	100°28'E	100°28'E
Latitude	1°39'S	0°30'S	0°18'S	0°18'S	0°18'S	0°17'S	0°22'S	0°22'S
SiO2	51.84	56.14	62.14	62.27	55.03	65.59	60.07	55.41
TiO2	1.10	0.89	0.61	0.64	0.73	0.14	0.78	0.96
Al2O3	19.05	18.05	16.54	16.39	17.00	11.22	17.24	16.91
Fe2O3	9.76	8.15	5.78	6.12	8.15	0.88	7.50	8.57
MnO	0.17	0.14	0.10	0.11	0.14	0.04	0.13	0.15
MgO	4.38	3.75	2.72	2.97	5.57	0.15	2.87	5.12
CaO	8.63	7.41	5.45	5.70	8.55	1.04	6.13	7.72
Na2O	3.55	3.24	3.18	3.28	2.49	2.69	3.53	3.38
K2O	1.10	1.30	2.52	2.44	1.39	3.50	2.40	1.97
P2O5	0.23	0.19	0.15	0.13	0.10	0.02	0.21	0.26
LOI	-0.33	0.55	0.51	0.20	0.49	15.04	-0.28	-0.47
Total	99.48	99.81	99.70	100.25	99.64	100.31	100.58	99.98
Mg#	51.11	51.74	52.30	53.07	61.42	28.42	47.13	58.19
Rb	25	45	117	47	51	153	81	58
Ba	233	265	422	439	235	550	425	408
Sr	517	375	310	255	280	122	393	414
Pb		9						
Cs	0.96	2.31						
Zr	120	157	187	96	105	96	209	166
Hf	3.01	3.95						
Nb	4	5	5	5	2	6	6	10
Ta	0.19	0.62						
Y	25	29	27	22	25	15	34	30
Th	3.27	5.6						
La	14	16.2						
Ce	31.9	37.5						
Nd	19.1	21.1						
Sm	4.87	5						
Eu	1.28	1.15						
Tb	0.83	0.73						
Ho	0.99	1.02						
Yb	2.1	2.6						
Lu	0.28	0.39						
Cr	15	17	33	45	214	1	5	80
Ni	14	12	13	20	34	1	8	32
V	259	193	121	131	212	2	138	190
Sc	31	25	17	18	30	2	18	23
87Sr/86Sr	0.70514	0.70630						
143Nd/144Nd	0.512652	0.512491						
208Pb/204Pb	39.001	39.265						
207Pb/204Pb	15.671	15.714						
206Pb/204Pb	18.701	18.837						

Table C2 cont. Whole-rock analyses of Indonesian Quaternary volcanics

	Sumatra						
Catalogue #	75275	75276	75277	75279	75280	75281	75282
Field #	SMG58	SMG59	SMG60	SMG62	SMG63	SMG64	SMG65A
Volcano	Marapi	Marapi	Marapi	Marapi	Marapi	Marapi	Marapi
Longitude	100°28'E	100°28'E	100°28'E	100°28'E	100°28'E	100°28'E	100°28'E
Latitude	0°22'S	0°22'S	0°22'S	0°22'S	0°22'S	0°22'S	0°22'S
SiO2	59.87	59.93	55.34	60.03	59.35	55.42	58.91
TiO2	0.81	0.78	0.99	0.79	0.81	0.95	0.81
Al2O3	16.92	16.84	16.77	17.03	17.12	17.03	17.07
Fe2O3	7.37	7.23	8.80	7.30	7.65	8.47	7.69
MnO	0.14	0.13	0.15	0.14	0.14	0.14	0.14
MgO	2.67	2.68	4.88	2.70	2.87	4.75	3.03
CaO	5.79	5.86	7.83	5.83	6.08	7.88	6.13
Na2O	3.32	3.54	3.26	3.58	3.50	3.22	3.66
K2O	2.60	2.51	1.95	2.46	2.34	1.92	2.34
P2O5	0.22	0.22	0.25	0.24	0.23	0.25	0.24
LOI	-0.13	-0.14	-0.28	-0.17	-0.27	0.15	-0.24
Total	99.58	99.58	99.94	99.93	99.82	100.18	99.78
Mg#	45.77	46.34	56.37	46.29	46.64	56.65	47.86
Rb	89	87	58	87	84	58	80
Ba	464	452	393	462	423	372	430
Sr	360	365	405	356	390	414	381
Pb			8				
Cs							
Zr	222	216	163	211	211	164	201
Hf							
Nb	6	6	11	6	7	11	5
Ta							
Y	35	33	28	33	35	30	35
Th			7				
La			20				
Ce			40				
Nd			22				
Sm							
Eu							
Tb							
Ho							
Yb							
Lu							
Cr	5	3	90	5	5	85	4
Ni	9	7	38	9	7	35	8
V	122	128	198	136	137	181	154
Sc	17	17	24	18	18	24	20
87Sr/86Sr			0.70446				
143Nd/144Nd			0.512782				
208Pb/204Pb			38.607				
207Pb/204Pb			15.602				
206Pb/204Pb			18.591				

Table C2 cont. Whole-rock analyses of Indonesian Quaternary volcanics

	Sumatra							
Catalogue #	75283	75284	75285	75288	75294	75295	75296	75297
Field #	SMG65B	SMG66	SMG67	SMG69	SMG72	SMG73	SMG74	SMG75
Volcano	Marapi	Marapi	Marapi	Tandikat	Tandikat	Singgalang	Close to Singgalang	Sirabungan
Longitude	100°28'E	100°27'E	100°27'E	100°20'E	100°16'E	100°17'E	100°18'E	100°14'E
Latitude	0°22'S	0°22'S	0°22'S	0°29'S	0°26'S	0°25'S	0°23'S	0°03'S
SiO2	59.22	55.14	58.25	58.21	59.06	56.72	59.21	56.39
TiO2	0.80	1.06	0.83	0.79	0.82	0.89	0.62	0.80
Al2O3	17.12	16.93	17.29	17.72	17.66	20.01	18.70	18.41
Fe2O3	7.55	8.60	7.71	7.56	7.22	6.60	5.82	7.51
MnO	0.14	0.15	0.14	0.15	0.14	0.13	0.16	0.14
MgO	2.92	5.06	3.25	3.18	2.82	2.11	2.50	3.52
CaO	6.16	8.09	6.43	7.07	6.45	8.06	5.17	7.50
Na2O	3.56	3.23	3.42	3.14	2.92	3.63	4.18	3.31
K2O	2.30	1.95	2.14	1.58	1.89	1.36	0.57	1.54
P2O5	0.22	0.26	0.22	0.20	0.20	0.22	0.22	0.23
LOI	-0.23	-0.33	-0.17	0.54	1.35	0.11	2.45	0.43
Total	99.76	100.14	99.51	100.14	100.53	99.84	99.60	99.78
Mg#	47.40	57.82	49.55	49.50	47.64	42.69	50.02	52.20
Rb	81	57	68	56	70	45	15	44
Ba	429	350	393	306	347	284	184	347
Sr	392	431	392	341	356	434	487	471
Pb								
Cs								
Zr	209	175	181	164	228	194	190	142
Hf								
Nb	7	14	8	4	6	6	4	6
Ta								
Y	36	30	30	28	39	39	29	51
Th								
La								
Ce								
Nd								
Sm								
Eu								
Tb								
Ho								
Yb								
Lu								
Cr	4	113	8	12	9	6	4	29
Ni	8	37	11	11	9	10	5	16
V	145	210	160	154	141	138	76	177
Sc	19	26	18	21	20	23	12	23
87Sr/86Sr								
143Nd/144Nd								
208Pb/204Pb								
207Pb/204Pb								
206Pb/204Pb								

Table C2 cont. Whole-rock analyses of Indonesian Quaternary volcanics

	Sumatra						
Catalogue #	75298	75299	75300	75301	75302	75305	75310
Field #	SMG76	SMG77	SMG78	SMG79	SMG80	SMG83	SMG88
Volcano	Batastinjaulaut	Close to Kumpulan	Close to Kumpulan	Close to Kumpulan	Sorik Marapi	Sorik Marapi	Bual Buali
Longitude	100°10'E	100°11'E	100°11'E	100°12'E	99°32'E	99°32'E	99°15'E
Latitude	0°04'S	0°04'S	0°04'S	0°04'S	0°40'N	0°41'N	1°34'N
SiO2	56.04	58.27	56.96	65.51	58.59	58.67	59.12
TiO2	0.77	0.75	0.64	0.49	0.68	0.68	0.77
Al2O3	17.79	18.20	16.41	16.03	17.76	17.11	16.86
Fe2O3	7.96	6.58	6.94	4.38	7.93	7.19	6.66
MnO	0.14	0.11	0.13	0.11	0.17	0.12	0.22
MgO	3.68	2.78	5.75	2.12	3.13	3.26	2.53
CaO	7.44	6.36	7.73	4.74	7.08	6.67	5.31
Na2O	3.26	3.76	3.34	3.82	3.20	3.09	3.62
K2O	1.63	1.80	1.61	2.70	1.64	1.94	2.21
P2O5	0.19	0.23	0.18	0.13	0.17	0.12	0.18
LOI	0.65	1.51	0.12	-0.11	0.02	0.67	2.62
Total	99.55	100.35	99.81	99.92	100.37	99.52	100.10
Mg#	51.86	49.61	65.87	53.00	47.91	51.37	46.95
Rb	49	57	55	86	55	67	74
Ba	348	435	455	578	304	349	400
Sr	455	480	393	348	347	342	281
Pb	10	9	10	16	10	8	10
Cs			1.91				
Zr	128	141	118	118	114	148	192
Hf			2.90				
Nb	5	5	5	7	3	4	6
Ta			1.47				
Y	36	24	18	18	26	31	31
Th			7.15		9	9	
La			20		16	21	
Ce			40.1		37	45	
Nd			18.6		19	21	
Sm			3.47				
Eu			0.93				
Tb			0.49				
Ho			0.72				
Yb			1.77				
Lu			0.23				
Cr	49	26	242	26	6	16	7
Ni	22	14	78	14	8	9	7
V	178	145	176	76	164	180	176
Sc	23	18	25	13	21	23	22
87Sr/86Sr			0.70512		0.70548		0.70702
143Nd/144Nd			0.512721		0.512573		0.512491
208Pb/204Pb			38.873		38.980		39.280
207Pb/204Pb			15.659		15.665		15.721
206Pb/204Pb			18.713		18.694		19.014

Table C2 cont. Whole-rock analyses of Indonesian Quaternary volcanics

	Sumatra							
Catalogue #	75311	75312	75313	75314	75315	75316	75317	75318
Field #	SMG89	SMG90	SMG91	SMG92	SMG93	SMG94	SMG95	SMG96
Volcano	Sibayak	Sibayak	Sibayak	Sinabung	Sinabung	Sinabung	Sinabung	Sinabung
Longitude	98°29'E	98°30'E	98°30'E	98°23'E	98°23'E	98°23'E	98°23'E	98°23'E
Latitude	3°15'N	3°15'N	3°15'N	3°10'N	3°10'N	3°10'N	3°10'N	3°10'N
SiO2	59.06	61.54	62.54	59.16	59.51	61.31	57.82	59.01
TiO2	0.61	0.60	0.59	0.65	0.66	0.70	0.69	0.64
Al2O3	17.41	16.90	16.54	17.64	17.71	14.53	17.69	17.43
Fe2O3	6.45	6.01	5.86	7.01	7.05	7.51	7.68	7.31
MnO	0.14	0.14	0.14	0.15	0.16	0.16	0.16	0.15
MgO	2.54	1.87	2.22	2.62	2.55	2.63	2.78	2.77
CaO	5.79	5.02	5.43	7.16	7.21	5.20	7.68	7.13
Na2O	2.91	2.77	2.94	3.09	3.03	2.65	2.89	3.23
K2O	2.24	2.65	2.75	1.83	1.98	2.13	1.79	1.84
P2O5	0.19	0.16	0.17	0.18	0.16	0.16	0.14	0.15
LOI	2.32	1.82	0.86	0.30	0.25	3.21	0.33	0.35
Total	99.66	99.48	100.04	99.79	100.27	100.19	99.65	100.01
Mg#	47.85	42.03	46.88	46.55	45.73	44.93	45.75	46.89
Rb	88	97	95	72	76	75	70	68
Ba	629	678	651	446	456	455	418	451
Sr	446	411	411	346	351	359	363	336
Pb								32
Cs								
Zr	135	146	133	140	146	145	143	139
Hf								
Nb	9	10	10	7	7	7	7	7
Ta								
Y	28	24	22	24	25	20	28	28
Th								9
La								24
Ce								54
Nd								23
Sm								
Eu								
Tb								
Ho								
Yb								
Lu								
Cr	11	5	5	5	5	5	5	4
Ni	9	5	6	8	7	6	8	7
V	138	114	93	161	150	152	167	158
Sc	18	16	15	16	17	20	20	18
87Sr/86Sr								0.70983
143Nd/144Nd								0.512230
208Pb/204Pb								39.545
207Pb/204Pb								15.774
206Pb/204Pb								18.861

Table C2 cont. Whole-rock analyses of Indonesian Quaternary volcanics

	Sumatra							
Catalogue #	75320	75321	75322	75323	75324	75325	75326	75327
Field #	SMG98	SMG99	SMG100	SMG101	SMG102	SMG103	SMG104	SMG105
Volcano	Sinabung	Sibayak	Sibayak	Sibayak	Sibayak	Close to Takengon	Close to Takengon	Close to Takengon
Longitude	98°23'E	98°28'E	98°28'E	98°29'E	98°29'E	96°47'E	96°47'E	96°47'E
Latitude	3°10'N	3°12'N	3°12'N	3°11'N	3°11'N	4°36'N	4°36'N	4°36'N
SiO2	59.42	60.89	61.76	57.08	60.67	62.41	62.65	62.46
TiO2	0.66	0.52	0.58	0.81	0.70	0.41	0.46	0.44
Al2O3	17.53	17.61	16.37	17.85	17.18	16.93	16.88	17.12
Fe2O3	7.18	5.39	5.92	7.64	6.69	5.11	5.50	5.35
MnO	0.16	0.13	0.13	0.16	0.14	0.14	0.15	0.14
MgO	2.54	2.07	2.25	2.94	2.46	1.72	1.85	1.93
CaO	7.00	3.13	5.54	7.38	6.35	5.55	5.89	5.98
Na2O	3.12	2.76	3.11	2.87	2.98	3.54	3.77	3.74
K2O	2.00	2.88	2.67	1.98	2.37	2.30	2.28	2.18
P2O5	0.17	0.19	0.17	0.18	0.16	0.18	0.21	0.14
LOI	0.27	4.53	1.13	0.95	0.26	1.63	0.44	0.20
Total	100.05	100.10	99.63	99.84	99.96	99.92	100.08	99.68
Mg#	45.18	47.22	46.96	47.27	46.14	43.95	43.94	45.67
Rb	73	103	102	71	87	76	71	69
Ba	455	687	612	538	596	670	671	677
Sr	345	268	418	424	383	535	567	553
Pb				17	26			
Cs					1.38			
Zr	144	158	139	178	184	109	99	101
Hf					4.15			
Nb	7	10	9	8	9	3	4	5
Ta					0.57			
Y	23	17	23	31	31	17	19	16
Th				9	9.89			
La				31	28.1			
Ce				62	60.4			
Nd				28	29.1			
Sm					5.23			
Eu					1.3			
Tb					0.84			
Ho					1.09			
Yb					2.72			
Lu					0.36			
Cr	4	3	7	7	4	8	5	6
Ni	8	6	8	8	6	6	6	7
V	147	105	120	172	141	93	98	96
Sc	17	11	15	20	17	11	13	12
87Sr/86Sr					0.71162			
143Nd/144Nd					0.512173			
208Pb/204Pb					39.539			
207Pb/204Pb					15.761			
206Pb/204Pb					18.882			

Table C2 cont. Whole-rock analyses of Indonesian Quaternary volcanics

	Sumatra							
Catalogue #	75328	75329	75330	75331	75332	75333	75334	75335
Field #	SMG106	SMG107	SMG108	SMG109	SMG110	SMG111	SMG112	SMG113
Volcano	Close to Takengon	Geureudong	Geureudong	Geureudong	Close to Bireuen	Close to Sare	Seulemium	Seulemium
Longitude	96°47'E	96°46'E	96°48'E	96°48'E	96°44'E	95°48'E	95°41'E	95°41'E
Latitude	4°36'N	4°44'N	4°45'N	4°45'N	4°57'N	5°23'N	5°22'N	5°22'N
SiO2	62.34	62.06	63.29	57.06	61.95	53.87	50.93	52.37
TiO2	0.45	0.44	0.41	0.71	0.46	0.80	0.72	0.77
Al2O3	17.15	17.16	16.75	17.69	16.98	17.41	16.30	19.06
Fe2O3	5.34	5.42	5.01	7.39	5.59	7.78	8.68	8.69
MnO	0.13	0.14	0.14	0.12	0.14	0.14	0.16	0.17
MgO	1.55	1.96	1.72	3.26	2.06	6.18	7.28	4.34
CaO	5.50	6.05	5.41	7.66	6.00	9.41	11.35	9.93
Na2O	3.72	3.71	3.80	3.36	3.72	2.90	2.36	2.92
K2O	2.45	2.04	2.13	1.77	2.13	1.03	0.60	0.89
P2O5	0.19	0.20	0.21	0.18	0.21	0.12	0.07	0.10
LOI	1.04	0.38	1.34	0.86	0.43	0.50	1.25	0.52
Total	99.86	99.56	100.21	100.06	99.67	100.14	99.70	99.76
Mg#	40.34	45.73	44.44	50.68	46.20	64.92	66.15	53.78
Rb	72	69	73	63	72	15	13	28
Ba	713	656	670	485	675	215	185	194
Sr	584	590	554	465	586	478	290	319
Pb		12	11	10	12	7		7
Cs					2.66	0.31		
Zr	113	107	111	120	110	53	69	75
Hf					2.56	1.37		
Nb	5	4	5	5	4	2	2	2
Ta					0.51	0.19		
Y	20	18	18	24	18	20	19	20
Th		10	12	8	11	3		2
La		24	28	23	20.5	6.88		7
Ce		48	51	44	43.4	15.6		16
Nd		21	22	19	19.4	10.3		11
Sm					3.59	2.73		
Eu					1	0.79		
Tb					0.54	0.45		
Ho					0.7	0.59		
Yb					1.82	1.34		
Lu					0.27	0.19		
Cr	6	5	9	20	6	173	241	16
Ni	6	5	7	14	5	66	45	16
V	99	101	88	216	103	305	271	253
Sc	13	12	11	24	13	39	53	30
87Sr/86Sr					0.70492	0.70398		0.70506
143Nd/144Nd					0.512614	0.512779		0.512722
208Pb/204Pb					38.820	38.581		39.146
207Pb/204Pb					15.634	15.600		15.696
206Pb/204Pb					18.658	18.396		18.750

Table C2 cont. Whole-rock analyses of Indonesian Quaternary volcanics

	Sumatra							
Catalogue #	75336	75337	75338	75339	75340	75341	75342	75343
Field #	SMG114	SMG115	SMG116	SMG117	SMG118	SMG119	SMG120	SMG121
Volcano	Seulemium	Seulemium	Seulemium	Seulemium	Seulemium	Seulemium	Seulemium	Weh Island
Longitude	95°41'E	95°41'E	95°41'E	95°41'E	95°41'E	95°41'E	95°41'E	95°18'E
Latitude	5°22'N	5°22'N	5°22'N	5°22'N	5°22'N	5°22'N	5°22'N	5°47'N
SiO2	52.10	55.17	59.73	50.36	52.36	60.46	57.64	62.85
TiO2	0.79	0.83	0.58	0.82	0.80	0.60	0.66	0.58
Al2O3	19.28	18.72	17.28	19.37	18.76	16.61	17.91	16.68
Fe2O3	8.88	7.23	6.20	9.11	8.89	6.21	7.53	5.80
MnO	0.17	0.15	0.15	0.17	0.19	0.14	0.17	0.11
MgO	4.53	3.26	2.53	4.91	4.49	2.45	2.87	2.41
CaO	10.20	7.61	6.48	9.34	9.07	6.23	6.76	5.71
Na2O	2.64	3.71	3.56	2.64	2.92	3.42	4.04	3.08
K2O	0.88	1.20	1.63	0.81	0.95	1.72	1.44	2.48
P2O5	0.11	0.14	0.12	0.14	0.12	0.11	0.30	0.11
LOI	0.76	1.85	1.62	1.86	0.85	1.56	0.51	0.46
Total	100.34	99.87	99.88	99.53	99.40	99.51	99.83	100.27
Mg#	54.31	51.23	48.74	55.67	54.06	47.89	47.03	49.19
Rb	25	22	44	24	28	54	31	134
Ba	189	509	373	221	233	380	320	300
Sr	320	365	329	295	323	286	378	240
Pb				6	7	12	12	19
Cs							0.81	
Zr	72	124	134	67	73	134	141	113
Hf							3.03	
Nb	1	4	3	1	2	2	4	3
Ta							0.33	
Y	20	20	19	20	22	20	30	22
Th				3	3	6	2.42	11
La				8	8	15	14.7	26
Ce				18	22	28	33	46
Nd				11	12	13	18.8	23
Sm							4.41	
Eu							1.26	
Tb							0.76	
Ho							1.02	
Yb							2.8	
Lu							0.38	
Cr	20	20	32	21	9	6	5	6
Ni	21	13	11	20	15	8	9	8
V	257	164	140	288	268	152	144	142
Sc	32	29	20	34	31	19	19	20
87Sr/86Sr							0.70516	0.70776
143Nd/144Nd							0.512743	0.512269
208Pb/204Pb							38.944	39.535
207Pb/204Pb							15.674	15.756
206Pb/204Pb							18.639	18.970

Table C2 cont. Whole-rock analyses of Indonesian Quaternary volcanics

	Sumatra							
Catalogue #	75344	75345	75346	75347	75348	75349	75350	75351
Field #	SMG122	SMG123	SMG124	SMG124B	SMG125	SMG126	SMG127	SMG128
Volcano	Weh Island	Weh Island	Weh Island	Weh Island	Weh Island	Weh Island	Weh Island	Weh Island
Longitude	95°18'E	95°19'E	95°18'E	95°19'E	95°18'E	95°18'E	95°18'E	95°18'E
Latitude	5°47'N	5°48'N	5°50'N	5°48'N	5°46'N	5°46'N	5°46'N	5°46'N
SiO2	61.99	62.64	56.75	57.00	63.10	64.19	64.95	63.84
TiO2	0.58	0.54	0.68	0.63	0.52	0.53	0.51	0.54
Al2O3	16.40	16.54	18.09	17.87	16.38	16.14	16.18	15.69
Fe2O3	5.55	5.41	7.59	7.26	5.42	5.38	4.51	5.11
MnO	0.11	0.12	0.15	0.16	0.11	0.10	0.09	0.10
MgO	2.27	2.17	3.54	3.47	2.22	2.06	1.21	1.39
CaO	5.57	5.64	7.64	7.48	5.42	5.35	5.52	5.57
Na2O	2.98	3.05	3.02	3.46	3.10	2.82	3.08	3.01
K2O	2.49	2.48	1.60	1.44	2.13	2.25	2.58	2.53
P2O5	0.12	0.13	0.13	0.14	0.16	0.13	0.17	0.10
LOI	1.69	0.78	1.06	0.77	1.79	1.23	1.05	1.51
Total	99.75	99.50	100.25	99.68	100.35	100.18	99.85	99.39
Mg#	48.79	48.31	52.08	52.69	48.83	47.15	38.46	38.79
Rb	128	129	80	73	165	108	150	179
Ba	285	278	187	177	296	301	275	294
Sr	229	235	285	295	245	244	236	231
Pb			16				20	17
Cs								
Zr	112	117	85	91	120	111	117	104
Hf								
Nb	2	2	3	3	4	4	3	2
Ta								
Y	19	19	22	21	17	18	16	22
Th			8				11	10
La			14				21	22
Ce			28				45	42
Nd			15				19	19
Sm								
Eu								
Tb								
Ho								
Yb								
Lu								
Cr	10	9	5	9	13	9	10	7
Ni	9	7	12	14	9	8	8	8
V	161	123	221	185	144	118	139	142
Sc	19	15	23	21	16	16	17	19
87Sr/86Sr			0.70664					
143Nd/144Nd			0.512463					
208Pb/204Pb			39.526					
207Pb/204Pb			15.751					
206Pb/204Pb			18.974					

Table C2 cont. Whole-rock analyses of Indonesian Quaternary volcanics

	Sumatra							
Catalogue #	75352	75353	75380	75381	75382	75383	75384	75385
Field #	SMG129	SMG130	SMG154	SMG155	SMG156	SMG157	SMG158	SMG159
Volcano	Weh Island	Weh Island	Kaba	Kaba	Kaba	Kaba	Kaba	Kaba
Longitude	95°15'E	95°15'E	102°37'E	102°37'E	102°37'E	102°37'E	102°37'E	102°37'E
Latitude	5°49'N	5°49'N	3°31'S	3°31'S	3°31'S	3°31'S	3°31'S	3°31'S
SiO2	61.20	62.50	63.03	63.21	62.97	62.52	56.90	56.58
TiO2	0.54	0.56	0.87	0.86	0.89	0.88	0.97	0.97
Al2O3	16.96	16.79	16.11	16.14	16.22	16.14	17.36	17.22
Fe2O3	5.87	5.54	5.70	5.68	5.89	5.79	8.12	8.18
MnO	0.12	0.10	0.12	0.12	0.12	0.12	0.15	0.14
MgO	2.43	1.74	1.87	1.89	2.10	2.02	4.04	4.15
CaO	5.70	4.70	4.35	4.24	4.70	4.37	7.23	7.27
Na2O	2.89	3.44	4.05	4.19	4.15	4.10	3.42	3.47
K2O	2.21	2.36	2.75	2.69	2.70	2.75	1.67	1.70
P2O5	0.13	0.11	0.25	0.27	0.24	0.25	0.26	0.30
LOI	1.64	1.83	0.39	0.37	0.15	0.42	-0.28	-0.29
Total	99.69	99.67	99.49	99.66	100.13	99.36	99.84	99.69
Mg#	49.10	42.25	43.32	43.67	45.38	44.84	53.69	54.17
Rb	110	129	108	116	112	112	65	61
Ba	258	307	434	434	415	438	287	289
Sr	240	221	285	295	209	305	417	391
Pb							12	
Cs				4.28				
Zr	117	131	284	295	283	290	179	174
Hf				6.94				
Nb	3	2	7	9	8	8	6	5
Ta				0.93				
Y	21	56	33	27	35	37	28	25
Th				13.05			7	
La				18.5			21	
Ce				42.6			47	
Nd				20.8			25	
Sm				4.97				
Eu				1.52				
Tb				0.84				
Ho				1.12				
Yb				2.78				
Lu				0.4				
Cr	8	6	10	11	12	9	43	41
Ni	8	9	9	9	8	7	28	28
V	136	128	114	110	109	112	188	193
Sc	16	17	19	19	20	20	26	26
87Sr/86Sr				0.70486			0.70473	
143Nd/144Nd				0.512643			0.512643	
208Pb/204Pb				39.058			39.052	
207Pb/204Pb				15.681			15.682	
206Pb/204Pb				18.712			18.703	

	Sumatra	
Catalogue #	75386	75387
Field #	SMG160	SMG160A
Volcano	Kaba	Kaba
Longitude	102°37'E	102°37'E
Latitude	3°31'S	3°31'S
SiO2	62.75	58.56
TiO2	1.17	0.94
Al2O3	15.35	16.85
Fe2O3	7.05	7.32
MnO	0.16	0.13
MgO	1.54	3.52
CaO	4.04	6.51
Na2O	4.40	3.79
K2O	3.18	2.08
P2O5	0.42	0.26
LOI	-0.20	-0.20
Total	99.86	99.76
Mg#	33.73	52.84
Rb	133	83
Ba	485	337
Sr	317	393
Pb	22	13
Cs		
Zr	340	218
Hf		
Nb	10	5
Ta		
Y	50	30
Th	16	11
La	38	25
Ce	88	55
Nd	48	27
Sm		
Eu		
Tb		
Ho		
Yb		
Lu		
Cr	1	27
Ni	5	20
V	53	160
Sc	23	23
87Sr/86Sr		
143Nd/144Nd		
208Pb/204Pb		
207Pb/204Pb		
206Pb/204Pb		

Table C3. Whole-rock analyses of Sumatran pre-Pliocene volcanics

Catalogue #	75243	75244	75245	75390	75392	75393
Field #	SMG28A	SMG28B	SMG29	BA1	BA8	BA9
Locality	Close to Muaradua	Close to Muaradua	Close to Baturaja	Southwest of Banda Aceh	Southwest of Banda Aceh	Southwest of Banda Aceh
Formation	Basalt complex	Basalt complex	Basalt complex	Bentaro Fm.	Bentaro Fm.	Bentaro Fm.
Age	Trias-Jura?	Trias-Jura?	Trias-Jura?	Jura-Creta	Jura-Creta	Jura-Creta
Longitude	104°09'E	104°09'E	104°11'E	95°15'E	95°19'E	95°19'E
Latitude	4°31'S	4°31'S	4°30'S	5°20'N	5°13'N	5°11'N
SiO2	49.46	49.00	51.88	50.52	51.22	53.47
TiO2	0.90	0.61	0.65	0.89	0.98	0.66
Al2O3	16.44	14.88	15.73	14.01	14.76	17.32
Fe2O3	8.79	8.99	9.11	10.62	11.54	7.12
MnO	0.17	0.17	0.19	0.17	0.17	0.15
MgO	7.75	9.34	8.06	6.60	4.66	3.85
CaO	11.35	11.85	11.09	9.45	8.77	5.82
Na2O	2.67	1.98	1.71	4.39	3.86	4.09
K2O	0.70	0.80	0.13	0.74	1.19	1.31
P2O5	0.22	0.10	0.17	0.22	0.27	0.25
LOI	1.36	1.91	1.70	2.60	2.33	6.26
Total	99.81	99.63	100.42	100.21	99.75	100.30
Mg#	67.26	70.76	67.33	59.15	48.48	55.75
Rb	15	18	3	7	18	
Ba	72	54	40	128	147	264
Sr	402	382	169	446	683	
Pb		4	2	3		
Cs						
Zr	90	62	62	60	61	
Hf						
Nb	5	1	1	3	3	
Ta						
Y	22	17	18	19	25	
Th			2	1		
La			9	6		
Ce			18	23		
Nd			10	15		
Sm						
Eu						
Tb						
Ho						
Yb						
Lu						
Cr	315	430	255	140	75	3
Ni	93	138	87	49	42	7
V	262	276	312	311	302	179
Sc	43	50	46	37	31	18
87Sr/86Sr		0.70389				
143Nd/144Nd		0.512921				
208Pb/204Pb		38.291				
207Pb/204Pb		15.539				
206Pb/204Pb		18.447				

Table C3 cont. Whole-rock analyses of Sumatran pre-Pliocene volcanics

Catalogue #	75394	75395	75396	75397	75399	75400
Field #	BA10	BA12	BA16	BA20	BA23	BA24
Volcano	Southwest of Banda Aceh	Southwest of Banda Aceh	Southwest of Banda Aceh	North of Calang	North of Calang	North of Calang
Formation	Bentaro Fm.	Bentaro Fm.	Bentaro Fm.	Calang Fm.	Calang Fm.	Calang Fm.
Age	Jura-Creta	Jura-Creta	Jura-Creta	Middle Miocene	Middle Miocene	Middle Miocene
Longitude	95°18'E	95°18'E	95°18'E	95°20'E	95°24'E	95°24'E
Latitude	5°04'N	5°07'N	5°09'N	5°03'N	4°56'N	4°56'N
SiO2	48.37	48.19	54.41	46.93	52.23	48.04
TiO2	1.09	1.12	0.75	0.83	0.92	1.53
Al2O3	15.05	19.50	18.00	13.18	19.13	17.22
Fe2O3	10.84	10.77	7.89	11.98	7.88	12.84
MnO	0.15	0.20	0.15	0.19	0.26	0.22
MgO	6.20	4.28	1.95	5.69	3.26	6.06
CaO	9.73	7.29	6.69	13.40	8.35	10.11
Na2O	3.78	3.37	5.74	2.85	3.41	3.03
K2O	0.45	2.26	0.94	1.45	0.52	0.69
P2O5	0.26	0.35	0.39	0.37	0.25	0.89
LOI	3.57	2.48	2.69	3.12	3.66	-0.14
Total	99.49	99.81	99.60	99.99	99.87	100.49
Mg#	57.13	48.08	36.54	52.53	49.08	52.37
Rb	6	43		19	13	18
Ba	108	435	164	62	163	213
Sr	389	808		352	424	388
Pb						4
Cs						0.57
Zr	85	54		52	103	84
Hf						2.29
Nb	4	4		1	4	2
Ta						0.41
Y	23	21		19	27	33
Th						1.93
La						14.6
Ce						35.2
Nd						21.9
Sm						6.09
Eu						1.63
Tb						1.09
Ho						1.24
Yb						2.73
Lu						0.36
Cr	126	5	32	169	9	88
Ni	48	18	17	40	10	41
V	364	364	163	300	231	418
Sc	32	28	18	36	27	35
87Sr/86Sr						0.70412
143Nd/144Nd						0.512835
208Pb/204Pb						38.614
207Pb/204Pb						15.608
206Pb/204Pb						18.458

Table C3 cont. Whole-rock analyses of Sumatran pre-Pliocene volcanics

Catalogue #	75401	75404	75405	75406	75407	75408
Field #	BA27	BA32	BA32B	BA33A	BA35A	BA35B
Volcano	Close to Calang	Close to Calang	Close to Calang	Close to Calang	Calang	Calang
Formation	Tangla Fm.	Unknown	Unknown	Unknown	Calang Fm.	Calang Fm.
Age	Early Miocene	Unknown	Unknown	Unknown	Middle Miocene	Middle Miocene
Longitude	95°25'E	95°45'E	95°45'E	95°45'E	95°34'E	95°34'E
Latitude	4°52'N	4°43'N	4°43'N	4°43'N	4°38'N	4°38'N
SiO2	59.17	56.52	52.80	51.73	56.95	57.64
TiO2	0.43	0.96	1.27	1.13	0.45	0.46
Al2O3	18.10	18.20	17.98	17.50	18.37	19.14
Fe2O3	5.81	6.22	8.21	10.19	5.68	6.13
MnO	0.23	0.10	0.16	0.19	0.12	0.15
MgO	1.56	1.88	2.81	4.20	3.17	3.42
CaO	5.42	5.71	7.45	8.06	7.13	7.04
Na2O	4.83	4.23	3.65	4.06	3.63	3.69
K2O	1.33	3.08	2.67	0.94	0.90	0.97
P2O5	0.36	0.45	0.93	0.34	0.19	0.15
LOI	2.30	2.13	1.92	1.50	3.77	1.20
Total	99.54	99.48	99.85	99.84	100.36	99.99
Mg#	38.48	41.32	44.36	48.99	56.53	56.52
Rb	29	101	104	21	14	17
Ba	456	520	515	315	300	298
Sr	634	580	564	633	502	528
Pb			15		5	
Cs						
Zr	114	251	395	113	76	72
Hf						
Nb	3	12	21	6	3	1
Ta						
Y	26	35	49	29	18	17
Th			12		1	
La					12	
Ce					29	
Nd					15	
Sm						
Eu						
Tb						
Ho						
Yb						
Lu						
Cr	2	13	38	10	25	20
Ni	3	14	25	20	23	17
V	46	124	149	271	99	107
Sc	8	15	19	32	15	16
87Sr/86Sr				0.70435		
143Nd/144Nd				0.512838		
208Pb/204Pb				38.299		
207Pb/204Pb				15.562		
206Pb/204Pb				18.329		

Appendix D

List of samples of volcanic and sedimentary rocks from the Northeastern Indian Ocean

The lithologic visual descriptions (e.g. basalt, clay) are simplified from the Initial Reports of the Deep Sea Drilling Project vol. 22 and 27 (1974), and do not necessarily correspond with the actual chemical composition. Descriptions of the non-DSDP/ODP samples are from ben Othman et al. (1989), Engel et al. (1965) and from cruise logs. Ages of volcanic rocks are based on the stratigraphic age of overlying sediments, magnetic anomalies, and analogy with nearby sites (Duncan 1991; Royer et al. 1991; Sager et al. 1992), except for the dolerite sill at site 211 (K/Ar dating of the sill - McDougall 1974) and Unit B at site 261 (minimum age deduced from the age of alteration material - Hart & Staudigel 1986). The ages reported for the Vema and DODO samples are the ages of the surrounding basement and are maximum ages only. Description of sites and depth in the column are from Initial Reports of the Deep Sea Drilling Project vol. 22 and 27 (1974), ben Othman et al. (1989), and cruise logs.

Table D. List of samples from the Northeastern Indian Ocean

Site	22 211			
Location	9° 46.53'S			
	102° 41.95'E			
Water depth	5535 m			
Total penetration	447 m			
Total length of cored section	142.5 m			
Total core recovered	67.21 m (47.2%)			
Acoustic basement:				
Depth	429 m			
Nature	Basalt			
Age of oldest sediment	Lower Campanian (83-65 Ma)			
Basement	Basalt			
Samples:				
DSDP 22 211/12-1:23-25	Volcanic	Diabase sill	409.2 m	71 my (K-Ar on biotite)
DSDP 22 211/12-1:125-127	Volcanic	Diabase sill	410.3 m	71 my (K-Ar on biotite)
DSDP 22 211/12-2:16-18	Volcanic	Diabase sill	410.7 m	71 my (K-Ar on biotite)
DSDP 22 211/12-2:112-115	Volcanic	Diabase sill	411.6 m	71 my (K-Ar on biotite)
DSDP 22 211/13-1:10-12	Sediment	Nanno ooze	418.1 m	Lower to Middle Campanian
DSDP 22 211/15-3:57-59	Volcanic	Basalt (Weathered amphibole-bearing basalt)	441.1 m	> 71 Ma
DSDP 22 211/15-4:70-73	Volcanic	Basalt (Weathered amphibole-bearing basalt)	442.7 m	> 71 Ma
DSDP 22 211/15-4:73-75	Volcanic	Basalt (Weathered amphibole-bearing basalt)	442.7 m	> 71 Ma
DSDP 22 211/15-4:94-96	Volcanic	Basalt (Weathered amphibole-bearing basalt)	443 m	> 71 Ma
Site	22 212			
Location	19° 11.34'S			
	99° 17.84'E			
Water depth	6240 m			
Total penetration	521 m			
Total length of cored section	366 m			
Total core recovered	174.3 m (47.6%)			
Acoustic basement:				
Depth	516 m			
Nature	Basalt			
Age of oldest sediment	Upper Cretaceous (95-65 Ma)			
Basement	Basalt			
Samples:				
DSDP 22 212/39-2:60-62	Volcanic	Basalt (glass)	518.1 m	> 95-65 Ma
DSDP 22 212/39-3:145-147	Volcanic	Basalt	520.5 m	> 95-65 Ma
Site	22 213			
Location	10° 12.71'S			
	93° 53.77'E			
Water depth	5611 m			
Total penetration	172.5 m			
Total length of cored section	172.5 m			
Total core recovered	145.5 m (84%)			
Acoustic basement:				
Depth	154.0 m			
Nature	Basalt			
Age of oldest sediment	Upper Paleocene (59-53 Ma)			
Basement	Basalt			
Samples:				
DSDP 22 213/1-3:30-32	Sediment	Rad diatom ooze	3.3 m	Quaternary
DSDP 22 213/1-4:67-69	Sediment	Rad diatom ooze	5.2 m	Quaternary
DSDP 22 213/7-2:88-90	Sediment	Clay rad rich diatom ooze /ash bearing clay rad rich diatom ooze	58.9 m	Upper Miocene
DSDP 22 213/7-5:71-73	Sediment	Clay rad rich diatom ooze /ash bearing clay rad rich diatom ooze	63.2 m	Upper Miocene

DSDP Site 213 (cont.)

DSDP 22 213/10-2:60-62	Sediment	Mn zeolite bearing clay	87.1 m	Middle Miocene
DSDP 22 213/13-4:91-93	Sediment	Mn-Fe oxides and zeolite rich clay	118.9 m	Middle Eocene
DSDP 22 213/16-2:57-59	Sediment	Nanno ooze	144.1 m	Upper Paleocene
DSDP 22 213/17-2:1-3	Volcanic	Basalt (glass)	153.0 m	> 59-53 Ma
DSDP 22 213/18-2:50-53	Volcanic	Basalt (glass)	161.5 m	> 59-53 Ma
DSDP 22 213/18-2:115-117	Volcanic	Basalt	162.2 m	> 59-53 Ma
DSDP 22 213/18-3:36-37	Volcanic	Basalt (glass)	162.8 m	> 59-53 Ma

Site	27 260
Location	16° 8.67'S
	110° 17.92'E
Water depth	5702 m
Total penetration	331 m
Total length of cored section	169.5 m
Total core recovered	56.7 m (33.5%)
Acoustic basement:	
Depth	322.4 m
Nature	Basalt
Age of oldest sediment	Albian (107-95 Ma)
Basement	Basalt
Samples:	

DSDP 27 260/18-2:140-142	Volcanic	Basalt	322.4 m	131 Ma
DSDP 27 260/20-1:16-18	Volcanic	Basalt	329.2 m	131 Ma

Site	27 261
Location	12° 56.83'S
	117° 53.56'E
Water depth	5667 m
Total penetration	579.5 m
Total length of cored section	342 m
Total core recovered	125.8 m (36.78%)
Acoustic basement:	
Depth	532.2 m
Nature	Basalt
Age of oldest sediment	Berriasian (135-128)
Basement	Basalt
Samples:	

DSDP 27 261/2-2:33-38	Sediment	Rad rich clay	11.4 m	Quaternary
DSDP 27 261/3-2:25-27	Sediment	Nanno ooze	49.3 m	Lower Pliocene
DSDP 27 261/4-1:99-101	Sediment	Nanno ooze	96 m	Upper Miocene
DSDP 27 261/6-2:25-27	Sediment	Clay	172.8 m	Coniacian
DSDP 27 261/8-5:20-22	Sediment	Clay	196.2 m	Coniacian
DSDP 27 261/14-1:75-77	Sediment	Claystone	247.7 m	Upper Aptian to Lower Albian
DSDP 27 261/22-5:21-24	Sediment	Claystone (semi lithified)	348.2 m	Aptian
DSDP 27 261/25-3:29-31	Sediment	Claystone	402.3 m	Aptian
DSDP 27 261/29-2:29-31	Sediment	Claystone (semi lithified)	467.3 m	Valanginian
DSDP 27 261/31-4:26-28	Sediment	Claystone	508.3 m	Valanginian
DSDP 27 261/32-2:58-61	Sediment	Claystone	524.6 m	Valanginian
DSDP 27 261/33cc 6-8	Volcanic	Basalt (Unit A)	533.7 m	159 Ma
DSDP 27 261/34-1:75-77	Volcanic	Basalt (Unit A)	534.8 m	159 Ma
DSDP 27 261/34-2:100-102	Volcanic	Basalt (Unit A)	536.5 m	159 Ma
DSDP 27 261/35-2:83-86	Volcanic	Basalt (Unit A)	543.9 m	159 Ma
DSDP 27 261/35-2:120-123	Volcanic	Basalt (Unit A)	544.2 m	159 Ma
DSDP 27 261/35-3:124-126	Volcanic	Basalt (Unit B)	545.7 m	>> 121 Ma
DSDP 27 261/35-4:102-105	Volcanic	Basalt (Unit B)	547 m	>> 121 Ma
DSDP 27 261/39-1:11-13	Volcanic	Basalt (Unit C)	570.1 m	159 Ma
DSDP 27 261/39-1:44-48	Volcanic	Basalt (Unit C)	570.5 m	159 Ma

Table D cont. List of samples from the Northeastern Indian Ocean

Dredged/short-cored samples

Sample name	Location		Nature	Lithology	Water depth	Depth in core	Age
V 28-341 115-118	9° 06'S	130° 13'E	Sediment	Biogenic	750 m	1.2 m	Quaternary?
RC 14-67 103-107	9 ° 28'S	122° 21'E	Sediment	Volcanogenic	3230 m	1 m	Quaternary?
V 28-343 63-67	12° 19'S	118° 18'E	Sediment	Clay Pelagic	5404 m	0.7 m	Quaternary?
V 28-343 325-326.5	12° 19'S	118° 18'E	Sediment	Clay Diatom	5404 m	3.3 m	Quaternary?
V 28-343 564-566	12° 19'S	118° 18'E	Sediment	Clay	5404 m	5.7 m	Quaternary?
V 28-343 750-751.5	12° 19'S	118° 18'E	Sediment	Clay	5404 m	7.5 m	Quaternary?
V 28-343 1050-1051.5	12° 19'S	118° 18'E	Sediment	Clay/Volcanic	5404 m	10.5 m	Quaternary?
V 28-343 1142-1143.5	12° 19'S	118° 18'E	Sediment	Clay	5404 m	11.4 m	Quaternary?
V 33-75 316-318	8° 25'S	107° 11'E	Sediment	Terrigenous/Biogenic	3396 m	3.2 m	Quaternary?
V 33-77 382-384	8° 07'S	106° 43'E	Sediment	Terrigenous/Biogenic	3014 m	3.8 m	Quaternary?
V 33-79 17-19	7° 54'S	106° 24'E	Sediment	Terrigenous	3000 m	0.2 m	Quaternary?
V 34-45 35-37	10° 23'S	94° 00'E	Sediment	Clay Pelagic	5577 m	0.4 m	Quaternary?
V 34-47 143-145.5	6° 06'S	90° 37'E	Sediment	Terrigenous	5288 m	1.5 m	Quaternary?
DODO 232E	5° 23'S	97° 29'E	Volcanic	Basalt	3558-4119 m	dredge	55 Ma?
DODO 232G "fresh"	5° 23'S	97° 29'E	Volcanic	Basalt	3558-4119 m	dredge	55 Ma?
DODO 232G alt.	5° 23'S	97° 29'E	Volcanic	Basalt	3558-4119 m	dredge	55 Ma?
DODO 232J	5° 23'S	97° 29'E	Volcanic	Basalt	3558-4119 m	dredge	55 Ma?
DODO 232K	5° 23'S	97° 29'E	Volcanic	Basalt	3558-4119 m	dredge	55 Ma?
DODO 232N	5° 23'S	97° 29'E	Volcanic	Basalt	3558-4119 m	dredge	55 Ma?
V 28 14A	11° 50'S	96° 58'E	Volcanic	Basalt	3506-2288 m	dredge	63 Ma?
V 28 14B	11° 50'S	96° 58'E	Volcanic	Basalt	3506-2288 m	dredge	63 Ma?
VM 28 RD 14-1	11° 50'S	96° 58'E	Volcanic	Basalt	3506-2288 m	dredge	63 Ma?
VM 28 RD 14-2	11° 50'S	96° 58'E	Volcanic	Basalt	3506-2288 m	dredge	63 Ma?
VM 28 RD 14-3	11° 50'S	96° 58'E	Volcanic	Basalt	3506-2288 m	dredge	63 Ma?
VM 28 RD 14-4 "fresh"	11° 50'S	96° 58'E	Volcanic	Basalt	3506-2288 m	dredge	63 Ma?
VM 28 RD 14-4 alt.	11° 50'S	96° 58'E	Volcanic	Basalt	3506-2288 m	dredge	63 Ma?
VM 28 RD 14-2 sediment	11° 50'S	96° 58'E	Sediment	Sediment	3506-2288 m	dredge	Quaternary?

Appendix E

Description of DSDP and ODP sites and dredge hauls in the Northeastern Indian Ocean

Site 22 211

The percentage of recovery for this site was rather low (47.2%) and the lithology of the sediments is very variable, ranging from Quaternary radiolarian- and diatom-rich oozes and ashes, to Pliocene sands, oozes, clays and silts, to Maastrichtian and Campanian nanno-rich clays and oozes and iron-rich ash (altered volcanic glass), which lie between a dolerite sill and basalt considered to be the upper part of the oceanic basement.

Including the new analyses reported in this thesis, twenty-one analyses come from this site, eight of which are from the dolerite sill, three from the sediments below the sill and ten from the basaltic basement. Also available is an average of thirty-three sediments and the average composition of trace elements in the clays.

The data available can therefore be regarded as representative of the different volcanic units and of the sedimentary units between them, but the composition of the sedimentary column is to be considered as largely unknown, both because of the paucity of data and because of the low percentage of recovery.

Three different volcanic units were recognised at this site. The upper unit is a dolerite sill, about 10 m thick, ophitic to subophitic in texture, with phenocrysts of plagioclase (40%), plum-coloured augite (20%), and phyllosilicates (serpentine, vermiculite and chlorite), with rare opaques and pyrite, biotite and amphibole. Early to Middle Campanian sediments were found at the base of the sill. The lower unit (basement) has been described as a weathered amphibole bearing basalt, fine to coarse grained, with variable texture and composition. Amphibolite intrusions, made of 80% amphibole, olivine and mica, and 20% groundmass and calcite, were found within this unit.

The dolerite samples studied in this thesis are fine to medium grained, with intergranular texture, and variable amounts of plagioclase and titanaugite, accessory opaques, biotite, pyrite, possibly some altered olivine, and secondary phyllosilicates, sericite and calcite. The degree of alteration is variable and strongly dependent on the grain size. Only one sample was considered to be fresh enough for Sr/Nd/Pb isotopic study.

The samples of the basement studied in this thesis are porphyritic, with dark brown, glassy to cryptocrystalline groundmasses, in some places fresh, in others completely to partially sericitised, with abundant opaques and pseudomorphs of eu- to subhedral plagioclase and olivine microphenocrysts. Some samples are variolitic, and some have cavities filled with celadonite and calcite. Rare titanaugite microcrysts, similar to those found in the sill, were found in some samples.

The unusual composition of the basalts of this site was recognised by several authors (Hekinian 1974; Sclater & Fisher 1974; Subbarao et al. 1977; Subbarao et al. 1979, and unpublished data therein), who pointed out that both the dolerite sill and the basement basalts are unlike MORB and similar to OIB basalts, and may somehow be more closely related to the Cocos and Christmas islands rather than to any mid-oceanic ridge system.

Both the sill and the basement rocks have high TiO_2 (> 2%), P_2O_5 (> 0.6) and alkali contents. The dolerite sill is nepheline-normative, and fairly "primitive", having relatively high Mg# (62-64) and Cr and Ni contents (respectively 300 and 140 ppm), whereas the basement basalts are generally nepheline-normative, but considerably more evolved (Mg# down to less than 50). The sill is also rich in K_2O in the sill (approximately 1.7-1.9 for Mg# ≈ 64), and has high LILE, LREE, and HFSE contents, with HFSE/HFSE and LILE/HFSE values typical of OIB.

Site 22 212

This site is situated in the deepest part of the Wharton Basin, SW of Christmas Island, at a water depth of 6240 m. Although the percentage of recovery was not very high (47.6%), the stratigraphy of the site is fairly well documented, and is almost totally made of nanno-oozes in the upper part (Middle Pliocene to Early Middle Miocene) and of nanno-chalk with layers of zeolitic clays in the lower part (Early-Middle Miocene to Upper Cretaceous). The lithology of this site is mainly made of carbonaceous material, and is fairly uniform.

Although the site is far away from the arc, the content of volcanogenic material in the upper part is very high, up to several percent in some layers (and volcanogenic material is common in the upper layers in most of the sites, and its amount increases nearer to the Sunda arc). The presence of calcareous material at a considerable depth at this site has been interpreted as due to rapid "flushes" of carbonate sediments from shallower waters.

Eighteen analyses are available for material from this site: four sediments (zeolite claystones) and fourteen volcanic rocks of the basement, including analyses of pillow margins and interiors, plus some analyses of fresh and altered glass. Unfortunately, no analyses from the carbonaceous sequence are available.

The volcanic basement cored in this site is a sequence of partially weathered and altered basaltic pillow lavas, with typical pillow lava texture and glassy areas rich in palagonite, brown glass, smectites and chlorite.

The samples of volcanic rocks examined in this thesis are yellow to dark brown devitrified glasses, many with unaltered euhedral plagioclase microphenocrysts and olivine microliths, rare clinopyroxene megacrysts (up to 5 mm), and relatively fresh glassy areas.

In contrast with those of site 22 211, the basalts from this site have low K_2O, P_2O_5, and TiO_2 (respectively < 0.7, < 0.03, and 0.5-0.6 in fresh samples), and also their trace element abundances closely resemble typical, little fractionated N-MORB (Hekinian 1974; Subbarao et al. 1979). The original composition of most of the analysed samples has been strongly modified by seawater/clay alteration.

Site 22 213

Site 213 is situated approximately 800 km SW of the coast of central Sumatra. Recovery was 84%, and the analyses available (sixteen, plus four averages) cover the recent (Quaternary to Upper Miocene) oozes (four analyses), the Middle Miocene to Lower Eocene? zeolite-rich clays (three analyses) and the Lower Eocene to Upper Paleocene oozes and the underlying clay-rich iron oxide sediments (one analysis each). The amount of volcanogenic material in the sediments has been estimated at up to 25% in the upper units. Six analyses of volcanic rocks and several analyses of glasses complete the available data set.

Due to the good percentage of recovery and to the good distribution of the samples along the stratigraphic column, this site is one of the best known sites in the area.

The volcanic basement has been interpreted as a sequence of basaltic pillow lavas, with typical pillow lava texture and variable amounts of plagioclase, clinopyroxene, palagonite and opaques. Although large variations have been observed between the crystalline and the glassy samples, the basalts from this site are geochemically similar to those from site 22 212, having low K_2O and P_2O_5, slightly depleted LREE, and composition typical of N-MORB.

The samples of volcanic rocks of this study are subophitic to glassy, moderately altered but with unaltered areas, with abundant plagioclase phenocrysts and microliths, and some very small olivines. Only one sample was considered to be fresh enough for Sr/Nd isotopic study.

Site 27 260

This site is situated about 1000 km S of central Jawa. The percentage of core recovery, 33.5%, was low, and the lithology is considered to be fairly variable. Neither the nine analyses nor the average of one hundred and eighteen analyses of sediments that have been published can be considered representative of the composition of the entire column, nor can the lithology of any single sedimentary unit be estimated.

The basement cored in this site was interpreted as a medium grained, intergranular to porphyritic basaltic sill, slightly vesiculated, with calcite and clay minerals in veins and filling vesicles. Phenocrysts and microphenocrysts are subhedral plagioclase (60%) showing normal zoning, anhedral clinopyroxene (25%), and magnetite (5%).

Samples from this site are tholeiites with a rather unusual composition, having high TiO_2 (1.8 to 2.1) but low K_2O and P_2O_5, low Rb but relatively high HFSE, and REE patterns similar to E-MORB, but more enriched.

Site 27 261

This is another site for which we have a very detailed set of information. Although the percentage of recovery was low (36.8%), the stratigraphy is very well known: Quaternary radiolarian- and diatom-rich clays, Lower Pliocene to Upper Miocene nanno-oozes and clays, Cretaceous clays and mainly claystones, resting on basaltic basement. The twenty analyses plus one average of eighty-six analyses of sediments accurately represent the overall lithology and the lithology of every single unit. Furthermore, seventeen analyses of the three units of basement basalts and three averages of trace elements (one for each basaltic unit) are available.

Three different volcanic units were recognised at this site. The upper unit (unit A) is interpreted as a poorly vesiculated, dark green-grey, fine to coarse grained basaltic sill, intruded between underlying basalt and Lower Cretaceous sediments. The unit is usually glomeroporphyritic, with olivine, replaced by smectite, and subhedral plagioclase and augite, with an intergranular to subophitic texture, and interstitial magnetite and alteration minerals. The middle unit (unit B) is a fine grained, highly fractured and strongly altered basalt, possibly a sill or a lava flow. The lower unit (unit C - basement) is a basal basaltic pillow breccia, with intersertal to intergranular texture, compositionally similar to unit A, but with very abundant clay minerals and calcite completely replacing augite and plagioclase.

The samples studied in this thesis of volcanic rocks from the three units are moderately to strongly altered, with variable amounts of clay minerals and celadonite. Only one sample from unit A, celadonite- and smectite-free, was considered to be fresh enough for Sr/Nd/Pb isotopic study.

The three units have two different geochemical compositions. Units A and C are rather strongly depleted in incompatible trace elements, and have low contents of TiO_2, K_2O, and P_2O_5 (in the fresh samples), and depleted LREE similar to N-MORB, whereas unit B has high HFSE, K_2O, and P_2O_5, and REE patterns similar to N-MORB, although considerably more enriched.

The relatively high $^{87}Sr/^{86}Sr$ (0.7039 to 0.7045) values reported for site 261 (unit B) and the other two sites located at the margins of the Wharton basin (259 and 260) may be due to alteration (Robinson & Whitford 1974; Frey et al. 1977). Whitford (1975, page 1299) observed that "if these ratios are a widespread feature of the oceanic crust which is being subducted to the north, then they may account for the Sr isotopic character of at least the arc tholeiites in Jawa".

Subbarao et al. (1979) noticed that these Sr isotope values fall within the range of MIOR basalts, and suggested that the high $^{87}Sr/^{86}Sr$ values are inherited from the source and not a consequence of secondary alteration. However, this interpretation is not in agreement with the currently accepted models of evolution of the Northeastern Indian Ocean, because it would imply that these basalts had a mantle plume component before the Kerguelen plume appeared in other marginal areas (see discussion in Chapter 3).

Dredged and short cored samples

V28-14A-B and VM 28 RD 14-1 to 4 are from a Lamont-Doherty dredge haul from the flanks of the Cocos Plateau, at a water depth of 3733 to 2428 m.

These samples (described in this thesis for the first time) are glassy to cryptocrystalline, strongly altered basalts, rich in opaques, with abundant zeolite, celadonite and calcite filling vesicles and replacing the original mineral phases (mainly plagioclase and clinopyroxene?), with thick surface deposits of manganese oxides and organogenic apatite (excluded from the analysed material).

Only one sample from this dredge was analysed for Sr/Nd/Pb isotopes, in an attempt to characterise the isotopic composition of basalts from this site.

VM 28 RD 14-4 "fresh" and VM 28 RD 14-4 "altered" are moderately and strongly altered fractions of the same dredged sample - taken about 5 cm apart. Sedimentary material adhering to basaltic sample VM 28 RD 14-2 is a loose clay: a thin black layer (oxides, Mn?) between this clay and the basalt was excluded from the analysed material.

DODO 232 E-G-J-K-N are dredge hauls from the flank of a large structure (a volcano, according to Engel et al. 1965) situated on the western flank of the Investigator Ridge, at a water depth of 4119 to 3558 m.

All these samples are moderately altered, except DODO 232N, vesiculated porphyritic basalts, with cryptocrystalline, partially sericitised groundmass with abundant plagioclase microliths and rare plagioclase and clinopyroxene microphenocrysts. Similar texture and degree of vesiculation have been observed in the Ninetyeast Ridge, and have been interpreted as evidence for shallow water or subaerial eruption.

Samples "DODO 232G altered" and "DODO 323G fresh" come from the same specimen, the altered part from the outside (less than 1 cm from the surface) and the fresh part from the interior of the same hand specimen. No differences in grain size, texture and degree of vesiculation are visible between the two parts, so the surface of the specimen is probably not a cooling surface: any compositional differences between the two parts may therefore be due to alteration. The differences are within the experimental uncertainty, although a greater difference was anticipated from the altered appearance of the exterior of the sample. Only one celadonite-free sample was considered to be fresh enough for Sr/Nd/Pb isotopic study.

Engel et al. (1965) first analysed the major element composition of these basalts, and noticed their high TiO_2, K_2O, and P_2O_5 compared with MORB. The high amount of vesicles (approximately 20 %) was considered as evidence for the sinking of the region of at least one kilometre, probably more, if the basalts were extruded in a shallow-water or subaerial environment. Based on the degree of alteration, Engel et al. (1965) suggested that the age of extrusion was not older than 30 Ma.

All the samples of sediments discussed in Chapter 4 analysed by ben Othman et al. (1989) and by McLennan et al. (1990), as well as the new analyses presented in this thesis for the same localities, are from short piston cores, and the bulk lithology of the site is therefore unknown. Only Nd isotope data were reported by Dia et al. (1992). Due to the shallow depth reached by these cores (usually a few metres or less), the maximum age of all these samples of sedimentary rocks is most likely to be Quaternary or, at most, Upper Pliocene.

Other DSDP and ODP sites (located in the Northeastern Indian Ocean, but for which no new analyses are reported in this thesis).

Site DSDP 26 256 and 26 257

Site 256 was cored at a depth of approximately 5400 m, south of site 212. The percentage of recovery of the 270 m of sediments drilled was 79%, but no analyses of sediments were found in the literature. Although very close to site 212, site 256 is totally made of detrital clays deposited in an

undisturbed deep-sea environment, ranging in age from Quaternary to Lower Cretaceous, the estimated age of the oldest sediments being just older (about 101 Ma) than in site 212 (80-100 Ma) (however, if, as seems to be, this site is genetically related to the Broken Ridge, then its age is likely to be much younger, in the range 50-60 Ma; see Royer et al. 1991). The drill then penetrated 19 m of fine- to coarse-grained olivine basalt, highly fractured and altered. At least four flows have been recognised, and eleven samples of this volcanic unit are included in this database.

Site 257 was cored at a water depth of approximately 5300 m in the south-easternmost part of the Wharton Basin. Like site 256, this core is almost totally made of detrital clays, with only minor amounts of calcareous material in the lower part. Again, as in site 256, volcanogenic material is absent. The percentage of recovery was 49%, but only one analysis of a Cretaceous? clay at the bottom of the sedimentary sequence was found in the literature.

The basement was reached at 262 m; at least seven flows of medium- to fine-grained olivine basalt, highly fractured and altered, have been described, and nineteen samples come from these flows.

The basalts from site 256 and the upper flow in site 257 are relatively enriched in TiO_2 (> 2.2 in site 256), and Zr (140-180 ppm), but have low K_2O and Ba, and REE patterns similar to DODO and DSDP 215. The older basalts in site 257 are considerably more depleted and resemble N-MORB, and were interpreted (Luyendyk 1974) as part of the earliest Early Cretaceous crust. Instead, the enriched basalts in site 256 and 257, similar to the basalts in the Ninetyeast Ridge rather than to the MORB from spreading centres, are believed to have formed just after the incipient rifting between Australia and Antarctica. However, according to Thompson et al. (1978), site 256 could be related to the volcanism responsible for the series of topographic highs that goes from the Broken Ridge to the vicinity of site 256, and no enriched basalts were described by Thompson et al. (1978) in site 257.

Sites DSDP 26 258, 27 259 and 27 263

These sites, although situated far from the arc, are very close to the Australian continent, and therefore they most likely represent the composition of continent-derived and shallow water sediments.

Site 258 was drilled in the northern flank of the Naturaliste Plateau, at a water depth of approximately 2800 m. Two cores (258A and 258B) penetrated 525 and 123 m of sediments respectively, of which 50% and 77% were recovered. The lithology is quite variable, ranging from Quaternary to Miocene nanno oozes, to Upper Cretaceous nanno chalks and silicified limestones, to Lower Cretaceous ferruginous detrital clays, with glauconite-rich sands and clays at the bottom of the sequence. The volcanic basement was not reached, and volcanogenic material is absent. Unfortunately, only one analysis of a Cretaceous clay is available for this site.

Site DSDP 27 259 was cored at a depth of approximately 4700 m some 100 km from the central coast of Western Australia. The upper section of the core (Quaternary to Upper Paleocene) is a sequence of nanno-oozes and zeolite-bearing clays and oozes; three samples, one for each lithology, come from this section. The lower (Cretaceous) part of the core is made of zeolitic clays, zeolite-bearing clays and oozes, and cristobalite and quartz clays, all the lithologies being represented by eight analyses. Four analyses of the volcanic basement and one average of the trace elements composition of the volcanic unit complete the data set. Due to the high percentage of recovery (71.9%) and to the good sampling coverage, this site too can be regarded as fairly well known.

Site DSDP 27 263 was cored at a depth of approximately 5000 m, between the Wallaby and the Exmouth Plateaux. The volcanic basement was not reached. The composition of this core ranges from recent (Quaternary to Upper Pliocene) nanno-oozes to Cretaceous clayey nanno-oozes, claystones and clays. All the different lithologies are represented by the ten published analyses.

The basalts of site 259 are quartz tholeiites strongly depleted in REE and with an N-MORB pattern - like in unit C of site 261 - and have low TiO_2, K_2O, and P_2O_5, and overall low abundances of both LILE and HFSE.

Site ODP 123 765 and 766

More than forty analyses of basalts and one hundred and forty of sediments come from site 765, cored at a water depth of approximately 5700 m in the southern part of the Argo Abyssal Plain, just north of the Swan Canyon and south of site DSDP 27 261. The 950 m thick sedimentary column at site 765 can be subdivided into two parts. The Cainozoic section is made essentially of calcareous turbidites, probably from the nearby Exmouth Plateau, while the Cretaceous section is dominated by pelagic clays. The earliest sediments are Early Berriasian to Lower Valanginian (Lower Cretaceous), in agreement with the stratigraphic age (and the absolute age measured on alteration minerals - see discussion in Chapter 3) of site 261. This is the only core in the NE Indian Ocean for which a systematic sampling of the sedimentary column has been carried out in order to estimate the average sediment composition. All the data discussed in this thesis from this site are from Ludden (1992), Ludden & Dionne (1992), Plank & Ludden (1992), and Ishiwatari (1992).

The volcanic basement at site 765 is made of pillow lavas and massive lava flows, with minor amounts of basaltic breccia, hyaloclastite, and a dolerite sill. The basalts are mostly aphyric, with plagioclase, rare olivine, and abundant clinopyroxene phenocrysts. Megacrysts of plagioclase and clinopyroxene, and fragments of gabbroic rocks - rather evolved (hypersthene-bearing) or primitive (with highly magnesian basaltic melt inclusions) - are common. Pebbles of basaltic rocks are found in conglomerate beds in the sedimentary column, mainly within a very thick Miocene turbidite.

Volcanic rocks were also cored at site 766, where massive Valanginian black siltstone was intruded by thin sills and a thick (at least 47 m) dolerite. The petrographic characteristics of these rocks are variable: the sills are moderately phyric (with plagioclase, clinopyroxene and olivine phenocrysts) and aphyric, whereas the dolerite is rather coarse-grained, with eu- to subhedral quartz.

The basalts of the basement at site 765 have low P_2O_5, K_2O, TiO_2, a REE pattern typical of N-MORB, and are very homogeneous throughout the sequence. The pebbles range in composition from depleted and primitive N-MORB to E-MORB. According to Ludden & Dionne (1992) the crust of this site is comparable with the new crust forming in the Red Sea, and was interpreted as the result of high degrees of mantle melting below a rifted continental lithosphere.

The composition of the different units at site 766 is very variable, but all the units seem to have variable HFSE but constant Ti/Zr values (approximately 120 - similar to sites 259, 260, and 261), and REE values ranging from N-MORB to rather enriched N-MORB (but less enriched than unit B in site 261).

According to Ludden & Dionne (1992) samples from site 765 have Sr, Nd, and Pb isotope values similar to those measured in site 261, and $^{87}Sr/^{86}Sr$ values in the range 0.7030 to 0.7033 were measured in site 766 (Ishiwatari 1992).

Site DSDP 27 262

This site was cored in the Timor Trough at a very short distance from Timor. Although the drill penetrated more than 400 m of sediments, the age of the deepest sediment recovered is Pliocene. The fifteen analyses (plus one average) published in the literature are representative of the lithologically uniform (radiolarian and foram clay-rich nanno-oozes and dolomites in the lower part of the column) young sediments.

Appendix F

Representative electron microprobe analyses of mineral phases in Indonesian volcanics

Note. Individual mineral grains are identified using the whole-rock sample number, followed by the number of the grain analysed (with reference to the number of grains for each sample mounted in a probe mount). For example, olivine 75379-49 indicates olivine grain 49 of sample 75379.

Olivine - disaggregated crystals

	75379-49	75379-50	75379-51	75379-52	75379-53	75379-20	75379-21	75379-22	75379-23
SiO2	40.94	41.13	41.05	40.56	40.33	40.71	40.80	41.00	40.71
FeO	9.99	10.74	9.58	9.74	11.32	10.20	10.00	9.89	10.03
MgO	49.23	48.37	49.16	48.06	47.75	49.07	48.61	48.72	48.78
CaO	0.10	0.07	0.05	0.07	0.07	0.06	0.09	0.07	0.07
Sum	100.25	100.31	99.83	98.43	99.47	100.04	99.48	99.68	99.59
Fo	89.78	88.92	90.14	89.79	88.26	89.55	89.65	89.77	89.65

	75379-24	75379-25	75379-26	75379-27	75379-28	75379-29	75379-30	75379-31	75379-32
SiO2	41.29	40.63	40.41	40.73	40.38	40.33	40.57	40.30	40.59
FeO	10.02	10.02	9.88	9.75	9.87	10.21	10.33	10.44	9.76
MgO	48.97	48.40	48.52	49.17	48.60	48.30	48.20	47.97	49.06
CaO	0.11	0.07	0.09	0.07	0.07	0.05	0.07	0.06	0.05
Sum	100.39	99.13	98.91	99.72	98.93	98.90	99.17	98.78	99.45
Fo	89.70	89.59	89.74	89.99	89.77	89.39	89.27	89.12	89.96

Phases in xenoliths

Olivines	75379-1	75379-2	75379-3	75379-5	75379-6
SiO2	40.47	40.25	40.66	40.62	40.64
FeO	9.74	10.12	9.89	9.49	9.72
MgO	48.78	48.27	49.03	48.85	48.84
CaO	0.11	0.07	0.11	0.06	0.06
Sum	99.09	98.72	99.69	99.01	99.26
Fo	89.92	89.48	89.83	90.17	89.95

Pyroxenes	75379-C1	75379-C2	75379-C3	75379-C4	75379-01	75379-03	75379-04	75379-05
SiO2	51.64	52.31	52.06	52.43	54.71	54.87	55.39	55.01
TiO2	0.51	0.53	0.56	0.49	0.17	0.09	0.13	0.19
Al2O3	7.48	7.25	7.24	7.29	5.39	5.27	5.28	5.22
FeO	2.91	3.05	3.03	3.03	6.64	6.28	6.46	6.46
MnO	0.08	0.04	0.06	0.05	0.04	0.03	0.07	0.06
MgO	15.40	15.46	15.29	15.52	33.21	33.22	33.27	33.37
CaO	19.68	19.42	19.40	19.25	0.73	0.74	0.71	0.77
Na2O	1.68	1.69	1.66	1.70	0.10	0.11	0.13	0.11
Total	99.37	99.75	99.29	99.75	100.98	100.60	101.44	101.18
mg#	0.90	0.90	0.90	0.90	0.90	0.90	0.90	0.90

Duplicate olivine analyses

	75379-5	75379-20	75379-21
SiO2	40.63	40.41	40.77
FeO	9.95	9.85	9.75
MnO	0.14	0.08	0.14
MgO	48.47	49.03	48.85
Cr2O3	0.00	0.00	0.00
CaO	0.07	0.06	0.07
NiO	0.40	0.47	0.38
Total	99.66	99.90	99.96
Fo	89.67	89.87	89.93

Table F1. Bukit Telor

Olivine	75416-2	75416-4	75416-5	75416-6	75416-7	75416-8	75416-10	75416-11	75416-12	75416-15	75416-16	75416-17	75416-19	75416-20	75416-21	75416-22	75416-23	75416-24	75416-25	75416-40
SiO2	40.10	40.62	40.62	39.82	40.37	39.78	39.73	40.56	37.83	40.51	39.74	37.75	39.30	40.33	40.78	40.49	40.06	40.45	40.20	38.86
FeO	11.82	10.60	11.24	14.07	11.35	12.08	13.29	11.46	25.46	9.50	11.31	25.95	16.61	11.60	10.22	12.58	14.76	12.15	11.79	20.63
MgO	47.97	49.22	48.44	46.09	48.33	47.65	45.99	48.42	36.65	49.65	47.96	36.12	43.69	48.35	49.07	47.69	45.75	47.77	47.82	40.95
CaO	0.23	0.20	0.23	0.18	0.20	0.26	0.27	0.21	0.11	0.20	0.21	0.09	0.13	0.26	0.21	0.14	0.24	0.23	0.22	0.29
Total	100.12	100.64	100.53	100.16	100.26	99.76	99.27	100.65	100.05	99.87	99.22	99.91	99.73	100.54	100.28	100.91	100.81	100.61	100.04	100.74
Fo	87.85	89.22	88.48	85.37	88.35	87.55	86.05	88.28	71.95	90.30	88.31	71.27	82.42	88.14	89.54	87.11	84.67	87.51	87.84	77.96

Olivine	75416-9	75416-13	75416-14	75416-18	75416-29	75416-39	75416-43	75416-45	75416-51
SiO2	39.94	39.84	40.24	40.41	40.70	41.00	38.64	40.56	38.18
FeO	12.07	13.83	12.08	10.93	12.47	9.94	18.48	11.78	21.19
MgO	47.46	45.92	47.51	48.80	47.65	49.45	41.85	48.14	39.67
CaO	0.16	0.26	0.19	0.20	0.22	0.21	0.21	0.24	0.22
Total	99.62	99.85	100.02	100.34	101.04	100.61	99.18	100.73	99.25
Fo	87.51	85.55	87.51	88.84	87.20	89.86	80.14	87.92	76.94

Spinel inclusions									
SiO2	0.26	0.17	0.18	0.38	0.12	0.60	0.19	0.12	0.13
TiO2	0.52	0.47	0.39	0.37	0.60	0.57	6.38	0.44	0.83
Al2O3	14.59	14.19	13.89	14.97	17.73	17.15	6.09	15.22	12.13
Cr2O3	46.64	46.36	45.78	47.68	42.71	45.44	22.26	47.28	41.93
Fe2O3	9.36	9.72	10.59	8.42	10.12	7.02	28.53	8.75	14.21
FeO	15.94	18.74	19.43	15.62	16.85	15.55	29.26	15.87	22.33
MnO	0.19	0.17	0.31	0.16	0.11	0.15	0.39	0.27	0.32
NiO	0.25	0.17	0.00	0.31	0.00	0.19	0.13	0.13	0.08
MgO	12.19	10.36	9.86	12.55	12.14	13.07	5.50	12.24	7.76
Total	99.94	100.34	100.43	100.46	100.38	99.74	98.73	100.33	99.72
mg #	0.577	0.496	0.475	0.589	0.562	0.600	0.251	0.579	0.383
cr#	0.682	0.687	0.689	0.681	0.618	0.640	0.710	0.676	0.699
Fe2+/Fe3+	1.891	2.142	2.039	2.061	1.850	2.461	1.139	2.015	1.746

Table F2. Galunggung

Olivine	75426-1	75426-2	75426-3	75426-4	75426-5	75426-6	75426-7	75426-8	75426-9	75426-10	75426-11	75426-28	75426-34	75426-45	75426-59	75426-60	75426-62
SiO2	38.89	38.73	38.70	37.47	38.64	38.72	38.59	38.41	38.41	38.72	38.39	38.88	38.40	38.10	38.50	38.16	38.72
FeO	19.66	19.66	19.08	25.26	19.27	18.75	20.08	18.89	19.59	18.77	18.54	18.55	20.11	22.08	19.76	19.05	19.02
MgO	40.86	40.91	41.56	35.84	41.40	41.87	41.06	41.76	40.32	41.95	40.74	40.91	40.16	38.42	40.85	40.35	41.50
CaO	0.16	0.19	0.15	0.21	0.18	0.19	0.17	0.17	0.16	0.19	0.16	0.17	0.13	0.19	0.15	0.23	0.18
Sum	99.57	99.49	99.49	98.78	99.49	99.53	99.90	99.23	98.48	99.63	97.84	98.51	98.80	98.79	99.26	97.79	99.42
Fo	78.74	78.76	79.51	71.66	79.29	79.92	78.47	79.76	78.57	79.93	79.66	79.71	78.06	75.62	78.64	79.05	79.54
Spinel inclusion																	
SiO2					0.14			0.09	0.09		0.09	0.14	0.07	0.10	0.08	0.08	0.06
TiO2					2.42			2.51	2.89		2.25	2.39	1.90	3.74	3.86	3.06	2.34
Al2O3					19.08			18.89	16.89		20.15	18.74	19.99	15.30	15.60	16.34	19.30
Cr2O3					28.28			27.14	25.83		28.28	27.00	28.69	27.05	25.86	26.82	28.05
Fe2O3					17.93			19.31	20.77		17.06	18.54	17.30	19.63	19.73	20.01	18.18
FeO					23.00			22.05	23.60		21.48	22.05	22.31	26.32	27.23	22.92	21.78
MnO					0.23			0.50	0.50		0.59	0.27	0.44	0.55	0.59	0.61	0.29
NiO					0.20			0.08	0.21		0.16	0.21	0.08	0.07	0.13	0.10	0.18
MgO					9.06			9.49	8.16		9.69	9.21	9.08	6.98	6.33	8.55	9.61
Total					100.34			100.06	98.94		99.75	98.54	99.85	99.74	99.41	98.50	99.79
mg #					0.41			0.43	0.38		0.45	0.43	0.42	0.32	0.29	0.40	0.44
cr#					0.50			0.49	0.51		0.48	0.49	0.49	0.54	0.53	0.52	0.49
Fe2+/Fe3+					1.43			1.27	1.26		1.40	1.32	1.43	1.49	1.53	1.27	1.33

Table F3. Kalimantan

Olivine	75333-2	75333-3	75333-4	75333-8	75333-9	75333-10	75333-12	75333-14	75333-15	75333-16	75333-17	75333-18	75333-19	75333-20	75300-2	75300-4	75300-5	75300-6	75300-7	75300-8	75300-9
SiO2	38.38	39.56	39.86	40.27	40.08	39.80	39.13	38.75	39.03	40.02	39.59	39.76	39.30	39.48	39.94	39.42	39.90	39.85	39.78	40.06	39.89
FeO	20.83	15.25	13.09	11.54	12.96	14.09	16.21	18.36	16.98	14.11	14.40	13.47	16.50	15.65	14.27	15.16	14.18	13.19	13.97	13.46	14.17
MgO	40.28	44.86	46.95	47.42	46.86	45.82	44.15	42.16	43.33	45.66	45.39	46.44	43.54	44.06	45.74	44.99	45.65	46.44	45.97	46.16	45.45
CaO	0.20	0.17	0.20	0.20	0.20	0.16	0.16	0.20	0.19	0.16	0.17	0.20	0.15	0.17	0.23	0.19	0.21	0.17	0.21	0.19	0.21
Total	99.69	99.84	100.11	99.43	100.10	99.87	99.65	99.47	99.53	99.95	99.55	99.88	99.49	99.36	100.18	99.77	99.95	99.65	99.93	99.87	99.73
Fo	77.51	83.98	86.47	87.99	86.56	85.29	82.92	80.36	81.98	85.22	84.89	86.00	82.47	83.38	85.10	84.10	85.16	86.26	85.43	85.93	85.11

Olivine	75300-10	75300-11	75300-12	75300-15	75300-17	75284-1	75284-2	75284-3	75284-4	75284-5	75284-6	75284-7	75284-8	75284-9	75284-10	75284-12	75284-13	75284-14	75284-15	75284-16	75284-17
SiO2	40.11	40.06	38.86	39.60	40.15	39.70	38.76	40.01	39.12	39.49	39.66	39.64	39.36	38.13	39.18	39.60	39.64	39.81	39.74	39.44	39.76
FeO	13.20	12.97	18.15	14.71	13.14	14.07	18.64	13.36	17.09	13.92	13.43	13.77	16.48	23.57	17.24	14.61	14.64	14.47	14.41	13.84	13.55
MgO	46.81	46.78	42.27	44.99	46.68	45.43	42.61	47.16	43.28	45.73	46.48	46.20	43.73	38.11	42.87	44.95	44.70	45.04	45.56	46.04	46.31
CaO	0.20	0.17	0.09	0.19	0.20	0.35	0.27	0.33	0.33	0.29	0.32	0.35	0.32	0.25	0.28	0.31	0.31	0.35	0.31	0.29	0.31
Total	100.32	99.98	99.37	99.50	100.16	99.55	100.28	100.87	99.83	99.44	99.90	99.96	99.88	100.06	99.57	99.47	99.29	99.67	100.02	99.61	99.92
Fo	86.34	86.53	80.59	84.49	86.36	85.20	80.29	86.28	81.86	85.41	86.05	85.67	82.55	74.24	81.58	84.57	84.47	84.73	84.93	85.56	85.90

Olivine	75284-18	75284-19	75284-20	75284-54	75273-1	75273-2	75273-3	75273-4	75273-5	75273-6	75273-7	75273-8	75273-9	75273-10	75273-11	75267-1	75267-2	75267-3	75267-4	75267-5	75267-6
SiO2	39.34	39.63	39.97	38.76	37.70	37.59	37.14	36.84	37.30	36.65	37.05	37.29	37.86	37.66	37.63	37.08	37.31	36.35	37.08	37.04	36.77
FeO	15.66	14.10	14.05	18.77	23.47	26.01	25.84	30.21	25.96	29.65	25.93	25.93	22.87	23.32	24.41	27.25	26.62	29.22	27.10	27.26	26.96
MgO	44.18	45.57	45.92	42.06	38.08	35.82	36.22	32.04	36.36	32.78	36.18	35.84	38.24	38.27	37.15	34.91	35.43	33.02	34.55	34.65	34.96
CaO	0.25	0.35	0.29	0.28	0.17	0.21	0.19	0.19	0.19	0.17	0.17	0.21	0.16	0.15	0.17	0.31	0.31	0.24	0.33	0.31	0.28
Total	99.43	99.65	100.23	99.88	99.43	99.64	99.38	99.27	99.81	99.25	99.33	99.28	99.13	99.40	99.36	99.55	99.66	98.83	99.07	99.26	98.96
Fo	83.41	85.21	85.35	79.97	74.30	71.05	71.41	65.40	71.39	66.33	71.31	71.12	74.87	74.52	73.06	69.53	70.34	66.82	69.44	69.37	69.80

Olivine	75267-7	75267-8	75267-9	75267-10	75237-1	75237-2	75237-3	75237-4	75237-5	75237-6	75237-7	75237-8	75237-9	75237-10
SiO2	37.23	37.05	36.86	37.15	38.96	38.96	38.88	37.65	38.55	38.36	38.57	39.41	38.86	38.94
FeO	26.68	27.18	27.46	27.37	17.64	17.16	17.56	22.73	18.83	19.14	19.88	15.79	17.99	17.54
MgO	35.34	35.31	34.45	34.39	43.10	43.12	42.72	38.51	41.32	41.16	40.66	44.28	42.45	42.84
CaO	0.25	0.28	0.32	0.28	0.23	0.24	0.20	0.27	0.24	0.23	0.20	0.19	0.23	0.20
Total	99.51	99.82	99.09	99.19	99.93	99.48	99.37	99.15	98.95	98.89	99.30	99.67	99.53	99.53
Fo	70.24	69.83	69.10	69.13	81.32	81.74	81.26	75.12	79.63	79.31	78.47	83.33	80.79	81.32

Table F4. Sumatran arc olivines

Olivine	75384-6a	75384-6b	75384-7	75384-13a	75384-13b	75384-16	75384-24	75384-26	75384-27	75384-31	75384-36	75333-1	75333-5
SiO2	39.05	38.93	39.21	39.13	39.25	39.11	38.98	38.19	39.33	38.71	38.88	40.89	40.28
FeO	17.60	17.41	17.27	17.44	17.88	17.80	17.90	20.82	18.71	17.81	18.31	9.60	11.99
MgO	43.29	42.68	42.92	43.10	42.61	42.98	42.90	40.51	42.30	42.56	42.53	49.63	47.94
CaO	0.20	0.17	0.20	0.21	0.24	0.19	0.20	0.20	0.20	0.21	0.19	0.15	0.16
Total	100.14	99.19	99.60	99.88	99.98	100.07	99.98	99.72	100.54	99.29	99.91	100.27	100.37
Fo	81.42	81.38	81.57	81.50	80.94	81.14	81.03	77.62	80.11	80.99	80.54	90.21	87.70
Spinel inclusion													
SiO2	0.14	0.09	0.10	0.11	0.10	0.12	0.08	0.07	0.07	0.07	0.03	0.09	0.07
TiO2	0.93	1.11	1.24	1.51	1.46	1.25	1.75	1.75	1.84	1.28	1.76	1.13	0.70
Al2O3	30.79	27.27	28.61	27.00	27.66	26.93	26.01	12.62	24.28	28.84	25.49	16.60	13.63
Cr2O3	18.51	21.24	19.46	19.60	18.69	21.68	16.76	15.55	18.88	19.90	18.99	39.43	44.29
Fe2O3	18.77	19.23	20.17	21.12	20.85	19.79	24.22	38.06	23.52	19.34	22.67	13.05	12.60
FeO	19.08	19.96	20.55	20.62	20.96	20.19	20.98	25.26	21.41	20.32	22.16	16.11	18.46
MnO	0.33	0.17	0.11	0.25	0.22	0.32	0.19	0.23	0.31	0.22	0.22	0.16	0.38
NiO	0.15	0.19	0.17	0.32	0.22	0.25	0.20	0.20	0.23	0.08	0.28	0.30	0.09
MgO	11.97	11.11	11.26	10.99	10.76	11.17	10.73	6.17	10.18	11.38	9.94	12.28	10.49
Total	100.67	100.37	101.67	101.52	100.92	101.69	100.92	99.91	100.72	101.43	101.54	99.15	100.71
mg #	0.53	0.50	0.49	0.49	0.48	0.50	0.48	0.30	0.46	0.50	0.44	0.58	0.50
cr#	0.29	0.34	0.31	0.33	0.31	0.35	0.30	0.45	0.34	0.32	0.33	0.61	0.69
Fe2+/Fe3+	1.13	1.15	1.13	1.09	1.12	1.13	0.96	0.74	1.01	1.17	1.09	1.37	1.63

Olivine	75333-6	75333-7	75333-11	75333-13	75333-24	75333-28	75333-30	75333-33	75300-1	75300-3	75300-6	75300-13	75300-14
SiO2	40.27	40.63	39.53	39.44	39.48	40.32	39.53	39.54	40.14	39.99	39.84	39.97	39.60
FeO	12.73	10.10	14.07	15.01	14.13	10.78	17.58	15.68	12.64	13.11	13.64	11.85	13.81
MgO	46.63	49.19	45.50	44.74	44.90	48.17	42.26	44.19	46.98	46.54	46.13	47.58	45.80
CaO	0.16	0.23	0.20	0.17	0.15	0.19	0.16	0.15	0.20	0.23	0.24	0.21	0.17
Total	99.78	100.15	99.30	99.37	98.66	99.45	99.53	99.56	99.97	99.88	99.85	99.62	99.39
Fo	86.72	89.67	85.22	84.16	84.99	88.84	81.07	83.40	86.88	86.35	85.77	87.73	85.53
Spinel inclusion													
SiO2	0.06	0.12	0.02	0.05	0.03	0.03	0.04	0.03	0.11	0.05	0.08	0.07	0.08
TiO2	0.71	0.57	1.11	0.83	1.85	0.40	0.76	1.46	0.49	0.57	0.57	0.47	0.45
Al2O3	12.69	13.35	8.10	12.81	9.40	9.91	10.33	8.69	25.55	24.99	23.90	26.13	24.19
Cr2O3	44.92	48.93	48.46	39.31	42.63	51.88	39.86	42.87	34.40	33.70	33.94	35.33	34.55
Fe2O3	11.17	8.15	12.08	16.83	16.48	9.09	18.39	15.98	9.74	11.39	11.58	9.30	11.40
FeO	21.28	17.52	23.01	22.42	22.26	19.28	24.17	24.65	15.90	16.31	16.85	14.86	17.43
MnO	0.45	0.37	0.33	0.22	0.41	0.30	0.41	0.37	0.11	0.17	0.27	0.33	0.18
NiO	0.09	0.25	0.11	0.05	0.10	0.11	0.19	0.17	0.22	0.14	0.23	0.28	0.17
MgO	8.30	10.87	7.09	7.91	8.31	9.37	6.22	6.22	13.22	13.01	12.32	13.94	12.19
Total	99.67	100.14	100.31	100.44	101.47	100.37	100.37	100.44	99.75	100.33	99.74	100.71	100.64
mg #	0.41	0.53	0.35	0.39	0.40	0.46	0.31	0.31	0.60	0.59	0.57	0.63	0.55
cr#	0.70	0.71	0.80	0.67	0.75	0.78	0.72	0.77	0.47	0.47	0.49	0.48	0.49
Fe2+/Fe3+	2.12	2.39	2.12	1.48	1.50	2.36	1.46	1.71	1.81	1.59	1.62	1.77	1.70

Olivine	75300-16	75300-18	75300-19	75300-20	75300-23	75300-26	75300-43	75300-49	75300-55	75284-11	75284-37	75284-39	75284-60
SiO2	39.99	39.63	39.58	39.73	39.68	40.06	39.94	40.23	40.10	39.89	38.62	39.36	39.85
FeO	12.55	12.67	12.56	13.53	13.02	11.85	12.38	12.89	11.51	13.71	18.54	15.02	13.98
MgO	47.42	46.73	46.99	45.55	46.47	47.49	47.22	46.85	47.87	45.91	42.04	44.71	45.65
CaO	0.17	0.24	0.21	0.23	0.21	0.25	0.20	0.25	0.17	0.32	0.31	0.32	0.36
Total	100.13	99.27	99.35	99.04	99.39	99.66	99.74	100.22	99.65	99.83	99.51	99.41	99.84
Fo	87.07	86.79	86.96	85.71	86.41	87.71	87.18	86.63	88.12	85.65	80.17	84.14	85.34
Spinel inclusion													
SiO2	0.10	0.10	0.06	0.10	0.09	0.10	0.09	0.10	0.10	0.08	0.09	0.09	0.11
TiO2	0.45	0.50	0.64	0.49	0.46	0.45	0.42	0.53	0.43	0.80	1.08	0.47	0.89
Al2O3	26.09	24.16	24.16	23.85	23.79	24.03	25.53	26.43	25.18	27.13	25.98	28.17	26.95
Cr2O3	33.79	35.00	35.39	34.49	35.67	36.90	34.64	33.34	37.38	31.38	32.29	30.39	30.38
Fe2O3	10.19	10.24	10.35	11.47	10.77	9.33	10.34	10.79	8.23	10.83	10.56	11.39	11.52
FeO	15.44	16.09	16.12	17.82	15.92	15.16	15.20	15.83	15.03	15.63	17.73	15.79	16.07
MnO	0.21	0.22	0.18	0.21	0.39	0.22	0.13	0.21	0.24	0.24	0.47	0.22	0.19
NiO	0.30	0.06	0.22	0.19	0.27	0.24	0.23	0.43	0.19	0.09	0.09	0.19	0.24
MgO	13.49	12.87	13.01	11.88	12.87	13.47	13.71	13.45	13.84	13.74	12.45	13.58	13.41
Total	100.06	99.24	100.13	100.50	100.23	99.90	100.29	101.11	100.61	99.92	100.74	100.29	99.75
mg #	0.61	0.59	0.59	0.54	0.59	0.61	0.62	0.60	0.62	0.61	0.56	0.61	0.60
cr#	0.46	0.49	0.50	0.49	0.50	0.51	0.48	0.46	0.50	0.44	0.45	0.42	0.43
Fe2+/Fe3+	1.68	1.75	1.73	1.73	1.64	1.81	1.63	1.63	2.03	1.60	1.86	1.54	1.55

Table F5. Sumatran arc olivine-spinel pairs

Olivine	75215-58	75215-1	75215-2	75215-3	75215-4	75215-6	75215-7	75215-8	75215-10	75215-12	75215-13	75215-14	75216-1	75216-3	75216-4	75216-5	75216-6	75216-7	75216-8	75216-9	75216-10
SiO2	39.69	39.14	39.15	39.43	39.33	39.66	39.41	39.38	39.63	39.88	39.28	39.53	39.55	39.94	40.06	40.01	39.94	39.92	40.27	40.09	40.00
FeO	13.95	15.90	14.09	13.84	13.70	14.05	14.02	14.15	14.09	13.96	14.40	13.22	16.10	15.67	14.04	14.44	15.28	15.90	14.28	14.23	14.70
MgO	45.88	44.18	45.15	45.40	45.71	45.47	45.59	45.57	45.62	45.79	45.04	45.52	44.11	44.96	45.74	45.29	44.32	43.81	45.78	45.66	45.17
CaO	0.23	0.18	0.17	0.17	0.16	0.20	0.22	0.20	0.20	0.21	0.18	0.20	0.24	0.20	0.21	0.18	0.21	0.21	0.22	0.22	0.20
Total	99.75	99.41	98.56	98.85	98.91	99.38	99.24	99.30	99.53	99.84	98.91	98.46	100.00	100.77	100.04	99.91	99.76	99.85	100.55	100.20	100.07
Fo	85.42	83.20	85.10	85.40	85.60	85.23	85.28	85.16	85.23	85.39	84.78	85.98	83.00	83.64	85.31	84.83	83.79	83.08	85.10	85.11	84.56

Olivine	75216-11	75216-12	75216-13	75216-14	75216-15	75216-16	75216-17	75360-2	75360-3	75360-7	75360-8	75360-9	75360-10	75360-11	75360-12	75360-13	75360-14	75360-15	75360-16	75360-17	75360-18
SiO2	40.06	40.28	40.03	40.06	39.87	40.07	39.85	40.10	39.92	39.69	40.33	39.87	40.26	40.45	39.36	40.04	39.68	39.99	39.36	39.41	40.05
FeO	14.15	14.11	15.02	15.75	14.61	15.24	15.01	14.35	13.76	14.90	13.15	13.77	13.36	14.31	15.84	14.58	16.00	14.16	17.78	17.43	14.55
MgO	45.39	46.01	44.85	44.24	45.30	44.52	44.19	45.80	45.86	44.78	46.46	45.44	45.73	45.57	43.94	44.80	44.23	45.11	42.54	42.82	45.18
CaO	0.22	0.18	0.22	0.20	0.20	0.19	0.17	0.19	0.20	0.22	0.22	0.21	0.23	0.20	0.20	0.21	0.27	0.19	0.27	0.21	0.20
Total	99.82	100.57	100.12	100.25	99.99	100.02	99.22	100.44	99.74	99.59	100.16	99.30	99.58	100.53	99.34	99.62	100.17	99.44	99.95	99.87	99.98
Fo	85.11	85.32	84.18	83.35	84.68	83.89	83.99	85.04	85.59	84.27	86.29	85.47	85.92	85.01	83.17	84.56	83.13	85.02	81.00	81.40	84.70

Olivine	75360-19	75365-1	75365-2	75365-3	75365-6	75365-7	75365-8	75365-9	75365-10	75365-11	75365-70	75365-69	75365-68	75365-67	75365-66	75365-65	75377-2	75377-3	75377-5	75377-8	75377-9
SiO2	39.26	39.90	40.20	39.87	40.12	39.88	39.95	39.79	40.03	39.76	39.83	39.77	39.96	39.70	40.05	40.04	39.80	39.86	39.94	39.06	39.27
FeO	17.33	15.74	14.34	14.45	14.34	14.13	15.91	15.99	13.98	14.74	14.56	16.18	14.24	15.55	13.91	15.00	13.76	14.02	13.12	13.93	13.46
MgO	42.94	44.49	45.39	45.74	45.66	45.46	43.90	43.65	45.89	45.32	45.19	44.10	45.83	44.52	45.08	45.23	45.68	45.82	46.16	45.42	45.90
CaO	0.19	0.21	0.18	0.21	0.21	0.18	0.19	0.20	0.21	0.20	0.22	0.23	0.18	0.19	0.19	0.20	0.22	0.23	0.21	0.24	0.18
Total	99.71	100.35	100.11	100.27	100.33	99.65	99.95	99.63	100.11	100.03	99.81	100.29	100.21	99.97	99.23	100.47	99.45	99.93	99.42	98.66	98.82
Fo	81.53	83.44	84.94	84.94	85.01	85.15	83.10	82.95	85.40	84.56	84.69	82.93	85.15	83.61	85.24	84.31	85.54	85.35	86.25	85.31	85.87

Olivine	75377-10	75377-11	75354-1	75354-2	75354-3	75354-4	75354-5	75354-7	75354-8	75354-9	75354-10	75354-58	75355-1	75355-3	75355-4	75355-5	75355-6	75355-7	75355-8	75355-10	75355-11
SiO2	39.01	39.54	39.29	38.99	39.15	39.36	38.69	39.41	39.30	39.55	38.98	39.51	39.31	39.19	39.33	39.45	39.56	39.19	39.30	39.24	39.76
FeO	15.01	13.29	14.29	15.14	14.41	15.14	17.62	15.00	14.58	14.27	15.28	13.88	15.89	15.15	16.03	14.40	14.15	16.30	15.31	15.45	13.82
MgO	44.29	45.87	45.79	44.59	45.12	44.97	42.50	44.53	45.08	45.34	44.35	45.32	44.14	44.97	44.32	44.91	45.22	43.94	44.22	44.18	45.84
CaO	0.17	0.22	0.21	0.18	0.17	0.20	0.21	0.16	0.24	0.20	0.21	0.21	0.18	0.20	0.19	0.19	0.18	0.19	0.17	0.23	0.16
Total	98.49	98.91	99.58	98.91	98.86	99.67	99.02	99.10	99.20	99.35	98.81	98.91	99.52	99.51	99.86	98.95	99.10	99.61	99.00	99.09	99.58
Fo	84.02	86.01	85.10	83.99	84.80	84.11	81.13	84.10	84.64	84.99	83.80	85.34	83.19	84.10	83.13	84.75	85.06	82.77	83.73	83.60	85.53

Table F6. Sukadana olivines

Olivine	75355-12	75355-13	75355-14	75355-15	75355-22	75361-1	75361-2	75361-3	75361-4	75361-7	75361-11	75361-12	75361-13	75361-14	75363-1	75363-2	75363-5	75363-6	75363-7	75363-10	75366-1
SiO2	39.47	39.80	39.60	39.41	39.77	39.39	39.02	39.27	39.18	38.87	39.49	39.37	39.29	39.35	39.83	39.51	39.90	39.94	39.88	40.04	39.80
FeO	14.69	14.08	14.35	15.40	14.66	15.63	16.87	15.07	16.70	17.43	16.27	16.36	15.73	15.26	14.91	14.79	14.34	14.81	14.52	14.90	14.35
MgO	45.13	45.70	45.31	43.63	45.02	43.94	42.97	44.17	43.63	42.46	43.14	43.53	44.39	44.96	44.69	44.92	45.37	45.19	45.12	44.77	44.46
CaO	0.19	0.17	0.00	0.11	0.20	0.10	0.20	0.21	0.16	0.23	0.19	0.20	0.19	0.19	0.21	0.21	0.21	0.20	0.24	0.24	0.22
Total	99.47	99.74	99.26	98.54	99.64	99.06	99.05	98.72	99.66	98.98	99.09	99.45	99.59	99.76	99.64	99.43	99.83	100.14	99.77	99.94	98.84
Fo	**84.56**	**85.26**	**84.91**	**83.47**	**84.56**	**83.36**	**81.95**	**83.93**	**82.32**	**81.28**	**82.53**	**82.58**	**83.41**	**84.00**	**84.23**	**84.40**	**84.93**	**84.47**	**84.71**	**84.26**	**84.66**

Olivine	75366-2	75366-3	75366-4	75366-5	75366-8	75366-9	75366-10	75366-11	75366-12	75366-13	75366-14	75366-15	75368-1	75368-3	75368-4	75368-5	75368-6	75368-7	75368-12	75369-1	75369-2
SiO2	39.81	40.04	39.99	39.81	39.88	39.82	39.93	39.84	39.76	39.77	40.08	39.79	40.11	39.83	39.77	39.61	40.10	40.27	39.30	39.24	38.66
FeO	13.94	14.06	13.93	14.00	14.13	14.67	13.82	14.00	14.28	13.83	14.19	14.92	14.54	14.84	14.47	14.84	14.48	14.28	16.83	15.15	16.67
MgO	45.79	45.42	45.46	45.58	45.41	45.29	45.93	45.20	45.12	45.31	45.79	44.64	44.82	45.58	45.22	44.61	45.59	45.21	42.94	44.26	43.24
CaO	0.22	0.21	0.19	0.21	0.20	0.21	0.18	0.21	0.23	0.18	0.21	0.21	0.24	0.22	0.20	0.29	0.20	0.20	0.26	0.01	0.17
Total	99.77	99.73	99.57	99.61	99.63	100.00	99.86	99.26	99.40	99.09	100.26	99.56	99.71	100.47	99.66	99.34	100.36	99.96	99.32	98.67	98.74
Fo	**85.41**	**85.20**	**85.33**	**85.29**	**85.14**	**84.62**	**85.55**	**85.19**	**84.92**	**85.38**	**85.19**	**84.21**	**84.60**	**84.55**	**84.78**	**84.27**	**84.87**	**84.94**	**81.97**	**83.89**	**82.21**

Olivine	75369-3	75369-4	75369-5	75369-6	75369-8	75369-10	75370-1	75370-2	75370-5	75370-6	75370-7	75370-8	75370-9	75370-10	75370-12	75371-1	75371-2	75371-3	75371-4	75371-5	75371-6
SiO2	38.87	38.13	39.47	39.40	39.12	39.45	38.96	39.28	39.40	39.23	39.09	39.04	39.08	39.11	38.86	39.34	39.36	39.12	39.28	38.94	39.15
FeO	17.25	19.40	14.50	15.57	16.06	14.85	16.47	14.81	14.56	15.21	14.88	14.98	14.65	14.73	16.18	14.36	14.62	15.05	14.88	16.08	15.31
MgO	42.32	40.73	44.33	43.67	43.04	44.45	43.28	44.00	44.74	44.35	44.49	44.46	44.64	44.44	43.76	44.85	44.92	44.40	44.07	43.26	44.48
CaO	0.18	0.22	0.16	0.19	0.18	0.19	0.18	0.19	0.18	0.20	0.16	0.16	0.16	0.16	0.22	0.19	0.18	0.22	0.20	0.20	0.19
Total	98.62	98.48	98.45	98.82	98.39	98.93	98.89	98.27	98.88	98.98	98.61	98.63	98.52	98.43	99.01	98.74	99.08	98.78	98.43	98.47	99.13
Fo	**81.38**	**78.91**	**84.49**	**83.33**	**82.69**	**84.21**	**82.40**	**84.12**	**84.55**	**83.86**	**84.20**	**84.10**	**84.45**	**84.32**	**82.82**	**84.77**	**84.55**	**84.02**	**84.07**	**82.75**	**83.81**

Olivine	75371-7	75371-8	75371-9	75371-10	75371-50	75372-2	75372-3	75372-4	75372-5	75372-6	75372-7	75372-8	75372-9	75372-10	75372-11	75372-12	75374-1	75374-2	75374-3	75374-4	75374-5
SiO2	39.18	38.94	39.57	38.93	39.19	39.54	39.17	39.23	39.12	39.19	39.07	38.97	39.36	39.07	39.06	39.25	39.04	39.26	39.54	39.22	39.17
FeO	14.66	15.66	14.85	14.77	15.39	15.02	15.57	14.44	14.98	15.31	15.21	15.60	14.88	15.59	14.90	14.94	17.09	15.74	15.99	16.56	14.57
MgO	45.11	43.69	44.81	44.40	44.04	44.81	44.01	44.49	44.42	44.19	44.09	43.76	44.66	43.51	44.55	44.29	43.08	43.89	44.31	43.75	45.38
CaO	0.21	0.16	0.19	0.19	0.20	0.18	0.18	0.19	0.19	0.19	0.17	0.20	0.18	0.17	0.19	0.19	0.00	0.20	0.19	0.21	0.22
Total	99.15	98.44	99.41	98.28	98.81	99.55	98.93	98.34	98.70	98.88	98.54	98.52	99.07	98.33	98.69	98.66	99.21	99.09	100.03	99.74	99.34
Fo	**84.58**	**83.25**	**84.32**	**84.27**	**83.61**	**84.17**	**83.44**	**84.59**	**84.09**	**83.72**	**83.78**	**83.33**	**84.25**	**83.26**	**84.20**	**84.08**	**81.79**	**83.25**	**83.15**	**82.48**	**84.73**

Table F6 cont. Sukadana olivines

Olivine	75374-7	75374-8	75374-9	75374-11	75374-12	75375-1	75375-2	75375-3	75375-5	75375-7	75375-8	75375-10	75376-1	75376-2	75376-3	75376-4	75376-5	75376-6	75376-7	75376-8	75376-9
SiO2	39.17	39.49	39.23	39.18	39.45	39.53	38.80	38.72	39.33	39.20	38.82	39.48	39.22	39.53	39.06	39.59	39.57	39.37	39.72	39.64	39.49
FeO	16.43	16.02	15.91	16.21	14.21	15.08	15.58	17.23	15.87	16.63	17.98	14.76	15.89	15.22	17.71	13.42	13.82	15.41	14.40	13.98	15.65
MgO	43.57	44.36	44.24	43.46	46.18	44.75	44.30	42.96	44.14	43.17	42.09	45.14	43.90	44.95	42.98	46.00	45.88	44.89	45.09	46.23	44.52
CaO	0.18	0.22	0.20	0.17	0.23	0.17	0.22	0.18	0.20	0.21	0.22	0.17	0.23	0.19	0.21	0.19	0.20	0.19	0.17	0.18	0.21
Total	99.34	100.08	99.58	99.01	100.06	99.53	98.89	99.09	99.54	99.21	99.11	99.54	99.24	99.89	99.95	99.19	99.47	99.85	99.38	100.02	99.86
Fo	82.53	83.15	83.21	82.69	85.28	84.10	83.52	81.63	83.21	82.22	80.66	84.50	83.11	84.03	81.22	85.93	85.54	83.85	84.80	85.50	83.52

Olivine	75376-10	75376-11	75376-12	75356-2	75356-4	75356-6	75356-8	75357-5	75357-6	75357-7	75357-10	75357-45	75358-45	75358-46	75358-48	75358-53	75358-34	75358-36	75358-37	75359-3	75359-5
SiO2	39.31	39.26	39.93	39.48	39.31	39.92	39.39	40.03	39.89	39.70	39.58	40.52	39.41	39.82	39.22	39.91	39.70	39.79	39.55	39.82	39.76
FeO	14.62	14.26	13.51	13.24	14.40	13.90	13.98	13.92	13.03	15.40	14.04	13.03	14.59	12.67	17.63	14.58	14.02	15.02	14.83	12.50	13.98
MgO	45.03	45.55	45.84	46.41	45.85	46.20	45.90	45.79	46.82	44.23	45.56	46.46	45.48	46.95	42.94	45.22	45.70	45.01	45.28	46.56	45.84
CaO	0.21	0.18	0.19	0.18	0.17	0.19	0.19	0.20	0.15	0.17	0.19	0.20	0.23	0.19	0.20	0.18	0.19	0.21	0.23	0.16	0.18
Total	99.17	99.24	99.47	99.31	99.73	100.21	99.45	99.94	99.88	99.50	99.36	100.21	99.71	99.62	99.98	99.89	99.60	100.03	99.88	99.04	99.75
Fo	84.59	85.06	85.81	86.20	85.02	85.55	85.41	85.42	86.49	83.66	85.26	86.40	84.74	86.85	81.28	84.67	85.32	84.23	84.48	86.90	85.39

Olivine	75359-7	75359-8	75359-9	75359-10	75359-11	75359-12	75359-13	75359-14	75359-20
SiO2	39.47	39.76	39.60	40.15	39.95	40.07	39.91	40.14	39.69
FeO	13.51	12.01	14.14	13.65	12.62	13.17	14.50	13.16	13.50
MgO	45.91	47.67	45.32	45.88	47.03	46.50	45.09	46.31	46.49
CaO	0.17	0.14	0.21	0.20	0.16	0.17	0.18	0.17	0.16
Total	99.06	99.57	99.26	99.88	99.75	99.91	99.68	99.78	99.84
Fo	85.83	87.62	85.10	85.69	86.92	86.28	84.71	86.24	85.99

Table F6 cont. Sukadana olivines

Olivine	75215-5	75215-9	75215-11	75215-15	75215-16	75215-29	75215-23	75215-41	75216-2	75216-26	75216-28	75216-30	75216-35	75216-41	75216-42	75360-1	75360-4	75360-5	75360-6	75360-22	75360-28
SiO2	39.61	39.17	39.03	39.50	38.95	39.00	38.47	39.36	39.82	39.74	39.54	39.07	39.95	39.87	39.80	39.82	39.95	39.97	39.88	39.97	39.54
FeO	14.44	14.77	16.27	15.87	16.73	14.85	16.76	15.10	16.46	15.36	15.99	17.20	15.18	14.57	14.93	15.79	14.09	13.79	13.93	14.86	17.44
MgO	45.40	45.41	43.86	44.14	42.65	45.23	42.52	44.55	43.53	44.40	44.21	42.95	44.57	44.80	44.80	44.25	45.21	45.81	46.44	45.48	43.30
CaO	0.20	0.17	0.23	0.22	0.22	0.20	0.26	0.28	0.21	0.23	0.24	0.21	0.27	0.22	0.22	0.22	0.21	0.23	0.22	0.20	0.24
Total	99.65	99.53	99.39	99.73	98.54	99.27	98.02	99.30	100.03	99.74	99.98	99.42	99.98	99.46	99.75	100.09	99.46	99.81	100.47	100.52	100.53
Fo	84.85	84.57	82.76	83.21	81.96	84.45	81.89	84.02	82.50	83.74	83.13	81.65	83.95	84.57	84.25	83.32	85.12	85.55	85.59	84.51	81.56
Spinel inclusion																					
SiO2	0.07	0.05	0.05	0.05	0.04	0.08	0.03	0.06	0.11	0.10	0.11	0.10	0.10	0.11	0.08	0.11	0.08	0.10	0.09	0.10	0.11
TiO2	2.91	3.16	3.88	2.94	3.59	3.00	3.21	3.20	4.30	3.37	3.32	3.83	3.29	2.90	2.84	2.79	1.93	1.93	1.77	3.22	3.21
Al2O3	18.77	18.29	18.06	17.97	17.51	18.36	17.82	19.31	16.58	18.09	17.91	17.33	17.55	19.08	18.79	19.02	22.88	23.04	23.60	18.57	18.43
Cr2O3	35.34	33.43	31.84	34.65	32.68	33.64	33.93	34.98	32.03	32.62	34.38	31.27	33.72	34.76	35.47	31.19	32.05	32.91	33.21	32.46	30.08
Fe2O3	11.68	12.82	12.56	12.80	13.60	12.89	12.54	10.29	13.82	13.41	12.21	14.02	13.07	11.04	11.75	14.86	11.72	10.69	11.14	14.06	15.25
FeO	18.85	19.28	21.38	20.25	21.15	20.28	20.71	19.90	21.67	19.62	20.40	22.08	19.89	19.85	19.14	20.48	17.52	17.55	16.87	19.66	21.70
MnO	0.19	0.23	0.24	0.18	0.32	0.25	0.20	0.14	0.26	0.19	0.10	0.27	0.05	0.26	0.24	0.13	0.10	0.15	0.17	0.34	0.20
NiO	0.31	0.21	0.16	0.26	0.08	0.22	0.29	0.16	0.31	0.27	0.33	0.33	0.09	0.22	0.37	0.26	0.36	0.40	0.44	0.37	0.29
MgO	11.91	11.52	10.51	10.94	10.60	10.93	10.59	11.48	10.56	11.46	11.09	9.96	11.40	11.21	11.70	10.80	12.47	12.47	13.06	11.45	10.04
Total	100.02	99.00	98.68	100.05	99.57	99.65	99.32	99.52	99.64	99.13	99.85	99.19	99.15	99.43	100.38	99.64	99.11	99.23	100.35	100.23	99.31
mg #	0.53	0.52	0.47	0.49	0.47	0.49	0.48	0.51	0.47	0.51	0.49	0.45	0.51	0.50	0.52	0.48	0.56	0.56	0.58	0.51	0.45
cr#	0.56	0.55	0.54	0.56	0.56	0.55	0.56	0.55	0.56	0.55	0.56	0.55	0.56	0.55	0.56	0.52	0.48	0.49	0.49	0.54	0.52
Fe2+/Fe3+	1.79	1.67	1.89	1.76	1.73	1.75	1.84	2.15	1.74	1.63	1.86	1.75	1.69	2.00	1.81	1.53	1.66	1.82	1.68	1.55	1.58

Table F7. Sukadana olivine-spinel pairs

Olivine	75360-30	75360-31	75360-35	75360-49	75365-5	75365-22	75377-4	75377-6	75377-7	75377-12	75377-15	75377-16	75354-6	75354-15	75354-23	75354-25	75354-40	75354-49	75354-31	75355-2	75355-9
SiO2	39.92	39.82	39.94	39.86	39.08	40.13	39.06	39.63	39.67	39.27	39.58	39.55	39.36	39.56	39.17	39.27	39.02	39.69	39.73	39.25	39.37
FeO	13.62	14.57	13.71	14.59	18.42	15.11	14.08	13.04	13.71	14.77	13.93	13.76	15.85	14.12	16.51	14.51	14.40	14.25	14.15	15.63	15.29
MgO	46.03	44.90	45.66	45.33	41.73	44.88	45.45	46.00	45.87	45.05	45.41	45.59	43.99	45.44	43.09	44.92	44.79	45.51	45.49	43.86	44.43
CaO	0.20	0.30	0.21	0.21	0.23	0.22	0.24	0.24	0.24	0.27	0.21	0.25	0.20	0.22	0.22	0.18	0.23	0.21	0.21	0.19	0.18
Total	99.77	99.59	99.52	100.00	99.46	100.34	98.83	98.91	99.49	99.36	99.13	99.14	99.40	99.33	98.99	98.88	98.45	99.65	99.58	98.92	99.27
Fo	85.76	84.60	85.58	84.70	80.15	84.11	85.19	86.28	85.63	84.46	85.31	85.51	83.18	85.16	82.31	84.65	84.71	85.05	85.14	83.34	83.81
Spinel inclusion																					
SiO2	0.10	0.06	0.09	0.14	0.10	0.11	0.09	0.08	0.10	0.06	0.11	0.13	0.08	0.09	0.04	0.10	0.08	0.15	0.08	0.14	0.15
TiO2	1.54	2.46	2.21	2.19	5.52	3.35	1.12	0.96	0.90	1.30	1.23	1.20	1.34	1.33	1.54	1.32	1.43	1.33	1.42	1.35	1.74
Al2O3	22.52	21.11	21.86	21.18	14.59	18.66	29.99	31.75	32.66	29.54	29.83	29.47	24.08	25.51	22.53	23.64	23.43	23.66	24.57	23.99	22.80
Cr2O3	35.06	32.44	34.22	32.94	31.28	33.55	28.54	29.96	27.80	28.31	28.26	29.08	33.09	32.25	32.91	33.42	33.01	33.65	33.13	33.88	32.47
Fe2O3	10.61	12.60	11.36	12.76	13.22	12.34	9.65	7.21	8.29	10.57	10.22	8.83	10.37	10.28	10.88	11.19	10.91	10.38	9.74	10.05	11.37
FeO	16.75	18.76	17.50	18.27	27.24	19.71	16.45	14.89	14.84	17.09	16.01	15.97	18.64	16.91	22.80	17.15	17.41	17.22	17.40	18.24	19.10
MnO	0.17	0.20	0.28	0.21	0.32	0.28	0.19	0.17	0.15	0.23	0.17	0.18	0.31	0.21	0.24	0.14	0.26	0.23	0.11	0.22	0.23
NiO	0.32	0.23	0.29	0.36	0.29	0.32	0.20	0.28	0.26	0.21	0.29	0.28	0.23	0.29	0.18	0.33	0.28	0.37	0.25	0.40	0.27
MgO	12.89	11.93	12.79	12.17	7.47	11.52	13.67	14.80	14.87	13.41	14.03	13.77	11.62	12.93	8.96	12.62	12.24	12.45	12.53	11.98	11.46
Total	99.96	99.79	100.60	100.22	100.03	99.84	99.91	100.11	99.87	100.72	100.15	98.91	99.76	99.80	100.08	99.91	99.05	99.44	99.22	100.26	99.59
mg #	0.58	0.53	0.57	0.54	0.33	0.51	0.60	0.64	0.64	0.58	0.61	0.61	0.53	0.58	0.41	0.57	0.56	0.56	0.56	0.54	0.52
cr#	0.51	0.51	0.51	0.51	0.59	0.55	0.39	0.39	0.36	0.39	0.39	0.40	0.48	0.46	0.49	0.49	0.49	0.49	0.47	0.49	0.49
Fe2+/Fe3+	1.75	1.65	1.71	1.59	2.29	1.77	1.89	2.30	1.99	1.80	1.74	2.01	2.00	1.83	2.33	1.70	1.77	1.84	1.99	2.02	1.87

Table F7 cont. Sukadana olivine-spinel pairs

Olivine	75355-17	75355-18	75355-22	75355-26	75361-5	75361-6	75361-8	75361-9	75361-10	75361-25	75361-27	75361-30	75361-32	75363-3	75363-4	75363-9	75363-11	75363-13	75363-16	75363-19	75363-24
SiO2	39.55	38.62	37.92	39.60	39.02	39.11	39.55	39.29	39.10	39.36	38.68	39.08	39.02	missing	39.65	39.91	39.80	39.97	40.00	39.85	39.76
FeO	14.84	19.67	24.38	16.97	16.50	16.68	15.48	17.13	16.47	16.51	18.61	15.90	15.67	analysis	14.39	14.90	15.04	14.61	14.68	15.22	14.61
MgO	44.97	40.78	37.17	43.02	43.13	43.48	44.00	42.72	43.35	43.38	41.73	43.92	43.86		45.14	45.07	44.48	45.02	44.82	44.49	45.07
CaO	0.17	0.15	0.22	0.19	0.21	0.20	0.21	0.23	0.20	0.20	0.20	0.22	0.22		0.19	0.24	0.23	0.22	0.21	0.23	0.21
Total	99.53	99.22	99.68	99.77	98.86	99.46	99.23	99.36	99.12	99.45	99.22	99.12	98.76		99.38	100.13	99.56	99.83	99.71	99.80	99.65
Fo	84.38	78.70	73.10	81.88	82.32	82.28	83.52	81.63	82.43	82.40	79.98	83.11	83.30		84.82	84.35	84.05	84.59	84.47	83.90	84.61
Spinel inclusion																					
SiO2	0.10	0.12	0.13	0.10	0.37	0.12	0.13	0.10	0.13	0.10	0.08	0.13	0.14	0.10	0.11	0.10	0.06	0.07	0.07	0.10	0.10
TiO2	1.32	1.38	2.18	7.51	1.58	0.93	1.02	1.14	0.91	1.14	0.94	0.97	1.04	1.12	1.01	1.00	1.13	1.04	1.09	1.33	0.93
Al2O3	23.88	23.12	23.07	7.73	29.60	26.63	27.85	27.28	27.12	26.58	27.10	27.73	27.61	24.09	24.85	25.74	25.76	24.84	24.49	23.29	25.18
Cr2O3	34.59	32.73	32.93	27.95	26.44	30.77	31.42	30.88	31.45	31.38	30.34	30.82	30.95	32.88	34.18	33.51	33.54	34.32	34.16	33.96	34.10
Fe2O3	9.77	10.82	10.91	19.16	9.66	10.72	9.11	8.91	9.68	9.72	9.90	9.37	10.02	10.54	9.06	8.74	8.65	9.04	9.91	10.02	9.17
FeO	17.59	21.48	18.56	31.97	19.34	18.12	16.98	18.55	17.50	17.88	20.10	16.99	17.42	17.62	16.95	17.29	17.23	16.95	16.83	18.70	16.54
MnO	0.13	0.15	0.16	0.20	0.23	0.17	0.18	0.16	0.23	0.12	0.20	0.22	0.20	0.00	0.14	0.09	0.15	0.00	0.24	0.29	0.05
NiO	0.36	0.37	0.36	0.09	0.19	0.37	0.33	0.24	0.41	0.33	0.28	0.36	0.30	0.24	0.28	0.38	0.13	0.12	0.13	0.29	0.26
MgO	12.41	9.77	12.28	4.92	12.16	12.03	13.04	11.88	12.43	12.29	10.77	12.80	12.84	12.15	12.60	12.45	12.66	12.77	12.79	11.39	12.94
Total	100.15	99.93	100.58	99.63	99.57	99.85	100.05	99.13	99.86	99.54	99.71	99.39	100.52	98.74	99.17	99.29	99.31	99.15	99.71	99.37	99.28
mg #	0.56	0.45	0.54	0.22	0.53	0.54	0.58	0.53	0.56	0.55	0.49	0.57	0.57	0.55	0.57	0.56	0.57	0.57	0.58	0.52	0.58
cr#	0.49	0.49	0.49	0.71	0.37	0.44	0.43	0.43	0.44	0.44	0.43	0.43	0.43	0.48	0.48	0.47	0.47	0.48	0.48	0.49	0.48
Fe2+/Fe3+	2.00	2.21	1.89	1.85	2.22	1.88	2.07	2.31	2.01	2.04	2.26	2.02	1.93	1.86	2.08	2.20	2.22	2.08	1.89	2.07	2.00

Table F7 cont. Sukadana olivine-spinel pairs

Olivine	75363-27	75366-6	75366-7	75366-20	75366-21	75366-38	75366-43	75366-45	75366-52	75368-2	75368-8	75368-9	75368-10	75368-11	75368-14	75368-16	75368-22	75369-9	75369-54	75370-3	75370-4
SiO2	39.85	39.75	39.78	39.96	39.75	39.53	39.84	39.90	39.90	39.60	39.65	40.18	39.61	39.53	39.84	39.62	39.81	39.22	38.94	38.93	39.20
FeO	14.79	13.90	14.21	14.33	14.12	16.21	15.10	14.98	14.45	17.72	14.55	15.64	16.52	15.76	14.18	14.26	14.36	16.12	15.76	15.49	15.79
MgO	44.91	45.50	44.94	45.52	44.99	43.62	45.21	44.65	45.33	41.99	45.33	44.27	43.04	44.03	44.72	45.16	44.94	43.25	43.65	43.57	43.83
CaO	0.20	0.22	0.26	0.21	0.23	0.23	0.22	0.23	0.22	0.24	0.22	0.21	0.30	0.21	0.19	0.24	0.24	0.19	0.19	0.20	0.21
Total	99.76	99.37	99.19	100.02	99.09	99.60	100.38	99.76	99.91	99.55	99.76	100.30	99.47	99.53	98.93	99.29	99.36	98.77	98.53	98.18	99.03
Fo	84.40	85.36	84.93	84.98	85.03	82.75	84.21	84.15	84.83	80.85	84.74	83.46	82.28	83.27	84.89	84.95	84.79	82.71	83.15	83.37	83.18
Spinel inclusion																					
SiO2	0.11	0.04	0.07	0.13	0.12	0.10	0.04	0.06	0.15	0.11	0.11	0.09	0.10	0.08	0.09	0.10	0.08	0.13	0.07	0.08	0.09
TiO2	1.05	1.02	1.13	1.01	0.99	1.06	0.97	1.07	0.97	2.30	0.95	1.26	1.32	1.09	0.95	0.95	1.05	1.44	1.35	1.42	1.35
Al2O3	24.80	24.72	25.60	25.78	24.99	24.29	24.47	23.44	24.25	20.14	25.41	23.64	24.02	23.35	24.64	24.36	24.97	23.96	25.20	25.84	24.29
Cr2O3	34.23	35.36	34.64	34.23	35.18	34.89	34.35	34.61	35.03	31.99	34.17	33.26	33.29	33.57	34.28	34.49	34.20	31.58	31.83	31.97	32.35
Fe2O3	9.00	9.14	7.73	8.47	8.28	8.49	10.10	10.48	9.06	12.24	9.26	10.16	10.00	10.83	9.39	9.73	8.75	11.06	9.97	9.01	10.52
FeO	17.54	16.44	16.66	16.86	16.74	18.13	16.67	17.23	16.80	22.95	17.09	18.60	19.37	19.23	16.50	16.95	16.86	18.87	18.45	17.94	18.02
MnO	0.26	0.16	0.15	0.20	0.06	0.22	0.20	0.27	0.20	0.32	0.26	0.15	0.29	0.21	0.17	0.16	0.13	0.25	0.06	0.12	0.16
NiO	0.29	0.41	0.31	0.17	0.38	0.20	0.42	0.15	0.31	0.09	0.28	0.17	0.27	0.28	0.24	0.37	0.27	0.31	0.31	0.40	0.28
MgO	12.22	13.00	12.90	12.94	12.83	11.79	12.67	12.35	12.64	8.89	12.66	11.51	11.13	11.01	12.79	12.52	12.63	11.37	11.82	12.16	11.97
Total	99.49	100.29	99.19	99.79	99.58	99.18	99.89	99.66	99.41	99.03	100.19	98.84	99.79	99.64	99.05	99.62	98.95	98.97	99.06	98.94	99.02
mg #	0.55	0.59	0.58	0.58	0.58	0.54	0.58	0.56	0.57	0.41	0.57	0.52	0.51	0.51	0.58	0.57	0.57	0.52	0.53	0.55	0.54
cr#	0.48	0.49	0.48	0.47	0.49	0.49	0.48	0.50	0.49	0.52	0.47	0.49	0.48	0.49	0.48	0.49	0.48	0.47	0.46	0.45	0.47
Fe2+/Fe3+	2.17	2.00	2.39	2.21	2.25	2.37	1.83	1.83	2.06	2.08	2.05	2.03	2.15	1.97	1.95	1.94	2.14	1.90	2.06	2.21	1.90

Table F7 cont. Sukadana olivine-spinel pairs

Olivine	75370-11	75370-14	75370-15	75370-19	75370-49	75371-49	75371-50	75372-21	75372-22	75372-30	75374-6	75374-10	75374-13	75374-21	75374-28	75374-44	75375-4	75375-6	75375-9	75375-11	75375-25
SiO2	39.37	38.30	38.43	39.38	38.95	39.15	38.34	39.10	38.92	38.87	38.80	39.23	39.12	39.27	39.88	39.17	39.14	39.27	39.04	39.20	39.37
FeO	15.70	19.97	20.01	15.54	15.99	14.81	19.76	16.31	18.70	16.32	15.92	15.19	16.55	15.58	13.40	16.36	16.34	15.47	16.31	16.13	16.90
MgO	43.56	39.67	40.40	43.84	43.76	44.58	40.36	43.85	40.49	42.20	42.99	44.80	43.80	44.08	46.42	43.69	43.83	44.73	43.86	43.42	43.31
CaO	0.20	0.22	0.23	0.21	0.22	0.20	0.26	0.19	0.19	0.21	0.26	0.19	0.21	0.23	0.20	0.26	0.20	0.20	0.25	0.23	0.23
Total	98.82	98.16	99.07	98.96	98.92	98.73	98.72	99.44	98.30	97.59	97.98	99.41	99.68	99.16	99.89	99.48	99.50	99.66	99.45	98.98	99.81
Fo	**83.18**	**77.97**	**78.25**	**83.41**	**82.98**	**84.29**	**78.45**	**82.73**	**79.41**	**82.17**	**82.79**	**84.01**	**82.50**	**83.45**	**86.06**	**82.63**	**82.70**	**83.75**	**82.74**	**82.75**	**82.04**
Spinel inclusion																					
SiO2	0.06	0.05	0.09	0.05	0.04	0.10	0.16	0.12	0.10	0.09	0.15	0.12	0.10	0.08	0.04	0.32	0.06	0.10	0.03	0.08	0.21
TiO2	1.30	2.73	3.64	1.35	1.49	1.27	1.30	1.38	1.31	1.18	1.67	1.13	2.13	0.94	0.98	1.57	0.86	0.92	0.97	1.02	1.07
Al2O3	22.24	20.30	18.57	24.42	23.55	23.47	23.85	22.57	22.02	22.43	22.79	26.86	20.03	24.15	26.46	21.71	24.41	25.48	24.85	25.20	24.45
Cr2O3	35.23	30.93	29.45	33.01	32.08	34.56	33.30	35.34	34.81	35.56	31.05	31.75	31.75	33.67	33.16	33.33	33.06	33.40	31.22	33.06	32.55
Fe2O3	9.45	12.05	13.00	10.49	11.67	9.75	9.47	9.51	9.95	9.93	12.32	9.48	14.72	10.57	9.63	11.83	10.85	10.13	11.78	10.22	10.86
FeO	17.79	25.63	26.51	17.49	18.61	17.53	18.92	18.17	20.55	18.23	20.13	17.19	19.81	17.87	15.56	22.33	18.43	17.76	18.01	18.31	19.36
MnO	0.03	0.31	0.24	0.21	0.28	0.17	0.22	0.20	0.20	0.08	0.17	0.07	0.31	0.15	0.25	0.25	0.16	0.26	0.24	0.09	0.08
NiO	0.21	0.22	0.21	0.49	0.37	0.31	0.33	0.31	0.24	0.43	0.22	0.27	0.25	0.28	0.18	0.37	0.27	0.46	0.31	0.28	0.25
MgO	11.80	7.42	7.10	12.29	11.52	12.22	11.26	11.77	10.13	11.61	10.73	12.90	10.91	11.94	13.76	9.55	11.53	12.19	11.69	11.97	11.36
Total	98.12	99.64	98.81	99.80	99.61	99.38	98.81	99.37	99.31	99.55	99.24	99.77	100.01	99.65	100.01	101.27	99.63	100.71	99.10	100.23	100.19
mg #	0.54	0.34	0.32	0.56	0.52	0.55	0.51	0.54	0.47	0.53	0.49	0.57	0.50	0.54	0.61	0.43	0.53	0.55	0.54	0.54	0.51
cr#	0.52	0.51	0.52	0.48	0.48	0.50	0.48	0.51	0.51	0.52	0.48	0.44	0.52	0.48	0.46	0.51	0.48	0.47	0.46	0.47	0.47
Fe2+/Fe3+	2.09	2.36	2.27	1.85	1.77	2.00	2.22	2.12	2.30	2.04	1.82	2.02	1.50	1.88	1.80	2.10	1.89	1.95	1.70	1.99	1.98

Table F7 cont. Sukadana olivine-spinel pairs

Olivine	75375-26	75375-29	75375-36	75375-47	75376-13	75376-28	75376-39	75376-44	75356-1	75356-3	75356-5	75356-7	75356-9	75356-10	75356-13	75356-17	75356-19	75357-1	75357-2	75357-3	75357-4
SiO2	38.84	39.31	39.12	39.09	39.51	39.19	39.80	39.25	39.81	39.67	39.22	39.95	39.74	39.20	39.73	39.92	39.69	39.30	39.99	39.54	39.64
FeO	17.17	15.18	17.69	16.58	14.03	16.30	14.55	15.18	14.78	14.10	16.05	13.98	13.61	14.12	14.47	13.92	14.28	14.49	13.16	15.02	14.25
MgO	43.25	44.25	42.48	43.53	45.48	43.37	44.99	43.98	44.25	45.89	43.22	45.71	46.02	45.50	44.61	46.12	45.73	45.57	46.56	45.07	45.36
CaO	0.23	0.21	0.20	0.21	0.25	0.20	0.21	0.22	0.20	0.17	0.23	0.16	0.18	0.19	0.19	0.21	0.17	0.20	0.19	0.21	0.18
Total	99.49	98.95	99.49	99.40	99.26	99.06	99.55	98.63	99.04	99.83	98.71	99.79	99.54	99.00	99.00	100.17	99.87	99.56	99.90	99.84	99.42
Fo	**81.78**	**83.86**	**81.06**	**82.39**	**85.25**	**82.58**	**84.64**	**83.77**	**84.22**	**85.30**	**82.76**	**85.36**	**85.77**	**85.17**	**84.60**	**85.51**	**85.09**	**84.86**	**86.31**	**84.25**	**85.01**
Spinel inclusion																					
SiO2	0.03	0.04	0.03	0.03	0.07	0.10	0.12	0.16	0.11	0.10	0.06	0.10	0.13	0.09	0.12	0.17	0.12	0.05	0.10	0.08	0.11
TiO2	0.94	1.06	0.91	1.52	0.84	1.31	0.94	1.28	1.20	1.14	1.78	1.02	0.99	1.16	1.07	0.96	1.27	1.21	1.39	1.42	1.56
Al2O3	25.32	24.88	23.34	22.44	26.86	22.92	27.16	25.91	19.06	20.43	19.00	21.81	22.73	20.81	20.04	22.70	22.07	21.19	21.04	21.94	21.87
Cr2O3	32.25	34.46	32.41	31.43	33.51	33.68	33.14	32.54	34.65	35.82	31.57	35.11	35.65	36.03	33.03	34.49	32.71	35.38	37.16	33.84	32.84
Fe2O3	11.18	9.06	12.93	13.64	8.97	11.07	8.93	9.14	14.78	12.50	16.69	11.52	10.27	11.01	15.49	10.98	13.19	12.38	10.47	12.83	13.09
FeO	18.96	18.08	19.85	19.65	16.23	19.03	16.69	17.84	18.94	18.99	21.30	18.07	17.17	18.64	19.25	17.45	18.30	18.37	17.18	18.57	18.21
MnO	0.25	0.26	0.24	0.27	0.17	0.22	0.15	0.19	0.14	0.19	0.27	0.13	0.21	0.30	0.27	0.22	0.11	0.22	0.20	0.24	0.30
NiO	0.34	0.12	0.21	0.27	0.28	0.13	0.22	0.27	0.46	0.30	0.28	0.19	0.16	0.39	0.39	0.25	0.46	0.33	0.31	0.39	0.41
MgO	11.41	12.03	10.66	10.90	13.36	11.37	13.32	12.42	10.86	11.09	9.72	11.69	12.37	11.01	10.67	12.04	11.59	11.56	12.43	11.66	11.77
Total	100.68	99.99	100.58	100.15	100.29	99.83	100.66	99.76	100.19	100.56	100.67	99.63	99.68	99.44	100.33	99.26	99.82	100.69	100.28	100.97	100.16
mg #	0.52	0.54	0.49	0.50	0.59	0.52	0.59	0.55	0.51	0.51	0.45	0.54	0.56	0.51	0.50	0.55	0.53	0.53	0.56	0.53	0.54
cr#	0.46	0.48	0.48	0.48	0.46	0.50	0.45	0.46	0.55	0.54	0.53	0.52	0.51	0.54	0.53	0.50	0.50	0.53	0.54	0.51	0.50
Fe2+/Fe3+	1.88	2.22	1.71	1.60	2.01	1.91	2.08	2.17	1.42	1.69	1.42	1.74	1.86	1.88	1.38	1.77	1.54	1.65	1.82	1.61	1.55

Table F7 cont. Sukadana olivine-spinel pairs

Olivine	75357-8	75357-9	75357-13	75357-17	75357-22	75357-24	75358-47	75358-49	75358-50	75358-51	75358-52	75358-35	75358-38	75358-39	75359-1	75359-2	75359-4	75359-6
SiO2	39.85	39.90	39.50	39.67	39.71	39.60	39.63	39.98	39.74	39.91	39.52	40.03	39.66	40.07	39.79	39.90	40.01	40.16
FeO	13.47	14.93	15.78	14.11	14.16	15.87	15.03	13.88	14.45	13.77	15.03	13.93	13.90	13.69	13.81	13.29	13.69	12.53
MgO	46.56	45.16	44.13	45.48	45.61	44.18	44.26	46.11	45.46	45.93	44.70	45.81	45.82	45.69	45.34	46.15	45.72	47.33
CaO	0.17	0.19	0.21	0.20	0.21	0.17	0.19	0.18	0.20	0.18	0.22	0.19	0.18	0.18	0.18	0.19	0.16	0.14
Total	100.05	100.17	99.62	99.45	99.68	99.82	99.11	100.15	99.85	99.79	99.47	99.96	99.56	99.63	99.12	99.52	99.58	100.16
Fo	86.04	84.35	83.29	85.17	85.17	83.22	83.99	85.54	84.86	85.60	84.13	85.42	85.45	85.61	85.40	86.09	85.61	87.06
Spinel inclusion																		
SiO2	0.06	0.11	0.09	0.08	0.41	0.12	0.05	0.10	0.05	0.08	0.05	0.08	0.08	0.07	0.08	0.05	0.04	0.06
TiO2	1.31	1.23	1.35	1.34	1.26	1.10	1.48	1.26	1.24	1.14	1.88	1.06	1.20	1.41	1.11	5.92	0.74	0.94
Al2O3	19.96	20.41	20.30	21.51	21.76	19.76	21.55	21.77	21.63	21.33	18.28	20.48	21.83	21.33	15.86	1.85	10.39	13.89
Cr2O3	37.65	35.17	34.92	35.54	35.72	36.92	33.49	35.75	37.17	36.85	34.64	37.16	36.33	34.71	23.24	1.97	24.40	20.92
Fe2O3	11.54	12.19	13.51	11.77	10.04	11.40	12.88	10.35	10.55	10.83	14.58	10.07	10.37	11.42	28.97	53.74	34.76	33.67
FeO	17.34	18.51	19.59	17.78	18.60	19.92	19.29	18.15	18.19	18.01	19.50	18.08	17.88	18.22	22.41	30.32	21.99	20.92
MnO	0.32	0.21	0.24	0.16	0.16	0.19	0.02	0.22	0.06	0.24	0.12	0.17	0.23	0.14	0.17	0.08	0.22	0.16
NiO	0.37	0.33	0.21	0.39	0.21	0.31	0.36	0.27	0.22	0.25	0.12	0.28	0.27	0.21	0.41	0.50	0.52	0.52
MgO	12.08	11.18	10.94	12.08	11.79	10.30	11.18	11.65	12.03	11.82	10.98	11.28	11.89	11.62	8.08	3.53	7.41	8.46
Total	100.63	99.34	101.14	100.65	99.95	100.02	100.30	99.53	101.14	100.54	100.15	98.66	100.08	99.13	100.33	97.96	100.47	99.53
mg #	0.55	0.52	0.50	0.55	0.53	0.48	0.51	0.53	0.54	0.54	0.50	0.53	0.54	0.53	0.39	0.17	0.38	0.42
cr#	0.56	0.54	0.54	0.53	0.52	0.56	0.51	0.52	0.54	0.54	0.56	0.55	0.53	0.52	0.50	0.42	0.61	0.50
Fe2+/Fe3+	1.67	1.69	1.61	1.68	2.06	1.94	1.67	1.95	1.92	1.85	1.49	1.99	1.92	1.77	0.86	0.63	0.70	0.69

Table F7 cont. Sukadana olivine-spinel pairs

Olivine	78129-5	78129-2	78129-38	78129-37	78129-36	78129-35	78129-34	78129-33	78129-31	78129-30	78129-29	78129-28	78129-27	78129-26	78129-24	78129-25	78129-22	78129-21	78129-45	78129-47	78129-48
SiO2	40.00	39.97	39.99	40.58	39.77	39.71	40.41	40.60	40.70	40.59	40.44	39.89	40.17	40.14	39.56	40.16	40.38	40.38	39.20	39.62	39.00
FeO	13.76	13.59	13.37	10.01	13.07	15.29	10.05	11.06	11.12	10.92	10.33	13.65	12.16	12.49	14.67	12.14	10.34	10.84	16.50	13.47	16.46
MgO	45.64	46.25	46.11	48.82	45.99	44.79	48.77	47.46	48.07	47.88	48.31	45.56	47.62	46.82	45.08	47.07	48.30	48.16	43.56	45.70	43.57
CaO	0.21	0.21	0.22	0.15	0.26	0.20	0.20	0.21	0.17	0.22	0.15	0.22	0.21	0.18	0.21	0.20	0.18	0.17	0.23	0.22	0.17
Total	99.61	100.02	99.70	99.54	99.09	99.99	99.43	99.32	100.06	99.61	99.23	99.32	100.17	99.64	99.53	99.56	99.21	99.56	99.49	99.01	99.19
Fo	**85.53**	**85.85**	**86.00**	**89.68**	**86.25**	**83.93**	**89.63**	**88.43**	**88.51**	**88.65**	**89.29**	**85.60**	**87.46**	**86.98**	**84.56**	**87.36**	**89.28**	**88.78**	**82.47**	**85.81**	**82.51**

Olivine	78129-83	78130-1	78130-2	78130-3	78130-4	78130-5	78130-6	78130-7	78130-8	78130-9	78130-10	78130-25	78130-13	78130-14	78130-16	78130-17	78130-18	78130-19	78130-20	78130-21	78130-22
SiO2	40.27	39.64	41.01	39.85	39.72	40.06	39.85	40.05	40.09	39.99	39.76	39.75	40.61	39.89	39.77	40.39	39.64	39.65	40.15	39.90	39.73
FeO	11.73	12.86	7.00	13.04	12.72	11.31	11.77	11.83	12.01	12.55	13.30	12.86	12.16	12.98	13.63	10.43	12.28	12.74	13.89	12.78	14.07
MgO	47.53	46.23	50.96	45.86	46.21	47.49	47.22	46.83	47.24	45.78	45.54	45.69	47.74	46.35	45.76	48.57	47.70	46.43	46.16	46.66	45.93
CaO	0.17	0.26	0.11	0.18	0.24	0.21	0.15	0.20	0.20	0.21	0.22	0.21	0.13	0.20	0.18	0.14	0.21	0.24	0.22	0.21	0.20
Total	99.70	98.99	99.07	98.94	98.90	99.07	98.99	98.91	99.54	98.53	98.82	98.51	100.65	99.42	99.34	99.53	99.83	99.06	100.41	99.55	99.92
Fo	**87.83**	**86.50**	**92.85**	**86.24**	**86.62**	**88.21**	**87.73**	**87.59**	**87.51**	**86.67**	**85.92**	**86.36**	**87.50**	**86.42**	**85.68**	**89.24**	**87.37**	**86.65**	**85.56**	**86.68**	**85.33**

Olivine	78130-23	78130-24	78130-26	78130-27	78130-28	78130-29	78130-30	78130-32	78130-33	78130-34	78130-35	78130-36	78130-37	78130-38	78130-40	78130-41	78130-42	78130-43	78130-46	78130-47	78130-48
SiO2	39.95	39.79	40.69	40.51	40.18	40.03	40.30	40.63	39.83	40.29	39.67	40.12	40.02	40.02	40.20	40.38	39.36	39.78	40.05	39.86	39.92
FeO	13.15	13.24	9.71	10.96	11.55	13.02	12.75	11.21	12.83	11.67	13.15	11.72	11.97	12.96	12.60	10.92	13.70	12.32	11.60	11.92	13.21
MgO	45.81	45.99	49.08	48.03	46.99	46.21	46.22	47.93	46.61	47.49	45.98	47.04	47.99	46.37	46.60	47.74	45.58	46.53	47.77	47.71	46.27
CaO	0.22	0.22	0.17	0.17	0.15	0.21	0.18	0.16	0.14	0.16	0.20	0.18	0.17	0.20	0.22	0.15	0.21	0.15	0.16	0.16	0.18
Total	99.12	99.24	99.66	99.67	98.88	99.46	99.46	99.93	99.41	99.61	98.99	99.06	100.15	99.55	99.62	99.20	98.85	98.78	99.59	99.65	99.58
Fo	**86.13**	**86.09**	**90.01**	**88.65**	**87.88**	**86.34**	**86.59**	**88.40**	**86.62**	**87.88**	**86.17**	**87.74**	**87.72**	**86.44**	**86.83**	**88.62**	**85.56**	**87.06**	**88.01**	**87.71**	**86.19**

Olivine	78130-51	78130-52	78130-57H	78130-58H	78130-66H	78130-77H	78130-80H	78130-83H	78130-87H	78130-90H	78130-92H	78130-94H	78130-96H	78131-2	78131-4	78131-6	78131-7	78131-9	78131-10	78131-11	78131-12
SiO2	39.77	39.55	40.58	40.02	40.89	40.52	40.26	41.20	40.40	40.87	40.21	40.10	40.89	39.64	40.13	40.57	40.30	39.71	39.99	39.85	40.60
FeO	13.61	13.48	8.81	12.30	8.16	10.60	10.91	7.23	11.43	8.62	11.59	11.65	9.56	14.50	12.86	11.55	12.44	15.71	14.21	14.32	12.13
MgO	45.93	45.73	49.79	47.10	51.03	48.12	48.04	51.39	47.46	49.99	47.36	47.61	49.93	45.75	47.56	48.72	48.24	45.29	47.07	46.74	48.23
CaO	0.23	0.22	0.14	0.15	0.12	0.17	0.15	0.11	0.16	0.09	0.16	0.15	0.10	0.22	0.19	0.21	0.18	0.22	0.18	0.18	0.23
Total	99.53	98.97	99.32	99.58	100.19	99.42	99.36	99.93	99.45	99.56	99.32	99.51	100.47	100.11	100.73	101.05	101.16	100.93	101.44	101.09	101.20
Fo	**85.75**	**85.80**	**90.97**	**87.22**	**91.77**	**88.99**	**88.70**	**92.69**	**88.09**	**91.18**	**87.92**	**87.93**	**90.30**	**84.90**	**86.83**	**88.26**	**87.36**	**83.71**	**85.52**	**85.33**	**87.63**

Table F8. Bukit Mapas olivines

Olivine	78131-13	78131-14	78131-15	78131-26	78132-2	78132-4	78132-6	78132-7	78132-8	78132-9	78132-11	78132-12	78132-13	78132-15	78132-16	78132-17	78132-18	78132-20	78132-22	78133-1	78133-2
SiO2	40.08	40.11	39.88	39.82	40.02	40.11	40.67	40.73	40.67	40.40	40.34	40.66	40.64	40.71	40.09	39.81	40.11	40.17	40.28	40.51	39.88
FeO	13.81	13.54	13.91	14.08	14.14	13.44	11.17	11.28	11.66	11.89	13.20	11.38	10.97	11.89	14.02	14.33	14.01	12.39	13.10	11.57	14.04
MgO	46.18	46.31	46.45	46.09	45.77	46.42	48.03	48.42	47.84	47.66	46.65	48.23	48.61	48.06	46.12	45.05	45.74	47.14	47.54	47.89	45.79
CaO	0.20	0.19	0.18	0.19	0.18	0.20	0.18	0.18	0.21	0.18	0.19	0.16	0.18	0.19	0.16	0.24	0.20	0.20	0.19	0.20	0.20
Total	100.27	100.15	100.41	100.18	100.11	100.17	100.05	100.61	100.38	100.13	100.39	100.42	100.40	100.85	100.38	99.44	100.06	99.90	101.11	100.18	99.91
Fo	**85.63**	**85.90**	**85.61**	**85.36**	**85.23**	**86.03**	**88.46**	**88.44**	**87.97**	**87.72**	**86.30**	**88.31**	**88.76**	**87.81**	**85.43**	**84.85**	**85.34**	**87.15**	**86.61**	**88.06**	**85.32**

Olivine	78133-3	78133-4	78133-5	78133-6	78133-7	78133-8	78133-9	78133-10	78133-11	78133-13	78133-14	78133-15	78133-16	78133-17	78133-18	78133-20	78133-42	78133-40	78133-59	78134-1	78134-6
SiO2	40.30	39.97	39.88	39.92	39.91	40.45	40.05	39.86	40.05	39.99	39.95	39.81	40.37	40.07	39.94	40.48	40.29	40.46	40.94	40.86	40.46
FeO	12.96	14.58	14.58	14.31	14.23	12.43	13.40	14.64	12.39	14.49	14.15	14.06	12.09	13.46	14.11	12.57	12.71	11.30	11.30	10.42	11.73
MgO	46.89	45.28	45.43	45.26	45.62	47.14	46.90	45.63	47.22	45.59	45.88	46.29	47.25	47.04	45.57	47.02	47.15	48.09	48.29	48.94	48.04
CaO	0.19	0.22	0.24	0.20	0.21	0.19	0.18	0.21	0.18	0.18	0.17	0.20	0.19	0.20	0.14	0.18	0.20	0.17	0.20	0.11	0.18
Total	100.34	100.04	100.13	99.70	99.97	100.21	100.52	100.34	99.84	100.24	100.15	100.36	99.91	100.77	99.76	100.25	100.36	100.02	100.73	100.33	100.41
Fo	**86.57**	**84.70**	**84.74**	**84.93**	**85.10**	**87.11**	**86.18**	**84.74**	**87.17**	**84.87**	**85.25**	**85.44**	**87.44**	**86.17**	**85.20**	**86.95**	**86.86**	**88.35**	**88.39**	**89.32**	**87.95**

Olivine	78134-8	78134-9	78134-10	78134-11	78134-12	78134-13	78134-14	78134-15	78134-16	78134-17	78134-18	78134-19
SiO2	40.27	40.17	40.41	40.01	39.89	40.70	41.13	40.18	39.62	40.38	40.20	40.30
FeO	13.44	12.48	12.18	14.22	13.74	11.02	8.55	12.92	15.52	12.47	13.64	11.73
MgO	46.97	47.33	47.77	45.90	45.91	48.27	50.23	46.94	44.64	47.36	46.19	47.61
CaO	0.18	0.20	0.19	0.19	0.23	0.12	0.10	0.20	0.22	0.18	0.22	0.18
Total	100.85	100.18	100.54	100.32	99.78	100.12	100.02	100.24	100.00	100.39	100.25	99.81
Fo	**86.17**	**87.11**	**87.49**	**85.19**	**85.62**	**88.64**	**91.28**	**86.62**	**83.67**	**87.13**	**85.78**	**87.86**

Table F8 cont. Bukit Mapas olivines

Olivine	78129-1	78129-32	78129-25	78129-23	78129-20	78129-69	78130-11	78130-12	78130-15	78130-39	78130-44	78130-45	78130-49	78130-50	78130-83H	78131-1	78131-3	78131-5	78131-8	78131-16
SiO2	39.94	40.47	40.12	40.08	39.94	40.37	40.05	40.54	39.80	39.85	39.77	39.83	39.32	40.64	40.50	39.98	39.93	39.35	40.04	39.85
FeO	13.18	11.06	12.15	11.48	14.14	10.31	13.29	8.70	12.99	13.22	12.97	12.77	13.54	8.39	10.33	13.89	13.88	14.95	14.13	14.39
MgO	46.27	47.59	46.72	47.40	45.23	48.80	45.32	49.23	45.96	45.37	45.74	45.90	44.82	49.86	49.01	46.54	46.63	45.14	46.07	45.71
CaO	0.21	0.18	0.20	0.21	0.20	0.18	0.23	0.20	0.28	0.28	0.22	0.22	0.22	0.22	0.16	0.17	0.22	0.19	0.18	0.22
Total	99.61	99.30	99.19	99.17	99.50	99.66	98.89	98.66	99.04	98.72	98.70	98.72	97.91	99.11	100.02	100.57	100.66	99.63	100.42	100.17
Fo	86.22	88.46	87.27	88.04	85.08	89.40	85.87	90.97	86.31	85.94	86.27	86.50	85.50	91.37	89.42	85.65	85.69	84.33	85.31	84.99
Spinel inclusion																				
SiO2	0.03	0.05	0.11	0.17	0.04	0.09	0.05	0.17	0.05	0.09	0.07	0.09	0.09	0.08	0.39	0.15	0.14	0.15	0.15	0.15
TiO2	0.96	0.58	0.67	0.52	0.67	0.48	0.52	0.29	0.98	0.97	0.96	0.87	0.71	0.37	0.22	0.94	0.89	1.30	0.61	0.73
Al2O3	18.23	14.70	16.62	14.57	15.07	14.55	14.59	10.31	17.16	16.83	17.40	18.09	14.13	11.59	7.91	16.45	17.29	17.51	15.54	15.33
Cr2O3	34.44	43.04	41.44	46.04	40.60	47.19	43.26	55.08	35.71	35.25	35.08	35.58	41.03	52.21	54.65	36.44	36.05	31.38	42.48	40.82
Fe2O3	17.34	13.06	12.59	10.07	14.18	10.23	12.33	6.55	17.11	17.31	16.95	15.97	14.68	8.08	6.09	16.82	16.52	18.25	12.20	13.63
FeO	17.89	17.31	17.08	17.96	19.70	15.42	18.24	13.72	18.33	19.13	18.49	17.69	18.29	13.65	20.36	19.60	18.77	23.49	18.57	19.32
MnO	0.36	0.17	0.43	0.34	0.41	0.26	0.51	0.47	0.38	0.23	0.49	0.60	0.62	0.34	0.52	0.21	0.15	0.40	0.27	0.20
NiO	0.33	0.20	0.16	0.05	0.04	0.08	0.13	0.25	0.26	0.09	0.01	0.09	0.14	0.01	0.02	0.14	0.21	0.01	0.21	0.13
MgO	11.31	11.27	11.65	10.98	9.74	12.60	10.35	12.76	11.00	10.55	10.85	11.30	10.31	13.08	8.16	10.37	10.92	7.95	10.62	10.24
Total	100.89	100.38	100.75	100.70	100.45	100.90	99.98	99.60	100.97	100.45	100.30	100.28	100.00	99.41	98.32	101.11	100.94	100.44	100.65	100.56
mg #	0.530	0.537	0.549	0.522	0.468	0.593	0.503	0.624	0.517	0.496	0.511	0.532	0.501	0.631	0.417	0.485	0.509	0.376	0.505	0.486
cr#	0.559	0.663	0.626	0.679	0.644	0.685	0.665	0.782	0.583	0.584	0.575	0.569	0.661	0.751	0.822	0.598	0.583	0.546	0.647	0.641
Fe2+/Fe3+	1.146	1.473	1.509	1.981	1.544	1.675	1.644	2.326	1.190	1.228	1.213	1.230	1.385	1.876	3.713	1.295	1.263	1.431	1.691	1.575

Table F9. Bukit Mapas olivine-spinel pairs

Olivine	78131-24	78131-30	78131-38	78131-41	78131-45	78132-3	78132-5	78132-7a	78132-10	78132-14	78132-19	78132-21	78132-24	78132-35	78133-12	78133-19	78133-21	78133-34	78133-43	78133-44
SiO2	40.06	40.01	40.22	39.81	40.03	40.86	39.53	40.59	40.55	40.40	39.99	40.37	40.00	39.80	40.30	40.46	40.39	40.20	39.91	40.26
FeO	14.07	12.09	13.00	13.93	14.96	10.95	16.43	12.53	12.04	13.38	12.47	13.20	13.75	16.84	14.31	12.41	12.10	12.98	13.98	12.46
MgO	46.19	47.48	47.05	46.10	45.52	48.25	43.85	47.16	47.10	46.54	47.33	46.68	45.96	43.21	45.82	47.53	47.45	46.68	45.84	46.90
CaO	0.22	0.17	0.19	0.22	0.21	0.17	0.19	0.19	0.21	0.19	0.19	0.18	0.21	0.18	0.20	0.20	0.19	0.21	0.20	0.20
Total	100.54	99.74	100.46	100.06	100.72	100.23	99.99	100.47	99.91	100.51	99.98	100.44	99.93	100.02	100.64	100.60	100.13	100.08	99.93	99.82
Fo	**85.40**	**87.50**	**86.58**	**85.50**	**84.43**	**88.70**	**82.62**	**87.02**	**87.45**	**86.11**	**87.12**	**86.30**	**85.62**	**82.06**	**85.09**	**87.22**	**87.48**	**86.50**	**85.39**	**87.02**
Spinel inclusion																				
SiO2	0.15	0.14	0.17	0.15	0.11	0.14	0.08	0.14	0.17	0.16	0.15	0.12	0.17	0.15	0.24	0.57	0.17	0.19	0.14	0.15
TiO2	0.87	0.69	0.63	0.98	1.62	0.57	0.96	0.61	0.51	0.60	0.62	0.57	1.00	0.85	0.97	0.67	0.57	0.61	0.82	0.62
Al2O3	16.47	15.96	15.39	16.41	14.62	16.56	16.75	15.46	15.65	16.53	15.75	13.60	18.47	16.81	14.48	16.21	15.95	16.19	15.93	16.58
Cr2O3	36.35	42.54	41.51	36.26	33.13	43.42	35.75	41.64	44.20	40.59	43.31	43.28	33.95	35.97	38.87	42.36	42.67	42.11	37.39	40.82
Fe2O3	16.46	11.77	13.17	16.56	18.95	11.51	16.48	13.61	11.07	12.27	11.73	13.84	17.36	16.81	16.10	11.35	11.62	12.15	16.34	13.28
FeO	18.95	17.50	20.84	19.51	24.34	16.28	21.25	18.75	17.48	18.76	17.80	19.09	18.36	21.48	19.99	17.84	17.26	18.08	19.05	16.84
MnO	0.18	0.16	0.18	0.25	0.37	0.15	0.24	0.22	0.23	0.23	0.26	0.15	0.30	0.26	0.27	0.19	0.17	0.19	0.26	0.15
NiO	0.10	0.24	0.07	0.19	0.14	0.00	0.00	0.13	0.13	0.22	0.19	0.13	0.06	0.00	0.14	0.15	0.31	0.32	0.11	0.21
MgO	10.60	11.41	9.45	10.28	7.19	12.51	9.28	10.68	11.44	10.44	11.26	10.22	11.42	9.29	9.95	11.75	11.41	11.08	10.46	11.91
Total	100.13	100.41	101.41	100.59	100.47	101.13	100.79	101.23	100.88	99.80	101.07	101.00	101.09	101.61	101.01	101.09	100.12	100.92	100.50	100.56
mg #	0.499	0.538	0.447	0.484	0.345	0.578	0.438	0.504	0.539	0.498	0.530	0.488	0.526	0.435	0.470	0.540	0.541	0.522	0.495	0.558
cr#	0.597	0.641	0.644	0.597	0.603	0.638	0.589	0.644	0.655	0.622	0.648	0.681	0.552	0.589	0.643	0.637	0.642	0.636	0.612	0.623
Fe2+/Fe3+	1.279	1.651	1.758	1.310	1.427	1.572	1.433	1.531	1.754	1.700	1.687	1.533	1.175	1.420	1.380	1.747	1.651	1.653	1.295	1.410

Table F9 cont. Bukit Mapas olivine-spinel pairs

Olivine	78133-51	78134-2	78134-3	78134-4	78134-5	78134-7	78134-20	78134-23	78134-30	78134-32	78134-36	78134-37	78134-43	78134-44	78134-45
SiO2	39.98	40.18	39.94	39.11	39.90	39.99	40.35	40.16	39.90	41.01	40.18	40.23	39.99	40.39	40.45
FeO	14.03	14.16	13.42	19.32	14.12	14.03	13.15	12.99	14.16	10.62	12.86	13.65	13.47	12.31	11.78
MgO	45.91	46.11	46.65	41.63	46.03	45.58	46.69	47.40	45.65	49.10	46.76	46.22	46.11	47.36	47.68
CaO	0.18	0.22	0.17	0.20	0.18	0.18	0.22	0.19	0.22	0.19	0.20	0.21	0.19	0.20	0.17
Total	100.10	100.67	100.18	100.26	100.22	99.77	100.42	100.74	99.93	100.92	99.99	100.31	99.75	100.26	100.07
Fo	**85.36**	**85.30**	**86.10**	**79.34**	**85.31**	**85.27**	**86.35**	**86.67**	**85.17**	**89.18**	**86.63**	**85.78**	**85.92**	**87.27**	**87.82**
Spinel inclusion															
SiO2	0.30	0.15	0.12	0.11	0.07	0.05	0.11	0.08	0.21	0.11	0.12	0.48	0.57	0.59	0.15
TiO2	0.84	0.86	1.04	0.64	0.92	0.69	0.88	0.63	1.12	0.54	0.66	1.03	0.91	0.58	0.60
Al2O3	17.12	14.88	17.67	12.58	13.52	24.71	17.03	15.44	17.98	15.22	15.62	17.47	17.65	15.80	16.09
Cr2O3	35.57	39.81	33.34	43.51	38.06	31.94	36.13	42.35	33.39	46.34	42.16	35.65	34.97	42.53	43.27
Fe2O3	16.19	15.05	18.26	13.08	16.68	13.93	16.60	13.04	17.52	10.11	12.88	16.20	15.90	11.60	12.11
FeO	19.50	19.46	18.23	23.89	22.43	17.13	18.05	17.55	19.10	15.43	17.38	19.40	19.20	17.79	16.59
MnO	0.24	0.28	0.26	0.30	0.31	0.33	0.21	0.39	0.24	0.17	0.37	0.32	0.23	0.26	0.24
NiO	0.17	0.11	0.13	0.13	0.11	0.22	0.00	0.08	0.08	0.10	0.22	0.18	0.14	0.19	0.19
MgO	10.37	10.17	11.20	6.96	7.85	12.60	11.29	11.26	10.90	12.74	11.35	10.97	10.97	11.60	12.15
Total	100.29	100.78	100.25	101.20	99.95	101.59	100.30	100.82	100.55	100.76	100.76	101.70	100.54	100.93	101.39
mg #	0.487	0.482	0.523	0.342	0.384	0.567	0.527	0.534	0.504	0.595	0.538	0.502	0.505	0.538	0.566
cr#	0.582	0.642	0.559	0.699	0.654	0.464	0.587	0.648	0.555	0.671	0.644	0.578	0.571	0.644	0.643
Fe2+/Fe3+	1.338	1.437	1.110	2.031	1.494	1.367	1.209	1.495	1.212	1.697	1.500	1.331	1.342	1.705	1.522

Table F9 cont. Bukit Mapas olivine-spinel pairs

Olivine	78133-42/1	78133-42/2	78133-10/1	78133-10/2	78133-10/3	78133-10/4	78133-10/5	78133-10/6	78133-62/1	78133-62/2	78129-65/1	78129-65/2	78129-76	78129-5a	78129-24	78129-27	78129-91	78129-8c	78129-7c
SiO2	40.41	39.87	39.69	39.99	39.92	39.93	39.93	39.89	40.06	39.79	40.02	40.09	39.42	39.93	40.34	39.86	39.70	40.37	40.15
FeO	13.03	14.29	13.65	13.74	13.49	13.73	13.86	13.99	13.84	14.44	8.18	9.16	13.97	14.51	12.19	14.20	13.83	9.98	11.64
MnO	0.15	0.20	0.31	0.22	0.20	0.21	0.17	0.23	0.19	0.13	0.08	0.13	0.28	0.28	0.18	0.23	0.35	0.21	0.23
MgO	46.81	45.33	45.36	45.70	45.53	45.37	45.82	45.82	45.79	45.46	49.97	49.30	45.30	45.01	47.06	45.90	45.25	48.68	47.13
Cr2O3	0.00	0.00	0.00	0.00	0.00	0.00	0.00	0.00	0.00	0.00	0.00	0.00	0.00	0.00	0.00	0.00	0.00	0.00	0.00
CaO	0.13	0.15	0.10	0.11	0.10	0.11	0.11	0.11	0.17	0.17	0.12	0.13	0.15	0.21	0.17	0.16	0.17	0.18	0.22
NiO	0.15	0.19	0.21	0.16	0.18	0.24	0.18	0.19	0.17	0.08	0.41	0.30	0.10	0.09	0.21	0.09	0.11	0.33	0.18
Total	100.68	100.03	99.31	99.92	99.42	99.59	100.09	100.24	100.23	100.07	98.79	99.12	99.21	100.03	100.15	100.43	99.41	99.75	99.55
Fo	86.49	84.97	85.56	85.57	85.74	85.48	85.49	85.38	85.50	84.87	91.59	90.56	85.25	84.68	87.31	85.21	85.36	89.69	87.84

Olivine	78129-70/1	78129-70/2	78133-4/1	78133-4/2	78133-5	78129-6a	78129-7a	78129-12a/1	78129-12a/2	78129-12a/3	78129-13a/1	78129-13a/2	78129-9a	78129-10a	78129-1	78129-2	78129-3/1	78129-3c/1	78129-3c/2
SiO2	40.30	40.04	39.89	39.53	39.46	39.04	39.85	39.73	39.56	40.35	39.05	39.00	39.28	39.96	40.11	40.19	40.50	39.97	40.62
FeO	12.80	13.01	13.19	12.72	13.15	13.51	11.43	12.12	12.57	13.18	14.28	13.72	14.12	11.50	15.33	14.00	12.47	10.79	8.78
MnO	0.28	0.30	0.26	0.20	0.15	0.20	0.14	0.17	0.17	0.11	0.20	0.29	0.16	0.21	0.24	0.23	0.18	0.15	0.17
MgO	46.73	46.90	46.63	46.94	46.65	46.41	47.82	47.34	47.04	46.03	45.91	46.28	46.02	47.77	44.81	45.37	46.54	47.53	49.75
Cr2O3	0.00	0.00	0.07	0.05	0.04	0.00	0.03	0.01	0.03	0.00	0.00	0.07	0.00	0.00	0.03	0.00	0.17	0.02	0.07
CaO	0.19	0.20	0.17	0.17	0.18	0.15	0.17	0.18	0.18	0.17	0.15	0.22	0.17	0.19	0.19	0.19	0.15	0.17	0.12
NiO	0.12	0.13	0.03	0.16	0.09	0.14	0.11	0.12	0.11	0.14	0.14	0.18	0.08	0.09	0.14	0.10	0.17	0.31	0.38
Total	100.42	100.58	100.24	99.76	99.72	99.46	99.55	99.68	99.66	99.98	99.73	99.76	99.82	99.71	100.84	100.08	100.18	98.94	99.88
Fo	86.68	86.53	86.31	86.80	86.35	85.97	88.18	87.44	86.97	86.16	85.15	85.74	85.32	88.11	83.90	85.25	86.93	88.71	91.00

Olivine	78129-3/2	78129-4	78129-5	78129-6	78129-7	78129-8/1	78129-8/2	78129-9/1	78129-9/2	78129-10	78129-11	78129-12	78129-13	78129-14	78129-15/1	78129-15/2	78129-17	78129-5c	78129-10c
SiO2	40.26	40.16	39.97	40.09	39.89	40.44	41.56	40.80	40.72	40.36	40.01	40.40	40.25	40.00	40.84	40.25	40.78	39.82	40.42
FeO	12.57	14.46	15.24	14.25	14.67	12.59	9.32	11.09	10.77	12.89	14.11	12.63	11.90	13.81	10.31	11.09	13.73	13.81	11.42
MnO	0.25	0.16	0.22	0.24	0.23	0.24	0.13	0.23	0.15	0.33	0.23	0.10	0.13	0.20	0.21	0.14	0.18	0.26	0.28
MgO	46.69	44.98	44.46	44.98	44.73	46.89	49.50	47.70	48.23	46.72	45.46	46.64	46.74	45.32	48.31	47.62	46.36	45.41	47.44
Cr2O3	0.02	0.00	0.03	0.06	0.01	0.08	0.06	0.02	0.05	0.02	0.02	0.02	0.01	0.03	0.07	0.00	0.03	0.00	0.03
CaO	0.15	0.25	0.19	0.19	0.21	0.19	0.14	0.19	0.15	0.17	0.21	0.17	0.18	0.18	0.17	0.19	0.15	0.22	0.17
NiO	0.09	0.12	0.08	0.10	0.12	0.20	0.24	0.19	0.17	0.13	0.15	0.11	0.16	0.18	0.26	0.20	0.14	0.13	0.16
Total	100.03	100.13	100.18	99.91	99.85	100.63	100.96	100.22	100.23	100.63	100.18	100.07	99.37	99.71	100.17	99.49	101.35	99.64	99.92
Fo	86.88	84.73	83.88	84.91	84.46	86.91	90.45	88.47	88.87	86.60	85.18	86.81	87.50	85.40	89.31	88.45	85.76	85.42	88.11

Table F10. Bukit Mapas - olivines for Al-spinel study

Spinel	78133-42/1	78133-10/1	78133-10/2	78133-10/3	78133-10/5	78133-10/6	78133-62/1	78133-62/2	78129-65/2	78129-76-1	78129-76-2	78129-76-3	78129-76-4	78129-5a
TiO2	0.34	0.51	0.45	0.45	0.43	0.43	0.84	0.84	0.27	0.23	0.26	0.25	0.26	0.39
Al2O3	54.76	38.43	37.74	37.61	39.43	38.22	16.59	16.71	10.00	57.31	56.64	56.35	56.26	54.60
Cr2O3	0.18	14.56	15.22	15.52	14.93	15.73	36.59	36.24	54.08	0.28	0.59	0.74	0.92	1.45
Fe2O3	14.06	15.16	15.31	15.67	14.42	14.57	15.80	15.68	7.08	10.97	11.28	11.09	11.04	11.74
FeO	12.14	15.39	14.99	14.95	14.80	15.25	18.97	19.50	15.15	11.01	11.41	11.21	11.43	12.20
MnO	0.16	0.17	0.20	0.17	0.14	0.10	0.37	0.33	0.28	0.14	0.18	0.13	0.06	0.11
NiO	0.21	0.19	0.20	0.21	0.20	0.28	0.00	0.06	0.15	0.16	0.07	0.06	0.16	0.16
MgO	18.73	15.00	14.91	15.06	15.33	14.87	10.42	10.29	11.68	19.44	19.26	19.22	19.12	18.88
Total	100.70	99.74	99.21	99.84	99.84	99.63	99.70	99.97	98.74	99.58	99.80	99.12	99.34	99.94
mg#	0.73	0.63	0.64	0.64	0.65	0.63	0.49	0.48	0.58	0.76	0.75	0.75	0.75	0.73
cr#	0.00	0.20	0.21	0.22	0.20	0.22	0.60	0.59	0.78	0.00	0.01	0.01	0.01	0.02
Fe2+/Fe3+	0.96	1.13	1.09	1.06	1.14	1.16	1.33	1.38	2.38	1.12	1.12	1.12	1.15	1.16
Fo (host olivine)	86.49	85.56	85.57	85.74	85.49	85.38	85.50	84.87	90.56	85.25	85.25	85.25	85.25	84.68

Spinel	78129-27	78129-70/2	78133-4/1	78133-4/2	78129-6a-1	78129-6a-2	78129-6a-3	78129-7a	78129-12a/1	78129-13a/1	78129-13a/2	78129-1-1	78129-1-2	78129-1-3
TiO2	0.57	0.78	0.37	0.88	0.83	0.69	0.72	0.79	0.83	0.30	0.89	0.75	0.66	0.67
Al2O3	50.85	16.52	39.13	18.79	54.56	55.35	54.76	17.02	17.61	50.40	16.63	56.96	55.68	54.79
Cr2O3	5.28	36.04	14.59	36.12	0.53	0.56	0.63	40.88	38.04	5.25	36.76	0.44	0.74	0.69
Fe2O3	12.57	15.19	16.21	14.89	12.58	12.30	12.76	11.99	14.02	13.18	15.51	12.51	12.83	12.49
FeO	12.59	16.86	13.36	18.37	12.25	12.08	12.44	16.80	17.53	13.29	19.05	12.00	11.21	12.35
MnO	0.30	0.25	0.07	0.26	0.13	0.05	0.09	0.29	0.19	0.17	0.36	0.12	0.09	0.12
NiO	0.16	0.03	0.18	0.09	0.14	0.09	0.18	0.08	0.00	0.09	0.13	0.31	0.22	0.22
MgO	18.20	11.24	16.10	11.14	18.63	18.89	18.60	11.73	11.48	17.31	10.07	19.52	19.63	18.53
Total	100.72	97.01	100.00	100.53	99.65	100.00	100.18	99.58	99.70	99.98	99.39	102.61	101.07	99.86
mg#	0.72	0.54	0.68	0.52	0.73	0.74	0.73	0.55	0.54	0.70	0.49	0.74	0.76	0.73
cr#	0.07	0.59	0.20	0.56	0.01	0.01	0.01	0.62	0.59	0.07	0.60	0.01	0.01	0.01
Fe2+/Fe3+	1.11	1.23	0.92	1.37	1.08	1.09	1.08	1.56	1.39	1.12	1.36	1.07	0.97	1.10
Fo (host olivine)	85.21	86.53	86.31	86.80	85.97	85.97	85.97	88.18	87.44	85.15	85.74	83.90	83.90	83.90

Table F11. Bukit Mapas - Al- and Cr-spinel inclusions for Al-spinel study

Spinel	78129-3/1	78129-4-1	78129-4-2	78129-5-1	78129-5-2	78129-5-3	78129-6	78129-7-1	78129-7-2	78129-8/1	78129-9/1-b	78129-9/1-c	78129-9/1-d	78129-9/1-e	78129-9/1-f
TiO2	0.68	0.55	0.53	0.28	0.27	0.33	1.10	0.60	0.27	0.78	0.69	0.59	0.53	0.66	0.41
Al2O3	15.95	56.10	56.33	55.92	55.60	56.11	18.23	57.27	57.25	13.88	19.02	15.02	14.78	20.14	50.53
Cr2O3	42.27	0.68	0.52	2.51	1.35	0.46	32.75	0.59	0.54	44.10	35.80	42.96	43.13	33.90	4.05
Fe2O3	12.31	14.01	12.60	11.28	13.74	13.92	17.88	11.68	12.00	12.91	16.42	13.31	13.57	17.27	15.92
FeO	17.04	11.99	11.42	12.07	12.15	11.86	19.76	11.91	11.83	17.16	16.56	16.94	16.92	16.95	11.86
MnO	0.27	0.15	0.11	0.15	0.18	0.08	0.21	0.17	0.03	0.32	0.31	0.26	0.21	0.25	0.13
NiO	0.04	0.16	0.13	0.18	0.19	0.17	0.20	0.14	0.14	0.09	0.00	0.17	0.13	0.12	0.20
MgO	11.52	19.50	19.52	18.84	18.96	19.30	10.13	19.40	19.33	11.33	12.31	11.46	11.46	12.25	18.62
Total	100.07	103.14	101.15	101.23	102.43	102.22	100.26	101.76	101.37	100.57	101.10	100.71	100.73	101.53	101.71
mg#	0.55	0.74	0.75	0.74	0.74	0.74	0.48	0.74	0.74	0.54	0.57	0.55	0.55	0.56	0.74
cr#	0.64	0.01	0.01	0.03	0.02	0.01	0.55	0.01	0.01	0.68	0.56	0.66	0.66	0.53	0.05
Fe2+/Fe3+	1.54	0.95	1.01	1.19	0.98	0.95	1.23	1.13	1.09	1.48	1.12	1.41	1.39	1.09	0.83
Fo (host olivine)	86.93	84.73	84.73	83.88	83.88	83.88	84.91	84.46	84.46	86.91	88.47	88.47	88.47	88.47	88.47

Spinel	78129-9/-1g	78129-9/2	78129-11	78129-14	78129-15/1	78129-17
TiO2	0.23	0.66	0.72	0.73	0.43	0.36
Al2O3	57.60	16.42	55.98	54.97	12.74	56.67
Cr2O3	0.22	42.88	0.47	0.58	51.02	0.79
Fe2O3	13.01	12.02	12.58	14.38	8.69	13.63
FeO	9.19	15.72	11.88	11.76	15.46	11.46
MnO	0.15	0.31	0.06	0.07	0.10	0.12
NiO	0.25	0.14	0.35	0.23	0.08	0.09
MgO	20.94	12.42	19.13	19.45	12.38	19.81
Total	101.58	100.56	101.11	102.17	100.91	102.92
mg#	0.80	0.58	0.74	0.75	0.59	0.76
cr#	0.00	0.64	0.01	0.01	0.73	0.01
Fe2+/Fe3+	0.78	1.45	1.05	0.91	1.98	0.93
Fo (host olivine)	88.47	88.87	85.18	85.40	89.31	85.76

Table F11 cont. Bukit Mapas - Al- and Cr-spinel inclusions for Al-spinel study

Pyroxene inclusions in olivine

Pyroxene	78133-62/2-1	78133-62/2-2	78129-24	78129-70/1	78129-7a	78129-12a/3	78129-9a
SiO2	45.17	45.67	51.37	51.27	51.60	52.05	49.05
TiO2	0.93	1.04	0.23	0.30	0.28	0.28	0.61
Al2O3	10.86	11.60	2.94	3.04	2.96	2.93	5.91
FeO	8.45	8.58	4.36	4.69	3.67	4.84	5.46
MnO	0.12	0.05	0.12	0.05	0.03	0.09	0.12
MgO	12.18	12.29	16.74	16.62	17.08	17.16	15.07
CaO	21.51	21.96	22.16	22.62	21.67	22.19	21.34
Na2O	0.35	0.42	0.26	0.24	0.26	0.24	0.29
Cr2O3	0.04	0.06	0.84	0.68	0.84	0.47	0.35
Total	99.61	101.67	99.02	99.51	98.38	100.23	98.19
Mg/Mg+Fe2+	0.72	0.72	0.87	0.86	0.89	0.86	0.83
Fo (host olivine)	**84.87**	**84.87**	**87.31**	**86.68**	**88.18**	**86.16**	**85.32**

Inclusions in cpx 78133-62/2-2

SiO2	29.14	35.73	38.76
TiO2	3.47	2.82	2.21
Al2O3	19.71	18.79	19.85
FeO	22.45	16.54	13.30
MnO	0.12	0.05	0.00
MgO	11.49	10.38	8.80
CaO	13.14	14.75	11.47
Na2O	0.72	1.30	1.76
K2O	0.19	0.37	0.79
P2O5	0.32	0.47	0.48
Total	100.78	101.28	97.52

Olivine inclusions in olivine 78129-65/1

SiO2	40.04	40.57
FeO	8.32	7.78
MnO	0.22	0.11
MgO	50.01	50.36
Cr2O3	0.00	0.00
CaO	0.13	0.15
NiO	0.34	0.36
Total	99.05	99.33
Fo	91.46	92.02
Fo (host olivine)	**91.95**	**91.95**

Table F12. Bukit Mapas - solid inclusions in olivine and pyroxene

Spinel	78133-5	78129-12a/2-1	78129-12a/2-clp	78129-12a/2-3	78129-12a/2-4	78129-12a/3
TiO2	0.31	0.74	0.52	0.40	0.55	0.38
Al2O3	57.56	16.18	58.80	58.79	57.00	57.76
Cr2O3	0.02	35.72	0.03	0.07	0.11	0.93
Fe2O3	10.76	17.99	10.09	10.20	11.14	10.89
FeO	11.87	18.15	11.48	11.40	11.93	9.52
MnO	0.11	0.25	0.16	0.07	0.11	0.00
NiO	0.09	0.00	0.13	0.13	0.21	0.15
MgO	18.96	10.76	19.61	19.72	19.04	20.70
Total	99.67	99.79	100.81	100.78	100.09	100.33
mg#	0.74	0.51	0.75	0.76	0.74	0.79
cr#	0.00	0.60	0.00	0.00	0.00	0.01
Fe2+/Fe3+	1.23	1.12	1.26	1.24	1.19	0.97
Fo (host olivine)	86.35	86.97	86.97	86.97	86.97	86.16

Spinel	78129-6-2	78129-8/2	78129-8c-1	78129-3c/1-1	78129-3c/2-1	78129-7c-1
TiO2	0.44	0.22	0.54	0.61	0.38	0.76
Al2O3	54.69	50.63	13.34	14.45	14.75	16.99
Cr2O3	0.77	0.30	46.02	42.62	48.00	34.20
Fe2O3	12.68	10.80	11.33	12.74	8.54	19.19
FeO	9.99	8.36	14.98	17.05	14.22	16.30
MnO	0.01	0.05	0.31	0.34	0.11	0.17
NiO	0.29	0.29	0.11	0.20	0.16	0.17
MgO	19.65	18.11	12.23	10.96	12.92	12.05
Total	98.51	88.76	98.86	98.96	99.07	99.84
mg#	0.78	0.79	59.28	53.41	61.84	56.86
cr#	0.01	0.00	69.83	66.43	68.58	57.45
Fe2+/Fe3+	0.88	0.86	1.47	1.49	1.85	0.94
Fo (host olivine)	84.91	90.45	89.69	88.71	91.00	87.84

Spinel	78129-7c-2	78129-8c-2	78129-3c/1-2	78129-3c/2-2
TiO2	0.29	0.31	0.43	0.17
Al2O3	56.33	56.84	58.82	61.63
Cr2O3	0.05	1.06	0.34	0.16
Fe2O3	12.72	12.48	9.58	6.96
FeO	10.65	6.83	8.89	6.10
MnO	0.17	0.07	0.11	0.07
NiO	0.19	0.33	0.36	0.42
MgO	19.55	22.09	20.85	22.61
Total	99.95	100.01	99.39	98.12
mg#	76.60	85.22	80.70	86.86
cr#	0.06	1.24	0.38	0.18
Fe2+/Fe3+	0.93	0.61	1.03	0.97
Fo (host olivine)	87.84	89.69	88.71	91.00

Table F13. Bukit Mapas - solid inclusions in melt inclusions

Spinel	78129-12a/1	78129-6-1
TiO2	0.69	0.56
Al2O3	51.33	14.39
Cr2O3	0.06	43.03
Fe2O3	12.46	13.11
FeO	13.73	16.11
MnO	0.08	0.27
NiO	0.09	0.11
MgO	16.29	11.65
Total	94.72	99.23
mg#	0.68	0.56
cr#	0.00	0.67
Fe2+/Fe3+	1.22	1.37
Fo (host olivine)	85.15	84.91

Spinel	78129-5c-1	78129-5c-2
TiO2	0.58	0.30
Al2O3	44.49	54.01
Cr2O3	0.03	0.05
Fe2O3	23.11	13.97
FeO	13.54	12.67
MnO	0.23	0.08
NiO	0.14	0.14
MgO	16.13	17.91
Total	98.24	99.11
mg#	67.98	71.60
cr#	0.05	0.06
Fe2+/Fe3+	0.65	1.01
Fo (host olivine)	85.42	85.42

Pyroxene	78129-12a/2	78129-12a/3
SiO2	45.25	50.09
TiO2	1.38	0.52
Al2O3	9.05	4.65
FeO	7.06	5.37
MnO	0.11	0.09
MgO	13.20	16.24
CaO	21.88	21.95
Na2O	0.29	0.26
Cr2O3	0.06	0.61
Total	98.28	99.78
Mg/Mg+Fe2+	0.77	0.84
Fo (host olivine)	86.97	86.16

Pyroxene	78129-10	78129-12
SiO2	45.81	47.39
TiO2	1.21	1.08
Al2O3	10.94	8.62
FeO	8.06	6.02
MnO	0.10	0.03
MgO	14.24	14.34
CaO	21.44	22.55
Na2O	0.36	0.25
Cr2O3	0.07	0.31
Total	102.23	100.59
Mg/Mg+Fe2+	0.76	0.81
Fo (host olivine)	86.60	86.81

Glass/Plagioclase	78129-12a/2	78129-3/2
SiO2	57.47	57.40
TiO2	0.71	0.28
Al2O3	25.22	26.29
FeO	1.38	1.17
MnO	0.00	0.04
MgO	0.56	0.91
CaO	1.52	1.08
Na2O	11.55	12.96
K2O	1.71	0.99
P2O5	0.94	0.85
Total	101.06	101.96

Table F13 cont. Bukit Mapas - solid inclusions in melt inclusions

Pyroxene	78129-13a/1	78129-10a	78129-3/2	78129-5	78129-4	78129-6/2
SiO2	43.30	43.97	40.18	40.82	43.92	45.92
TiO2	0.77	1.76	1.78	1.98	1.71	1.12
Al2O3	15.11	11.27	13.46	14.57	10.77	9.94
FeO	8.56	7.97	11.26	9.14	7.88	6.36
MnO	0.07	0.07	0.07	0.06	0.02	0.00
MgO	8.80	11.74	11.79	10.42	13.92	13.10
CaO	20.00	22.31	20.73	21.97	20.70	22.82
Na2O	0.97	0.31	0.35	0.26	0.37	0.29
Cr2O3	0.00	0.02	0.04	0.06	0.05	0.04
Total	97.59	99.42	99.65	99.27	99.33	99.59
Mg/Mg+Fe2+	0.65	0.72	0.65	0.67	0.76	0.79
Fo	85.15	88.11	86.88	83.88	84.91	90.45
(host olivine)						

Pyroxene	78129-13	78129-3c/2	78129-5c	78129-10c	78133-62/2
SiO2	45.23	46.19	41.31	41.73	45.42
TiO2	1.12	1.35	1.95	0.88	0.99
Al2O3	9.63	10.27	14.19	16.08	11.23
FeO	7.40	5.51	9.48	7.21	8.52
MnO	0.02	0.03	0.03	0.06	0.09
MgO	12.96	13.51	10.00	10.15	12.24
CaO	22.84	22.87	22.57	22.70	21.74
Na2O	0.22	0.36	0.28	0.29	0.39
Cr2O3	0.16	0.02	0.02	0.00	0.05
Total	99.57	100.12	99.83	99.09	100.64
Mg/Mg+Fe2+	0.76	81.38	65.29	71.52	71.92
Fo	87.50	91.00	85.42	88.11	84.88
(host olivine)					

Glass/Plagioclase	78129-15/2
SiO2	58.34
TiO2	0.39
Al2O3	25.84
FeO	0.52
MnO	0.00
MgO	0.08
CaO	0.84
Na2O	13.72
K2O	0.85
P2O5	0.56
Total	101.15

Table F13 cont. Bukit Mapas - solid inclusions in melt inclusions

Pyroxene phenocryst	78129-25	78130-30	78130-29	78130-28
SiO2	53.24	51.14	52.55	51.80
TiO2	0.19	0.35	0.23	0.22
Al2O3	2.40	3.75	2.61	3.52
FeO	3.89	4.78	4.82	4.23
MnO	0.05	0.11	0.07	0.06
MgO	17.72	16.14	16.54	16.45
CaO	21.99	22.55	22.13	22.25
Na2O	0.23	0.19	0.17	0.21
Total	99.70	98.99	99.13	98.74
Mg/Mg+Fe2+	0.89	0.86	0.86	0.87

Table F14. Bukit Mapas - clinopyroxene phenocrysts